

MECHANICAL PROPERTIES OF TANK CAR STEELS RETIRED FROM THE FLEET

FINAL REPORT

SwRI® Project No. 18.12240
Foster-Miller Subcontract SUB3-00022
Volpe Contract No. DDTS.060183.000.801

Prepared by

Peter C. McKeighan

Prepared for

Foster-Miller Inc.
350 Second Ave.
Waltham, MA 02154-1196

August 2008



SOUTHWEST RESEARCH INSTITUTE®
SAN ANTONIO HOUSTON WASHINGTON, DC

MECHANICAL PROPERTIES OF TANK CAR STEELS RETIRED FROM THE FLEET

FINAL REPORT

SwRI® Project No. 18.12240
Foster-Miller Subcontract SUB3-00022
Volpe Contract No. DDTS.060183.000.801

Prepared by

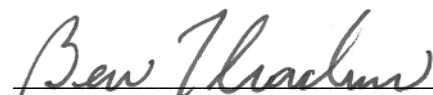
Peter C. McKeighan

Prepared for

Foster-Miller Inc.
350 Second Ave.
Waltham, MA 02154-1196

August 2008

APPROVED:



Ben H. Thacker, Ph.D., Director
Materials Engineering Department

TABLE OF CONTENTS

Section	Page
List of Tables	v
List of Figures.....	vii
Executive Summary	xiii
1.0 Introduction.....	1
1.1 Pressure Tank Car Fleet in the United States.....	2
1.2 Statistical Variables Concerning Tank Car Steel.....	3
1.3 Previous Steel Property Testing Performed for GATX	5
2.0 Previous Vintage Tank Car Fracture Toughness Testing	13
2.1 Scope of the Testing.....	13
2.2 Testing Procedures.....	14
2.3 Summary of Results.....	15
3.0 Pedigree of In-service Vintage Tank Car Materials	27
3.1 Material Identification Scheme.....	27
3.2 Material Sources and Description.....	27
3.3 Subdividing the Fleet of Tank Cars	29
4.0 Material Characterization Testing of Vintage Materials	49
4.1 Material Processing.....	49
4.2 Material Characterization Test Procedures.....	49
4.3 Results of Material Characterization	51
4.4 Comparison with TC128-B Material Specifications.....	53
5.0 Pendulum Impact Testing of Bulk Fracture Behavior	79
5.1 Background.....	79
5.2 Pendulum Test Method Details.....	80
5.3 Effect of Specimen Thickness and Width on BFCM Energy (sharpest tup)	83
5.4 BFCM Energy of Vintage Tank Car Material (sharpest tup)	84
5.5 Sharp versus Blunt Impactor Tup	85
5.6 Effect of Specimen Thickness on BFCM Energy (bluntest tup)	86
5.7 Stalling the BFCM – Effect of Initial Angle on BFCM Energy (bluntest tup).....	87
6.0 Fracture Testing of Retired Vintage Materials	117
6.1 Preliminary Matrix of Conditions.....	117
6.2 Differences between Current Testing and Previous GATX Minot Testing.....	118
6.3 Fracture Toughness Test Specimens.....	119
6.4 Toughness Test Procedures.....	119

TABLE OF CONTENTS (Continued)

Section	Page
6.5	Preliminary Assessments of High Rate Test Frame Performance 120
6.6	Necessity for Backup Load Measurement (Grip Strain Gages)..... 122
6.7	Analysis Methodology for the High Rate Fracture Toughness Test Data 123
6.8	High Rate Fracture Toughness Test Data 124
6.9	Fracture Surfaces 126
6.10	Fracture Toughness Variation of TC128-B with Date of Fabrication 127
6.11	Global Averages for Fleet Subsets..... 129
6.12	Toughness Correlations 130
7.0	Limitations of Fracture Toughness Data..... 165
7.1	Toughness Methodology Utilized Herein..... 165
7.2	Toughness Magnitude and CVN Correlations to Fracture Toughness 167
7.3	Accommodating Nonlinear (Ductile) Fracture 169
7.4	Accommodating Linear (Brittle) Fracture 171
7.5	Structural Relevance of Test Results 172
7.6	Significance of Dynamic Fracture Toughness to Tank Car Structural Integrity..... 173
8.0	Summary 185
9.0	References..... 189
APPENDIX A – Data from High Rate Fracture Toughness Tests A-1	
APPENDIX B – NTSB Assessment..... B-1	

LIST OF TABLES

Table	Page
1-1 Makeup of the pressure tank car fleet as of 2005 (UMLER, April 2005 data).....	7
2-1 Tabulated fracture toughness test results for the twelve different Minot tank car plate conditions evaluated.....	17
2-2 Tabulated fracture toughness test results for the pieces excised from scrapped tank cars	18
3-1 Cars available for materials testing (including teardown material and Minot-related plates)	31
3-2 Steel pieces from the different scrapped cars provided in support of this effort	32
3-3 Steel pieces from the car sills (teardown effort) and from those tested during the GATX-sponsored Minot work.....	33
3-4 Alphabetical listing of the different tank cars describing features and characteristics of each	34
4-1 Tensile properties for most of the TC128-B plate material	56
4-2 Tensile properties for teardown, Minot and post-1989 TC128-B material	57
4-3 Composition properties for most of the TC128-B plate material	58
4-4 Composition properties for teardown, Minot and post-1989 TC128-B material.....	59
4-5 CVN energy properties for most of the TC128-B plate material.....	60
4-6 CVN energy properties for teardown, Minot and post-1989 TC128-B material	61
4-7 Statistical analysis (averages and standard deviations) of TC128-B material characterization testing	62
4-8 Tensile property and chemical specifications for TC128-B	63
5-1 Test plates and specimens required for Volpe fracture toughness testing	88
5-2 Comparison of properties between the two baseline normalized TC128-B materials	89

LIST OF TABLES *(Continued)*

Table	Page
5-3	BFCM test results assessing the influence of specimen dimensions (normalized TC128-B circa 1999 from tank head offal).....90
5-4	BFCM test results assessing the difference between different railroad tank car materials fabricated at different times.....91
5-5	BFCM energy levels for the different thickness conditions tested (wider tup)92
5-6	BFCM results examining the effect of different initial energy states (drop heights) on BFCM energy.....93
5-7	Energies and speeds for the different drop heights.....93
6-1	Basic test matrix for high rate fracture toughness testing of a given car condition.....132
6-2	Test plates and compact-tension specimen required for high rate fracture testing.....133
6-3	Matrix of test specimen ID number, date tested, specimen dimensions and flow stress.....134
6-4	Tabulated fracture toughness test results for the different test conditions evaluated135
6-5	Tabulated fracture toughness test results for the different test conditions evaluated136
6-6	Tabulated fracture toughness test results for the different test conditions evaluated137
6-7	Tabulated fracture toughness test results for the different test conditions evaluated138
6-8	Tabulated fracture toughness test results for the different test conditions evaluated139
6-9	Statistical summary of the fracture toughness test data140
7-1	Different forms of the equation relating CVN to fracture toughness (K is in $\text{ksi}\sqrt{\text{in}}$ and CVN is energy in ft-lbs).....175

LIST OF FIGURES

Figure	Page
1-1 Number of pressure tank cars in service as a function of when they were built.....	8
1-2 Cumulative number of pressure tank cars with year produced.....	9
1-3 Description of the materials involved in the pre-1989 pressure tank car fleet	10
1-4 Description of the tank cars available compared to the cumulative number of cars produced.....	11
2-1 The tank car stub sill farm at SwRI from which the two car segments were removed.....	19
2-2 Torch-cutting removing segments from the tank cars	19
2-3 Wreckage from tank cars involved in the Minot accident (Glenwood, MN)	20
2-4 Definition of the orientation of fracture toughness samples in the shell	20
2-5 Tensile property variation with material examined	21
2-6 CVN fracture toughness variation with material examined.....	22
2-7 Typical recorded data for brittle and ductile examples of fracture toughness tests.....	23
2-8 Variation in average high rate fracture toughness as a function of temperature and material (error bars ± 2 std. devs.)	24
2-9 Correlation between fracture toughness and CVN energy for tests at 0°F	25
3-1 Cross-referencing system used to identify steel pieces in all subsequent testing	43
3-2 Different tank car pieces including (a) car stub sill segments from the teardown study in the “stub sill farm” and (b) different pieces of the Minot steel.....	44
3-3 Tank car cut-up instructions and schematic (supplied by Union Tank Car Company).....	45
3-4 Collection of plates received, representative marking and torching smaller pieces out of the plate	46

LIST OF FIGURES *(Continued)*

Figure	Page
3-5 Comparison between the available tank cars and the cumulative car manufacture for the pre-1989 fleet	47
3-6 Temperatures selected for CVN tests (overlaid with NTSB data from Minot report).....	48
4-1 Room temperature tensile yield and ultimate strength for different vintage TC128-B conditions	64
4-2 Room temperature tensile elongation and reduction of area for different vintage TC128-B conditions.....	65
4-3 CVN toughness at -50° and 0° F for different vintage TC128-B conditions.....	66
4-4 CVN toughness at 50°F for different vintage TC128-B conditions	67
4-5 Influence of carbon content on room temperature strength for vintage TC128-B	68
4-6 Room temperature tensile and yield strength for different normalized TC128-B and other material types	69
4-7 Room temperature tensile elongation and reduction of area for normalized TC128-B and other material types.....	70
4-8 CVN toughness at -50°F, 0°F and 50°F for different materials and post-1989 TC128-B conditions.....	71
4-9 Strength properties of vintage TC128-B as a function of when manufactured	72
4-10 Ductility properties of vintage TC128-B as a function of when manufactured.....	73
4-11 CVN toughness properties of vintage TC128-B as a function of when manufactured.....	74
4-12 CVN toughness at 50°F of vintage TC128-B as a function of when manufactured.....	75
4-13 CVN toughness at 0°F of vintage TC128-B as a function of when manufactured.....	76
4-14 CVN toughness at -50°F of vintage TC128-B as a function of when manufactured	77

LIST OF FIGURES *(Continued)*

Figure	Page
5-1	BFCM specimen with self-engaging trapezoidal end and 6-inch long center section94
5-2	Broadest face width (0.5-inch) impact tup.....94
5-3	Medium face width (0.5-inch) impact tup95
5-4	Sharp face width (0.125-inch) impact tup.....95
5-5	Different photographic views of the BFCM facility with a specimen mounted in the test fixture96
5-6	Modern-vintage normalized plate with BFCM specimens extracted97
5-7	The original BFCM arm bent after attempting to fracture the first specimen97
5-8	Pre-test calibration of arm weight and CG position for (a) generation 1 and (b) re-designed BFCM98
5-9	Worn tups after a number of different uses99
5-10	Measured strain response on the back of the specimen behind impactor99
5-11	Typical BFCM fracture surfaces (sharpest tup).....100
5-12	Deformation observed in a blunt impact specimen.....100
5-13	Effect of specimen width on the pendulum impact energy (sharpest tup).....101
5-14	Effect of specimen thickness on the pendulum impact energy (sharpest tup).....102
5-15	Raw BFCM energy for different tank car steels103
5-16	Thickness normalized BFCM energy for different tank car steels104
5-17	Thickness normalized BFCM energy as a function of UTS105
5-18	Thickness normalized BFCM energy as a function of flow strength106
5-19	Thickness normalized BFCM energy as a function of CVN energy107

LIST OF FIGURES *(Continued)*

Figure	Page
5-20 Thickness normalized BFCM energy as a function of elongation.....	108
5-21 Thickness normalized BFCM energy as a function of percent RA	109
5-22 Thickness normalized BFCM energy as a function of a quantity proportional to area under the engineering stress-strain curve	110
5-23 Thickness normalized BFCM energy as a function of a quantity proportional to area under the true stress-strain curve.....	111
5-24 Additional comparisons between sharp and blunt tups.....	112
5-25 Blunt tup results plotted as previously showing a data band for the sharp tup.....	113
5-26 Blunt versus sharp striker tup energy results as a function of specimen thickness	114
5-27 Comparison between the specimen that stalled the machine and a failed specimen	115
6-1 Nominal compact tension specimen dimensions	141
6-2 Modified compact tensile specimen to accommodate eddy current transducer	142
6-3 Cold-box setup (before and after taping with thermal insulating tape) with temperature controller and Nicolet high speed digital storage oscilloscope.....	143
6-4 Compact tension specimen with load line displacement gage, front face clip gage and back face strain gage	144
6-5 Slack adapter to achieve highest rate loading occurring by oversize grip holes	145
6-6 Instrumentation mounted on specimen including back face strain gage, eddy current transducer on the load-line, front face mounted extensometer and grip strain gages.....	145
6-7 Immediately after a high rate, low temperature fracture test with frost formed on the fracture surface and the eddy current transducer exposed	146
6-8 The data generated during the Minot testing was examined to establish the relationship between applied stress intensity factor rate (K-rate), actuator rate and strain rate.....	147

LIST OF FIGURES *(Continued)*

Figure	Page
6-9 The initial LVDT displacement nonlinearity is overcome with a slack adapter.....	148
6-10 High rate frame stroke (average rate of 60 inch/second).....	148
6-11 Example dynamic load cell data (pink signals) that necessitated developing the grip load cell derived from local strain gages.....	149
6-12 Excellent correlation between grip gages and load cell.....	150
6-13 Transducer signals versus time for several pre-tests.....	151
6-14 Load versus COD/BFS for several pre-tests (load derived from grip strain gages).....	152
6-15 Example data from a “brittle” fracture toughness test.....	153
6-16 Example data from a “ductile” fracture toughness test.....	154
6-17 Fracture surfaces from several A212-B specimens	155
6-18 Fracture surfaces from several normalized post-1989 vintage TC128-B materials	156
6-19 Fracture surfaces from several early vintage TC128-B materials	157
6-20 Fracture surfaces from several later vintage TC128-B materials	158
6-21 Fracture toughness plotted as a function of year for the different classifications of materials.....	159
6-22 Fracture toughness average for the different ages/materials at 0°F.....	160
6-23 Fracture toughness average for the different ages/materials at -50°F	161
6-24 CVN energy and fracture toughness variation with sulfur content.....	162
6-25 Fracture toughness variation with thickness normalized BFCM energy	163
6-26 Fracture toughness as a function of CVN energy (at relevant temperature).....	164

LIST OF FIGURES *(Continued)*

Figure		Page
7-1	Variation in toughness as a function of temperature and loading rate.....	176
7-2	Two plots indicating the lower bound relations from Roberts and Newton.....	177
7-3	Comparison between expected compliance (based on crack length) to measured compliance	178
7-4	Sample nonlinear data where the majority of the nonlinearity is plastic zone growth for two different tests/materials.....	179
7-5	Attempt to analyze a troublesome load-displacement diagram	180
7-6	Analysis of another questionable load-displacement diagram resulting in lowered toughness.....	181
7-7	Fracture test data set only made suitable for analysis by smoothing the dynamic nature of the load data.....	182
7-8	Variation of limit load ratio (ratio of max load to the limit load of the specimen) for all tests.....	183

Executive Summary

As a consequence of several recent tank car accidents, the structural integrity of railroad tank cars has come under greater scrutiny, especially the older portion of the fleet fabricated prior to steel normalization requirements. The purpose of this program was to obtain samples of the steel used for tank car shell and head fabrication in the current tank car fleet. Once obtained, the dynamic fracture toughness of a subset of material was determined as well as basic material characterization of all samples. The process of gathering the samples required coordinating with the fleet operators and railroads to obtain pieces of tank cars as they were retired from the fleet. Fleet retirements occur with tank cars of all ages and for numerous reasons unrelated to material issues.

In total, steel samples from thirty-four tank cars were received and tested. These thirty-four tank cars yielded sixty-one different pre-1989 TC128-B conditions (40 shell and 21 head samples), three tank cars yielded seven different post-1989 TC128-B conditions (4 shell and 3 head samples), and six tank cars yielded mixed material (A212, A515 and A285 steel) conditions (6 shell and 5 head samples). All samples were subjected to basic material characterization, tensile property evaluation, chemical makeup, and Charpy v-notch toughness at three temperatures. Dynamic fracture toughness tests were performed at both 0°F and -50°F on a subset of the selected materials and conditions (100 total tests on pieces from 16 tank cars). In addition, some full thickness, unnotched specimen impact testing was performed in a novel pendulum test setup to assess puncture resistance (analysis of these tests is still ongoing).

The vast majority of the TC128-B samples extracted from retired tank cars met current TC128-B material specifications. Elemental composition requirements were satisfied in 97% of the population whereas the required tensile properties were satisfied in 82% of the population. Interpreting the dynamic toughness tests required dividing the pre-1989 fleet into quartiles and testing three tank cars per quartile. Considering the 0°F dynamic fracture toughness results for the pre-1989 fleet, 100% of the oldest two quartiles, 58% of the second youngest quartile, and 83% of the youngest quartile exhibited adequate or better fracture toughness (defined as a toughness greater than 50 ksi√in). Dynamic toughness at -50°F was adequate for 83% of two quartiles, but the other two quartiles exhibited lower toughness with only 33-50% exhibiting adequate properties.

If these results are used for fleet management decisions, it is likely essential to further sample the newest 50% of the pre-1989 fleet. Finally, until toughness can be related to public risk, it is extraordinarily difficult to utilize these results for mitigating risk.

This page intentionally left blank.

1.0 INTRODUCTION

Railroad tank cars are a common type of railcar, accounting for approximately one in every seven cars in the North American Fleet [1]. A large percentage of the tank car fleet carries hazardous materials (HAZMAT) that are flammable, corrosive, poisonous, or pose toxic inhalation danger to the public. As described in the Transportation Research Board (TRB) report [1], the safety of the tank car fleet has been continually improved by Department of Transportation (DOT) regulation and industry through improvements of the physical tank car as well as the operating environment. The TRB report further states that as of 1994, only one person had died as a result of hazardous material release from a tank car since 1980, compared with more than 40 fatalities during the 1970s.

However, the structural integrity of railroad tank cars has come under greater scrutiny due to several recent incidents and accidents:

- *Minot, North Dakota (1/18/2002)* – A freight train moving at approximately 40 mph derailed and five tank cars containing anhydrous ammonia failed catastrophically, resulting in one fatality, \$2M in property damage and \$8M in environmental remediation [2].
- *Macdona, Texas (6/28/2004)* – Two freight trains collided, resulting in three fatalities and a breach in a tank car containing chlorine. Although the NTSB report is not yet fully complete and is believed to be due imminently, some work regarding the materials involved has been released [3].
- *Graniteville, South Carolina (1/6/2005)* – A freight train traveling at about 40 mph collided with a parked train resulting in a release of chlorine gas. Nine fatalities occurred in this accident [4].

In the late 1980s, the American Association of Railroads (AAR) recommended practices changed to require all subsequent pressure cars to be fabricated from normalized TC128-B steel. Prior to 1989, non-normalized steel was used, especially in the shells of the car. Non-normalized steel has a higher transition temperature and potentially lower fracture toughness when compared to normalized steel. The tank cars involved in the three accidents described above included both older- and newer-vintage tank cars. However, all of the catastrophic failures involved in the Minot accident were older-vintage (pre-1989) tank cars.

The National Transportation Safety Board (NTSB) report issued as a consequence of the Minot accident [2] had seven recommendations to the Federal Railroad Administration (FRA). Four of these recommendations concerned either materials or the dynamic forces involved in the accidents (which directly relate to material performance). In particular, the most critical recommendation in terms of this project is the following:

- *“Conduct a comprehensive analysis to determine the impact resistance of the steels in the shells of pressure cars constructed before 1989. At a minimum, the safety analysis should include the results of dynamic fracture toughness tests and/or the results of nondestructive testing techniques that provide information on material ductility and fracture toughness. The data should come from a statistically representative sampling of the shells of the pre-1989 pressure tank car fleet.”*

This recommendation provided the basic motivation for this program. Simply stated, the objective of the project is to perform the testing and analysis required to satisfy the above NTSB recommendation. The approach includes analyzing available data, procuring samples of the pre-1989 tank car fleet, testing the steel, summarizing the results, and identifying pertinent implications. Integral in this effort was the involvement of the AAR Tank Car Committee Task Force T79.32 examining tank car steel properties. These industry volunteers provided the material required in this work.

1.1 Pressure Tank Car Fleet in the United States

To respond to the charge recommended by the NTSB and described earlier, it is first important to understand the vintage and materials involved in the construction of pressure tank cars. The TRB report [1] provides a snapshot of the tank car fleet in 1993 that suggests approximately 55% of the full fleet of tank cars transports HAZMAT and about 44% of this HAZMAT fleet consists of pressure cars. The complete distribution of pressure cars in the fleet in 2005 is shown in Table 1-1 as a function of build date and the material utilized in the tank car. These data, extracted from the Universal Machine Language Equipment Register (UMLER) database, are further analyzed in Figures 1-1 through 1-4.

It is important to note that the data contained in Table 1-1 and plotted in Figures 1-1 through 1-4 represent the current makeup of the fleet as of the date indicated. First, Figure 1-1

provides detail regarding the number of pressure cars in service as a function of build date. For most years, the distribution is populated by 500-1000 tank cars for that year of manufacture. However, there are exceptions for the oldest tank cars and for a period of time in the mid-1980s when tank car production appeared less.

These data describing the makeup of the fleet are further examined on a cumulative number of pressure tank cars in Figure 1-2. Approximately 75% of the pressure car fleet was manufactured prior to 1998. Moreover, $\frac{1}{4}$ of the full fleet was produced before 1976 and $\frac{1}{2}$ before 1990. In terms of materials (Figure 1-3), 93% of the pressure car fleet are manufactured from TC128-B and 4% from A212B. The remaining 3% are fabricated from other materials, including A515, A516 and A285C as the most numerous choices in this small percentage of the fleet.

1.2 Statistical Variables Concerning Tank Car Steel

Examining the tank car fleet as a whole, there are a number of obvious variables involved in the 60,000+ pressure cars. These variables include such things as:

- tank car manufacturer
- date of fabrication
- steel manufacturers and mill sites
- steel plate thickness
- type of steel
- shell and head locations
- position where the steel is extracted from the car (A-end or B-end heads, or different rings along the length of the car)
- commodity carried
- service life history and overall usage of the tank car
- design idiosyncrasies of the tank car.

These variables act to complicate the sampling strategy required to assess overall steel properties in the fleet. If the list above is examined, the concept of a specific car having a single material property characteristic is obviously a misnomer. Each car has its own distribution of toughness properties that is related in some way to the fleet distribution of properties.

Nevertheless, some of these issues can be easily dealt with; for instance, shell/head locations can be sampled from the same car. Certificates of construction for candidate tank cars also will list the manufacturer, date of manufacture (roughly), type of steel, and steel thickness. The UMLER database will also indicate what commodity was carried in the tank car. However, in some cases records are simply not available (e.g. material lots associated with a given car or steel manufacturer) or cannot be made available for competitive reasons (e.g. makeup of the tank car fleet in terms of car manufacturer). Service life history, overall usage of the tank car (miles traveled and other anomalies that occurred over the life of the car) and design idiosyncrasies are also variables that can not be measured with the data available.

Given these limitations, an engineering approach was taken to procuring the materials involved in this work. First, industry participants in the AAR Tank Car Committee Task Force T79.32 were requested to make steel available from tank cars. These tank cars were being scrapped either because they were too old (and hence no longer economically viable) or they had been involved in an accident and hence were being scrapped¹. Second, material that was available at Southwest Research Institute (SwRI) from previous projects was re-examined in the context of the goals for this program. The cars available are shown with the fleet population in Figure 1-4.

This methodology implies that the steel coupons obtained from tank cars are random in occurrence and, therefore, not guaranteed to be representative of the full pre-1989 pressure tank car fleet. Without additional data other than that noted above, it is difficult to definitively state whether the sampling that is available is representative of the fleet. Furthermore, one fundamental assumption in the approach utilized is that steel properties do not degrade with service use, or time in service. If, for instance, we were evaluating the fatigue performance of the steel where applied loading cycles would consume fatigue life, this approach would be fundamentally flawed. However, it is assumed that the fracture toughness of the steel does not

¹ When a car had been involved in an accident, special care was taken to ensure that the material supplied was not in an area where the accident affected the material properties. For instance, if a car was involved in a serious fire, no material was used from it due to concern about how the fire might affect steel properties. On the other hand, if the car derailed, material was supplied from that car as long as it was not dented or heavily deformed or near a region that was. Obviously, the tank cars involved in the Minot accident were exceptions to this case since samples were typically extracted adjacent to catastrophic failure or denting.

degrade with service use and the properties measured are consistent with the overall, original quality of the steel supplied.

In theory, if a sufficient sampling of the tank car fleet were made, it could be possible to measure behavior and make conclusions regarding how material performance changes as a function of each different year of manufacture. This would likely take multiple samples per year (assume for argument, ten samples per year from a range of suppliers) with an overall span of 25 years (1964 to 1988). The scope of this outlined effort, 250 different tank cars with potentially different head and shell locations, is simply beyond the current tank car samples available, time allowed and budgetary constraints for this effort.

A more modest approach has been taken to sampling available tank cars, driven to some extent by the samples that have been made available. The hypothesis that is being tested is that refinements in steel fabrication have led to a gradual improvement of properties over time. By the end of this program, we want to definitively understand behavior over a decade, or possibly half of a decade. Therefore, the goal has been to procure a tank car for roughly each year of manufacture represented in the current pressure car fleet. This has been the approach utilized when candidate tank cars have become available and been considered for this program. The goal is to be able to understand how properties have changed over a number of years, not on a year-to-year basis. This is an important characteristic and limitation of the current work detailed herein.

1.3 Previous Steel Property Testing Performed for GATX

During the summer of 2005, SwRI was retained by GATX to provide fracture toughness testing of tank car steel in support of ongoing litigation concerned with the 2002 Minot tank car accident described in the introduction of this report. This work is particularly germane to the focus of this program and has provided a framework for the approach utilized. Due to the relevance of this work, GATX has fully approved sharing the results with the AAR Tank Car Committee Task Force T79.32 examining tank car steel properties. Hence, the results obtained during this GATX-sponsored program have been fully integrated into this overall effort. This

leveraging is significant because the GATX funding was approximately 50% of the total authorized to date for the FRA work detailed in this report.

Four recent documents detail the work performed for GATX and these documents were provided to members of the Task Force:

- An extended executive summary of the GATX work [5]
- A methodology for interpreting the resulting fracture toughness magnitudes [6]
- A report detailing material property and fracture toughness measurements on exemplar (similar) steel from tank cars that were similar to the mid-1970s vintage cars involved in Minot [7]
- A second report detailing material property and fracture toughness measurements on artifact steel (extracted from the wrecked Minot tank cars) [8].

In summary, the scope of the work outlined in these references included evaluations of TC128-B material properties from modern normalized plate, two older pressure cars (1967 and 1971) and six Minot tank cars (1976 and 1978 vintage). A number of different locations (head and shell, A- and B-end of the cars) were examined as well as properties from shells that fractured and adjacent plates welded to the fractured shells. In total, nine conditions were examined from tank cars not involved in Minot and twelve conditions from the Minot tank cars. The primary material property evaluated was a high rate fracture toughness (K-based) measure, although chemistries, tensile properties, and Charpy V-notch (CVN) toughnesses were also examined to a limited extent. This Minot-related work is important because: (a) it is anticipated that all subsequent evaluations of tank car steel will be performed in a similar manner to the GATX-sponsored work, and (b) the Minot-related material results will be leveraged into the current program to provide the fullest picture possible of the mechanical properties of the tank car fleet.

The next section of this report more fully discusses the GATX work that was performed previous to this work yet providing a framework for the testing.

Table 1-1. Makeup of the pressure tank car fleet as of 2005 (UMLER, April 2005 data).

Year	Not Listed	ASTM A516 Gr 70	AAR TC128 Gr B	ASTM A515 Gr 70	ASTM A285 Gr C	ASTM A212 A Gr	ASTM A212 Gr B	AAR TC128 A Gr	ASTM A240 T304L	ASTM A537	Other
1956	9	0	0	0	0	0	0	0	0	0	0
1957	43	0	0	0	2	0	0	0	0	0	3
1958	30	0	0	0	2	0	3	0	0	0	1
1959	4	0	0	0	1	0	0	0	0	0	0
1960	4	0	0	0	5	0	10	0	0	0	0
1961	14	0	0	0	2	1	25	0	0	0	0
1962	56	0	0	0	0	0	30	0	0	0	0
1963	41	0	0	0	0	0	42	0	0	0	0
1964	214	0	8	0	5	2	123	11	0	0	0
1965	156	0	58	0	4	0	237	41	0	0	0
1966	330	0	575	5	3	0	145	3	0	0	1
1967	398	5	971	2	11	0	17	0	0	0	0
1968	244	8	1109	14	2	0	1	0	0	0	4
1969	578	3	1330	6	3	0	2	0	0	0	5
1970	532	5	1351	7	5	0	12	0	0	0	0
1971	398	0	693	0	1	0	2	0	0	0	0
1972	266	3	177	22	0	0	0	0	0	0	0
1973	266	0	633	0	0	0	0	0	0	0	0
1974	329	19	557	0	0	0	0	0	0	2	0
1975	177	8	864	24	0	0	0	0	0	2	0
1976	465	0	770	1	1	0	0	0	0	0	0
1977	740	0	1072	0	2	0	0	0	0	0	2
1978	498	27	1322	0	2	0	0	0	0	8	0
1979	791	6	1395	0	1	0	0	0	0	0	0
1980	728	8	2134	0	0	0	8	0	0	4	0
1981	506	0	1334	6	0	0	0	0	0	10	0
1982	166	0	367	0	0	0	0	0	0	0	0
1983	11	20	59	0	2	0	0	0	0	0	0
1984	107	0	137	0	0	0	0	0	0	0	0
1985	98	0	209	0	0	0	0	0	0	0	0
1986	30	25	189	0	1	0	0	0	0	0	0
1987	24	36	387	0	0	0	0	0	0	0	0
1988	105	10	1062	0	0	0	0	0	0	0	0
1989	72	18	748	0	0	0	0	5	0	0	0
1990	384	58	865	0	0	0	0	0	0	0	0
1991	328	12	1168	0	0	0	0	0	0	0	0
1992	390	5	959	0	0	0	0	0	0	0	0
1993	30	0	893	0	0	0	0	0	0	0	12
1994	170	0	725	0	0	0	0	0	3	0	0
1995	774	0	1380	0	0	0	0	18	0	0	0
1996	399	105	3318	0	0	0	0	72	0	0	0
1997	71	0	2060	0	0	0	0	14	0	0	0
1998	0	22	2822	0	0	0	0	0	7	0	0
1999	0	37	1776	0	0	0	0	0	15	0	0
2000	0	49	1983	0	0	0	0	0	3	0	0
2001	0	34	1774	0	0	0	0	0	0	0	0
2002	0	15	1358	0	0	0	0	0	0	0	0
2003	0	14	2640								
2004	0	0	3985								
2005	0	0	2098								
2006	0	0	426								
Total	10976	552	49741	87	55	3	657	164	28	26	28
Percent	17.61	0.89	79.82	0.14	0.09	0.00	1.05	0.26	0.04	0.04	0.04

Reference: J.W. Cardinal, P.C. McKeighan, W.N. Caldwell, and J.R. Billing, "Low Temperature Impact Effect on Tank Cars," Transport Canada Report No. TP 14139E, July 2003, p. 6.

Update by PGK 7/19/2005 using 2005 April UMLER data

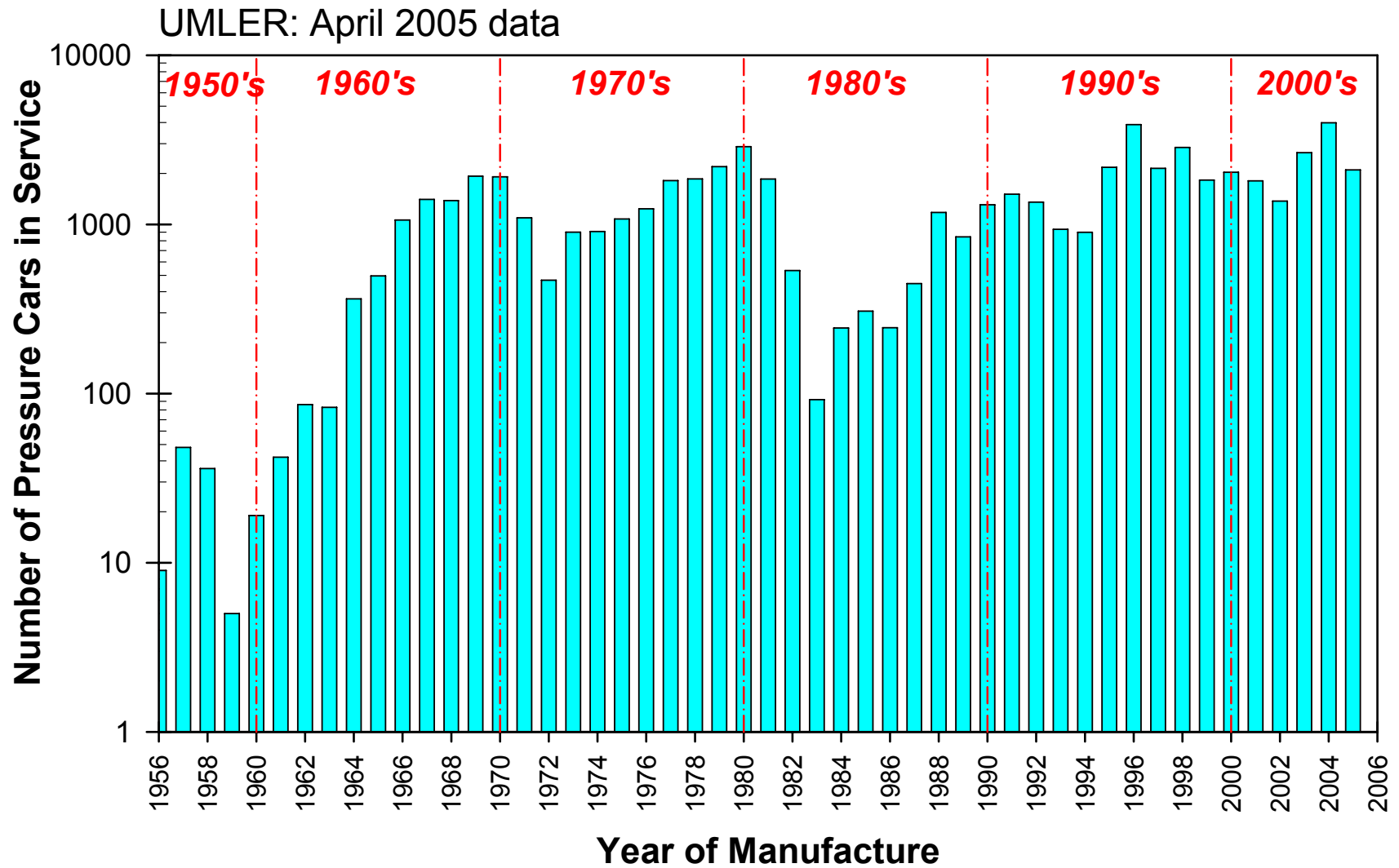


Figure 1-1. Number of pressure tank cars in service as a function of when they were built.

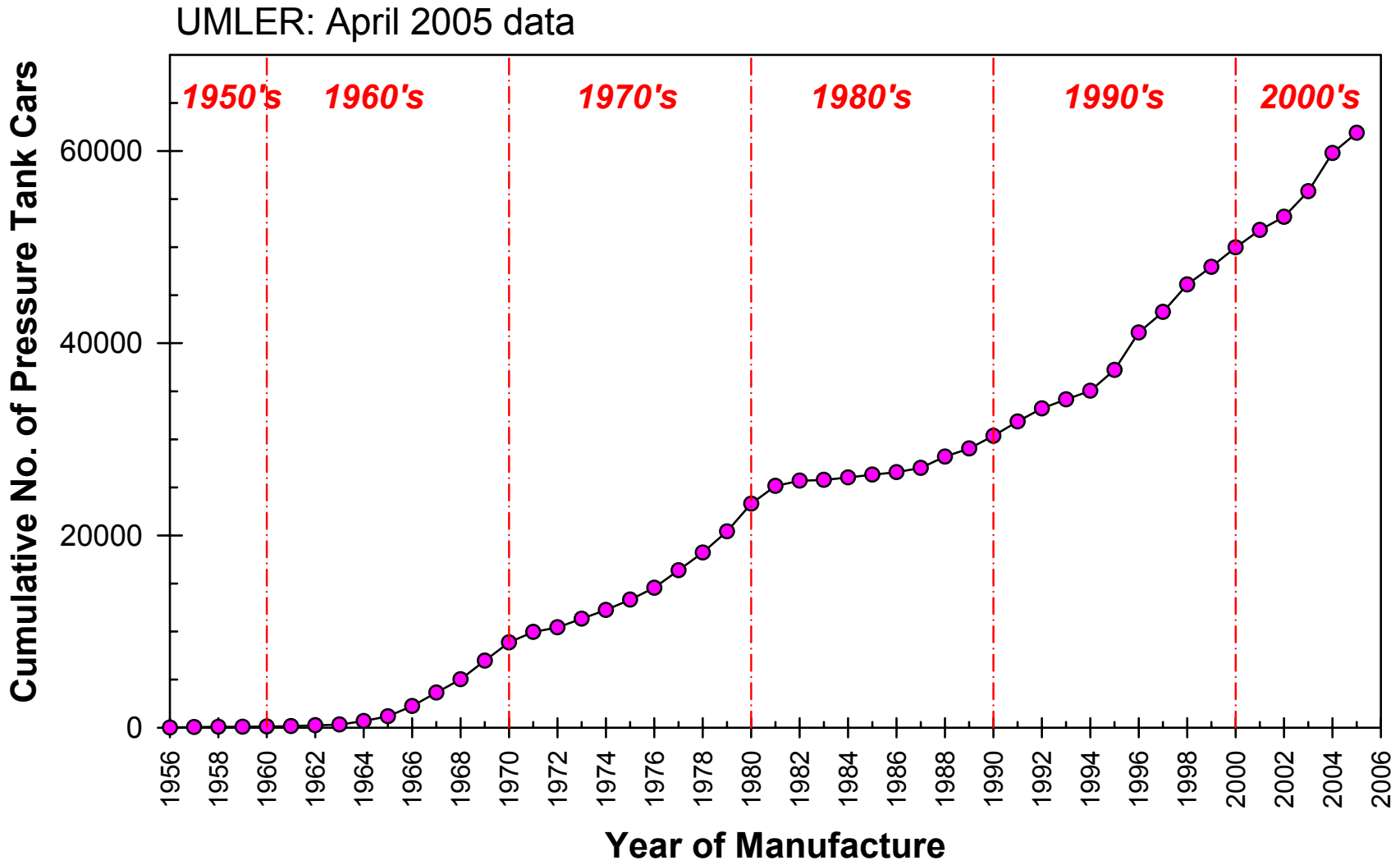


Figure 1-2. Cumulative number of pressure tank cars with year produced.

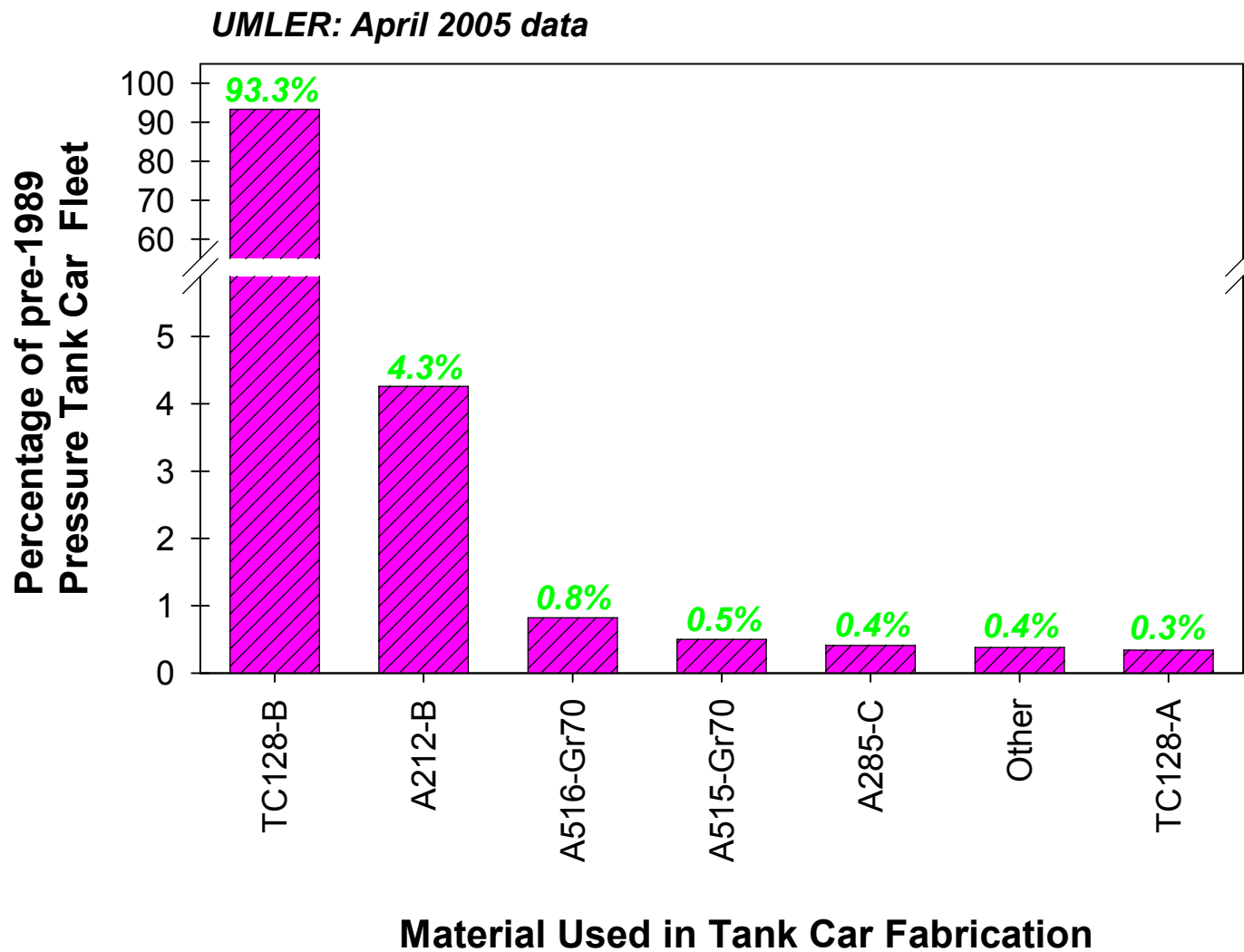


Figure 1-3. Description of the materials involved in the pre-1989 pressure tank car fleet.

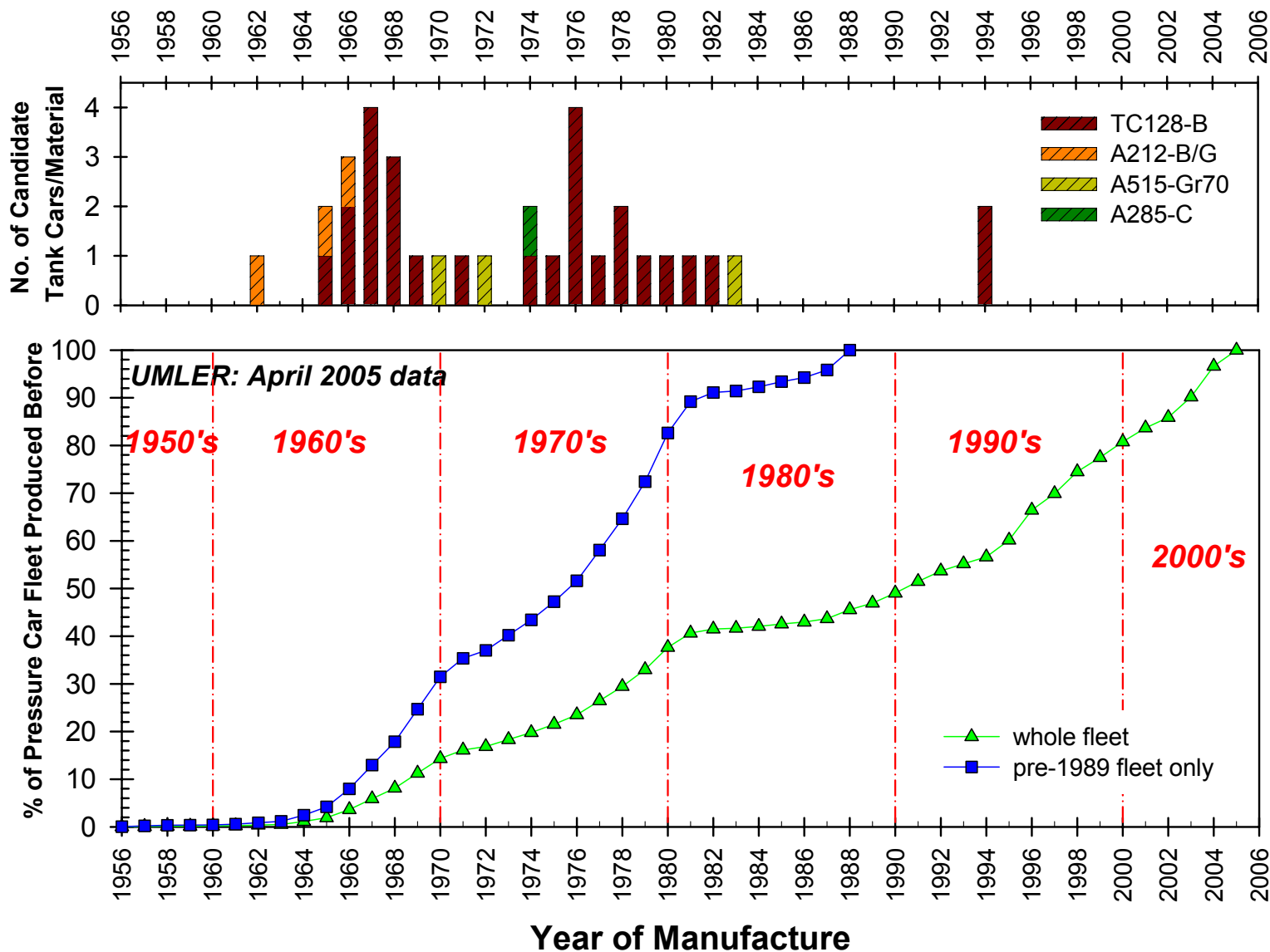


Figure 1-4. Description of the tank cars available compared to the cumulative number of cars produced.

This page intentionally left blank.

2.0 PREVIOUS VINTAGE TANK CAR FRACTURE TOUGHNESS TESTING

In January 2002, Canadian Pacific Railway freight train 292-16 derailed 31 of its 112 cars near Minot, ND. Fifteen of the thirty-one derailed cars were pressure tank cars containing anhydrous ammonia. The first seven tank cars that derailed lost all of their lading due to ruptures and/or punctures, with the remaining eight tank cars sustaining less severe damage. As a consequence of this accident, mechanical testing was performed on portions of the steels shells from six of the seven cars that sustained the most serious damage. These tank cars were all manufactured between 1976-1978. In addition to the shell testing performed on the six artifact cars, similar mechanical testing was performed on two exemplar tank cars fabricated in 1967 and 1971. The purpose of this section of the report is to detail this work since the later work was generally modeled after what was done in support of the Minot investigation.

2.1 Scope of the Testing

This work was initiated at SwRI and sponsored by GATX. The mechanical test data summarized are contained in two reports, both issued in June 2005 with the subtitles:

- Phase A – Pre-1989 GATX Tank Cars and Modern Vintage Plate [7]
- Phase B – Tank Cars Involved in the 2002 Minot Incident [8].

By special agreement, GATX has granted release of these data for the overall benefit of the T79.32 Task Force (combined, the two references [7] and [8] include over sixty pages of text and nearly 90 pages of supporting information in Appendices).

Testing was initially performed on two exemplar cars extracted from the SwRI tank car sill collection (see Figure 2-1). This sill “farm” corresponds to the material remaining from a teardown analysis performed in 2001 and detailed in reference [9]. A variety of material conditions and locations were considered during this testing, with samples extracted from the existing hardware as shown in Figure 2-2. Two exemplar tank cars were considered during this Phase A of the work. Testing was performed on portions of the tank car head (presumably

normalized during hot forming), the shell, and from both A- and B-ends of the tank cars (seven material conditions). In addition, testing was also performed on modern vintage, normalized TC128-B plate.

The second Phase B portion of the work focused on portions of tank cars from the Minot incident. The Minot hardware was on a site in Minnesota pictorially depicted in Figure 2-3. For the six artifact cars considered in Phase B, multiple positions were examined in the tank car shell sampling different plates that make up the tank car shell. More specifically, testing was performed on (a) portions of the shell that exhibited a fracture during the accident, (b) adjacent shell plates next to the plate that fractured and (c) dented shell plates. In total, twelve different material sources were tested from these six artifact cars.

2.2 Testing Procedures

A series of basic material characterization tests were performed on test samples extracted from the artifact and exemplary cars. These tests included the following:

- *Elemental Composition* – The weight percent of standard TC128-B constituents (C, Mn, P, S, Si, Cu, Ni, Cr, Mo, V) were measured along with other elements of interest (Al, Nb, Ti, B, N and Sn). These compositional measurements were performed on samples from all tested plates.
- *Tensile Testing* – Standard ASTM E8 tests were performed at room temperature and 0°F for the two exemplar tank cars. For the six artifact cars, tensile testing was performed at room temperature only. All evaluated material conditions were tensile tested with the focus on transverse plate properties.

Two types of fracture toughness tests were performed on the material: the steel industry standard Charpy v-notch (CVN) test as per ASTM E23 and a fracture mechanics toughness test based on ASTM E399. CVN toughness measurements (three replicates) were performed at 0°F, again for all material conditions (seven for the two exemplar cars, one for the modern normalized plate and twelve for the six artifact tank cars). Specimens were oriented with the primary loading direction in the transverse direction with the crack growing longitudinally (orientation consistent with circumferential failure of the tank). For reference, this orientation is shown in

additional detail in Figure 2-4. In the case of the three tank heads evaluated in the exemplar tank cars, one arbitrary orientation (undefined due to uncertainty of the original plate orientation during head forming) was tested.

Fracture toughness tests using a fracture mechanics based approach and yielding a critical stress intensity factor were also performed. The test method, based on the K_{Ic} test method and yielding a K_{max} toughness parameter, calculated from peak applied load (assuming no crack advance), provides a toughness measure that can be used in fracture mechanics design calculations to predict the onset of instability. The fracture tests performed in this manner perturbed the following variables:

- *loading rate*: quasistatic loading conditions were employed, as well as high rate loading (in this context, high rate loading corresponds to actuator speeds of 10-13 inch/second). Observed specimen strain rates (remote from the crack tip) were 0.5-1.0 inch/inch/second which implies stress rates of 15,000-30,000 ksi/second and stress intensity factor rates of 14,000-22,000 ksi $\sqrt{\text{in}}$ /second. The vast majority of the tests were performed at high rate.
- *temperature range*: room temperature to -100°F, with the majority of the tests performed at ambient (at the time of the accident estimated to be 37°F) or 0°F.

In the case where material toughness was high (usually where $K_{max} > 90$ ksi $\sqrt{\text{in}}$) and non-linearity was observed in the load-displacement data, an elastic-plastic J_{max} toughness (and equivalent K_{Jmax}) was derived from the data utilizing an energy-to-fracture approach.

2.3 Summary of Results

Of the twenty material conditions sampled, nineteen of the twenty met the elemental composition requirements of TC128-B. The only exception was one shell sample that exhibited carbon levels slightly higher than specification. A summary of the tensile properties observed is shown in Figure 2-5. Comparison to the standard AAR specification is problematic because the specification is for longitudinal properties whereas the test samples were oriented in the transverse direction. CVN fracture toughness measurements (at 0°F) are shown in Figure 2-6 to range from <5 ft-lbs to >35 ft-lbs for head material (presumably normalized). Two exemplar

tank car material conditions demonstrated toughness levels <5 ft-lbs, one from tank shell and one, surprisingly, from a tank head.

Two examples of the type of data observed during high rate testing are shown in Figure 2-7. The upper two plots in Figure 2-7 exhibit brittle behavior whereas in the lower two plots a more ductile behavior is exhibited. Brittle behavior tended to result in an immediate load decrease upon achieving peak load as the crack races across the specimen rapidly. However, in the case of the more damage tolerant, higher energy ductile behavior, the load tended to remain high as the crack gradually tears through the material. Summaries of the Phase A and B testing are provided in Tables 2-1 and 2-2, respectively.

The high rate K_{\max} or $K_{J\max}$ fracture toughnesses shown in Figure 2-8 are in excess of 50 $\text{ksi}\sqrt{\text{in}}$ with some values approaching 300 $\text{ksi}\sqrt{\text{in}}$. Some weak dependence of high rate fracture properties as a function of CVN toughness was also observed as shown in Figure 2-9. Keep in mind, however, that these data include both upper and lower shelf data. The relationships shown in Figure 2-9 assume a direct correlation of CVN to fracture toughness at a given temperature, so no transition temperature shift is necessary.

Table 2-1. Tabulated fracture toughness test results for the twelve different Minot tank car plate conditions evaluated.

Car ID No.	Plate Region	Test Temp	Spec. ID No.	ϵ rate, in/in/sec	Krate, ksi $\sqrt{\text{in}}$ /sec	v/P, mil/kip	Compl Ratio	Limit Ratio	Kmax, ksi $\sqrt{\text{in}}$	Percent Plastic J	Jmax, ksi-in	KJmax, ksi $\sqrt{\text{in}}$	KJ/Kmx Ratio
PLMX 4504	fracture	37°F	24F-2	0.66	22,696	3.10	0.98	0.79	79.1	<0	–	–	–
			24F-3	0.71	23,528	3.54	1.08	0.71	70.4	<0	–	–	–
		0°F	24F-1	0.54	18,816	3.23	0.99	0.69	68.7	<0	–	–	–
	adjacent	37°F	24A-2	0.62	21,027	3.61	1.05	0.93	93.1	<0	–	–	–
			24A-3	0.76	25,235	3.57	1.06	0.82	82.9	<0	–	–	–
0°F		24A-1	0.66	23,932	3.06	0.91	0.58	58.9	<0	–	–	–	
GATX 47814	fracture	37°F	19F-1	0.81	25,161	3.61	1.10	1.13	97.3	44	0.514	130	1.34
			19F-3	0.85	25,137	3.43	1.06	1.11	96.4	45	0.517	131	1.35
		0°F	19F-2	0.77	24,636	3.40	1.04	1.01	87.8	<0	–	–	–
	adjacent	37°F	19A-1	0.75	22,406	3.20	1.00	1.17	100.1	60	0.761	158	1.58
			0°F	19A-2	0.84	25,338	3.36	1.04	1.24	105.3	59	0.823	165
		19A-3	0.79	25,776	3.43	1.05	1.13	95.8	<0	–	–	–	
	dented	37°F	19D-2	0.81	23,526	3.12	1.00	1.11	101.1	65	0.882	171	1.69
			19D-3	0.83	24,684	3.47	1.09	1.12	101.2	57	0.728	155	1.53
0°F		19D-1	0.81	23,887	3.57	1.09	1.11	99.6	21	0.379	112	1.12	
GATX 47982	fracture	37°F	22F-3	0.82	23,631	3.25	1.04	1.26	99.5	73	1.129	193	1.94
			22F-1	0.85	23,418	3.30	1.07	1.23	97.5	73	1.051	186	1.91
		0°F	22F-2	0.79	24,358	3.08	0.97	1.30	102.4	37	0.505	129	1.26
	adjacent	37°F	22A-1	0.82	25,920	3.12	0.96	1.13	115.3	55	0.899	172	1.49
			22A-3	0.82	24,619	3.44	1.08	1.11	113.5	50	0.787	161	1.42
0°F		22A-2	0.68	22,820	3.12	0.98	0.73	74.3	<0	–	–	–	
PLMX 4644	dented	37°F	18D-2	0.73	19,493	3.40	1.04	1.23	103.2	61	0.826	165	1.60
			18D-3	1.07	25,158	3.57	1.08	1.30	109.3	68	1.141	194	1.77
		0°F	18D-1	0.82	21,941	3.30	1.05	1.19	100.3	46	0.570	137	1.37
	adjacent	37°F	18A-3	0.82	25,419	3.50	1.07	1.15	109.7	45	0.666	148	1.35
0°F			18A-2	0.81	26,045	3.30	1.01	1.22	116.0	44	0.727	155	1.33
GATX 49248	dented	37°F	21D-3	0.83	24,760	3.71	1.15	1.19	98.0	53	0.615	142	1.45
		0°F	21D-1	0.81	24,913	3.46	1.07	1.25	102.3	44	0.572	137	1.34
GATX 47837	fracture	37°F	20F-2	0.85	23,970	3.32	1.03	1.15	101.3	67	0.938	176	1.74
			20F-3	0.95	25,040	3.49	1.05	1.19	99.8	72	1.089	189	1.90
		0°F	20F-1	0.77	25,039	3.15	0.96	1.14	95.9	<0	–	–	–
	adjacent	37°F	20A-1	0.82	24,031	3.21	1.03	1.19	102.8	65	0.920	174	1.69
			20A-3	0.94	24,217	3.11	0.99	1.16	101.1	60	0.782	161	1.59
0°F		20A-2	0.69	22,351	3.38	1.02	0.83	70.3	27	0.206	83	1.17	

Table 2-2. Tabulated fracture toughness test results for the pieces excised from scrapped tank cars.

Matl Source	Posn in Car	Car End	Test Rate	Test Temp	Spec ID No.	Rate, in/sec	ϵ Rate, in/in/sec	Krate, ksi/in/sec	Kmax, ksi/in	v/P, mil/kip	Compl Ratio	Limit Ratio	Jmax, ksi-in	Percent Plastic J	KJmax, ksi/in	KJ/K Ratio	
GATX 25008	shell	A	quasi	RT	8-AS-1	0.41(10 ⁻³)	0.20(10 ⁻⁴)	0.64	82.2	3.30	1.06	0.92	0.718	71	154	1.87	
				0°	8-AS-10	0.83(10 ⁻³)	0.35(10 ⁻⁴)	1.15	85.1	3.13	1.07	0.89	0.697	69	152	1.78	
					8-AS-8	0.82(10 ⁻³)	0.29(10 ⁻⁴)	0.93	79.6	3.08	1.18	0.81	0.617	69	143	1.79	
			high	RT	8-AS-2	12.1	0.57	17,293	97.8	3.05	1.06	1.06	0.581	50	139	1.42	
					8-AS-7	n/a	0.64	19,531	100.2	2.96	1.10	1.08	0.664	54	148	1.48	
				0°	8-AS-5	13.1	0.66	20,820	97.3	3.08	1.02	1.02	0.245	-17	90	0.92	
				8-AS-3	13.0	0.66	20,718	107.5	2.80	0.93	1.13	0.721	51	154	1.43		
			-50°	8-AS-4	10.1	0.40	14,014	55.9	3.11	1.04	0.58	0.093	-2	55	0.99		
			-100°	8-AS-6	8.7	0.35	12,504	42.1	3.05	1.04	0.44	0.072	26	49	1.16		
		B	high	0°	8-BS-8	n/a	0.49	16,925	56.0	2.90	0.95	0.58	0.072	-33	49	0.87	
	head	B	high	0°	8-BH-1	n/a	0.56	17,201	120.0	3.02	1.10	1.21	0.728	40	155	1.29	
					8-BH-4	n/a	0.67	20,966	120.0	2.67	0.94	1.22	0.775	44	160	1.33	
				-50°	8-BH-3	n/a	n/a	19,028	129.1	2.98	1.10	1.30	0.795	36	162	1.25	
	head	A	high	0°	8-AH-1	n/a	0.68	21,561	109.9	2.83	0.99	1.06	0.369	1	110	1.00	
					8-AH-4	n/a	0.68	21,238	123.9	2.88	1.00	1.20	0.831	44	166	1.34	
	hd+90°	A	high	0°	8-AHP-1	n/a	0.68	21,293	118.9	2.95	1.02	1.16	0.656	35	147	1.24	
				8-AHP-2	n/a	0.63	20,165	119.6	2.78	0.98	1.15	0.662	34	148	1.23		
GATX 91467	shell	B	quasi	0°	7-BS-4	0.83(10 ⁻³)	0.32(10 ⁻⁴)	1.02	84.5	2.21	1.13	1.05	1.108	80	191	2.26	
					7-BS-8	0.81(10 ⁻³)	0.28(10 ⁻⁴)	1.00	86.1	2.14	1.10	1.05	1.341	83	210	2.44	
					7-BS-10	n/a	0.56	16,326	95.1	2.27	1.06	1.17	1.554	82	226	2.38	
			high	RT	7-BS-7	n/a	0.68	16,419	95.2	2.52	1.11	1.19	1.616	83	231	2.43	
					7-BS-2	12.1	0.56	16,588	106.2	2.18	1.03	1.33	1.226	72	201	1.89	
				0°	7-BS-3	12.5	0.55	16,925	97.5	2.12	1.02	1.24	0.226	-8	94	0.96	
				7-BS-6	12.2	0.49	16,491	83.8	2.15	0.99	1.08	0.152	-40	71	0.84		
			-100°	7-BS-10	10.9	0.41	14,340	75.5	2.24	1.02	0.96	0.058	-3	75	0.99		
		A	high	0°	7-AS-1	n/a	0.51	14,405	66.4	1.95	0.98	0.84	0.100	-34	57	0.86	
					7-AS-2	n/a	0.45	15,430	67.3	1.94	0.95	0.73	0.130	-6	66	0.97	
	-50°			7-AS-4	n/a	0.38	13,126	47.2	2.13	1.02	0.52	0.057	-18	43	0.92		
				7-AS-3	n/a	0.41	14,178	46.0	2.05	1.00	0.50	0.047	-35	40	0.86		
	head	B	high	0°	7-BH-1	n/a	0.53	17,748	78.4	2.69	1.09	0.79	0.158	-18	72	0.92	
					7-BH-2	n/a	0.64	18,640	93.7	2.69	1.11	0.93	0.160	-67	73	0.77	
				7-BH-3	n/a	0.59	17,341	56.4	2.32	0.99	0.56	<0	-	-	-		
-50°				7-BH-3	n/a	0.59	17,341	56.4	2.32	0.99	0.56	<0	-	-	-		
Virgin Plate	n/a	n/a	quasi	0°	TP-3	n/a	0.34(10 ⁻⁴)	1.13	100.6	2.40	1.04	1.09	2.062	85	261	2.59	
					TP-10	n/a	0.29(10 ⁻⁴)	1.08	99.6	2.46	1.08	1.08	2.224	86	271	2.72	
				high	RT	TP-2	n/a	0.63	18,822	110.8	2.29	0.99	1.25	2.511	85	288	2.60
						TP-6	n/a	0.61	18,719	111.1	2.25	0.99	1.24	2.120	82	264	2.38
			0°	TP-1	n/a	0.44	14,718	96.9	2.33	1.01	1.05	0.218	-31	85	0.87		
				TP-4	n/a	0.60	19,035	121.0	2.48	1.05	1.32	0.812	45	164	1.35		
				-50°	TP-7	n/a	0.55	18,556	105.3	2.26	0.97	1.15	0.267	-26	94	0.89	
					TP-9	n/a	0.49	17,340	89.3	2.24	0.99	0.96	0.179	-35	77	0.86	



Figure 2-1. The tank car stub sill farm at SwRI from which the two car segments were removed.



Figure 2-2. Torch-cutting removing segments from the tank cars.



Figure 2-3. Wreckage from tank cars involved in the Minot accident (Glenwood, MN).

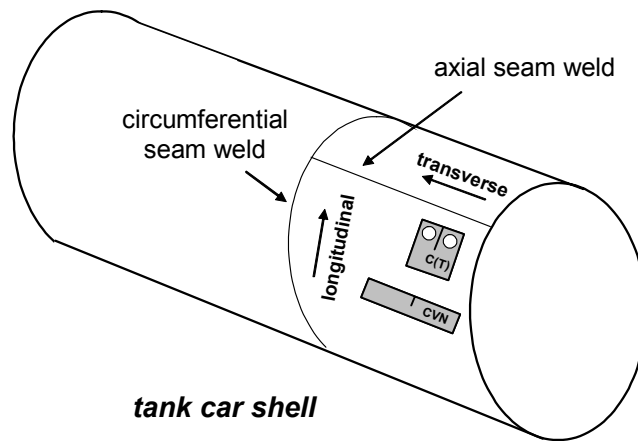


Figure 2-4. Definition of the orientation of fracture toughness samples in the shell.

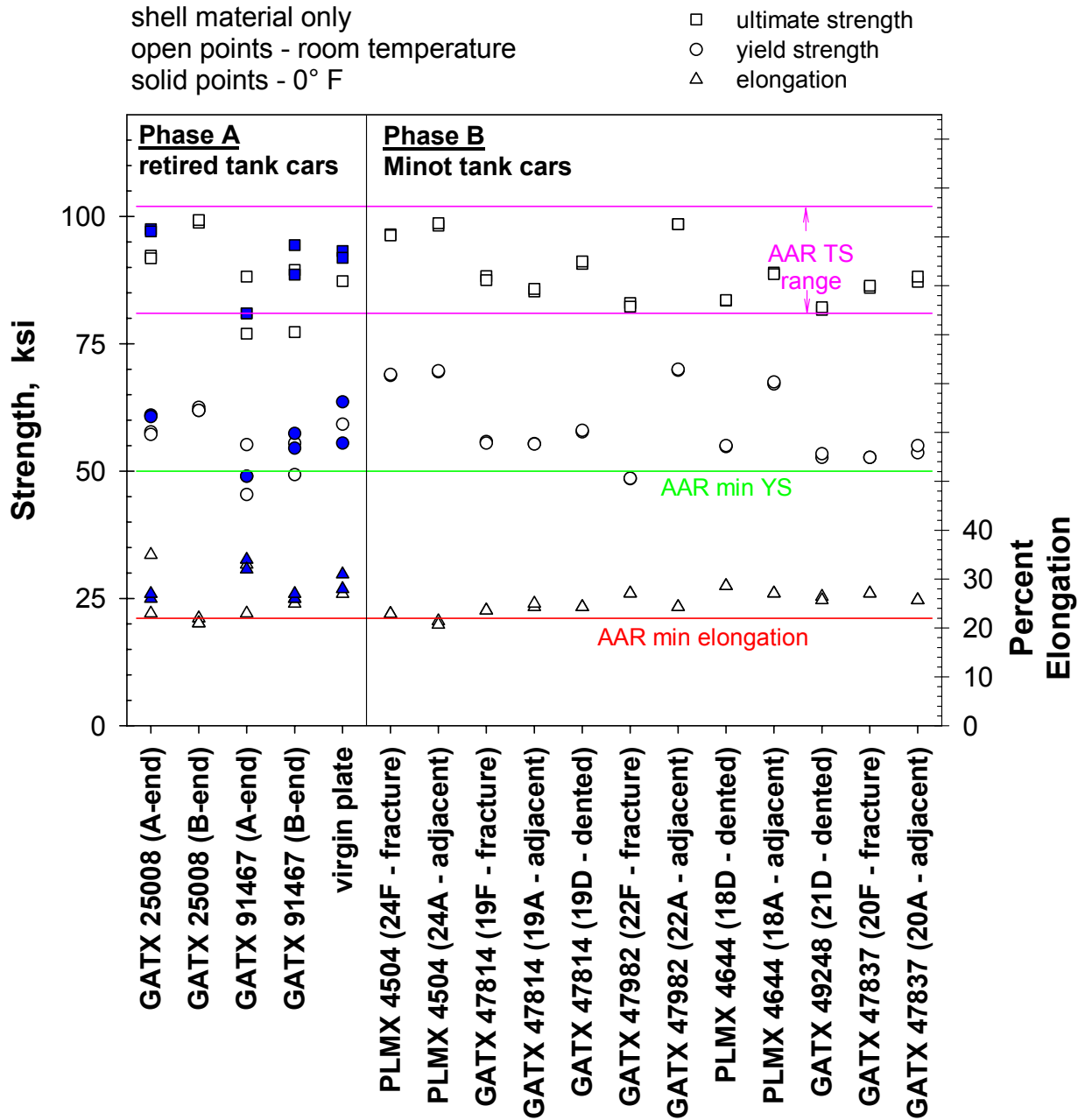


Figure 2-5. Tensile property variation with material examined. Note that the AAR specification applies for the longitudinal orientation whereas the samples tested were orthogonal to this orientation.

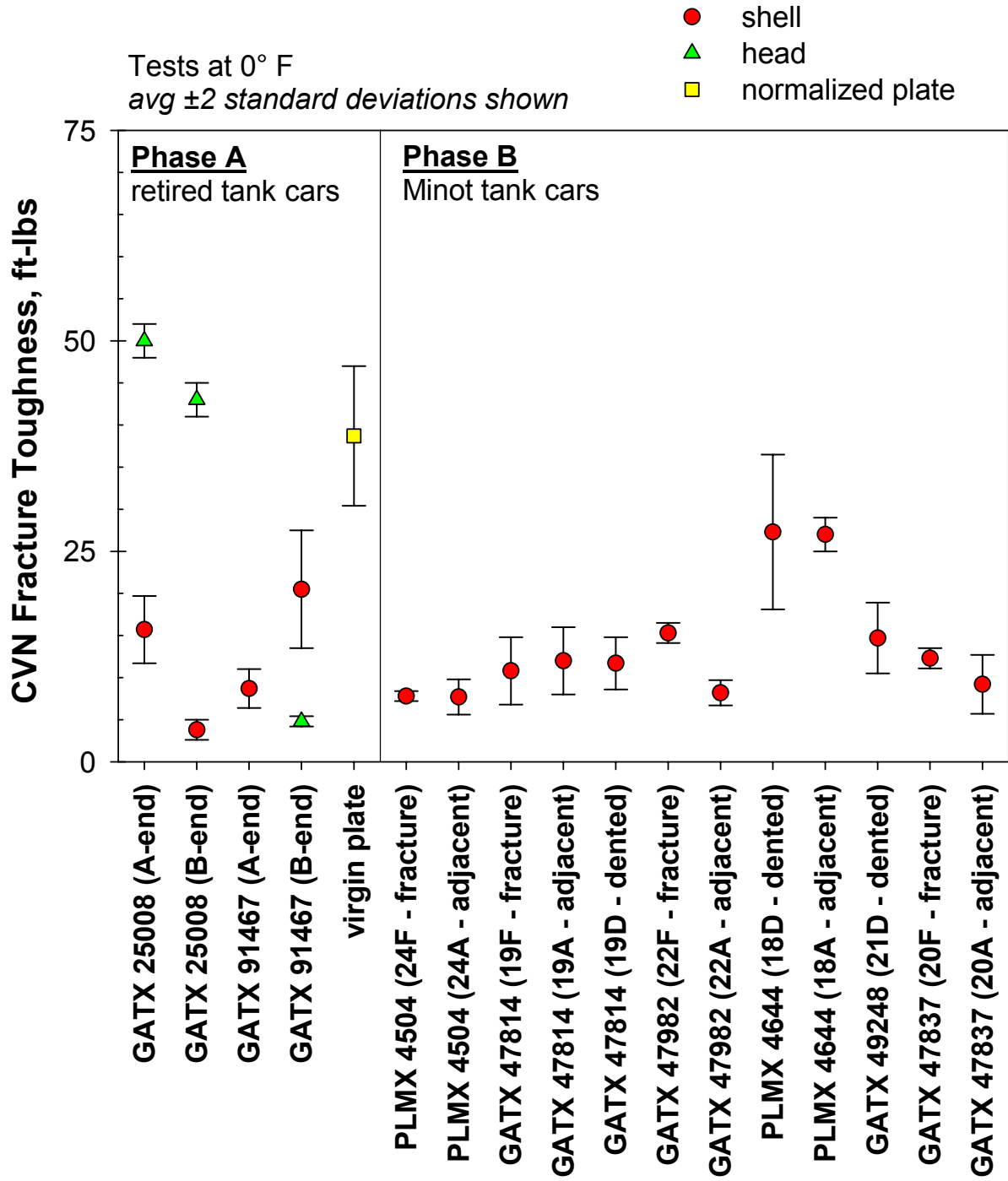


Figure 2-6. CVN fracture toughness variation with material examined.

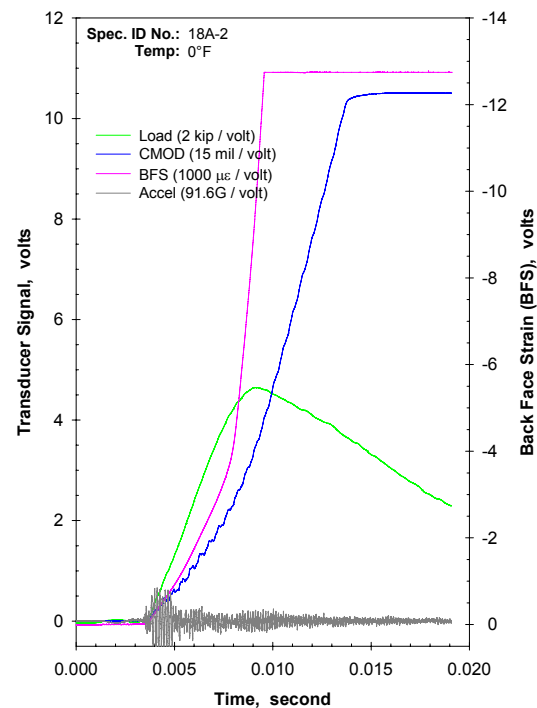
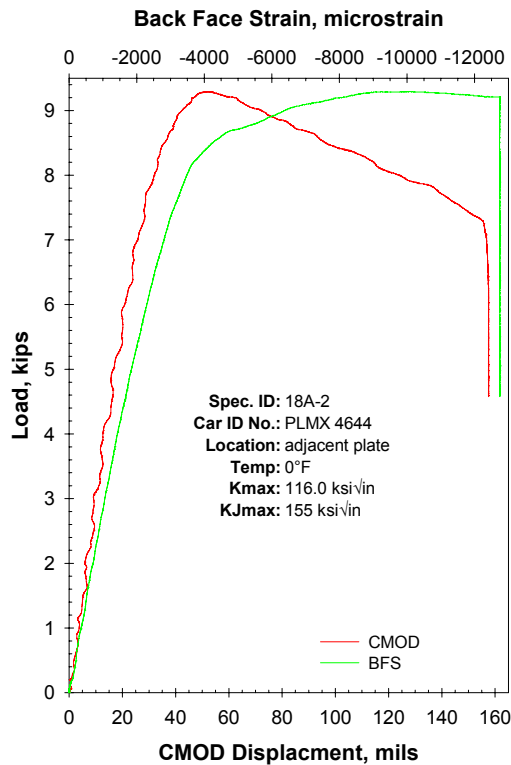
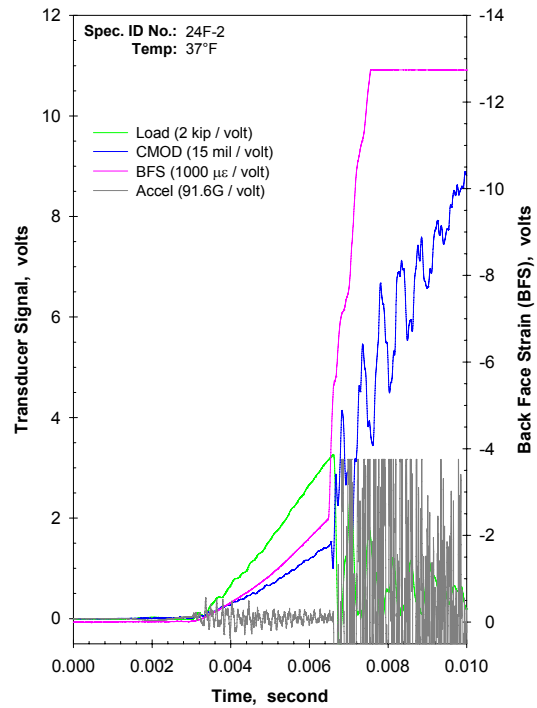
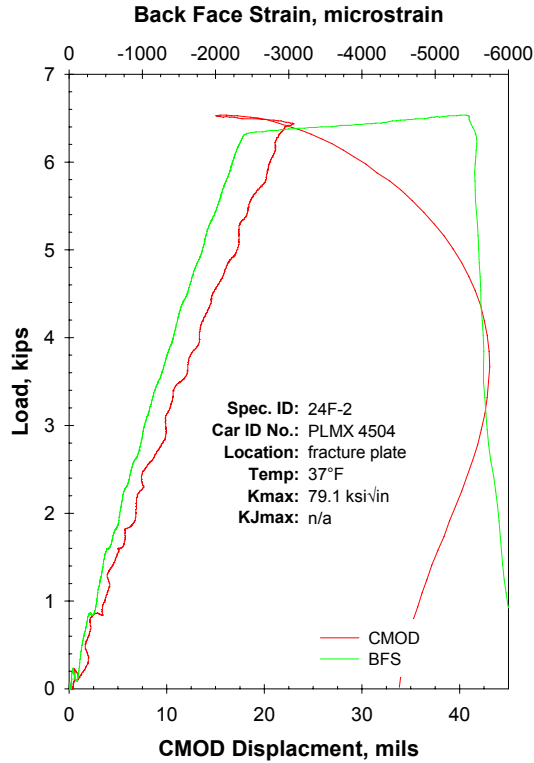


Figure 2-7. Typical recorded data for brittle (top) and ductile (bottom) examples of fracture toughness tests.

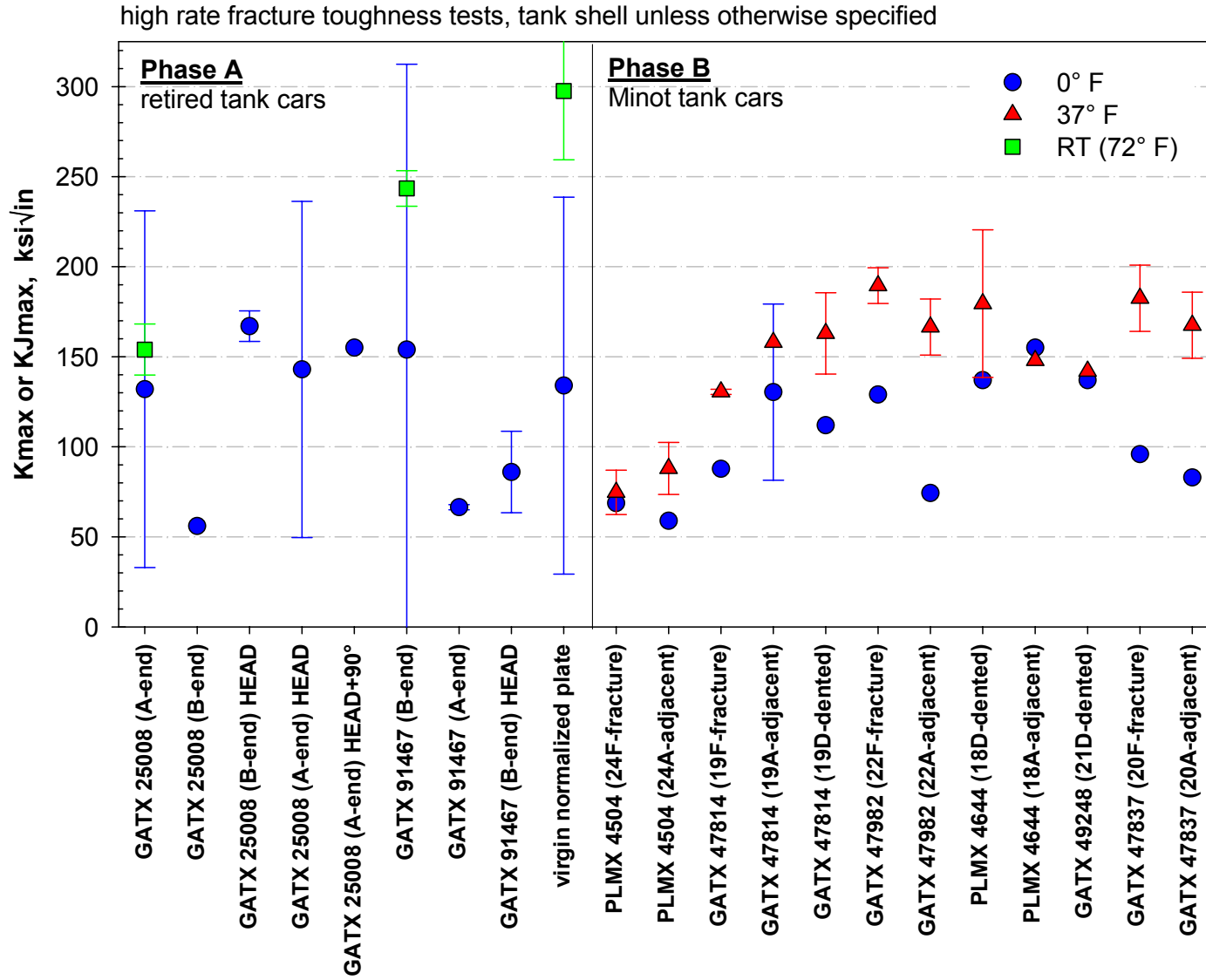


Figure 2-8. Variation in average high rate fracture toughness as a function of temperature and material (error bars ±2 std. devs.).

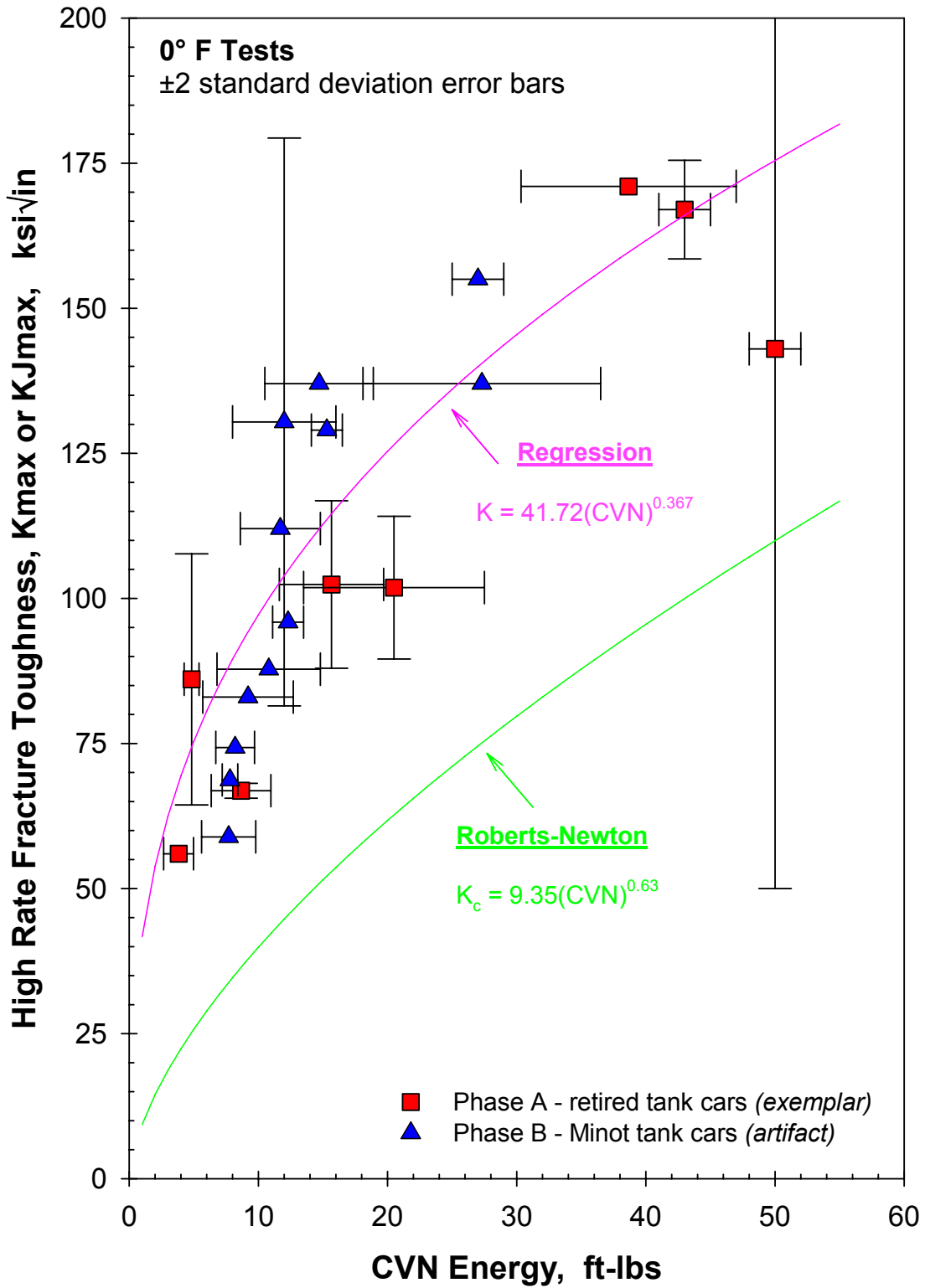


Figure 2-9. Correlation between fracture toughness and CVN energy for tests at 0°F.

This page intentionally left blank.

3.0 PEDIGREE OF IN-SERVICE VINTAGE TANK CAR MATERIALS

The purpose of this section of the report is to fully identify the sources and characteristics of the different materials involved in this program.

3.1 Material Identification Scheme

There were enough different materials involved in this program that necessitated a simple yet effective method of differentiating materials. The specific tank car materials involved in the program are outlined in Table 3-1. This includes twenty plates supplied specifically for this program as well as eight sills (A and B end of each) from the teardown and six different Minot tank cars. Each of the different car conditions (identified by a tank car ID number or reporting mark) has a build date indicated in Table 3-1.

The sizes of the different pieces of material are described fully in Table 3-2 (plates) and Table 3-3 (teardown and Minot material). There is also a “new ID” indicated in one of the columns on the right-hand-side (in Tables 3-2 and 3-3). This new ID consists of a year code for the first two digits that is then followed by an alpha identifier. The key to relate the year code and alpha to a specific tank car is provided in Figure 3-1. Hence, the first two numbers indicate the year of manufacture with an alpha-identifier (A, B, C or D) simply indicating the different cars as shown. This is followed by either S (shell) or H (head) to further identify the material. If different locations were available on the same car, an alpha-identifier (A or B) is also attached to the material condition. In some cases, other IDs at the end differentiate material condition (D = dented plate as used in the earlier Minot work).

3.2 Material Sources and Descriptions

Material was extracted from three specific sources. In the case of the teardown sills and Minot material (see Figure 3-2), these components were already on hand and extracting pieces suitable for fabricating test specimens was trivial. During the teardown, GATX and Union Tank Car Company donated stub sills from both ends of eight cars due to be retired from service.

These sill ends were then examined and subjected to a teardown inspection. Although the teardown focused on the sills, there typically was sufficient material available from around the sills to sample both the head and shell. Photographs of the collection of these sills with head and shell attached are shown in Figure 3-2. The second source of material was the GATX Minot-related work (also see Figure 3-2) and the final source was cars supplied by the industry partners in this program over approximately the past year.

It is worth briefly reviewing how tank car material was obtained from a given tank car. First, the tank car industry was made aware of the work underway at SwRI and solicited for donations of material (usually at Tank Car Committee Meetings and the like). Once a possible tank car had been identified, the industry representative typically called SwRI and asked whether the car was a suitable candidate. The primary driver for making this choice was the year of fabrication, tank head and shell material and manufacturer of the tank car. Assuming the car was a suitable candidate, cutting instructions such as that in Figure 3-3 were supplied (these instructions in Figure 3-3 were supplied by Union Tank Car). Note that the instructions and schematic in Figure 3-3 indicate two shell segments (from different rings) and one head segment. Sometimes only a single shell segment was available after cutting. The collection of plates at SwRI, along with typical marking and subsequent cutting, is indicated in Figure 3-4. When smaller segments were cut from the plate, a zone of around the torched area was discarded due to uncertain microstructure. This zone was typically at least two thicknesses and sometimes up to four thicknesses wide.

The steel material from the thirty-four tank cars are identified in Table 3-1. The first eight lines of Table 3-1 are the car segments that were supplied during the teardown analysis. Note that four of these tank cars are not pressure cars. However, materials from these cars are still valuable since they represent materials that are used sparsely in the pressure tank car fleet (although the thickness of the shells and heads in the pressure car designs are greater than in the non-pressure cars). The next six lines of Table 3-1 correspond to the cars that were involved in the Minot-related work. The next twenty cars (marked as candidate material) represent the specific cars donated by industry for this work.

The data in Table 3-1 is further shown in Figure 3-5 comparing the available tank cars with the distribution of the tank car fleet. Of particular interest is how well the current population of tank cars represents the fleet of pre-1989 tank cars. First, examining the pre-1989 fleet, 25% of the fleet was fabricated in the 1960s, 47% of the fleet in the 1970s and 28% of the fleet in the 1980s. Since TC128-B is the predominant material in the fleet (making up 93% of the pre-1989 pressure car fleet), it is worthwhile examining the distribution of available TC128-B material. The first sample available is in 1965 with only 2.5% of the pre-1989 pressure car fleet fabricated before 1965. Conversely, the newest TC128-B available is from 1981 after which only 11% of the pre-1989 fleet was manufactured. Therefore, the TC128-B samples obtained represent approximately 85% of the pre-1989 pressure car fleet. There is, however, a bit of a gap in the available data for the early 1970s (representing about 10% of the pre-1989 fleet). It would also still be beneficial if some TC128-B samples in the 1982-1988 range could be obtained.

3.3 Subdividing the Fleet of Tank Cars

The data contained in Table 3-1 clearly indicate that an excellent cross-section of the fleet is available for analysis. Thirty-two different tank cars were included in this work. A further description of the thirty-two is provided in Table 3-4, where the pedigree of the tank car is fully described. Included in these thirty-two different tank cars is a total of seventy-two distinct conditions (where a distinct condition might imply head or shell, A-end or B-end positions and the like). However, practical resource limitations imply that not all seventy-two conditions will be able to be fully examined for both mechanical properties and fracture toughness. The danger with attempting to examine all conditions is that this type of single-minded approach could end up yielding considerable data but little insight and understanding of what the data suggests. The alternate approach was to perform screening tests on the materials to help down-select the conditions where high rate fracture toughness tests will be performed. Screening tests, consisting of mechanical property testing (composition, tensile properties and CVN toughness), were performed on all steel materials.

To assist in interpreting the data, the tank car fleet is split up into four nominally equal subdivisions as described in Figure 3-5. Recall this data is from the UMLER database snapshot

in April 2005 (see Table 1-1). As this program progressed, there was anecdotal evidence that the rate of scrapping older cars was increasing dramatically. Nevertheless, an updated UMLER run was not able to be procured to provide a more accurate snapshot of the fleet that was tested (at least in terms of current fleet makeup). The subdivisions described in Figure 3-5 were nominally setup to equally represent the fleet; more specifically, the target for each subdivision is 25% of the fleet. As the data in Figure 3-5 suggests:

- 1st quarter (subset A) – tank cars fabricated before 1970 and representing 25% of the fleet
- 2nd quarter (subset B) – tank cars fabricated between 1970-1976 (inclusive) representing 25-52% of the total fleet
- 3rd quarter (subset C) – tank cars fabricated between 1977-1979 (inclusive) representing 52-72% of the total fleet
- 4th quarter (subset D) – tank cars fabricated after 1979 and representing the final 28% of the fleet.

The availability of material conditions is not sufficient to indicate year-by-year material trends. More practically it is believed that conclusions regarding material property variations may be able to be made in context of the above four subdivisions.

During the previous Minot work, the primary temperatures examined during testing were 0°F and 37°F. For this work, the temperatures of interest were -50°, 0° and 50°F (CVN only, fracture toughness testing was performed at the two lower temperatures and tensile properties were measured only at room temperature). It is believed that these three temperatures are minimally sufficient to provide a sense of how properties vary with temperature (hence, to differentiate lower and upper shelf behavior). For reference, these temperature conditions are shown in Figure 3-6 overlaid with some NTSB-generated transition temperature curves.

Table 3-1. Cars available for materials testing (including teardown material and Minot-related plates). The highlighted entries are not pre-1989 TC128-B.

Status	Tank Car ID No.	ID No.	Builder	Material	Org (when supplied)	DOT Class.	Build Date	Commodity	Plates Recvd	
									shell	head
old teardown material	GATX 91554	67b	GATX	TC128-B	teardowns (2001)	112A340W	1967	anhyd ammonia	2	2
	GATX 55905	66a	GATX	TC128-B	teardowns (2001)	112J340W	1966	anhyd ammonia	2	2
	GATX 25008	71a	GATX	TC128-B	teardowns (2001)	112A340W	1971	LPG-butane mix	2	2
	GATX 91467	67a	GATX	TC128-B	teardowns (2001)	105A500W	1967	chlorine/sulfur	2	2
	UTLX 14439	74a	Union	A285-C	teardowns (2001)	111A100W2	1974	sulfuric acid	2	2
	GATX 50863	70a	GATX	A515-Gr70	teardowns (2001)	111A100W1	1970	50% caustic soda	2	2
	GATX 16108	83a	GATX	A515-Gr70	teardowns (2001)	111A100W1	1983	molten sulfur	2	2
	GATX 9746	65a	GATX	A212-B	teardowns (2001)	111A340W	1965	unknown	2	2
tested (GATX Minot Work)	PLMX 4504	76a	Rich (Trin)	TC128-B	CP (Minot accident)	105A300W	1976	anhyd ammonia	2	none
	GATX 47814	76b	GATX	TC128-B	CP (Minot accident)	105A300W	1976	anhyd ammonia	3	none
	GATX 47982	76c	GATX	TC128-B	CP (Minot accident)	105A300W	1976	anhyd ammonia	2	none
	PLMX 4644	78a	Rich (Trin)	TC128-B	CP (Minot accident)	105A300W	1978	anhyd ammonia	2	none
	GATX 49248	77a	GATX	TC128-B	CP (Minot accident)	105A300W	1977	anhyd ammonia	1	none
	GATX 47837	76d	GATX	TC128-B	CP (Minot accident)	105A300W	1976	anhyd ammonia	2	none
plates received	UTLX 80681	65b	Union	M-128	Union (Apr 04)	112J340W	1965	LPG	1	1
	UTLX 28744	74b	Union	TC128-B	Union (Apr 04)	105J500W	1974	chlorine	1	1
	TGAX 331007	75a	ACF	TC128-B	ARI (May 05)	112S340W	1975	anhyd ammonia	1	1
	CGTX 64270	78b	Hawk-Sid	TC128-B	TC (June 05)	112J340W	1978	LPG	1	1
	GATX 92593	68a	GATX	TC128-B	GATX (July 05)	112J340W	1968	propane	1	1
	GATX 97833	66b	GATX	TC128-B	GATX (July 05)	112A340W	1966	anhyd ammonia	1	1
	CGTX 64251	67c	CGTX	TC128-B	GATX (July 05)	112S340W	1967	liq hydroC gas	1	1
	CGTX 63699	66c	GATX	A212-B	GATX (July 05)	112J340W	1966	liq hydroC gas	1	1
	UTLX 89348	67d	Union	TC128-B	Union (Aug 05)	112J340W	1967	LPG	2	1
	UTLX 95454	69a	Union	TC128-B	Union (Sept 05)	112J340W	1969	LPG	2	1
	PROX 89773	68b	Union	TC128-B	BNSF (Dec 05)	112J340W	1968	LPG	2	1
	PROX 81231	68c	Union	TC128-B	BNSF (Dec 05)	112J340W	1968	LPG	2	2
	UTLX 83551	62a	Union	A212-G	UP (Jan 06)	112S400W	1962	LPG	none	1*
	PROX 83469	80a	Procor	TC128-B	CSX (Apr 06)	105A500W	1980	chlorine	1	1
	GAMX 4115	79a	ACF	TC128-B	KCSR (Apr 06)	105A500W	1979	chlorine	2	1
	TAEX 143	72a	Rich (Trin)	A515-Gr70	FRA (May 06)	111A100W1	1972	fertilizer	1	none
	HOKX 8453	82a	GATX	TC128-B	Occ. Chem (May 06)	105A500W	1982	chlorine	2	1
	HOKX 8373	81a	ACF	TC128-B	Occ. Chem (Oct 06)	105A500W	1981	chlorine	2	1
	PROX 31153	94a	Procor	TC128-B (N)	BNSF (May 06)	112J340W	1994	LPG	2	1
	PROX 31218	94b	Procor	TC128-B (N)	BNSF (May 06)	112J340W	1994	LPG	2	1

Table 3-2. Steel pieces from the different scrapped cars provided in support of this effort.

Rep. Mark/Car No	Builder	Material Type	Date	C-O-C	NewID	Plate Size (in)
UTLX 80681	Union	M-128	1965	✓	65b-SA	24½(A) x 24
					65b-HA	23 x 22¾
UTLX 28744	Union	TC128-B	1974	✓	74b-SA	24(A) x 24
					74b-HA	24 x 24
TGAX 331007	ACF	TC128-B	1975	✓	75a-SA	35½(A) x 34
					75a-HA	35½ x 34½
CGTX 64270	Hawk-Sid	TC128-B	1978	✓	78b-SA	19½(A) x 13
					78b-HA	24 x 14
GATX 92593	GATX	TC128-B	1968	✓	68a-SA	24¾(A) x 23½
					68a-HA	23½ x 23
GATX 97833	GATX	TC128-B	1966	✓	66b-SA	23½ (A) x 24
					66b-HA	24¼ x 23¾
CGTX 64251	CGTX	TC128-B	1967	✓	67c-SA	24¼(A) x 24
					67c-HA	24¾ x 24¼
CGTX 63699	CGTX	A212-B	1966	✓	66c-SA	23¾(A) x 22½
					66c-HA	22½ x 22¼
UTLX 89348	Union	TC128-B	1967	✓	67d-SA	35½(A) x 32¼
					67d-SB	31½(A) x 30½
					67d-HA	35½ x 31
UTLX 95454	Union	TC128-B	1969	✓	69a-SA	35¾(A) x 35½
					69a-SB	36(A) x 35¾
					69a-HA	36 x 35¾
PROX 89773	Union	TC128-B	1968	✓	68b-SA	36(A) x 35¼
					68b-SB	36(A) x 35
					68b-HA	36 x 35¾
PROX 81231	Union	TC128-B	1968	✓	68c-SA	37¼(A) x 37½
					68c-SB	36 (A) x 36
					68c-HA	36½ x 35½
					68c-HB	35½ x 34½
UTLX 83551	Union	A212-G	1962	✓	62a-HA	8 x 11
PROX 83469	Procor	TC128-B	1980	✓	80a-SA	37½(A) x 34
					80a-HA	36¾ x 35¾
GAMX 4115		TC128-B	1979	✓	79a-SA	39½(A) x 42
					79a-SB	49(A) x 38
					79a-HA	45 x 43
TAEX 143	Trinity	A515-Gr70	1972	✓	72a-SA	26½(A) x 25
HOKX 8453	GATX	TC128-B	1982	✓	82a-SA	36(A) x 34½
					82a-SB	35¼(A) x 35
					82a-HA	36½ x 36½
HOKX 8373	ACF	TC128-B	1981	✓	81a-SA	37(A) x 34½
					81a-SB	39(A) x 33
					81a-HA	36 x 35½
PROX 31153	Procor	TC128-B (N)	1994	✓	94a-SA	35¾(A) x 35
					94a-SB	36¼(A) x 36
					94a-HA	36 x 35½
PROX 31218	Procor	TC128-B (N)	1994	✓	94b-SA	36¼(A) x 35½
					94b-SB	36(A) x 35½
					94b-HA	35¾ x 35½

Table 3-3. Steel pieces from the car sills (teardown effort) and from those tested during the GATX-sponsored Minot work.

Status	Rep. Mark or Car No.	Car Builder	Material Type	Date	C-O-C	NewID	Plate Size (in)
Car	GATX 91554	GATX	TC128-B	1967	✓	67b-SA 67b-HA	11½ (A) x 23 14 x 17
Sills	GATX 55905	GATX	TC128-B	1966	✓	66a-SA 66a-HA	14 (A) x 22 irregular
	UTLX 14439	Union	A285-C	1974	✓	74a-SA 74a-HA	28½ (A) x 10 irregular
	GATX 50863	GATX	A515-Gr70	1970	✓	70a-SA 70a-HA	9 (A) x 30 18 x 15
	GATX 16108	GATX	A515-Gr70	1983	✓	83a-SA 83a-HA	14 (A) x 26½ 13½ x 14½
	GATX 9746	GATX	A212-B	1965	✓	65a-SA 65a-HA	13½(A) x 32½ 14 x 12½
	Tested (Minot work)	PLMX 4504	Rich (Trinity)	TC128-B	1976	✓	76a-SA(F) 76a-SB(A)
GATX 47814		GATX	TC128-B	1976	✓	76b-SA(F) 76b-SB(A) 76b-SC(D)	
GATX 47982		GATX	TC128-B	1976	✓	76c-SA(F) 76c-SB(A)	
PLMX 4644		Rich (Trinity)	TC128-B	1978	✓	78a-SA(D) 78a-SB(A)	
GATX 49248		GATX	TC128-B	1977	✓	77a-SA(D)	
GATX 47837		GATX	TC128-B	1976	✓	76d-SA(F) 76d-SB(A)	

Table 3-4. Alphabetical listing of the different tank cars describing features and characteristics of each

Car ID No:	CGTX 63699	CGTX 64251	CGTX 64270	GAMX 4115
<i>DOT Stencil:</i>	DOT 112J340-W	DOT 112S340-W	DOT 112J340W	105A500W (105J500W)
<i>Capacity (gal):</i>	33552	33666	33756	17360
	LIQUEFIED	ANHYDROUS		
<i>Commodity:</i>	HYDROCARBON GAS	AMMONIA	LPG	Chlorine
<i>Build Date:</i>	1966	1967	Nov 1978	1978/1979
			Hawker Siddeley	
<i>Manufacturer:</i>	CGTX	GATX	Canada	ACF
<i>Build Order No:</i>	CO1980	8041		18-15333
<i>Certif. of Const.:</i>	20542	21383	A-788501-A	Z781500 (Z781200)
<i>Insulation:</i>	None	None	Fibrefrax 0.65"	urethane foam
<i>Light Wgt (lbs):</i>	113,900	101,800	99,800	82,500
<i>Gross Rail Load (lbs):</i>	263,000	263,000	263,000	263,000
<i>Coils:</i>	None	None		None
<i>Tank Wall (inch):</i>	0.7986	0.653	0.625	0.7751
<i>Tank ID (inch):</i>	104.25 / 118.375	112	119	100.4498
<i>Tank Material:</i>	A212-B	TC128-B (FQS)	TC-128	TC 128 Gr. B
<i>Head Wall (inch):</i>	0.7033	0.653	0.625	13/16
<i>Head Material:</i>	A212-B	TC128-B (FQS)	TC-128	TC 128 Gr. B
<i>Underframe:</i>	GAT095	GATX098	unknown	ACF 200
<i>Mileage:</i>	637772	396483	unknown	unknown
<i>Inspections:</i>	TT, Rule 88B, SS3 in 2000,	TT, Rule 88B, SS3 in 2000,	unknown	unknown
<i>Why Scrapped:</i>	unknown	unknown	derailment	unknown
<i>Location Scrapped:</i>	Sarnia, Canada	Sarnia, Canada	Québec, Canada	unknown

Table 3-4. continued...

Car ID No:	GATX 16108	GATX 25008	GATX 47814	GATX 47837
<i>DOT Stencil:</i>	111A100 W 1	112A340 W	105A300W	105A300W
<i>Capacity (gal):</i>	13890	33697	33687	33687
<i>Commodity:</i>	molten sulfur	propane-butane mixture	LPG, Anhydrous Ammonia, Butadiene	LPG, Anhydrous Ammonia, Butadiene
<i>Build Date:</i>	Nov 1983	Oct 1971	1976	1976
<i>Manufacturer:</i>	General American	General American	General American	General American
<i>Build Order No:</i>	10938	9144	unknown	unknown
<i>Certif. of Const.:</i>	A833044	25624	F763017	F763017
<i>Insulation:</i>	fiberglass, 6 in.	ceramic, 0.5 in.	GWB 3/4"	GWB 3/4"
<i>Light Wgt (lbs):</i>	59,100	98,200	95,800	95,800
<i>Gross Rail Load (lbs):</i>	263,000	263,000	263,000	263,000
<i>Coils:</i>	14 - exterior	none	n/a	n/a
<i>Tank Wall (inch):</i>	0.4375	0.6244	0.5625	0.5625
<i>Tank ID (inch):</i>	99	119	119	119
<i>Tank Material:</i>	A515 Gr. 70	TC128 Gr. B	TC128B	TC128B
<i>Head Wall (inch):</i>	0.4375	n/a	0.5625	0.5625
<i>Head Material:</i>	A515 Gr. 70	unknown	TC128B	TC128B
<i>Underframe:</i>	GAT020	GAT098A (9801)	unknown	unknown
<i>Mileage:</i>	308797	145861	unknown	unknown
<i>Inspections:</i>	No cracks (SS-2)	Six cracks reported in SS-2 ranging 1-5" long.	unknown	unknown
<i>Why Scrapped:</i>	unknown	unknown	accident	accident
<i>Location Scrapped:</i>	Industrial Scrap	Industrial Scrap	Minot, ND	Minot, ND

Table 3-4. continued...

Car ID No:	GATX 47982	GATX 49248	GATX 50863	GATX 55905
<i>DOT Stencil:</i>	105A300W	105A300W	111A100 W 1	112J340 W
<i>Capacity (gal):</i>	33687	33687	16243	33635
<i>Commodity:</i>	LPG, Anhydrous	LPG, Anhydrous	50% caustic soda	anhydrous ammonia
<i>Build Date:</i>	Ammonia, Butadiene 1976	Ammonia, Butadiene 1977	May 1970	Jul 1966
<i>Manufacturer:</i>	General American	General American	General American	General American
<i>Build Order No:</i>	unknown	unknown	8883	7624
<i>Certif. of Const.:</i>	F763019	F773076	24299	20220
<i>Insulation:</i>	4" comp. glass wool	4" comp. glass wool	fiberglass, 6 in.	ceramic, 0.5 in.
<i>Light Wgt (lbs):</i>	95,800	96,200	63,300	105,600
<i>Gross Rail Load (lbs):</i>	263,000	263,000	263,000	263,000
<i>Coils:</i>	n/a	n/a	8 - exterior	none
<i>Tank Wall (inch):</i>	0.5625	0.5625	0.4375	0.653
<i>Tank ID (inch):</i>	119	119	102	112
<i>Tank Material:</i>	TC128B	TC128B	A515 Gr. 70	TC128 Gr. B
<i>Head Wall (inch):</i>	0.5625	0.5625	0.500	n/a
<i>Head Material:</i>	TC128B	TC128B	A515 Gr. 70	unknown
<i>Underframe:</i>	unknown	unknown	GAT098A (9801)	GAT097
<i>Mileage:</i>	unknown	unknown	224335	191677
<i>Inspections:</i>	unknown	unknown	Five cracks reported in SS-2 ranging 1-3" long. unknown	Two SS-2's identified several cracks. too many cracks
<i>Why Scrapped:</i>	accident	accident		
<i>Location Scrapped:</i>	Minot, ND	Minot, ND	Industrial Scrap	Waskom, TX

Table 3-4. continued...

Car ID No:	GATX 91467	GATX 91554	GATX 92593	GATX 9746
<i>DOT Stencil:</i>	105A500 W	112A340 W	DOT 112J340-W	111A100 W 1
<i>Capacity (gal):</i>	16527	33652	33636	20494
<i>Commodity:</i>	chlorine converted to sulfur	anhydrous ammonia	PROPANE	unknown
<i>Build Date:</i>	Oct 1967	Dec 1967	1968	Mar 1965
<i>Manufacturer:</i>	General American	General American	GATX	General American
<i>Build Order No:</i>	7986	8094	8418	7237
<i>Certif. of Const.:</i>	21391	21383	22765-A	19395
<i>Insulation:</i>	polyurethane, 4 in.	ceramic, 0.5 in.	None	none
<i>Light Wgt (lbs):</i>	82,600	105,600	100,600	64,600
<i>Gross Rail Load (lbs):</i>	263,000	263,000	263,000	263,000
<i>Coils:</i>	none	none	None	16 - interior
<i>Tank Wall (inch):</i>	0.787	0.653	0.625	0.4375
<i>Tank ID (inch):</i>	102	112	119	102
<i>Tank Material:</i>	TC128 Gr. B	TC128 Gr. B	TC128-B (FQS)	A212 Gr. B
<i>Head Wall (inch):</i>	n/a	n/a	0.625	n/a
<i>Head Material:</i>	unknown	unknown	TC128-B (FQS)	unknown
<i>Underframe:</i>	GAT098A (9801)	GAT098A (9801)	GATX098	GAT101A
<i>Mileage:</i>	63,560 (reset)	320615	266923	222055
<i>Inspections:</i>	One 8" long crack recorded in SS-2	Sixteen cracks in SS-2 ranging 2-6" long.	SS3 in 2003, TT in 1995	Two 4" long cracks recorded in SS-2.
<i>Why Scrapped:</i>	unknown	unknown	unknown	unknown
<i>Location Scrapped:</i>	Waskom, TX	Industrial Scrap	Red Deer, Canada	Industrial Scrap

Table 3-4. continued...

Car ID No:	GATX 97833	HOKX 8373	HOKX 8453	PLMX 4504
<i>DOT Stencil:</i>	DOT 112A340-W	DOT 105A500W	DOT 105A500W	105A300W
<i>Capacity (gal):</i>	33651	17360	17368	33,500 (nominal)
	LIQUEFIED			LPG, Anhydrous
<i>Commodity:</i>	HYDROCARBON GAS	Chlorine	Chlorine	Ammonia, Butadiene
<i>Build Date:</i>	1967	29646	30011	1976
				Richmond Tank Car
<i>Manufacturer:</i>	GATX	ACF	GATX	Company (Trinity Tank)
<i>Build Order No:</i>	7810	unknown	10764	unknown
<i>Certif. of Const.:</i>	21366	A811020	F-823015	A754015
<i>Insulation:</i>	None	4" Urethane Foam	4" Urethane Foam	2-3" urethane
<i>Light Wgt (lbs):</i>	90,500	83,000	82,000	99,000
<i>Gross Rail Load (lbs):</i>	263,000	263,000	263,000	263,000
<i>Coils:</i>	None	N/A	N/A	n/a
<i>Tank Wall (inch):</i>	0.653	0.7751	0.7874	0.5625
<i>Tank ID (inch):</i>	112	100.4	102"	114.875
<i>Tank Material:</i>	TC128-B (FQS)	TC-128 Grade B	TC-128 Grade B	TC128B
<i>Head Wall (inch):</i>	0.653	0.8125	0.8125	0.5625
<i>Head Material:</i>	TC128-B (FQS)	TC-128 Grade B	TC-128 Grade B	TC128B
<i>Underframe:</i>	GATX097	unknown	GATX Type 98	unknown
<i>Mileage:</i>	229464	unknown	unknown	unknown
<i>Inspections:</i>	SS3 in 1997, HM-201 in 1999	unknown	unknown	unknown
<i>Why Scrapped:</i>	unknown	Hurricane Katrina	Hurricane Katrina	accident
<i>Location Scrapped:</i>	Red Deer, Canada	New Orleans Area	New Orleans Area	Minot, ND

Table 3-4. continued...

Car ID No:	PLMX 4644	PROX 31153	PROX 31218	PROX 81231
<i>DOT Stencil:</i>	105A300W	112J340W	112J340W	DOT 112J340W
<i>Capacity (gal):</i>	34,000 (nominal) LPG, Anhydrous	33866	33970	33988
<i>Commodity:</i>	Ammonia, Butadiene	Butadiene	Butadiene	LPG
<i>Build Date:</i>	1978 Richmond Tank Car Company (Trinity Tank)	Oct '94	Nov '94	25112
<i>Manufacturer:</i>	UTC	UTC	UTC	UTC
<i>Build Order No:</i>	unknown	5036B	5036B	A-4190
<i>Certif. of Const.:</i>	F774D12	F947045A	F947045A	22566
<i>Insulation:</i>	2-1/4" urethane	Fiberfrax	Fiberfrax	1/2" fiberfrax
<i>Light Wgt (lbs):</i>	100,300	99,100	99,100	102,800
<i>Gross Rail Load (lbs):</i>	263,000	263,000	263,000	263,000
<i>Coils:</i>	n/a	No	No	n/a
<i>Tank Wall (inch):</i>	0.5625	0.618"	0.618"	11/16"
<i>Tank ID (inch):</i>	114.875	117.875"	117.875"	117.925"
<i>Tank Material:</i>	TC122B	TC-128-BN	TC-128-BN	AAR TC 128 Gr B
<i>Head Wall (inch):</i>	0.5625 min	0.6875"	0.6875"	11/16"
<i>Head Material:</i>	TC122B	TC-128-BN	TC-128-BN	AAR TC 128 Gr B
<i>Underframe:</i>	unknown	No	No	Stub Sill
<i>Mileage:</i>	unknown	332200	299500	563700
<i>Inspections:</i>	unknown	TNK QUAL 12/04	TNK QUAL 10/04	tank test 10/98, safety valve 6/03
<i>Why Scrapped:</i>	accident	unknown	unknown	destroyed in derailment
<i>Location Scrapped:</i>	Minot, ND	unknown	unknown	Hutchinson KS

Table 3-4. continued...

Car ID No:	PROX 83469	PROX 89773	TAEX 143	TGAX 331007
<i>DOT Stencil:</i>	105A500W	DOT 112J340W	111A100W1	112S340W
<i>Capacity (gal):</i>	17300	33731	20,800 (nominal) fertilizer at time of accident	33,729 GAL
<i>Commodity:</i>	Chlorine	LPG/AA	26299	Anhydrous Ammonia
<i>Build Date:</i>	29465	25020	Richmond Tank Car Company (Trinity Tank)	July 1975
<i>Manufacturer:</i>	Procor Ltd	UTC	unknown	ACF
<i>Build Order No:</i>	4570	A-4173	26200"A"	A751058
<i>Certif. of Const.:</i>	F808806	21968	n/a	None
<i>Insulation:</i>	4" urethane foam	3/4" fiberous	60,200	88,600 lbs
<i>Light Wgt (lbs):</i>	81,900	102,000	263,000	174,400 lbs
<i>Gross Rail Load (lbs):</i>	263,000	263,000	n/a	None
<i>Coils:</i>		n/a	0.4375	.625"
<i>Tank Wall (inch):</i>	0.779	.6875"	108.75	118.75"
<i>Tank ID (inch):</i>	101	117.925	A-515 Grade 70	AAR TC-128 Grade "B"
<i>Tank Material:</i>	128B	TC-128 Gr B	unknown	.625"
<i>Head Wall (inch):</i>	0.779	.6875"	unknown	AAR TC-128 Grade "B"
<i>Head Material:</i>	128B	TC-128 Gr B	unknown	Stub Sill Z
<i>Underframe:</i>	unknown	STUBSILL (PROZBN)	unknown	unknown
<i>Mileage:</i>	322236	574000	unknown	unknown
<i>Inspections:</i>		tank test 1996, safety valve 2001	unknown	unknown
<i>Why Scrapped:</i>	unknown	destroyed in derailment	accident	age
<i>Location Scrapped:</i>	unknown	Denver Colorado	The Andersons	Birmingham, AL

Table 3-4. continued...

Car ID No:	UTLX 14439	UTLX 28744	UTLX 80681
<i>DOT Stencil:</i>	111A100W2	DOT 105J500W	DOT 112J340W
<i>Capacity (gal):</i>	13702	17458	33842
<i>Commodity:</i>	sulfuric acid	chlorine	LPG
<i>Build Date:</i>	Sep 1974	27364	24047
<i>Manufacturer:</i>	Union Tank Car (East Chicago)	Union Tank Car	Union Tank Car
<i>Build Order No:</i>	Approp. 3411A	Appro. 3467	Appro. 1945
<i>Certif. of Const.:</i>	A-747001	A747089	18857
<i>Insulation:</i>	none	4" urethane foam	1" mineral wool
<i>Light Wgt (lbs):</i>	56,200	81,600	106,900
<i>Gross Rail Load (lbs):</i>	263,000	263,000	263,000
<i>Coils:</i>	none	none	none
<i>Tank Wall (inch):</i>	0.5625	0.779	0.6875
<i>Tank ID (inch):</i>	104.875	100.75	104.625 at head, 116.625 at center
<i>Tank Material:</i>	ASTM A285-C	TC128 GR B	M-128 (0.25% max C)
<i>Head Wall (inch):</i>	n/a	UTL-ZBN	n/a
<i>Head Material:</i>	unknown	unknown	unknown
<i>Underframe:</i>	UTL-ZBD (100" ohang)	unknown	UTL-ZBR
<i>Mileage:</i>	unknown	unknown	418000
<i>Inspections:</i>	Single 4" long crack recorded in SS-2.	Two inspections with no cracks found.	One 2" crack found on SS-2 inspection.
<i>Why Scrapped:</i>	Railroad damage	repair estimate exceeded repair limit	age of car
<i>Location Scrapped:</i>	Cleveland, TX	Marion, OH	El Dorado, KS

Table 3-4. continued...

Car ID No:	UTLX 83551	UTLX 89348	UTLX 95454
<i>DOT Stencil:</i>	DOT 112S400W	DOT 112J340W	DOT 112J340W
<i>Capacity (gal):</i>	Approx. 22,500	33557	34053
<i>Commodity:</i>	LPG	LPG	LPG
<i>Build Date:</i>	22647	24807	25235
<i>Manufacturer:</i>	UTC	UTC	UTC
<i>Build Order No:</i>	1383	3016	3103
<i>Certif. of Const.:</i>	15225A	21171	22591
<i>Insulation:</i>	None	None	None
<i>Light Wgt (lbs):</i>	85,300	102,500	101,200
<i>Gross Rail Load (lbs):</i>	263,000	263,000	263,000
<i>Coils:</i>	None	None	None
<i>Tank Wall (inch):</i>	25/32"	11/16"	5/8"
<i>Tank ID (inch):</i>	97-7/16"	117.925"	118.05"
<i>Tank Material:</i>	ASTM A-212 Gr. G	TC-128 Gr. B	TC-128 Gr. B
<i>Head Wall (inch):</i>	25/32"	11/16"	11/16"
<i>Head Material:</i>	ASTM A-212 Gr. G	TC-128 Gr. B	TC-128 Gr. B
<i>Underframe:</i>	UTL-FBR	UTL-ZBN	UTL-ZBN
<i>Mileage:</i>	unknown	319390	354385
<i>Inspections:</i>	unknown	Two 2" long cracks on SS-2	One 4" long crack recorded on SS-2.
<i>Why Scrapped:</i>	derailment	age of car	age of car
<i>Location Scrapped:</i>	Eastland, TX	Marion, OH	Evanston, WY

Tank Car Material Cross Referencing

Key = **Minot samples**
Teardown sample (evaluated during Minot investigation)
Teardown sample
Builder or railroad supplied

Year Built	ID Description alphanumeric)					
	No.	a	b	c	d	
1962	62	=	UTLX 83551			
1963	63	=				
1964	64	=				
1965	65	=	GATX 9746	UTLX 80681		
1966	66	=	GATX 55905	GATX 97833	CGTX 63699	
1967	67	=	GATX 91467	GATX 91554	CGTX 64251	UTLX 89348
1968	68	=	GATX 92593	PROX 89773	PROX 81231	
1969	69	=	UTLX 95454			
1970	70	=	GATX 50863			
1971	71	=	GATX 25008			
1972	72	=	TAEX 143			
1973	73	=				
1974	74	=	UTLX 14439	UTLX 28744		
1975	75	=	TGAX 331007			
1976	76	=	PLMX 4504	GATX 47814	GATX 47982	GATX 47837
1977	77	=	GATX 49248			
1978	78	=	PLMX 4644	CGTX 64270		
1979	79	=	GAMX 4115			
1980	80	=	PROX 83469			
1981	81	=	HOKX 8373			
1982	82	=	HOKX 8453			
1983	83	=	GATX 16108			
1984	84	=				
1985	85	=				
1986	86	=				
1987	87	=				
1988	88	=				
1994	94	=	PROX 31153	PROX 31218		

Figure 3-1. Cross-referencing system used to identify steel pieces in all subsequent testing. For instance, the combination of vertical and horizontal column to form 76c implies that material so-marked is from tank car GATX 47982 (and color coding indicates that this was a Minot sample).

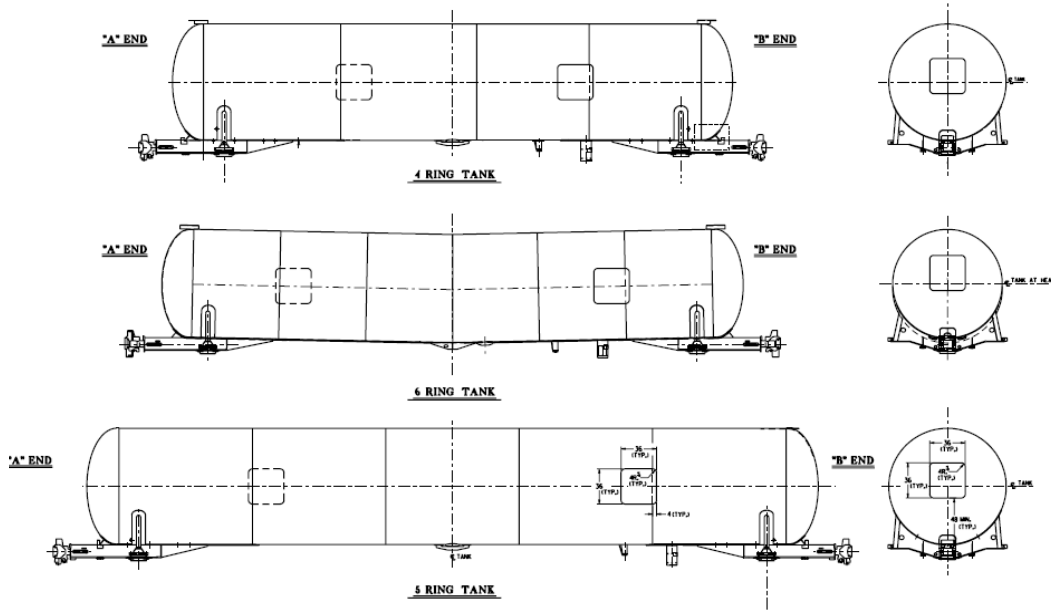


(a)



(b)

Figure 3-2. Different tank car pieces including (a) car stub sill segments from the teardown study in the “stub sill farm” and (b) different pieces of the Minot steel.



SHOP INSTRUCTIONS
Sample Tank Car Sections for SWRI
 P-60277-05 Rev A
 9/13/05

Please have the sections described below cut from the tank before it is sent to scrap.

- One 3'x3' section of the head. The bottom of the section is to be at least 4 feet above the top of the stub sill. Corners of the section are to have a 4 inch radius, +/- 1 inch.
- Two 3'x3' sections of shell, from different shell rings. Cut one of these from each side of the tank, AR and BL corners to keep the car marks and numbers intact. Locate the section such that it is centered from top to bottom. Take about 4 inches of the end shell ring and the rest of the 3 foot length from the 2nd shell ring in from the end. This will result in a girth weld being included along one edge. Corners of the section are to have a 4 inch radius, +/- 1 inch.
- When samples are cut in this way, cars can be shipped directly to scrap dealer without adding tank reinforcement.
- After the above sections have been removed, jacket material must be tacked in place over the holes to prevent kids or vandals from entering or tossing anything into the car, while it is in transit to the scrap dealer.

Charge this work to Project 60277

Send material to:
 Peter C. McKeighan
 Southwest Research Institute
 Manager - Mechanical Testing Section
 Materials Engineering Department
 6220 Culebra Road
 San Antonio, TX 78238-5166
pmckeighan@swri.org
 Phone: 210-522-3617

Figure 3-3. Tank car cut-up instructions and schematic (supplied by Union Tank Car Company).

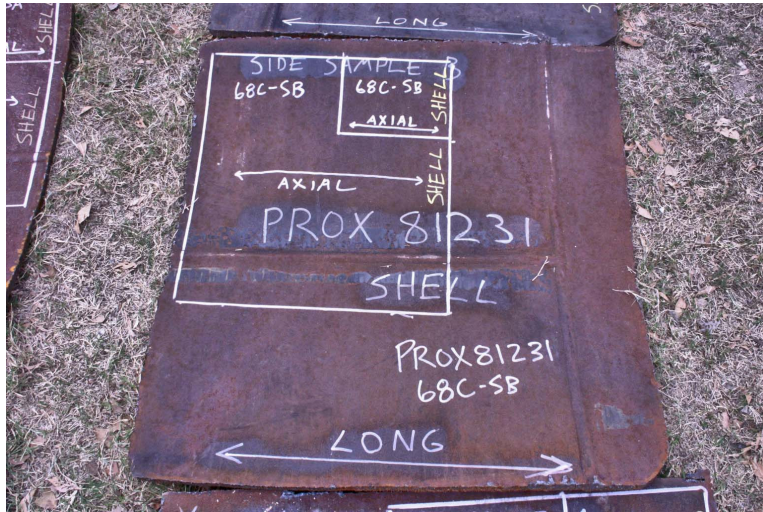


Figure 3-4. Collection of plates received, representative marking and torching smaller pieces out of the plate.

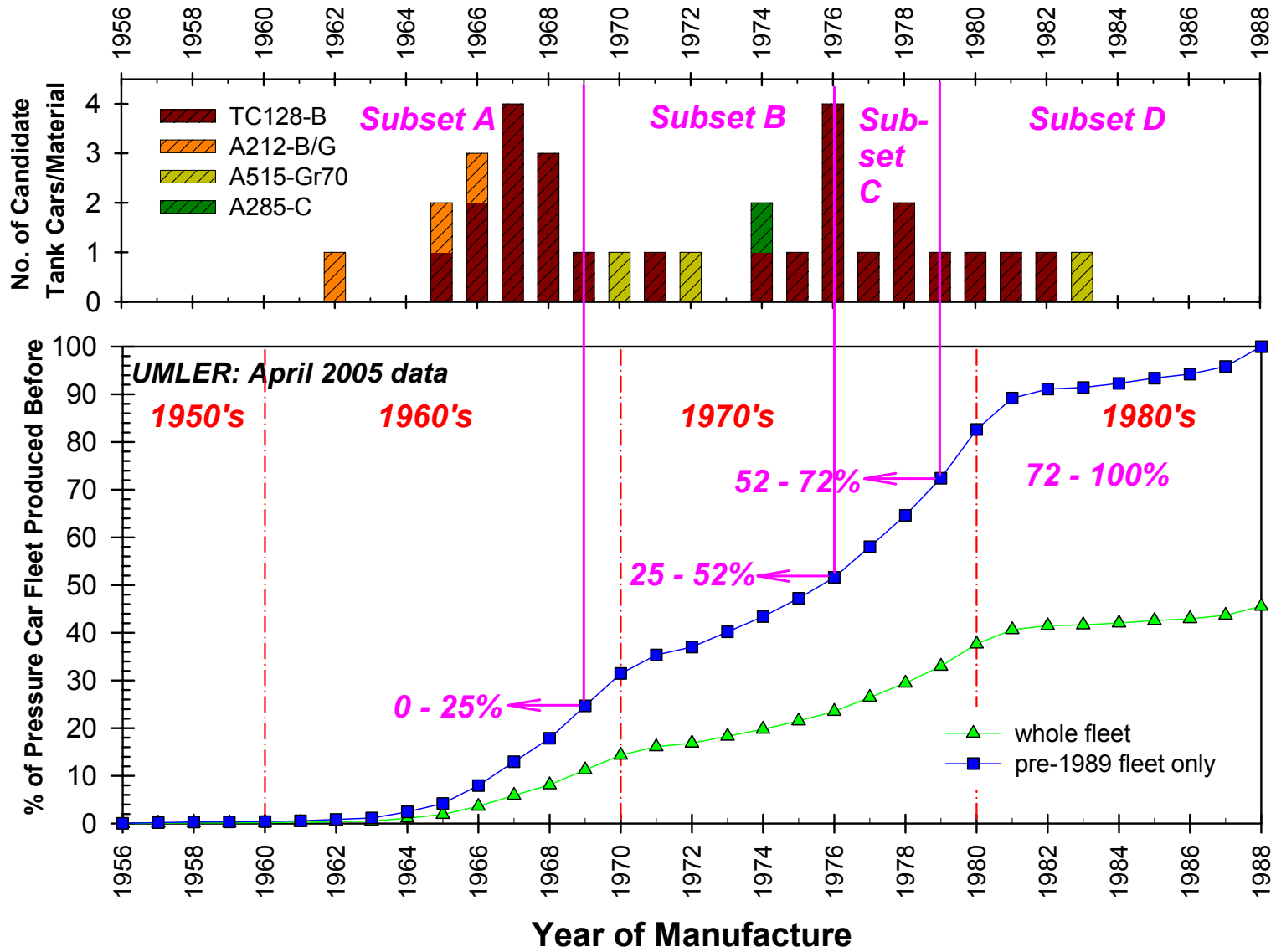


Figure 3-5. Comparison between the available tank cars and the cumulative car manufacture for the pre-1989 fleet.

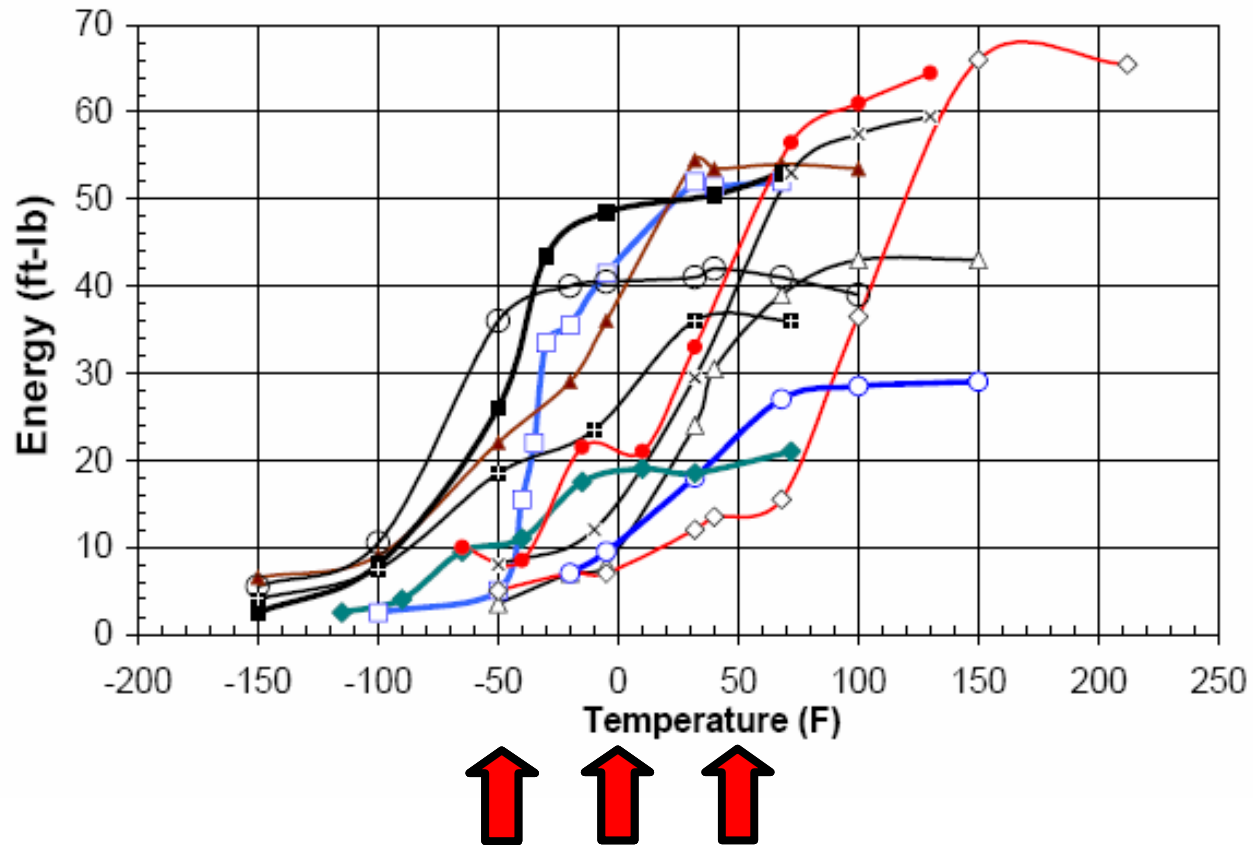


Figure 3-6. Temperatures selected for CVN tests (overlaid with NTSB data from Minot report).

4.0 MATERIAL CHARACTERIZATION TESTING OF VINTAGE MATERIALS

The previous section of the report described in detail the pedigree of the materials involved in this study. The focus of this section is the basic material characterization testing. This includes the tensile testing, chemistry testing and CVN fracture toughness testing.

4.1 Material Processing

Once the plate segments were received and logged into the database, they were marked with identifiers and stored with the other tank car material. Sometimes material was in the form of plate segments, whereas other times larger pieces of the structure were available. Some pieces were as small as a shoebox whereas in other cases the resulting plate was more on the order of 6' x 6'. The most common form of material delivery was a piece approximately 3' x 3'.

Two subset pieces were removed from the received plates. The first subset was a piece suitable for performing the basic material characterization testing and the second piece was reserved for further testing (usually fracture toughness testing). The plates were photographed before piece removal with the markings shown on each plate and then after documenting the removal of the segment. Redundant marking was employed to ensure that no piece would get "lost" or not have its pedigree known.

4.2 Material Characterization Test Procedures

Basic material characterization was performed by a subcontractor, Staveley Services (Glendale Heights, IL). SwRI has had extensive experience with Staveley (now part of Bodycote) and were confident that the required testing could be performed proficiently. All tank car pieces and conditions not previously evaluated were characterized in terms of:

- tensile properties – ASTM A370²
- CVN fracture toughness – ASTM A23³
- chemical (elemental) analysis – ASTM E415⁴.

The tensile properties of interest were ultimate and yield strength, percent elongation at failure and reduction of area. The customary gage length utilized was a 2-inch gage length, although material limitations occasionally required testing subsize (1-inch or 1.4-inch) gage length specimens. The tensile specimens were oriented transverse to the primary plate axis for the shell specimens. In the case of the pieces of head, they were arbitrarily removed since the orientation of the plate prior to hot pressing the head was not known. Two replicate specimens were tested in all cases.

Although the standard for CVN testing (E23) typically requires three samples for each temperature, the excellent repeatability observed herein allowed testing only two CVN samples at each of the three different temperatures. In a limited number of cases, a third replicate was, however, required if variability was too high or results made little sense. CVN specimens from the shell material were oriented with the primary axis of the specimen in the transverse plate direction and the crack direction orthogonal (and in the plate longitudinal direction). For the head, the orientation was again arbitrary (see discussion above for the tensile specimens). The primary axis (long axis) of the CVN specimen was the axis along which tensile properties were measured.

Finally, when performing the chemical analysis, particular attention was paid to sixteen elements, even though the TC128-B composition specification requires controlling only nine distinct elements.

² ASTM A370-05: Standard Test Methods and Definitions for Mechanical Testing of Steel Products.

³ ASTM A23-05: Standard Test Methods for Notched Bar Impact Testing of Metallic Materials.

⁴ ASTM E415-99a(2005): Standard Test Method for Optical Emission Vacuum Spectrometric Analysis of Carbon and Low-Alloy Steel.

4.3 Results of Material Characterization

The material characterization results are provided in tabular format in Tables 4-1 through 4-6. For each distinct property, two tables are provided: the first is for TC128-B material provided specifically for this program and the second is for material considered in the Minot work, during the teardown or other non-TC128-B material donated to this effort. More specifically,

- tensile properties (two replicates) are shown in Tables 4-1 and 4-2
- composition properties are included in Tables 4-3 and 4-4
- CVN toughnesses are included in Tables 4-5 and 4-6 (two replicates, except in the case of the Minot specimens, three replicates).

A summarizing statistical analysis is provided in Table 4-7, examining only the pre-1989 TC128-B samples considered in this study. This summary encompasses all key tensile and CVN properties and provides the relevant average and standard deviation as well as the sample size. The statistical analysis considers all samples as well as the four subsets roughly examining 25% intervals of the fleet.

Although tabulated summaries are important for completeness, it is difficult to draw any conclusions from only tabulated numbers. It is usually more effective in this case to plot the results and examine the inter-relationships between the data in some spatial sense. Therefore, plots are provided examining tensile and CVN data in Figures 4-1 through 4-14.

Strength is plotted in Figure 4-1 as a function of condition evaluated along the x-axis. Several observations are notable. First, in conditions where a low or high yield strength is observed, typically the same trend manifests itself for ultimate strength. Second, it is interesting to note that some conditions have a significant spread indicated for ± 2 standard deviations. These are conditions where a third replicate specimen may have been warranted (but not tested). In general, yield strength varies from 50-70 ksi and ultimate strength from 75-100 ksi. A similar

plot, but this time in terms of the two ductility measures, is provided in Figure 4-2. Percent elongation tends to range from 20-30% and reduction of area from 45-65%.

Plots for CVN toughness are indicated in Figures 4-3 for +50°F and 0°F and in Figure 4-4 for -50°F. A close examination of the data clearly illustrates the toughness decrease with decreasing temperature. Wide scatter in the data is evident at the two higher temperatures. However, for the lowest temperature condition (-50°F), the toughness has decreased significantly and typically lie below 20 ft-lbs.

It is not uncommon to observe a link between carbon content and tensile properties. In an effort to understand this trend for TC128-B material, Figure 4-5 indicates how ultimate and yield strength vary with carbon content. Put simply, there does not appear to be much, if any, correlation between strength and carbon content. The data in Figure 4-5 does not appear to exhibit a systematic trend in any direction.

The focus of the plots so far has been on pre-1989 TC128-B material. Post-1989 TC128-B material as well as other older materials are shown in Figures 4-6, 4-7 and 4-8 for strength, ductility and CVN toughness, respectively. Clearly the yield and ultimate strengths of the A212 and A515 materials are fairly low (40-45 ksi for YS and 70-80 ksi for UTS) as observed in Figure 4-6. The ductilities depicted in Figure 4-7 do not appear too far from that observed in the pre-1989 TC128-B. CVN fracture toughness is markedly low for the non-TC128-B material in Figure 4-8, especially at the lowest temperature. A quite large variation in fracture toughness is particularly evident for the post-1989 normalized TC128-B in Figure 4-8.

The statistical summary data from Table 4-7 is plotted in Figures 4-9, 4-10 and 4-11 for strength, ductility and CVN toughness, respectively. For each interval (and variable) examined, three distinct points are indicated: analysis of the average and ± 2 standard deviations for all (head and shell), shell-only and head-only conditions. This plot also allows examining trends with time, at least in terms of averages. Several observations are notable:

- In terms of average value and including the ± 2 std. dev. range, no definitive change is observed in (a) either measure of strength (yield and ultimate) or (b) either measure of ductility.
- The head material tends to exhibit slightly elevated yield strength when compared with the shell.
- There is no clearly definitive statistical trend of ultimate strength differences between the head and shell condition.
- Regardless of which measure of ductility that is used, the shell is slightly lower (2-5% absolute) than the head.

The CVN toughness data shown in Figure 4-11 tends to exhibit a significant amount of scatter. Hence, it is difficult to more definitively observe any clear difference between the different conditions and the relevant toughness data.

To further understand differences between head and shell, the CVN energy data is plotted as a function of build year in Figures 4-12, 4-13 and 4-14 for the +50°F, 0°F and -50°F conditions, respectively. It should be noted that the faint gray dots along the x-axis indicate car conditions that are available (but not necessarily tested). Presenting the data in this manner allows assessing data variation by year (recall the previous comparison was performed with the Table 4-7 data on the basis of averages and standard deviations). Nevertheless, the overall conclusion is the same; none of the data in Figures 4-12 through 4-13 appears to exhibit any systematic trend with build year. The scatter in the data tends to be greater than any year-to-year trend that is apparent in the data.

4.4 Comparison with TC128-B Material Specifications

Chemical and tensile property definitions are available for TC128-B and summarized in Table 4-8. However, the reader is cautioned that these specifications are current specifications and their applicability to vintage steel that was fabricated in some cases over 40 years ago is not clear. Also, some of the tank car samples involved in this study were not pressure cars, and the applicability of the M1002 specifications to these conditions is unknown. Nevertheless, as

described in Table 4-7, a total of 61 TC128-B conditions were examined: 40 shell conditions and 21 head conditions.

The critical observation is that regardless of specification applicability, the vast majority of the steel extracted from retired tank cars met current chemistry specifications. This is especially true for the chemical analyses. Only two deviations are noted in the TC128-B conditions described in Table 4-3 and 4-4. In one case, the carbon content was 0.32 wt % as opposed to criteria of <0.29 wt % (1971 vintage, 71a-SB). In another case, the sulfur content was 0.05% wt % as opposed to the criteria of < 0.04% (1981 vintage, 81a-HA). No other chemical content disparities were observed. In summary, 59 of 61 samples (97%) met composition requirements of TC128-B.

A larger number of retired tank car samples were observed outside the allowable bounds on tensile properties. First, considering yield strength (the YS specification is >50 ksi), two tank car conditions were observed slightly under the limit:

- a 1976 shell, 76c-SA(F) with both replicate specimens approximately 48 ksi
- a 1967 shell, 67a-SB with one of two replicate samples with a YS of 45 ksi.

The ductility requirement is a percent elongation that exceeds 22%. Three tank cars exhibited elongations less than the minimum and in the range of 19-21% (67d-SB, 76a-SB(a) and 18b-SA).

The UTS requirement is the range 81-101 ksi and deviations were noted in the sixty-one samples on both sides of the range. First, considering the high levels, two tank car conditions exhibited strengths in the range of 101-103 ksi (78b-SA and 81a-SA). Seven tank car conditions manifested UTS levels under 81 ksi. These seven (67a-SB, 68a-HA, 68b-SA, 68b-SB, 68c-SA, 74b-SA and 74b-HA) typically had both replicate specimens exhibiting strengths on the order of 77-80 ksi. However, in one case (68b-SA) both replicate specimens yielded UTS levels of about 74 ksi.

So, in summary, given requirements on ductility, ultimate and yield strengths, eleven cars did not exhibit tensile properties within the specifications indicated in Table 4-8. The remaining 82% of the samples tested did meet the properties required.

Table 4-1. Tensile properties for most of the TC128-B plate material.

Matl Type	Build Date	Matl ID No.	Trial No. 1				Trial No. 2			
			σ_{YS} , ksi	σ_{TS} , ksi	elong, %	RA, %	σ_{YS} , ksi	σ_{TS} , ksi	elong, %	RA, %
M-128	1965	65b-SA	62.0	92.5	23.5	50.9	63.4	92.8	23.5	52.0
		65b-HA	62.1	96.7	22.9	61.3	64.4	99.5	25.0	58.8
TC128-B	1966	66a-SA	64.2	88.2	24.5	47.3	61.0	87.5	23.5	47.1
		66a-HA	62.6	84.1	30.5	60.2	61.5	83.2	30.0	60.6
TC128-B	1966	66b-SA	54.8	86.2	26.5	54.1	54.0	85.9	26.5	54.2
		66b-HA	63.3	85.8	31.5	66.9	64.9	87.2	30.0	66.1
TC128-B	1967	67b-SA	67.3	95.6	22.0	45.4	68.1	96.0	21.5	45.2
		67b-HA	57.2	86.8	28.0	57.0	57.4	86.3	28.5	59.3
TC128-B	1967	67c-SA	57.1	83.9	26.5	53.1	58.4	84.3	26.0	51.7
		67c-HA	60.7	90.6	24.0	57.7	60.0	92.3	24.0	57.3
TC128-B	1967	67d-SA	68.5	98.0	21.5	44.2	67.1	97.3	21.5	45.2
		67d-SB	69.8	96.4	19.3	42.2	71.7	96.8	19.3	44.3
		67d-HA	60.9	88.4	31.0	64.1	60.5	88.5	30.5	63.5
TC128-B	1968	68a-SA	67.1	93.2	24.5	50.3	65.5	93.2	24.0	49.4
		68a-HA	57.6	78.3	32.5	64.1	58.7	77.7	33.0	64.8
TC128-B	1968	68b-SA	51.0	74.1	29.0	51.3	51.2	73.9	29.0	52.4
		68b-SB	53.7	77.3	29.5	53.2	52.8	77.6	28.5	51.4
		68b-HA	60.5	83.3	31.0	62.5	62.0	83.3	30.0	63.1
TC128-B	1968	68c-SA	55.5	80.6	27.5	61.2	55.5	80.4	26.5	60.7
		68c-SB	50.3	84.1	24.0	46.7	50.6	85.7	26.0	46.5
		68c-HA	60.8	87.0	29.0	60.8	62.8	87.1	29.0	61.1
		68c-HB	64.6	86.3	30.0	62.5	62.1	86.5	30.0	61.2
TC128-B	1969	69a-SA	55.3	90.2	24.0	47.4	59.5	90.1	24.0	46.9
		69a-SB	59.0	89.1	24.0	46.5	59.6	88.9	24.0	45.6
		69a-HA	64.0	84.4	30.0	65.7	63.8	84.9	29.5	66.4
TC128-B	1974	74b-SA	51.7	78.1	27.5	48.4	52.1	78.2	27.5	47.0
		74b-HA	57.8	78.3	30.0	63.1	54.0	78.2	32.0	64.0
TC128-B	1975	75a-SA	73.9	98.8	23.0	48.3	76.0	98.8	23.0	47.2
		75a-HA	66.4	88.8	28.5	52.9	66.2	89.4	27.0	51.0
TC128-B	1978	78b-SA	71.5	102.3	21.0	46.7	72.6	102.8	21.5	46.5
		78b-HA	61.6	91.5	23.5	54.6	61.3	91.7	24.5	52.8
TC128-B	1979	79a-SA	62.0	89.0	24.0	51.1	63.0	89.2	23.0	50.4
		79a-SB	65.1	90.0	23.0	47.3	65.6	90.4	22.0	47.1
		79a-HA	66.9	89.9	30.0	64.6	66.8	90.1	29.0	62.8
TC128-B	1980	80a-SA	54.4	82.5	30.5	62.6	54.4	82.9	31.0	61.4
		80a-HA	53.9	81.1	34.0	72.0	53.8	81.1	34.0	71.0
TC128B	1981	81a-SA	73.8	100.1	23.0	46.3	74.4	100.5	22.0	46.8
		81a-SB	74.3	101.4	22.0	44.9	74.7	101.3	22.0	45.8
		81a-HA	64.0	88.2	30.0	63.0	63.3	88.6	30.0	64.1
TC128-B	1982	82a-SA	57.6	88.1	25.0	48.0	57.6	87.9	25.0	45.1
		82a-SB	64.1	91.3	23.0	42.8	62.7	70.8	23.0	43.8
		82a-HA	65.3	89.2	27.0	64.0	72.9	95.1	29.0	63.7

Table 4-2. Tensile properties for teardown, Minot and post-1989 TC128-B material.

Matl Type	Build Date	Matl ID No.	Trial No. 1				Trial No. 2			
			σ_{ys} , ksi	σ_{TS} , ksi	elong, %	RA, %	σ_{ys} , ksi	σ_{TS} , ksi	elong, %	RA, %
TC128-B	1976	76a-SA(F)	68.8	96.5	22.9	51.8	69.0	96.3	22.9	50.9
		76a-SB(A)	69.5	98.2	21.4	51.0	69.7	98.7	20.7	47.9
TC128-B	1976	76b-SA(F)	55.8	88.3	23.6	44.6	55.5	87.5	23.6	45.3
		76b-SB(A)	55.4	85.3	24.3	52.1	55.3	85.8	25.0	51.7
		76b-SC(D)	57.7	90.7	24.3	49.7	58.0	91.2	24.3	49.0
TC128-B	1976	76c-SA(F)	48.5	83.0	27.1	56.8	48.6	82.3	27.1	54.9
		76c-SB(A)	69.8	98.5	24.3	48.9	70.0	98.5	21.3	49.4
TC128-B	1976	76d-SA(F)	52.7	86.0	27.1	52.3	52.7	86.4	27.1	52.9
		76d-SB(A)	53.6	87.2	25.7	52.9	55.0	88.1	25.7	51.2
TC128-B	1977	77a-SA(D)	52.7	81.7	26.4	49.4	53.4	82.2	25.7	48.0
TC128-B	1978	78a-SA(D)	55.0	83.5	28.6	62.0	54.8	83.6	28.6	64.8
		78a-SB(A)	67.1	89.0	27.1	52.9	67.5	88.7	27.1	53.1
TC128-B	1967	67a-SA	55.5	89.5	25.0	48.0	54.5	88.6	26.0	49.0
		67a-SB	45.4	77.0	33.0	60.0	55.2	88.2	23.0	55.0
		67a-HA	63.0	96.7	27.0	62.0	62.6	96.8	27.0	62.0
TC128-B	1971	71a-SA	57.7	92.3	23.0	52.0	57.2	91.8	35.0	58.0
		71a-SB	62.5	99.2	22.0	47.0	61.9	98.8	21.0	46.0
		71a-HA	67.2	91.9	30.0	66.0	70.7	93.3	30.0	66.0
		71a-HB	64.0	88.2	33.0	60.0	61.7	87.7	32.0	64.0
TC128-B (normalized)	1994	94a-SA	55.6	79.6	30.0	58.2	55.3	79.6	30.0	57.8
		94a-SB	53.8	79.5	34.0	67.5	53.6	79.5	34.5	69.0
		94a-HA	54.7	82.5	34.5	69.9	51.5	78.8	35.0	71.8
TC128-B (normalized)	1994	94b-SA	54.7	81.2	30.0	48.6	55.2	81.7	29.0	48.4
		94b-SB	59.4	86.0	26.0	57.8	59.9	85.8	25.0	57.5
		94b-HA	53.5	80.5	34.0	69.8	53.6	80.4	36.0	71.3
TC128-B (normalized)	1999	TP	59.2	87.3	27.0	59.0	n/a	n/a	n/a	n/a
A212-B	1965	65a-SA	44.7	74.3	32.0	59.9	43.9	74.1	32.0	58.7
		65a-HA	49.2	85.3	29.0	62.8	46.3	83.7	29.0	61.2
A212-B	1966	66c-SA	39.9	72.4	29.0	48.5	42.9	72.5	29.0	47.7
		66c-HA	54.8	74.3	35.0	59.3	52.0	74.5	32.0	58.9
A515-Gr70	1970	70a-SA	44.0	72.0	33.6	60.3	43.8	71.9	29.3	55.3
		70a-HA	44.3	79.5	30.0	60.3	45.1	80.0	29.3	60.2
A515-Gr70	1972	72a-SA	47.7	76.9	31.5	49.0	42.8	75.3	33.0	49.8
A285-C	1974	74a-SA	37.0	58.4	36.4	63.4	40.5	58.2	36.4	64.1
		74a-HA	46.8	61.1	35.0	66.1	46.6	61.1	33.6	65.6
A515-Gr70	1983	83a-SA	43.6	75.3	31.0	59.5	44.9	75.6	32.0	59.7
		83a-HA	45.6	75.2	27.0	70.4	41.8	78.7	30.0	67.2

Table 4-3. Composition properties for most of the TC128-B plate material.

Matl Type	Build Date	Matl ID No.	Chemical Composition (in weight percent)															
			Si	Mn	C	P	S	Ni	Cr	Mo	Cu	Al	V	B	Ti	Sn	N	Cb
M-128	1965	65b-SA	0.24	1.27	0.24	0.01	0.02	0.20	0.17	0.01	0.02	0.04	0.05	<0.0005	<0.01	<0.01	0.0027	<0.01
		65b-HA	0.26	1.32	0.23	0.01	0.02	0.19	0.17	0.02	0.05	0.04	0.05	<0.0005	<0.01	<0.01	0.003	<0.01
TC128-B	1966	66a-SA	0.21	1.28	0.24	0.01	0.02	0.20	0.04	0.04	0.08	0.02	0.04	<0.0005	<0.01	<0.01	0.0037	<0.01
		66a-HA	0.21	1.24	0.24	0.01	0.02	0.20	0.05	0.05	0.08	0.03	0.04	<0.0005	<0.01	<0.01	0.0016	<0.01
TC128-B	1966	66b-SA	0.23	1.34	0.21	0.01	0.02	0.11	0.16	0.01	0.28	0.05	<0.01	<0.0005	<0.01	<0.01	0.0046	<0.01
		66b-HA	0.21	1.29	0.21	0.01	0.02	0.21	0.04	0.05	0.08	0.02	0.05	<0.0005	<0.01	<0.01	0.0044	<0.01
TC128-B	1967	67b-SA	0.24	1.41	0.23	0.01	0.02	0.19	0.05	0.06	0.05	0.02	0.04	<0.0005	<0.01	<0.01	0.0018	<0.01
		67b-HA	0.20	1.28	0.20	0.01	0.02	0.18	0.05	0.04	0.02	0.01	0.03	<0.0005	<0.01	<0.01	0.0033	<0.01
TC128-B	1967	67c-SA	0.24	1.21	0.21	0.01	0.02	0.11	0.18	0.01	0.25	<0.01	<0.01	<0.0005	0.02	<0.01	0.0034	<0.01
		67c-HA	0.18	1.20	0.25	0.01	0.02	0.19	0.04	0.05	0.13	0.01	0.04	<0.0005	<0.01	<0.01	0.0031	<0.01
TC128-B	1967	67d-SA	0.18	1.29	0.24	0.03	0.02	0.16	0.08	0.06	0.07	0.01	0.04	<0.0005	<0.01	<0.01	0.0043	<0.01
		67d-SB	0.22	1.33	0.23	0.02	0.02	0.16	0.08	0.06	0.07	0.01	0.04	<0.0005	<0.01	<0.01	0.04	<0.01
		67d-HA	0.30	1.26	0.28	0.01	0.01	0.11	0.05	0.02	0.12	<0.01	<0.01	<0.0005	<0.01	<0.01	0.0077	<0.01
TC128-B	1968	68a-SA	0.23	1.37	0.24	0.01	0.01	0.18	0.06	0.04	0.04	0.02	0.04	<0.0005	<0.01	<0.01	0.0043	<0.01
		68a-HA	0.19	1.22	0.20	0.01	0.02	0.15	0.07	0.04	0.02	0.02	0.04	<0.0005	<0.01	<0.01	0.0035	<0.01
TC128-B	1968	68b-SA	0.21	1.24	0.21	0.01	0.03	0.02	0.03	0.01	0.02	0.06	0.05	<0.0005	<0.01	<0.01	0.0049	<0.01
		68b-SB	0.22	1.43	0.24	0.01	0.03	0.03	0.03	0.01	0.02	0.08	0.04	<0.0005	<0.01	<0.01	0.0054	<0.01
		68b-HA	0.24	1.34	0.24	0.03	0.02	0.23	0.05	0.03	0.04	0.03	0.01	<0.0005	<0.01	<0.01	0.0066	<0.01
TC128-B	1968	68c-SA	0.22	1.12	0.20	0.01	0.02	0.23	0.17	0.07	0.27	0.01	<0.01	<0.0005	<0.01	<0.01	0.0031	<0.01
		68c-SB	0.24	1.18	0.22	0.01	0.02	0.06	0.18	0.02	0.02	0.07	0.03	<0.0005	<0.01	<0.01	0.0017	<0.01
		68c-HA	0.24	1.31	0.22	0.03	0.02	0.20	0.02	0.01	0.05	0.03	0.01	<0.0005	<0.01	<0.01	0.004	<0.01
		68c-HB	0.27	1.47	0.27	0.02	0.02	0.17	0.04	0.02	0.03	0.03	0.01	<0.0005	<0.01	<0.01	0.0036	<0.01
TC128-B	1969	69a-SA	0.27	1.36	0.27	0.02	0.02	0.19	0.06	0.01	0.06	0.01	<0.01	<0.0005	<0.01	<0.01	0.0046	<0.01
		69a-SB	0.28	1.45	0.24	0.03	0.02	0.20	0.07	0.02	0.06	0.04	0.01	<0.0005	<0.01	<0.01	0.003	<0.01
		69a-HA	0.26	1.24	0.21	0.01	0.02	0.19	0.23	0.07	0.23	0.05	<0.01	<0.0005	<0.01	<0.01	0.0016	<0.01
TC128-B	1974	74b-SA	0.20	1.26	0.22	0.01	0.02	0.19	0.21	0.07	0.01	0.03	<0.01	<0.0005	<0.01	<0.01	0.0061	<0.01
		74b-HA	0.24	1.43	0.21	0.02	0.01	0.14	0.04	0.02	0.02	0.03	<0.01	<0.0005	<0.01	<0.01	0.0027	<0.01
TC128-B	1975	75a-SA	0.24	1.28	0.20	0.01	0.02	0.21	0.17	0.07	0.31	0.04	0.05	<0.0005	<0.01	<0.01	0.0077	<0.01
		75a-HA	0.26	1.42	0.23	0.01	0.03	0.19	0.20	0.07	0.06	0.07	0.03	<0.0005	<0.01	<0.01	0.0019	<0.01
TC128-B	1978	78b-SA	0.24	1.30	0.22	0.01	0.02	0.20	0.21	0.04	0.21	0.04	0.07	<0.0005	<0.01	<0.01	0.0069	<0.01
		78b-HA	0.22	1.20	0.18	0.01	0.01	0.16	0.18	0.04	0.22	0.03	0.07	<0.0005	<0.01	<0.01	0.007	<0.01
TC128-B	1979	79a-SA	0.26	1.32	0.20	0.01	0.03	0.14	0.10	0.04	0.19	0.04	0.06	<0.0005	<0.01	0.01	0.0093	<0.01
		79a-SB	0.25	1.29	0.19	0.01	0.03	0.16	0.10	0.04	0.18	0.03	0.06	<0.0005	<0.01	0.01	0.0078	<0.01
		79a-HA	0.32	1.12	0.24	0.01	0.02	0.14	0.19	0.06	0.28	0.01	0.08	0.001	<0.01	0.02	0.0108	<0.01
TC128-B	1980	80a-SA	0.41	1.47	0.24	0.02	0.01	0.01	0.03	0.01	0.02	0.06	0.04	<0.0005	<0.01	<0.01	0.0055	<0.01
		80a-HA	0.38	1.45	0.22	0.02	0.01	0.02	0.04	0.01	0.02	0.06	0.04	<0.0005	<0.01	<0.01	0.006	<0.01
TC128B	1981	81a-SA	0.22	1.23	0.22	0.02	0.02	0.16	0.19	0.06	0.28	0.01	0.04	<0.0005	<0.01	<0.01	0.0111	<0.01
		81a-SB	0.22	1.21	0.26	0.02	0.01	0.16	0.19	0.07	0.28	0.01	0.01	<0.0005	<0.01	<0.01	0.0109	<0.01
		81a-HA	0.23	1.25	0.26	0.02	0.05	0.21	0.19	0.06	0.27	0.03	0.05	<0.0005	<0.01	<0.01	0.0081	<0.01
TC128-B	1982	82a-SA	0.23	1.32	0.26	0.01	0.03	0.23	0.18	0.05	0.26	0.01	<0.01	<0.0005	<0.01	0.01	0.0106	<0.01
		82a-SB	0.23	1.32	0.26	0.01	0.03	0.24	0.17	0.05	0.27	0.01	<0.01	<0.0005	<0.01	0.01	0.0106	<0.01
		82a-HA	0.24	1.31	0.24	0.01	0.02	0.23	0.02	0.05	0.26	0.01	0.05	<0.0005	<0.01	<0.01	0.0109	<0.01

Table 4-4. Composition properties for teardown, Minot and post-1989 TC128-B material.

Matl Type	Build Date	Matl ID No.	Chemical Composition (in weight percent)															
			Si	Mn	C	P	S	Ni	Cr	Mo	Cu	Al	V	B	Ti	Sn	N	Cb
TC128-B	1976	76a-SA(F)	0.22	1.26	0.20	0.01	0.02	0.21	0.15	0.04	0.24	0.02	0.04	<0.0005	<0.01	0.1	0.0107	<0.01
		76a-SB(A)	0.23	1.26	0.21	0.01	0.02	0.21	0.15	0.04	0.25	0.02	0.04	<0.0005	<0.01	<0.01	0.0118	<0.01
TC128-B	1976	76b-SA(F)	0.24	1.41	0.23	0.02	0.02	0.20	0.22	0.06	0.02	0.07	<0.01	<0.0005	<0.01	<0.01	0.0077	<0.01
		76b-SB(A)	0.24	1.21	0.21	0.01	0.02	0.18	0.17	0.02	0.28	0.03	<0.01	<0.0005	<0.01	<0.01	0.0111	<0.01
		76b-SC(D)	0.25	1.32	0.25	0.01	0.03	0.18	0.18	0.02	0.30	0.03	<0.01	<0.0005	<0.01	<0.01	0.0127	<0.01
TC128-B	1976	76c-SA(F)	0.21	1.29	0.22	0.01	0.01	0.18	0.20	0.06	0.02	0.04	<0.01	<0.0005	<0.01	<0.01	0.0085	<0.01
		76c-SB(A)	0.24	1.31	0.23	0.01	0.04	0.20	0.16	0.01	0.24	0.01	0.05	<0.0005	<0.01	<0.01	0.1000	<0.01
TC128-B	1976	76d-SA(F)	0.20	1.16	0.25	0.01	0.02	0.19	0.15	0.01	0.02	0.02	<0.01	<0.0005	<0.01	<0.01	0.0114	<0.01
		76d-SB(A)	0.25	1.28	0.21	0.03	0.02	0.17	0.16	0.02	0.27	0.03	<0.01	<0.0005	<0.01	<0.01	0.0114	0.01
TC128-B	1977	77a-SA(D)	0.21	1.22	0.18	0.01	0.02	0.19	0.16	0.01	0.24	0.04	<0.01	<0.0005	<0.01	<0.01	0.0118	<0.01
TC128-B	1978	78a-SA(D)	0.26	1.38	0.21	0.01	0.01	0.21	0.10	0.03	0.01	0.04	<0.01	<0.005	<0.01	<0.01	0.0080	<0.01
		78a-SB(A)	0.28	1.24	0.17	0.02	0.01	0.01	0.01	<.01	<.01	0.04	0.06	<0.0005	<0.01	<0.01	0.0068	0.03
TC128-B	1967	67a-SA	0.26	1.33	0.24	0.01	0.02	0.11	0.15	0.01	0.24	0.03	<0.01	<0.0005	<0.01	<0.01	0.0050	<0.01
		67a-SB	0.25	1.23	0.18	0.01	0.02	0.12	0.14	<.01	0.24	0.04	<0.01	<0.0005	<0.01	<0.01	0.0040	<0.01
		67a-HA	0.22	1.40	0.24	0.01	0.02	0.19	0.06	0.01	0.05	0.02	0.03	<0.0005	<0.01	<0.01	0.0050	<0.01
TC128-B	1971	71a-SA	0.23	1.26	0.27	0.01	0.02	0.19	0.20	0.02	0.23	0.03	<0.01	<0.0005	<0.01	<0.01	0.0090	<0.01
		71a-SB	0.26	1.28	0.32	0.02	0.03	0.19	0.22	0.02	0.28	0.03	<0.01	<0.0005	<0.01	<0.01	0.0070	<0.01
		71a-HA	0.21	1.21	0.26	0.02	0.02	0.18	0.22	0.02	0.28	<0.01	0.02	<0.0005	<0.01	<0.01	0.0090	<0.01
		71a-HB	0.21	1.33	0.24	0.01	0.02	0.16	0.19	<.01	0.18	0.02	0.04	<0.0005	<0.01	<0.01	0.0090	<0.01
TC128-B (normalized)	1994	94a-SA	0.38	1.24	0.22	0.02	0.01	0.03	0.22	0.07	<.01	0.04	0.04	<0.005	<0.01	<0.01	0.0068	<0.01
		94a-SB	0.34	1.23	0.24	0.01	0.01	0.02	0.16	0.06	<.01	0.03	0.03	<0.0005	<0.01	<0.01	0.0055	<0.01
		94a-HA	0.35	1.27	0.24	0.01	0.01	0.03	0.20	0.07	0.01	0.05	0.04	<0.0005	<0.01	<0.01	0.0076	<0.01
TC128-B (normalized)	1994	94b-SA	0.36	1.29	0.23	0.03	0.02	0.01	0.22	0.07	0.01	0.04	0.04	<0.0005	<0.01	<0.01	0.0047	<0.01
		94b-SB	0.35	1.30	0.24	0.02	0.03	0.04	0.25	0.07	0.02	0.03	0.07	0.001	<0.01	<0.01	0.0059	<0.01
		94b-HA	0.34	1.24	0.23	0.01	0.01	0.03	0.21	0.07	0.03	0.07	0.04	<0.0005	<0.01	<0.01	0.0068	<0.01
TC128-B (normalized)	1999	TP	0.41	1.41	0.21	0.01	0.01	<.01	0.01	0.05	<.01	0.03	0.06	<0.0005	<0.01	<0.01	0.0050	<0.01
A212-B	1965	65a-SA	0.18	0.84	0.27	0.01	0.02	0.04	0.04	0.02	0.03	<0.01	<0.01	<0.0005	<0.01	<0.01	0.0017	<0.01
		65a-HA	0.20	0.89	0.30	0.02	0.03	0.03	0.06	0.01	0.03	<0.01	<0.01	<0.0005	<0.01	<0.01	0.0045	<0.01
A212-B	1966	66c-SA	0.22	0.72	0.28	0.01	0.03	0.02	0.08	0.01	0.05	0.03	<0.01	<0.0005	<0.01	<0.01	0.0030	<0.01
		66c-HA	0.28	0.76	0.24	0.01	0.02	0.04	0.06	0.02	0.14	0.05	<0.01	<0.0005	0.01	<0.01	0.0045	<0.01
A515-Gr70	1970	70a-SA	0.19	0.76	0.24	0.01	0.02	0.03	0.05	0.02	0.03	<0.01	<0.01	<0.0005	<0.01	<0.01	0.0050	<0.01
		70a-HA	0.19	0.78	0.28	0.01	0.02	0.04	0.04	0.01	0.04	<0.01	<0.01	<0.0005	<0.01	<0.01	0.0022	<0.01
A515-Gr70	1972	72a-SA	0.22	0.71	0.24	0.01	0.02	0.09	0.11	0.02	0.11	<0.01	<0.01	<0.0005	<0.01	0.01	0.0055	<0.01
A285-C	1974	74a-SA	0.14	0.62	0.15	0.02	0.02	0.01	0.01	0.01	0.01	<0.01	<0.01	<0.0005	<0.01	<0.01	0.0025	<0.01
		74a-HA	0.06	0.60	0.18	0.01	0.02	0.02	0.01	0.01	0.01	<0.01	<0.01	<0.0005	<0.01	<0.01	0.0023	<0.01
A515-Gr70	1983	83a-SA	0.22	1.00	0.23	0.01	0.02	0.02	0.04	0.01	0.02	<0.01	<0.01	<0.0005	<0.01	<0.01	0.0012	<0.01
		83a-HA	0.18	1.07	0.22	0.01	0.02	0.01	0.02	0.01	0.04	<0.01	<0.01	<0.0005	<0.01	<0.01	0.0073	<0.01

Table 4-5. CVN energy properties for most of the TC128-B plate material.

Matl Type	Build Date	Matl ID No.	CVN energy (ft-lbs)						
			+50°F		0°F			-50°F	
			trial 1	trial 2	trial 1	trial 2	trial 3	trial 1	trial 2
M-128	1965	65b-SA	11	16	7	7	n/a	3	2
		65b-HA	12	10	11	10	n/a	3	3
TC128-B	1966	66a-SA	22	23	7	13	n/a	5	4
		66a-HA	40	42	26	25	n/a	6	10
TC128-B	1966	66b-SA	23	21	11	10	n/a	5	8
		66b-HA	69	64	66	69	n/a	18	18
TC128-B	1967	67b-SA	15	15	7	10	n/a	5	5
		67b-HA	23	29	12	14	n/a	10	9
TC128-B	1967	67c-SA	20	20	11	8	n/a	2	4
		67c-HA	31	38	7	26	n/a	10	3
TC128-B	1967	67d-SA	10	11	5	6	n/a	2	2
		67d-SB	22	18	10	11	n/a	3	4
		67d-HA	63	66	44	48	n/a	24	16
TC128-B	1968	68a-SA	12	16	8	7	n/a	4	4
		68a-HA	54	49	53	49	n/a	30	24
TC128-B	1968	68b-SA	25	27	24	24	n/a	13	7
		68b-SB	28	27	26	26	n/a	13	19
		68b-HA	40	43	25	24	n/a	16	13
TC128-B	1968	68c-SA	35	35	23	26	n/a	9	10
		68c-SB	11	16	8	5	n/a	4	4
		68c-HA	46	42	20	24	n/a	10	10
		68c-HB	103	65	27	34	n/a	14	10
TC128-B	1969	69a-SA	21	21	11	11	n/a	3	3
		69a-SB	23	21	10	9	n/a	3	3
		69a-HA	73	71	57	43	n/a	24	28
TC128-B	1974	74b-SA	25	25	22	25	n/a	4	7
		74b-HA	54	49	39	35	n/a	7	18
TC128-B	1975	75a-SA	12	12	10	10	n/a	5	5
		75a-HA	27	27	27	27	n/a	19	16
TC128-B	1978	78b-SA	8	7	8	4	n/a	5	4
		78b-HA	16	17	12	13	n/a	5	6
TC128-B	1979	79a-SA	12	11	7.5	9.5	n/a	4.5	4
		79a-SB	15	13	7.5	10	n/a	2	7.5
		79a-HA	106	121	36	37	n/a	19	48
TC128-B	1980	80a-SA	48	43	23	21	n/a	16.5	10
		80a-HA	105	140	101	70	n/a	42	40
TC128B	1981	81a-SA	9	10	6	6	n/a	3	2
		81a-SB	9	9	4	4	n/a	4	2
		81a-HA	56	50	33	43	n/a	17	13
TC128-B	1982	82a-SA	25	23	11.5	12	n/a	4.5	5.5
		82a-SB	18	19	9	11	n/a	4	4
		82a-HA	59	58	59	60	n/a	26	24

Table 4-6 CVN energy properties for teardown, Minot and post-1989 TC128-B material.

Matl Type	Build Date	Matl ID No.	CVN energy (ft-lbs)						
			+50°F		0°F			-50°F	
			trial 1	trial 2	trial 1	trial 2	trial 3	trial 1	trial 2
TC128-B	1976	76a-SA(F)	14	11	8	8	7.5	7.5	5.5
		76a-SB(A)	11	13	8	8.5	6.5	7	5
TC128-B	1976	76b-SA(F)	19	20	12	12	8.5	6.5	7
		76b-SB(A)	31	32	10	14	12	7	5
		76b-SC(D)	26	25	13	10	12	3.5	5
TC128-B	1976	76c-SA(F)	31	22	15	16	15	9	9.5
		76c-SB(A)	22	28	8	9	7.5	2.5	3.5
TC128-B	1976	76d-SA(F)	19	19	13	12	12	5	5.5
		76d-SB(A)	13	12.5	11	9	7.5	3	2
TC128-B	1977	77a-SA(D)	25	22	13	17	14	9.5	9.5
TC128-B	1978	78a-SA(D)	42	38	30	30	22	23	22
		78a-SB(A)	40	41	28	27	26	19	13
TC128-B	1967	67a-SA	34	27	10	8	8	8	9
		67a-SB	n/a	n/a	16.5	23	22	n/a	n/a
		67a-HA	n/a	n/a	4.5	5	5	n/a	n/a
TC128-B	1971	71a-SA	n/a	n/a	13.5	17.5	16	n/a	n/a
		71a-SB	n/a	n/a	3.5	4.5	3.5	n/a	n/a
		71a-HA	n/a	n/a	49	50	51	n/a	n/a
		71a-HB	n/a	n/a	42	44	43	n/a	n/a
TC128-B (normalized)	1994	94a-SA	38	41	32	25	n/a	11	16
		94a-SB	117	71	85	75	n/a	39	25
		94a-HA	116	152	92	94	n/a	54	62
TC128-B (normalized)	1994	94b-SA	37	37	20	22	n/a	14.5	5
		94b-SB	32	28	17	21	n/a	8.5	8.5
		94b-HA	138	120	91	93	n/a	42	31
TC128-B (normalized)	1999	TP	n/a	n/a	34	42	40	n/a	n/a
A212-B	1965	65a-SA	20	17	4	4	n/a	2	2
		65a-HA	6	6	3	3	n/a	2	2
A212-B	1966	66c-SA	23	23	10	8	n/a	4	5
		66c-HA	46	45	41	33	n/a	16	19
A515-Gr70	1970	70a-SA	16	15	4	4	n/a	2	2
		70a-HA	8	8	4	3	n/a	2	2
A515-Gr70	1972	72a-SA	19	17.5	3	4	n/a	1	1
A285-C	1974	74a-SA	14	16	5	4	n/a	2	2
		74a-HA	10	9	3	4	n/a	2	2
A515-Gr70	1983	83a-SA	20	20	10	8	n/a	2	3
		83a-HA	44	45.3	34.7	6.7	n/a	2.7	8

Table 4-7. Statistical analysis (averages and standard deviations) of TC128-B material characterization testing.

Subset A: 1969 and before build date, 25% of the pre-1989 pressure car fleet
Subset B: 1970 to 1976 build date, 25-52% (27% total) of the pre-1989 pressure car fleet
Subset C: 1977 to 1979 build date, 52-72% (20% total) of the pre-1989 pressure car fleet
Subset D: 1980 and later build date, 28% of the pre-1989 pressure car fleet

Data Set	Tank Posn	# Cars (conds)	UTS, ksi			YS, ksi			Elong, percent			RA, percent			CVN at +50°F			CVN at 0°F			CVN at -50°F		
			N	avg	2SD	N	avg	2SD	N	avg	2SD	N	avg	2SD	N	avg	2SD	N	avg	2SD	N	avg	2SD
all	H&S	25 (61)	122	88.8	13.45	122	61.1	13.33	122	26.3	7.15	122	54.3	14.78	110	31.9	49.07	141	19.9	33.60	110	9.8	17.58
	S-only	25 (40)	80	89.3	14.72	80	60.5	15.31	80	24.8	5.90	80	50.2	9.81	74	21.0	18.77	96	12.5	13.55	74	6.3	9.18
	H-only	19 (21)	42	87.7	10.45	42	62.3	8.01	42	29.2	5.52	42	62.1	8.69	36	54.4	60.69	45	35.5	41.43	36	16.9	21.83
A	H&S	11 (28)	56	87.6	12.56	56	60.0	10.87	56	26.6	6.93	56	55.1	14.56	52	32.7	40.94	59	19.6	31.84	52	9.2	14.52
	S-only	11(16)	32	87.6	13.75	32	58.9	13.49	32	24.9	5.95	32	50.0	9.66	30	20.9	13.93	34	12.6	13.93	30	5.7	7.94
	H-only	11 (12)	24	87.6	11.06	24	61.6	4.50	24	28.9	5.37	24	62.0	5.69	22	48.8	43.82	25	29.1	39.06	22	14.0	15.98
B	H&S	7 (17)	34	90.0	13.37	34	60.8	15.39	34	26.0	7.39	34	52.8	12.07	26	23.1	21.56	47	17.4	26.92	26	6.9	8.76
	S-only	7 (13)	26	90.9	13.58	26	59.9	16.34	26	24.6	6.00	26	50.3	6.67	22	20.1	14.16	37	11.1	9.08	22	5.5	3.94
	H-only	3 (4)	8	87.0	11.37	8	63.5	10.89	8	30.3	3.96	8	60.9	11.68	4	39.3	28.58	10	40.7	17.51	4	15.0	10.95
C	H&S	4 (8)	16	89.7	11.98	16	62.9	12.40	16	25.3	5.78	16	53.4	13.14	16	33.4	67.27	19	18.5	21.00	16	12.6	23.45
	S-only	4 (6)	12	89.4	13.88	12	62.5	14.01	12	24.8	5.49	12	51.6	11.96	12	22.8	27.72	15	16.9	18.71	12	10.3	14.77
	H-only	2 (2)	4	90.8	1.87	4	64.2	6.23	4	26.8	6.45	4	58.7	11.73	4	65.0	112.68	4	24.5	27.74	4	19.5	40.08
D	H&S	3 (8)	16	89.4	17.43	16	63.8	16.16	16	26.9	8.63	16	55.3	21.27	16	42.6	73.86	16	29.6	58.10	16	13.6	26.36
	S-only	3 (5)	10	90.7	20.55	10	64.8	17.48	10	24.7	6.80	10	48.8	14.28	10	21.3	28.27	10	10.8	13.28	10	5.6	8.94
	H-only	3 (3)	6	87.2	10.72	6	62.2	14.60	6	30.7	5.61	6	66.3	8.12	6	78.0	72.67	6	61.0	47.28	6	27.0	23.66
normalized		3 (7)	13	81.7	5.71	13	55.4	5.14	13	31.2	7.47	13	62.0	16.62	12	77.3	94.95	15	52.2	63.22	12	26.4	38.33

Cars = Number of unique tank cars, conds = unique material conditions, H = head, S = shell, avg = average, 2σ = 2 std. deviations

Table 4-8. Tensile property and chemical specifications for TC128-B [4].

Property	Allowable
Transverse Ultimate Tensile Strength (ksi):	81 – 101
Transverse Yield Strength (ksi):	>50
Transverse Elongation (%):	>22

Elemental Constituent	Weight Percent Allowed*
carbon	< 0.29
chromium	< 0.25
copper	< 0.35
manganese	0.92 – 1.62 (thick)
molybdenum	< 0.08
nickel	< 0.25
phosphorous	< 0.035
silicon	0.13 – 0.55 (thick)
sulfur	< 0.04
vanadium	< 0.08
iron	remainder

* M1002 (1992) specification for the product (ladle) analysis

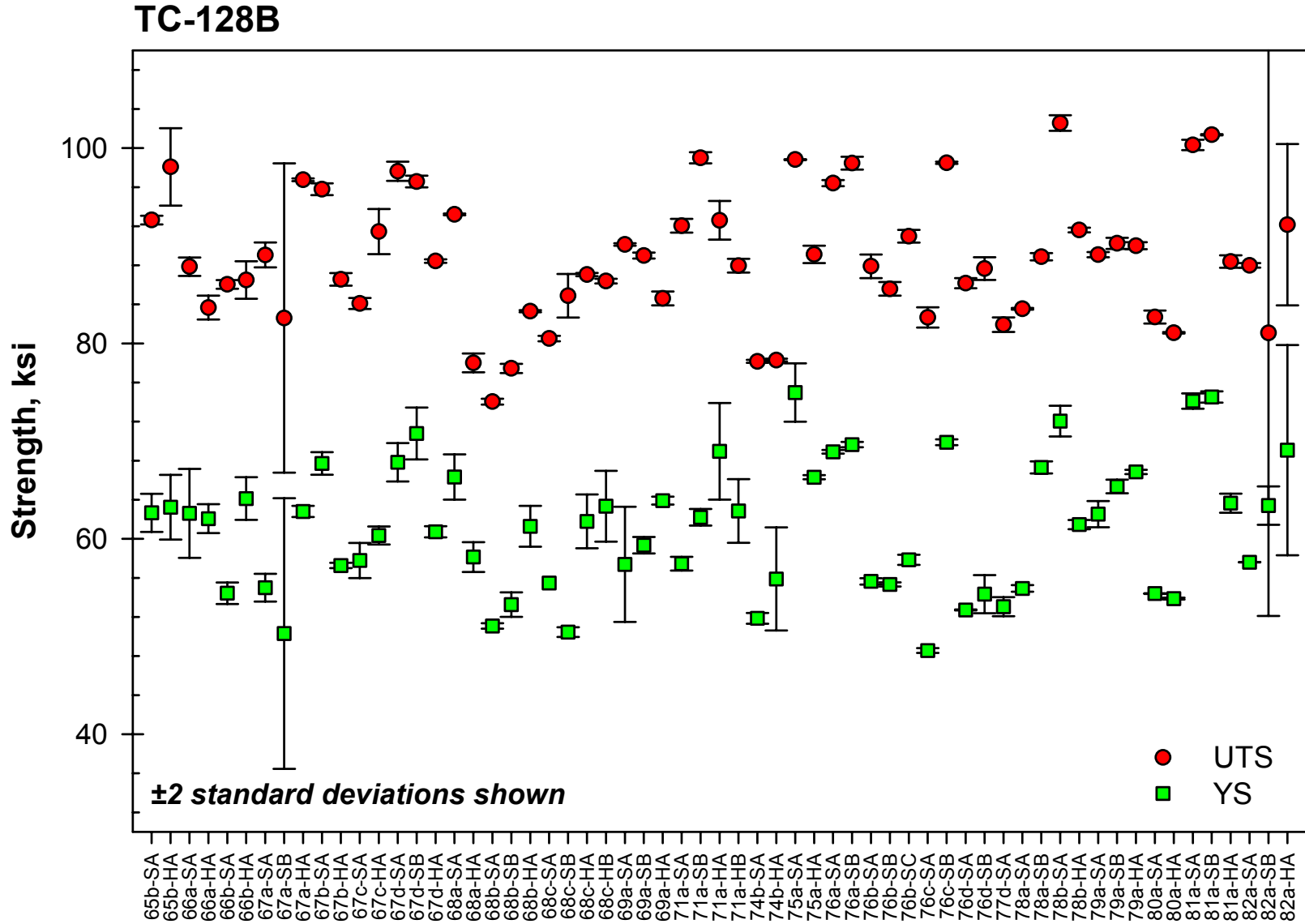


Figure 4-1. Room temperature tensile yield and ultimate strength for different vintage TC128-B conditions.

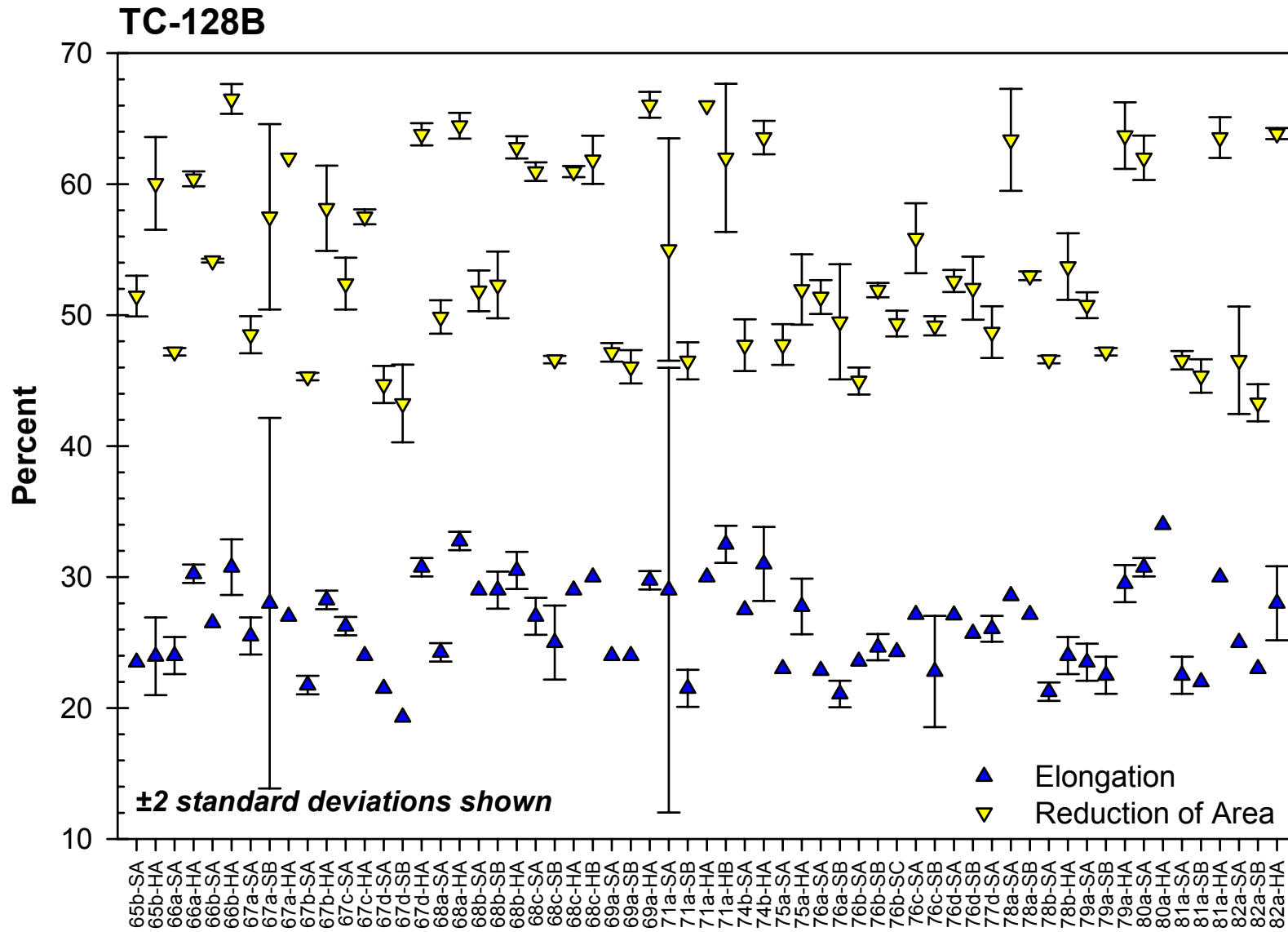


Figure 4-2. Room temperature tensile elongation and reduction of area for different vintage TC128-B conditions.

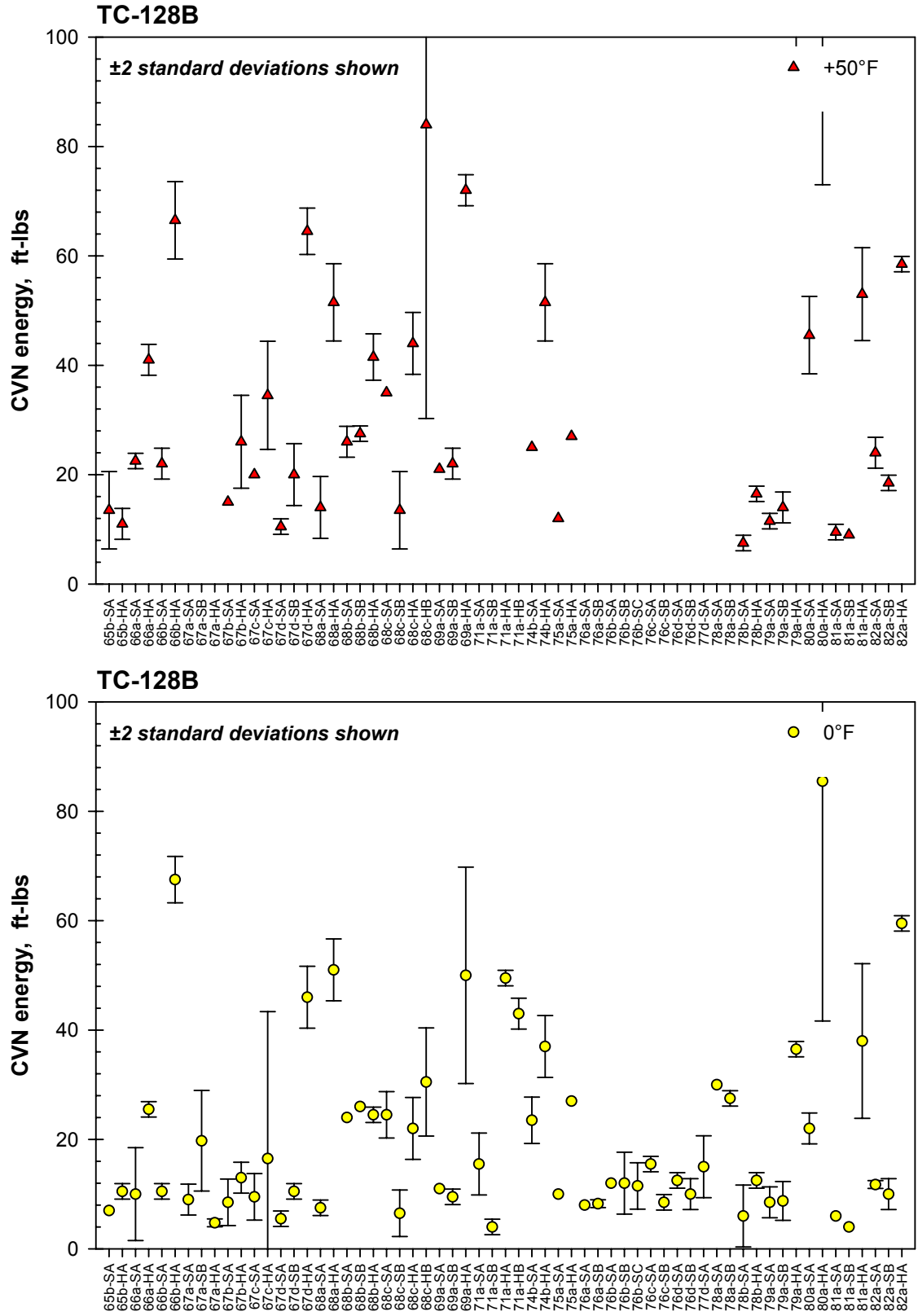


Figure 4-3. CVN toughness at -50° and 0° F for different vintage TC128-B conditions.

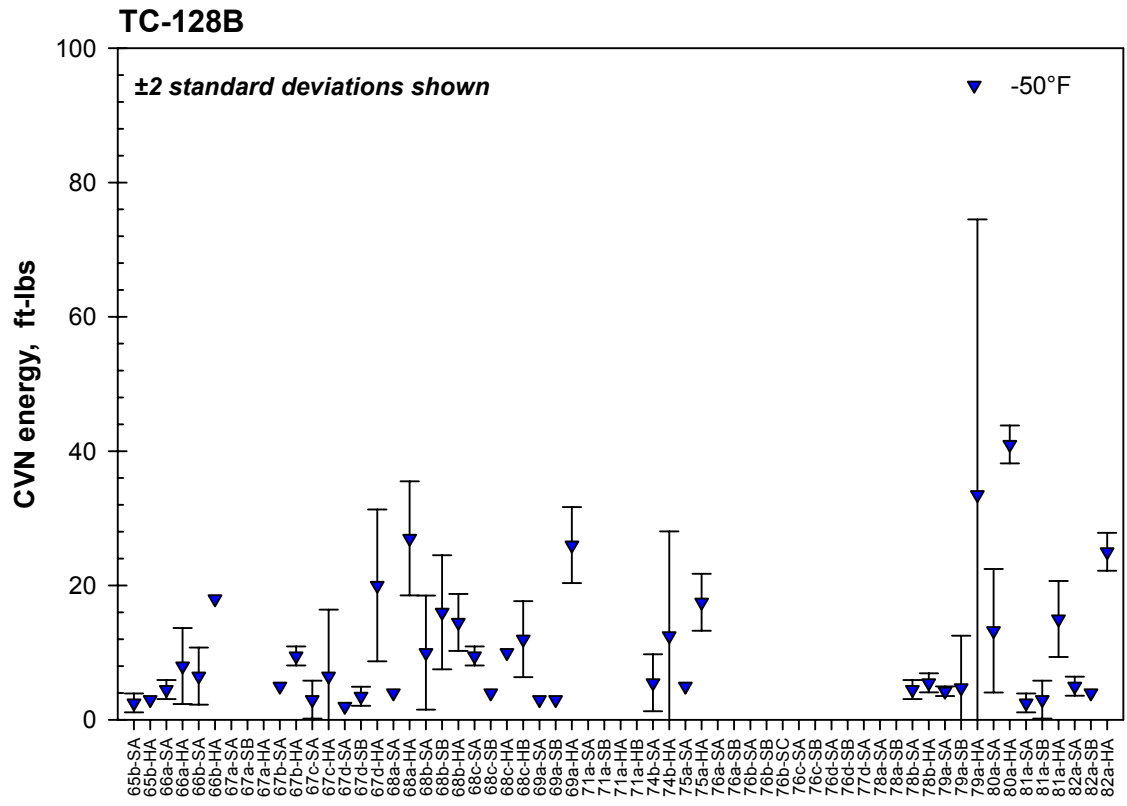


Figure 4-4. CVN toughness at 50°F for different vintage TC128-B conditions.

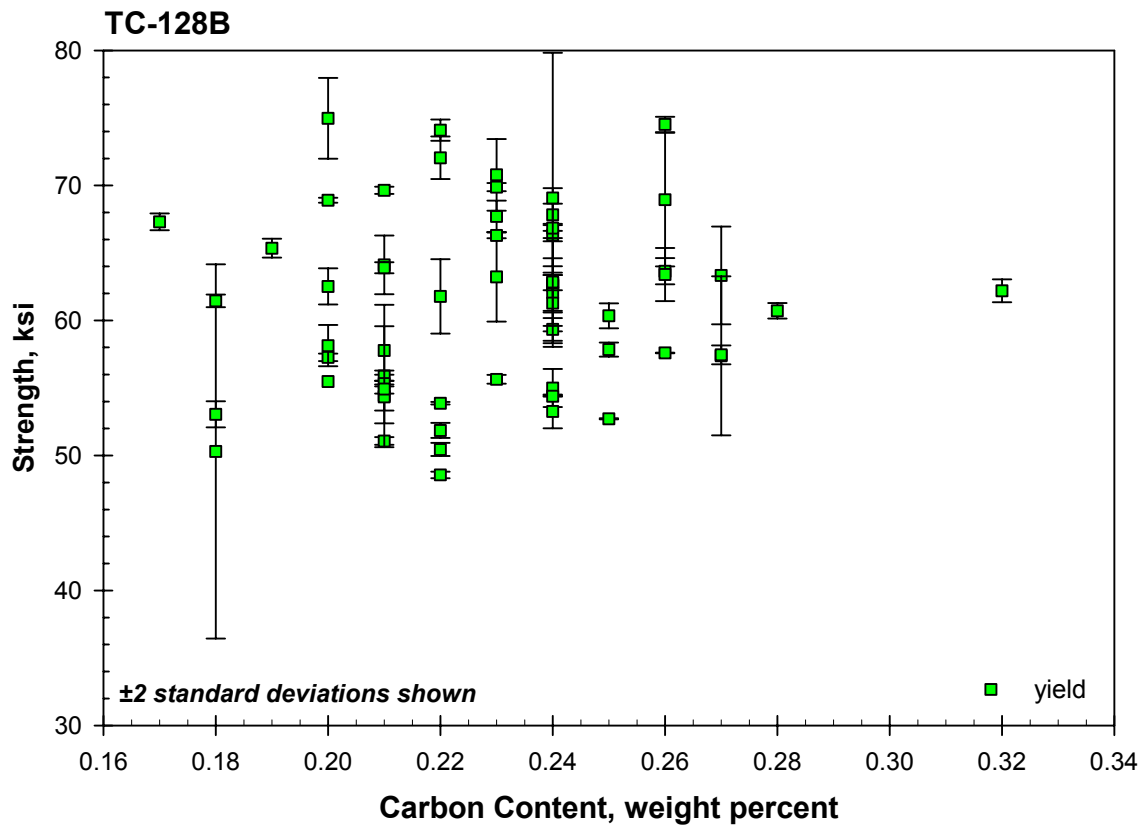
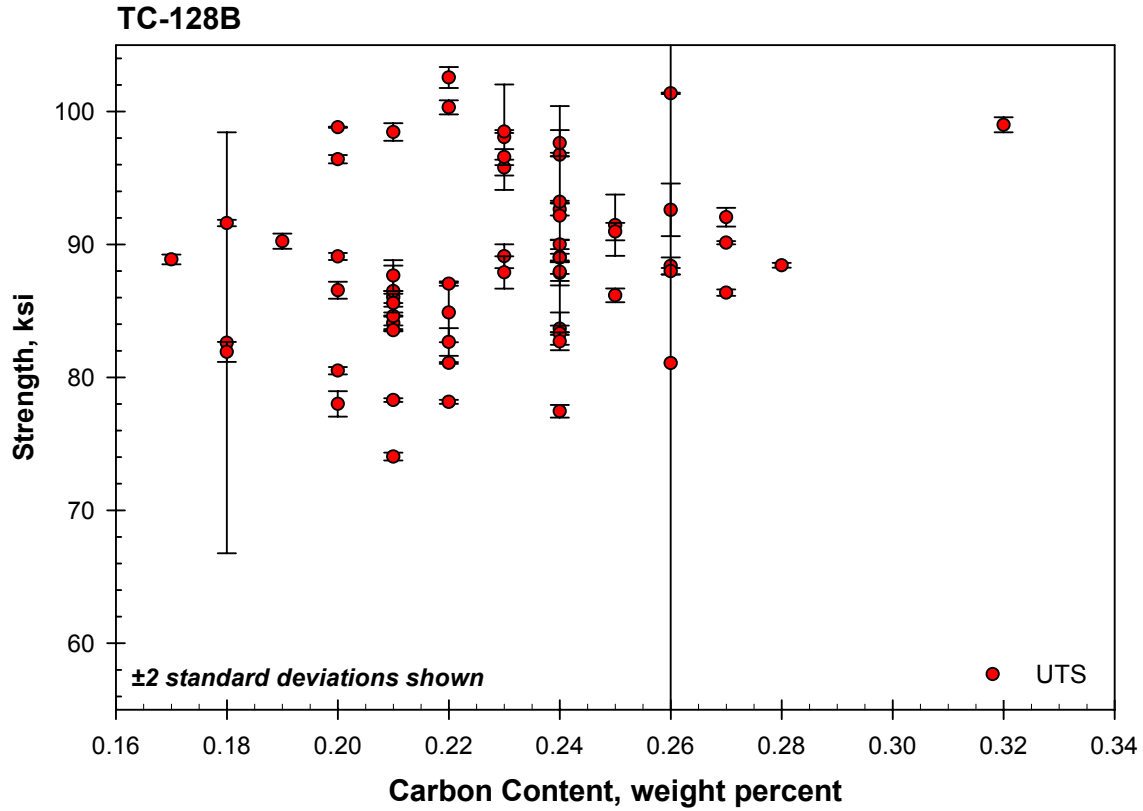


Figure 4-5. Influence of carbon content on room temperature strength for vintage TC128-B.

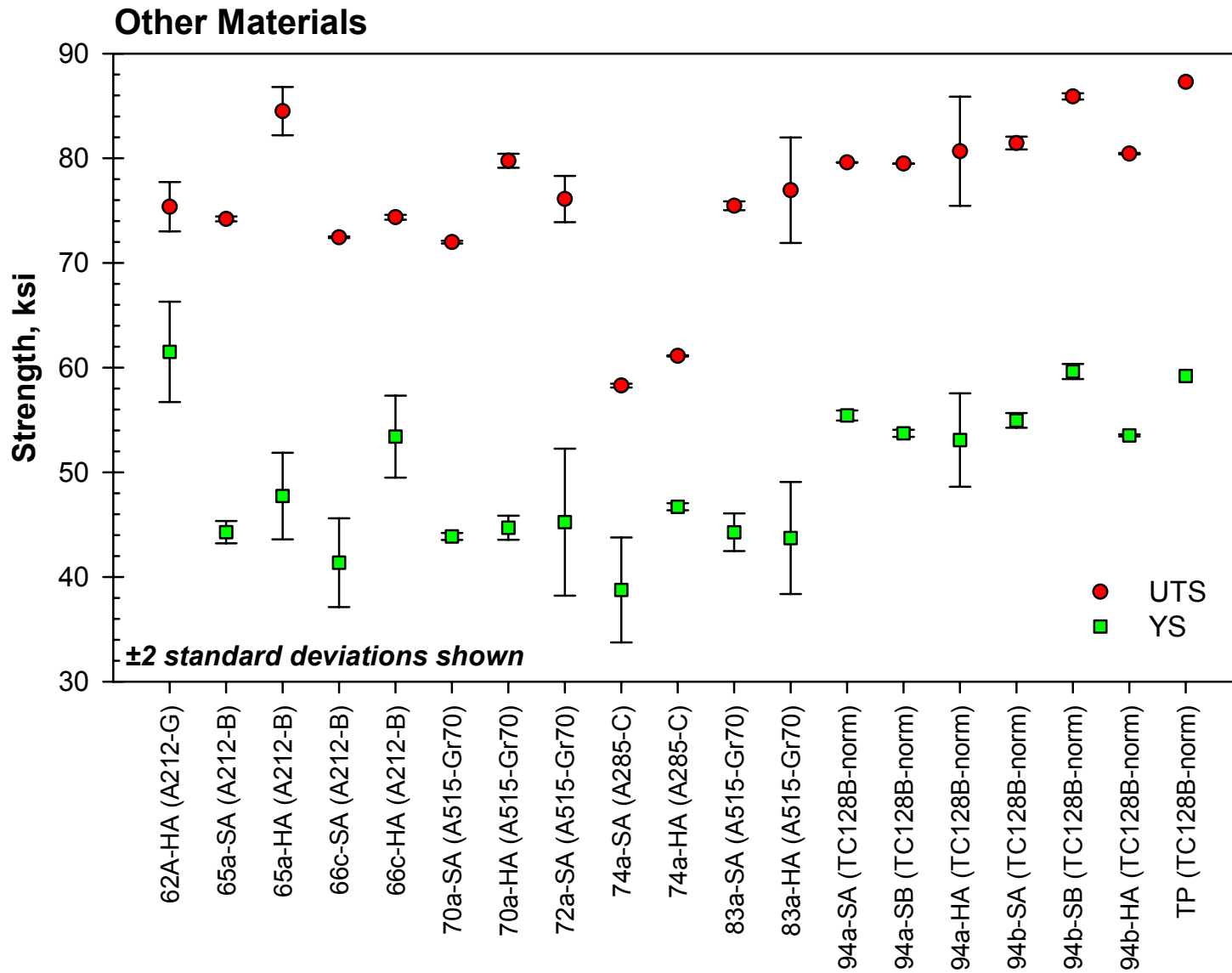


Figure 4-6. Room temperature tensile and yield strength for different normalized TC128-B and other material types.

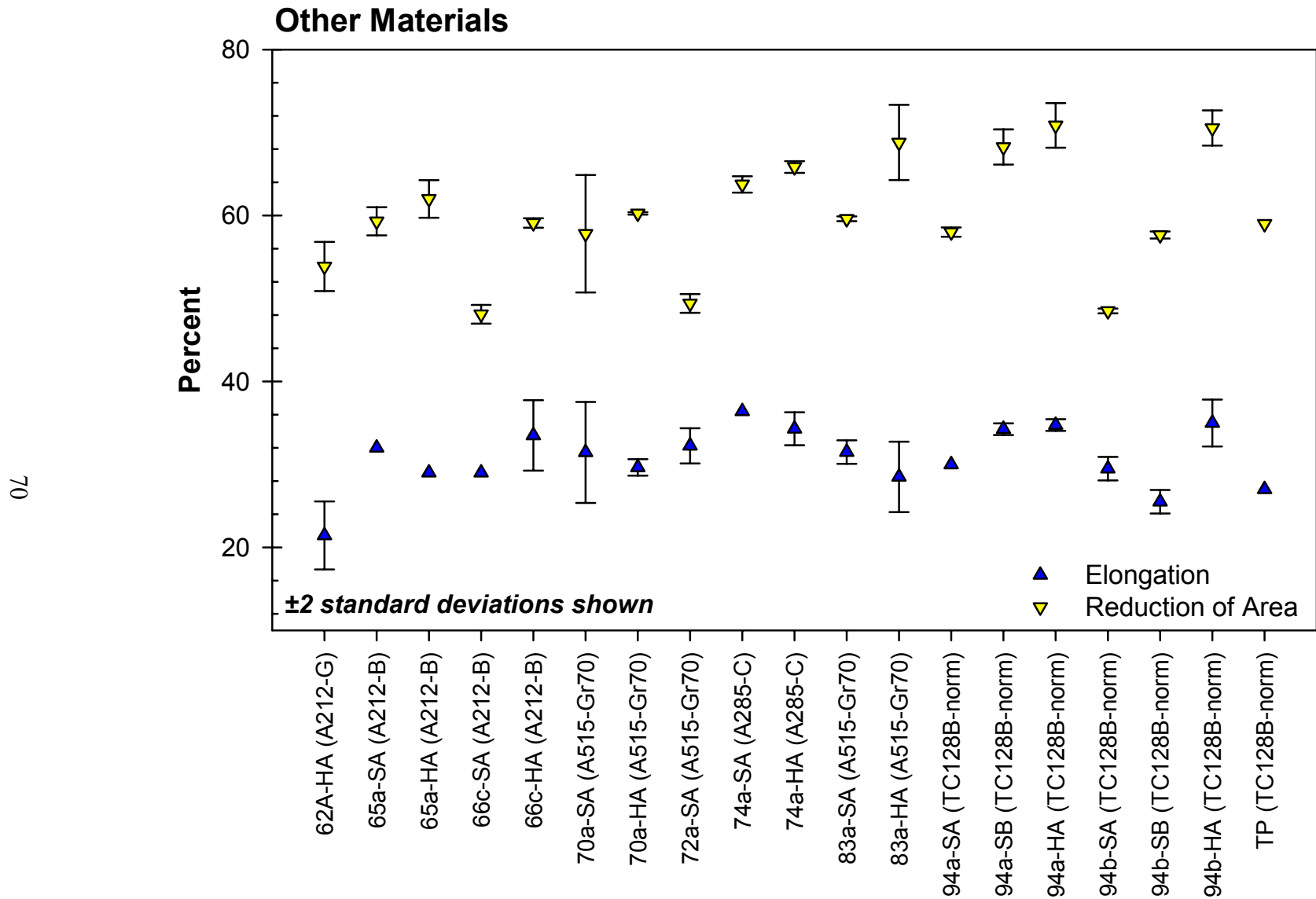


Figure 4-7. Room temperature tensile elongation and reduction of area for normalized TC128-B and other material types.

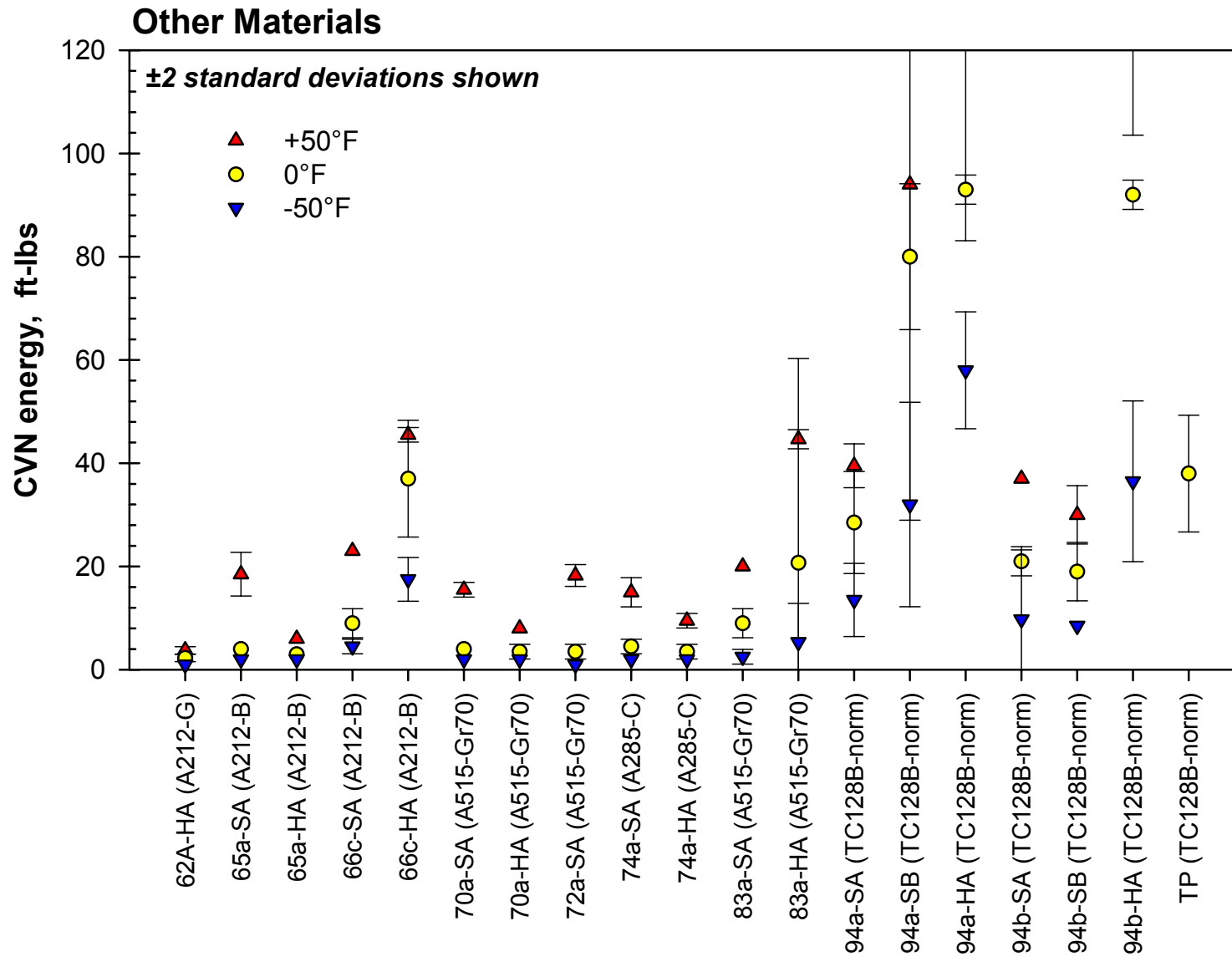


Figure 4-8. CVN toughness at -50°F, 0°F and 50°F for different materials and post-1989 TC128-B conditions.

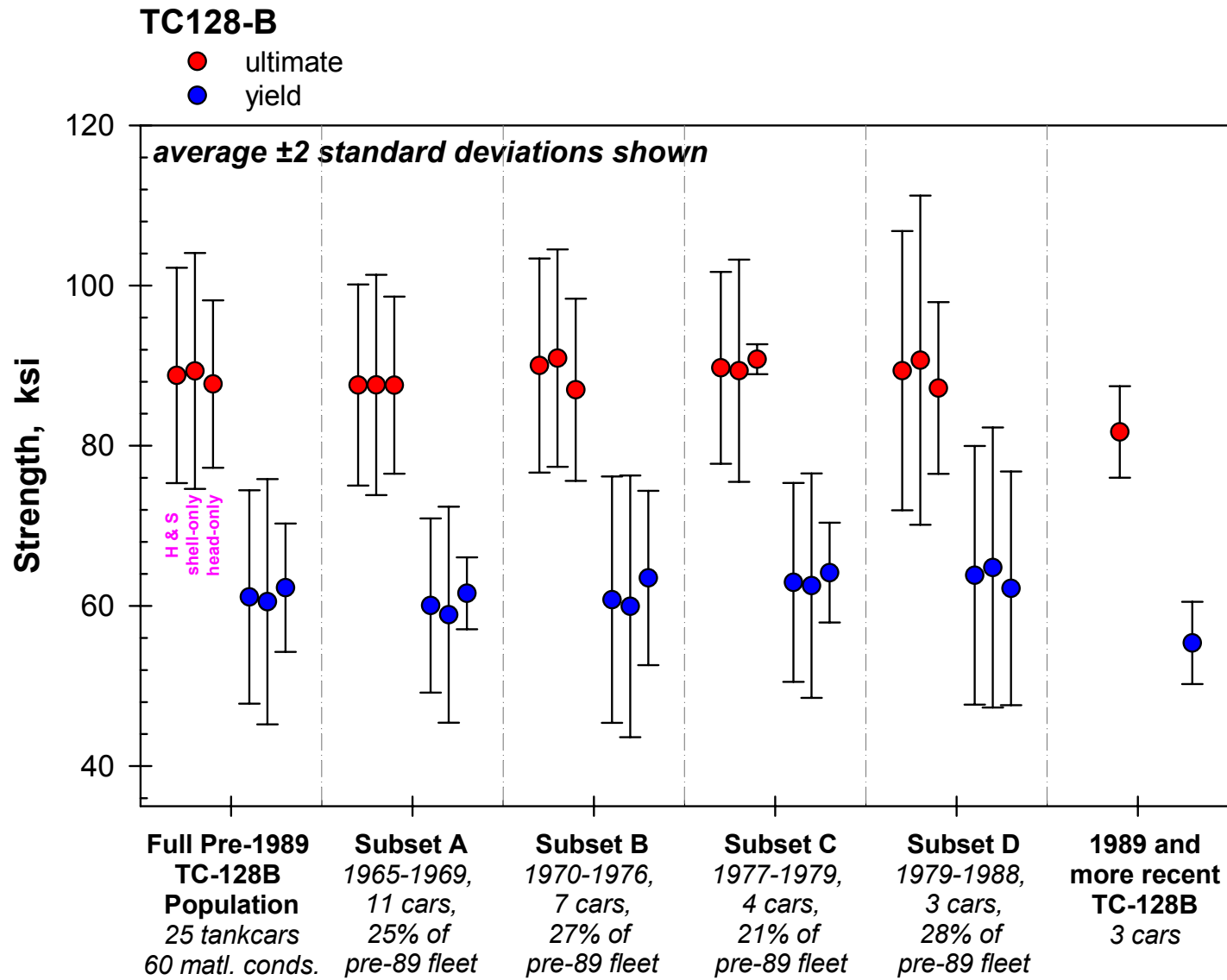


Figure 4-9. Strength properties of vintage TC128-B as a function of when manufactured.

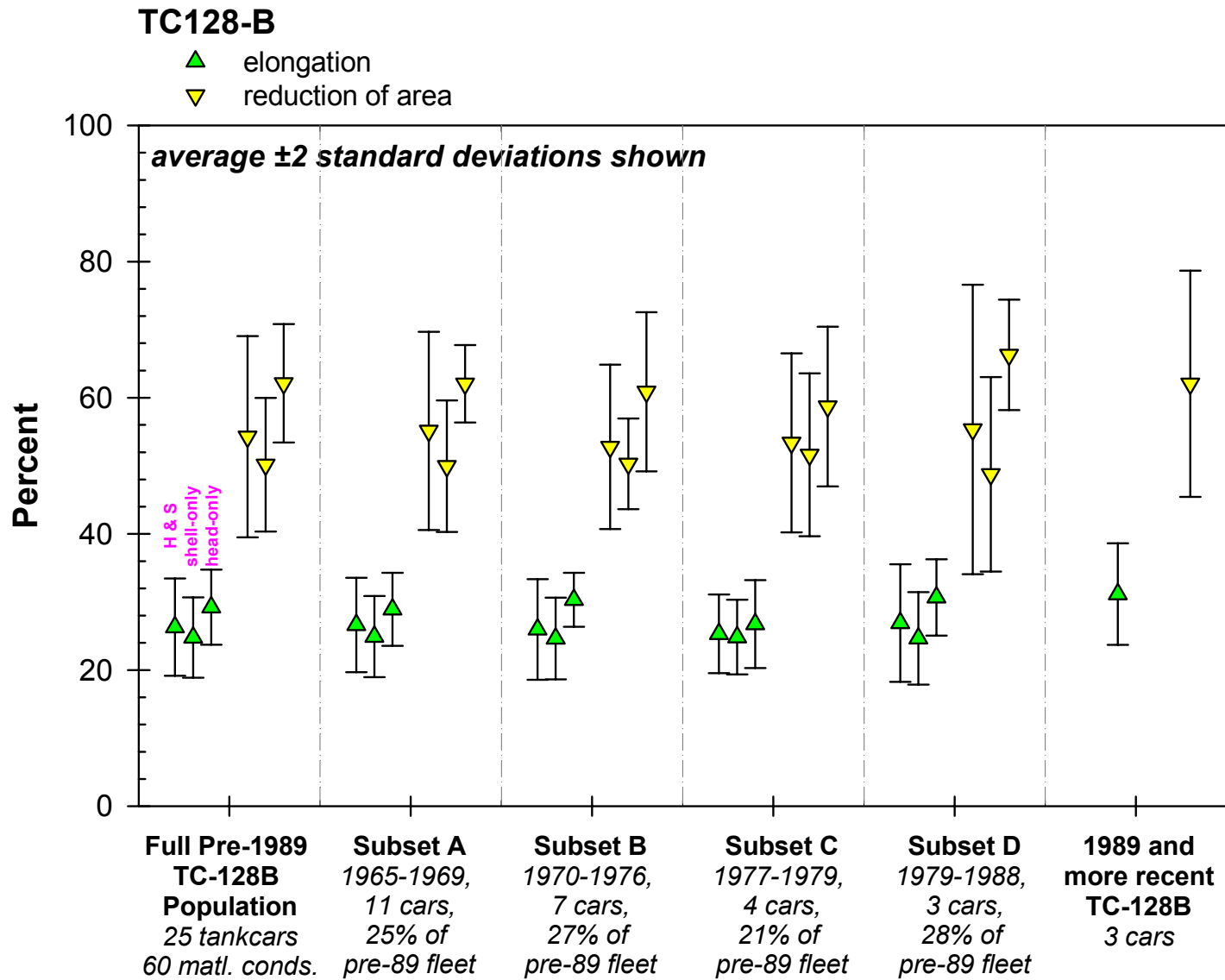


Figure 4-10. Ductility properties of vintage TC128-B as a function of when manufactured.

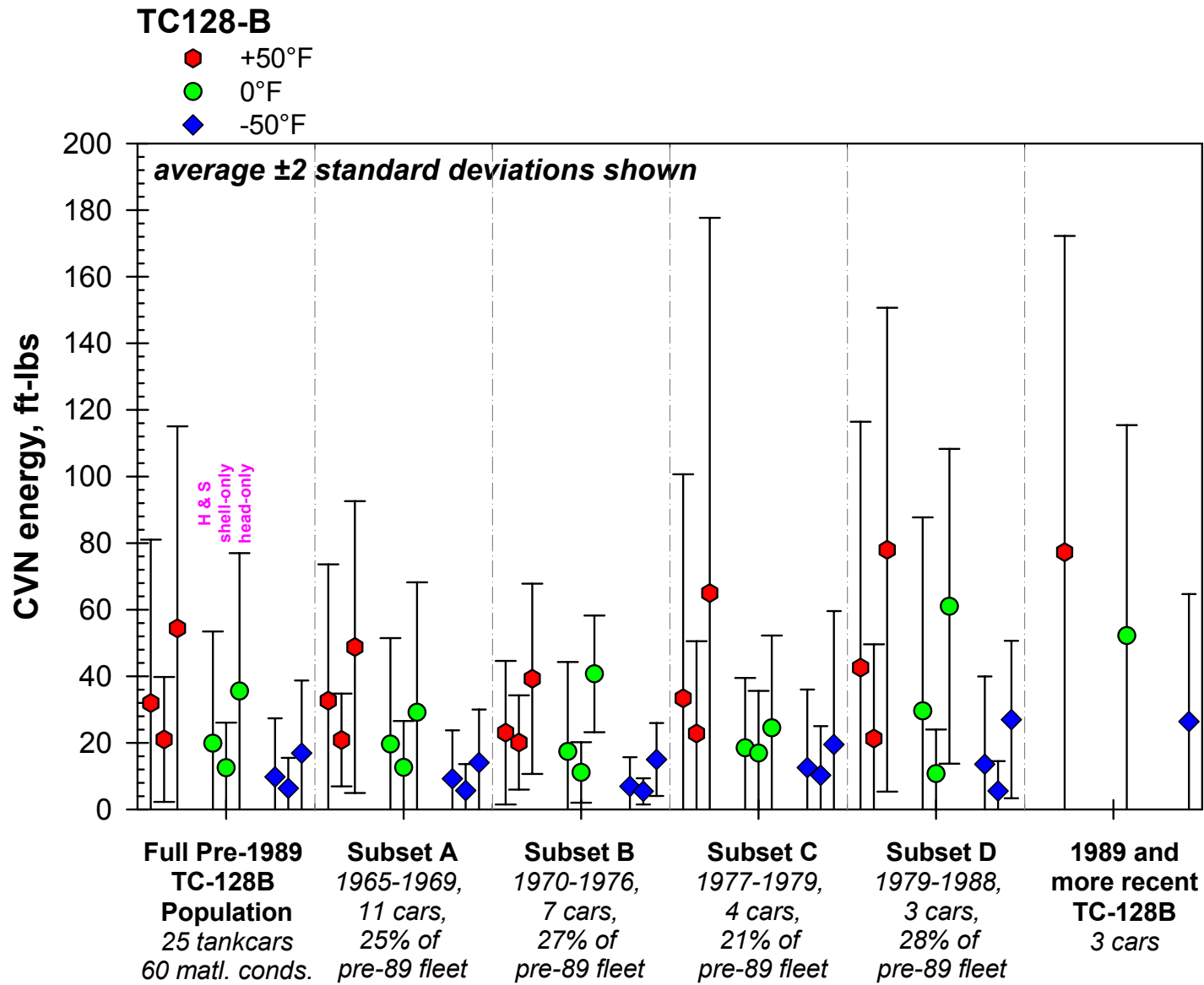


Figure 4-11. CVN toughness properties of vintage TC128-B as a function of when manufactured.

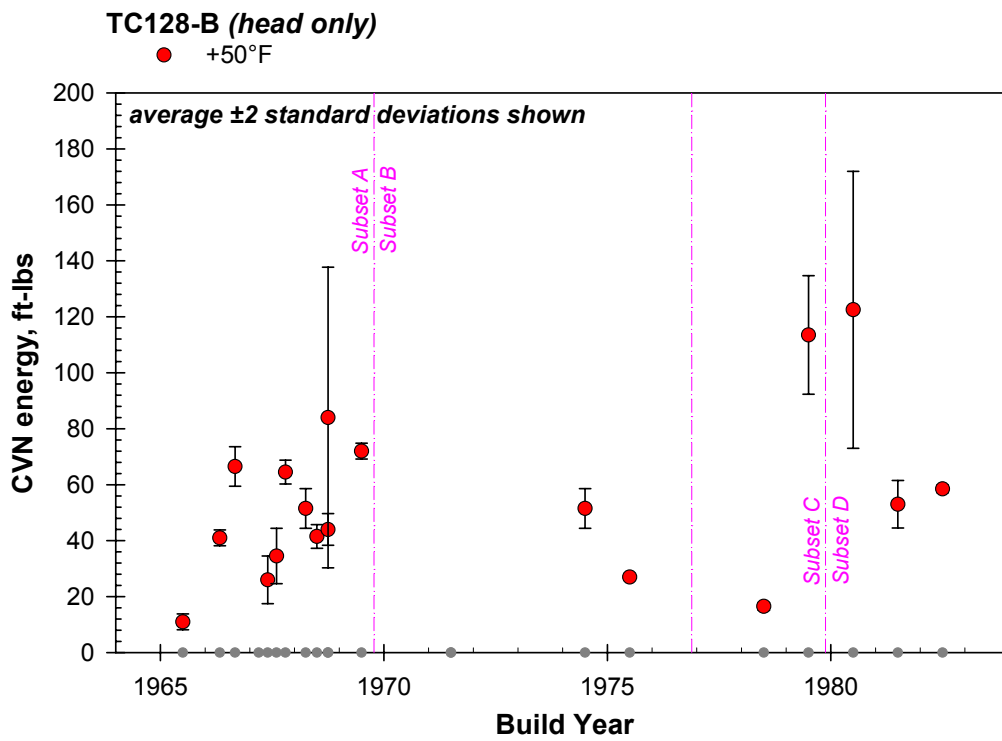
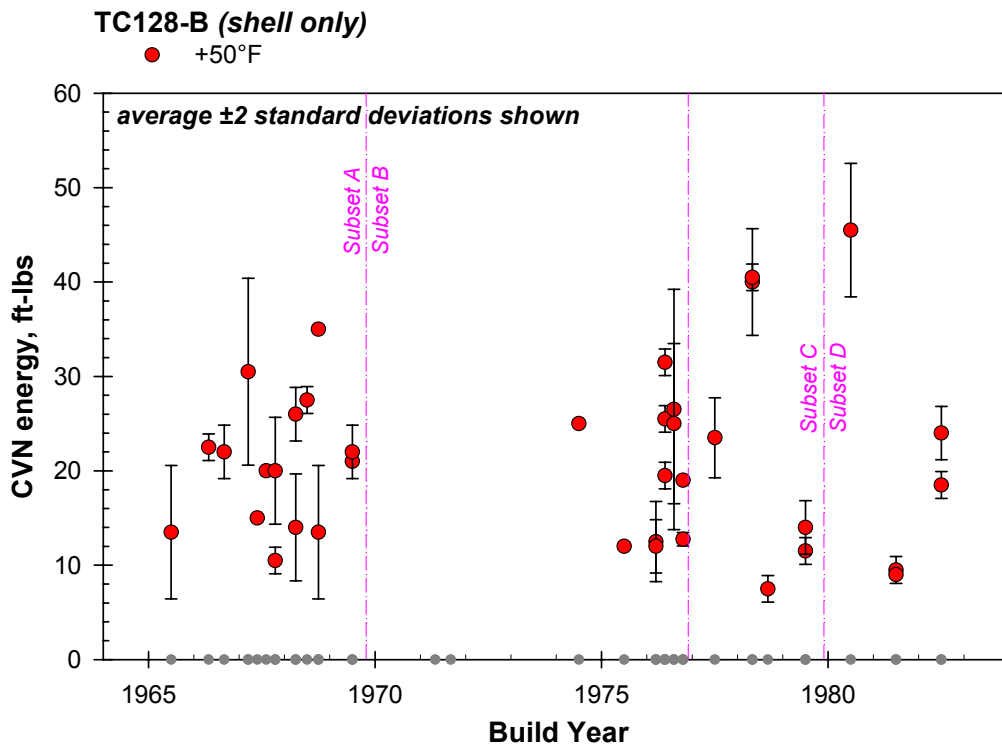


Figure 4-12. CVN toughness at 50°F of vintage TC128-B as a function of when manufactured.

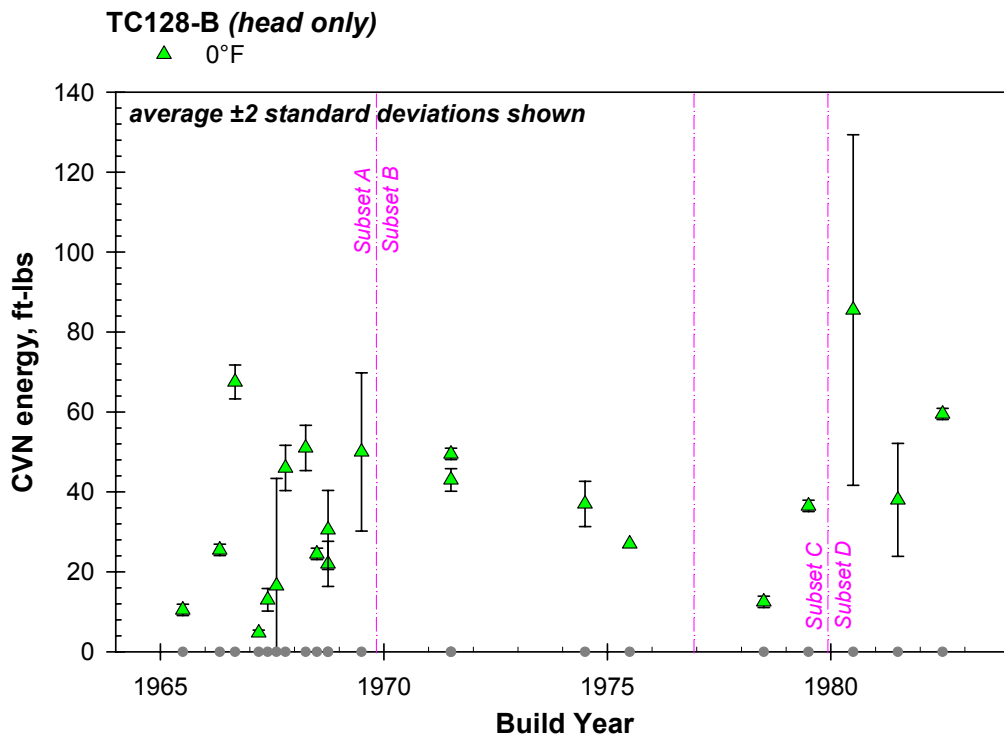
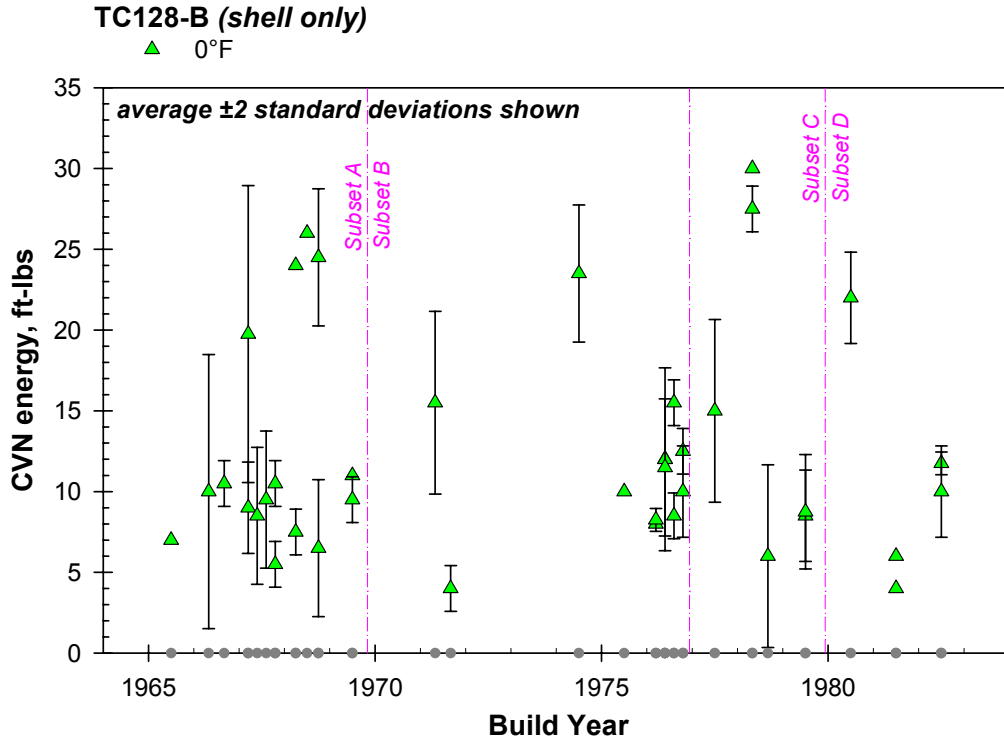


Figure 4-13. CVN toughness at 0°F of vintage TC128-B as a function of when manufactured.

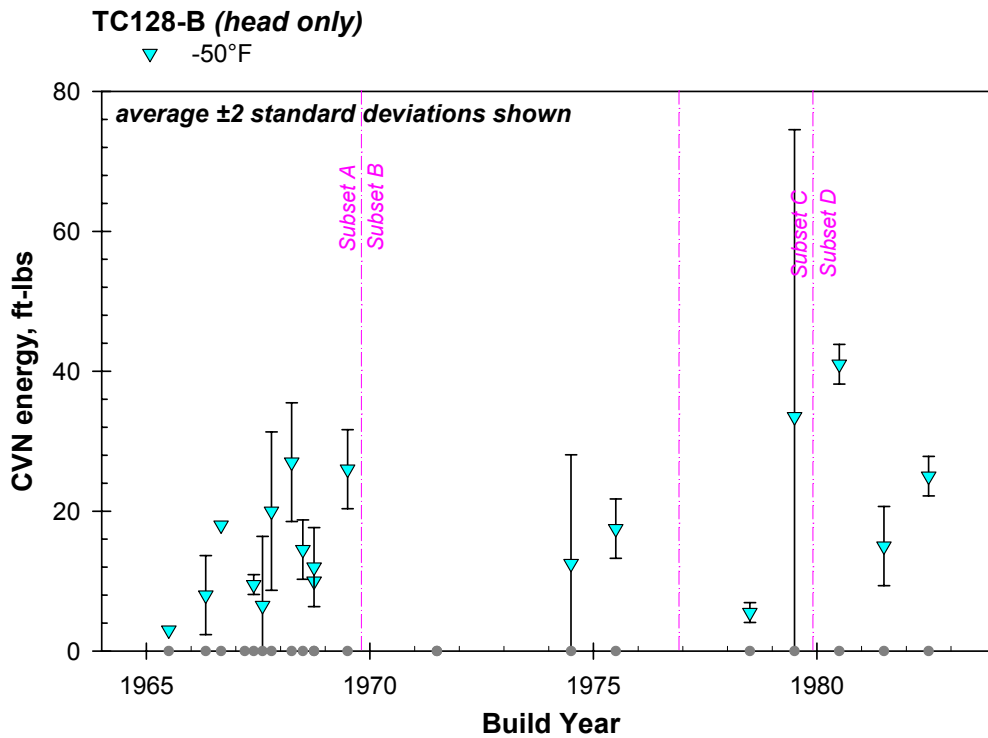
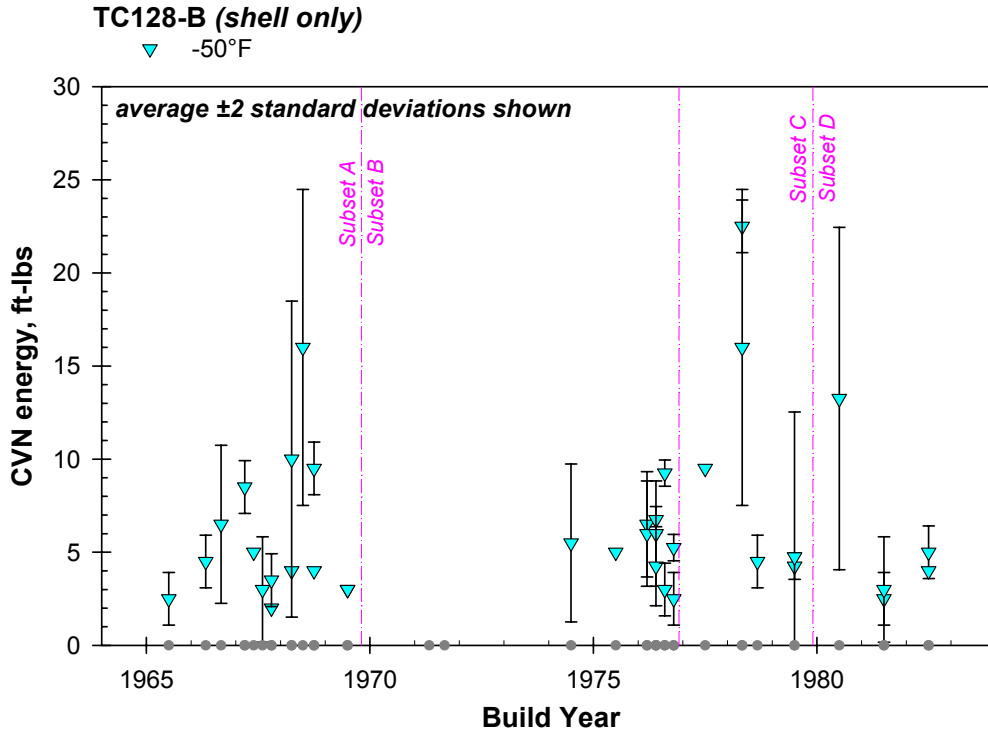


Figure 4-14. CVN toughness at -50°F of vintage TC128-B as a function of when manufactured.

This page intentionally left blank.

5.0 PENDULUM IMPACT TESTING OF BULK FRACTURE BEHAVIOR

The previous chapters of this report have described the pedigree and mechanical properties of the steel material removed from retired tank cars. The properties described that are used to characterize the steel are all determined using ASTM standard test methods. What is described in this portion of the report is a highly nonstandard pendulum impact test that was developed to quantify the puncture behavior of the steel. Since this test is nonstandard, considerable attention is paid to the rationale for the test method, fully describing the experimental techniques and understanding the structural nature of the test.

5.1 Background

The past thirty years of steels research for the tank car industry has focused on brittle fracture resistance and low temperature CVN toughness. Anderson and Kirkpatrick [10] contend that tank car fracture occurs first with ductile puncture and then with a crack that grows from a puncture. Anecdotal evidence from the Minot accident suggests that this is true. In examining the catastrophic fracture surfaces, nearly all included a tank shell dent and puncture. In fact, the NTSB clearly indicated in the Minot investigation [2] that cracks did not initiate at stress concentrations or welds; rather, crack nucleation occurred in parent metal plate away from any discontinuities or design elements. Anderson and Kirkpatrick argue in reference [10] that the focus should be on increasing upper shelf toughness, since this in part will increase the brittle, lower shelf toughness behavior as well.

It is believed that this argument has merit and the underlying material characteristic that is critical in most accident and derailment situations is puncture resistance. Improved steel properties can increase puncture resistance, but the absence of engineering models for predicting puncture resistance makes achieving increased puncture resistance difficult. Without practical models, the underlying material properties that need to be optimized for puncture resistance are not known. In fact, problems in modeling are not the only issue since there are no readily acceptable ASTM or industry tests currently available for measuring puncture behavior.

Given this, the goal of the pendulum test work was to develop a “poor man’s” puncture test suitable for screening material conditions and assessing puncture behavior. The test must be relatively simple, inexpensive and rapid to perform. The key to the test technique, however, is analytical modeling provided by Anderson in the follow-on program to that in reference [10]. In fact, the work described here was funded not only by Volpe through this project but also by the Chlorine Institute in support of Anderson’s ongoing puncture program.

5.2 Pendulum Test Method Details

The test concept utilized is that of a high energy pendulum impact on an oversize Charpy specimen that does not have a notch in it. However, without a notch, a CVN specimen would simply be folded around the impact tup and the specimen would then slip through the two outer bend supports as it folded. The method utilized here is performed on what is termed the Bulk Fracture Charpy Machine (BFCM) where the ends of the specimen are held fixed as the impact load is applied via a pendulum. Furthermore, in establishing the goals of the test method there also was a desire to (a) maximize the width of the specimen and (b) test at full thickness. A drawing of the 1-inch wide by full thickness (in the case of the calibration specimens, 0.77-inch) specimen is shown in Figure 5-1. Initially it was believed that maximum energy would be not greater than 5,000 to 10,000 ft-lbs to fail the specimen when impacted.

The optimum impact tup geometry was not known prior to testing. Therefore, three different tup geometries were designed and fabricated. One flat impact tup geometry, based loosely on a CVN tup, was developed as shown in Figure 5-2. Intermediate and sharp (0.125-inch wide face) tups were also fabricated from hardened (HRC 45) 4130 steel. The drawings for these tups are shown in Figure 5-3 and 5-4. Testing was initiated using the sharpest tup since it was expected that this tup size would require the minimum amount of energy to fail the specimen. Test specimens were fabricated from vintage tank car material as described in Table 5-1. Not all conditions examined with C(T) specimens in the fracture toughness testing were examined on the BFCM. As shown in the last column in Table 5-1, a subset of the total samples were examined in the pendulum impact tester. In addition to the vintage samples, specimens suitable for the BFCM were fabricated from plate left over from a previous Volpe

program [11] that examined the fatigue crack growth properties of normalized, TC128-B tank head material. Specimens were extracted from tank head plate material as shown in Figure 5-6. These plate material samples were used for BFCM calibration purposes in a series of experiments that will be described below. Two different plates from the previous Volpe program were utilized. The measured tensile and CVN toughness of the two plates are described more fully in Table 5-2.

The BFCM frame and fixtures are shown in Figure 5-5. The machine was adapted from a 25-year-old machine at SwRI that was no longer being used. Many of the basic machine components were refurbished, including the truck brake mounted on the axle and designed to stop the motion of the pendulum when desired. One of the key questions before testing began was the condition of the bearings. To test this, the arm was cocked 120° and released. Using the angle measure plate, the rebound angle was measured and for a minimum of 20 swings, it had not degraded by a measurable amount (the angle measure plate is calibrated in 1° increments, implying measurement precision on the order of 0.25-0.50°). When the frame was refurbished, the arm weight was 677-lbs and the total maximum stored energy was 4900 ft-lbs. This was not believed to be high enough, so 464-lbs was added to the arm to result in a total stored energy of approximately 8200 ft-lbs.

A test is performed in the BFCM by first cocking the arm. The nominal angle for the cocked arm was 120° as shown in the photograph in the upper right-hand side of Figure 5-5. The pendulum hammer is then dropped and the BFCM specimen is impacted. From a 120° angle, the impact speed is approximately 15 mph. During the impact, the hammer loses some energy and the rebound angle (after passing through the specimen) is less than the beginning angle. A pointer on the angle measurement disk records maximum angle observed during the test and a calculation is then made to determine energy dissipated during fracture. This is the only data nominally recorded during impact failure of a BFCM specimen.

Unfortunately, the first pendulum impact (with the blunt impactor) stalled the arm without failing the specimen. Adding the mass to the arm resulted in an overload of the arm and severe bending as shown in Figure 5-7. Therefore, a new, much more structurally resilient arm was

designed and fabricated. In addition, 1240-lbs of steel was also added to the arm, bringing the total pendulum arm weight up to nearly 2400-lbs and almost 16,000 ft-lbs of stored energy at 120° of cocked arc.

Prior to testing an impact specimen with either the new or the old pendulum arm configuration, a calibration was performed to measure the weight and center-of-gravity position for the arm. In this calibration, a load cell was attached to the pendulum and the pendulum was lifted, stopping periodically to measure load. Knowing the kinematics of the measurement positions and the geometry allowed calculating the product $W \cdot R$, where W is the weight (measured with a load cell by hanging the arm vertically prior to installation) and R is the radial position of the center-of-gravity (CG). The results from these calibrations are shown in Figure 5-8. In theory, the product $W \cdot R$ should be constant and a close examination of Figure 5-8 suggests that the product is indeed fairly constant. The uncertainty in the position of the CG is only on the order of ± 0.5 -inch ($\pm 1\%$ of the total length), which is virtually unmeasurable. Furthermore, it is interesting to note that the Generation 1 arm (pre-bending) CG is 57.2-inch whereas the re-designed arm had a CG measurement of 52.45-inch (due presumably to the large footprint for the mass added to the arm).

Prior to testing the BFCM, there was concern regarding the durability of the impact tup. Although the tup was fairly hard (45 HRC), its durability was suspect due to the enormous energy transmitted through a relatively small area. The thought of having a disposable tup for every test was considered as the worst-case scenario. As it turned out, tup durability was not too bad as the photographs of the worn tups shown in Figure 5-9 indicate. On balance, the observed wear was excellent and the replacement schedule of every 20 impacts was established and adhered to during testing.

High-speed data acquisition was utilized on a BFCM specimen with a strain gage mounted opposite the sharpest tup. The resulting strain data from this test is shown in Figure 5-10. Note that strain data past the peak strain is suspect due to the likely debonding of the strain gage. It is also unlikely that the peak measured strain corresponds to the peak strain for the same reasons. Nevertheless, the primary use of the strain gage is the information that it gives regarding loading

rate. The loading rate in the BFCM specimen is on the order of 60 inch/inch/second with the impact velocity of approximately 15 mph. This information is useful from the viewpoint of quantifying overall behavior and relating experimental to analytical results.

Photographs of fracture surfaces as well as a deformed BFCM specimen are indicated in Figures 5-11 and 5-12. The fracture surfaces in Figure 5-11 clearly indicate a region where the striker tip smears the material followed by a region where the material pulls apart. The region where the material pulls apart appears similar to the fracture surfaces created during the high rate fracture testing. The deformation observed in the BFCM specimens was significant, as shown in Figure 5-12. Note that this specimen was one that was struck with the broadest (flattest) impact tip. Initial calculations suggested that the elongation in the specimen along its primary axis was on the order of 15-20%.

Testing was performed with the BFCM on a number of mini-projects investigating different aspects of the machine, the resulting energy measurements and different tank car materials. These mini-projects and their results are the focus of the next series of sections of the report.

5.3 Effect of Specimen Thickness and Width on BFCM Energy (sharpest tip)

The pendulum impact test described here is a structural test. Structural tests differ from material tests in that there is not a “material property” that results from the test. What results is a property that is somewhat dependent upon the boundary conditions applied to the specimen and oftentimes also the geometry of the specimen. Therefore, the first series of BFCM tests are designed to understand how specimen dimensions impact the measured energy level. This is important from the point of view of thickness since the thickness of the vintage materials evaluated varies by nearly a factor of 2x. To understand this, the width and thickness of normalized TC128-B specimens were varied and tested in the BFCM. Drop angles of 120° were employed with an arm length of 52.45-inch and a pendulum weight of 2378-lbs. The tabulated results are indicated in Table 5-3 with the resulting data also indicated in Figures 5-13 and 5-14.

Intuition suggests that the influence of specimen width should be linear since during impact the stress state is a combined axial (P/A) and bending (My/I). If we assume energy is linearly related to stress, elementary theory suggests that axial load varies linearly with width ($1/A$) and quadratically (y/I) with thickness. Indeed, as the data indicates in Figure 5-13, the trend of energy with specimen width is indeed linear. The deviation from linearity is fairly low, on the order of 5% or less (r^2 error for this fit is 0.992). What is interesting, however, is the zero intercept. The fit indicated would suggest that a specimen that has a width of 0-inch would have a nonzero energy which is clearly not physically possible. As expected, the data plotted in Figure 5-14 clearly follows a 2nd order fit although there is some deviation evident at the lower end of the curve. It is notable, too, that the intercept in this case is virtually zero (-84.7 ft-lbs). Furthermore, the r^2 error for this fit is excellent at 0.989.

These tests have indicated that BFCM energy appears to directly scale with stress state in the specimen.

5.4 BFCM Energy of Vintage Tank Car Material (sharpest tup)

The BFCM data for the examination of different tank car steels is shown in Table 5-4. The raw energy is plotted versus material condition in Figure 5-15. The toughest material is modern normalized TC128-B whereas the lowest energy to fail is the 1965 vintage A212-B. It is interesting to note that the 1966 vintage A212-B exhibits a 3x higher BFCM energy when compared to the earlier vintage material. Nevertheless, the data in Figure 5-15 indicates a 4x difference in energy level between the extremes.

Whereas the data in Figure 5-15 clearly indicates overall differences in structural energy to failure, it is somewhat unfair to judge material differences since there were also thickness differences involved. The data plotted in Figure 5-14 clearly provides a normalization strategy that can account for different thicknesses. This approach, using a BFCM energy normalized by the square of thickness, is employed in Figure 5-16. Once the thickness disparity is accounted for, the materials all appear to yield energies more on par with each other. The disparity

observed with the A212 also vanishes. It is interesting to observe no consistent trend with the TC128-B data, although there is a fair amount of overall scatter in the average energy results.

One of the key variables with the different tank car steels is the different mechanical properties involved. In a further effort to understand this effect, a series of plots were made to understand if BFCM energy varies in some manner with mechanical properties. These plots, shown in Figures 5-17 through 5-23, provide some insight into what the BFCM energy measure corresponds to. A weak correlation is evident when comparing BFCM energy to either UTS or flow stress (Figures 5-17 and 5-18) although variability levels are fairly high. Less correlation is evident when either CVN (Figure 5-19) or ductility measures (elongation in Figure 5-20 and RA in Figure 5-21) are considered. The final quantity examined is strain energy, which can be thought of as the area under a stress strain curve. Correlations are provided on both an engineering strain and true strain basis in Figures 5-22 and 5-23, respectively. The strongest correlation evident is clearly observed with the true strain approach in Figure 5-23.

These empirical correlations suggest that BFCM energy may be weakly related to strain energy, or alternatively flow stress.

5.5 Sharp versus Blunt Impactor Tup

During testing, modeling performed at SRT-Quest (Ted Anderson's company) suggested that the blunter tup may be better than the sharp tup. Therefore, some testing was also performed using the blunt tup. Before changing over, the following results were obtained:

- sharp tup, $E = 6160$ ft-lbs
- medium tup, $E = 6126$ ft-lbs
- blunt tup, $E = 6868$ ft-lbs

where all of the above results are two test averages and E corresponds to BFCM energy. These results agree with intuition that the blunt tup should require higher energy levels to push the tup

through the material. However, the results for the sharp and medium tup are curious and not believed to statistically indicate any difference between the two.

Additional data comparing sharp and blunt tups are included in Figure 5-24. Note that some of this data was focused on generated properties for other materials (HPS 70, HPS 100 and A710). Differences in energy of greater than the 10% noted above are typically observed. Levels more on the order of 15-25% are evident. The blunt impactor results in Figure 5-24 are further examined in Figure 5-25 contrasting the data band (sharp impactor) to the points shown for the blunt impactor. It appears that the blunt tup data generally lies within the given range, although the slope might appear slightly different for the blunter tup data.

5.6 Effect of Specimen Thickness on BFCM Energy (bluntest tup)

Given a 10-25% energy increase when transitioning from a sharp to a blunt impactor tup, the question that is then raised is: How is the specimen thickness dependence investigated earlier influenced by the different impactor tup? Whenever a characteristic dimension is changed, differences can arise since the ratio between characteristic dimensions often controls underlying behavior. For instance, with a fixed thickness, the difference between two different impactor tups is likely related to a fundamental length measure associated with each tup. It is important to understand differences associated with each dimensional variable.

The thickness effect on BFCM energy was examined with the data included in Table 5-5 and plotted (with earlier results) in Figure 5-26. The resulting curve is remarkably similar to the earlier curve, albeit offset by a certain extent. The implication of the data in Figure 5-26 is that regardless of impactor tup, when taking thicknesses into account the relevant normalization scheme is to divide by thickness squared.

5.7 Stalling the BFCM – Effect of Initial Pendulum Angle on BFCM Energy (bluntest tup)

The last structural-related BFCM task undertaken was an examination of the influence of initial energy level on final measured energy level for a failed specimen. Understanding this effect is important to more fully comprehend the quantities measured in the BFCM and to ensure that the measured energy is not dependent on initial energy level.

Two things change when the initial angle is varied from the nominal 120° drop angle (recall, all testing to date has been performed at 120° with an arm center-of-gravity length of 52.45-inch and an arm weight of 2378 lbs). First, the initial energy state changes and then the impact speed also varies. In general, the measured energy level in a fractured specimen should not depend upon the initial energy state unless there is some type of bias or offset in our equipment. However, the speed could actually affect properties since initial angle influences the applied strain rate.

The testing performed was with the second baseline calibration material that, as described in the last report, exhibits an average BFCM energy of 7003 ft-lbs and a range (over four specimens) from 6800-7200 ft-lbs. The drop angle was gradually decreased until the pendulum was stalled and the specimen broke in two pieces. When this occurred, we ratcheted back up to the previous angle where failure occurred to ensure failure again occurred.

The data indicated in Table 5-6 indicates that stall occurred at the 62.5° drop where the energy level was 5600 ft-lbs (the unfailed specimen is shown in Figure 5-27). Moreover, the initial drop angles included in Table 5-6 are further described in Table 5-7 in terms of drop energy and speed of impact. The data shows that over a 50% change in initial energy and a 40% decrease in impact velocity, no systematic change is noted in BFCM energy. All of the energy levels indicated in Table 5-6 are within the average ± 2 standard deviations.

Table 5-1. Test plates and specimens required for Volpe fracture toughness testing (last column refers to the BFCM specimens fabricated for testing).

Material Source and Description	Tank Car ID No.	Car Builder	Build Year	Remnant Piece ID No.	No. of Specimens....	
					C(T)'s	BFCM Bowties
TC128B-Subset A <i>(oldest fleet quartile)</i>	GATX 97833	GATX	1966	66b-SA	2 + 1 spare	
	GATX 55905	GATX	1966	66a-SA 66a-HA	2 + 1 spare 2 + 1 spare	
	PROX 89773	Union	1968	68b-SA 68b-SB 68b-HA	2 + 1 spare 2 + 1 spare 2 + 1 spare	3 3
TC128B-Subset B <i>(2nd oldest fleet quartile)</i>	UTLX 28744	Union	1974	74b-SA 74b-HA	2 + 1 spare 2 + 1 spare	3
	TGAX 331007	ACF	1975	75a-SA 75a-HA	2 + 1 spare 2 + 1 spare	3
	GATX 47814	GATX	1976	76b-SA(F) 76b-SA(A)	2 + 2 spare 2 + 2 spare	
TC128B-Subset C <i>(2nd youngest fleet quartile)</i>	CGTX 64270	Hawk-Sid	1978	78b-SA 78b-HA	2 + 1 spare 2 + 1 spare	
	GATX 49248	GATX	1977	77a-SA(D)	2 + 2 spare	
	GAMX 4115	ACF	1979	79a-SA 79a-SB 79a-HA	2 + 1 spare 2 + 1 spare 2 + 1 spare	3 3
TC128B-Subset D <i>(youngest fleet quartile)</i>	PROX 83469	Procor	1980	80a-SA 80a-HA	2 + 1 spare 2 + 1 spare	
	HOKX 8373	ACF	1981	81a-SB	2 + 1 spare	
	HOKX 8453	GATX	1982	82a-SA 82a-SB 82a-HA	2 + 1 spare 2 + 1 spare 2 + 1 spare	3 3
TC128B-normalized <i>(new material)</i>	PROX 31153	Procor	1994	94a-SA 94a-SB 94a-HA	2 + 2 spare 2 + 2 spare 2 + 1 spare	3 3
	PROX 31218	Procor	1994	94b-SA 94b-HA	2 2	3
A212-B <i>(older material)</i>	GATX 9746	GATX	1965	65a-HA 65a-SA	2 + 1 spare 2 + 1 spare	3
	CGTX 63699	GATX	1966	66c-SA 66c-HA	2 2	3

Table 5-2. Comparison of properties between the two baseline normalized TC128B materials (the prefix attached to the specimen IDs fabricated from the old plate was BFCM whereas for the new it was N).

Plate Descrip	Plate Orient	RT CVN's (ft-lbs)		Tensile Properties				Miscellaneous Comments
		energies	avg	UTS, ksi	YS, ksi	elong, %	RA, %	
old	L	96, 58, 69	74	87.3	59.2	27	59	BFCM spec. ID no.'s "BFCM"*
	T	47, 50, 49	49	n/a	n/a	n/a	n/a	
new	L	84, 87, 100	90	91.3	64.8	28	59	BFCM spec. ID no.'s "N"
	T	49, 53 54	52	89.8	63.6	27	57	

* The definition of a BFCM sample in the longitudinal orientation is one whose major tensile axis (the long axis of the specimen) is in the L-direction and the impactor strikes in the orthogonal T-direction (hence, the material is cut along the T-axis).

Table 5-3. BFCM test results assessing the influence of specimen dimensions (normalized TC128-B circa 1999 from tank head offal).

Preliminary BFCM Testing to Establish the Influence of Specimen Dimensions										
Specimen ID	Thickness in	Width in	Area in ²	Temp F	Tup	Initial Angle deg	Final Angle deg	Energy, ft-lbs	Average E, ft-lbs	Std. Dev. E, ft-lbs
BFCM-A-P	0.8000	1.0000	0.800	75-85	Thin_1	120	85.50	6013.1	6159.9	170.47
BFCM-A-1	0.8090	1.0015	0.810	75-85	Thin_2	120	83.75	6329.2		
BFCM-A-2	0.8100	1.0150	0.822	75-85	Thin_2	120	85.50	6013.1		
BFCM-A-3	0.8095	1.0075	0.816	86-88	Thin_1	120	84.00	6284.1		
BFCM-B-1	0.8055	0.7535	0.607	75-85	Thin_2	120	94.50	4382.0	4502.6	138.27
BFCM-B-2	0.8105	0.7510	0.609	86-88	Thin_2	120	94.00	4472.4		
BFCM-B-3	0.8175	0.7510	0.614	86-88	Thin_1	120	93.00	4653.5		
BFCM-C-1	0.8085	0.5025	0.406	75-85	Thin_2	120	104.25	2638.8	2609.5	91.40
BFCM-C-2	0.8110	0.5005	0.406	86-88	Thin_2	120	105.00	2507.1		
BFCM-C-3	0.8145	0.5000	0.407	86-88	Thin_1	120	104.00	2682.7		
BFCM-D-1	0.7520	1.0095	0.759	75-85	Thin_2	120	88.25	5515.0	5484.8	26.18
BFCM-D-2	0.7540	1.0100	0.762	86-88	Thin_2	120	88.50	5469.7		
BFCM-D-3	0.7510	1.0160	0.763	86-88	Thin_1	120	88.50	5469.7		
BFCM-E-1	0.6260	1.0110	0.633	75-85	Thin_2	120	99.00	3571.4	3736.0	144.28
BFCM-E-2	0.6250	1.0085	0.630	86-88	Thin_1	120	97.50	3840.7		
BFCM-E-3	0.6220	1.0070	0.626	86-88	Thin_1	120	97.75	3795.8		
BFCM-F-1	0.5030	1.0045	0.505	75-85	Thin_1	120	107.50	2071.7	1971.0	108.47
BFCM-F-2	0.5030	1.0040	0.505	75-85	Thin_1	120	108.75	1856.2		
BFCM-F-3	0.5010	1.0090	0.506	75-85	Thin_1	120	108.00	1985.3		
BFCM-G-1	0.3735	1.0105	0.377	75-85	Thin_1	120	113.00	1135.9	1080.4	96.06
BFCM-G-2	0.3650	1.0105	0.369	75-85	Thin_1	120	114.00	969.5		
BFCM-G-3	0.3715	1.0100	0.375	75-85	Thin_1	120	113.00	1135.9		
BFCM-H-1	0.1905	1.0010	0.191	75-85	Thin_1	120	116.00	640.6	572.9	62.08
BFCM-H-2	0.1905	1.0065	0.192	75-85	Thin_1	120	116.50	559.3		
BFCM-H-3	0.1905	1.0075	0.192	75-85	Thin_1	120	116.75	518.7		

Table 5-4. BFCM test results assessing the difference between different railroad tank car materials fabricated at different times.

BFCM Testing - Volpe												
Tank Car ID No.	Specimen ID	Thickness in	Width in	Date	Test Order	Temp F	Tup	Initial Angle deg	Final Angle deg	Energy ft-lbs	Average E, ft-lbs	Std. Dev. E, ft-lbs
PROX 89773	B-68B-SA-1	0.6800	1.0150	4/11/2007	1	90-100	Thin_3	120	101.00	3214.1	3347.9	133.9
	B-68B-SA-2	0.6820	1.0055	4/11/2007	2	90-100	Thin_3	120	99.50	3481.9		
	B-68B-SA-3	0.6750	1.0060	4/11/2007	3	90-100	Thin_3	120	100.25	3347.8		
	B-68B-SB-1	0.7060	1.0005	4/11/2007	4	90-100	Thin_3	120	98.50	3661.1	3616.3	118.6
	B-68B-SB-2	0.7090	1.0185	4/11/2007	5	90-100	Thin_3	120	98.25	3705.9		
	B-68B-SB-3	0.6845	1.0215	4/11/2007	6	90-100	Thin_3	120	99.50	3481.9		
UTLX 28744	B-74B-SA-1	0.7845	1.0095	4/11/2007	7	90-100	Thin_3	120	94.50	4382.0	3875.1	957.4
	B-74B-SA-2	0.7880	1.0095	4/11/2007	8	90-100	Thin_3	120	103.50	2770.9		
	B-74B-SA-3	0.7900	1.0135	4/11/2007	9	90-100	Thin_3	120	94.00	4472.4		
TGAX 331007	B-75A-SA-1	0.6430	1.0080	4/11/2007	10	90-100	Thin_3	120	99.00	3571.4	3541.6	51.7
	B-75A-SA-2	0.6490	1.0140	4/11/2007	11	90-100	Thin_3	120	99.00	3571.4		
	B-75A-SA-3	0.6430	1.0110	4/11/2007	12	90-100	Thin_3	120	99.50	3481.9		
GAMX 4115	B-79A-SA-1	0.7865	1.0125	4/11/2007	13	90-100	Thin_3	120	89.50	5288.3	5258.0	52.4
	B-79A-SA-2	0.7920	1.0085	4/11/2007	14	90-100	Thin_3	120	90.00	5197.5		
	B-79A-SA-3	0.7795	1.0030	4/11/2007	15	90-100	Thin_3	120	89.50	5288.3		
	B-79A-SB-1	0.7890	1.0020	4/11/2007	16	90-100	Thin_4	120	95.50	4201.2	4820.1	536.4
	B-79A-SB-2	0.7820	1.0070	4/11/2007	17	90-100	Thin_4	120	90.50	5106.8		
	B-79A-SB-3	0.7890	1.0095	4/11/2007	18	90-100	Thin_4	120	90.25	5152.2		
HOKX 8453	B-82A-SA-1	0.8035	1.0100	4/12/2007	19	75-85	Thin_4	120	90.75	5061.5	5122.0	145.8
	B-82A-SA-2	0.8060	1.0125	4/12/2007	20	75-85	Thin_4	120	91.00	5016.1		
	B-82A-SA-3	0.8015	1.0080	4/12/2007	21	75-85	Thin_4	120	89.50	5288.3		
	B-82A-SB-1	0.8090	1.0105	4/12/2007	22	75-85	Thin_4	120	93.00	4653.5	4759.4	396.0
	B-82A-SB-2	0.8125	1.0145	4/12/2007	23	75-85	Thin_4	120	94.25	4427.2		
	B-82A-SB-3	0.8110	1.0045	4/12/2007	24	75-85	Thin_4	120	90.00	5197.5		
PROX 31153	B-94A-SA-1	0.6325	1.0100	4/12/2007	25	75-85	Thin_4	120	101.50	3125.1	3110.3	25.6
	B-94A-SA-2	0.6300	1.0030	4/12/2007	26	75-85	Thin_4	120	101.50	3125.1		
	B-94A-SA-3	0.6285	1.0050	4/12/2007	27	75-85	Thin_4	120	101.75	3080.7		
	B-94A-SB-1	0.6225	1.0140	4/12/2007	28	75-85	Thin_4	120	101.50	3125.1	3110.3	67.9
	B-94A-SB-2	0.6300	1.0100	4/12/2007	29	75-85	Thin_4	120	101.25	3169.6		
	B-94A-SB-3	0.6265	1.0035	4/12/2007	30	75-85	Thin_4	120	102.00	3036.3		
PROX 31218	B-94B-SA-1	0.6350	1.0135	4/12/2007	31	75-85	Thin_4	120	101.00	3214.1	3169.6	44.5
	B-94B-SA-2	0.6320	1.0090	4/12/2007	32	75-85	Thin_4	120	101.50	3125.1		
	B-94B-SA-3	0.6285	1.0065	4/12/2007	33	75-85	Thin_4	120	101.25	3169.6		
GATX 9746	B-65A-SA-1	0.4505	1.0440	4/12/2007	34	75-85	Thin_4	120	111.00	1472.3	1472.4	84.7
	B-65A-SA-2	0.4500	1.0260	4/12/2007	35	75-85	Thin_4	120	110.50	1557.1		
	B-65A-SA-3	0.4505	1.0205	4/12/2007	36	75-85	Thin_2	120	111.50	1387.7		
CGTX 63699	B-66C-SA-1	0.8345	1.0230	4/12/2007	37	75-85	Thin_2	120	91.50	4925.4	4940.6	69.3
	B-66C-SA-2	0.8280	1.0080	4/12/2007	38	75-85	Thin_2	120	91.75	4880.1		
	B-66C-SA-3	0.8290	1.0070	4/12/2007	39	75-85	Thin_2	120	91.00	5016.1		

Table 5-5. BFCM energy levels for the different thickness conditions tested (wider tup).

BFCM Testing to Establish the Influence of Specimen Dimensions, Large Tup, Calibration Plate 2											
Specimen ID	Thickness in	Width in	Date	Test Order	Temp F	Tup	Initial Angle deg	Final Angle deg	Energy ft-lbs	Average E, ft-lbs	Std. Dev. E, ft-lbs
**BFCM-A-12	0.8240	1.0195	4/18/2007	older	70-80	Large_1	120	81.25	6778.9	6733.7	249.9
**BFCM-A-13	0.8315	1.0200	4/18/2007	older	70-80	Large_1	120	80.25	6958.0		
**BFCM-A-14	0.7840	1.0110	5/4/2007	older	80-90	Large_1	120	83.00	6464.4		
N-A-1	0.8205	1.0145	5/8/2007	*23	80-90	Large_1	120	80.50	6913.2	7002.5	163.1
N-A-2	0.8215	1.0115	5/8/2007	*24	80-90	Large_1	120	79.00	7181.0		
N-A-3	0.8180	1.0130	5/8/2007	*25	80-90	Large_1	120	79.50	7091.9		
N-A-4	0.8270	1.0085	5/16/2007	1	80-90	Large_2	120	81.00	6823.7		
N-B-1	0.6265	1.0090	5/16/2007	2	80-90	Large_2	120	94.50	4382.0	4276.5	113.7
N-B-2	0.6250	1.0125	5/16/2007	3	80-90	Large_2	120	95.00	4291.6		
N-B-3	0.6255	1.0065	5/16/2007	4	80-90	Large_2	120	95.75	4156.1		
N-C-1	0.5005	1.0035	5/16/2007	5	80-90	Large_2	120	101.50	3125.1	3169.6	44.49
N-C-2	0.5005	1.0050	5/16/2007	6	80-90	Large_2	120	101.25	3169.6		
N-C-3	0.5045	1.0100	5/16/2007	7	80-90	Large_2	120	101.00	3214.1		
N-D-1	0.3760	1.0085	5/16/2007	8	80-90	Large_2	120	106.00	2332.3	2303.2	25.16
N-D-2	0.3770	1.0085	5/16/2007	9	80-90	Large_2	120	106.25	2288.7		
N-D-3	0.3755	1.0075	5/16/2007	10	80-90	Large_2	120	106.25	2288.7		
N-E-1	0.2540	1.0000	5/16/2007	11	80-90	Large_2	120	111.00	1472.3	1430.0	73.16
N-E-2	0.2490	0.9950	5/16/2007	12	80-90	Large_2	120	111.75	1345.6		
N-E-3	0.2505	1.0120	5/16/2007	13	80-90	Large_2	120	111.00	1472.3		

* test order number is in reference to the high purity test matrix

** these tests were performed on the old baseline material (all other data is from the new baseline plate)

Table 5-6. BFCM results examining the effect of different initial energy states (drop heights) on BFCM energy.

BFCM Testing- Hammer Stall, Large Tup, Calibration Plate 2									
Specimen ID	Thickness in	Width in	Date	Test Order	Temp F	Tup	Initial Angle deg	Final Angle deg	Energy ft-lbs
N-A-5	0.8130	1.0110	5/22/2007	1	70-80	Large_3	116.50	76.75	7020.8
N-A-6	0.8170	1.0110	5/22/2007	2	70-80	Large_3	104.50	63.00	7322.0
N-A-7	0.8195	1.0155	5/22/2007	3	70-80	Large_3	93.50	50.00	7316.4
N-A-8	0.8225	1.0165	5/22/2007	4	70-80	Large_3	82.50	34.00	7261.1
N-A-9	0.8225	1.0135	5/22/2007	5	70-80	Large_3	71.00	14.00	6702.0
N-A-10	0.8280	1.0110	5/22/2007	6	70-80	Large_3	62.50	STALL, NO BREAK	>5600
N-A-11	0.8185	1.0115	5/22/2007	7	70-80	Large_3	71.00	8.00	6909.6

93

Table 5-7. Energies and speeds for the different drop heights (values in parentheses are percent of the baseline 120° drop angle).

Initial Drop Angle, °	Initial Potential Energy, ft-lbs	Impact Speed, mph
120	15593 (100%)	14.0 (100%)
116.5	15033 (96%)	13.8 (98%)
104.5	12998 (83%)	12.8 (91%)
93.5	11030 (70%)	11.8 (84%)
82.5	9038 (58%)	10.7 (76%)
71.0	7010 (45%)	9.4 (67%)
62.5	5595 (36%)	8.4 (60%)

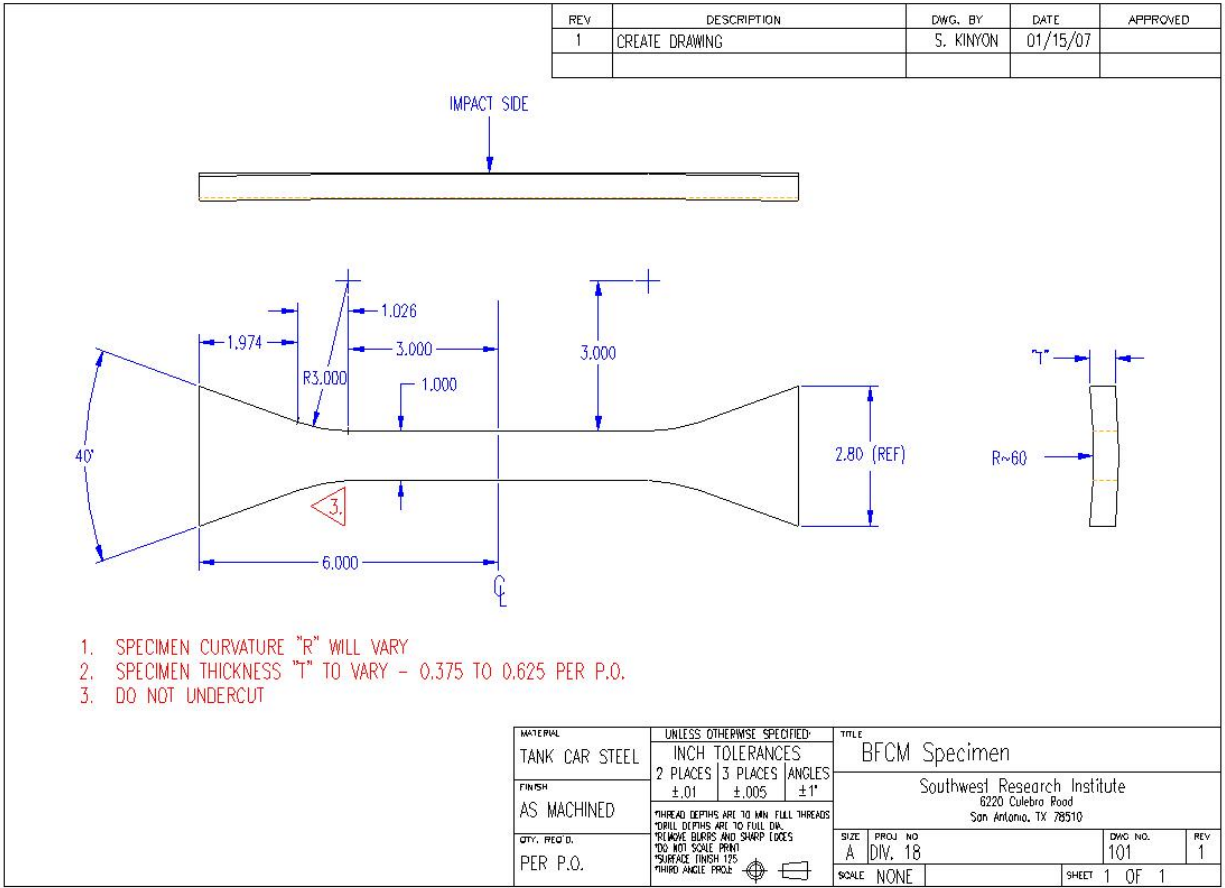


Figure 5-1. BFCM specimen with self-engaging trapezoidal end and 6-inch long center section.

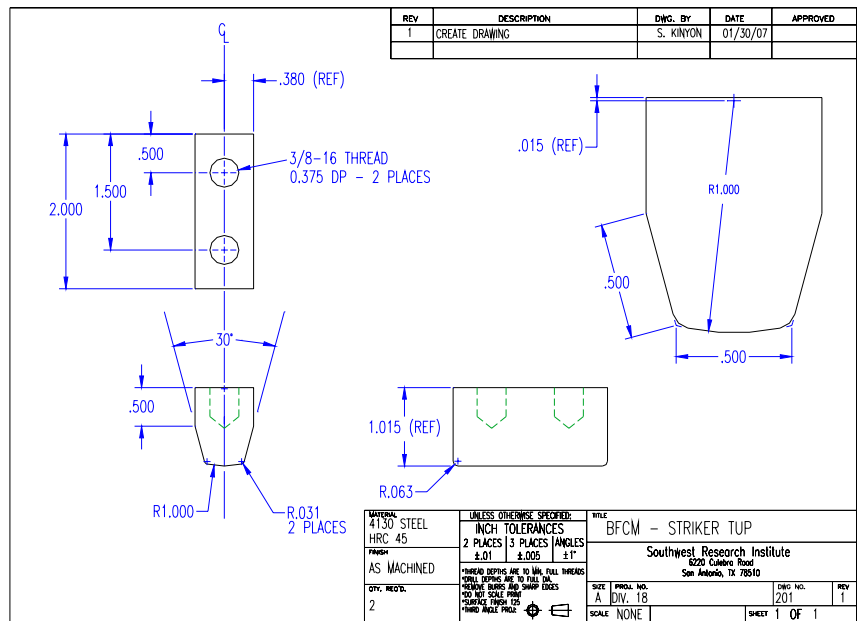


Figure 5-2. Broadest face width (0.5-inch) impact tup.

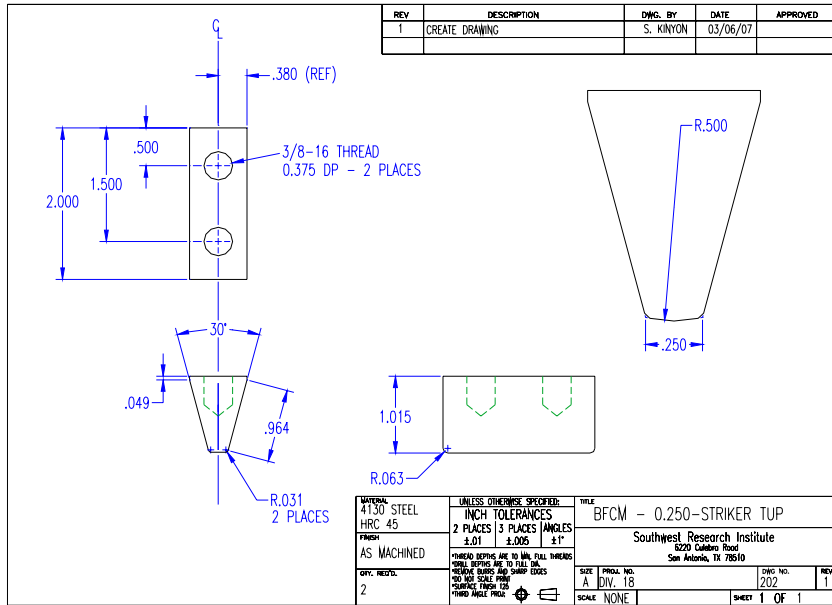


Figure 5-3. Medium face width (0.5-inch) impact tup.

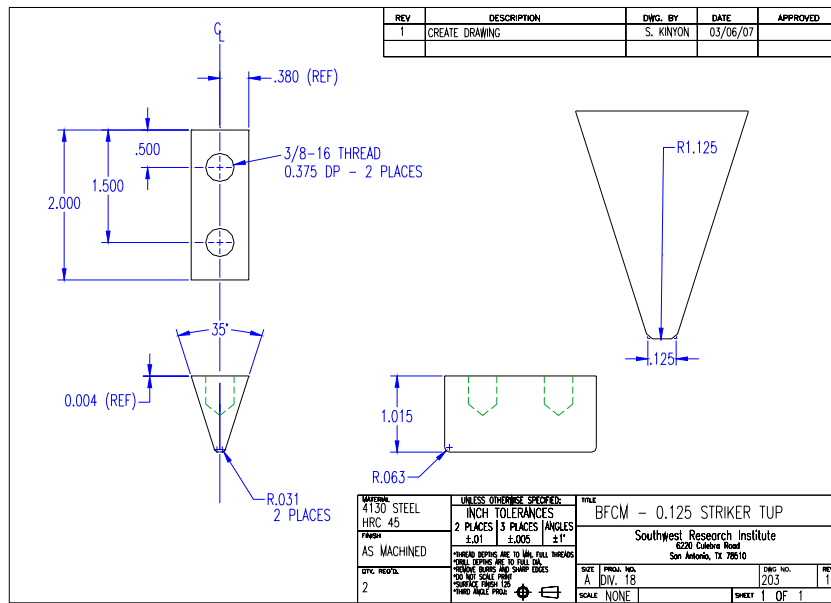


Figure 5-4. Sharp face width (0.125-inch) impact tup.



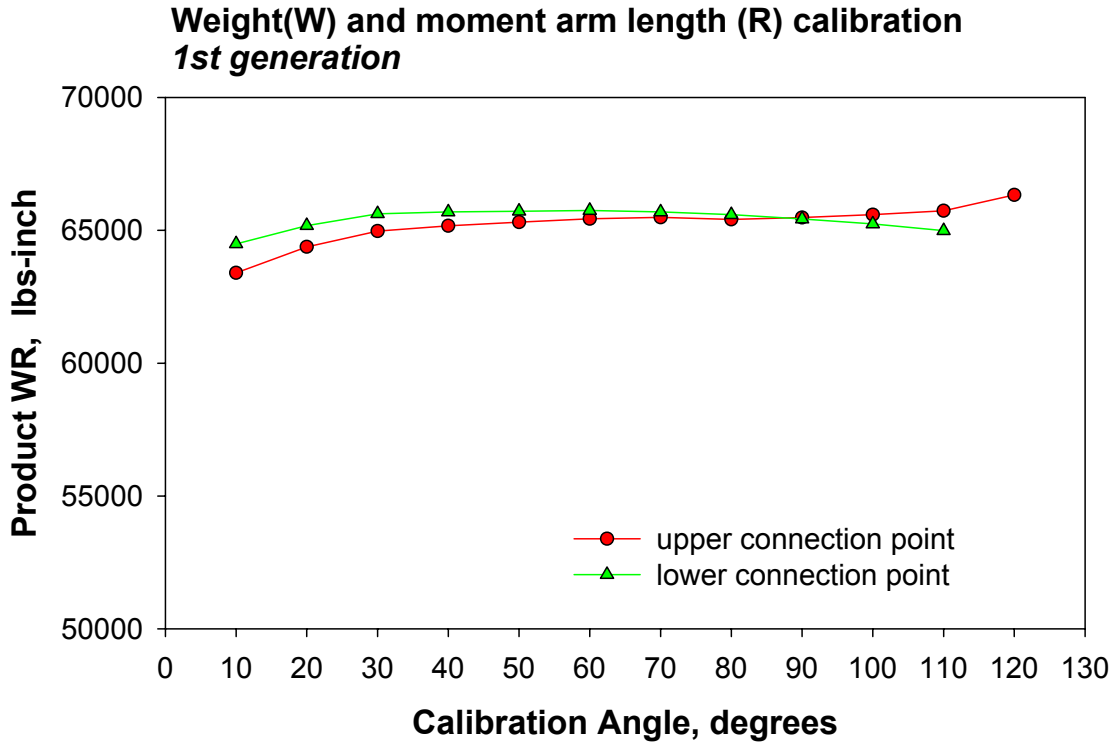
Figure 5-5. Different photographic views of the BFCM facility with a specimen mounted in the test fixture.



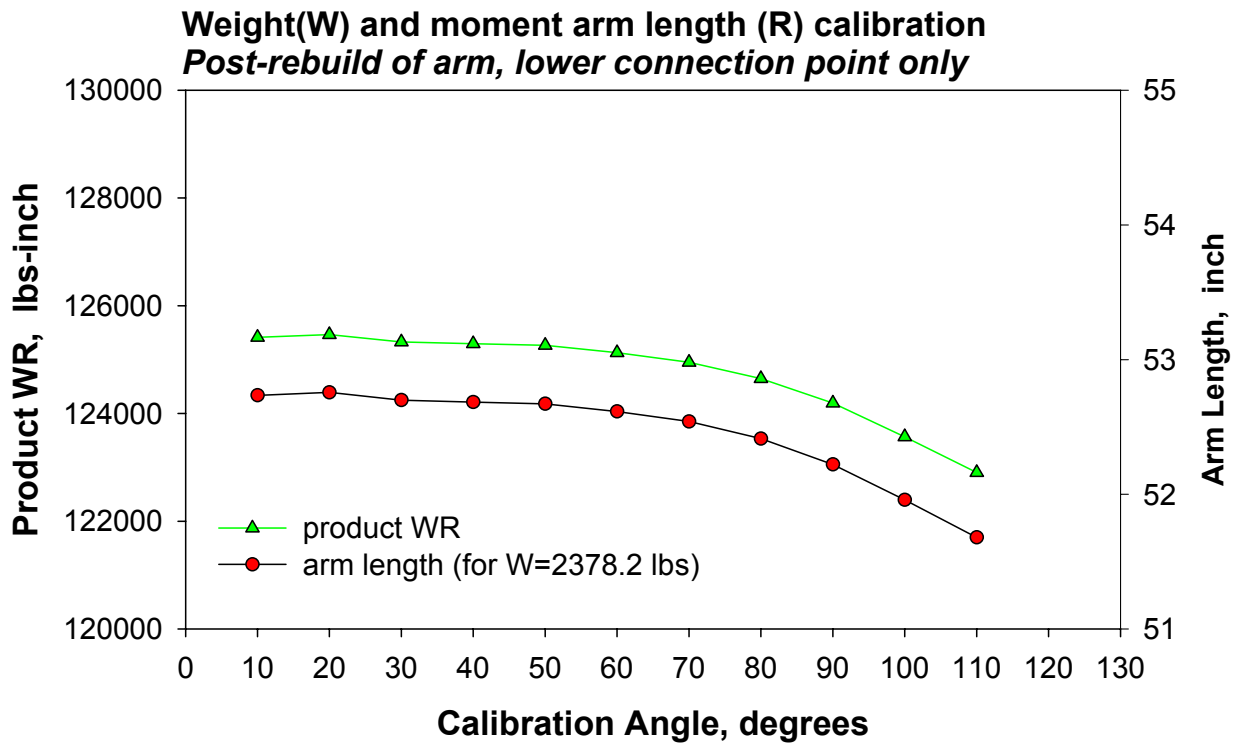
Figure 5-6. Modern-vintage normalized plate with BFCM specimens extracted.



Figure 5-7. The original BFCM arm bent after attempting to fracture the first specimen.



(a)



(b)

Figure 5-8. Pre-test calibration of arm weight and CG position for (a) generation 1 and (b) re-designed BFCM.



Figure 5-9. Worn tups after a number of different uses.

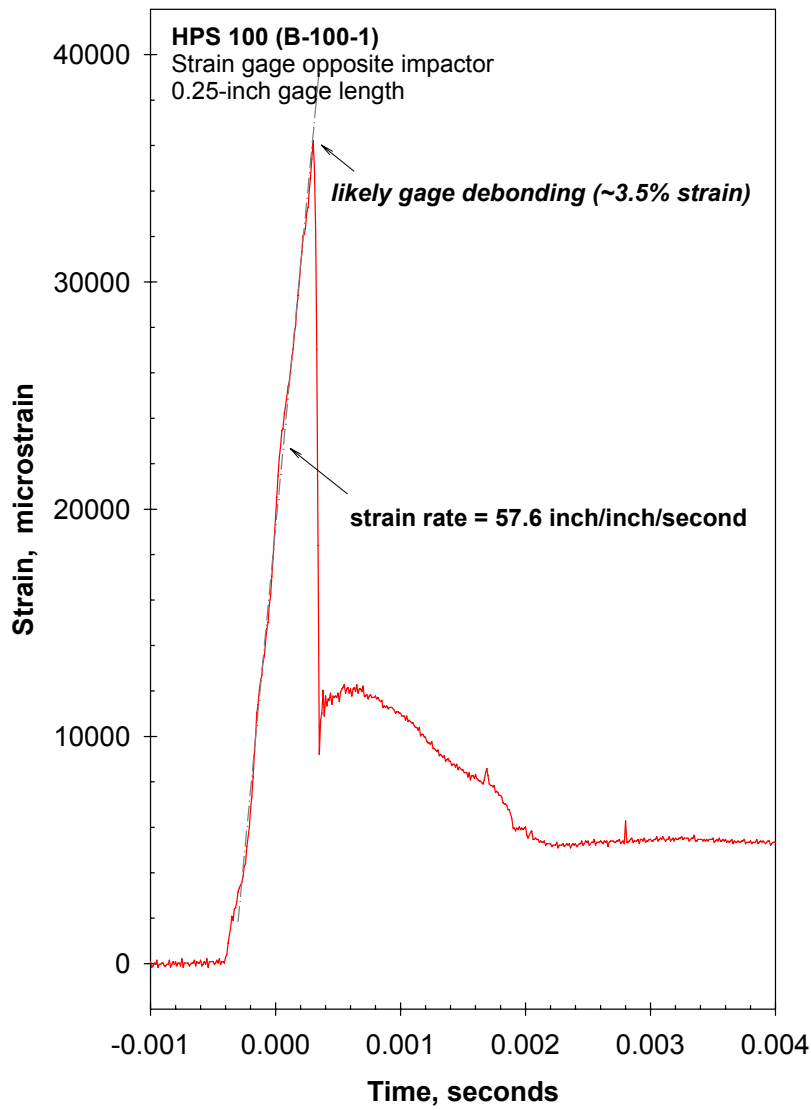


Figure 5-10. Measured strain response on the back of the specimen behind impactor.

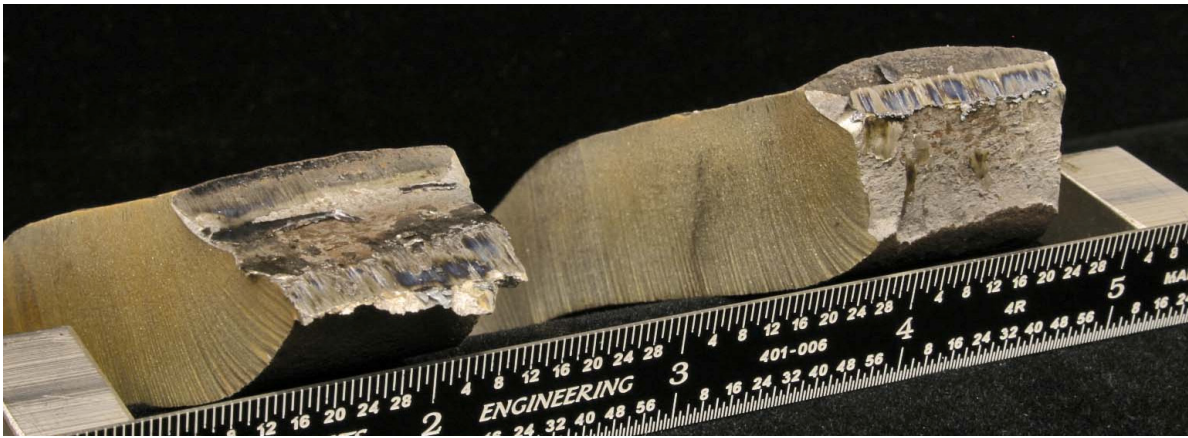
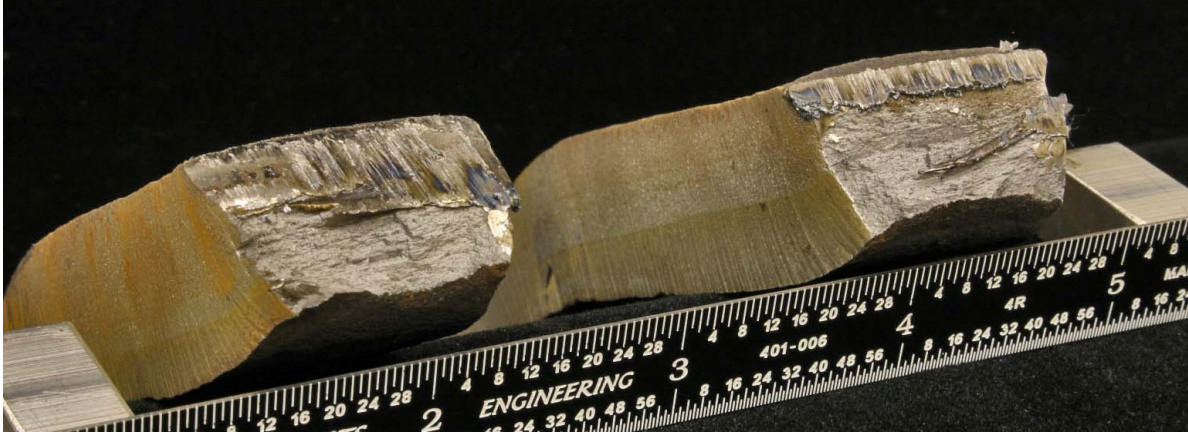


Figure 5-11. Typical BFCM fracture surfaces (sharpest top).



Figure 5-12. Deformation observed in a blunt impact specimen.

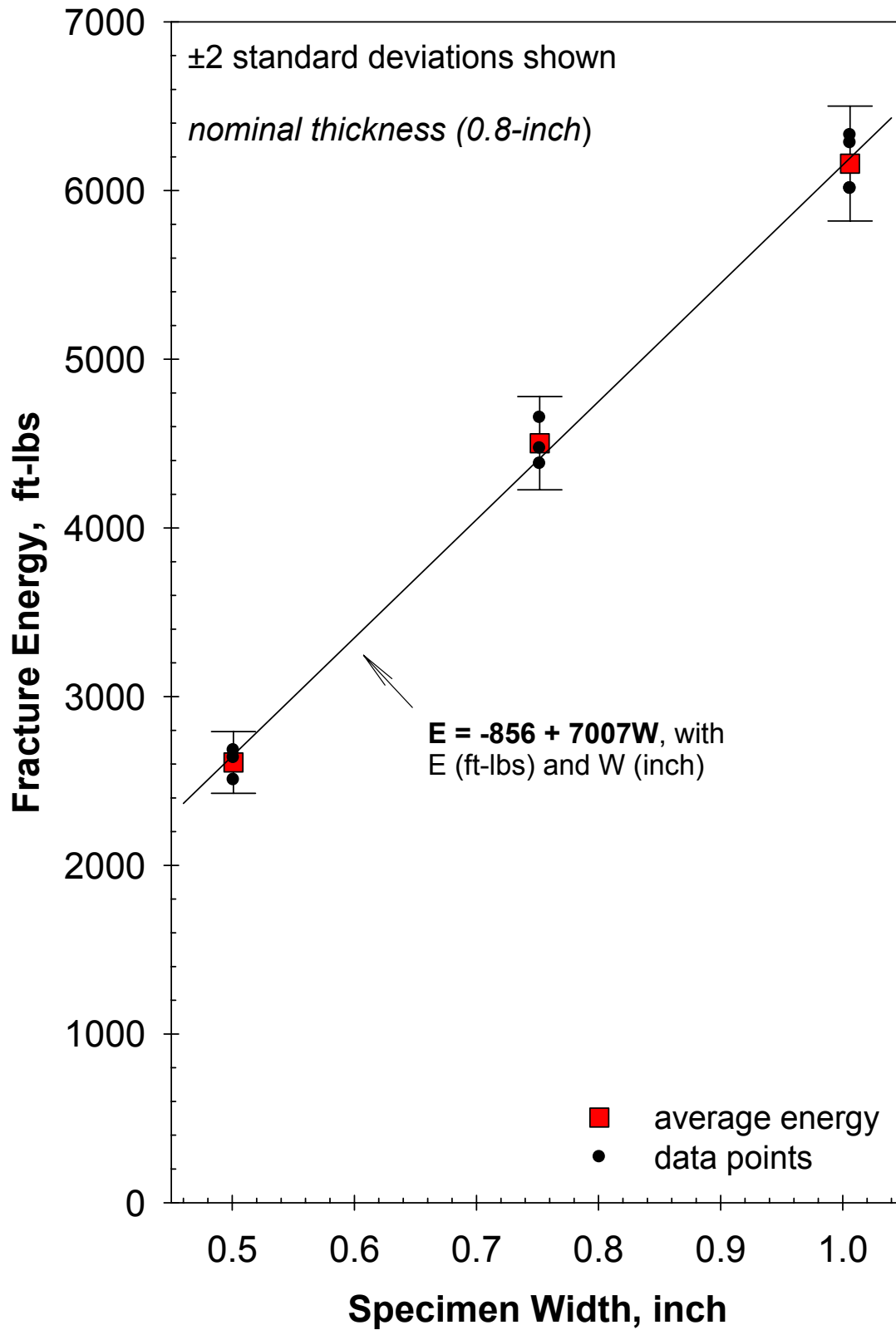


Figure 5-13. Effect of specimen width on the pendulum impact energy (sharpest tup).

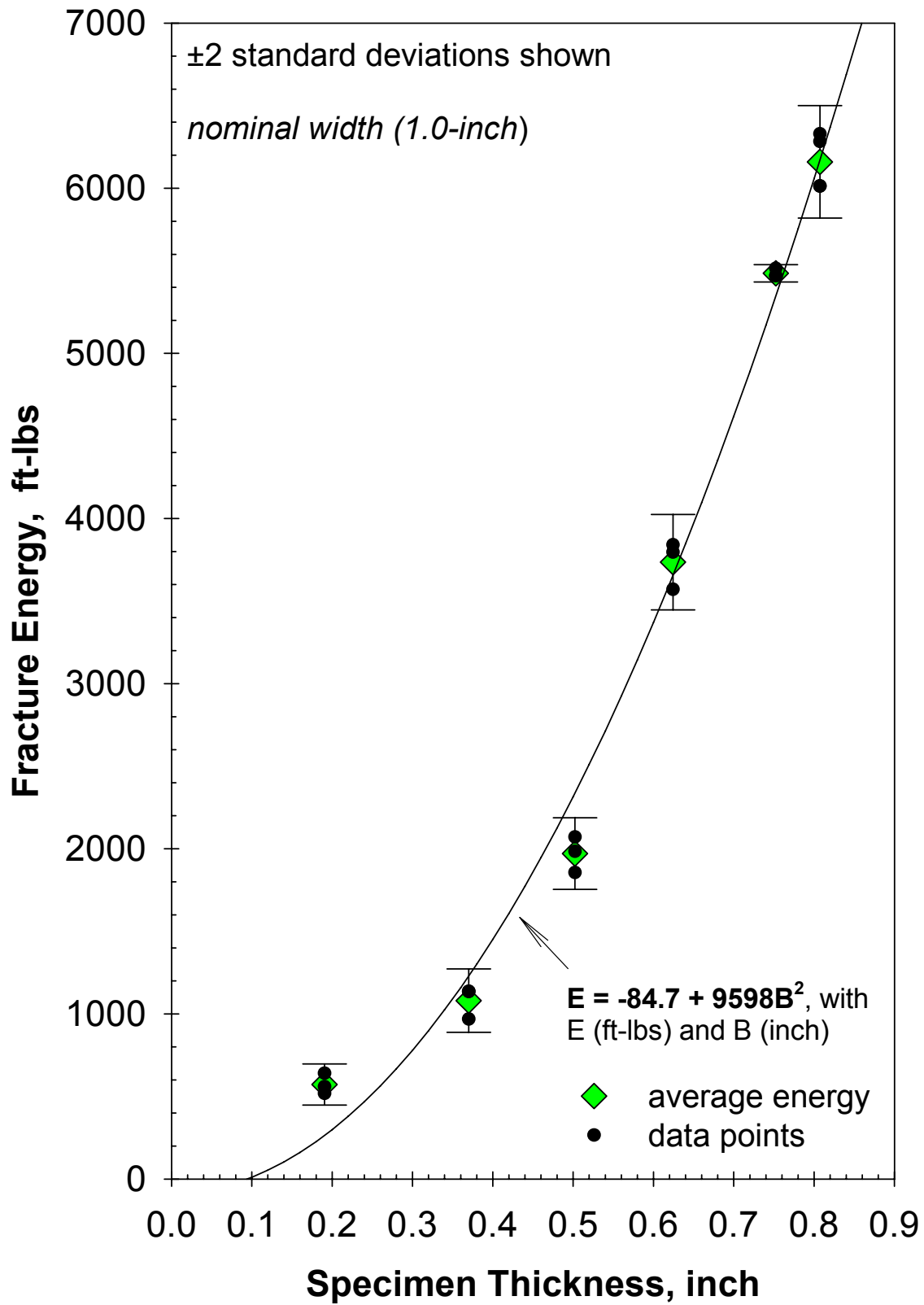


Figure 5-14. Effect of specimen thickness on the pendulum impact energy (sharpest tup).

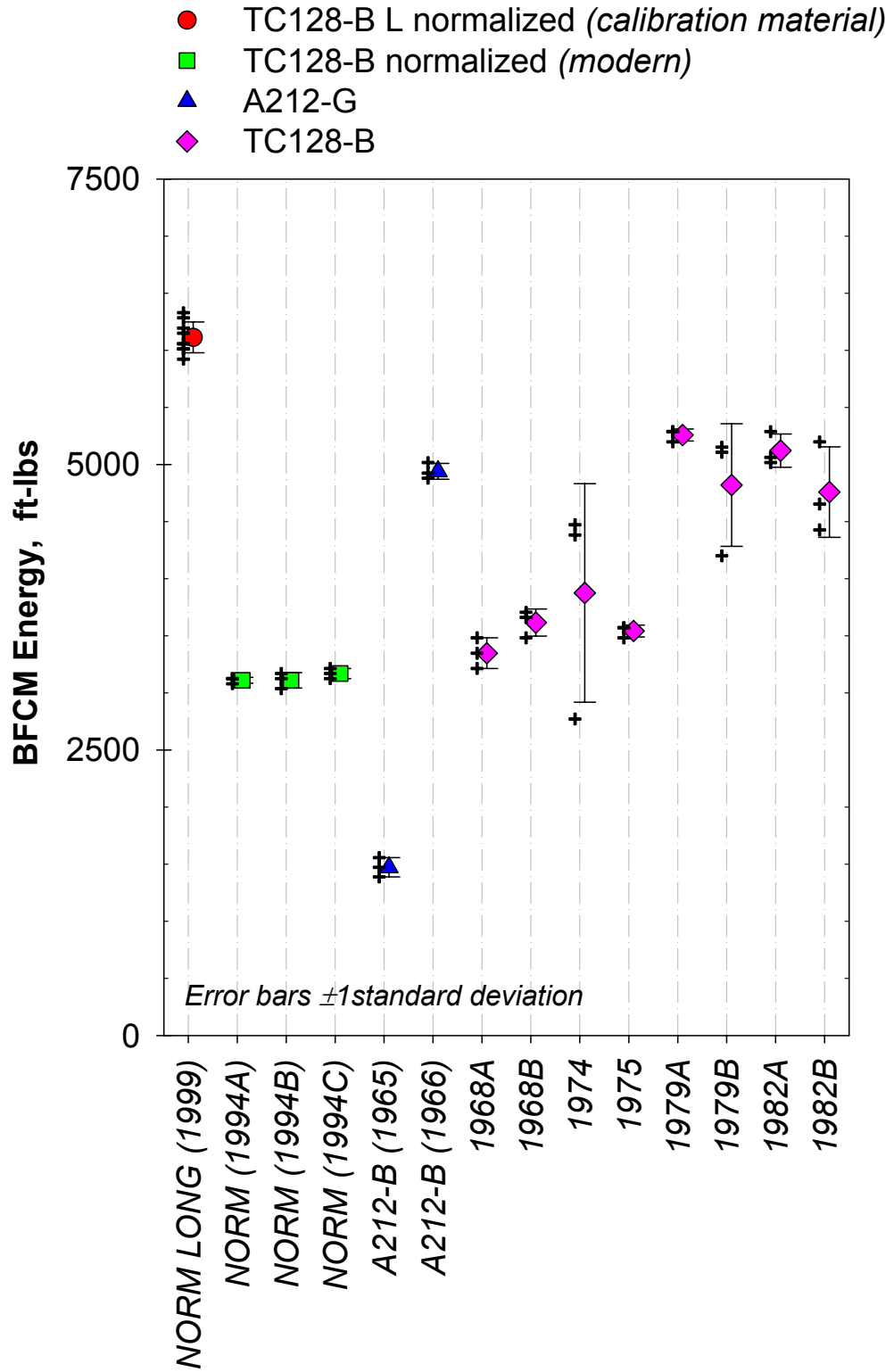


Figure 5-15. Raw BFCM energy for different tank car steels.

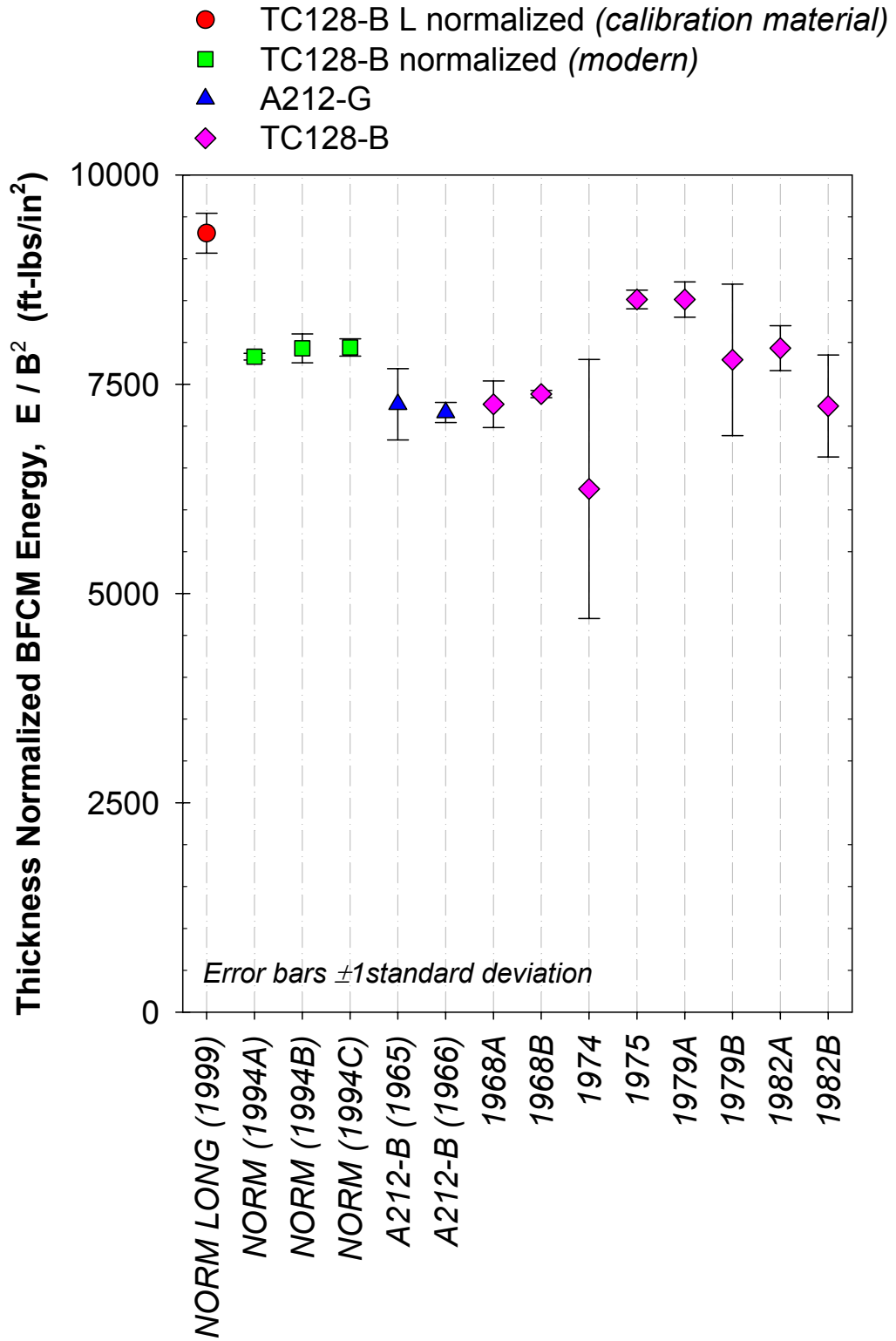


Figure 5-16. Thickness normalized BFCM energy for different tank car steels.

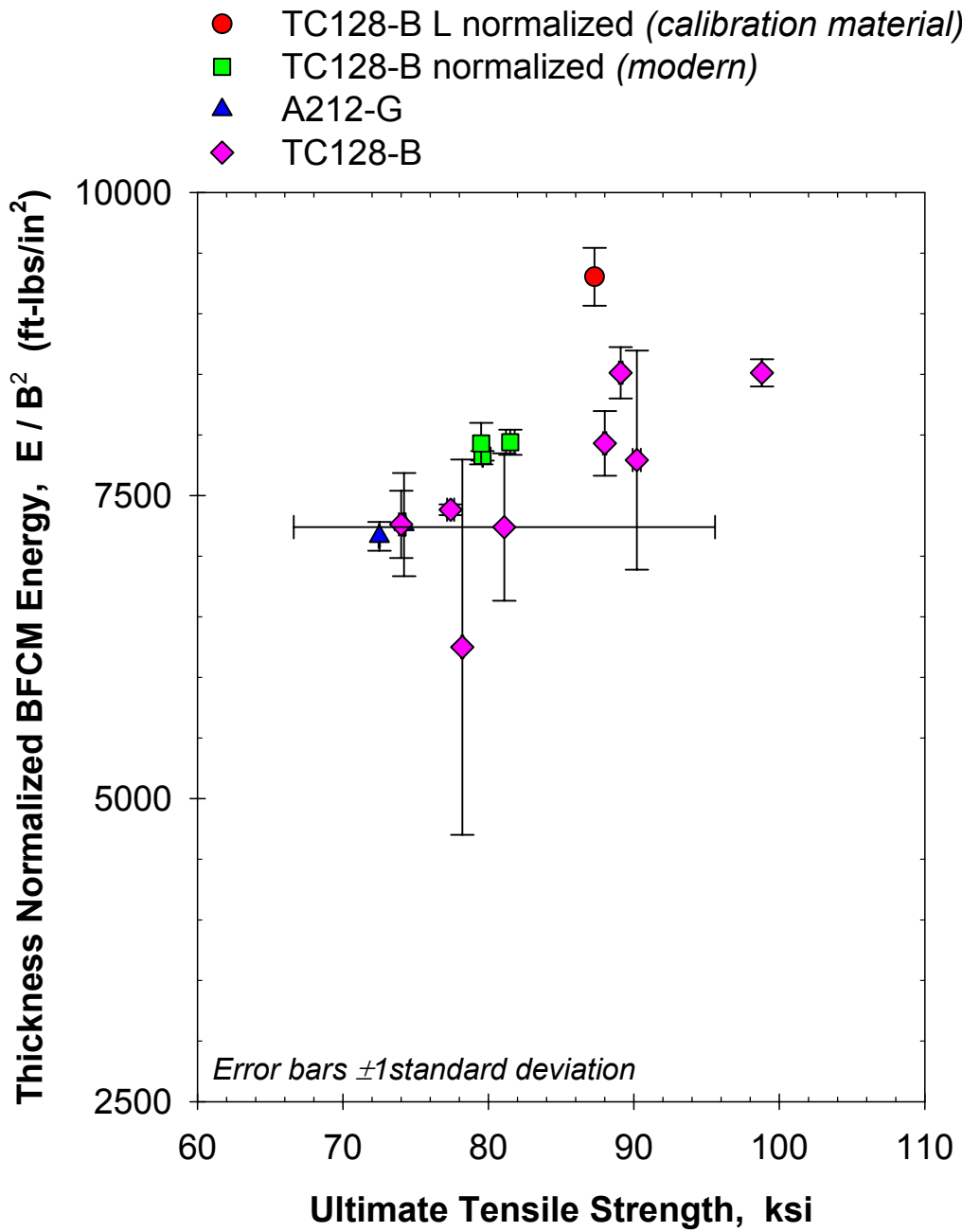


Figure 5-17. Thickness normalized BFCM energy as a function of UTS.

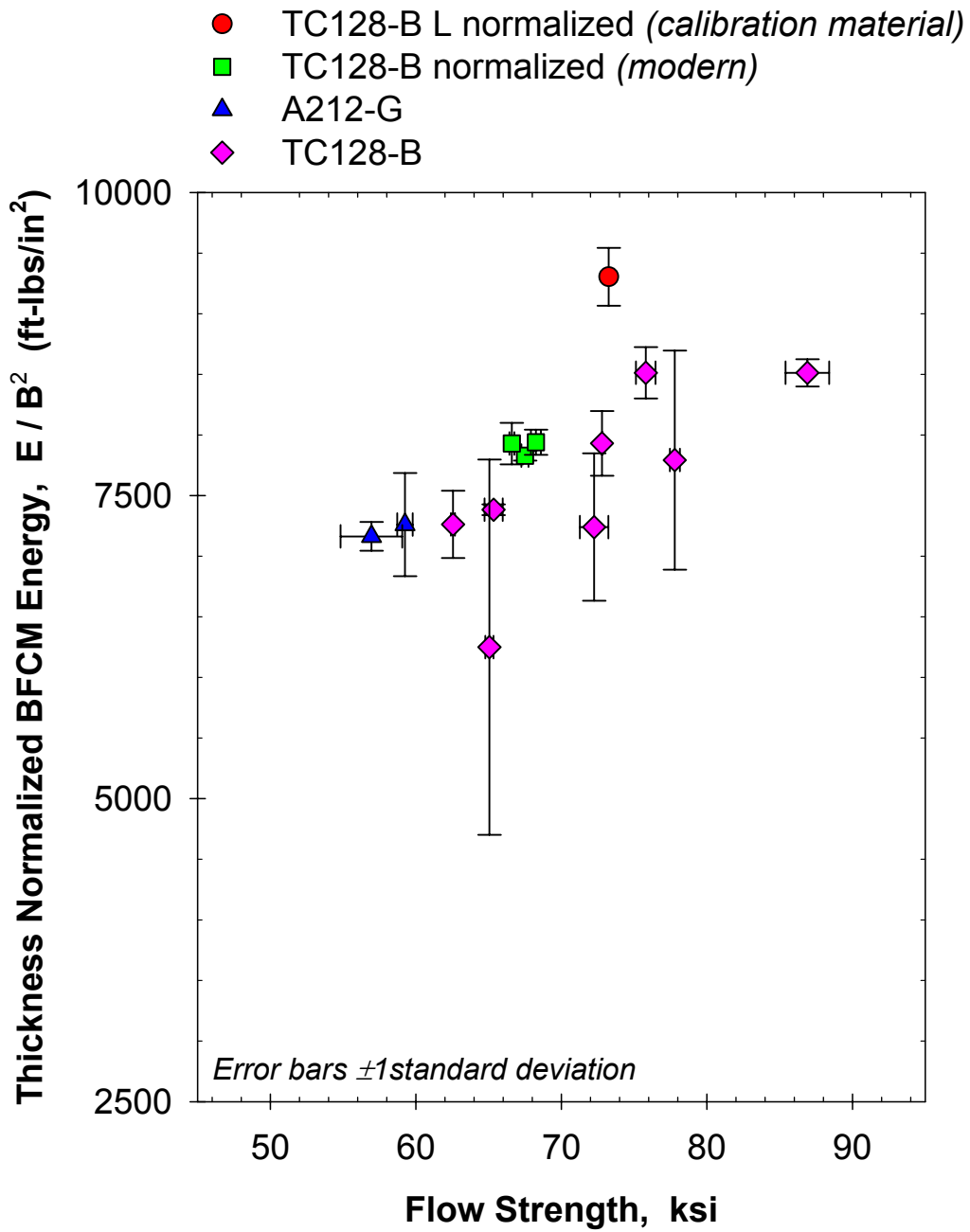


Figure 5-18. Thickness normalized BFCM energy as a function of flow strength.

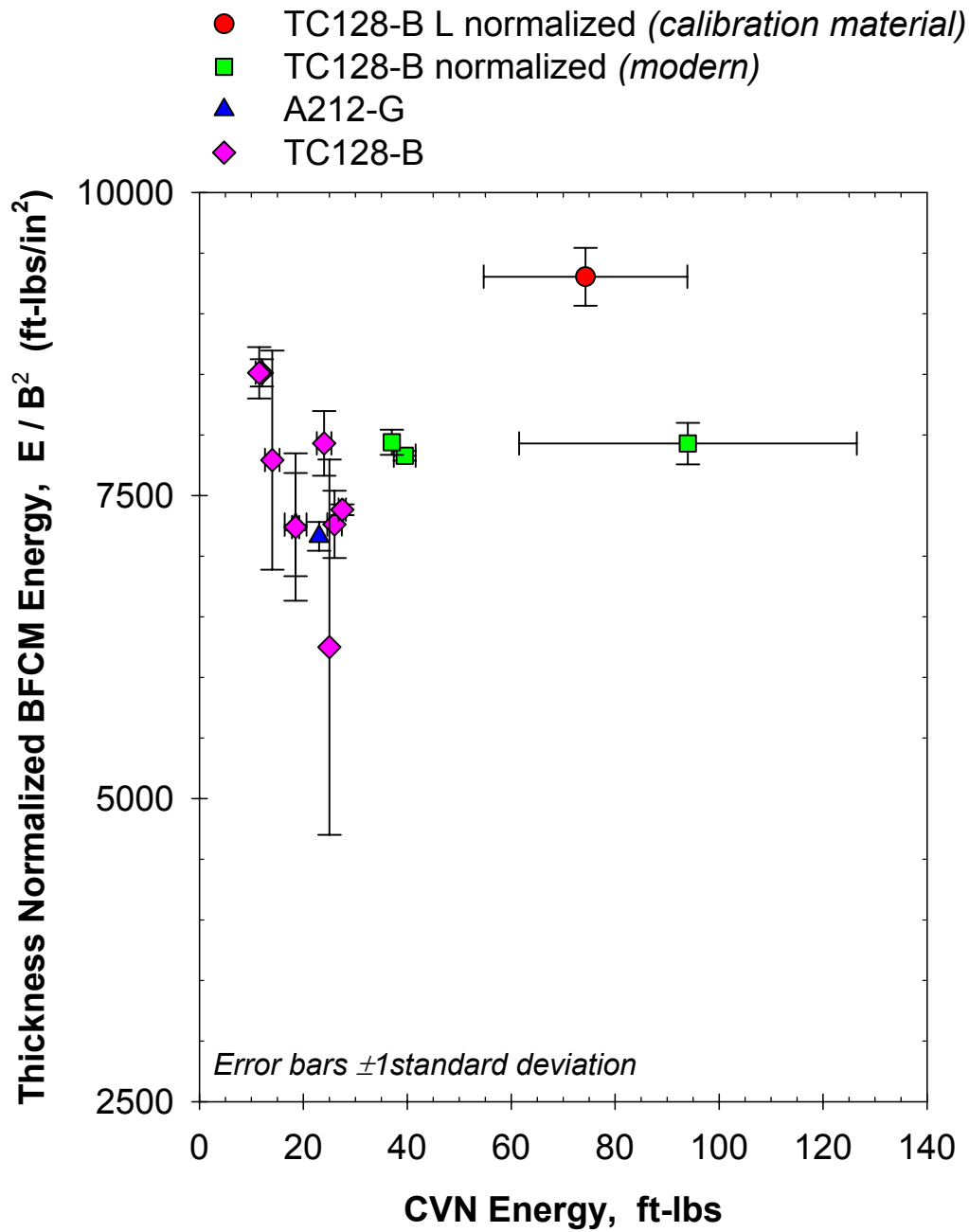


Figure 5-19. Thickness normalized BFCM energy as a function of CVN energy.

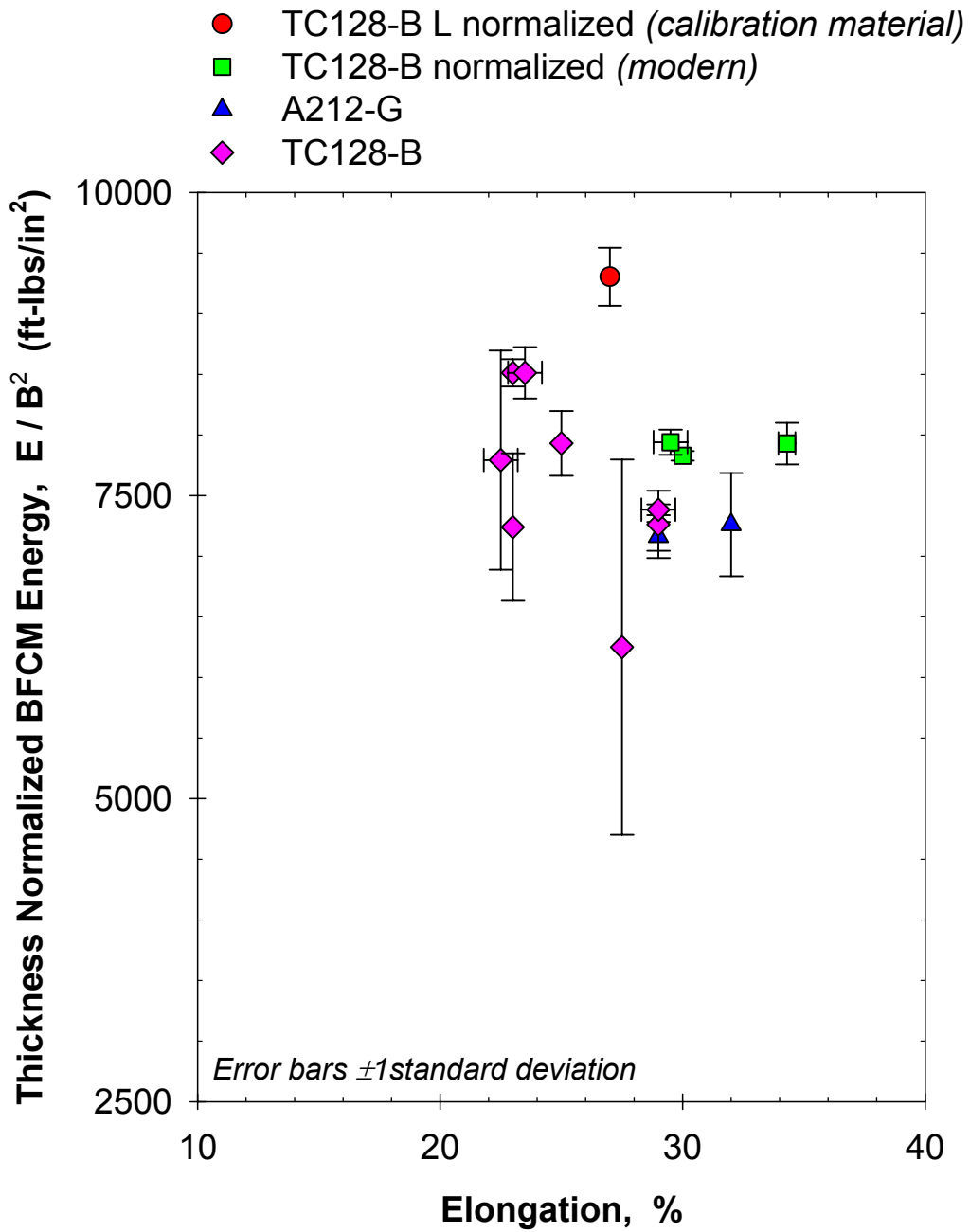


Figure 5-20. Thickness normalized BFCM energy as a function of elongation.

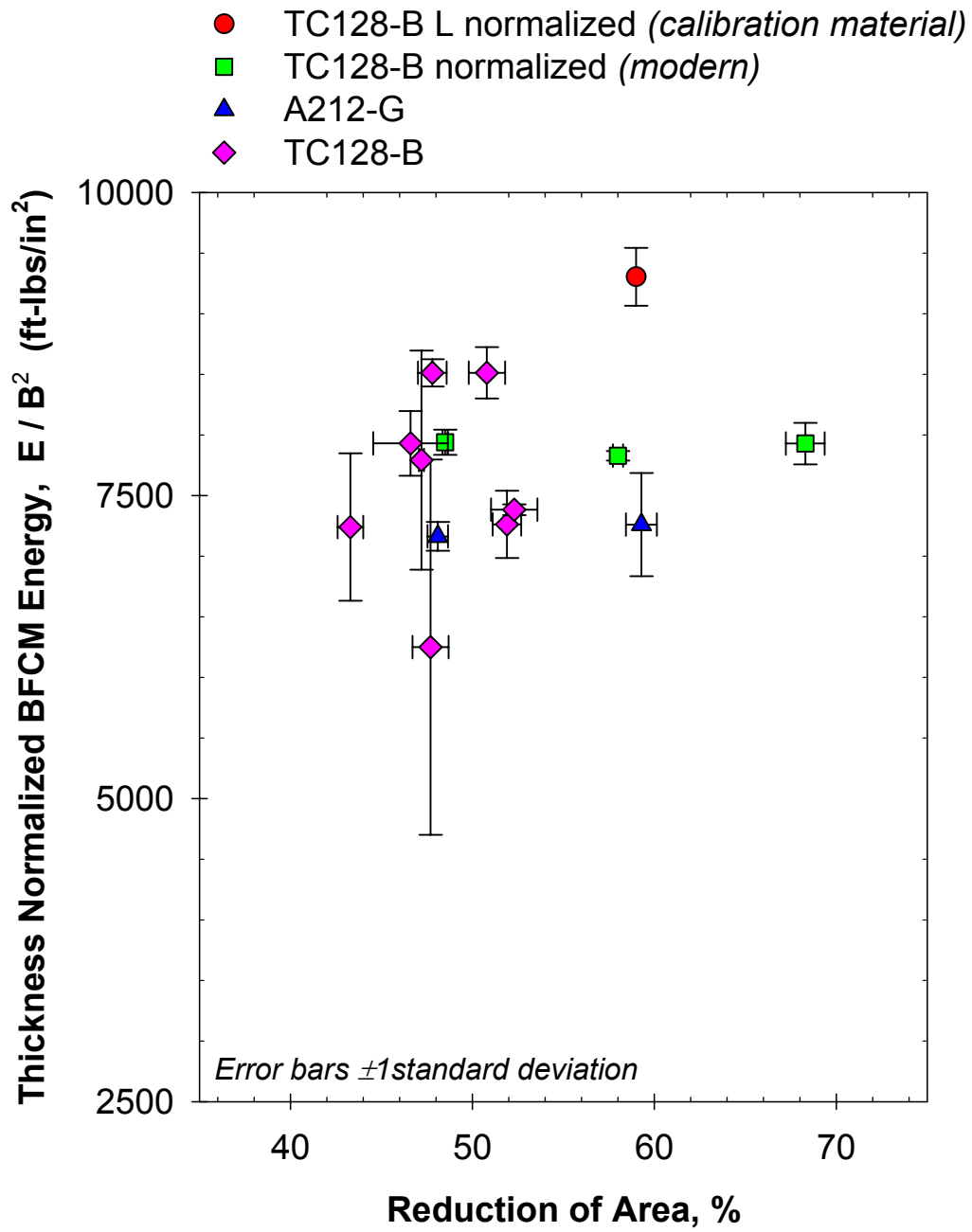


Figure 5-21. Thickness normalized BFCM energy as a function of percent RA.

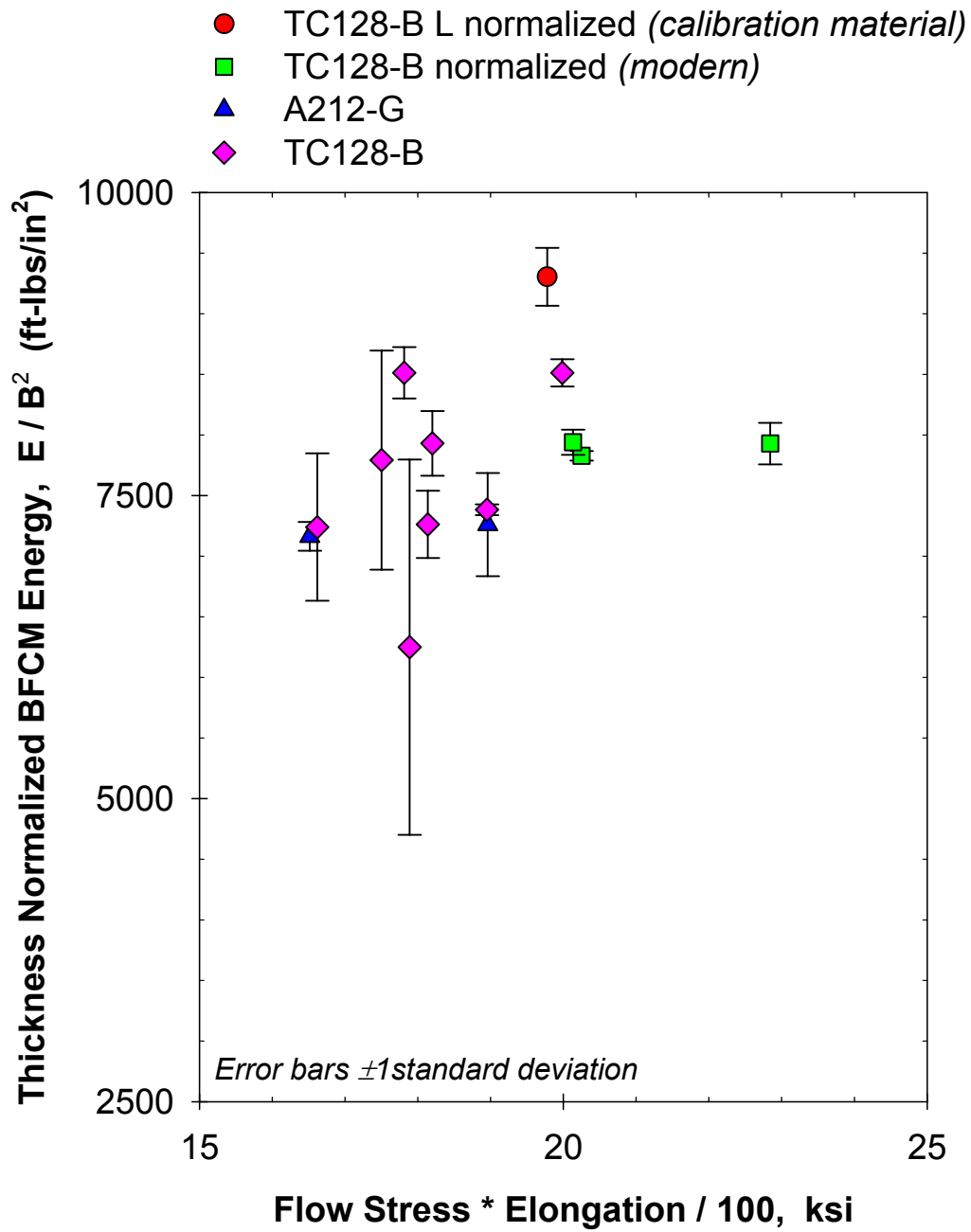


Figure 5-22. Thickness normalized BFCM energy as a function of a quantity proportional to area under the engineering stress-strain curve.

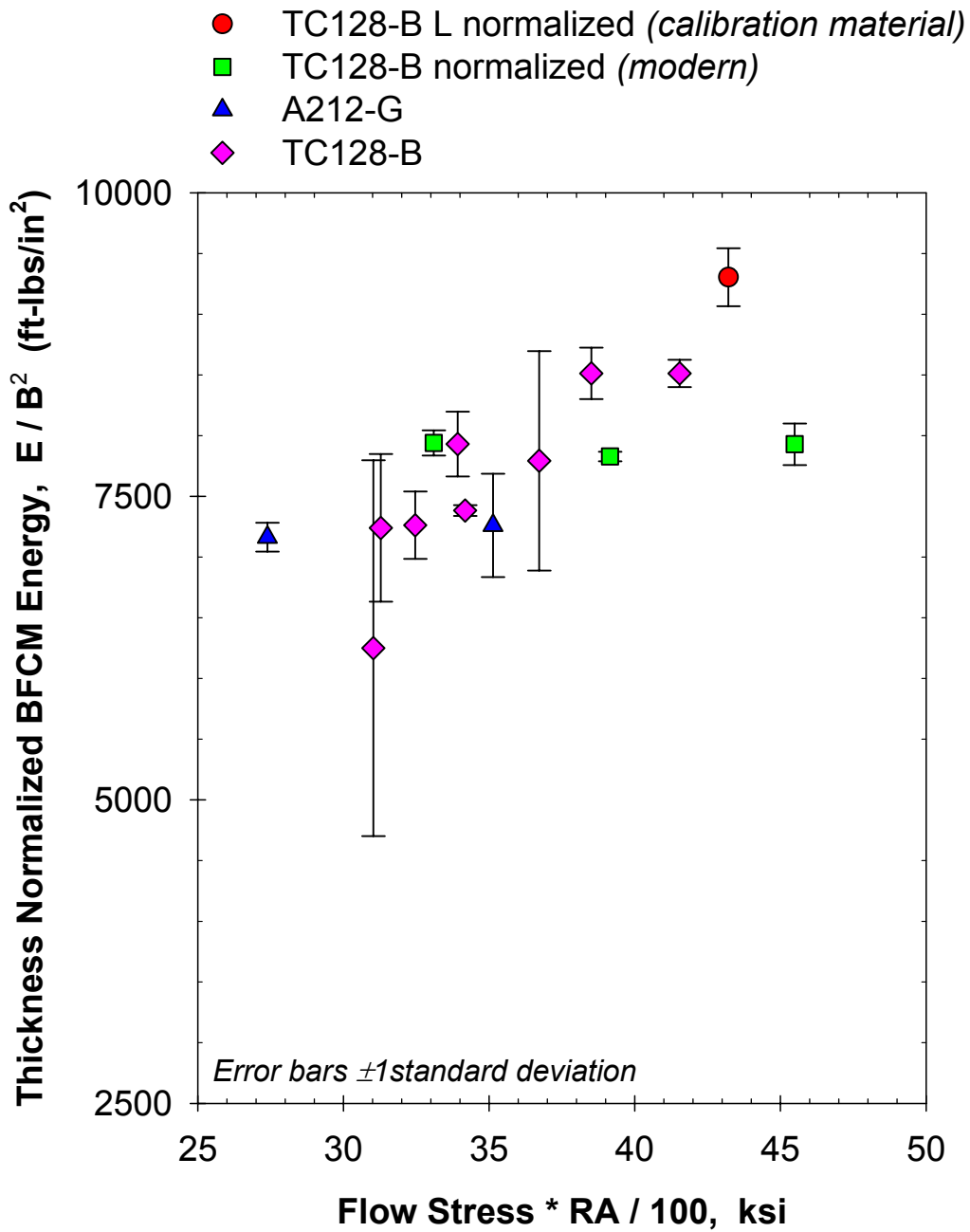


Figure 5-23. Thickness normalized BFCM energy as a function of a quantity proportional to area under the true stress-strain curve.

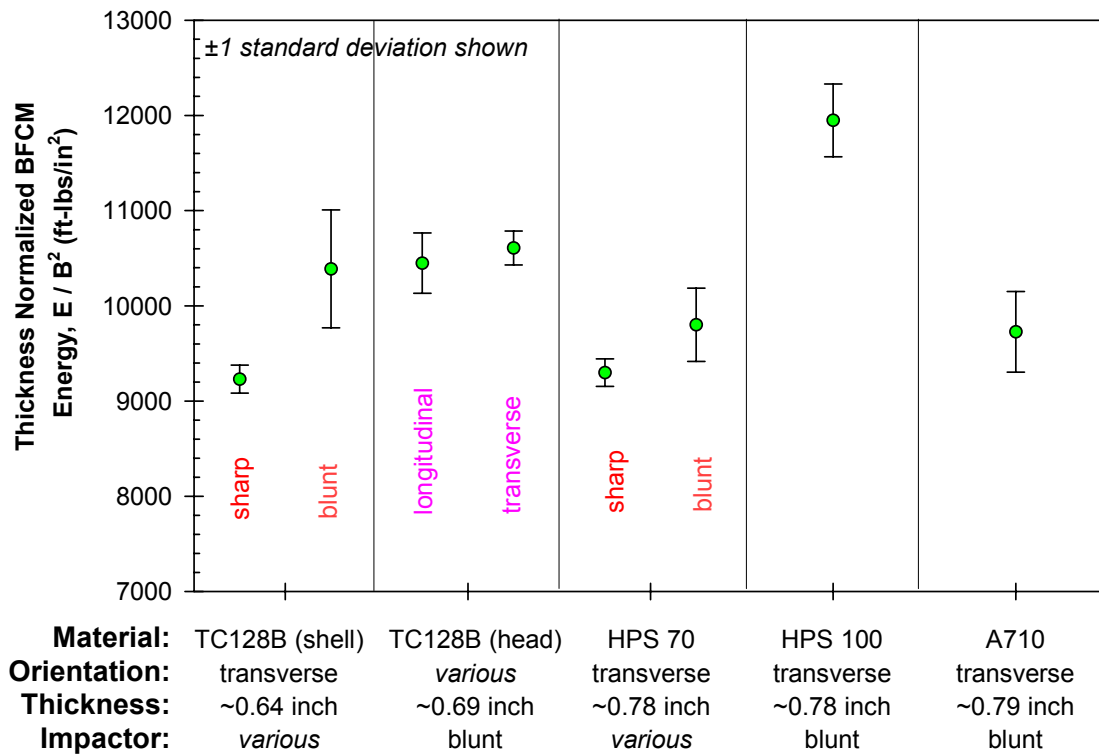
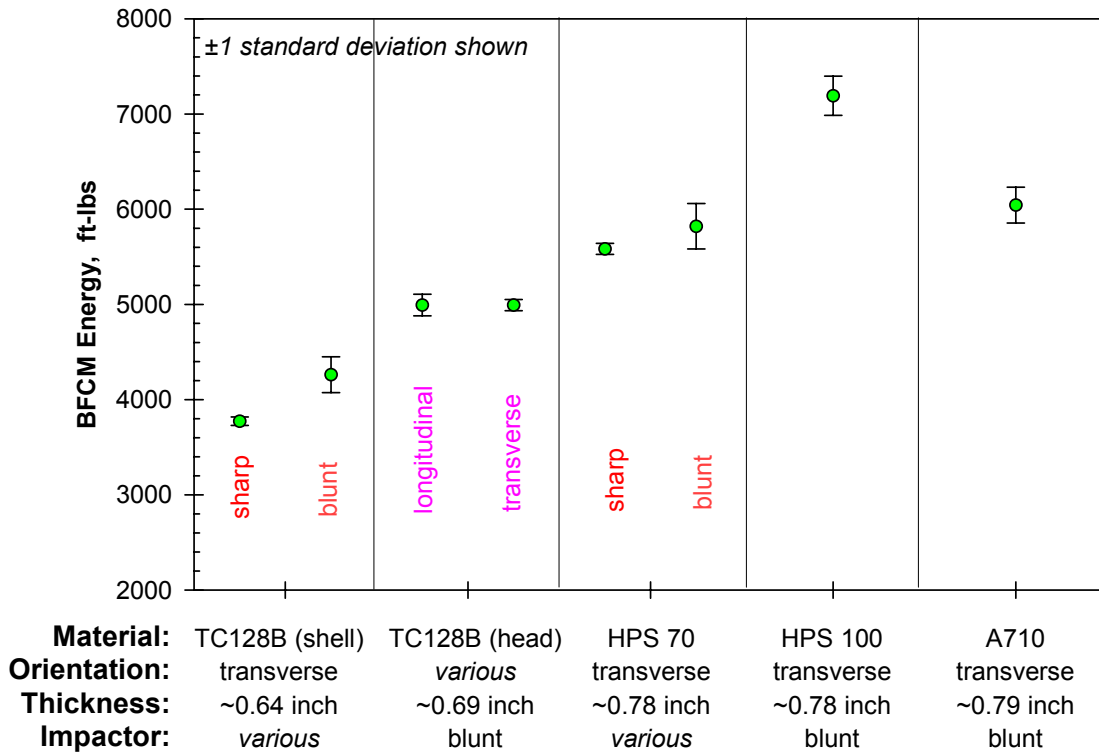


Figure 5-24. Additional comparisons between sharp and blunt tups.

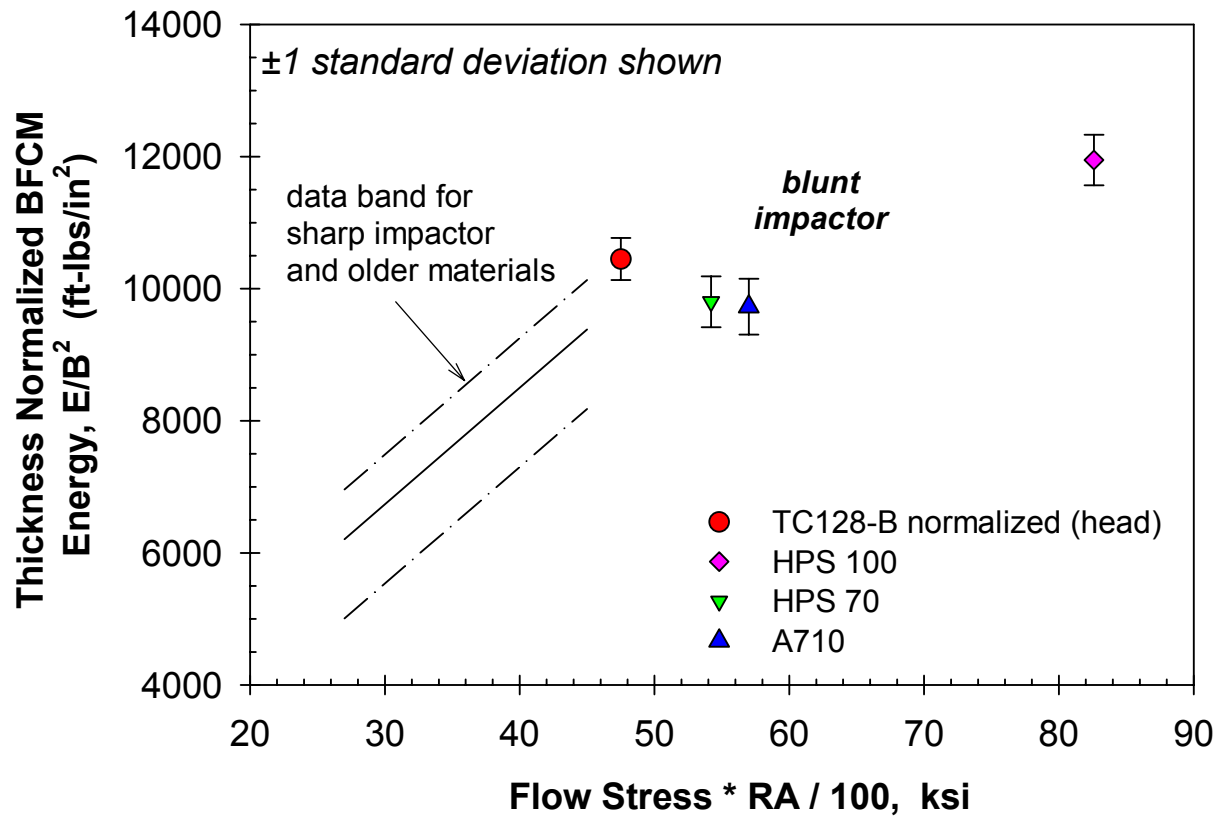


Figure 5-25. Blunt tup results plotted as previously showing a data band for the sharp tup.

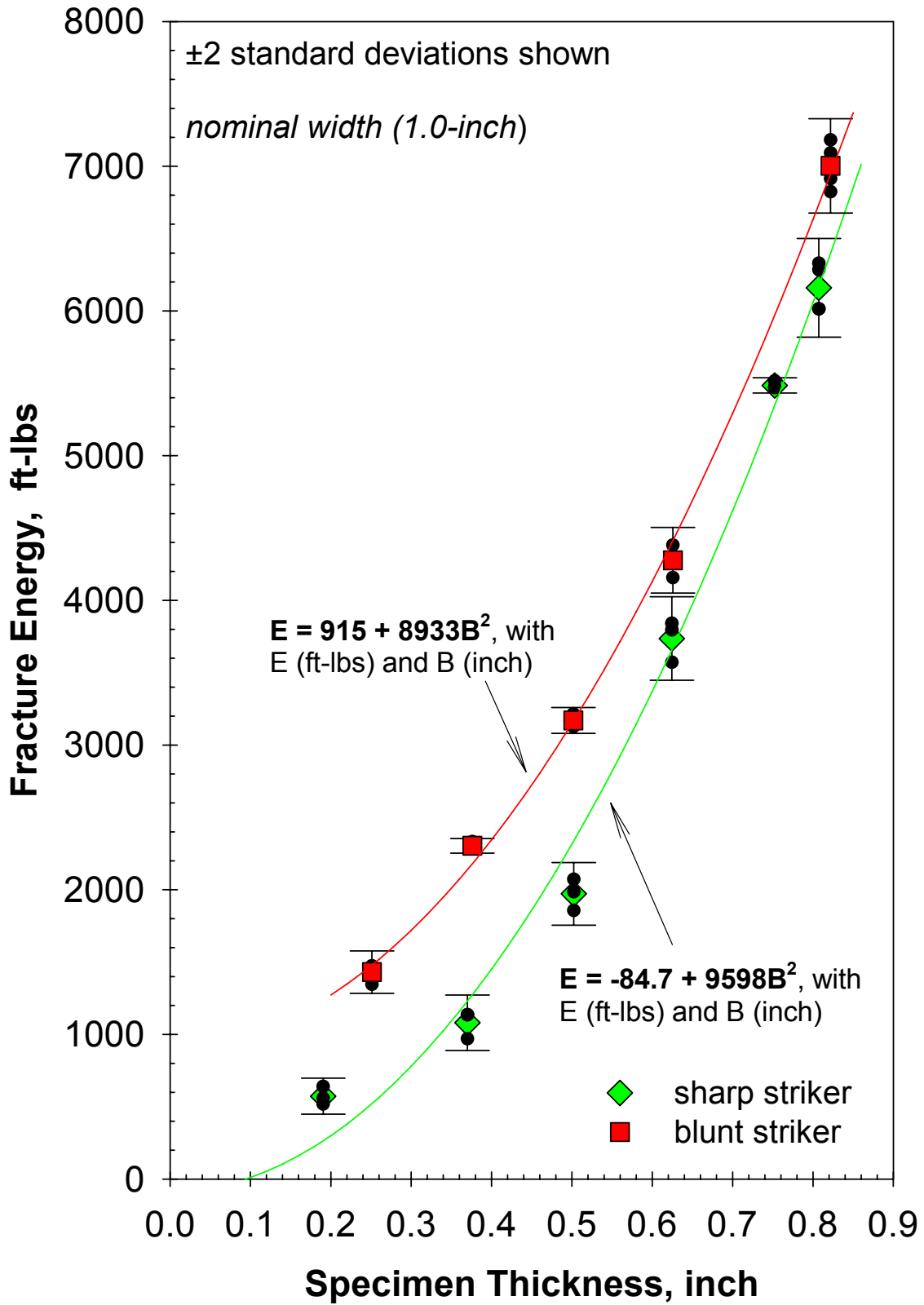


Figure 5-26. Blunt versus sharp striker tup energy results as a function of specimen thickness.



Figure 5-27. Comparison between the specimen that stalled the machine and a failed specimen.

This page intentionally left blank.

6.0 FRACTURE TESTING OF RETIRED VINTAGE MATERIALS

The previous sections of this report have focused on the pedigree of the material and the resulting material properties. The focus of this section of the report is the high rate fracture toughness measurements. These tests represent the most critical testing involved with this program since these tests specifically address the NTSB's concerns described earlier.

6.1 Preliminary Matrix of Conditions

Once the mechanical testing was complete, the program team met and discussed what fracture testing would be performed. There was some hope that the material characterization work might help guide this process. However, as indicated earlier there did not appear to be a transient (time-based) change in tensile, composition, or CVN toughness numbers, given the degree of variability observed. Therefore, the measured properties were not able to be used to directly guide choices for fracture toughness testing. In theory, it would be useful to sample every year available. In practice, this was not possible with the program resources available. Instead, the approach taken (as described earlier) was to classify the fleet in a number of blocks or subsets. In this case, the fleet was broken up into four 25% intervals (in terms of year). Each one of these subsets represents a period of interest.

Budget was available to perform about seventy-five high rate, low temperature fracture tests. Therefore, the test matrix needed to be about this size. Recall that each car condition available typically includes a head and two shell locations. Since the focus was on realistic lower bound conditions, the primary temperature of interest would be 0°F, with a limited amount of interest also in -50°F. Since sampling was minimized, it was believed that assessing the worst-case lower bound toughness at -50°F could mitigate the minimal testing performed by giving a sense of lowest toughness properties in the tail of the distribution. Therefore, the basic matrix of test conditions is shown in Table 6-1.

It is impractical to test all material conditions that are available. Nevertheless, as shown in earlier sections 93% of the fleet is TC128-B with A212-B making up another 4%. It was deemed

sufficient that these two be evaluated since testing these two materials would cover 97% of the fleet. Recall that there are four pre-1989 TC128-B conditions, a post-1989 TC128-B condition (so comparisons could be made to the more modern component of the fleet) and also A212-B. Given these six conditions and the matrix of six tests shown in Table 6-1 as well as two tank cars per condition results in approximately 70 tests. This was the basic approach used to develop the matrix of conditions shown in Table 6-2. Note that spare specimens were also being fabricated to perform additional replicate testing since the decision was made to not perform replicate testing in the nominal matrix of conditions.

In the end, one hundred high rate, low temperature fracture toughness tests were performed. All spare specimens were tested, typically providing replicate test data at 0°F.

6.2 Differences between Current Testing and Previous GATX Minot Testing

The previous GATX Minot tests were used as a model to design the current testing. However, the Minot tests only evaluated a very narrow range of years; the focus herein was to extend the years examined. The Minot fracture tests were also concerned with two conditions: 37°F and 0°F. Testing here, as described earlier, was focused on lower temperatures at higher strain rates.

As will be described in a later section, the desire here was to perform testing at a higher strain rate. Unfortunately, this caused inconsistent behavior in some instrumentation that necessitated using different transducers. Therefore, it was necessary to implement a local load cell by instrumenting the clevis that pin loaded the specimen. The higher rates also resulted in higher order dynamics in the clip gage on the front face of the specimen rendering it useless. To overcome this, a load-line displacement transducer based on eddy current technology was implemented and used. Other than these changes, the methods used and applied are similar to the methods described in the GATX Minot reports [7,8].

6.3 Fracture Toughness Test Specimens

A nominal 2-inch wide fracture toughness specimen, similar to that used in the GATX Minot work, is depicted in Figure 6-1. The specimen used in this study was quite similar, but a small cutout was provided along the crack plane and forward of the load-line to accommodate an eddy current transducer. This cutout is shown in the specimen drawing in Figure 6-2. A chevron was milled into the specimen to promote early crack initiation and ease precracking.

The specimen thickness utilized was the maximum possible with the curved specimens. Flats were milled to maximize thickness. As indicated in Table 6-3, the thickness ranged from 0.35-inch to 0.75-inch. Most specimens, however, were on the order of 0.5-0.6 inch thick.

6.4 Toughness Test Procedures

Testing was nominally performed in accordance with the relevant ASTM E399⁵ test procedure. All testing was performed under high rate (open servo loop) loading conditions. Furthermore, all testing (except preliminary tests evaluating data acquisition and other setup issues) was performed at low temperature in a Styrofoam enclosure shown in Figure 6-3. The temperature controller and Nicolet digital storage oscilloscope (DSO) is also shown in Figure 6-3. All data were recorded on the high speed Nicolet SIGMA 90-8 DSO system.

The instrumentation mounted on the compact tension specimen are evident in Figure 6-4. The compact tension specimen was pin-loaded with a standard fracture mechanics clevis machined oversize to provide a slack adapter. A photograph of the oversize hole and pin arrangement is shown in Figure 6-5. A slack adapter allows the actuator to pick up speed so that when the pins engage the specimen, the actuator rate is constant and at the level necessary to perform the tests. Without a slack adapter, there typically is an initial period of variable (slower) rate. The slack adapter allows higher loading rates to be achieved.

⁵ E399-06: Standard Test Method for Linear-Elastic Plane-Strain Fracture Toughness K_{Ic} of Metallic Materials.

Instrumentation utilized during testing included a load measuring transducer (load cell), displacement gage on the front face of the specimen (clip gage), strain gage on the back face of the specimen, two strain gages mounted on the clevis grips (backup load measurement) and a special eddy current displacement transducer on the load-line of the specimen (see Figure 6-4). Note, too, that the fuzzy wire in Figure 6-4 and Figure 6-6 is a thermocouple welded on the front face of the compact tension specimen. The clevis-mounted strain gage (one of the two) for backup load measurement is also evident by carefully examining Figure 6-6.

Prior to performing a fracture toughness test, the specimen is fatigue cycled to initiate and propagate a crack at the machined chevron notch. These precracking procedures were performed under room temperature and lab air conditions at an applied K_{\max} that did not exceed 16 ksi $\sqrt{\text{in}}$. During precracking, load was shed to keep K_{\max} below the level indicated. Precracking was completed once the crack had grown to a width normalized length a/W in excess of 0.45 (and typically not greater than 0.5).

The specimen was then chilled with liquid nitrogen and a temperature controller prior to testing. It typically would take approximately two hours to cool and stabilize a specimen when starting from room temperature. A number of specimens were typically put in the cold box to increase thermal mass and decrease the time required between specimens. Once cool, fracture testing was then rapidly performed resulting in a fracture similar to that shown in Figure 6-7.

6.5 Preliminary Assessments of High Rate Test Frame Performance

Some preliminary work to prepare for the high rate fracture toughness testing was also performed. First, the dynamic capability demonstrated during the previous Minot-related work was examined. The strain rate applied work during these dynamic fracture toughness tests (computed on the back face of the compact tension specimen) was typically in the range of 0.5-1.0 in/in/sec. The actuator rate achieved during these tests was on the order of 15-20 inch/sec. The plots, shown in Figure 6-8, show the clear relationship between actuator rate (the controlled variable) and the resulting strain and stress intensity factor rates. The empirical relationships

shown in the plots can be used to some extent to control machine performance and achieve specific loading rates.

The obvious key question is: What is the desired strain rate and how much does it matter where it is measured? We know, for example, that the measurement at the back face of the specimen is lower than strain rate at the crack tip. In fact, the “effective stress concentration” at the crack tip is very high. For engineering purposes, we can estimate it as 3x of what is happening on the back face, but this level still is likely conservatively low. What is the strain rate during an accident? Volpe is currently performing work to understand forces and strains in a train accident. Nevertheless, the Volpe program manager for this project provided an estimate of 30-35 in/in/sec [12]. This strain rate range was determined by performing a dynamic simulation and also estimating crack speeds and dent sizes (40 mph, 20-inch dent). Assuming that back face strain is 1/3 of that at the crack tip implies that a good target strain rate is 10 in/in/sec.

Between the GATX Minot work and this current work, the high rate equipment available in the SwRI lab was upgraded to improve the dynamic response and allow testing at a faster rate. The first step of the equipment upgrade concerned modifications to the servovalve assembly. A higher flow 3-stage valve (90 gpm) was installed immediately adjacent to the actuator. Bigger supply hoses were purchased and installed along with larger levels of hydraulic accumulation (2 gallon on the pressure input and 1.5 gallon on the return). The electronic components in the controller related to valve operation were also upgraded and the system tuned in an optimum manner.

The performance of this upgraded frame is indicated in Figure 6-9 and Figure 6-10. The response shown in Figure 6-9 with an initial nonlinear (slower) region is overcome by installing the slack adapter in the load train (see Figure 6-5) to allow the actuator to achieve top speed before loading the specimen. The dynamic response of the frame is further shown in Figure 6-10 indicating the optimum, highest speed of 60 inch/sec. This actuator rate is approximately 3-4x faster than achieved in the Minot work. However, it is about 2-4x slower than the desired 10 in/in/sec.

6.6 Necessity for Backup Load Measurement (Grip Strain Gages)

One consequence of increasing the actuator rate and overall dynamic loading was periodic, poor load cell data. Dynamic effects were not manifested every single test, but when they did occur they rendered the load cell data nearly unusable (without some significant smoothing). An example of this is shown in Figure 6-11. The signal with the large periodic component (pink color) is from the load cell. This type of dynamic effect is not uncommon. For instance, this effect is widely seen when analyzing high rate split Hopkinson pressure bar data derived from strain gages. The dynamic effect is often the result of a stress wave reflecting back and forth along the load train. There are many ways to minimize the impact of this type of transient; one common method is to fit the signal with a Fourier polynomial. Although this smooths the data, the peak load derived from the data is clearly questionable, especially with the magnitude of the harmonic in Figure 6-11.

One way to overcome this dynamic effect is to decrease the length of the load train attached to the load cell. Therefore, an alternate load cell was configured by attaching strain gages to the clevis grip (see Figure 6-6). This alternate load cell was statically calibrated and then used in a dynamic manner during testing. Although the new clevis load cell (denoted grip strain gage) did not entirely eliminate dynamic effects, the data shown in Figure 6-11 clearly indicate that the magnitude of the dynamic component in the grip load cell is small (see black and gray signals in Figure 6-11) and less than 5% peak load near the peak.

Several other examples of dynamic data are indicated in Figures 6-12 and 6-13. In these cases, the dynamic effect of the conventional load cell appears smaller than before, but the effect near the peak appears greater in several instances. This is contrasted to the steady clevis load cell (denoted grip strain gage) data evident in Figures 6-12 and 6-13. The peak load derived from the conventional load cell is approximately 10% higher than that derived from the clevis load cell. Clearly the clevis load cell signal is steadier and more believable than the upper load train mounted conventional load cell.

The resulting load-displacement and load-strain data from the tests in Figure 6-13 are shown in Figure 6-14. In these cases, the load is derived from the grip strain gages (clevis load cell). The resulting load-displacement data derived from the clevis load cell are suitable for standard fracture toughness test analysis software. Incidentally, the dynamic problems associated with the clip gage (measuring front face displacement) are evident from the green traces in Figure 6-14.

6.7 Analysis Methodology for the High Rate Fracture Toughness Test Data

The K_{Ic} fracture test is best suited for brittle, linear-elastic behavior where at maximum load the crack reaches instability and instantaneously tears through the remaining specimen ligament. In practice, however, these conditions are highly dependent upon the actual material behavior and the observed ductility. Conditions can sometimes develop when higher levels of plasticity are observed near the peak applied load. This is indicative of failure where the limit load of the specimen is often reached or exceeded and higher levels of nonlinearity are observed in the load-displacement traces.

During analysis of K_{Ic} fracture tests, the initial portion of the load-displacement diagram is fit and an offset method applied to the data to determine the fracture load used to calculate the K_{Ic} value. However, under high rate loading conditions, the integrity of the load-displacement behavior is often less than optimum (due primarily to dynamic effects from the displacement measurement transducer), hence making this type of analysis approach ineffective and often impossible insofar as yielding meaningful numbers in a consistent manner. Therefore, during this testing the toughness that is reported is a K_{max} toughness corresponding to the applied stress intensity factor calculated using the initial crack length (measured post-test and corresponding to the length at the end of precracking) and the maximum applied load observed during the fracture test. Utilizing the K_{max} approach eliminates applying judgment to less than optimum data and hence minimizes unfair bias creeping into the calculations and results because the occurrence and magnitude associated with the peak load is definitively known. As a cautionary note, it must be remembered that high rate fracture toughness values are not the most accurate measurements;

the price paid in achieving the high rate loading conditions is some data fidelity. The K_{\max} toughness parameter is a structurally relevant measure of fracture behavior.

If any plasticity is occurring, this K_{\max} approach yields a highly conservative (i.e. lower bound) toughness since it does not include any ductile tearing or load-displacement energy that occurred prior to achieving peak load. If, however, the behavior is brittle, the K_{\max} toughness can yield slightly non-conservative results if the upper end of the load-displacement curve has begun to flatten somewhat. This issue, and the implications, will be explored in greater detail in the next chapter.

For conditions when higher levels of non-linearity are evident in the load displacement behavior, an alternative approach can be taken based on the methods described in ASTM E1820⁶ where the area under the load-displacement diagram is used to augment the fracture toughness measurement. The integral steps applied in this approach included:

- calculating a J value where $J = K^2(1-\nu^2)/E + J_{\text{plastic}}$ incrementally at each load-displacement point with $J_{\text{plastic}} = \eta A_{\text{plastic}}/Bb_o$ (see E1820 for definition of terms)
- continuing this process and summing until maximum load to yield a J_{\max} value (J_{\max} can also be converted to the “equivalent” linear-elastic parameter $K_{J_{\max}} = [J_{\max}E/(1-\nu^2)]^{0.5}$).

This approach yields an alternate engineering method for quantifying toughness assuming that the crack has not advanced by the peak applied load. It allows for including the influence of load-displacement nonlinearity before peak load. A key assumption is that negligible tearing has occurred at peak load, though.

6.8 High Rate Fracture Toughness Test Data

The raw and processed test data for the 100 fracture toughness tests performed during this program are detailed in Appendix A of this report. In this Appendix, two plots are shown: a time history plot showing each transducer recorded during the test and the resulting load-displacement

⁶ E1820-06: Standard Test Method for Measurement of Fracture Toughness.

and load-strain trace from the data. Two typical examples of for brittle and ductile behavior are shown in Figures 6-15 and 6-16, respectively. In the case of the first test (79a-SB-2 in Figure 6-15), the test was performed at -50°F whereas the second test (74b-SA-3 in Figure 6-16) was at 0°F. In the case of the first test (Figure 6-15), observed crack opening displacement (COD, measured on the load-line) is less than 10 mils. This is contrasted to the more ductile second case where maximum crack opening displacement is in excess of 100 mils.

The test data for each experiment are shown for the six subsets of materials examined in this program and shown in Tables 6-4 through 6-8. Although these tables are detailed and somewhat “busy”, the essence of each test is summarized in this tabular format. The quantities included in Tables 6-4 through 6-8 are further described below:

- *Rate* – Measured actuator rate derived from the recorded LVDT signal
- *ε rate* – Measured strain rate derived from the strain gage mounted on the back face of the C(T) specimen (it should be noted that the crack tip strain rate will be higher than this arbitrary measured level)
- *Krate* – Applied stress intensity rate derived from the observed load rate and the relevant K-calibration for the C(T) specimen. This quantity was calculated over typically the 10-75% region of the load-displacement response
- *Compl Ratio* – Ratio of the measured compliance with the theoretical compliance for that crack length (all load-line compliances). These two quantities should typically be within $\pm 10\%$ (0.9-1.1). The measured compliance was calculated over the region that corresponds to the best linearity in the signal
- *Limit Ratio* – Ratio of the maximum observed load to the plane-stress limit load of the C(T) specimen (a value greater than unity suggests that limit load for the specimen was exceeded)
- *Kmax* – Maximum applied stress intensity factor assuming no crack advance and based on the peak load observed in the fracture test
- *Percent Plastic J* – percent of J_{\max} due to the area under the load-displacement trace (a percent plastic J of 0 implies a linear elastic test)
- *Jmax* – calculated J_{\max} from test start to maximum applied load using the analysis procedure described previously (this analysis accounts for enhanced plasticity and ductile fracture)

- *KJmax* – conversion of J_{\max} value to the linear elastic equivalent using the conventional $[J_{\max}E / (1-\nu^2)]^{1/2}$
- *KJ/Kmx Ratio* – ratio between $K_{J_{\max}}$ and K_{\max} which, similar to percent plastic J, is indicative of the degree of ductile fracture observed (values >1 indicate that the area under the load-displacement curve contributed to higher toughness levels).

The tests that exhibited brittle behavior do not have any values indicated to the right of K_{\max} in Tables 6-4 through 6-8. Conversely, those that had nonlinearity in their load-displacement trace have the rightmost portion of Tables 6-4 through 6-8 filled in.

6.9 Fracture Surfaces

Some typical fracture surfaces are indicated in Figures 6-17 through 6-20. Two views are shown for each fracture surface. The top view is a straight-on top view whereas the bottom is a more isometric view. Both are useful for understanding images and features on fracture surfaces.

The three indicated in Figure 6-17 are A212-B specimens. Fracture behavior appeared fairly featureless, smooth and without shear lips in 65a-HA-2 and 66c-SA-1. This is contrasted to a higher energy fracture in 66c-HA-1 with splitting through-the-thickness and a rougher, more wood-like fracture surface. Note, too, the extent of through-thickness displacement and necking in the sample on the lower left of Figure 6-17.

Four examples of post-1989 normalized TC128-B fractures are shown in Figure 6-18. The two specimens on the right-hand side are both brittle failures with featureless fracture surfaces and little ductility at -50°F. The two photographs on the right side, however, exhibit higher energy ductile fracture with plasticity and shear lips evident. In both cases the initiation site at the end of the crack tip can be traced to near mid-thickness by following the flow lines back to the origin of fracture.

Different vintage TC128-B materials are included in Figures 6-19 and 6-20. In general, the woodier specimens tend to exhibit a rougher fracture surface, through-thickness splitting and

higher levels of ductility. All of these features likely contribute to a higher toughness. The variety observed in TC128-B is no more apparent than for the bottom two fracture surfaces in Figure 6-20. The fracture on the left is nearly a classic featureless, flat and brittle “plane strain” fracture whereas the one on the right is rough, with significant through-thickness splitting (which consumes energy) and significant dimple formation and necking apparent.

6.10 Fracture Toughness Variation of TC128-B with Date of Fabrication

In an attempt to understand toughness variation with time, the TC128-B dynamic fracture toughness is plotted as a function of material condition in Figure 6-21. In a given test, if no plasticity was evident, the K_{max} toughness is plotted; whereas in the case of nonlinearity, K_{Jmax} is plotted. Not surprisingly, the level of scatter tends to obscure any definitive findings. However, several observations are apparent. Before making these observations, though, it is worth revisiting reference [6] in the context of understanding toughness magnitudes. In this document, Anderson and McKeighan lay out criteria for interpreting these results. The classifications for the different toughness magnitudes include:

- 25-50 $\text{ksi}\sqrt{\text{in}}$ – poor toughness
- 50-100 $\text{ksi}\sqrt{\text{in}}$ – adequate toughness
- 100-200 $\text{ksi}\sqrt{\text{in}}$ – good toughness
- >200 $\text{ksi}\sqrt{\text{in}}$ – excellent toughness.

Given these ranges, the vast majority of the data in Figure 6-21 fall into the adequate or good category. A limited number of samples fall into the poor magnitude, but these are mostly confined to lowest (-50°F) temperature results. A cursory examination of Figure 6-21 suggests no clear trend in toughness. However, a closer examination of the data does appear to suggest that the newest 50% of the fleet tends to exhibit slightly lower toughness than the oldest 50%. This is especially true in the Subset C period of the data and to a lesser extent during Subset D. The logical question that should be asked is whether this program has sufficient sampling to draw this conclusion. This is certainly an open issue worthy of debate. Keep in mind the

engineering approach used. In a sense, the study performed is a screening study that could potentially suggest that more sampling is necessary.

The data contained in Tables 6-4 through 6-8 and plotted in Figure 6-21 can be further analyzed. For example, consider the following observations concerning the pre-1989 TC128-B material:

- Subset A – 100% of 0°F tests exhibit adequate or better toughness, 50% of -50°F tests exhibit adequate or better toughness
- Subset B – 100% of 0°F tests exhibit adequate or better toughness, 83% of -50°F tests exhibit adequate or better toughness
- Subset C – 58% of 0°F tests exhibit adequate or better toughness, 33% of -50°F tests exhibit adequate or better toughness
- Subset D – 83% of 0°F tests exhibit adequate or better toughness, 83% of -50°F tests exhibit adequate or better toughness.

Considering the two other materials, along similar lines the following can be observed:

- Post-1989 TC128-B (normalized) – 100% of 0°F tests exhibit adequate or better toughness, 80% of -50°F tests exhibit adequate or better toughness
- A212-B – 67% of 0°F tests exhibit adequate or better toughness, 25% of -50°F tests exhibit adequate or better toughness.

There is no question that all materials involved in this program can clearly exhibit good or excellent toughness levels. Nevertheless, the extent of scatter observed in toughness level is fairly large. What is concerning is that with a modest number of specimens and fairly sparse sampling, this program has managed to yield toughness data with unacceptably low levels of toughness. This observation is an especially nagging concern in the context of the few samples that have been tested for a given subset of the tank car fleet.

6.11 Global Averages for Fleet Subsets

Yet another way to look at these data is in a global sense, examining the statistics associated with each subset of material. Recall that the subsets examined different vintage pre-1989 TC128-B, post-1989 normalized TC128-B or A212-B. Averages and standard deviations can then be compared and contrasted. The relevant statistical data is provided in Table 6-9 and plots of these data supplied in Figures 6-22 and 6-23. Note that the difference between Figure 6-22 and Figure 6-23 is different temperatures; 0°F and -50°F, respectively. The histogram at the top of the toughness plot provides a sense of the number of samples associated with each condition. Note also that the bars represent only ± 1 standard deviation.

There is no question that for TC128-B material subset A and B (the oldest 50% of the fleet), the global average behavior at 0°F is of a higher magnitude toughness than observed in the youngest 50% of the fleet. This is counter-intuitive and suggests that the newer vintage fleet is not as tough as the older vintage fleet. Nevertheless, the broad standard deviations clearly suggest that the toughness variability is too high to conclude that this is a statistically significant finding.

The data in Figure 6-22 at 0°F also shows that the poorest performing material is the A212-B. Average toughness values are lower than observed in any of the other materials and the lower bound levels also the lowest when taking into account variability. Clearly any type of TC128-B outperforms the A212-B material. The wide variability and low average also suggests that a large percentage of the A212-B fleet will exhibit “poor” toughness levels.

One advantage with the post-1989 normalized TC128-B is that the apparent variability in toughness appears less than with the older vintage TC128-B. Although the average toughness observed with the newer vintage, normalized material is not significantly different from the pre-1989 fleet (the averages are actually less than observed in the older 50% of the fleet), the smaller standard deviation band means that the lower bound toughness when subtracting 2 standard deviations still is in excess of 50 ksi $\sqrt{\text{in}}$. This suggests that the post-1989 normalized material outperforms all other materials or conditions in Figure 6-22.

Material performance in Figure 6-23 for -50°F is generally poor with low average values. The sample size is small too, and this presumably influences the standard deviation bands indicated. A similar trend is observed as with the 0°F data though, with higher average toughness for the oldest half of the fleet when compared to the younger half. On balance, the best behaving material at -50°F is the post-1989, normalized TC128-B. However, it is clear that if the error bar were extended to ± 2 standard deviations, the range would dip below 50 ksi $\sqrt{\text{in}}$ and into the poor toughness regime.

6.12 Toughness Correlations

Increasing sulfur content acts to reduce fracture toughness on the upper shelf according to Anderson and Kirkpatrick [10]. In reference [10], the plot shown in Figure 6-24(a) is shown depicting the GATX Minot Charpy toughness data at +50°F. If the pre-1989 data points are removed from this plot, a clear trend is observable of increasing Charpy toughness as sulfur content decreases. Nevertheless, a similar trend is clearly not evident with the 0°F data shown in Figure 6-24(b). Undoubtedly, some of the lower toughness data points are not on the upper shelf, but the majority in excess of certainly 100 ksi $\sqrt{\text{in}}$ likely are. If data only in excess of this level is considered in Figure 6-24(b), the trend is the opposite direction: increasing toughness with increasing sulfur content. In summary, the data generated and plotted in Figure 6-24 does not support the argument that lower sulfur content increases toughness.

In the last chapter of this report where the BFCM data was presented, correlations between BFCM energy and different mechanical properties were shown. The most promising relationship seemed to be an increase in BFCM energy and area under the stress-strain curve, represented by the product of flow stress and reduction of area. There was not a clear link between BFCM energy and CVN energy. However, the data measured and shown in Figure 6-25 suggests little or no correlation between BFCM energy and fracture toughness. However, any possible relationship might be masked by the scatter observed in the fracture toughness testing. In addition, the 80°F BFCM energies are compared with 0°F toughness tests (clearly not an optimum comparison).

CVN energy is related to K_{\max} or $K_{J\max}$ toughness in Figure 6-26 for high rate loading conditions at 0°F and -50°F. Also shown on the plot are the results from both of the GATX Minot studies, references [7] and [8], and the regression detailed therein. As expected, as CVN energy increases so does the high rate fracture toughness. For reference, the measured toughness data for TC128-B does exceed the lower bound Roberts-Newton relationship [12]. This relation, developed for lower shelf or transition behavior, is indicated in Figure 6-26 and described by Barsom and Rolfe [13]. The Roberts-Newton relationship continues to perform a reasonable job as a *lower bound* estimate of fracture toughness even though there are some data that lie beneath the curve. In fact, the Roberts-Newton relationship does an excellent job of representing toughness data less than 75 ksi $\sqrt{\text{in}}$ or less than 30 ft-lbs CVN energy. According to Figure 3-6 (NTSB Minot CVN data), energies less than 30 ft-lbs are in the transition or lower shelf for 11 of 13 materials.

Table 6-1. Basic test matrix for high rate fracture toughness testing of a given car condition.

Material Source	Test Temperature	
	lowest (-50°F)	intermediate (0°F)
head	1 test	1 test
shell – “A” position	1 test	1 test
shell – “B” position	1 test	1 test

Table 6-2. Test plates and compact-tension specimen required for high rate fracture testing.

Material Source and Description	Tank Car ID No.	Car Builder	Build Year	Piece ID No.	No of C(T)'s
TC128B-Subset A <i>(oldest fleet quartile)</i>	GATX 97833	GATX	1966	66b-SA	2 + 1 spare
	GATX 55905	GATX	1966	66a-SA	2 + 1 spare
				66a-HA	2 + 1 spare
PROX 89773	Union	1968	68b-SA 68b-SB 68b-HA	2 + 1 spare 2 + 1 spare 2 + 1 spare	
TC128B-Subset B <i>(2nd oldest fleet quartile)</i>	UTLX 28744	Union	1974	74b-SA 74b-HA	2 + 1 spare 2 + 1 spare
	TGAX 331007	ACF	1975	75a-SA 75a-HA	2 + 1 spare 2 + 1 spare
	GATX 47814	GATX	1976	76b-SA(F) 76b-SA(A)	2 + 2 spare 2 + 2 spare
TC128B-Subset C <i>(2nd youngest fleet quartile)</i>	CGTX 64270	Hawk-Sid	1978	78b-SA 78b-HA	2 + 1 spare 2 + 1 spare
	GATX 49248	GATX	1977	77a-SA(D)	2 + 2 spare
	GAMX 4115	ACF	1979	79a-SA	2 + 1 spare
79a-SB				2 + 1 spare	
79a-HA				2 + 1 spare	
TC128B-Subset D <i>(youngest fleet quartile)</i>	PROX 83469	Procor	1980	80a-SA 80a-HA	2 + 1 spare 2 + 1 spare
	HOKX 8373	ACF	1981	81a-SB	2 + 1 spare
	HOKX 8453	GATX	1982	82a-SA	2 + 1 spare
82a-SB				2 + 1 spare	
82a-HA				2 + 1 spare	
TC128B-normalized <i>(new material)</i>	PROX 31153	Procor	1994	94a-SA	2 + 2 spare
				94a-SB	2 + 2 spare
94a-HA				2 + 1 spare	
	PROX 31218	Procor	1994	94b-SA	2
				94b-HA	2
A212-B <i>(older material)</i>	GATX 9746	GATX	1965	65a-HA 65a-SA	2 + 1 spare 2 + 1 spare
	CGTX 63699	GATX	1966	66c-SA	2
66c-HA				2	

Table 6-3. Matrix of test specimen ID number, date tested, specimen dimensions and flow stress.

spec ID No.	test temp, °F	test date	W, inch	B, inch	crack len a, inch	σflow, ksi
65A-HA -1	0	5/17	2.001	0.358	1.018	66.1
65A-HA -2	-50	5/22	2.001	0.356	1.013	
65A-HA -3	0	6/3	2.002	0.356	1.017	
65A-SA -1	0	5/23	2.001	0.408	1.018	59.2
65A-SA -2	-50	5/22	2.001	0.407	1.013	
65A-SA -3	0	6/3	2.002	0.408	0.995	
66A-HA -1	0	5/24	1.998	0.591	1.012	72.9
66A-HA -2	-50	5/24	1.999	0.591	1.073	
66A-HA -3	0	6/1	2.001	0.590	1.021	
66A-SA -1	0	5/17	1.999	0.617	1.032	75.2
66A-SA -2	-50	5/22	2.000	0.617	0.990	
66A-SA -3	0	6/1	2.000	0.616	1.018	
66B-SA-1	0	6/3	1.992	0.620	1.000	70.2
66B-SA-2	-50	5/21	1.984	0.620	1.000	
66B-SA-3	0	5/16	1.993	0.621	1.006	
66C-HA-1	0	5/23	2.002	0.746	1.023	63.9
66C-HA-2	-50	5/22	2.002	0.742	1.036	
66C-SA-1	0	5/23	2.001	0.749	1.043	56.9
66C-SA-2	-50	5/22	2.002	0.750	1.039	
68B-HA-1	0	5/23	2.000	0.630	1.005	
68B-HA-2	-50	5/22	2.002	0.630	1.008	
68B-HA-3	0	6/1	2.002	0.630	1.015	
68B-SA-1	0	5/17	2.001	0.594	1.020	62.6
68B-SA-2	-50	5/22	2.000	0.594	0.992	
68B-SA-3	0	6/1	1.997	0.595	0.993	
68B-SB-1	0	5/24	2.001	0.620	0.990	65.4
68B-SB-2	-50	5/24	2.001	0.620	1.001	
68B-SB-3	0	6/1	1.998	0.620	0.993	
74B-HA-1	0	5/23	2.003	0.752	1.023	67.1
74B-HA-2	-50	5/23	2.002	0.753	1.032	
74B-HA-3	0	6/1	2.000	0.752	1.020	
74B-SA-1	0	5/23	1.999	0.695	1.020	65.0
74B-SA-2	-50	5/24	2.002	0.696	1.010	
74B-SA-3	0	6/3	2.000	0.695	1.019	
75A-HA-1	0	5/23	2.000	0.594	1.006	77.7
75A-HA-2	-50	5/22	2.002	0.594	0.995	
75A-HA-3	0	6/1	1.997	0.594	0.992	
75A-SA-1	0	5/23	2.002	0.546	1.007	86.9
75A-SA-2	-50	5/22	2.001	0.549	1.002	
75A-SA-3	0	6/3	2.000	0.552	1.002	
76B-SA-1	0	5/17	2.004	0.493	1.017	70.5
76B-SA-2	-50	5/21	2.001	0.493	1.017	
76B-SA-3	0	6/4	2.002	0.490	1.000	
76B-SA-4	0	6/1	2.000	0.491	1.019	
76B-SF-1	0	5/24	2.002	0.493	0.994	71.8
76B-SF-2	-50	5/24	2.001	0.493	1.002	
76B-SF-3	0	6/3	2.001	0.494	1.001	
76B-SF-4	0	6/4	2.001	0.494	1.015	
77A-SD-1	0	6/4	2.002	0.491	1.005	67.5
77A-SD-2	-50	5/22	2.001	0.491	0.999	
77A-SD-3	0	6/3	1.999	0.491	1.004	
77A-SD-4	0	5/16	2.003	0.491	1.013	

spec ID No.	test temp, °F	test date	W, inch	B, inch	crack len a, inch	σflow, ksi
78B-HA -1	0	5/23	1.999	0.602	1.019	76.5
78B-HA -2	-50	5/24	1.999	0.601	1.035	
78B-HA -3	0	6/1	1.998	0.6025	1.035	
78B-SA -1	0	5/17	1.996	0.6225	1.026	87.3
78B-SA -2	-50	5/21	1.999	0.6125	1.011	
78B-SA -3	0	5/30	1.997	0.622	1.018	
79A-HA-1	0	5/23	2.005	0.725	1.015	78.4
79A-HA-2	-50	5/24	2.000	0.724	1.023	
79A-HA-3	0	5/30	2.000	0.725	1.015	
79A-SA-1	0	5/17	2.003	0.695	1.030	75.8
79A-SA-2	-50	5/21	2.003	0.704	1.021	
79A-SA-3	0	5/30	2.002	0.702	1.020	
79A-SB-1	0	5/16	1.999	0.704	1.030	77.8
79A-SB-2	-50	5/18	1.998	0.704	1.041	
79A-SB-3	0	5/30	1.996	0.704	1.025	
80A-HA-1	0	5/16	2.000	0.727	1.017	67.5
80A-HA-2	-50	5/18	2.002	0.727	1.016	
80A-HA-3	0	5/30	1.997	0.727	1.010	
80A-SA-1	0	5/17	2.001	0.704	1.019	68.5
80A-SA-2	-50	5/22	1.998	0.702	1.014	
80A-SA-3	0	5/30	2.001	0.704	1.012	
81A-SB-1	0	5/16	2.003	0.695	1.012	87.9
81A-SB-2	-50	5/21	2.001	0.695	1.029	
81A-SB-3	0	5/30	2.002	0.696	1.021	
82A-SB-1	0	5/16	2.001	0.742	1.016	72.2
82A-SB-2	-50	5/18	2.000	0.747	1.035	
82A-SB-3	0	5/30	1.999	0.745	1.010	
82A-HA-1	0	5/16	1.999	0.726	1.002	80.6
82A-HA-2	-50	5/21	1.999	0.724	1.024	
82A-HA-3	0	5/30	2.001	0.725	1.005	
82A-SA-1	0	5/18	1.999	0.746	1.036	72.8
82A-SA-2	-50	5/18	1.997	0.752	1.038	
82A-SA-3	0	5/30	2.000	0.746	1.034	
94A-SB1	0	5/16	2.003	0.546	1.015	66.6
94A-SB-2	-50	5/21	2.002	0.549	1.005	
94A-SB-3	0	5/30	2.001	0.548	1.001	
94A-SB-4	0	5/2	2.002	0.546	1.009	66.9
94A-HA-1	0	5/16	1.995	0.594	1.023	
94A-HA-2	-50	5/18	2.001	0.594	1.021	
94A-HA-3	0	5/30	2.001	0.594	1.012	
94A-SA-1	0	5/17	2.000	0.549	1.016	67.5
94A-SA-2	-50	5/22	2.002	0.547	0.991	
94A-SA-3	0	5/30	2.001	0.549	1.003	
94A-SA-4	0	6/4	1.998	0.546	1.008	
94B-HA-1	0	5/24	2.001	0.594	1.009	67.0
94B-HA-2	-50	5/24	2.000	0.594	1.009	
94B-SA-1	0	5/16	1.999	0.547	1.017	68.2
94B-SA-2	-50	5/22	2.003	0.547	1.000	

Table 6-4. Tabulated fracture toughness test results for the different test conditions evaluated.

Matl Source	Build Year	Spec ID No.	Test Temp	Rate, in/sec	ϵ rate, in/in/sec	Krate, ksi $\sqrt{\text{in}}$ /sec	Compl Ratio	Limit Ratio	Kmax, ksi $\sqrt{\text{in}}$	Percent Plastic J	Jmax, ksi-in	KJmax, ksi $\sqrt{\text{in}}$	KJ/Kmx Ratio
TC128-B Subset A	1966	66b-SA-3	0°	59.1	2.66	84K	1.01	1.01	83.1	<0	-	-	-
		66b-SA-1	0°	57.8	3.33	103K	0.96	0.96	79.7	<0	-	-	-
		66b-SA-2	-50°	55.4	1.84	54K	1.13	0.55	45.9	<0	-	-	-
	1966	66a-SA-1	0°	57.1	2.58	82K	1.10	0.94	82.0	73	0.754	158	1.92
		66a-SA-3	0°	61.5	2.31	71K	1.09	0.85	75.0	<0	-	-	-
		66a-SA-2	-50°	60.4	2.55	97K	1.20	0.53	47.5	<0	-	-	-
		66a-HA-1	0°	59.0	3.16	90K	n/a	1.30	111.4	<0	-	-	-
		66a-HA-3	0°	61.1	3.70	102K	1.06	1.32	112.5	<0	-	-	-
		66a-HA-2	-50°	55.0	2.11	58K	1.08	0.75	61.8	<0	-	-	-
	1968	68b-SA-1	0°	57.4	3.32	93K	1.07	1.47	107.6	60	0.871	170	1.57
		68b-SA-3	0°	60.7	3.06	86K	1.03	1.54	115.1	37	0.638	145	1.26
		68b-SA-2	-50°	55.7	2.80	82K	1.13	0.84	62.8	46	0.222	86	1.36
		68b-SB-1	0°	57.5	2.95	85K	1.07	1.35	105.8	39	0.558	136	1.28
		68b-SB-3	0°	62.4	3.63	110K	1.08	1.37	107.1	57	0.802	163	1.52
		68b-SB-2	-50°	52.4	2.91	85K	1.10	1.30	101.3	62	0.819	164	1.62
		68b-HA-1	0°	58.9	3.51	112K	0.95	1.09	93.3	<0	-	-	-
		68b-HA-3	0°	58.9	2.24	66K	1.03	0.80	68.2	<0	-	-	-
	68b-HA-2	-50°	53.6	6.07	73K	0.97	0.56	47.7	<0	-	-	-	

Table 6-5. Tabulated fracture toughness test results for the different test conditions evaluated.

Matl Source	Build Year	Spec ID No.	Test Temp	Rate, in/sec	ϵ rate, in/in/sec	Krate, ksi $\sqrt{\text{in}}$ /sec	Compl Ratio	Limit Ratio	Kmax, ksi $\sqrt{\text{in}}$	Percent Plastic J	Jmax, ksi-in	KJmax, ksi $\sqrt{\text{in}}$	KJ/Kmx Ratio
TC128-B Subset B	1974	74b-SA-1	0°	59.7	3.44	102K	1.06	1.36	103.5	42	0.555	135	1.31
		74b-SA-3	0°	59.6	3.27	97K	0.98	1.34	102.3	43	0.552	135	1.32
		74b-SA-2	-50°	54.1	4.44	81K	n/a	0.8	59.5	<0	-	-	-
		74b-HA-1	0°	60.6	2.98	90K	1.03	1.35	106.4	<0	-	-	-
		74b-HA-3	0°	61.8	3.02	87K	1.04	1.21	95.2	<0	-	-	-
		74b-HA-2	-50°	54.9	1.82	54K	1.02	0.83	65.0	<0	-	-	-
	1975	75a-SA-1	0°	56.1	1.64	46K	n/a	0.54	55.9	<0	-	-	-
		75a-SA-3	0°	39.9	3.32	116K	0.95	0.75	77.8	<0	-	-	-
		75a-SA-2	-50°	58.7	2.54	74K	1.07	0.34	35.1	<0	-	-	-
		75a-HA-1	0°	55.6	3.24	101K	0.95	1.23	113.1	49	0.768	159	1.41
		75a-HA-3	0°	58.1	3.22	94K	1.01	1.22	112.6	64	1.073	188	1.67
		75a-HA-2	-50°	55.0	3.19	92K	1.04	1.23	113.8	57	0.909	173	1.52
	1976	76b-SF-1	0°	59.0	3.64	105K	1.09	1.19	101.7	43	0.550	135	1.32
		76b-SF-3	0°	59.2	3.93	119K	1.01	1.18	102.3	28	0.439	120	1.18
		76b-SF-4	0°	60.3	3.80	115K	1.01	1.20	101.4	55	0.687	151	1.48
		76b-SF-2	-50°	58.6	2.28	70K	1.09	0.84	72.0	<0	-	-	-
		76b-SA-1	0°	56.7	3.21	100K	1.03	1.31	108.8	61	0.930	175	1.61
		76b-SA-3	0°	60.1	3.66	99K	1.18	0.99	82.8	<0	-	-	-
		76b-SA-4	0°	55.2	8.14	174K	1.05	1.09	90.3	<0	-	-	-
		76b-SA-2	-50°	59.7	3.74	88K	0.85	0.69	57.4	<0	-	-	-

Table 6-6. Tabulated fracture toughness test results for the different test conditions evaluated.

Matl Source	Build Year	Spec ID No.	Test Temp	Rate, in/sec	ϵ rate, in/in/sec	Krate, ksi $\sqrt{\text{in}}$ /sec	Compl Ratio	Limit Ratio	Kmax, ksi $\sqrt{\text{in}}$	Percent Plastic J	Jmax, ksi-in	KJmax, ksi $\sqrt{\text{in}}$	KJ/Kmx Ratio
TC128-B Subset C	1977	77a-SD-4	0°	55.7	2.81	82K	1.09	1.28	101.8	34	0.479	126	1.23
		77a-SD-1	0°	62.1	2.99	87K	1.00	1.13	90.6	58	0.595	140	1.55
		77a-SD-3	0°	58.1	3.82	112K	1.04	1.33	106.2	<0	-	-	-
		77a-SD-2	-50°	56.9	3.13	100K	0.90	0.91	72.7	<0	-	-	-
	1978	78b-SA-1	0°	54.5	2.40	73K	1.01	0.46	47.1	<0	-	-	-
		78b-SA-3	0°	56.1	1.17	37K	0.94	0.48	49.4	<0	-	-	-
		78b-SA-2	-50°	56.0	1.60	49K	0.99	0.35	35.8	<0	-	-	-
		78b-HA-1	0°	58.9	2.03	80K	0.96	0.55	49.4	<0	-	-	-
		78b-HA-3	0°	56.4	3.67	88K	1.03	0.55	48.9	<0	-	-	-
		78b-HA-2	-50°	61.3	1.72	57K	n/a	0.46	41.1	<0	-	-	-
	1979	79a-SA-1	0°	57.2	1.83	55K	1.09	0.70	62.2	<0	-	-	-
		79a-SA-3	0°	63.2	2.88	86K	1.06	0.67	59.5	<0	-	-	-
		79a-SA-2	-50°	56.4	1.28	34K	1.20	0.41	36.6	<0	-	-	-
		79a-SB-1	0°	56.1	1.72	52K	1.05	0.57	51.3	<0	-	-	-
		79a-SB-3	0°	59.0	2.04	16K	1.29	0.52	46.8	<0	-	-	-
		79a-SB-2	-50°	53.3	1.68	53K	1.08	0.49	44.1	<0	-	-	-
		79a-HA-1	0°	63.9	2.95	92K	1.03	1.21	112.2	<0	-	-	-
		79a-HA-3	0°	61.7	3.39	102K	1.04	1.20	110.8	<0	-	-	-
	79a-HA-2	-50°	58.3	2.62	92K	1.00	0.87	79.5	<0	-	-	-	

Table 6-7. Tabulated fracture toughness test results for the different test conditions evaluated.

Matl Source	Build Year	Spec ID No.	Test Temp	Rate, in/sec	ϵ rate, in/in/sec	Krate, ksi $\sqrt{\text{in}}$ /sec	Compl Ratio	Limit Ratio	Kmax, ksi $\sqrt{\text{in}}$	Percent Plastic J	Jmax, ksi-in	KJmax, ksi $\sqrt{\text{in}}$	KJ/Kmx Ratio
TC128-B Subset D	1980	80a-SA-1	0°	59.0	3.01	101K	1.09	1.24	99.3	<0	-	-	-
		80a-SA-3	0°	65.1	2.84	85K	1.16	1.15	92.5	<0	-	-	-
		80a-SA-2	-50°	57.3	2.16	72K	1.03	0.64	51.5	<0	-	-	-
		80a-HA-1	0°	56.0	3.84	59K	1.19	0.95	75.5	53	0.368	110	1.46
		80a-HA-3	0°	60.3	3.31	100K	1.07	1.42	112.6	24	0.509	130	1.15
		80a-HA-2	-50°	57.9	3.08	97K	1.07	1.16	91.7	<0	-	-	-
	1981	81a-SB-1	0°	54.3	1.42	48K	0.97	0.45	46.8	<0	-	-	-
		81a-SB-3	0°	61.6	1.78	55K	n/a	0.37	37.8	<0	-	-	-
		81a-SB-2	-50°	54.6	1.77	51K	1.05	0.30	30.9	<0	-	-	-
	1982	82a-SA-1	0°	51.9	2.61	78K	1.03	1.16	97.5	22	0.370	110	1.13
		82a-SA-3	0°	62.0	2.78	79K	1.04	0.81	68.5	<0	-	-	-
		82a-SA-2	-50°	55.4	2.26	66K	1.08	0.66	55.8	<0	-	-	-
		82a-SB-1	0°	56.8	2.13	68K	1.06	0.84	71.0	42	0.261	93	1.31
		82a-SB-3	0°	59.2	2.38	64K	1.09	0.75	64.2	68	0.395	114	1.78
		82a-SB-2	-50°	55.9	2.14	64K	1.06	0.62	52.0	<0	-	-	-
		82a-HA-1	0°	58.5	2.97	86K	1.04	1.35	129.0	53	1.081	189	1.46
		82a-HA-3	0°	61.3	3.44	93K	1.03	1.36	130.2	64	1.431	217	1.67
	82a-HA-2	-50°	54.1	2.80	77K	0.99	0.91	87.2	<0	-	-	-	

Table 6-8. Tabulated fracture toughness test results for the different test conditions evaluated.

Matl Source	Build Year	Spec ID No.	Test Temp	Rate, in/sec	ϵ rate, in/in/sec	Krate, ksi $\sqrt{\text{in}}$ /sec	Compl Ratio	Limit Ratio	Kmax, ksi $\sqrt{\text{in}}$	Percent Plastic J	Jmax, ksi-in	KJmax, ksi $\sqrt{\text{in}}$	KJ/Kmx Ratio
TC128-B normalized	1994	94a-SA-1	0°	56.5	3.19	102K	0.96	1.31	103.8	18	0.399	115	1.11
		94a-SA-3	0°	60.5	3.30	108K	1.03	1.21	96.5	<0	-	-	-
		94a-SA-4	0°	57.3	3.40	109K	n/a	0.97	77.5	<0	-	-	-
		94a-SA-2	-50°	59.8	2.80	99K	0.98	0.71	57.8	<0	-	-	-
		94a-SB-1	0°	56.9	2.90	88K	1.07	1.30	101.6	<0	-	-	-
		94a-SB-3	0°	62.0	2.98	90K	0.98	1.08	85.6	<0	-	-	-
		94a-SB-4	0°	60.6	3.73	131K	0.97	1.23	96.4	<0	-	-	-
		94a-SB-2	-50°	55.6	2.47	76K	0.99	0.86	67.6	<0	-	-	-
		94a-HA-1	0°	55.6	2.83	88K	0.96	1.47	114.9	41	0.677	149	1.30
	94a-HA-3	0°	63.6	2.73	87K	0.98	1.44	113.4	37	0.618	143	1.26	
	94a-HA-2	-50°	54.9	2.49	77K	1.03	0.91	71.0	<0	-	-	-	
	1994	94b-SA-1	0°	59.3	2.98	96K	0.97	1.23	98.0	<0	-	-	-
		94b-SA-2	-50°	57.3	1.27	61K	1.12	0.56	44.9	<0	-	-	-
		94b-HA-1	0°	58.6	4.00	114K	n/a	1.40	110.9	<0	-	-	-
94b-HA-2		-50°	54.5	1.77	55K	1.02	0.76	60.1	<0	-	-	-	
A212-B	1965	65a-SA-1	0°	59.7	2.15	79K	1.04	0.65	45.4	<0	-	-	-
		65a-SA-3	0°	58.0	2.22	65K	1.04	0.79	56.0	<0	-	-	-
		65a-SA-2	-50°	59.8	2.85	88K	n/a	0.60	41.7	<0	-	-	-
		65a-HA-1	0°	58.3	3.28	91K	1.08	0.74	57.6	26	0.136	67	1.16
		65a-HA-3	0°	56.6	1.63	55K	n/a	0.54	41.6	<0	-	-	-
		65a-HA-2	-50°	57.3	1.85	38K	n/a	0.51	39.4	<0	-	-	-
	1966	66c-SA-1	0°	59.9	1.60	42K	1.12	0.77	50.4	<0	-	-	-
		66c-SA-2	-50°	56.6	1.13	28K	1.05	0.60	39.7	<0	-	-	-
		66c-HA-1	0°	54.7	2.62	72K	1.03	1.43	106.7	50	0.685	150	1.41
66c-HA-2		-50°	55.9	2.94	101K	1.07	0.82	60.4	<0	-	-	-	

Table 6-9. Statistical summary of the fracture toughness test data.

Material Source	Quantity	Kmax or KJmax at 0°F			Kmax or KJmax at -50°F		
		all	shell-only	head-only	all	shell-only	head-only
TC128-B Subset A	<i>count:</i>	12	8	4	6	4	2
	<i>max:</i>	170.0	170.0	112.5	164.0	164.0	61.8
	<i>min:</i>	68.2	75.0	68.2	45.9	45.9	47.7
	<i>average:</i>	116.3	126.2	96.4	75.5	85.9	54.8
	<i>std dev:</i>	37.0	40.3	20.7	46.0	55.3	10.0
TC128-B Subset B	<i>count:</i>	14	10	4	6	4	2
	<i>max:</i>	188.0	175.0	188.0	173.0	72.0	173.0
	<i>min:</i>	55.9	55.9	95.2	35.1	35.1	65.0
	<i>average:</i>	121.9	115.8	137.2	77.0	56.0	119.0
	<i>std dev:</i>	38.9	37.5	43.9	48.6	15.4	76.4
TC128-B Subset C	<i>count:</i>	13	9	4	6	4	2
	<i>max:</i>	140.0	140.0	112.2	79.5	72.7	79.5
	<i>min:</i>	46.8	46.8	48.9	35.8	35.8	41.1
	<i>average:</i>	77.7	76.5	80.3	51.6	47.3	60.3
	<i>std dev:</i>	35.2	37.0	36.0	19.3	17.3	27.2
TC128-B Subset D	<i>count:</i>	12	8	4	6	4	2
	<i>max:</i>	217.0	114.0	217.0	91.7	55.8	91.7
	<i>min:</i>	37.8	37.8	110.0	30.9	30.9	87.2
	<i>average:</i>	109.0	82.7	161.5	61.5	47.6	89.5
	<i>std dev:</i>	52.0	28.6	49.9	23.4	11.3	3.2
TC128-B Normalized	<i>count:</i>	10	7	3	5	4	1
	<i>max:</i>	149	115	149	71	67.6	71
	<i>min:</i>	77.5	77.5	110.9	44.9	44.9	71.0
	<i>average:</i>	107.4	95.8	134.3	60.3	57.6	71.0
	<i>std dev:</i>	23.1	11.9	20.5	10.1	9.4	n/a
A212-B	<i>count:</i>	6	3	3	4	2	2
	<i>max:</i>	150	56	150	60.4	41.7	60.4
	<i>min:</i>	41.6	45.4	41.6	39.4	39.7	39.4
	<i>average:</i>	68.4	50.6	86.2	45.3	40.7	49.9
	<i>std dev:</i>	41.0	5.3	56.7	10.1	1.4	14.8

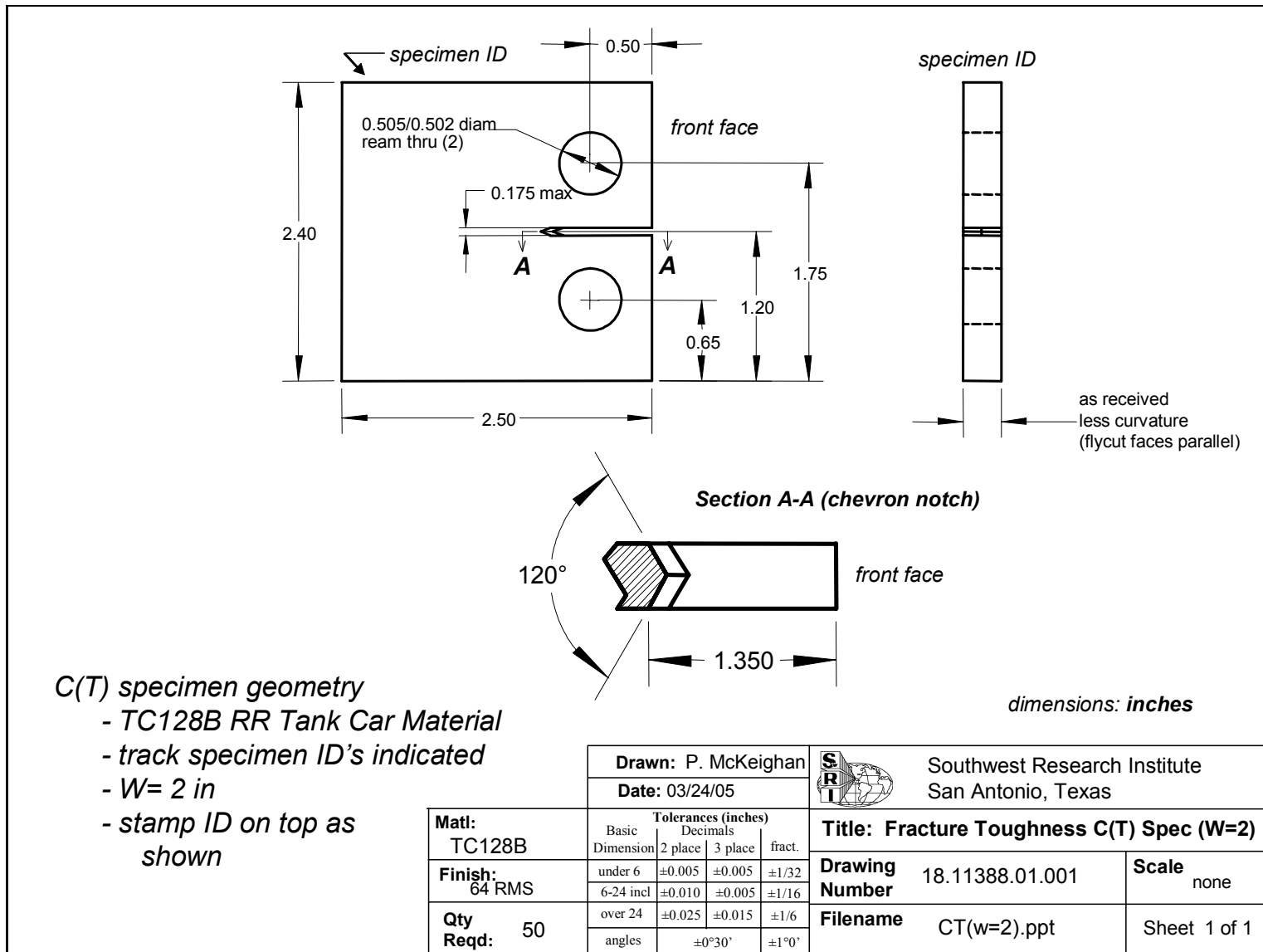


Figure 6-1. Nominal compact tension specimen dimensions.

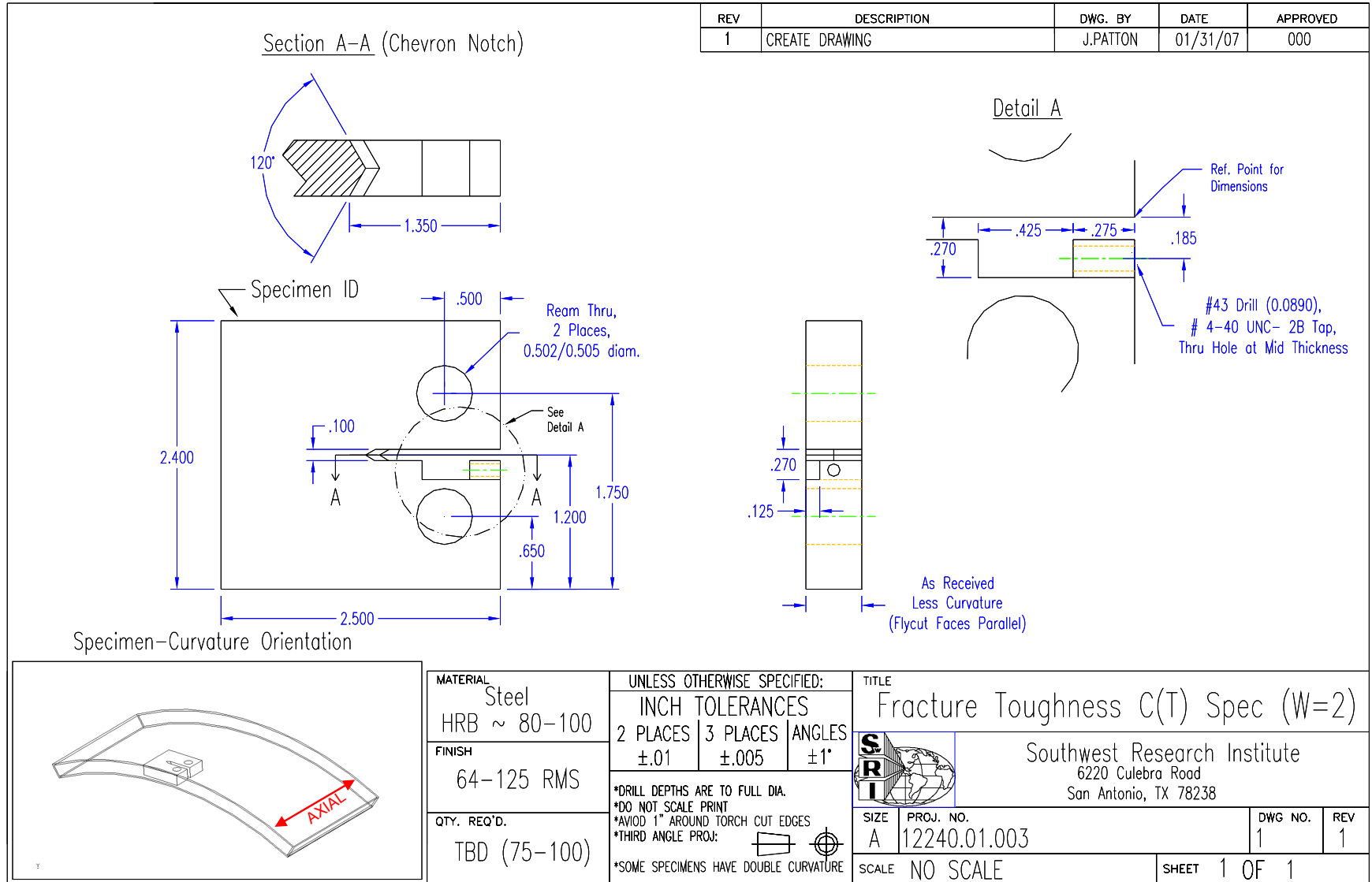


Figure 6-2. Modified compact tensile specimen to accommodate eddy current transducer.

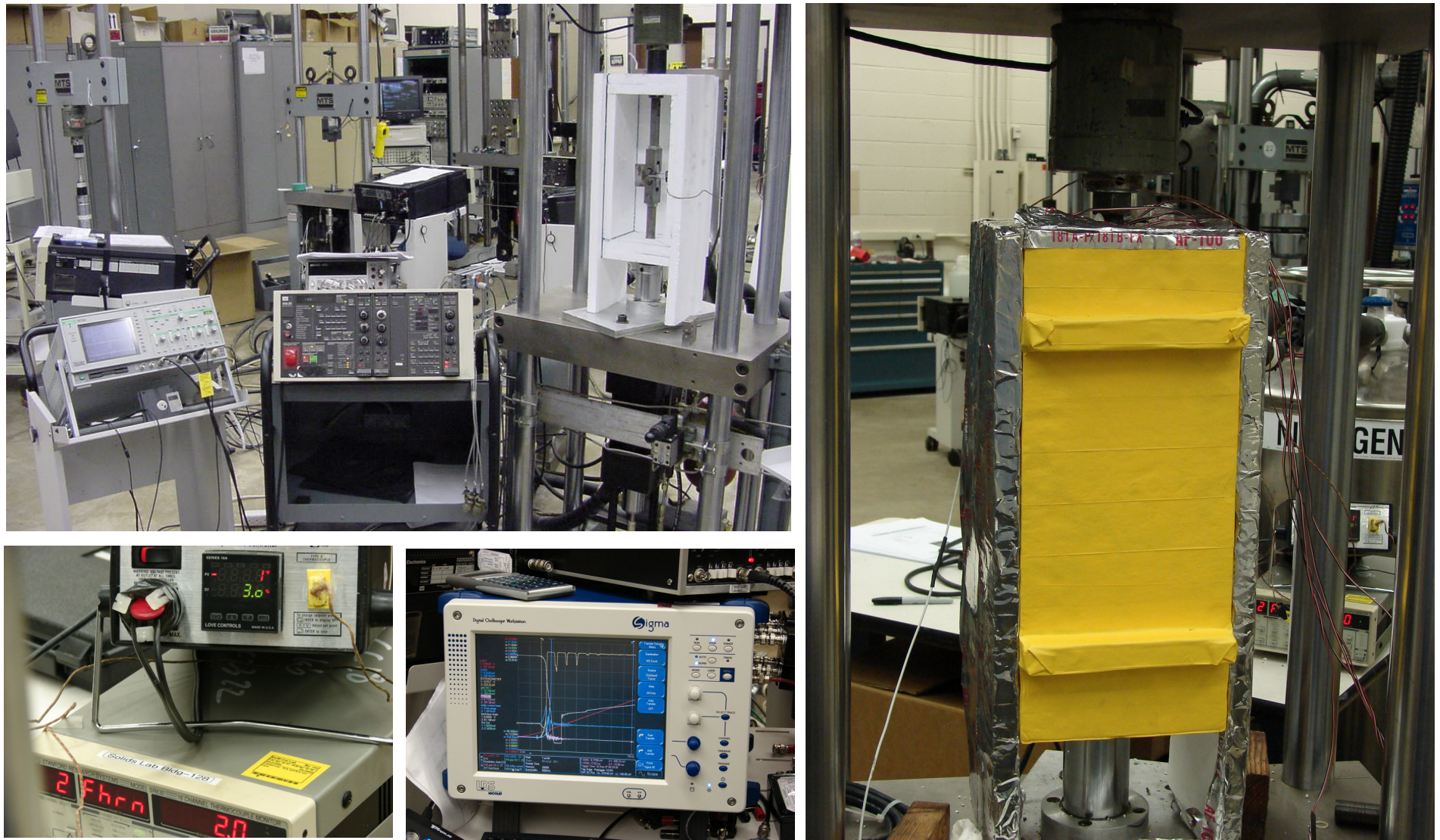


Figure 6-3. Cold-box setup (before and after taping with thermal insulating tape) with temperature controller and Nicolet high speed digital storage oscilloscope.

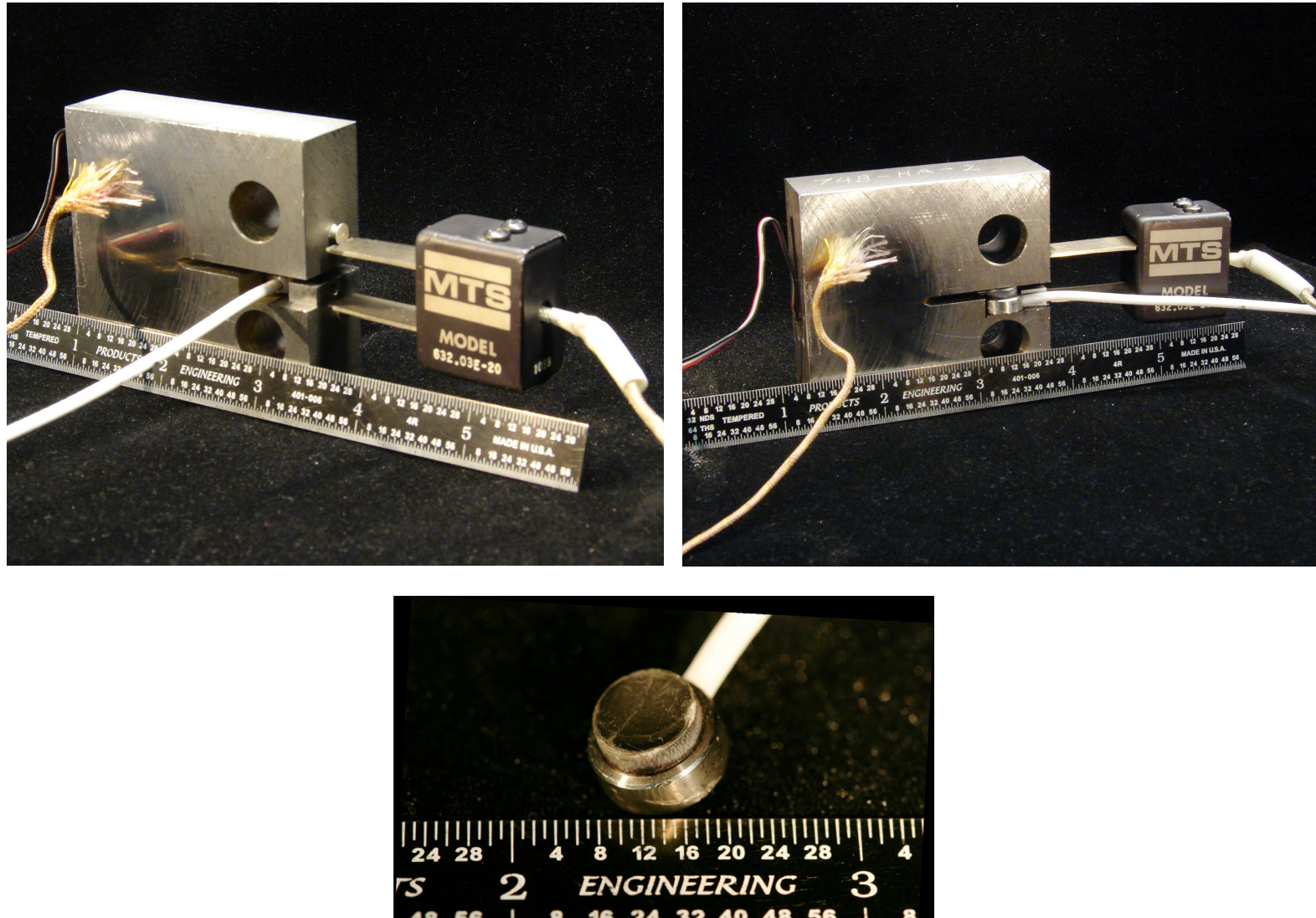


Figure 6-4. Compact tension specimen with load line displacement gage, front face clip gage and back face strain gage.

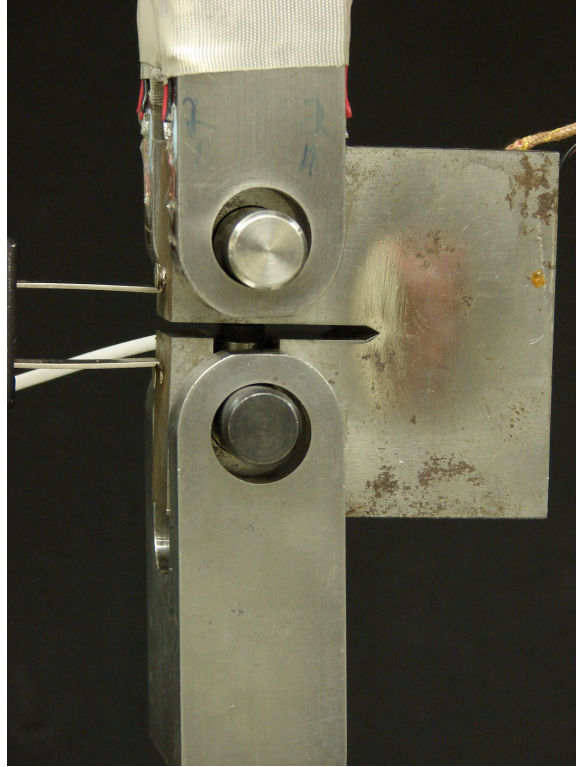


Figure 6-5. Slack adapter to achieve highest rate loading occurring by oversize grip holes.

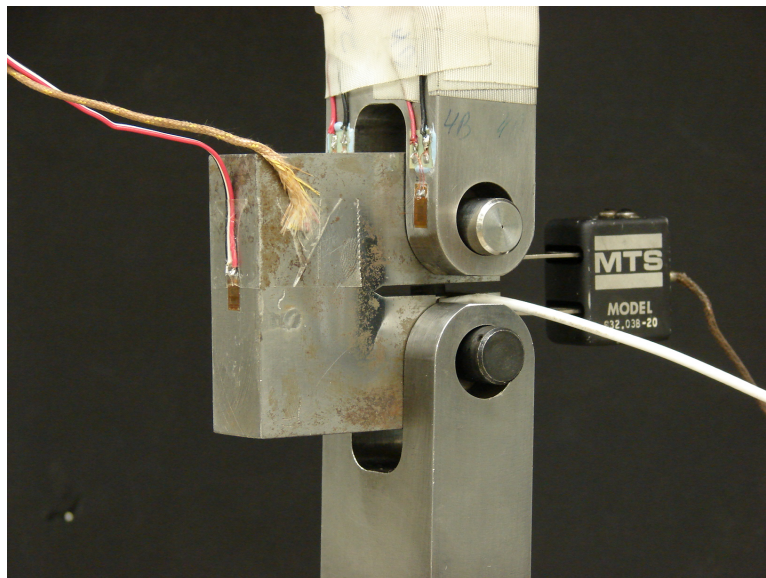


Figure 6-6. Instrumentation mounted on specimen including back face strain gage, eddy current transducer on the load-line, front face mounted extensometer and grip strain gages.

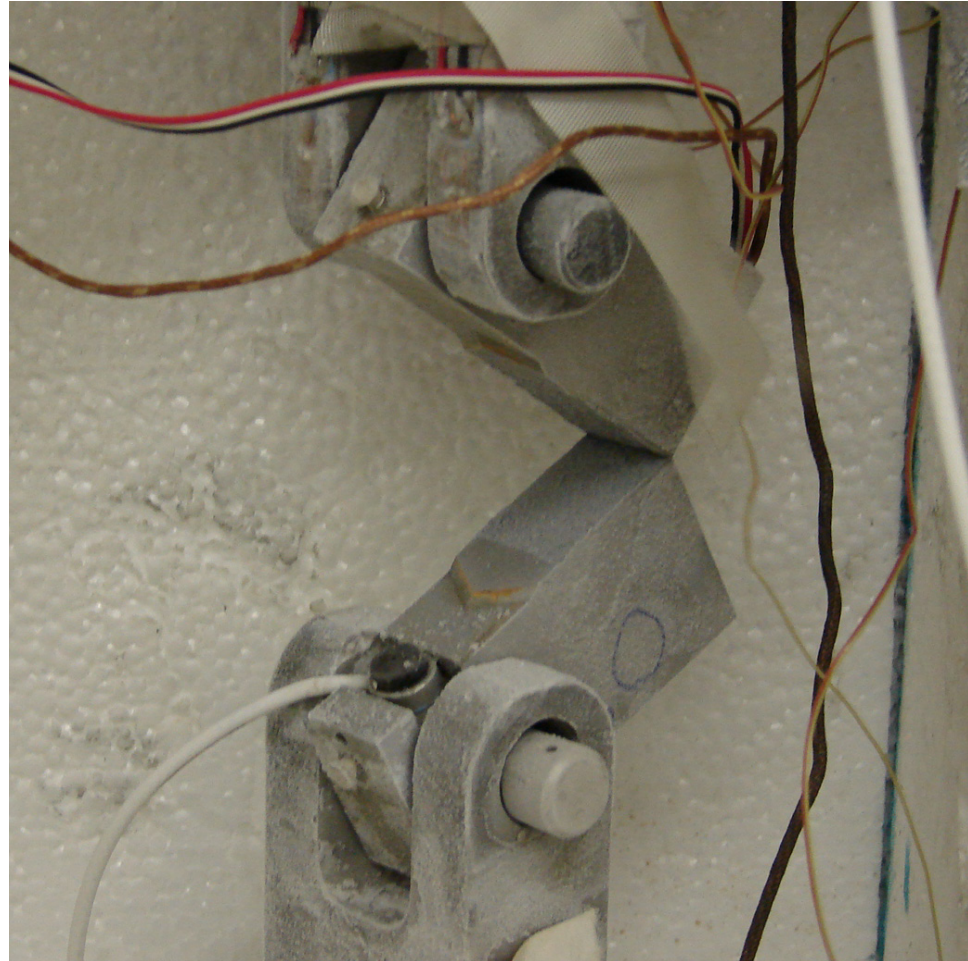
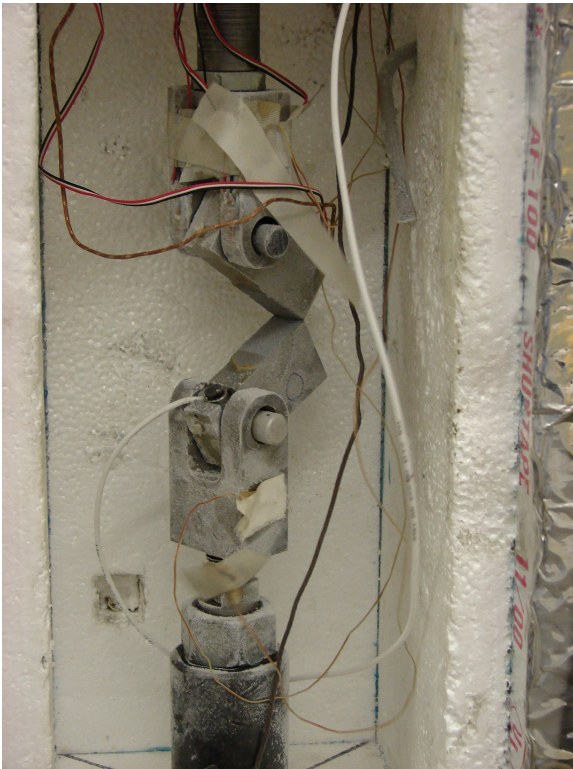


Figure 6-7. Immediately after a high rate, low temperature fracture test with frost formed on the fracture surface and the eddy current transducer exposed.

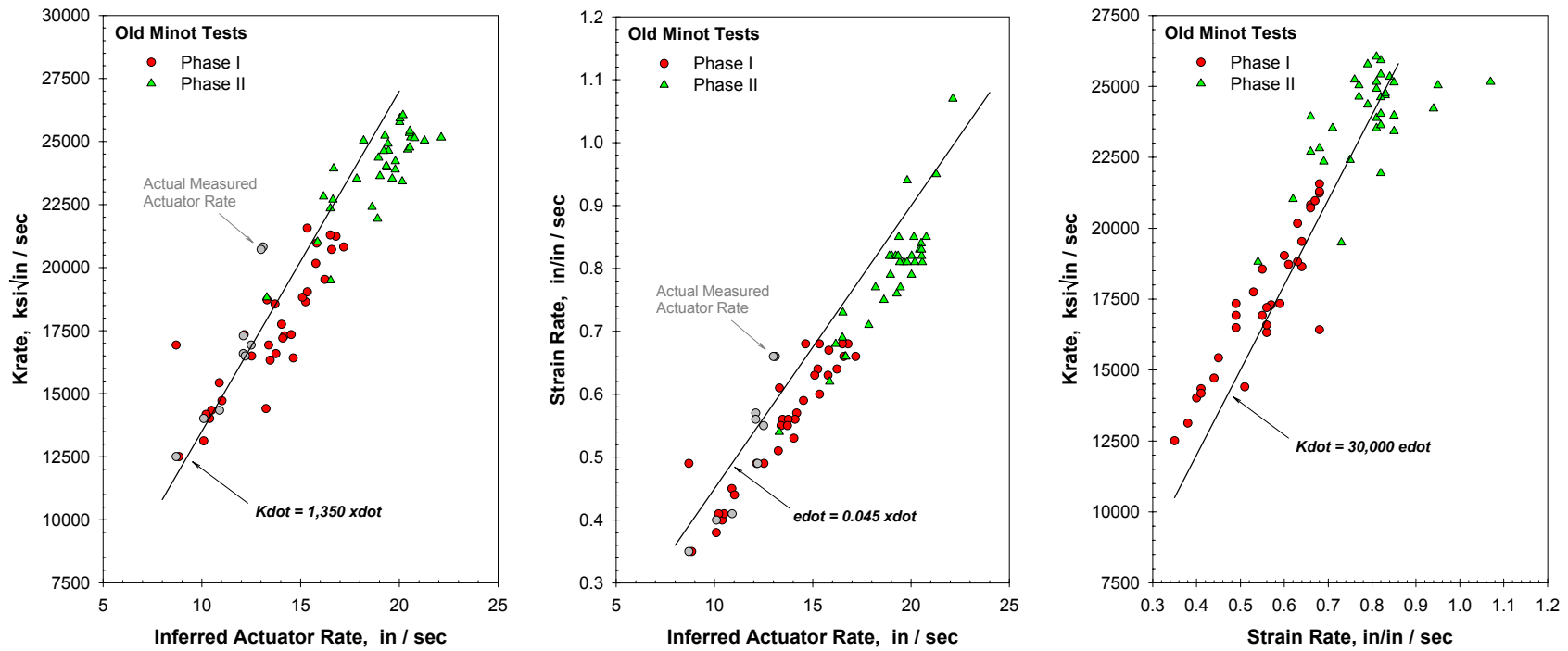


Figure 6-8. The data generated during the Minot testing was examined to establish the relationship between applied stress intensity factor rate (K-rate), actuator rate and strain rate.

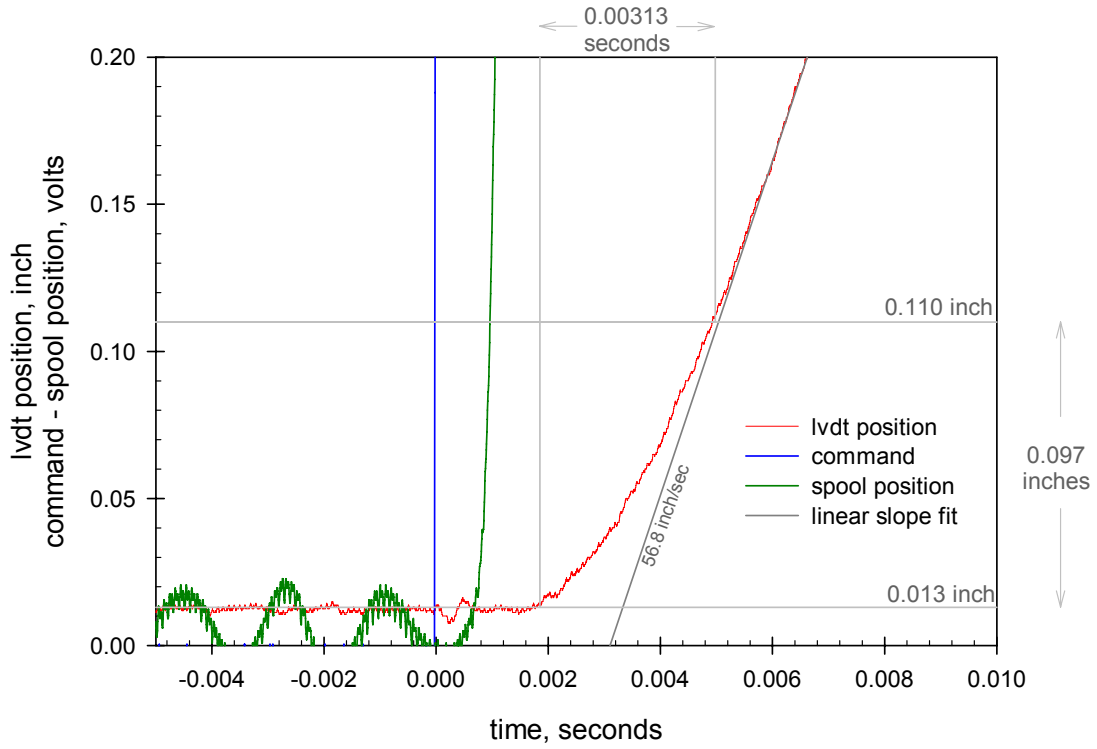


Figure 6-9. The initial LVDT displacement nonlinearity is overcome with a slack adapter.

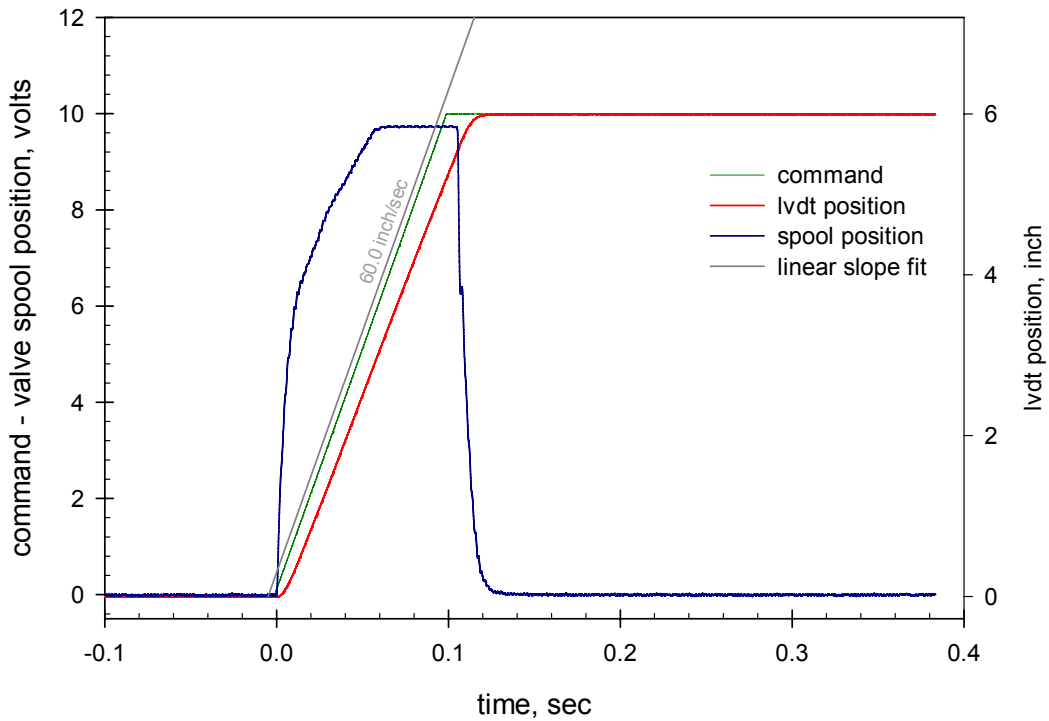


Figure 6-10. High rate frame stroke (average rate of 60 inch/second).

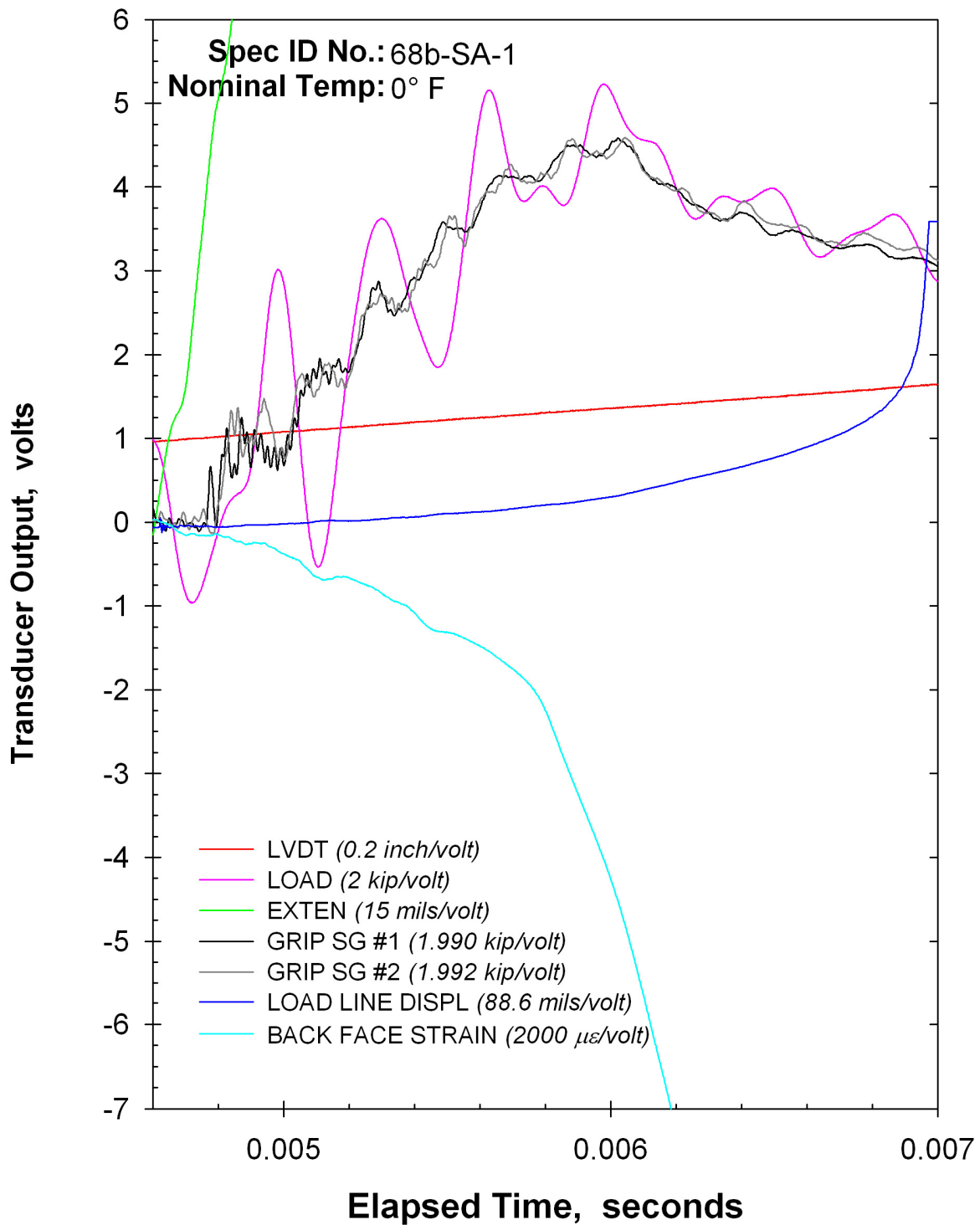


Figure 6-11. Example dynamic load cell data (pink signals) that necessitated developing the grip load cell derived from local strain gages.

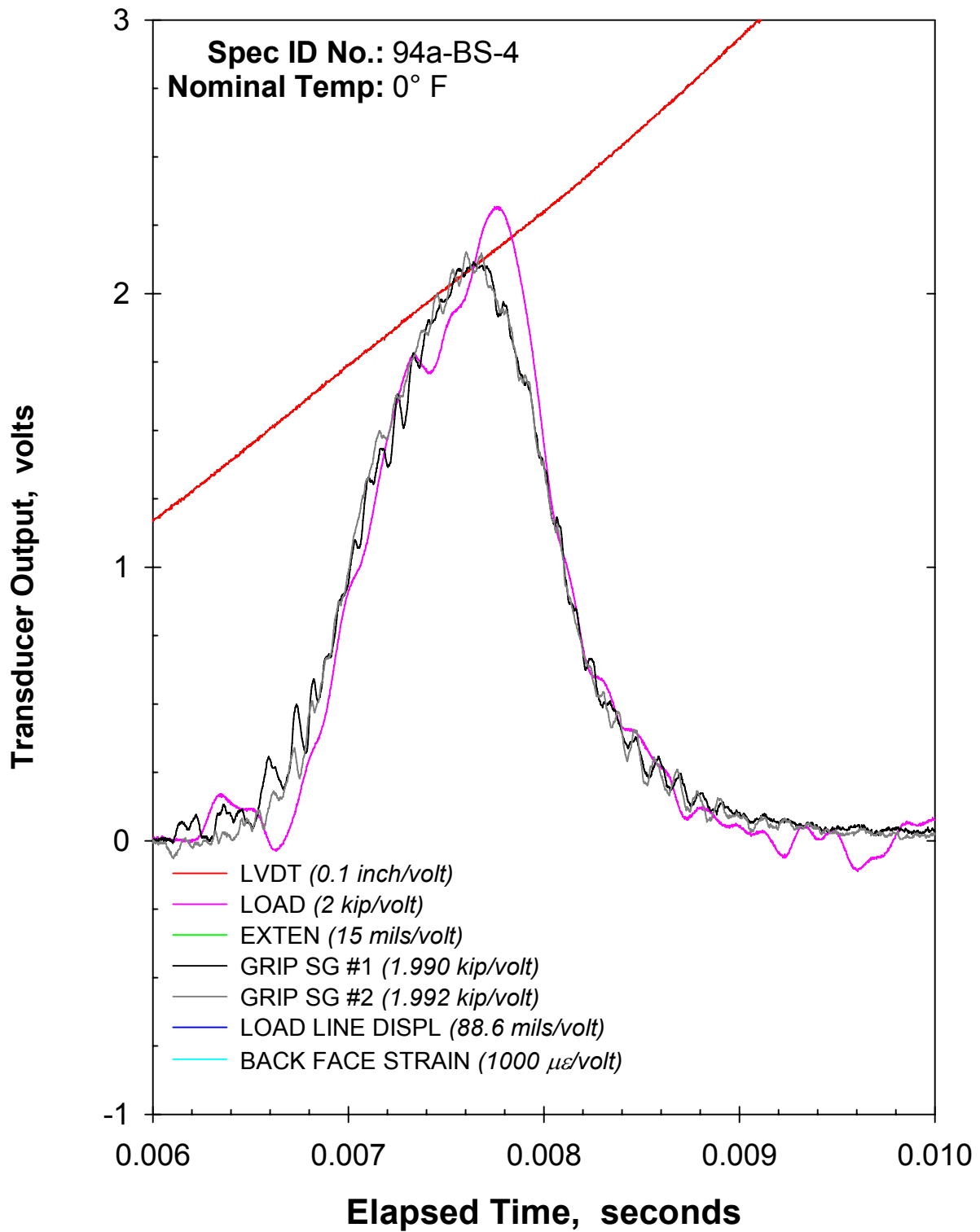


Figure 6-12. Excellent correlation between grip gages and load cell.

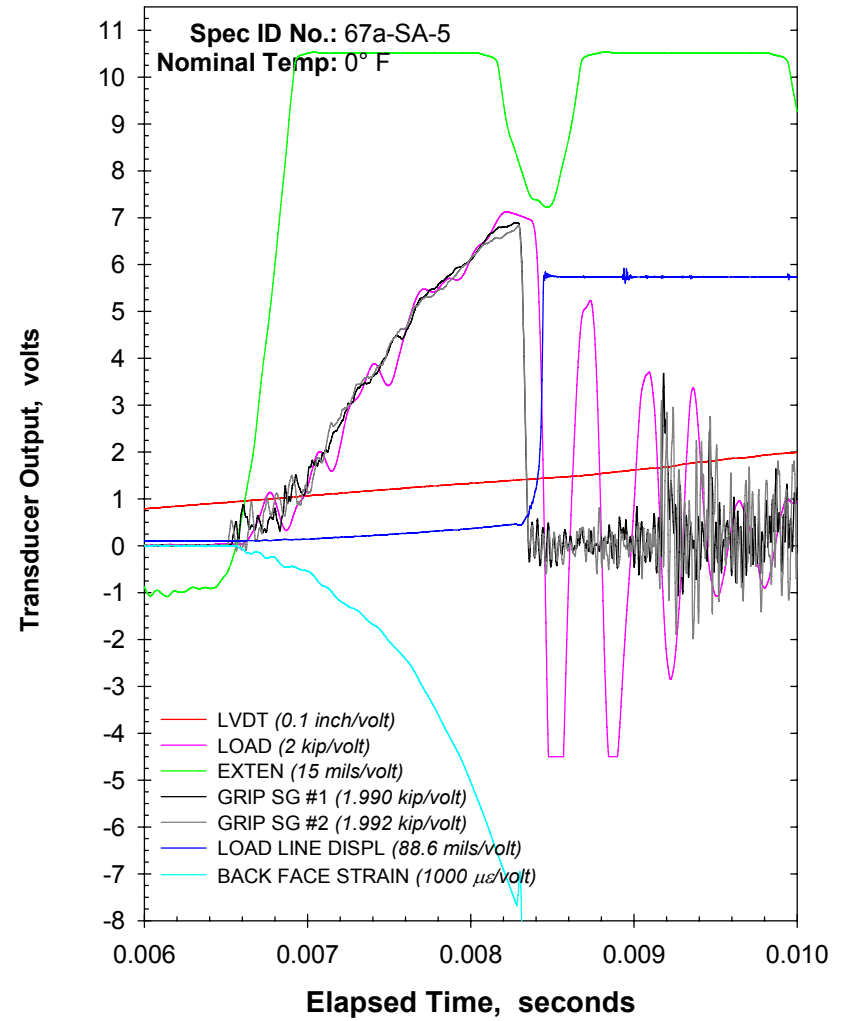
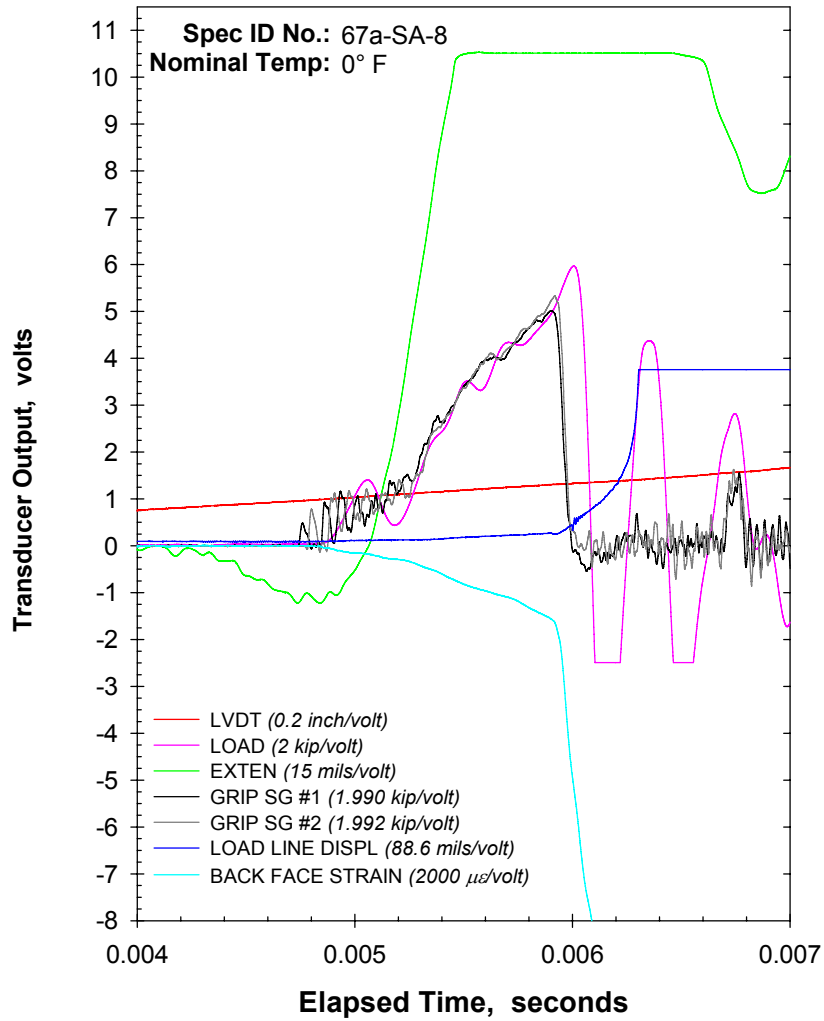


Figure 6-13. Transducer signals versus time for several pre-tests.

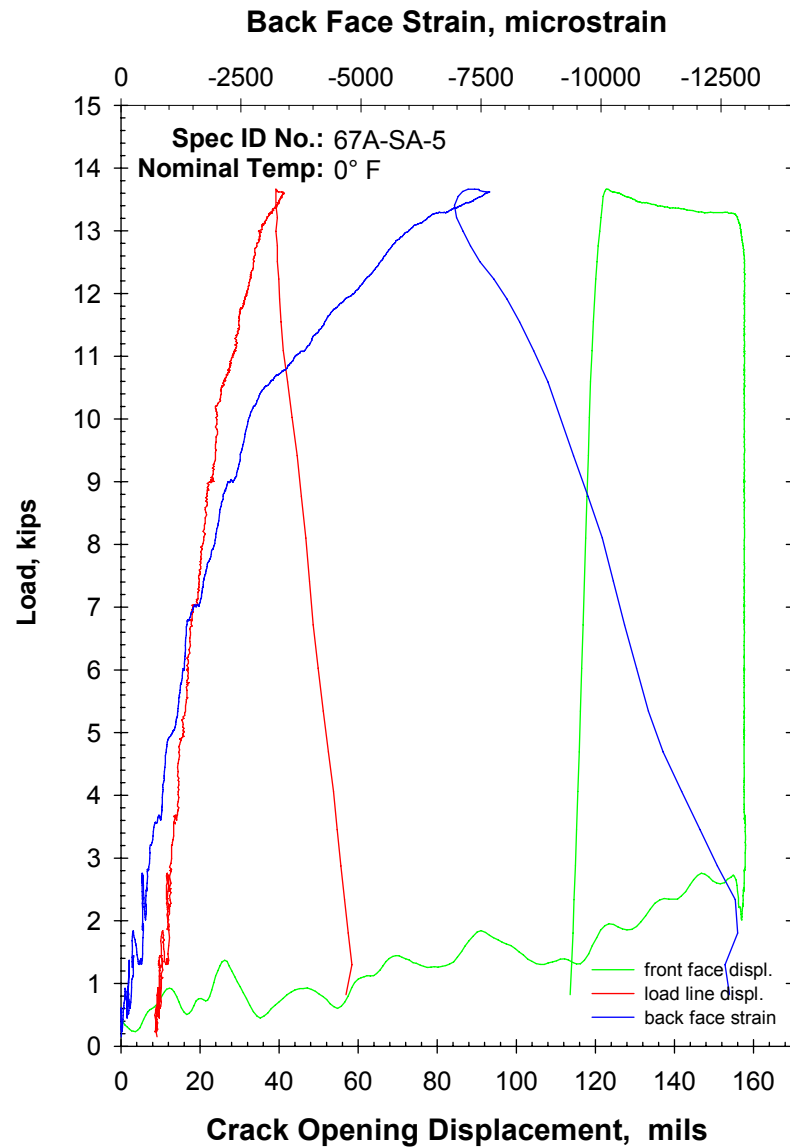
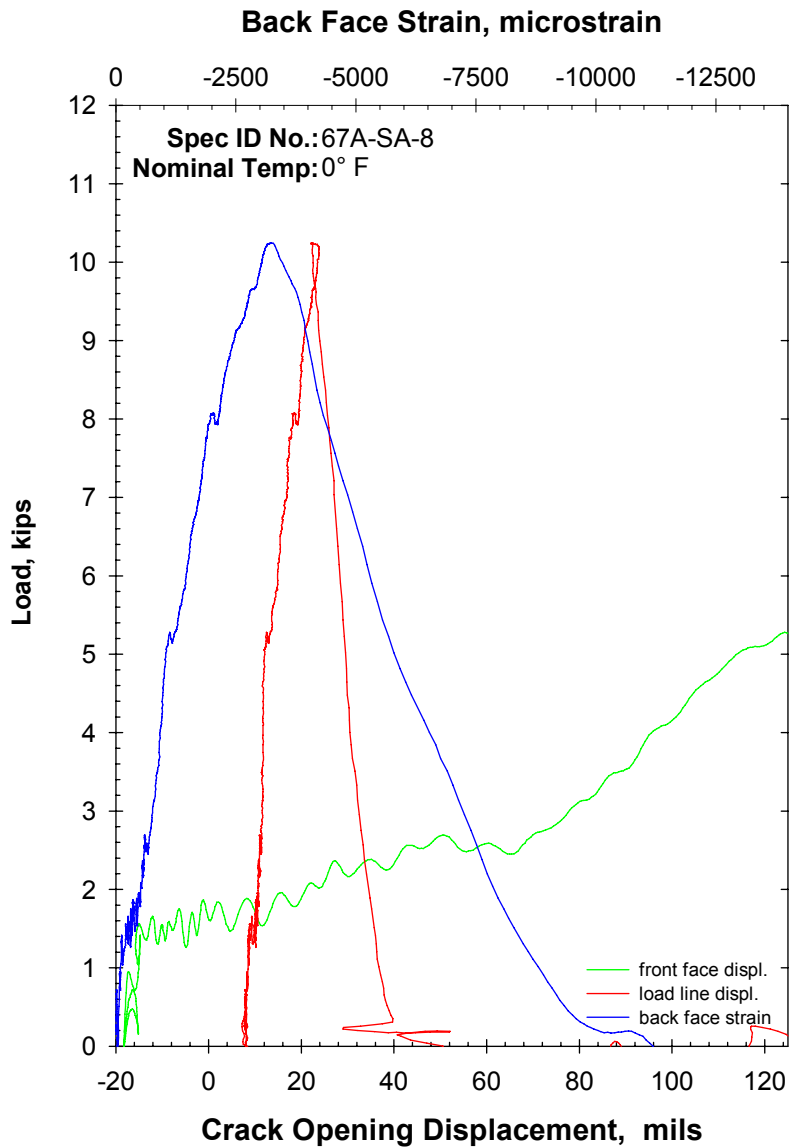


Figure 6-14. Load versus COD/BFS for several pre-tests (load derived from grip strain gages).

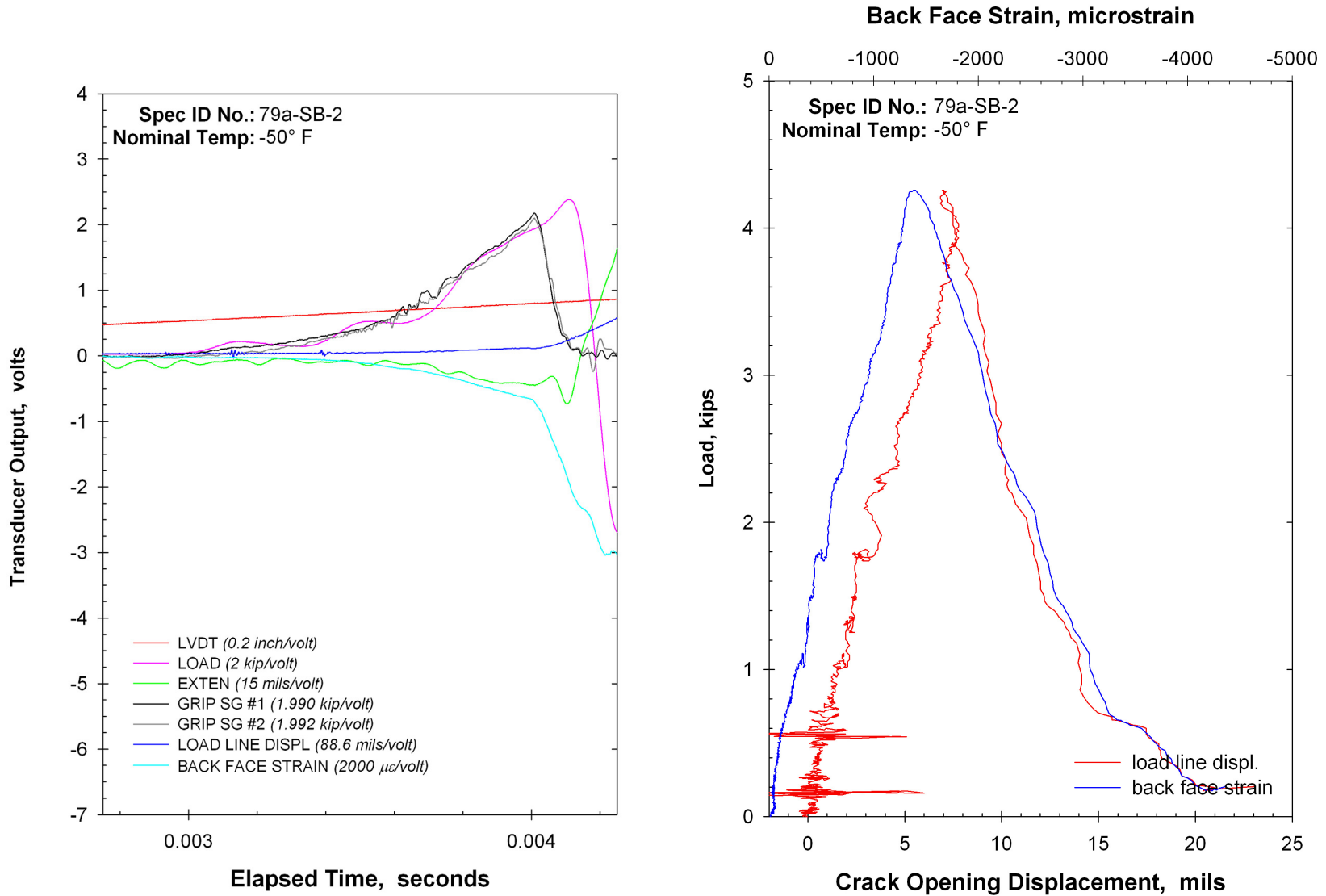


Figure 6-15. Example data from a “brittle” fracture toughness test.

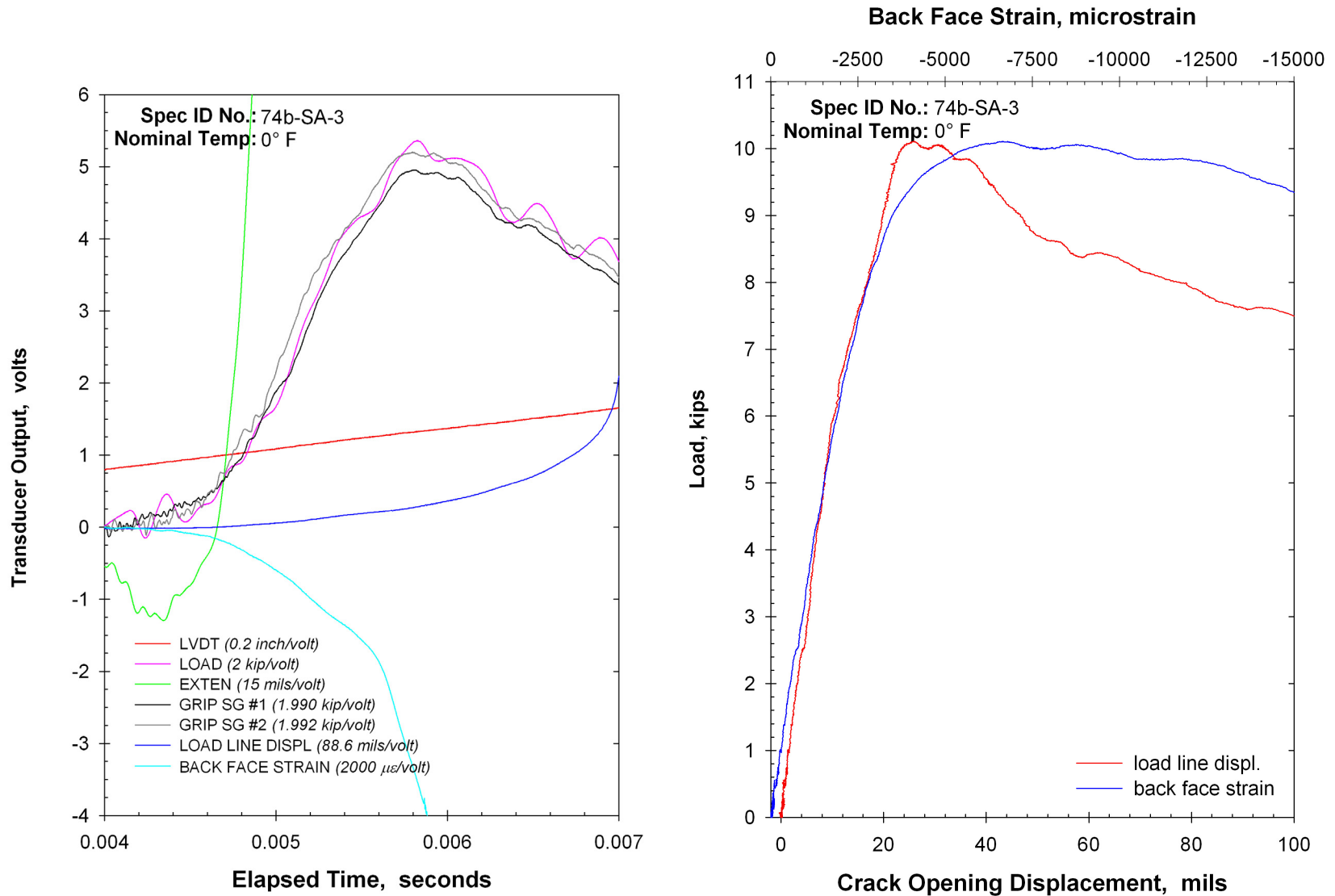
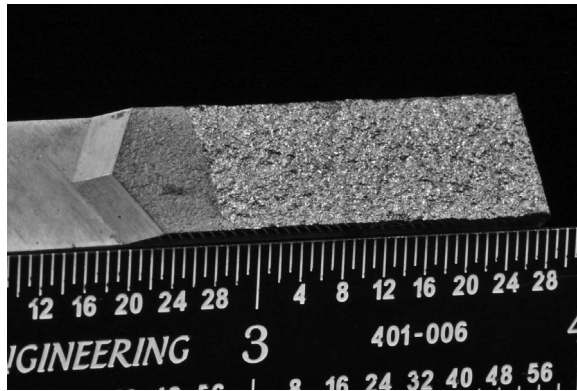
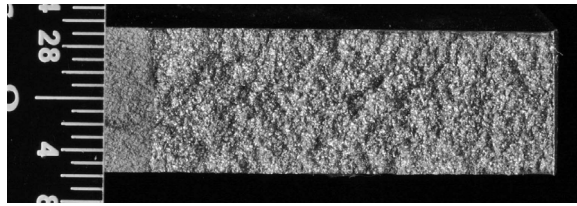
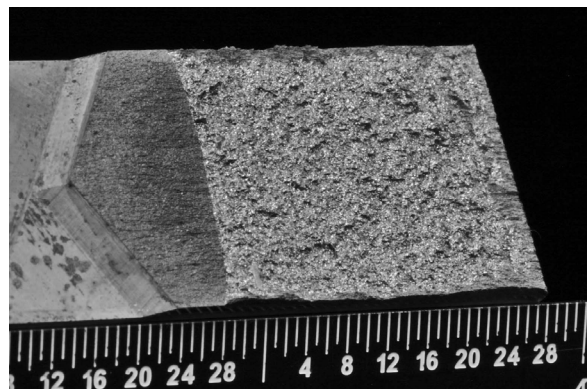
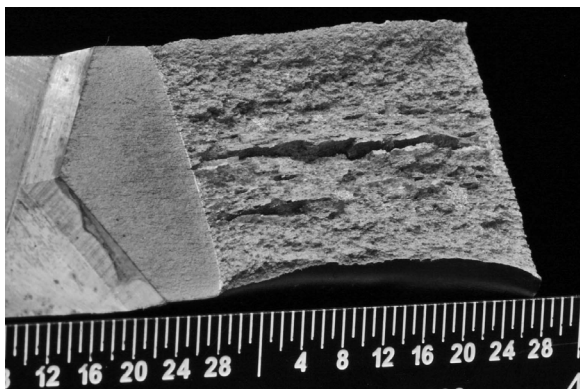
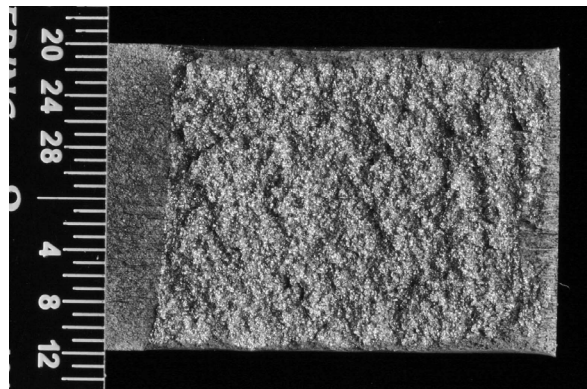
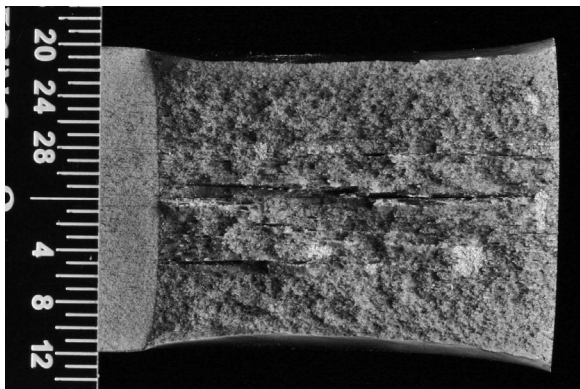


Figure 6-16. Example data from a “ductile” fracture toughness test.



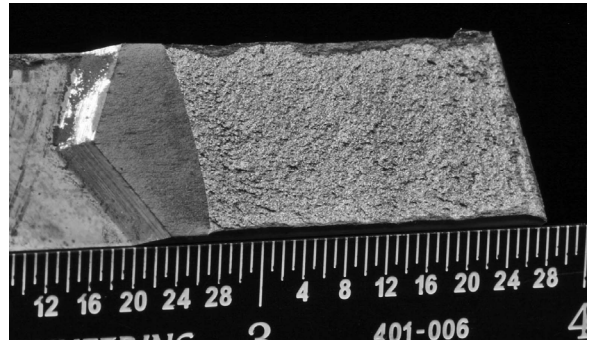
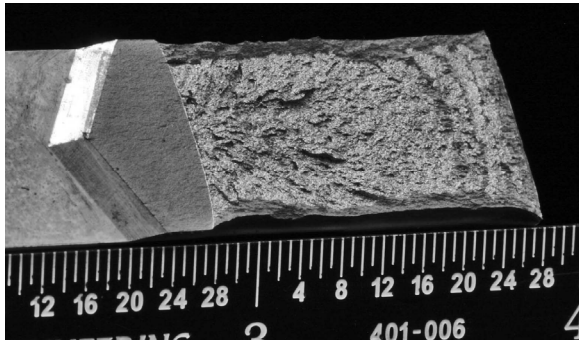
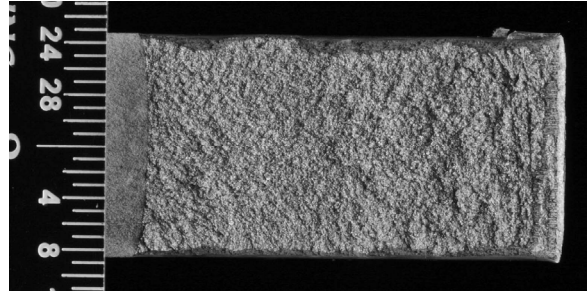
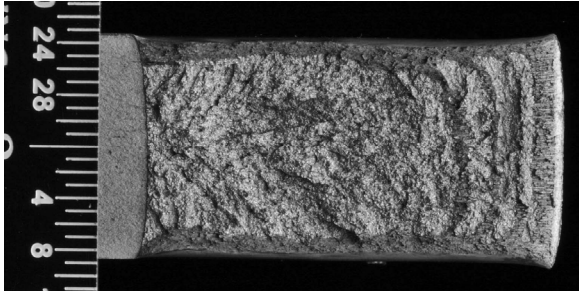
65a-HA-2 ($T=-50^{\circ}F$, $K_{Jmax} = 39.4 \text{ ksi } \sqrt{in}$)



66c-HA-1 ($T=0^{\circ}F$, $K_{Jmax} = 106.7 \text{ ksi } \sqrt{in}$)

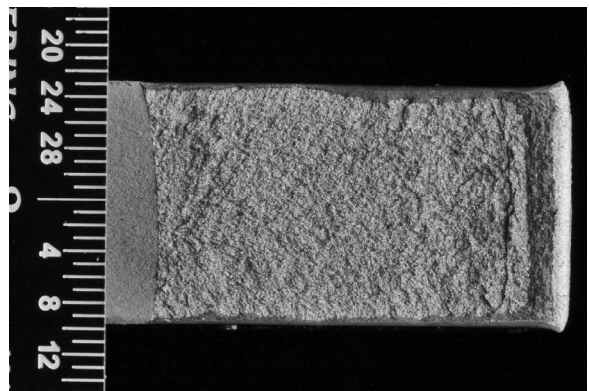
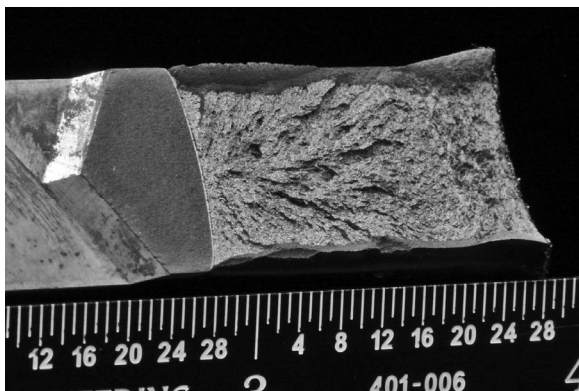
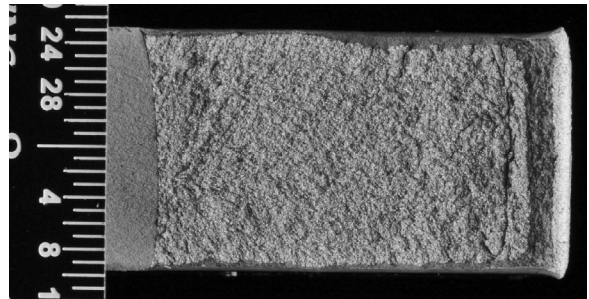
66c-SA-1 ($T=0^{\circ}F$, $K_{Jmax} = 50.4 \text{ ksi } \sqrt{in}$)

Figure 6-17. Fracture surfaces from several A212-B specimens.



94a-SA-1 ($T=0^{\circ}\text{F}$, $K_{Jmax} = 103.8 \text{ ksi } \sqrt{\text{in}}$)

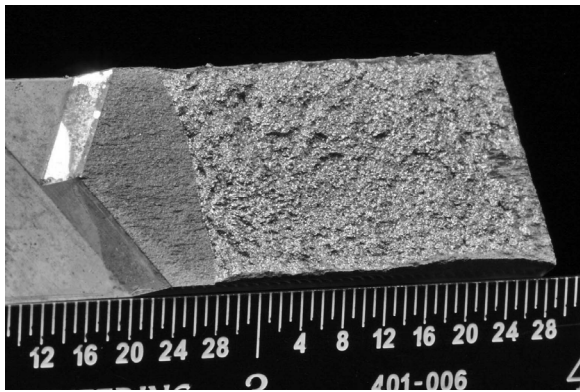
94a-SA-2 ($T=-50^{\circ}\text{F}$, $K_{Jmax} = 57.8 \text{ ksi } \sqrt{\text{in}}$)



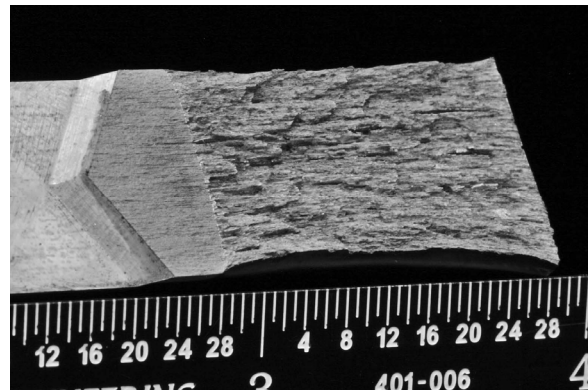
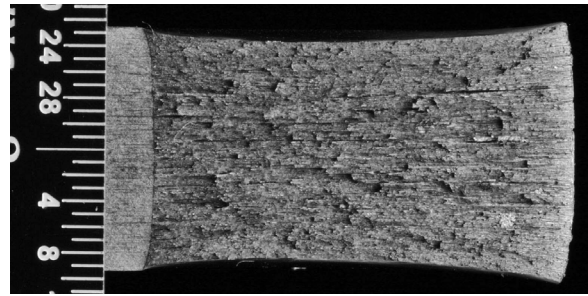
94a-HA-3 ($T=0^{\circ}\text{F}$, $K_{Jmax} = 113.4 \text{ ksi } \sqrt{\text{in}}$)

94b-HA-2 ($T=-50^{\circ}\text{F}$, $K_{Jmax} = 60.1 \text{ ksi } \sqrt{\text{in}}$)

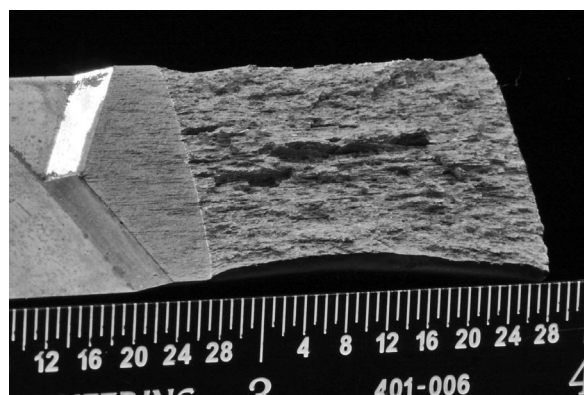
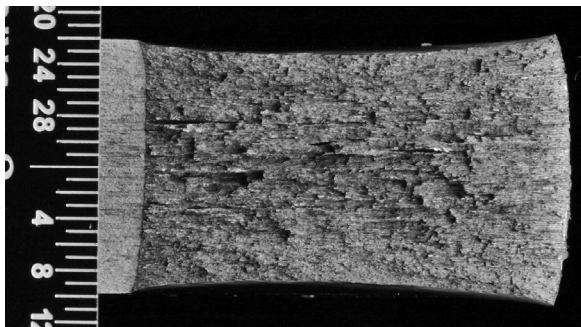
Figure 6-18. Fracture surfaces from several normalized post-1989 vintage TC128-B materials.



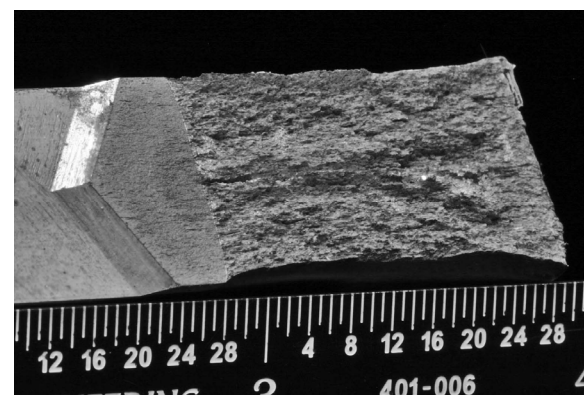
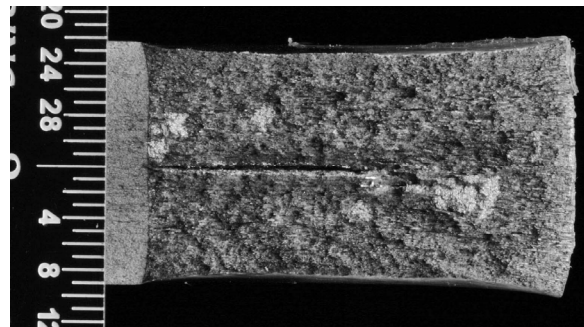
66b-SA-1 ($T=0^{\circ}\text{F}$, $K_{Jmax} = 79.7 \text{ ksi}\sqrt{\text{in}}$)



68b-SA-1 ($T=0^{\circ}\text{F}$, $K_{Jmax} = 107.6 \text{ ksi}\sqrt{\text{in}}$)

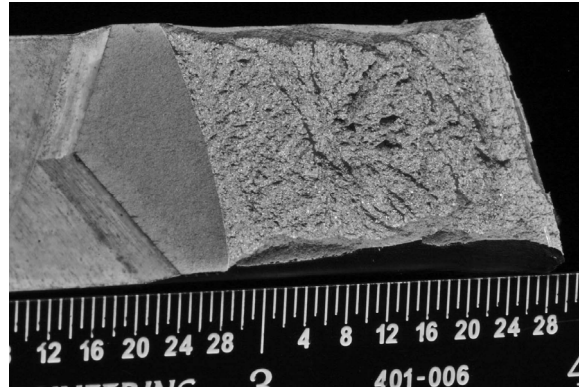


68b-SB-1 ($T=0^{\circ}\text{F}$, $K_{Jmax} = 105.8 \text{ ksi}\sqrt{\text{in}}$)

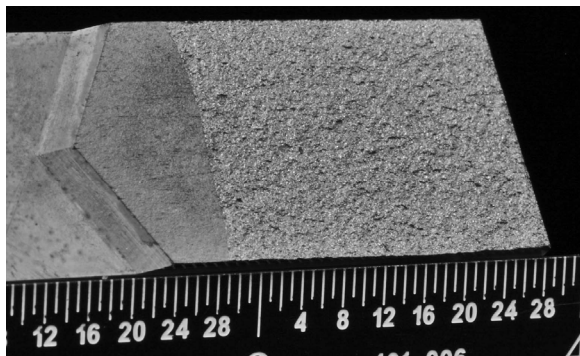
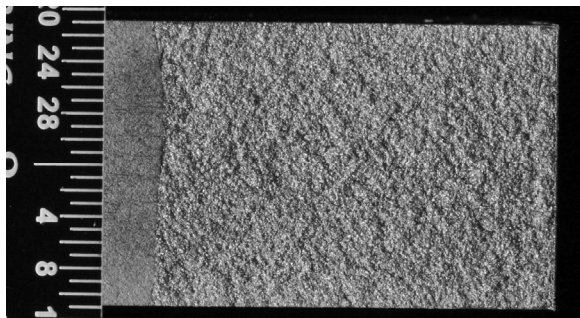


75a-HA-2 ($T=-50^{\circ}\text{F}$, $K_{Jmax} = 113.8 \text{ ksi}\sqrt{\text{in}}$)

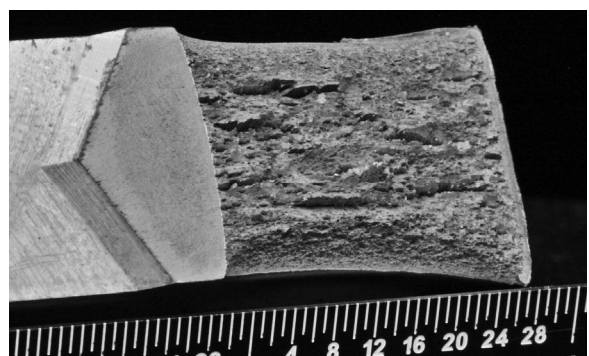
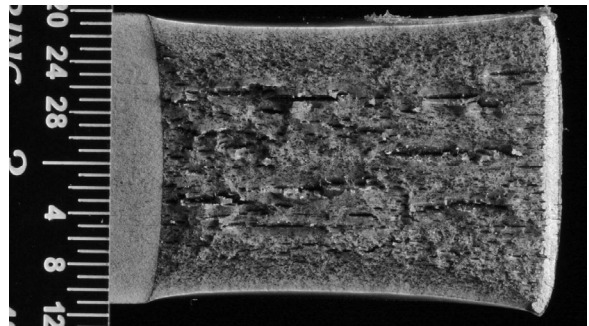
Figure 6-19. Fracture surfaces from several early vintage TC128-B materials.



80a-HA-2 ($T=-50^{\circ}\text{F}$, $K_{Jmax} = 91.7 \text{ ksi } \sqrt{\text{in}}$)



81a-SB-2 ($T=-50^{\circ}\text{F}$, $K_{Jmax} = 30.9 \text{ ksi } \sqrt{\text{in}}$)



82a-HA-3 ($T=0^{\circ}\text{F}$, $K_{Jmax} = 130.2 \text{ ksi } \sqrt{\text{in}}$)

Figure 6-20. Fracture surfaces from several later vintage TC128-B materials.

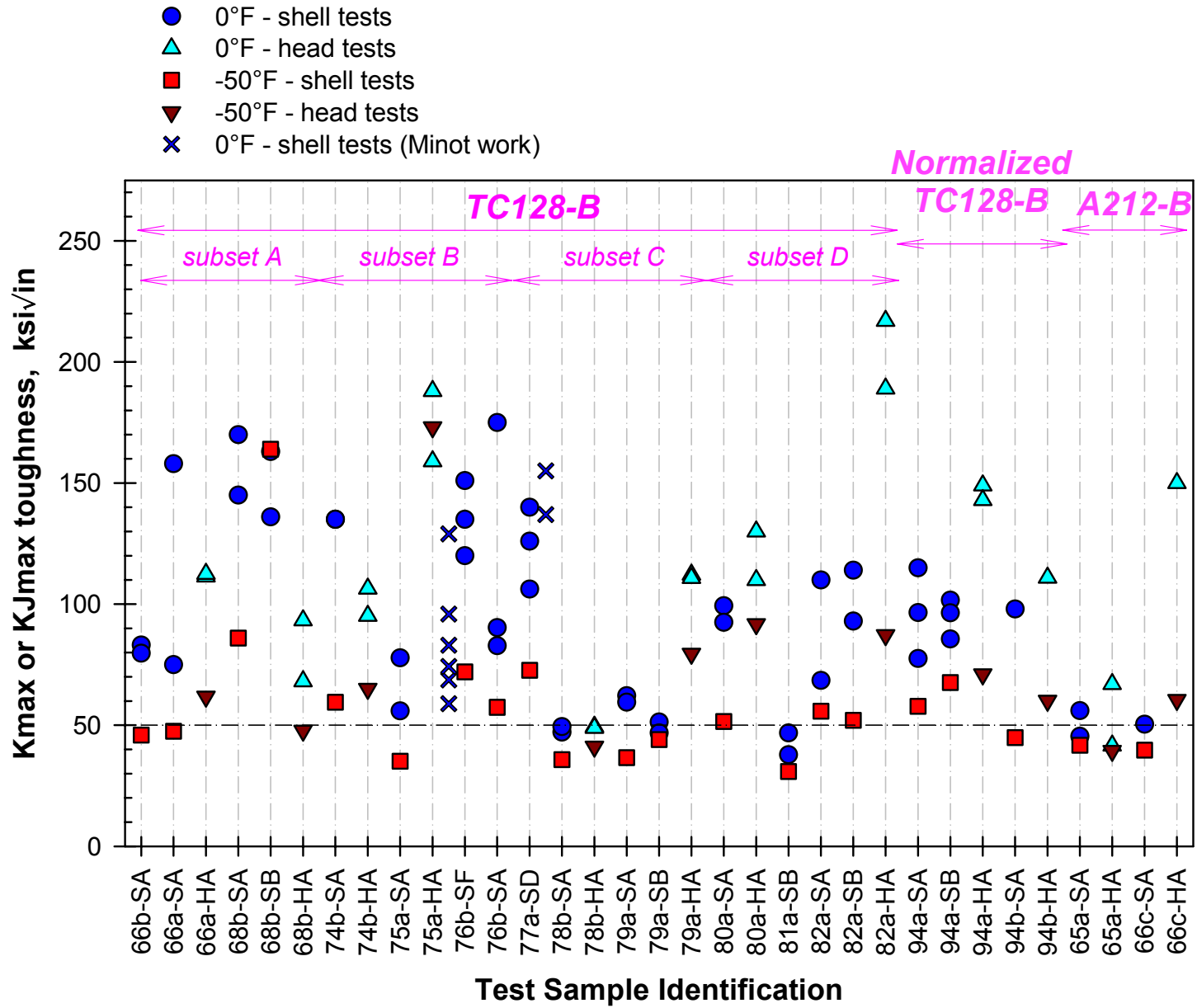


Figure 6-21. Fracture toughness plotted as a function of year for the different classifications of materials.

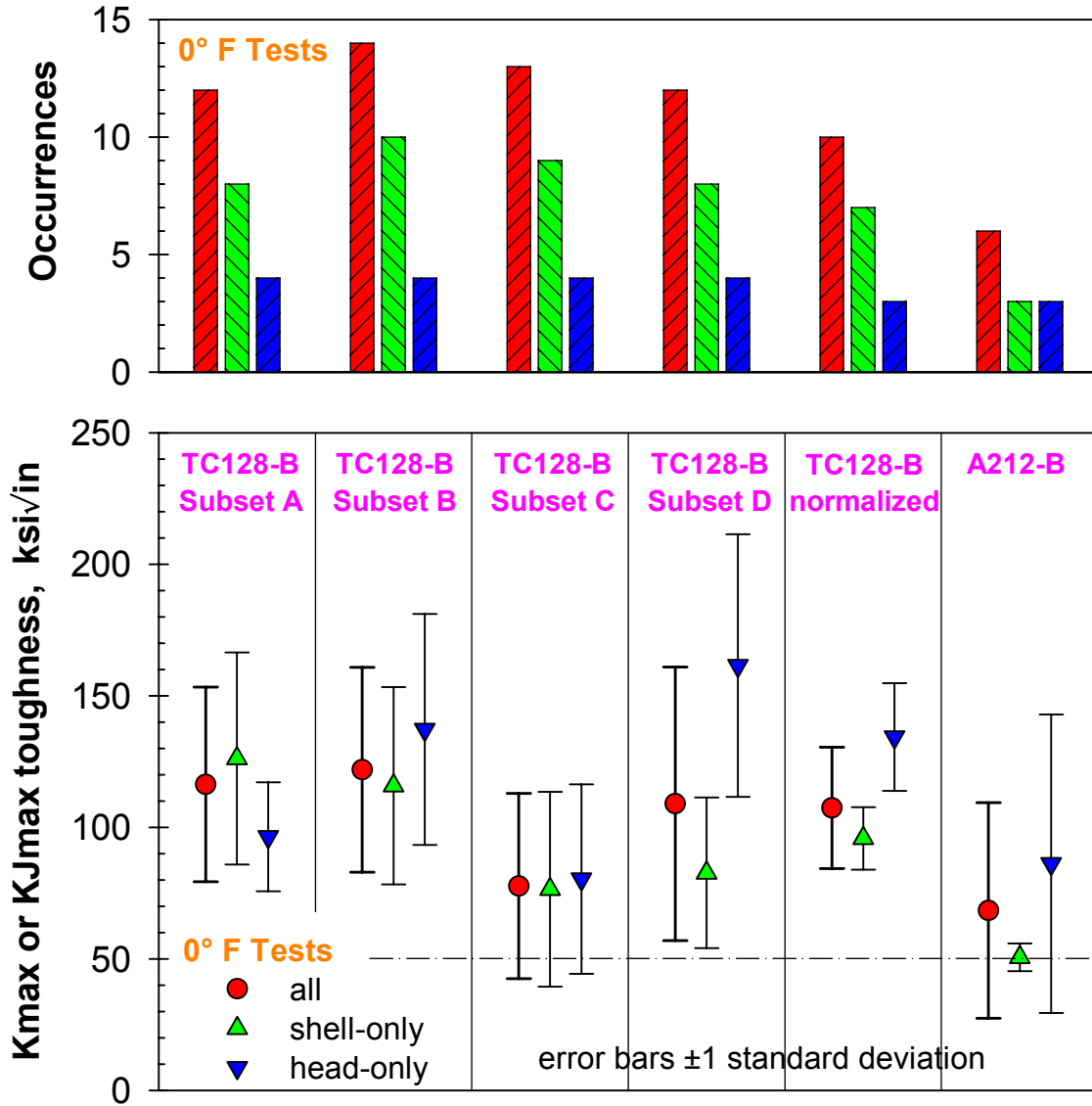


Figure 6-22. Fracture toughness average for the different ages/materials at 0°F.

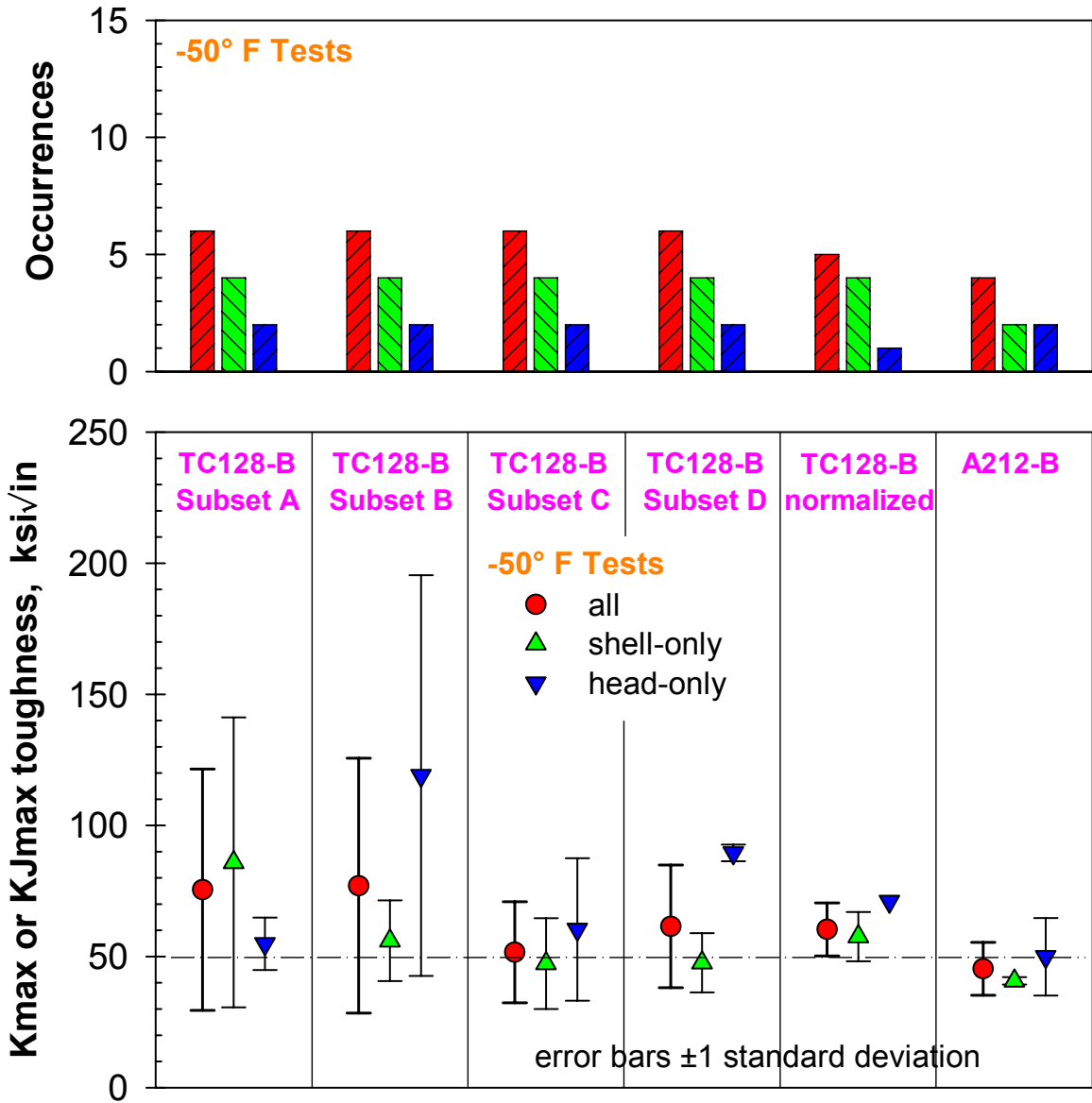
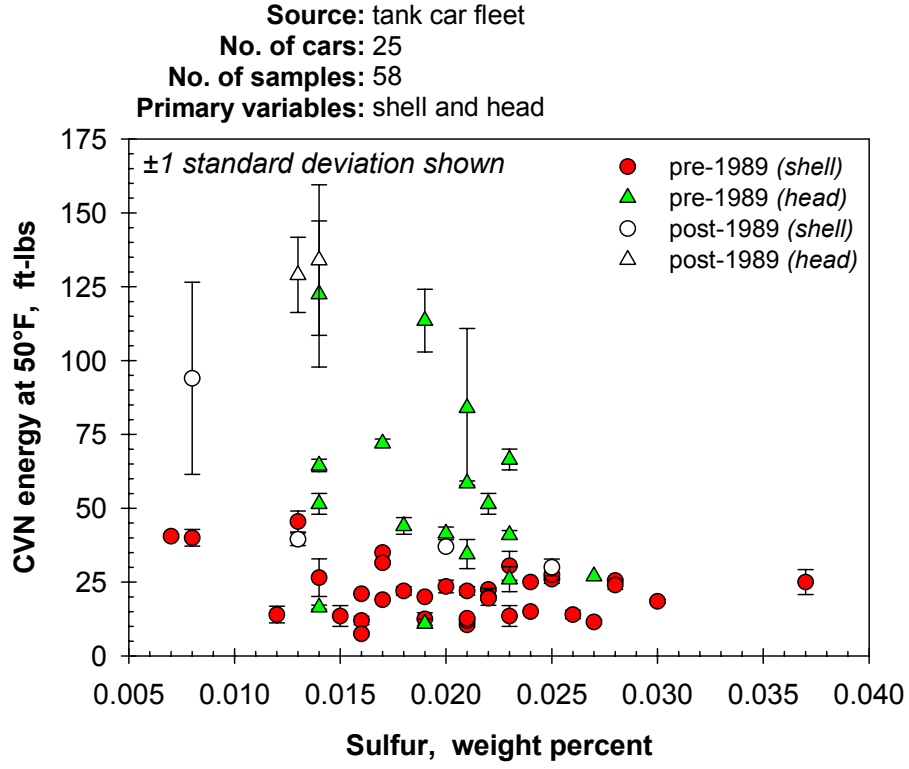
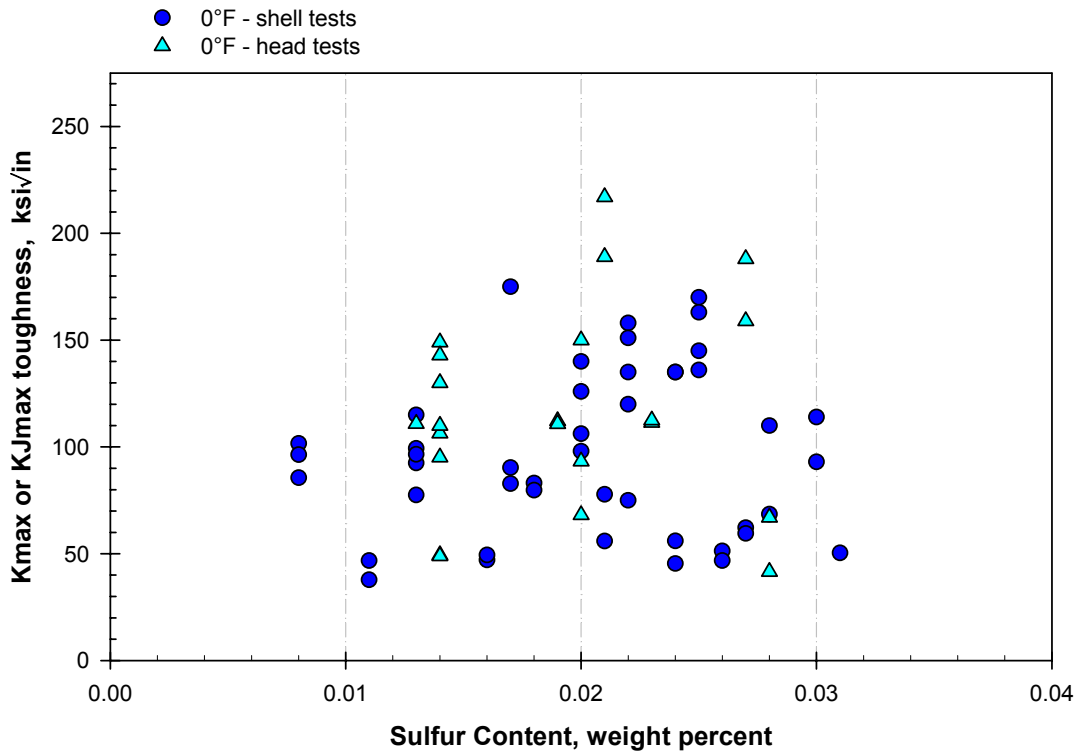


Figure 6-23. Fracture toughness average for the different ages/materials at -50°F.



(a)



(b)

Figure 6-24. CVN energy and fracture toughness variation with sulfur content.

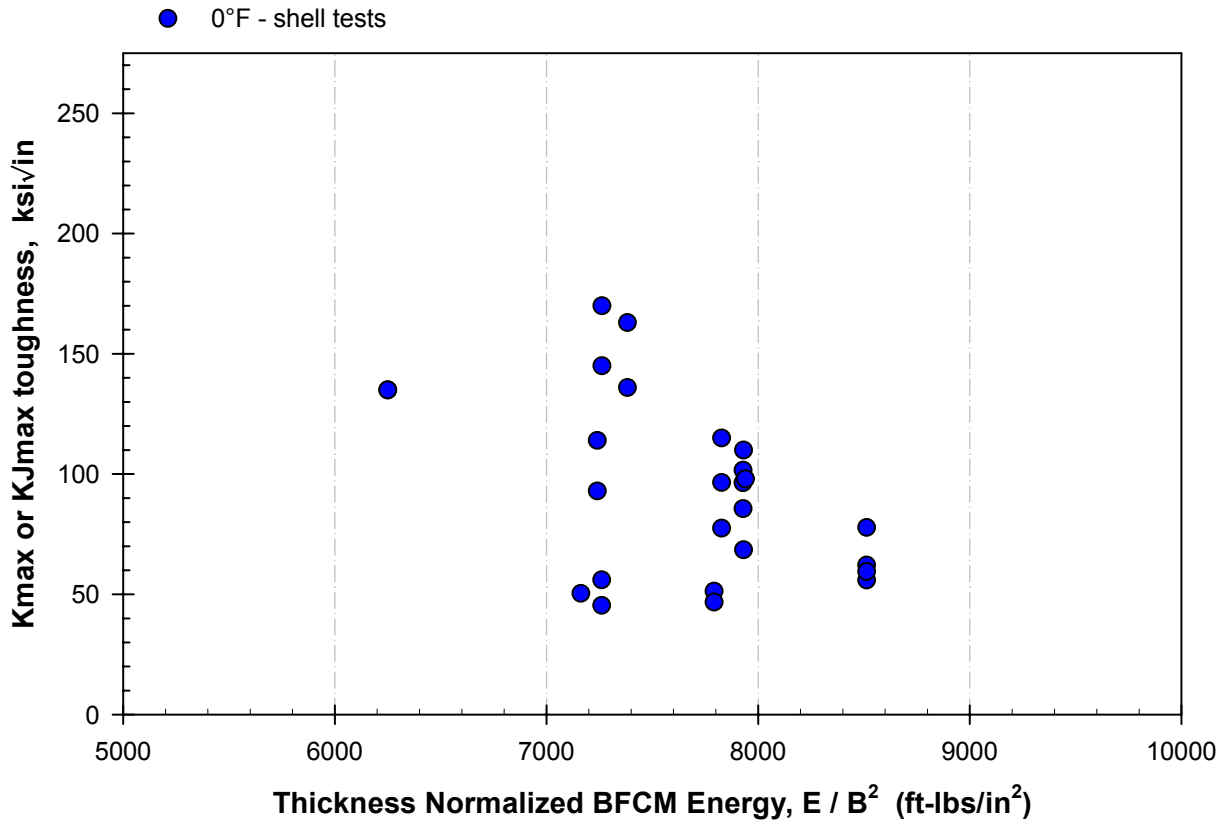


Figure 6-25. Fracture toughness variation with thickness normalized BFCM energy.

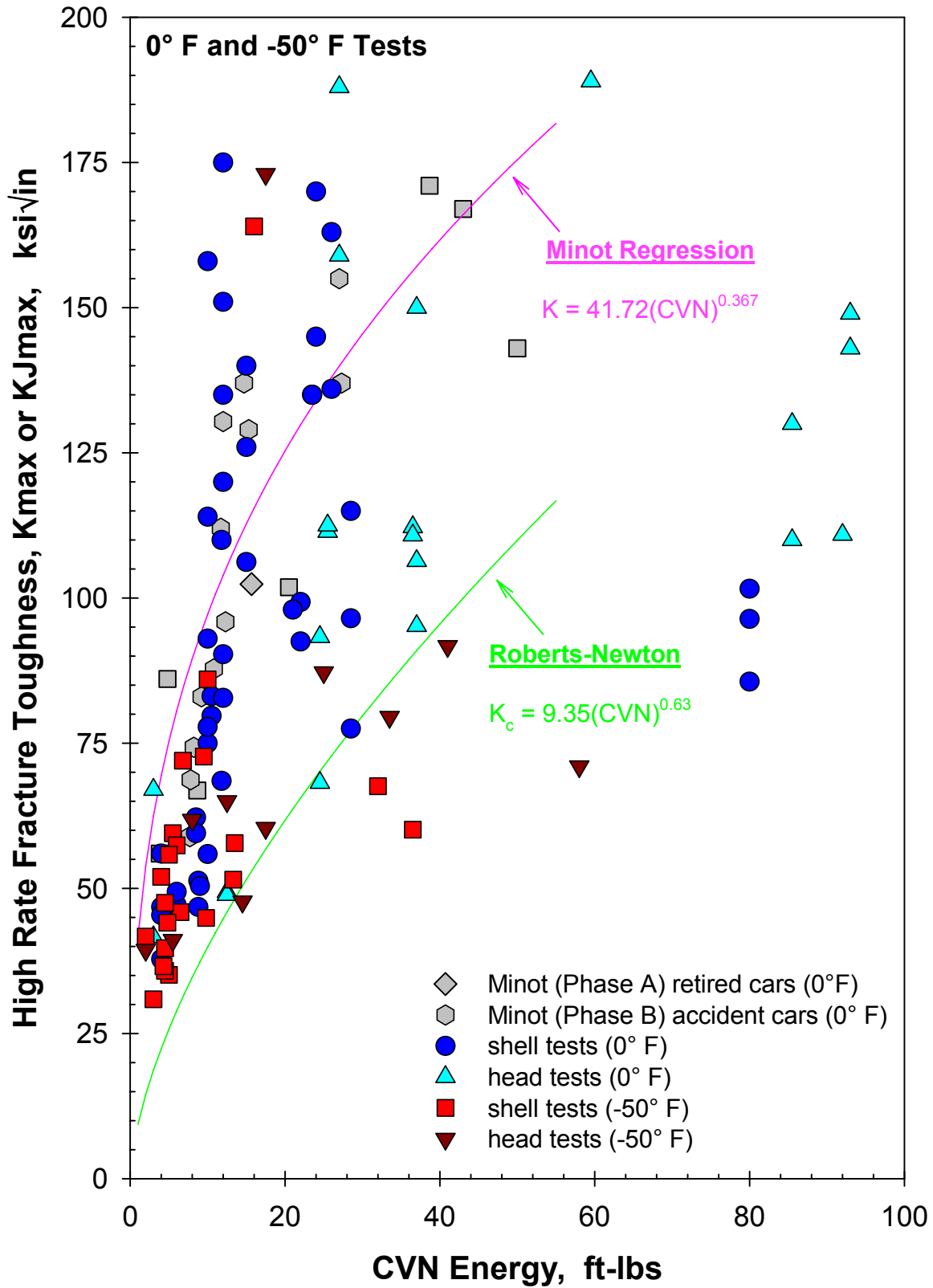


Figure 6-26. Fracture toughness as a function of CVN energy (at relevant temperature).

7.0 LIMITATIONS OF FRACTURE TOUGHNESS DATA

A recent NTSB document, entitled “NTSB Assessment of the Significance of Fracture Toughness on Tank Car Safety in Railroad Accidents,” authored by Alan Kushner is reproduced in whole in Appendix B. In this document, Dr. Kushner raises a number of excellent points regarding the data produced during SwRI’s GATX-sponsored Minot work. Since similar test and analysis methodologies were utilized during this program, this chapter is devoted to fully clarifying any confusion that may exist from this or earlier reports.

7.1 Toughness Methodology Utilized Herein

The test methods utilized herein tended to be somewhat non-standard. This results in some confusion regarding the type of test performed during this testing. This confusion is probably based on the fact that no specific test standard was applicable to the conditions that were necessary to evaluate. The purpose of this section is to ensure that a full understanding exists for exactly what procedures were applied during the testing and analysis.

When faced with performing an ASTM-valid fracture toughness test, there are basically four choices of toughness parameters available. These measures include:

- *K_{IC} fracture toughness (ASTM E399)* – typically used when a material exhibits low energy, mostly brittle fracture where plane strain conditions dominate and plasticity effects are low (best for thick structure with low amounts of plasticity)
- *K_c fracture toughness (E561)* – a wide panel, thin material test well suited for assessing conditions where plasticity plays an important role but the crack tends to remain stationary or enveloped in the plastic zone during testing (best for thin sheet applications like a wing skin)
- *CTOD fracture toughness (E1290)* – popular in the offshore industry and in Europe and quantifies crack-tip opening displacement (CTOD) values at one or more of several crack extension events. Useful for materials spanning brittle to ductile behavior
- *J_{IC} (or similar J-based) fracture toughness (E1820)* – an elastic-plastic test method using both K-based and J-based (extracting data from the energy, or area under a

load-displacement curve) methods and also including the effect of slow, stable crack advance (tearing) in the specimen (best for high energy, moderate strength materials).

Given these four approaches, the second one is germane to thin panel fracture, clearly not the case that we have here. Therefore, the choices are either a K-based or J-based approach (in a sense CTOD can be viewed as a special case of J for ductile behavior and K_{Ic} for brittle, although it tends to lack the rigor that the other toughness measures have). Items that also need to be factored in include: (a) the material tested herein is thinner than typical for plane-strain conditions, (b) it is curved so we are practically limited in specimen size, and (c) testing is occurring at both low temperature and at elevated loading rate with strain rates approaching 5 inch/inch/second. The high strain rate has serious implications with regard to transducer performance and data integrity. Applying a J-based testing method requires highly accurate crack extension measurements which are not practical when time to peak load is 1/1000th of a second. The implication: it should be self evident, **none** of the accepted, ASTM-codified test methods apply to the peculiar test conditions performed herein.

The testing method applied was a combined method utilizing some aspects of the K_{Ic} test and some aspects of the J_{Ic} test. The route that was taken was a combination of both, and the toughness parameter resulting depended upon the behavior exhibited in the test, as discussed below:

OPTION 1 (Linear-Elastic) – If the fracture was “linear” with little deviation in the load-displacement curve from linearity (calculated by comparing the area under the load-displacement curve with the area under the compliance line defining the most linear region of the data), an approach akin to K_{Ic} was utilized. A standard K_{Ic} analysis was not employed because the load-displacement data from the high rate tests generally did not have the fidelity to differentiate a K_{Ic} value. The author did not want to inject test engineer bias into having to “interpret” a test and “throw out” portions of the data based on judgment; instead, the bias-free maximum load approach was used.

OPTION 2 (Elastic-Plastic) – If extensive non-linearity was apparent in the data, an approach was taken where a J-value was calculated based upon the current K and the area

under the load-displacement curve (see Section 6.7 for more detail on this method). It should be noted that displacement was measured during this program with an eddy current transducer which was immune to dynamic effects but had less overall resolution than a conventional clip gage (hence, load-displacement traces for these faster tests did not have the fidelity that the Minot tests had). Calculation was continued until the maximum load was reached where calculation was stopped and J was converted to its linear-elastic equivalent $K_{J_{max}}$ so results could be compared between the two approaches. This method is identical to that employed in E1820, except crack length is not known (to plot a J-R curve). Rather, the assumption that is made is that crack advance prior to peak load is minimal, which is not an unreasonable assumption for an engineering measurement of toughness.

Is this approach and are these tests ASTM valid? Unfortunately not, but this is clearly a consequence of the conditions under which data was required. In fact, there is no standard that could yield a fracture toughness of more relevance in this setup with its inherent peculiarities.

7.2 Toughness Magnitude and CVN Correlations to Fracture Toughness

Two issues of concern to Kushner in the NTSB document included in Appendix B were (a) the observation of dynamic toughness in excess of quasistatic toughness and (b) the higher dynamic toughness level than expected from measured CVN energy.

The trend of toughness with temperature and loading rate is reproduced in Figure 7-1 from Barsom's text [14]. Confusion can arise because loading rate effectively shifts transition temperature. In the case of lower shelf behavior where temperature is less than NDT, one would expect dynamic toughness to be less than static toughness. This is contrasted to the upper shelf situation where high rate dynamic toughness exceeds quasistatic fracture toughness. No conclusions can be made in the intermediate range.

Given this, the obvious question is: In what regime were the tank car steels operating? With the observed variability, tests were effectively on the lower shelf, in transition, and near the upper shelf. In fact, a close examination of the fracture surfaces indicated in Figures 6-17 to 6-

20 show a clear transition occurring. At toughnesses less than 60 ksi√in, classic cleavage fracture can be observed. This is contrasted to the woody, rough, high plasticity fractures occurring at toughnesses in excess of 80 ksi√in. Although cleavage was likely still occurring to some extent, the fracture was of mixed mode. All of this uncertainty contributes to a situation where dynamic toughness could be either higher or lower than quasistatic toughness. Frankly, with the scatter observed it is not clear to the author that there is any statistical significance to the slight difference noted by Kushner.

A recent review of fracture toughness correlations [15] summarized the relationships used to link CVN energy to fracture toughness. In total, thirty-one published correlations are available. These correlations exist for a wide variety of conditions: some for lower shelf only, lower shelf and transition, upper shelf only, etc. Some correlations are also better suited to specific materials or welds-only.

Many of the correlations are used in design and as such must be operating as a lower bound estimate linking the two parameters. A summary of three of the different correlations is included in Table 7-1. Kushner in Appendix B uses the Corten-Sailors relationship [16] to provide an explanation for why he believes SwRI fracture toughness magnitudes are higher than expected. Kushner also asserts that the Roberts-Newton correlation supports this finding.

Two plots are shown in Figure 7-2 extracted from the Roberts and Newton paper [13]. In the text of the paper, Roberts and Newton clearly state that the expression in Figure 6-26 is a lower bound to the expressions observed in Figure 7-2(a). A similar lower bound can be established for K_{Ic} (see Table 7-1). A close examination of Figure 7-2 clearly indicates that this expression is indeed acting as a lower bound to the experimental test data. This is precisely the same finding noted when Figure 6-26 was discussed in the context of the data and the Roberts and Newton relationship. The data in Figure 6-26 further validates exactly what the correlation was intended to do: act as a lower bound. Since the correlations are indeed lower bound, the observation of higher toughness levels during SwRI testing is expected.

Finally, Kushner further asserts that the toughness values predicted from the Corten-Sailors correlation [16] suggest that the toughness observed in SwRI dynamic testing is too high. A close examination of reference [15] indicates that the CVN energy value necessary in the Corten-Sailors expression, also Kushner's Eqn. 6 (Appendix B), is that from a fatigue pre-cracked CVN specimen. Since CVN specimens were not precracking during this testing, this correlation therefore does not apply and it can not be used to judge toughness magnitude for this case.

7.3 Accommodating Nonlinear (Ductile) Fracture

The increase in loading rate obtained in the latest round of testing resulted in a loss in some fidelity in the crack opening displacement measurements. Probably more than anything, the data tended to vary significantly from test to test, exhibiting both high quality as well as poor quality. Presumably, the quality depended upon uncontrolled laboratory factors.

This is not to say that the eddy current gage did not yield satisfactory displacement data. In general it did. One of the things that is always examined during analysis of the fracture test data is the measured compliance of the specimen. Compliance is the first indicator of whether loads and displacements are in accordance with expectation. Given a specific crack length (and of course specimen design), compliance, the reciprocal of stiffness, is simply a function of the specimen geometry. A comparison of measured compliance with theoretical compliance is indicated in Figure 7-3 for all of the tests performed. Compliance has been observed to generally vary in the range of $\pm 10\%$. As shown in Figure 7-3, the vast majority of the tests satisfied this criteria. Less than 10% of the total number of tests were outside the $\pm 10\%$ boundary (furthermore, ASTM does not view this as a criterion and only requires reporting if it is outside the bounds). This lends credence to the load and displacement measurements made here. In general, excellent consistency was observed between the displacement gage and the strain gage; hence providing yet another indicator of the integrity of both measurements.

In Appendix B, Kushner applies the K_{Ic} analysis methodology to two tests included in the Minot investigation with K_{max} toughnesses on the order of 100-110 ksi \sqrt{in} . These tests were both dominated by plasticity and hence with nonlinear load-displacement curves. The resulting K_{Jmax}

toughnesses were on the order of 165-170 ksi $\sqrt{\text{in}}$. In the Minot report, the $K_{J_{\text{max}}}$ magnitude was used to represent the toughness for both of these tests. Analyzing a plasticity dominated test using a K_{Ic} slope-offset method as Kushner did is incorrect. For instance, the linear elastic fracture mechanics (LEFM) K parameter has little or no meaning in these tests since the limit load at peak load is exceeded in both tests (by greater than 10% for each). In the analysis methods applied, nearly 75% of the resulting toughness was a consequence of area under the load-displacement curve. Analyzing this test with the K_{Ic} slope-offset method is meaningless in the context of fracture behavior.

Second, there are many causes for nonlinearity in the load-displacement diagram and not all are a consequence of crack advance. To further understand this, test data is presented from two other programs unrelated to this current testing (this is not TC128-B material). Data from a K-R curve is presented in Figure 7-4(a) for a structural alloy tested in a wide panel arrangement and in Figure 7-4(b) for a lower toughness/strength material in a C(T) configuration. In Figure 7-4(a), the black curve is the recorded load-displacement behavior with a significant amount of nonlinearity. For the two other curves, different plastic zone size corrections are applied to “straighten” the data. The methods employed are in accordance with a technique described by Bucci et al. [17]. A close examination indicates that in both plots in Figure 7-4 the plastic zone size corrections effectively linearize the data, hence validating in these two cases that the large plastic zone growth was a primary cause for nonlinearity. In the case of Figure 7-4(a), the toughness of this material was much the same as TC128-B: on the order of 125 ksi $\sqrt{\text{in}}$. For Figure 7-4(b), the yield strength was more comparable to TC128-B. Nevertheless, both of these examples clearly indicate that nonlinearity is not only caused by crack advance, and applying a simple, K_{Ic} type slope-offset analysis approach with the load-displacement data is incorrect. This is especially true in the case of materials that have toughnesses in excess of 50 ksi $\sqrt{\text{in}}$ due to the resulting size of the plastic zone.

7.4 Accommodating Linear (Brittle) Fracture

In general, two types of behaviors were observed during this testing. High energy, more ductile fracture as described in the last section or lower energy, brittle failure with significantly lower toughness magnitude. Kushner in Appendix B correctly notes that regardless of whether a K_{\max} or K_{Ic} approach is used to analyze the lowest toughness data, the magnitude of the resulting toughness is not changed significantly. He also notes that the Minot tests would also likely satisfy the ASTM validity checks. However, it should be noted that the ASTM K_{Ic} analysis methodology necessitates fairly stringent signal fidelity in the crack opening displacement data that typically was not present in this data. It was absent since the COD gage needed to accommodate (and be calibrated for) displacement behavior to 200 mils (as opposed to 5 mils for brittle behavior) and the test duration was on the order of 2-3 milliseconds. The rapid nature of the test results in a loss of displacement signal and load signal fidelity that makes a standard K_{Ic} analysis methodology problematic.

To further understand this, the load-displacement signals from three of the lowest toughness tests are further examined in Figures 7-5 through 7-7. These three tests include:

- 81a-SB-3, a 0°F test that yielded $K_{\max} = 37.8 \text{ ksi}\sqrt{\text{in}}$ (the lowest observed toughness)
- 78b-HA-1, a 0°F test that yielded $K_{\max} = 49.4 \text{ ksi}\sqrt{\text{in}}$
- 81a-SB-1, a 0°F test that yielded $K_{\max} = 46.8 \text{ ksi}\sqrt{\text{in}}$.

Included in these tests are both irregular and well-behaved load-displacement diagrams. The dynamic effects (signal periodicity) in the load data are first reduced by smoothing the load-time signal with a 3x2 Fourier polynomial. The plots shown in Figures 7-5 through 7-7 include both original signal and smoothed behavior.

In the case of 81a-SB-3 in Figure 7-5, the smoothing results in a load-displacement signal that is not well tailored to any further analysis. This is contrasted to the behavior noted in Figure 7-6 where a bilinear load-COD result is obtained. Analysis using a conventional K_{Ic} technique would suggest a significantly lower toughness magnitude, reduced approximately 50%

from the peak level. Is this effect real? On balance, considering the alternatives, this approach for analyzing the data was rejected and not employed for the tests herein for several reasons. First, the data does not meet the load-displacement “smoothness” requirements of the rapid rate annex in ASTM E399. The smoothing technique applied is not included in the ASTM analysis procedure. Finally, it is believed that this approach requires injecting too much qualitative data processing (e.g. bias) into the analysis process. However, some tests yielded data that could be analyzed using the ASTM K_{Ic} method to a degree at least. An example of this is shown in Figure 7-7 where the original signal violated the data smoothness requirements of the rapid rate annex. After smoothing, as shown in Figure 7-7, the data was able to be analyzed and the resulting K_{Ic} toughness was virtually identical to analysis using the K_{max} approach.

7.5 Structural Relevance of Test Results

The testing performed herein has generated structural results, not material property results. There is clear structural dependence as part of these results and the data would be expected to exhibit size effects.

A clear indication of the structural nature of the test results can be obtained by examining the column labeled “limit ratio” in Tables 6-4 to 6-8. For convenience, these data are plotted in Figure 7-8 for each of the test conditions. The limit ratio is the percent of limit load for the specimen at the maximum applied load. A value of 0.8 would imply that at the maximum load, the specimen sustained 80% of the limit load possible with that specimen/material combination. Conversely, a value of 1.25 would imply that the load was at 125% of limit load. Had the test specimens been larger, the limit load ratio would likely have been less. However, these specimens were about as large as possible without significantly thinning the specimen and not testing full wall thickness (i.e. they would have been too curved to test to bigger dimensions).

Also shown in Figure 7-8 is a line at a limit ratio of 0.67. For the specimens that were beneath this line, K-based linear-elastic fracture mechanics applies. For the tests above the line, plasticity conditions dominated and an elastic-plastic parameter governed toughness (such as the

K_{Jmax} parameter). K_{Ic} is clearly an unsuitable test method or toughness quantifier for this regime and for the majority of the tests performed.

It is likely that plane-strain dominance was observed in the test specimen involved in this program. The first clear indication of this is the extent of flat fracture (without shear lips) observed in the specimen and documented in Figures 6-17 to 6-20. Although the specimens are flat, at high applied K -levels a significant amount of through-thickness “necking” is observed. Nevertheless, the most recent version of E399 has relaxed the thickness requirement. In fact, there currently is no thickness requirement, but a remaining ligament size requirement of $2.5(K_{Ic}/\sigma_{YS})^2$ is still present in the standard.

7.6 Significance of Dynamic Fracture Toughness to Tank Car Structural Integrity

Kushner provides an extensive discussion in the NTSB document contained in Appendix B related to the significance of dynamic fracture toughness to the tank car integrity program. He makes several excellent points regarding the significance of toughness. Since the NTSB recommendations that led to the work detailed here, there has been a considerable amount of work done to try to better understand what occurs in a tank car accident. We have the benefit today of making use of that expertise when examining the structural integrity issues.

Static strength, or possibly fracture toughness, is a driver if the tank is ever allowed to “go hydraulic solid” in an accident. In other words, “hydraulic solid” occurs when denting is sufficient to take-up the outage in the tank car’s product. Hence, it is the condition when further impact and shell deformation is resisted by a fluid with no more gaseous head. This is likely the situation that rockets tank car pieces thousands of feet in the most violent accidents that occur.

For the more typical accident, shell and head puncture are the critical occurrences that must be avoided. Despite what others have publicly stated, an individual with extensive failure analysis experience was given access to the Minot wreckage and he made the observation that most if not all of the fractures that he saw on the different tank cars involved also had some form of puncture in or adjacent to them. His belief was that the first step in the failure process for

most of the Minot cars was likely puncture and the second step, given sufficient energy, was separation of the tank.

Unfortunately, we do not yet have a good understanding of what material properties contribute to enhanced puncture resistance. Some of the work required to better understand this is currently underway, and initial findings appear somewhat promising in terms of better understanding what parameters drive puncture. Properties such as a materials fracture toughness and static strength likely play some type of role; however, the significance of these roles is not yet clear since the physics-based models for puncture have not been developed.

Table 7-1. Different forms of the equation relating CVN to fracture toughness (K is in ksi $\sqrt{\text{in}}$ and CVN is energy in ft-lbs).

$K_x = A(CVN)^B$			Comments	Reference
Toughness K_x	A	B		Source
dynamic K_{Id}	15.87	0.375	Kushner NTSB document, eqn. 4	Corten and Sailors [16]
quasistatic K_{Ic}	9.35	0.65	Figure 6-26 and Figure 7-2(a) in this report	Roberts and Newton [13]
dynamic K_{Id}	21.6	0.17	Figure 7-2(b) in this report	Roberts and Newton [13]

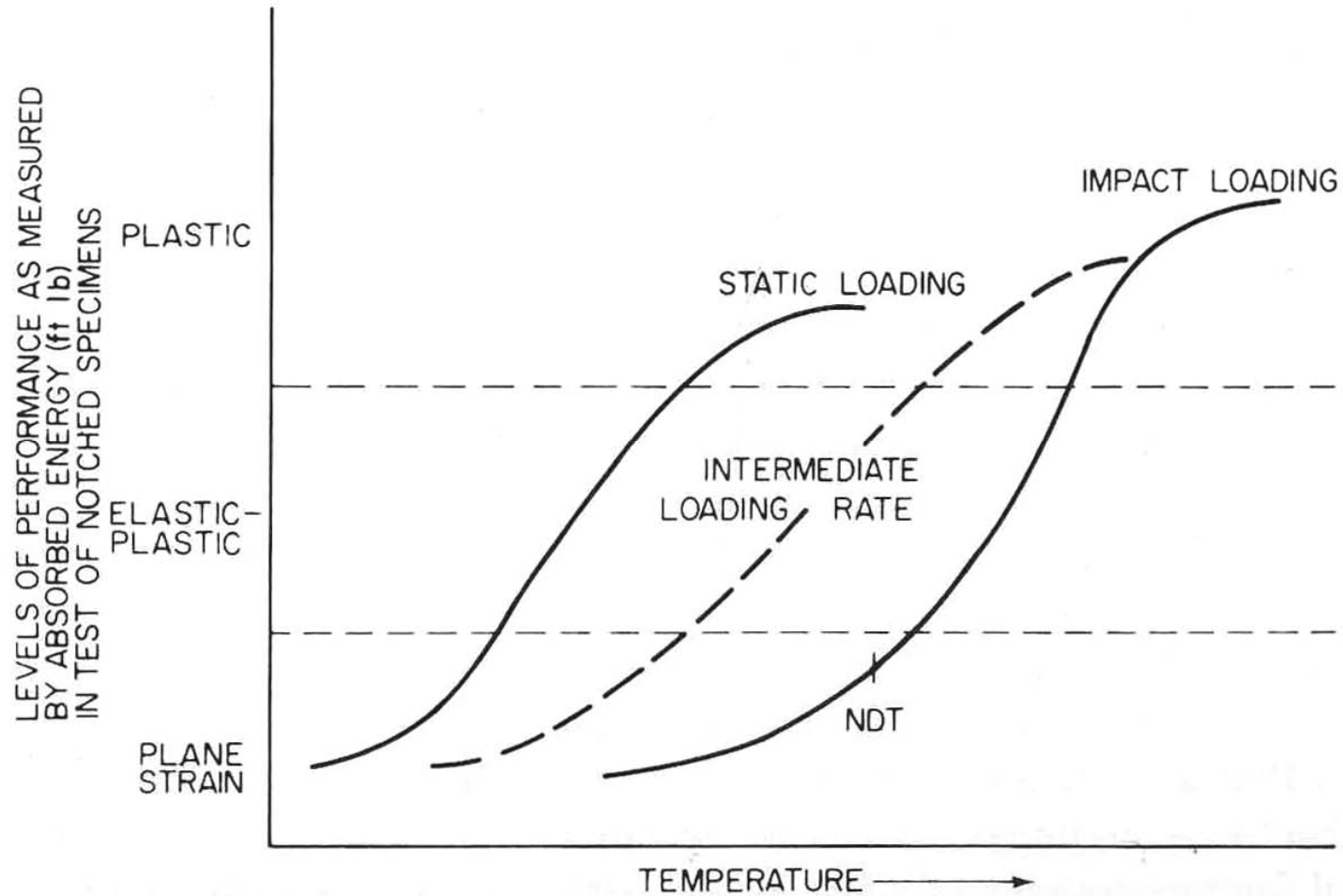
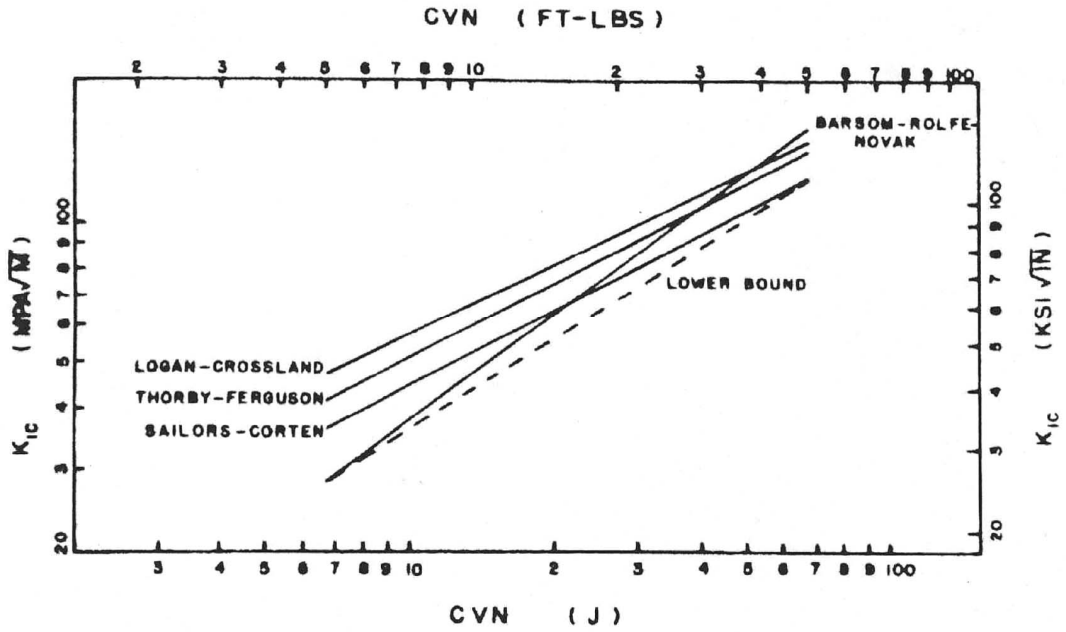
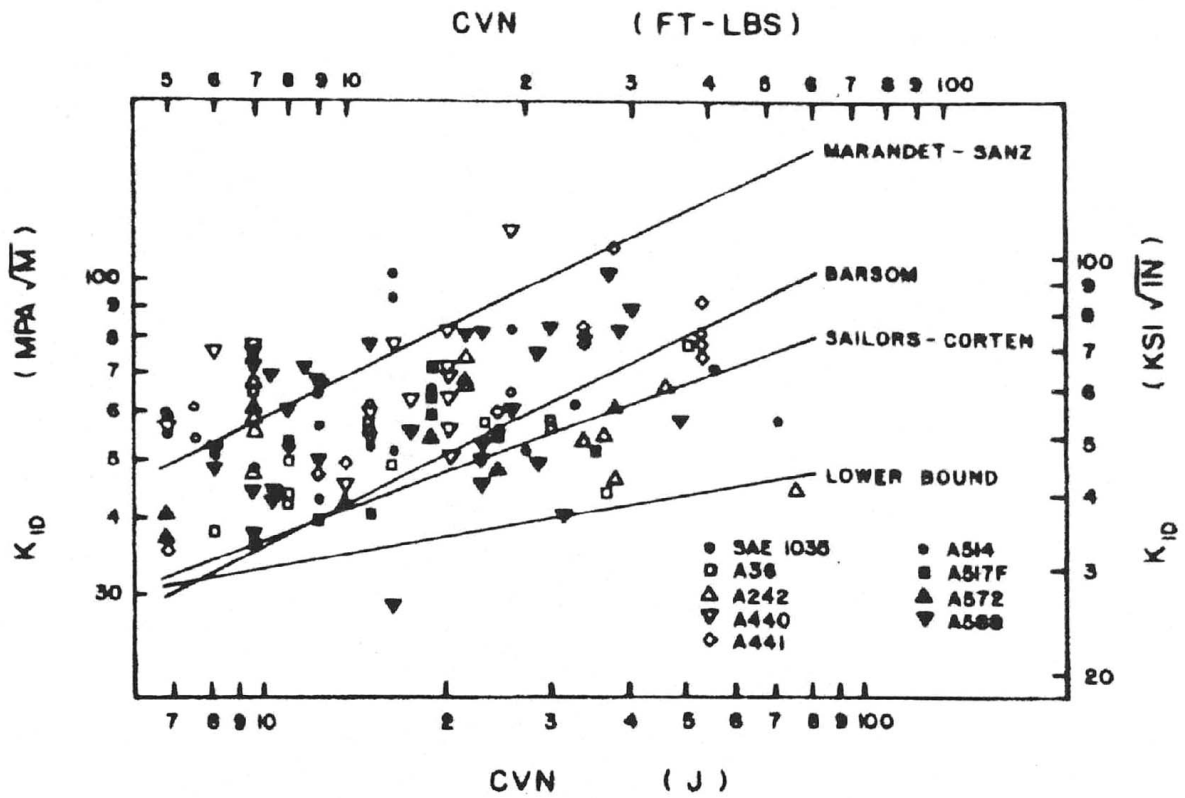


Figure 7-1. Variation in toughness as a function of temperature and loading rate (from reference [14]).



(a)



(b)

Figure 7-2. Two plots indicating the lower bound relations from Roberts and Newton [13].

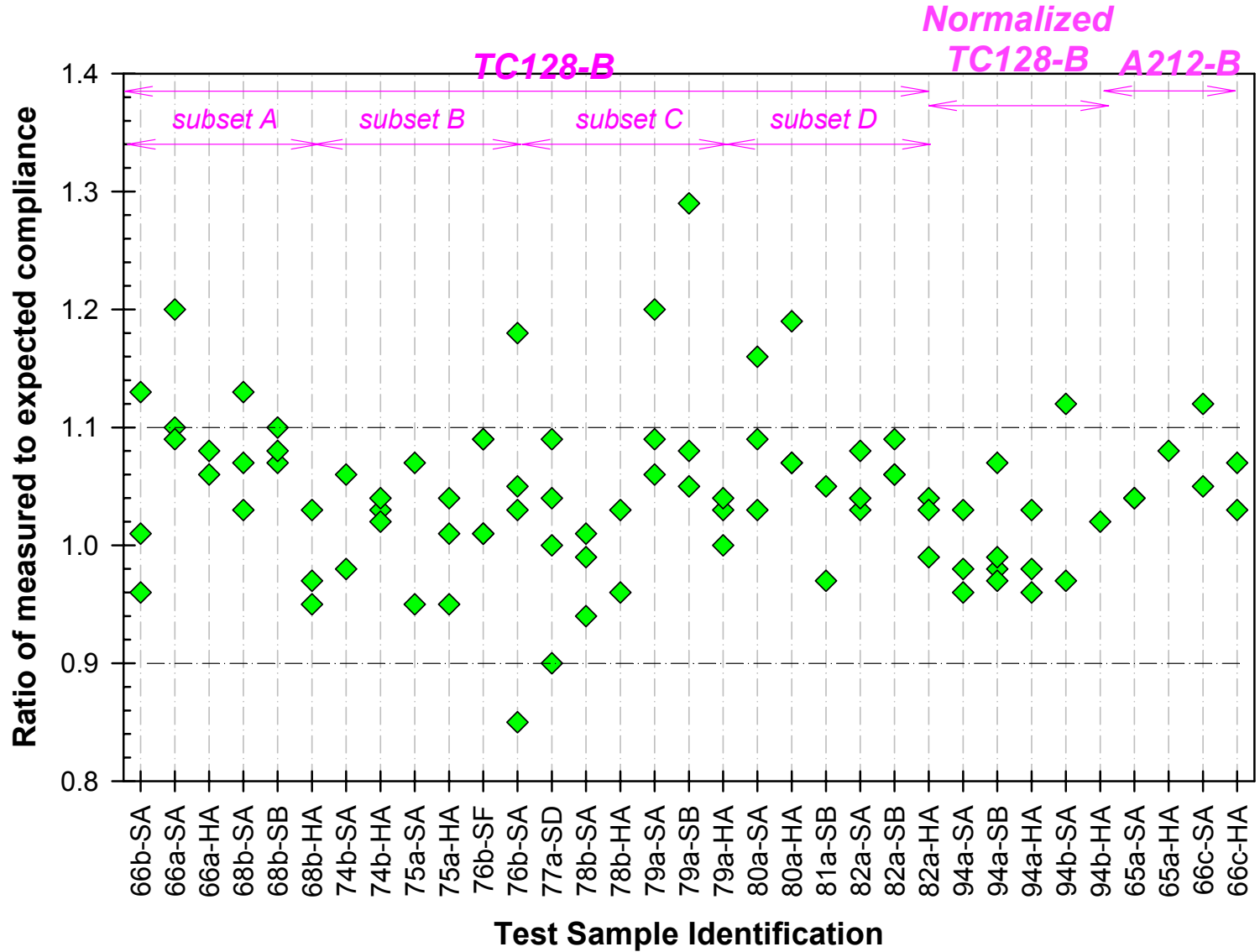


Figure 7-3. Comparison between expected compliance (based on crack length) to measured compliance.

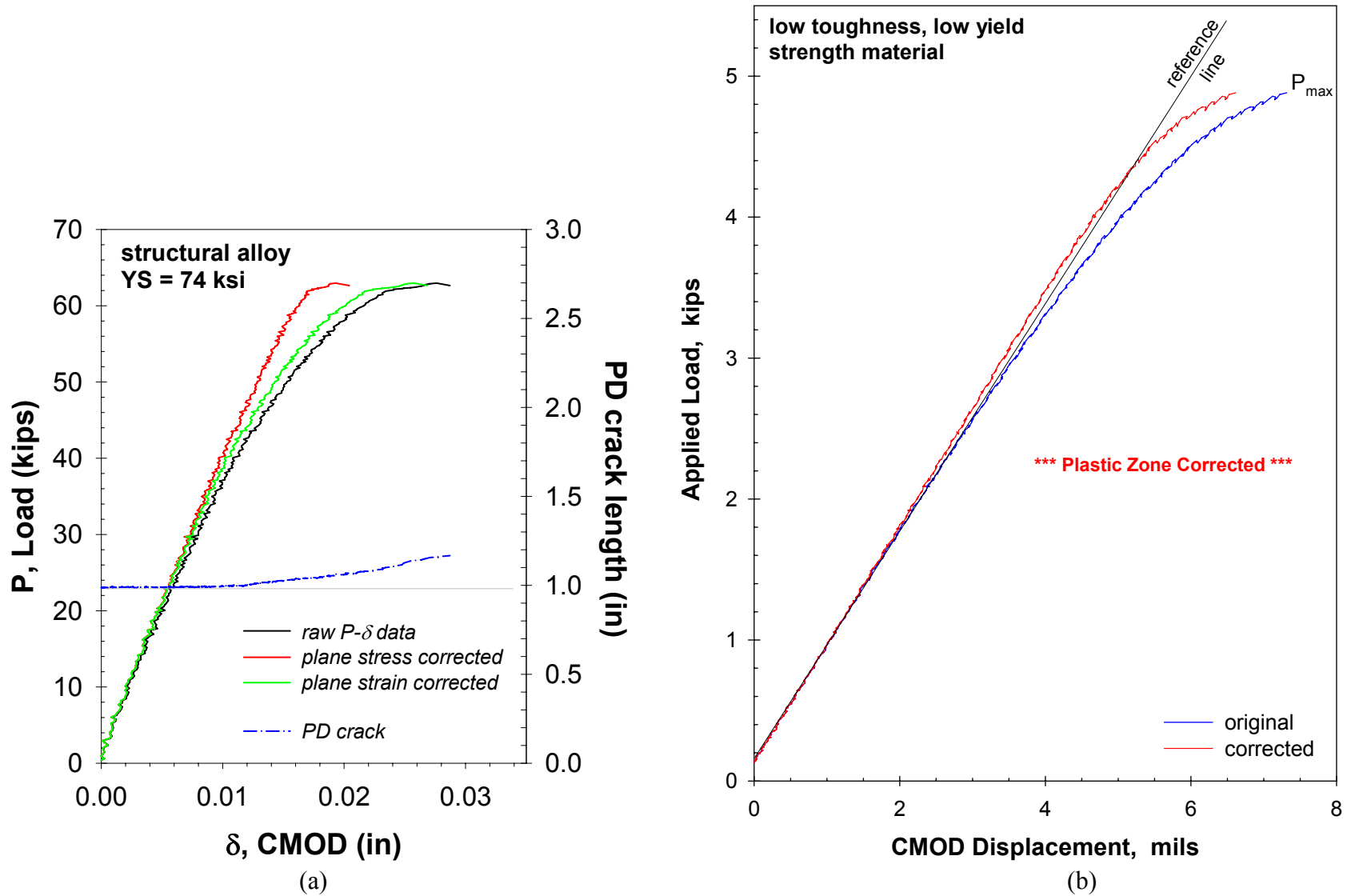
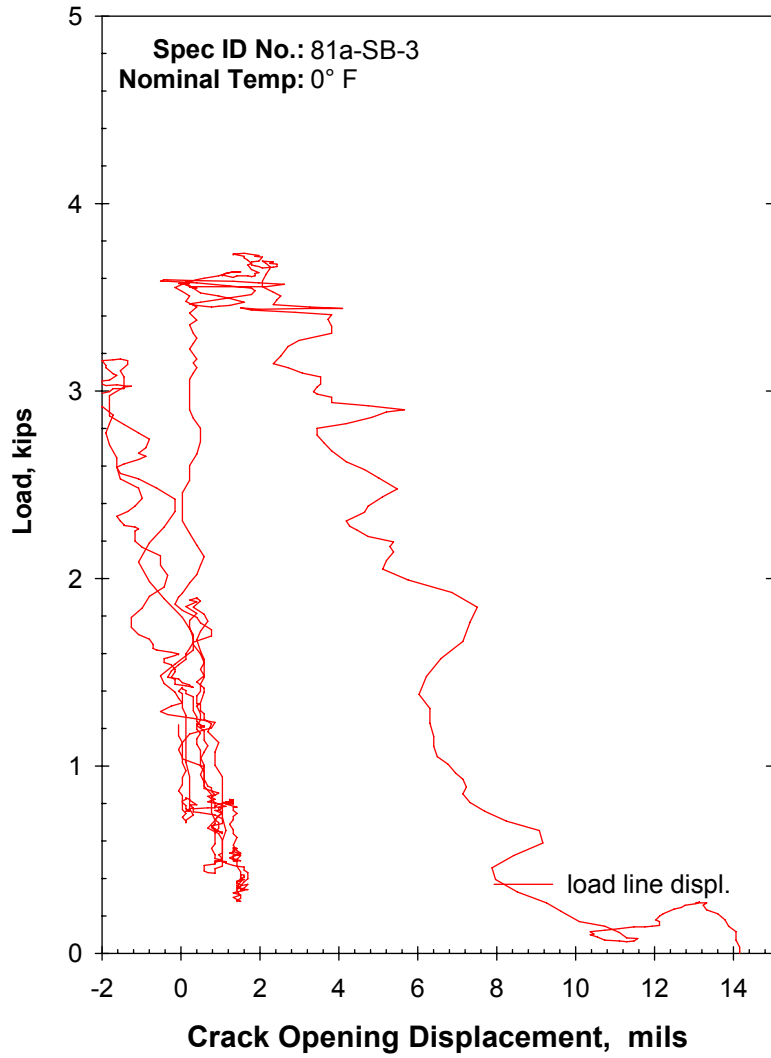
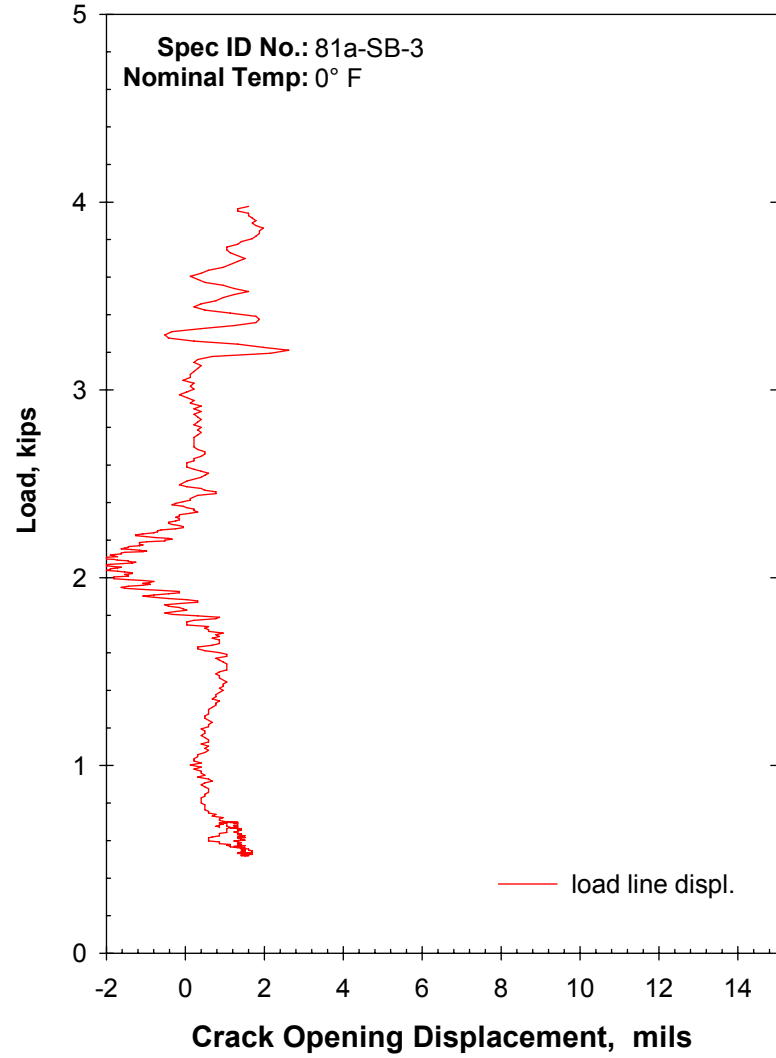


Figure 7-4. Sample nonlinear data where the majority of the nonlinearity is plastic zone growth for two different tests/materials.

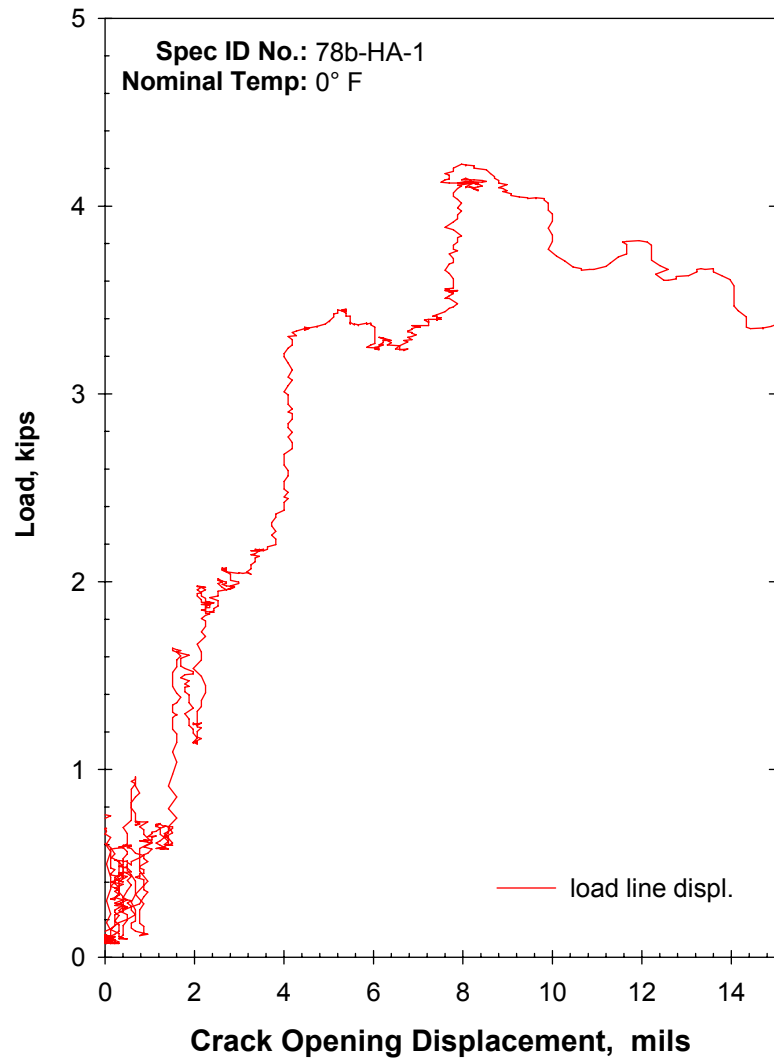


(a) original uncorrected

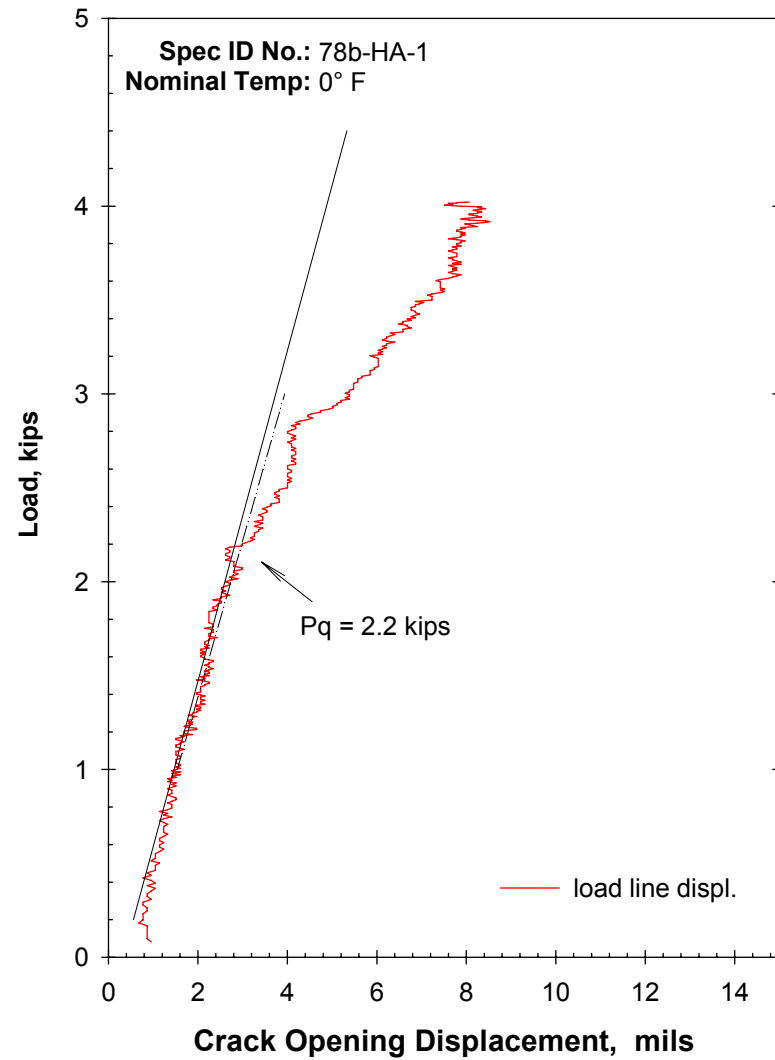


(b) after Fourier polynomial load smoothin

Figure 7-5. Attempt to analyze a troublesome load-displacement diagram.

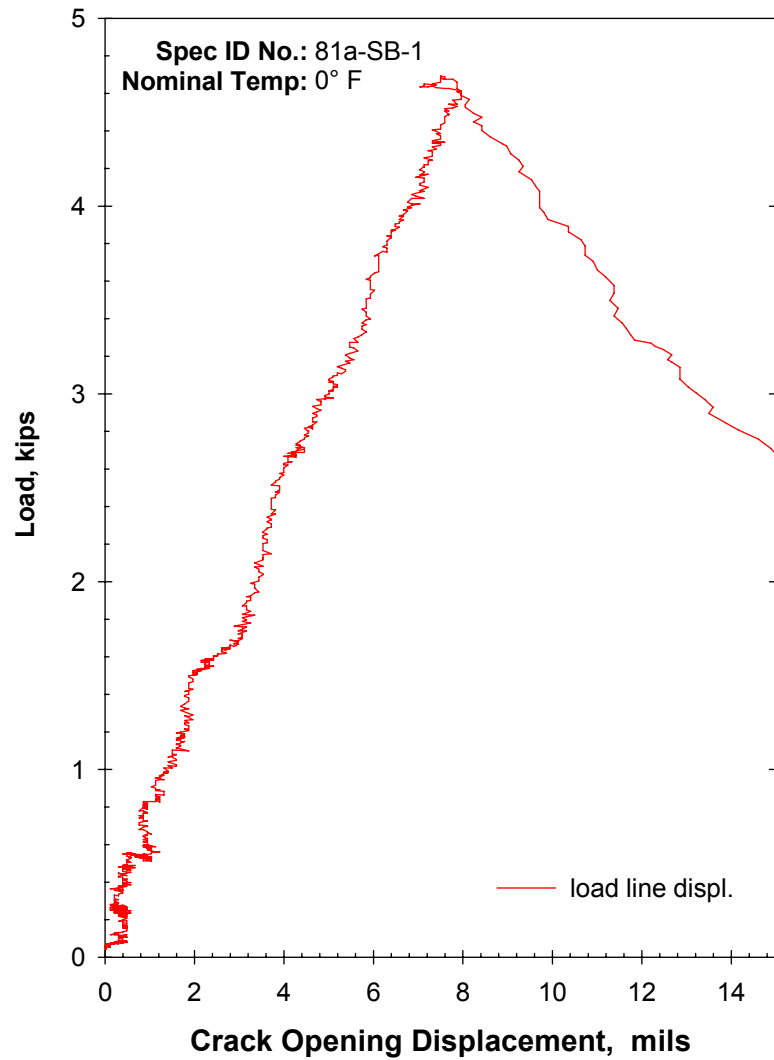


(a) original uncorrected

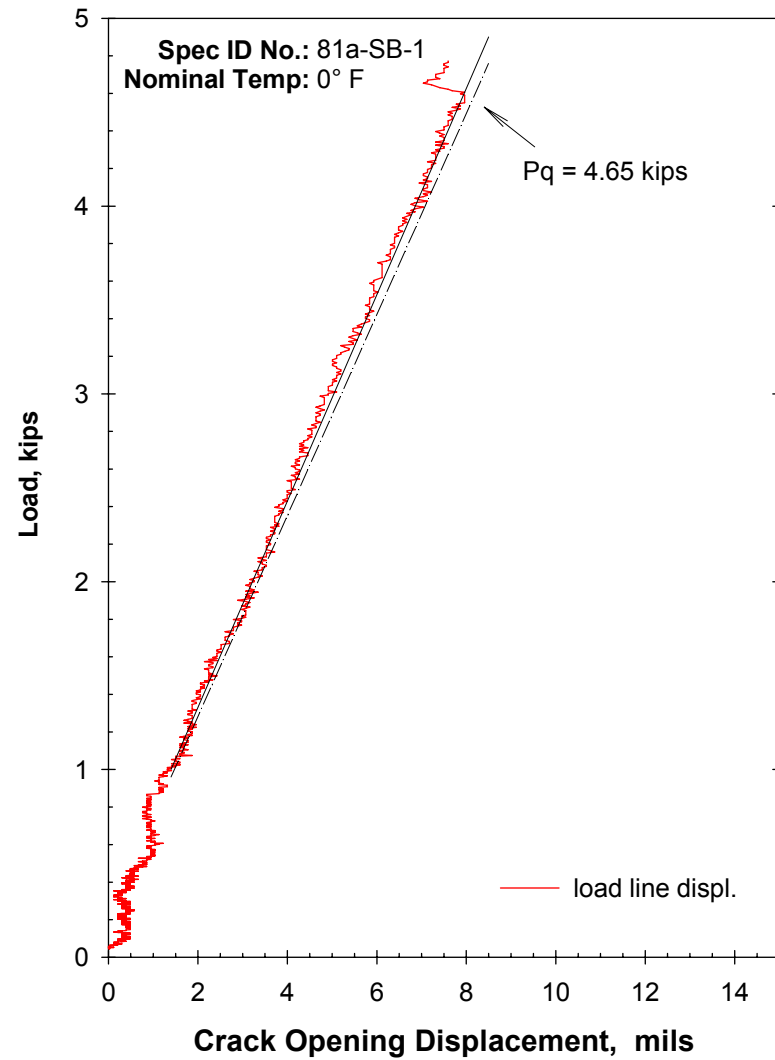


(b) after Fourier polynomial load smoothing

Figure 7-6. Analysis of another questionable load-displacement diagram resulting in lowered toughness.



(a) original uncorrected



(b) after Fourier polynomial load smoothing

Figure 7-7. Fracture test data set only made suitable for analysis by smoothing the dynamic nature of the load data.

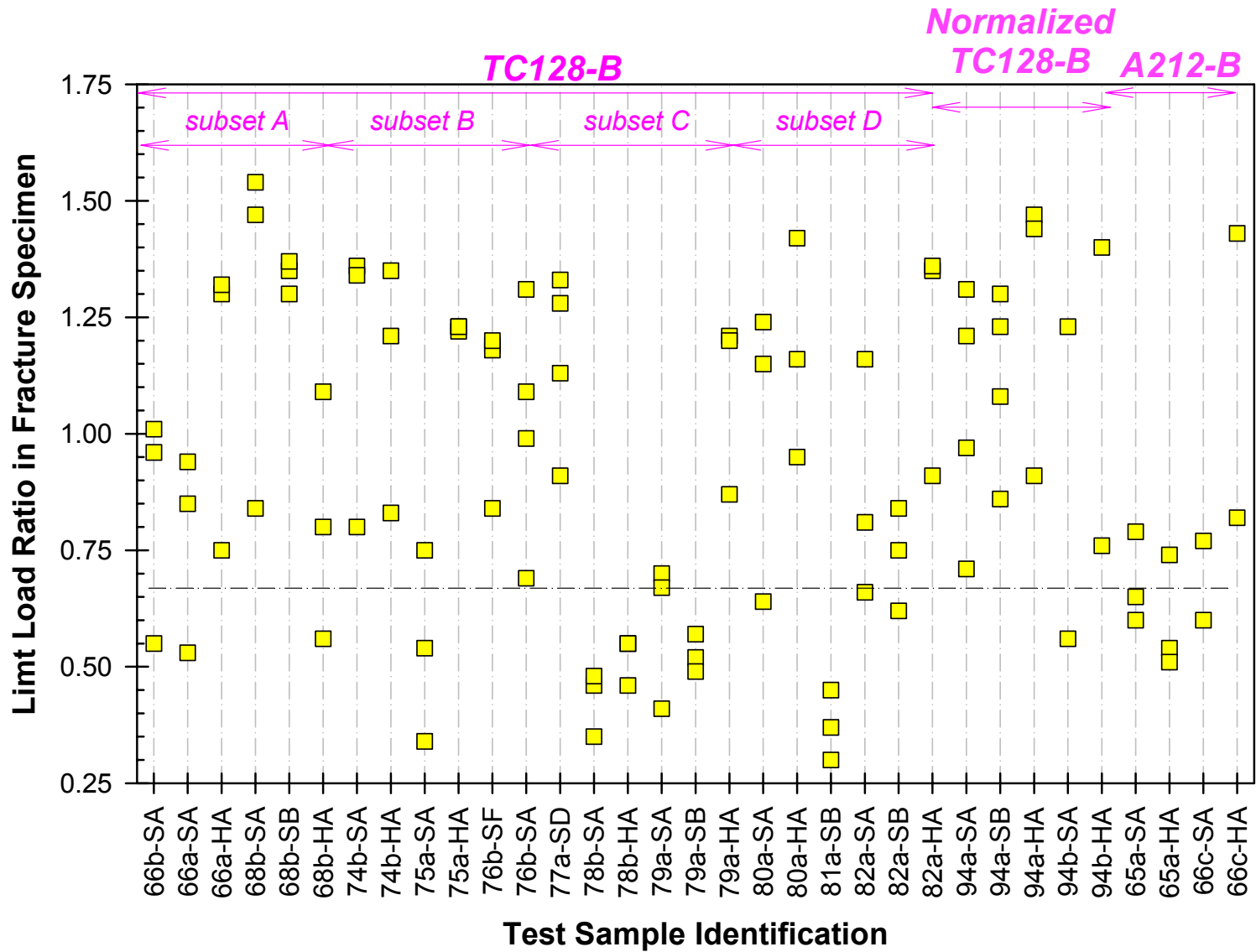


Figure 7-8. Variation of limit load ratio (ratio of max load to the limit load of the specimen) for all tests.

This page intentionally left blank.

8.0 SUMMARY

The focus of this program has been to first collect a representative sample of material from retired tank cars so that the material characterization of the current fleet could be quantified. With the critical assistance of the tank car industry and railroad operators, this was achieved and pieces from thirty-four tank cars were received and tested. This testing has yielded the following conclusions:

- 1) No clear trend was observed between chemical, tensile or CVN toughness properties and tank car build date. In total, sixty-one different pre-1989 TC128-B conditions were examined. Eighteen other conditions were examined including non-TC128-B material as well as post-1989 normalized TC128-B.
- 2) The vast majority of the TC128-B samples extracted from retired tank cars met current TC128-B material specifications.
- 3) Fifty-nine of sixty-one samples satisfied the chemistry requirements for TC128-B. In one case, the two anomalies included high carbon content, and in the other case, high sulfur content.
- 4) Eighty-two percent of the tank car samples met tensile property requirements for TC128-B. Two TC128-B conditions exhibited slightly lower yield strengths than allowed. Three tank car conditions exhibited slightly lower ductility than allowed. Nine tank car conditions violated the required range of ultimate strength (two exceeded and seven were less).
- 5) No trend was observed between strength properties and sulfur content for TC128-B.
- 6) A novel, pendulum impact test methodology on uncracked, full-thickness specimens was applied to selected tank car material conditions. The resulting fracture energy appeared to scale with the area under a true stress-strain curve. Varying the impactor geometry resulted in only slight (10-15%) changes in fracture energy.

- 7) The pre-1989 tank car fleet was subdivided into $\frac{1}{4}$ life segments and high rate, low temperature fracture toughness testing was performed on samples from the different life segments. Criteria recommended by Anderson and McKeighan were used to quantify toughness performance. Considering the oldest 25% of the pre-1989 fleet, 100% of the 0°F and 50% of the -50°F tests exhibited adequate or better toughness. Considering the second oldest 25% of the pre-1989 fleet, 100% of the 0°F and 83% of the -50°F tests exhibited adequate or better toughness. Considering the second newest 25% of the pre-1989 fleet, 58% of the 0°F and 33% of the -50°F tests exhibited adequate or better toughness. Considering the newest 25% of the pre-1989 fleet, 83% of the 0°F and 83% of the -50°F tests exhibited adequate or better toughness.
- 8) Testing was also performed on newer TC128-B material as well as A212-B material. Considering the post-1989 vintage, normalized TC128-B material, 100% of the 0°F and 80% of the -50°F tests exhibited adequate or better toughness. Considering the A212-B material, 67% of the 0°F and 25% of the -50°F tests exhibited adequate or better toughness.
- 9) The extent of scatter observed in the fracture toughness testing was quite large. This obscures making definitive conclusions regarding toughness variation with time.
- 10) Dynamic fracture toughness did not correlate with either sulfur content or full thickness, unnotched specimen, pendulum impact fracture energy test data.
- 11) Although the curved plate, high rate, low temperature loading conditions detailed make obtaining ASTM-standard toughness measures problematic to obtain, the fracture testing herein has provided an excellent estimate of the range and variation observed with dynamic fracture toughness in the fleet.

Based on these observations, there are recommendations that can be drawn from this work:

- 1) Practical limitations restricted the amount of material that could be fracture tested. As originally set up, this program was intended to screen the samples available so as to determine whether additional testing might be required. If the results from this program are intended to be used for fleet management decisions (i.e. which cars to retire), it is likely essential to further sample the newest 50% of the pre-1989 fleet.
- 2) It is essential to understand the link between fracture toughness and puncture resistance to properly utilize the results from this program. For instance, it is not yet clear what the implication of having tank cars in the current fleet with fracture toughnesses less than $50 \text{ ksi}\sqrt{\text{in}}$ is from the perspective of public risk for commodity release. Until toughness can be related to risk, it is extraordinarily difficult to utilize these results for risk mitigation.

This page intentionally left blank.

9.0 REFERENCES

- [1] “Ensuring Railroad Tank Car Safety,” Transportation Research Board Special Report 243, National Research Council, 1994.
- [2] “Derailment of Canadian Pacific Railway Freight Train 292-16 and Subsequent Release of Anhydrous Ammonia Near Minot, North Dakota (1/18/2002),” National Transportation Safety Board, Railroad Accident Report, NTSB/RAR-04/01, PB2004-916301, Notation 7461A, March 2004.
- [3] “Collision of Union Pacific Railroad Train MHOTU-23 With BNSF Railway Company Train MEAP-TUL-126-D With Subsequent Derailment and Hazardous Materials Release Macdona, Texas (June 28, 2004),” National Transportation Safety Board, Railroad Accident Report, NTSB/RAR-06/03, PB2006-916303, Notation 7675D, July 2006.
- [4] “Collision of Norfolk Southern Freight Train 192 with Standing Norfolk Southern Local Train P22 with Subsequent Hazardous Materials Release at Graniteville, South Carolina (1/06/2005),” National Transportation Safety Board, Railroad Accident Report, NTSB/RAR-05/04, PB2005-916304, Notation 7710A, November 2005.
- [5] McKeighan, P. C., “High Rate Fracture Toughness, Tensile Properties, CVN and Composition of Various TC-128B Steels,” Extended Executive Summary, August 2005.
- [6] Anderson, T. L. and McKeighan, P. C., “Interpreting Fracture Toughness Magnitudes of Tank Car Steels: Relating K-based Toughness Range with Material Adequacy,” August 2005.
- [7] McKeighan, P. C., “High Rate Fracture Toughness, Tensile Properties, CVN and Composition of Various TC-128B Steels, Phase A: Pre-1989 GATX Tank Cars and Modern Vintage Plate,” Interim Report, Southwest Research Institute Project No. 18.11388, June 2005.
- [8] McKeighan, P. C., “High Rate Fracture Toughness, Tensile Properties, CVN and Composition of Various TC-128B Steels, Phase B: Tank Cars Involved in the 2002 Minot Incident,” Interim Report, Southwest Research Institute Project No. 18.11388, June 2005.
- [9] Warke, R. W., McKeighan, P. C. and Cardinal, J. W., “Teardown Inspections of Cracked Stub Sills,” Final Report, Southwest Research Institute Project No. 18-06965-080, RPI-AAR Report No. RA 01-02, October 2001.
- [10] Anderson, T. L. and Kirkpatrick, S. W., “Quantifying and Enhancing Puncture Resistance in Railroad Tank Cars Carrying Hazardous Materials – Phase I: Preliminary Study,” Final Report for the Chlorine Institute, Structural Reliability Technology, Inc. and Applied Research Associates, Inc., August 2006.

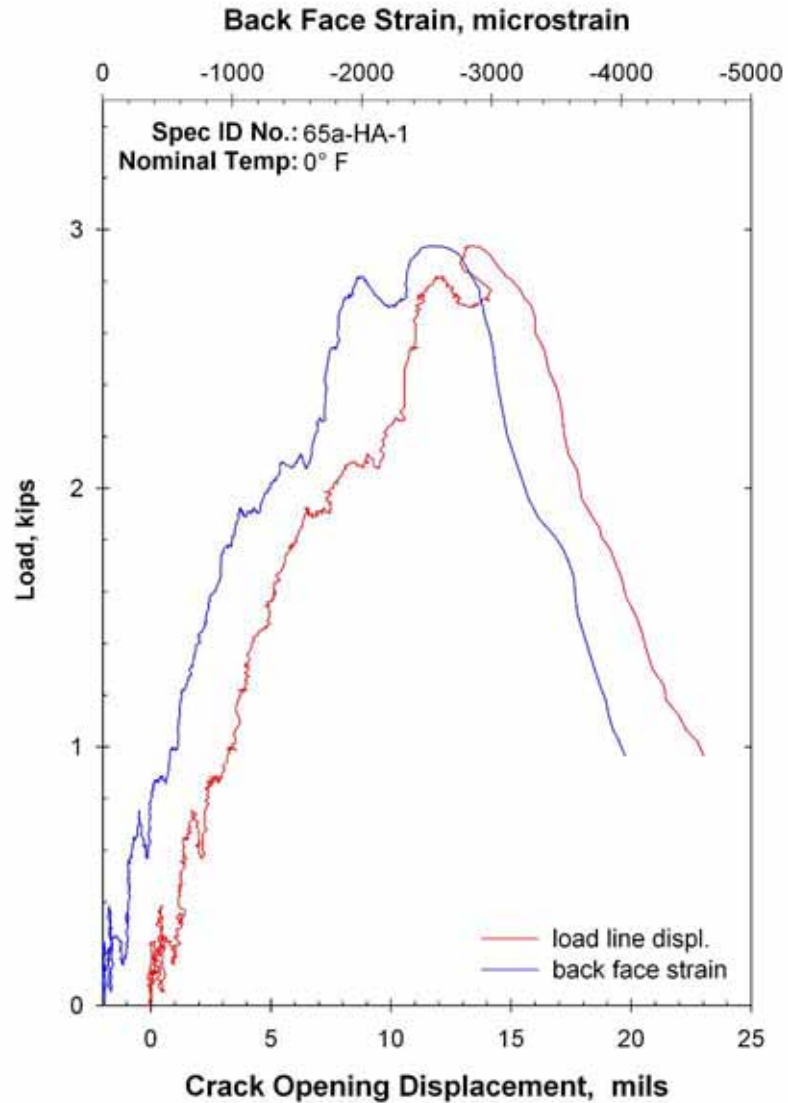
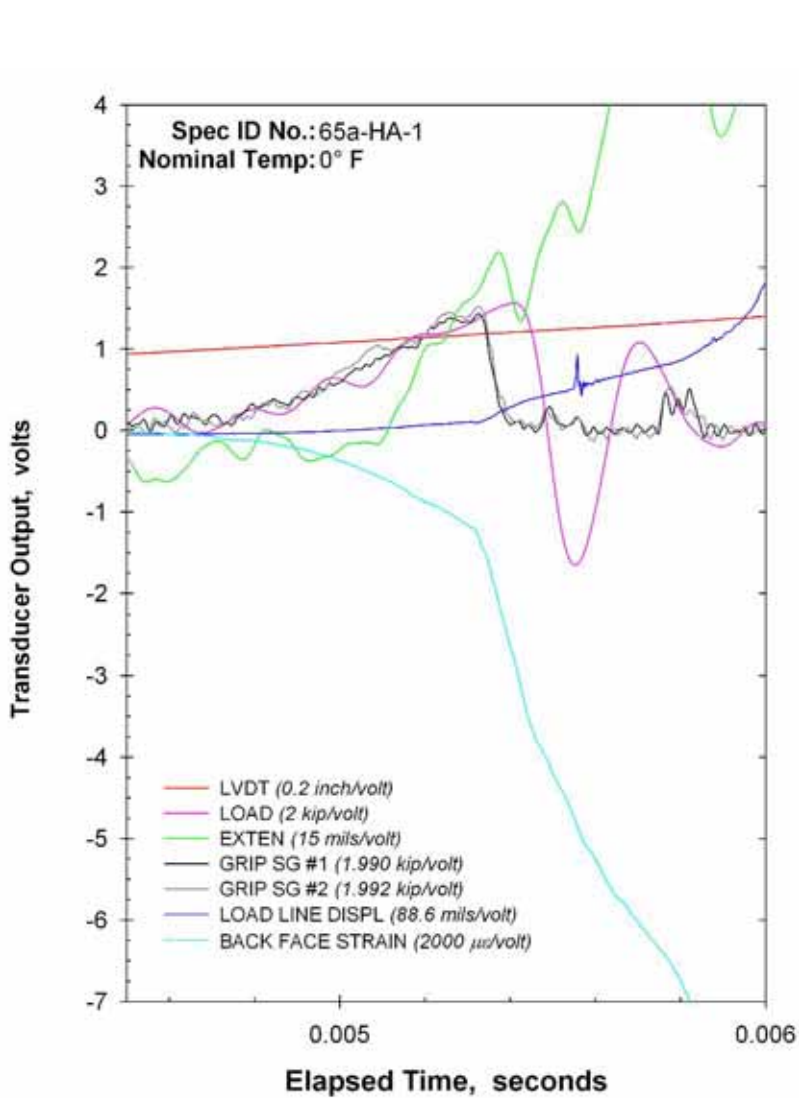
- [11] McKeighan, P. C. and Feiger, J. H., "Fatigue Crack Growth Behavior of Tank Car Steel TC128-B Subjected to Various Environments," Final Report, Southwest Research Institute Project No. 18.03630, performed for the Volpe National Transportation Systems Center, September 2001.
- [12] Email dated 10/31/06 from David Y. Jeong.
- [13] Roberts, R. and Newton, C., "Interpretive Report on Small-Scale Test Correlations with K_{Ic} Data," Welding Research Council Bulletin, 265, 1981, pp. 1-18.
- [14] Barsom, J. M. and Rolfe, S. T., Fracture and Fatigue Control in Structures: Applications of Fracture Mechanics, Prentice-Hall Publishers, Second Edition, 1987.
- [15] Phall, R., Macdonald, K. A. and Brown, P. A., "Correlations between Fracture Toughness and Charpy Impact Energy," TWI Journal, Vol. 6, No. 3, 1997.
- [16] Sailors, R. H. and Corten, H. T., "Relationship between Material Fracture Toughness using Fracture Mechanics and Transition Temperature Tests," Fracture Toughness, Proceedings of the 1971 National Symposium on Fracture Mechanics, Part II, ASTM STP 514, ASTM, 1972, pp. 164-191.
- [17] Bucci, R. J., Paris, P. C., Landes, J. D. and Rice, J. R., "J Integral Estimation Procedures," Fracture Toughness, Proceedings of the 1971 National Symposium on Fracture Mechanics, Part II, ASTM STP 514, American Society for Testing and Materials, 1972, pp. 40-69.

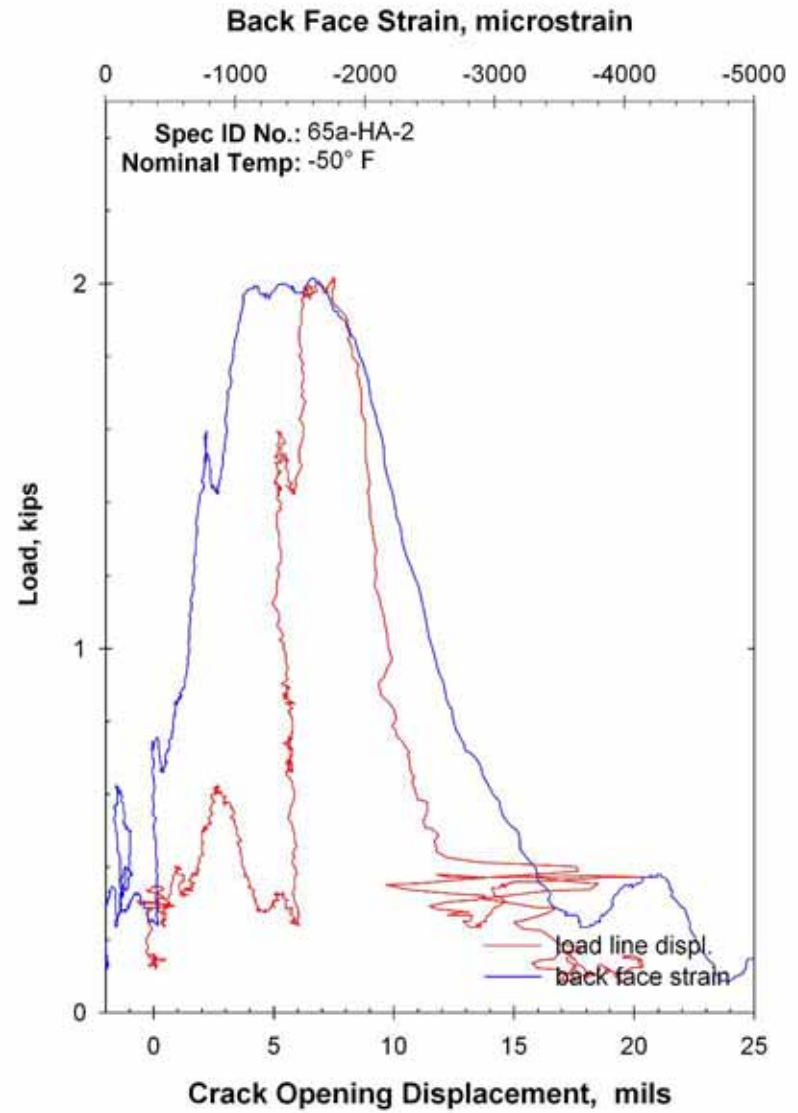
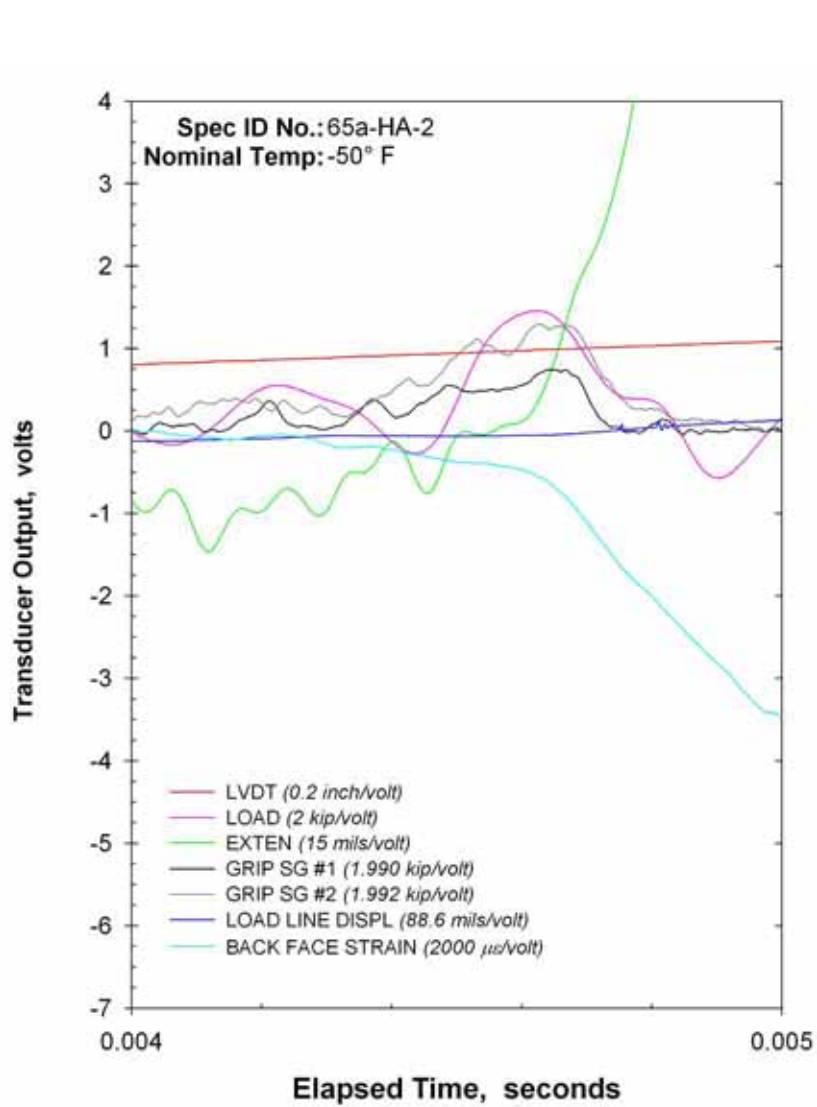
APPENDIX A

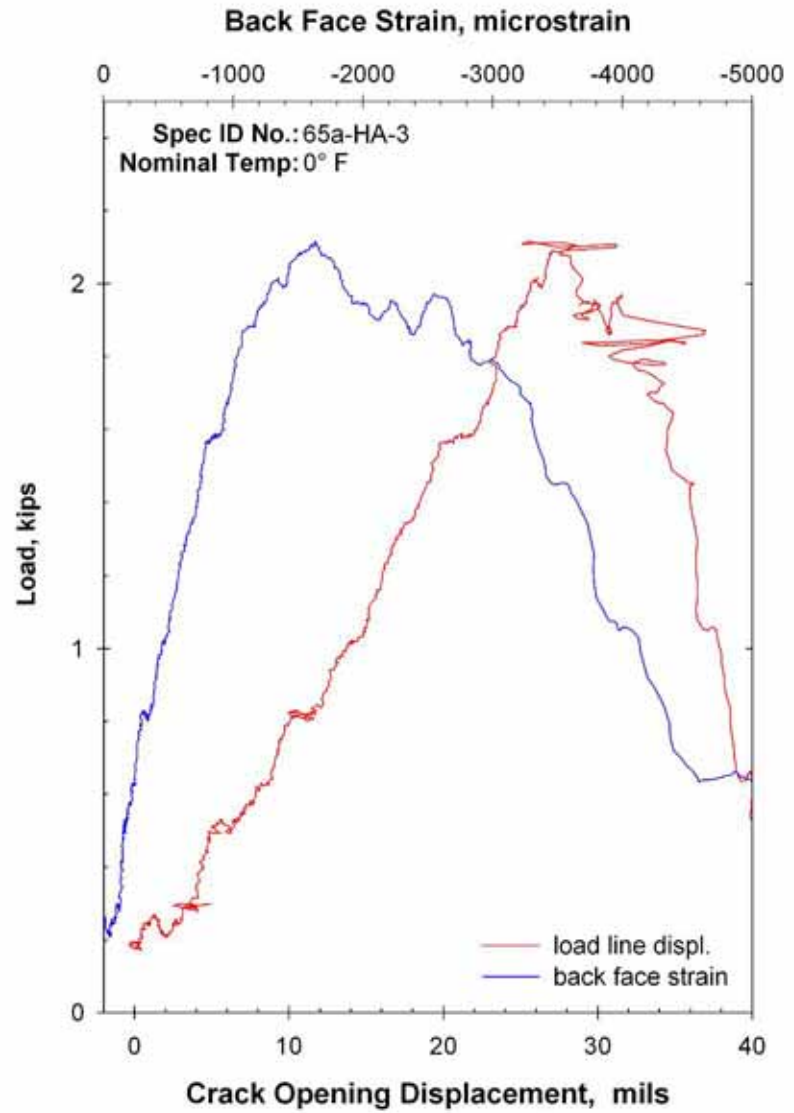
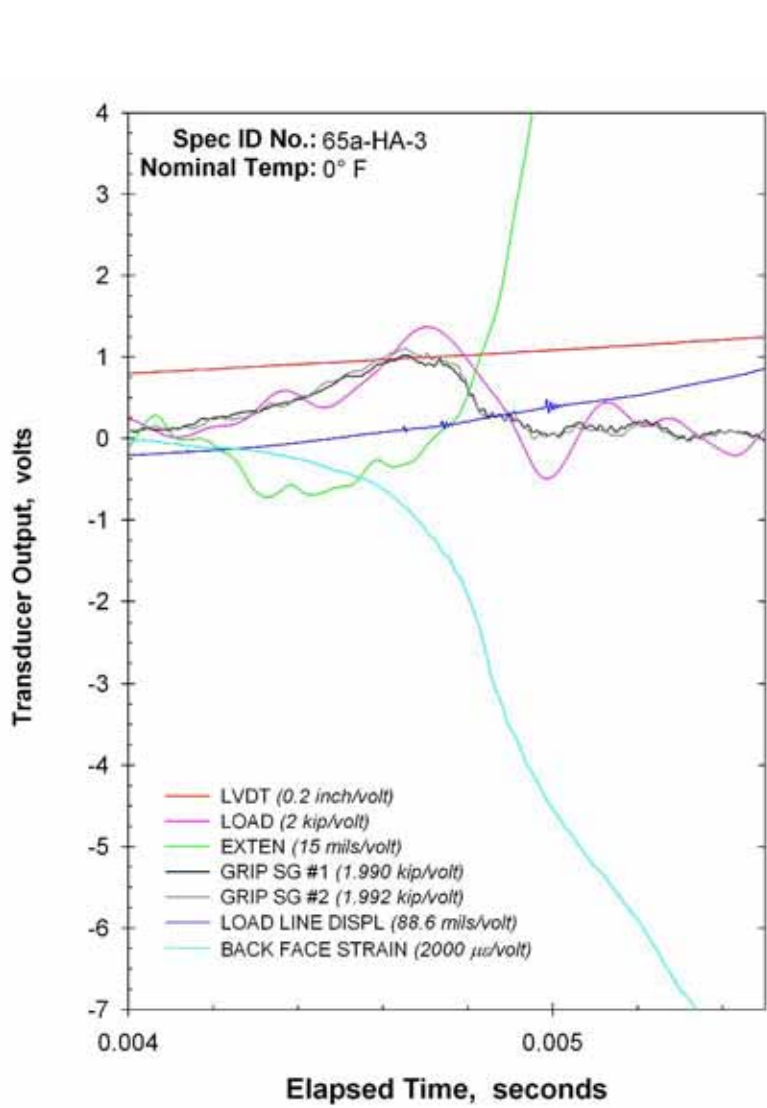
Data from High Rate Fracture Toughness Tests

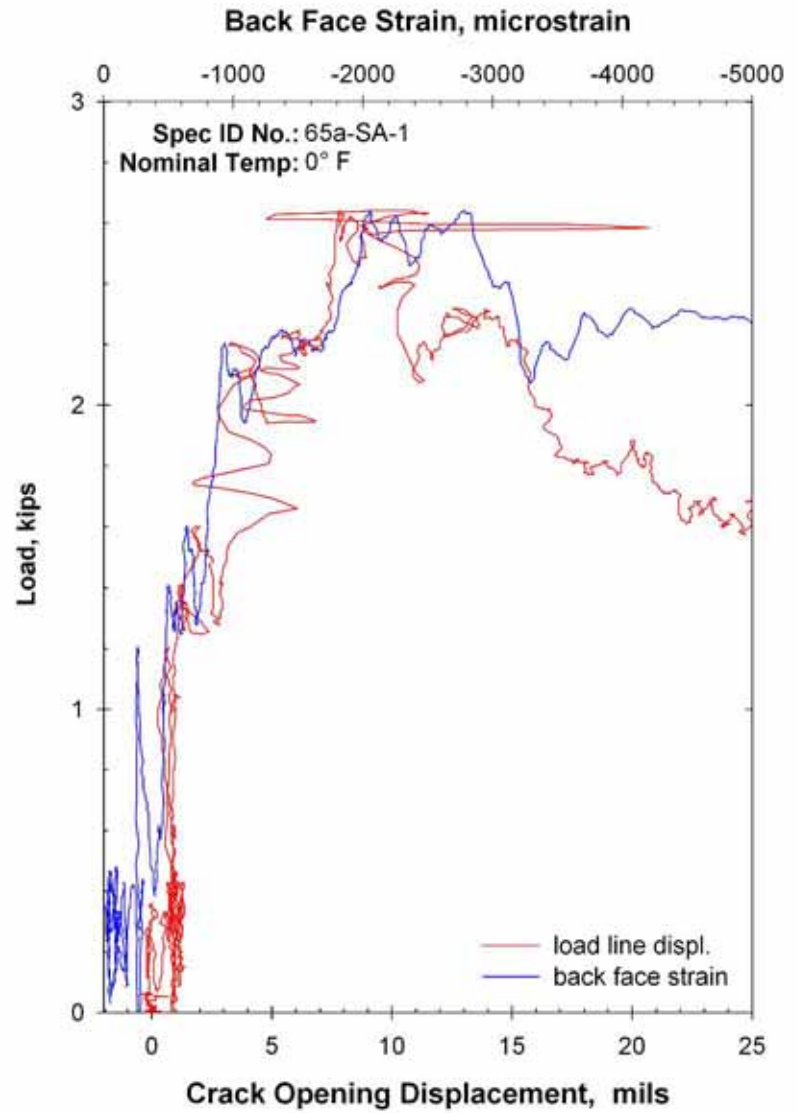
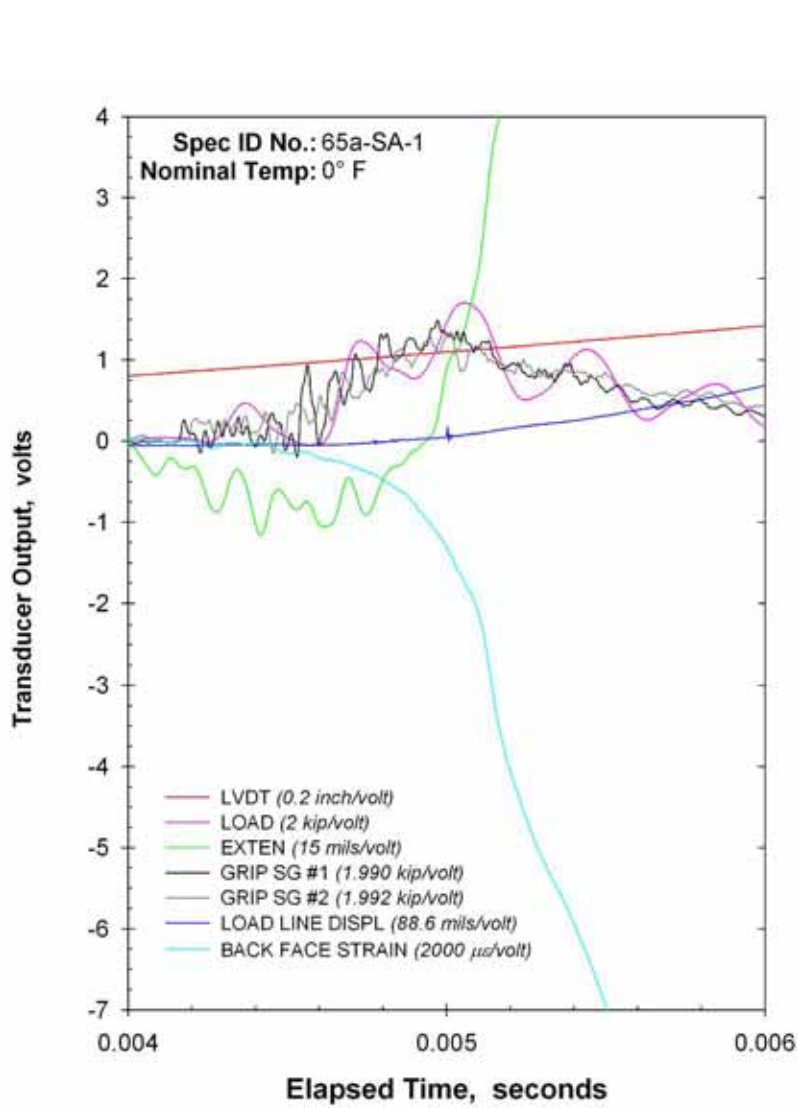
Transducer signals versus time and load versus strain/displacement

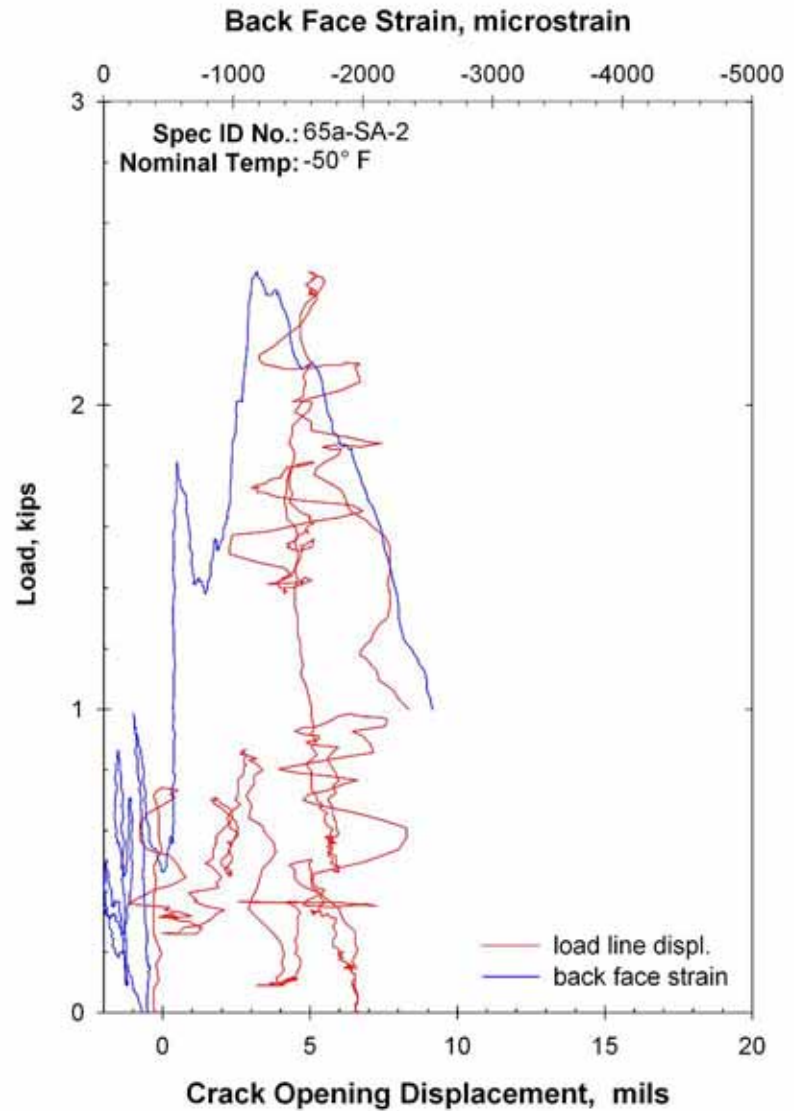
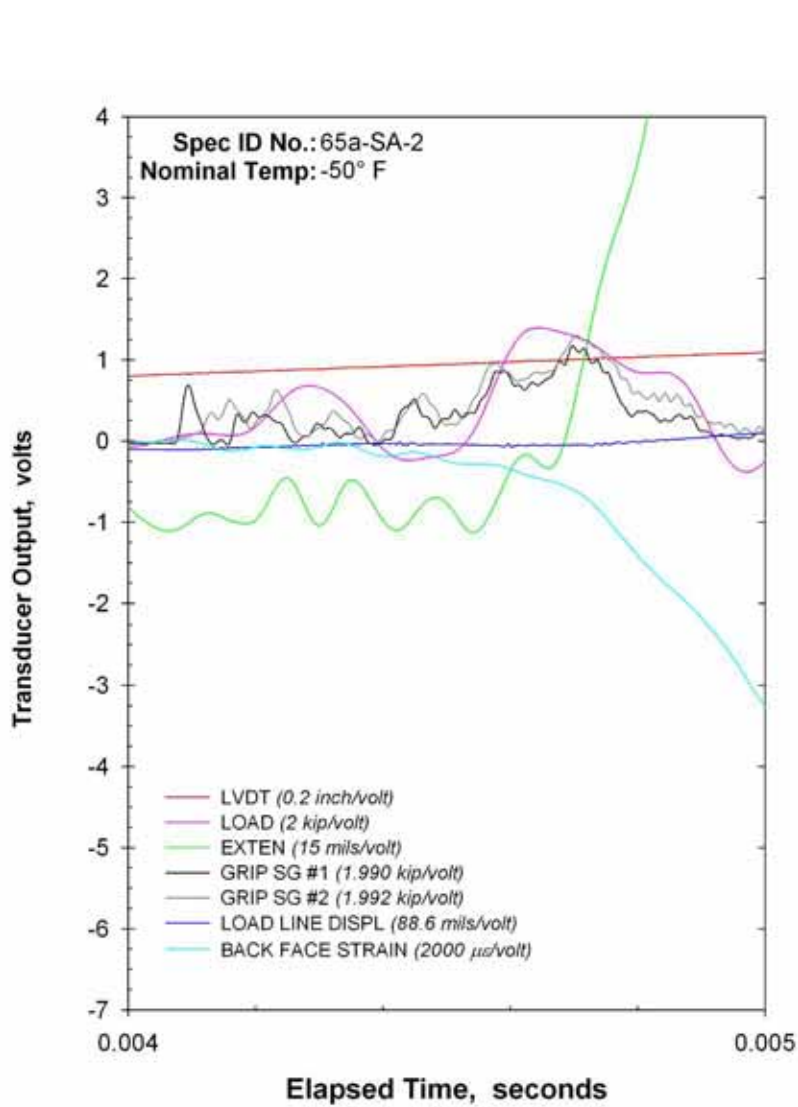
This page intentionally left blank.

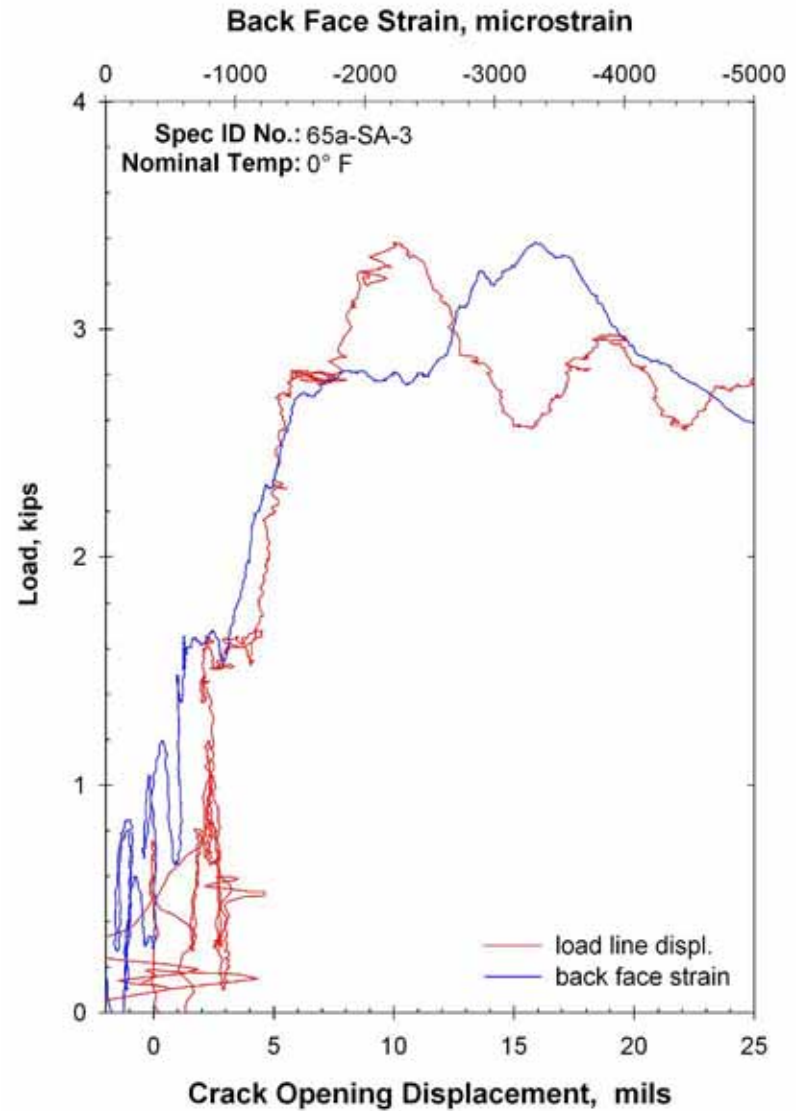
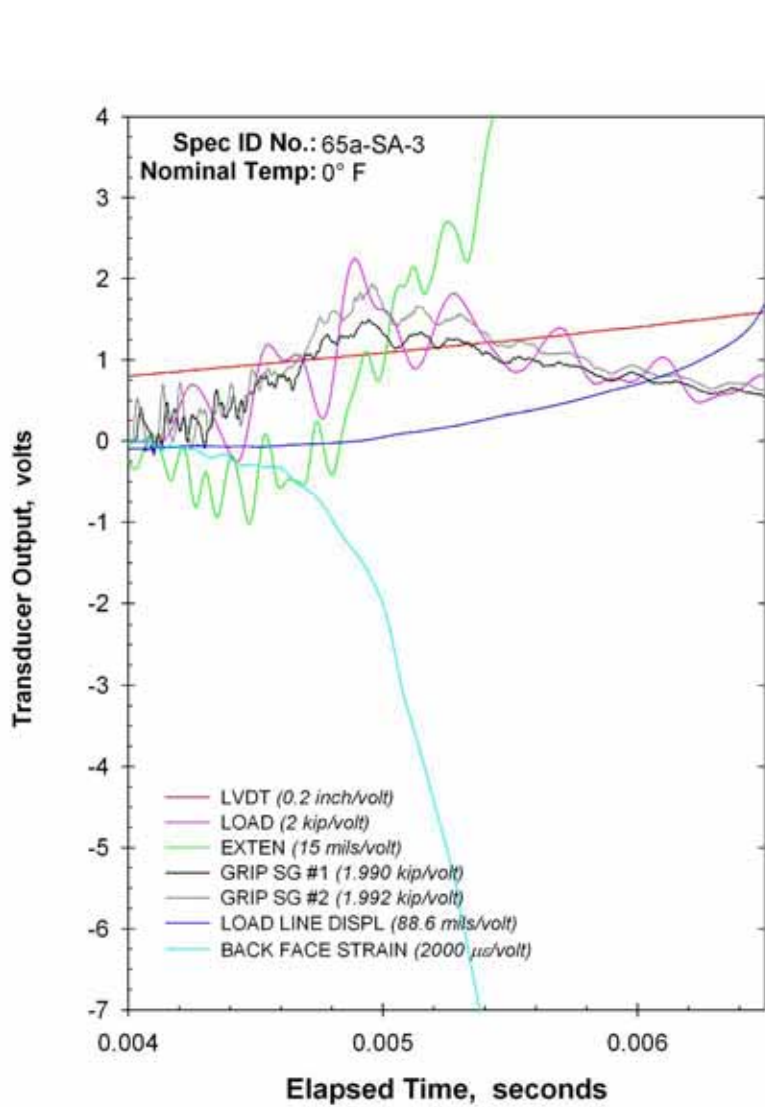


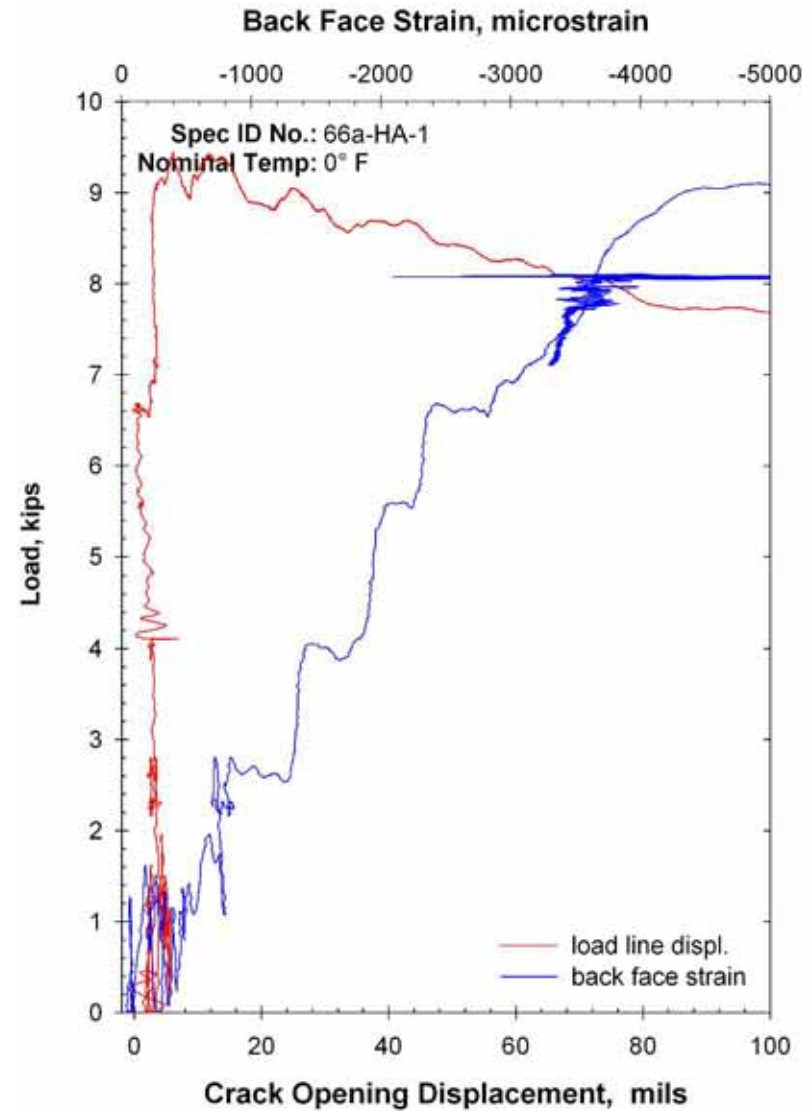
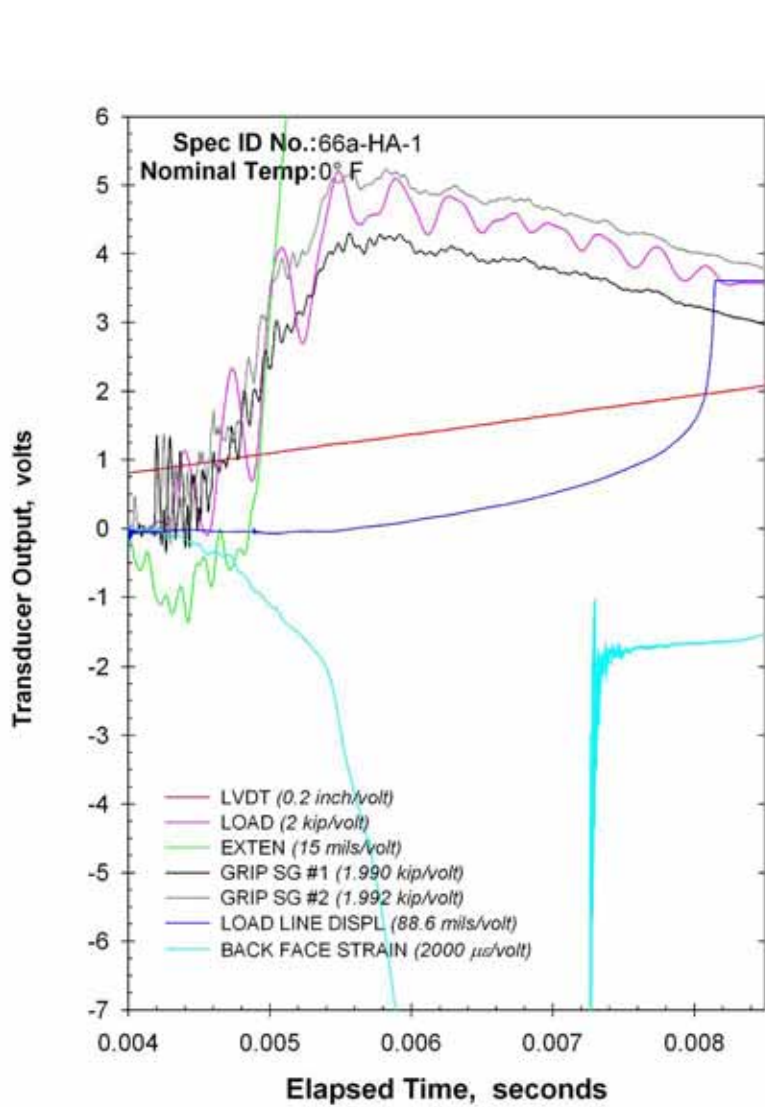


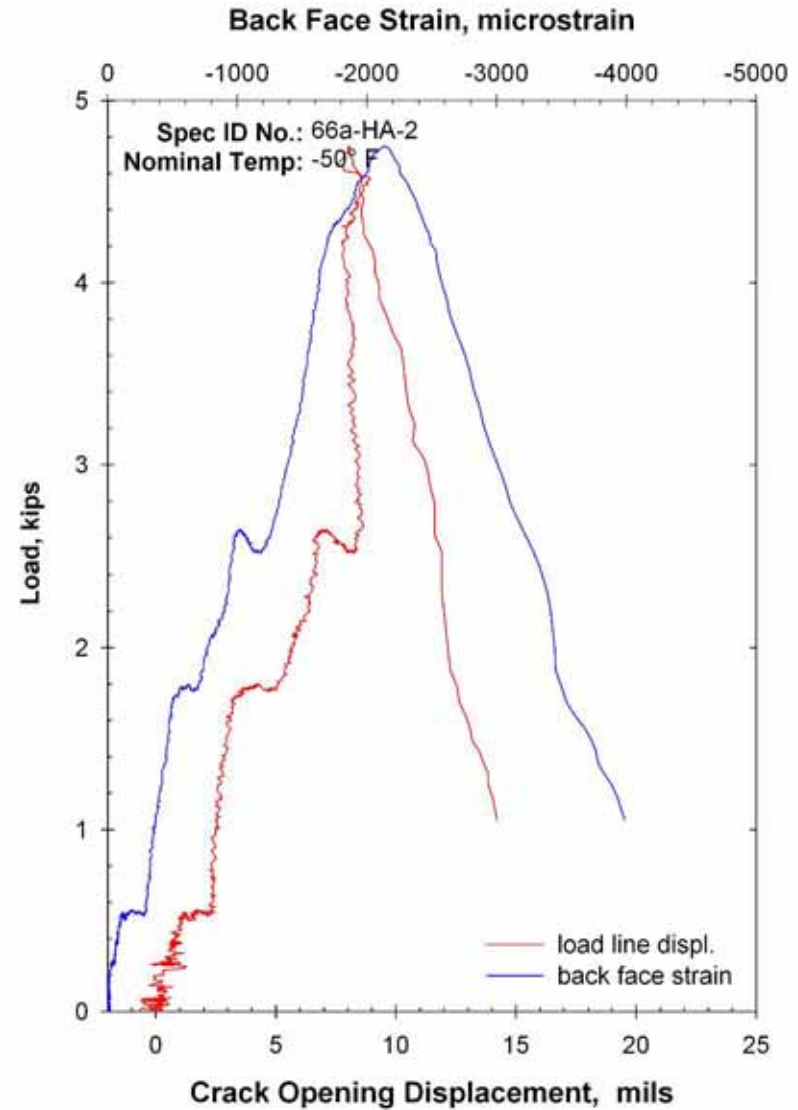
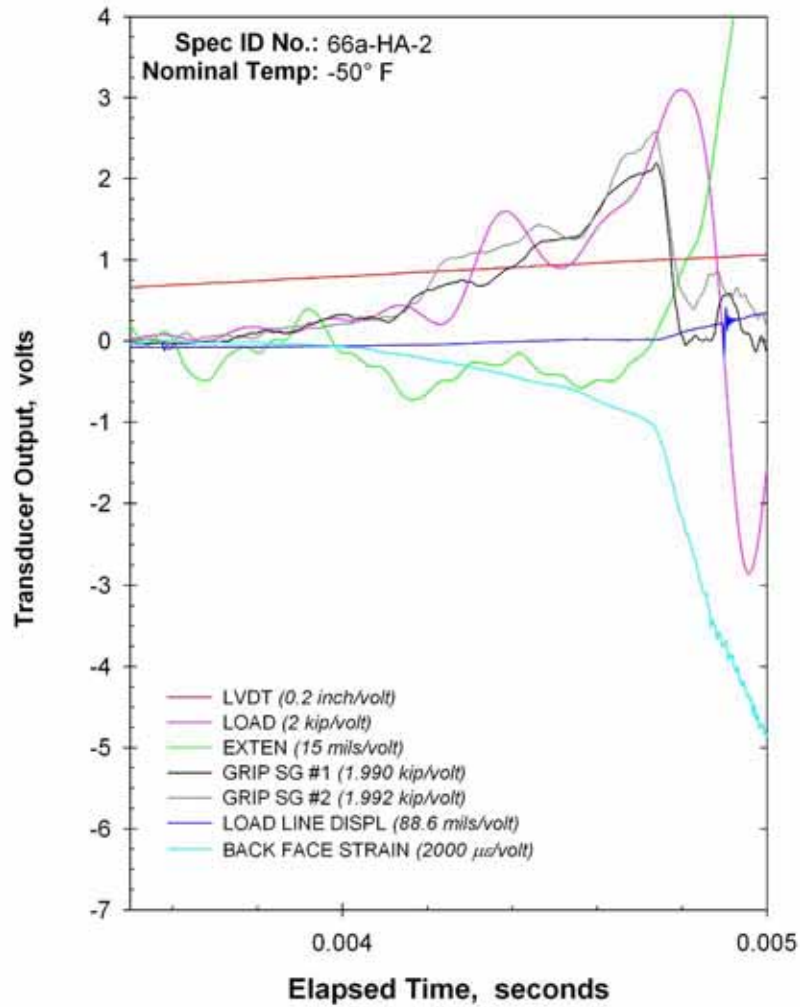


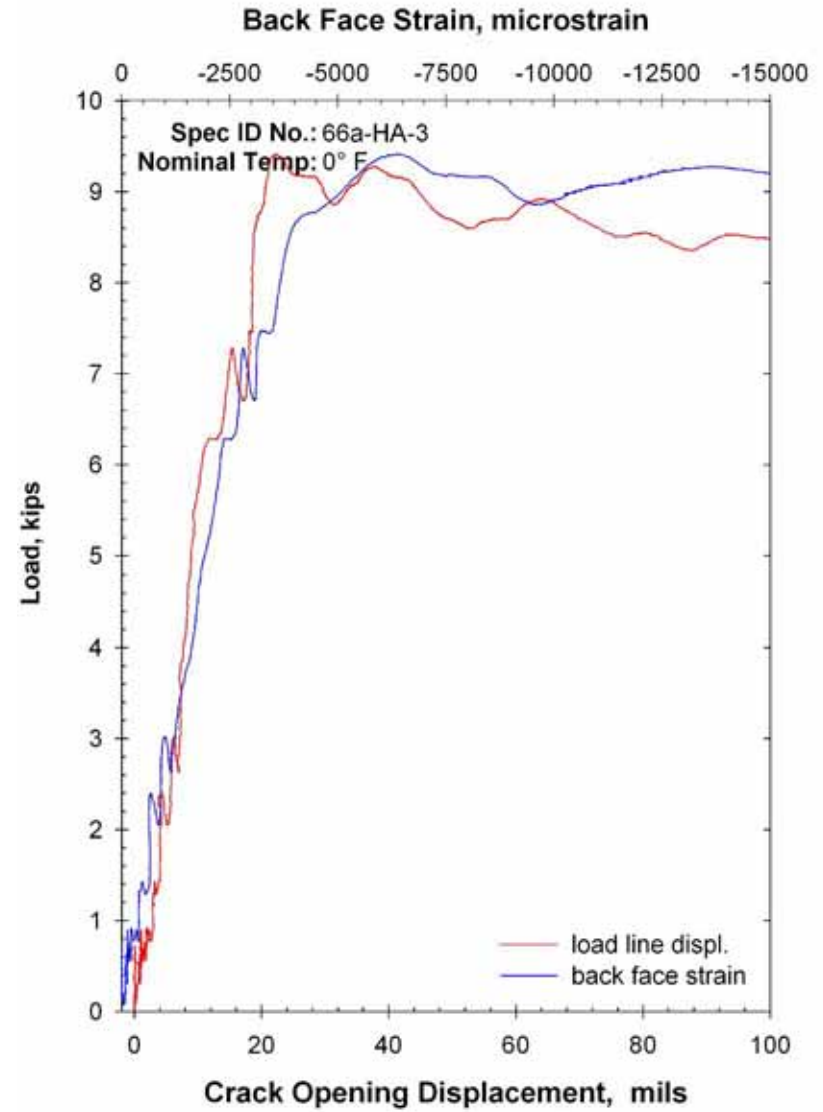
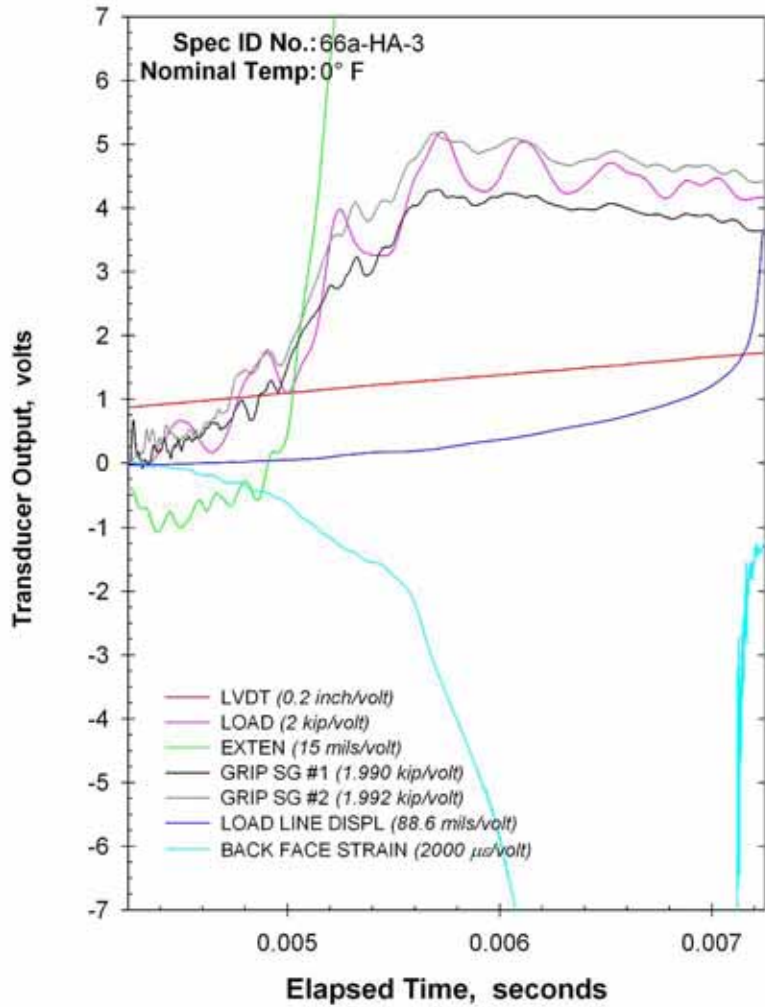


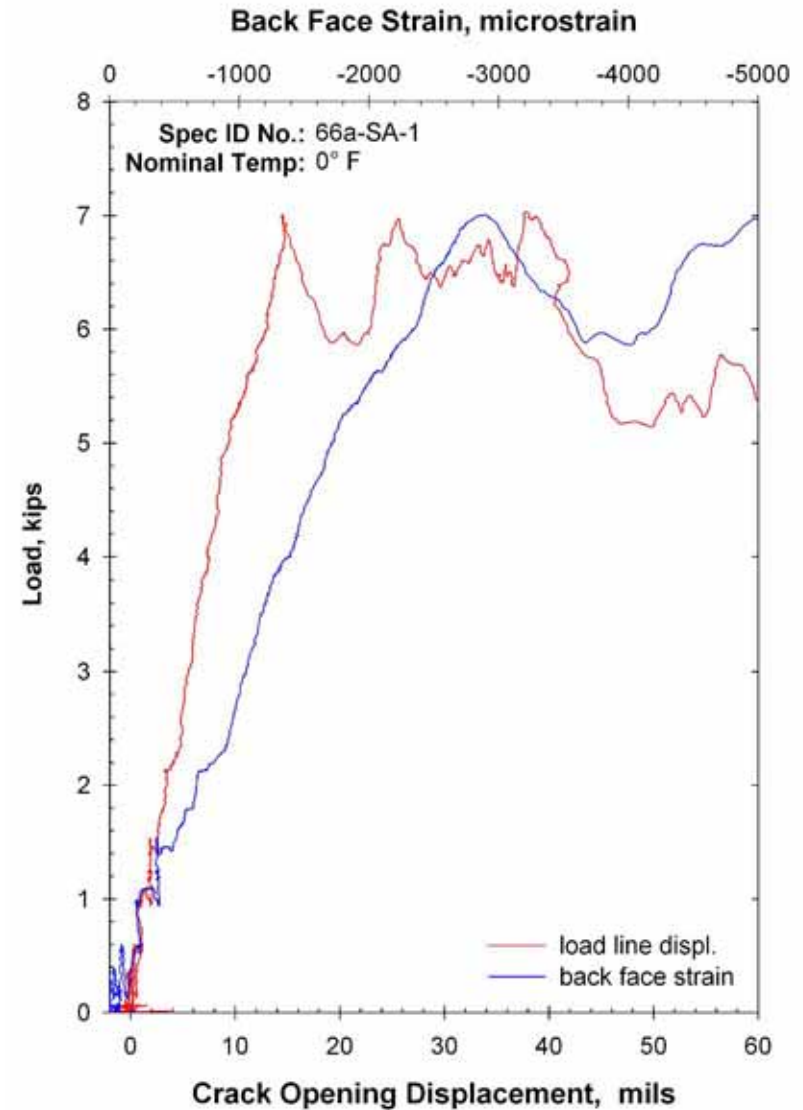
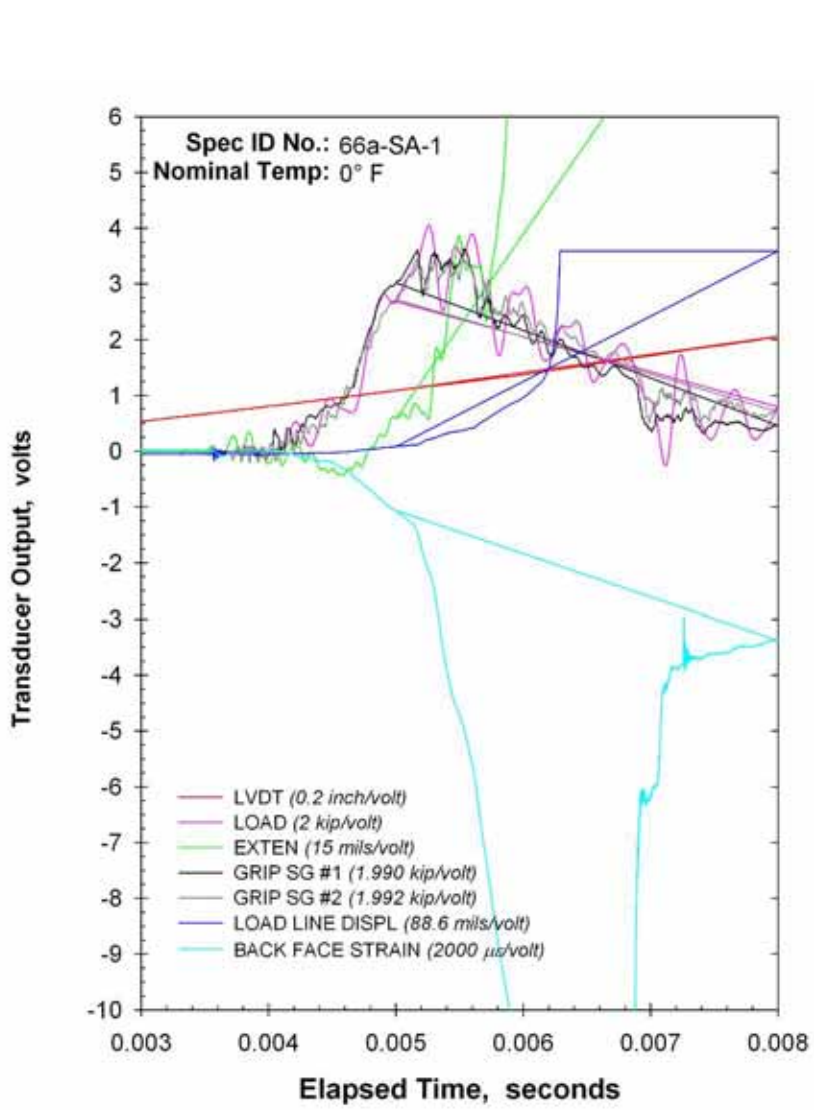


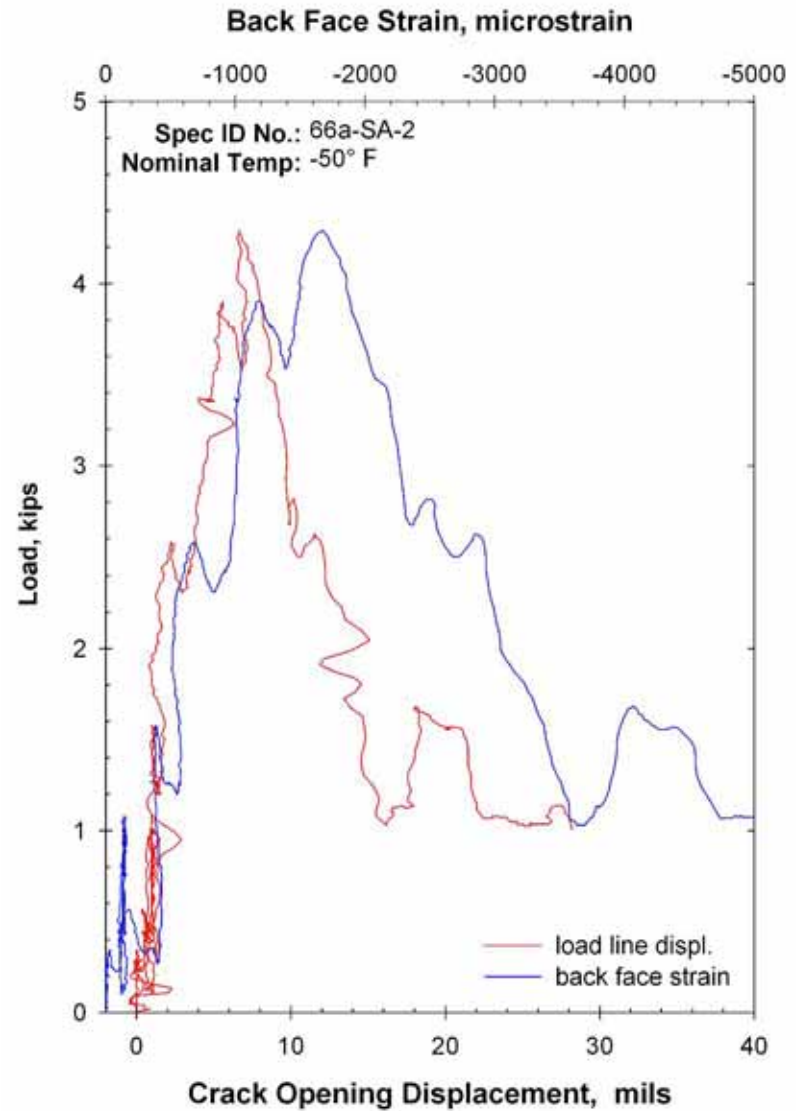
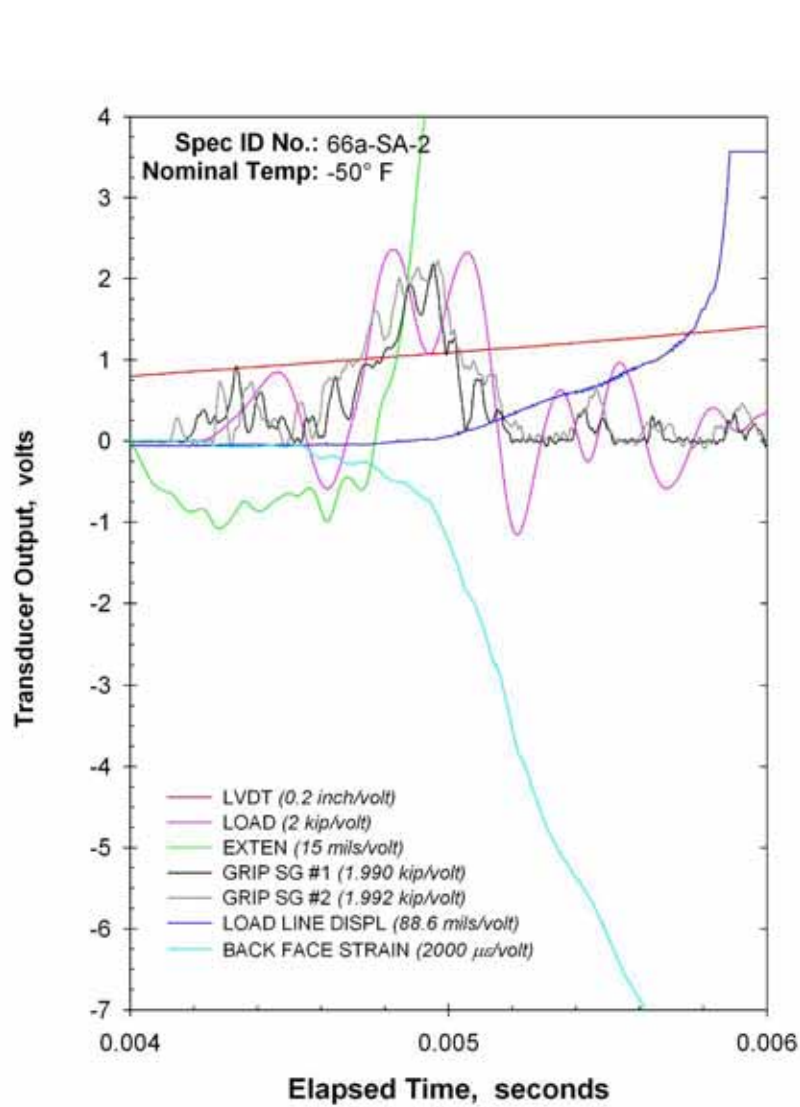


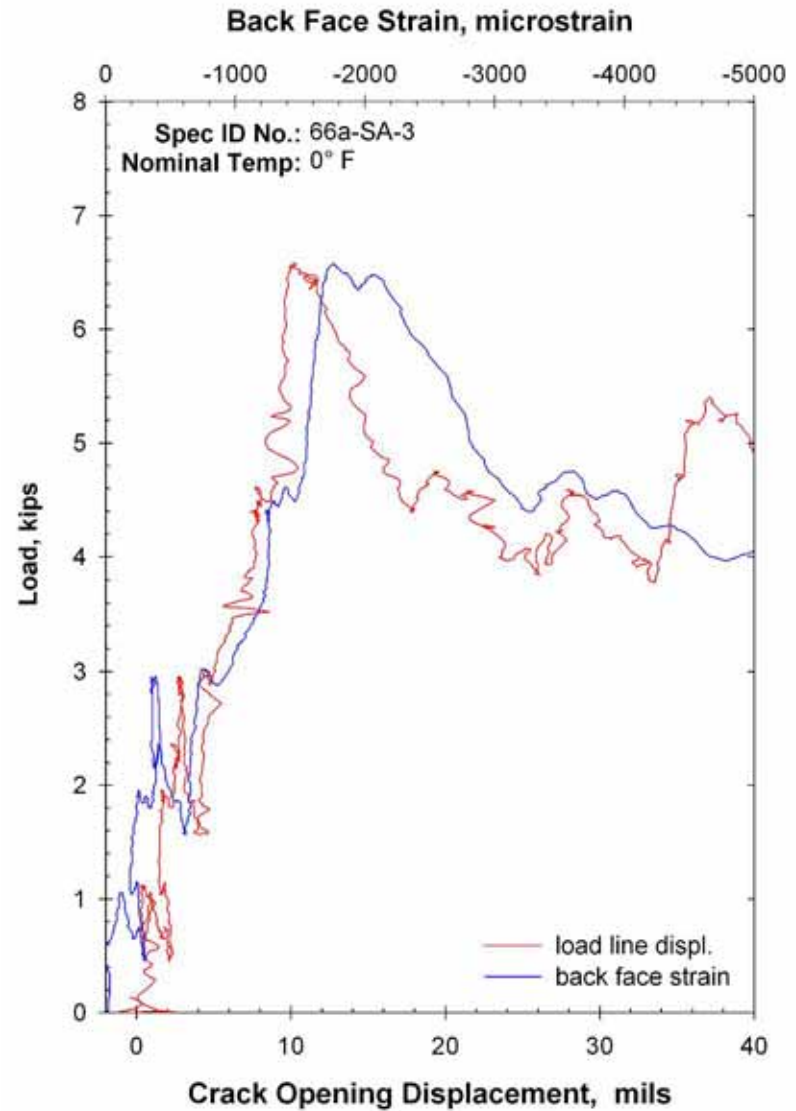
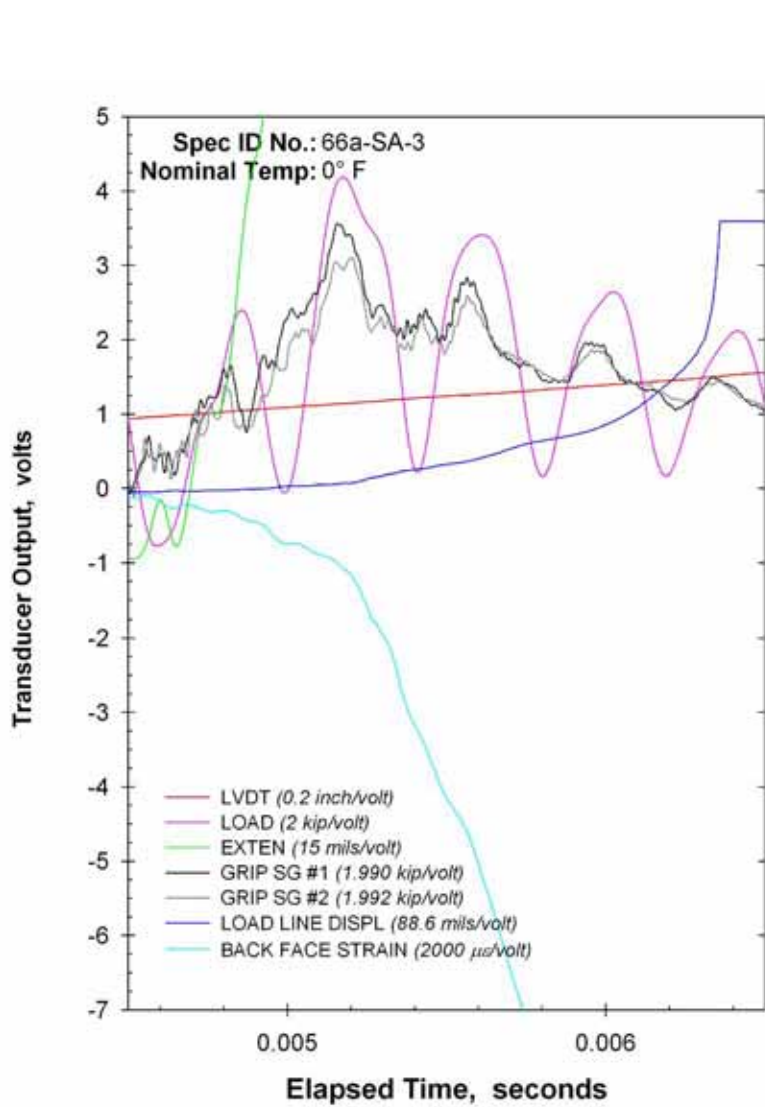


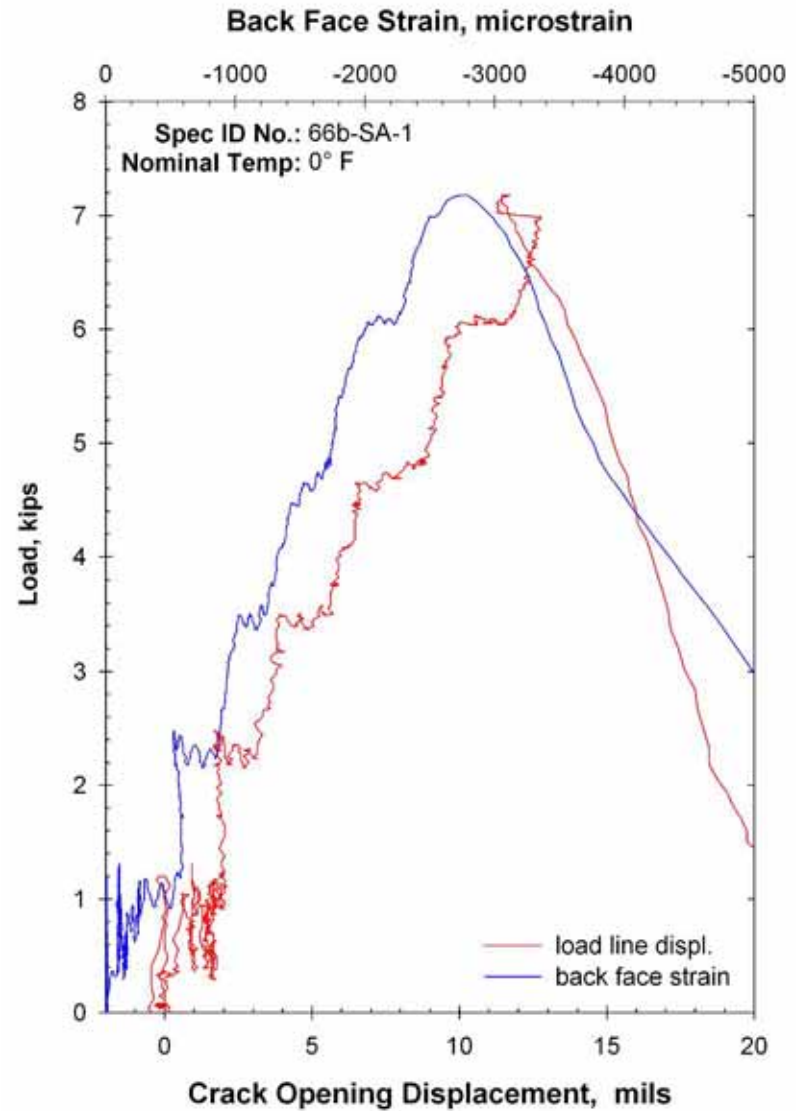
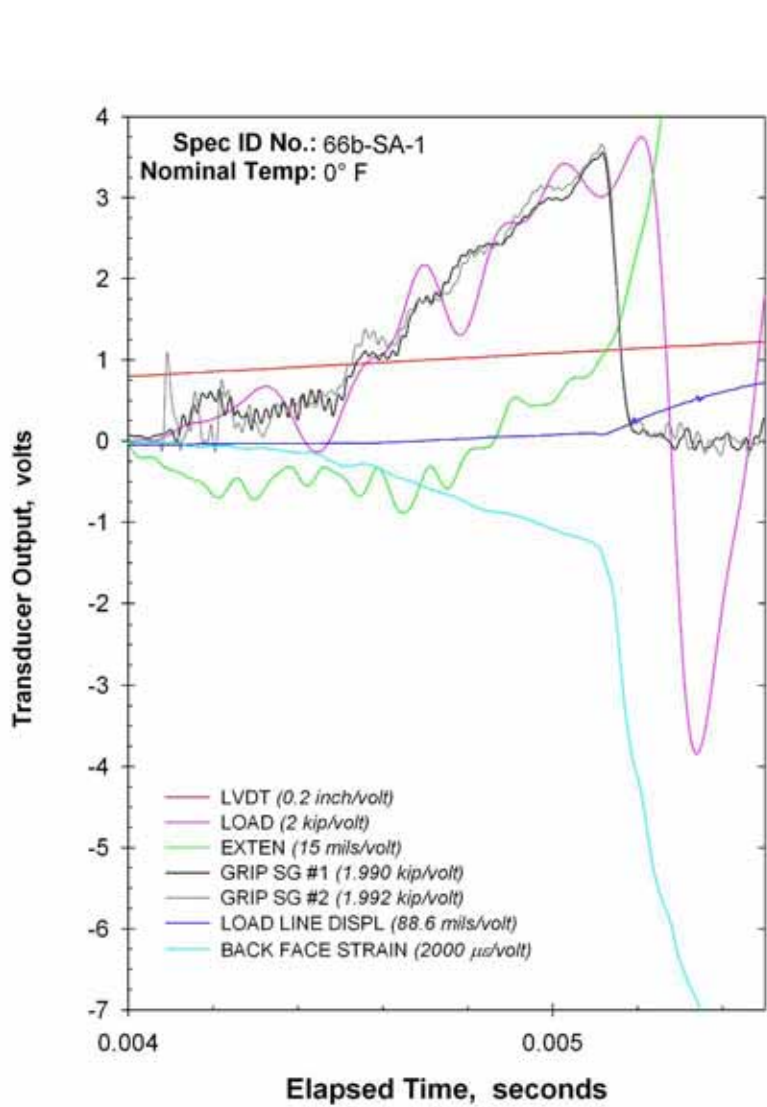


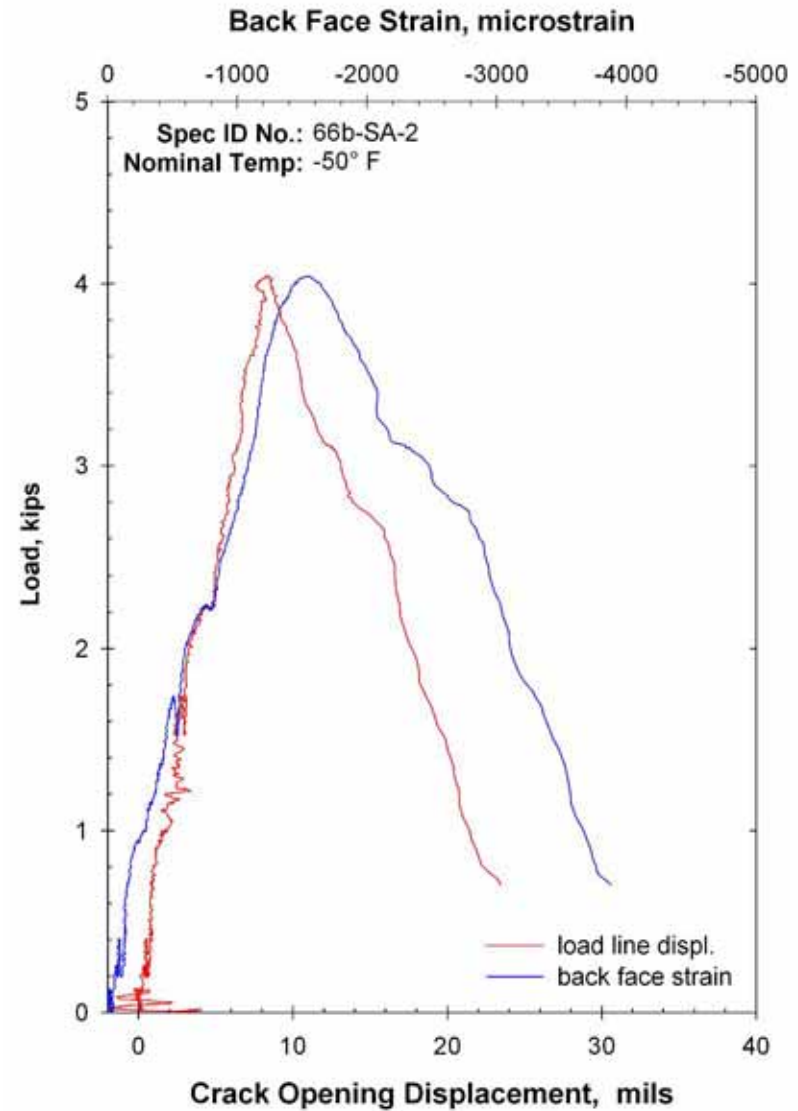
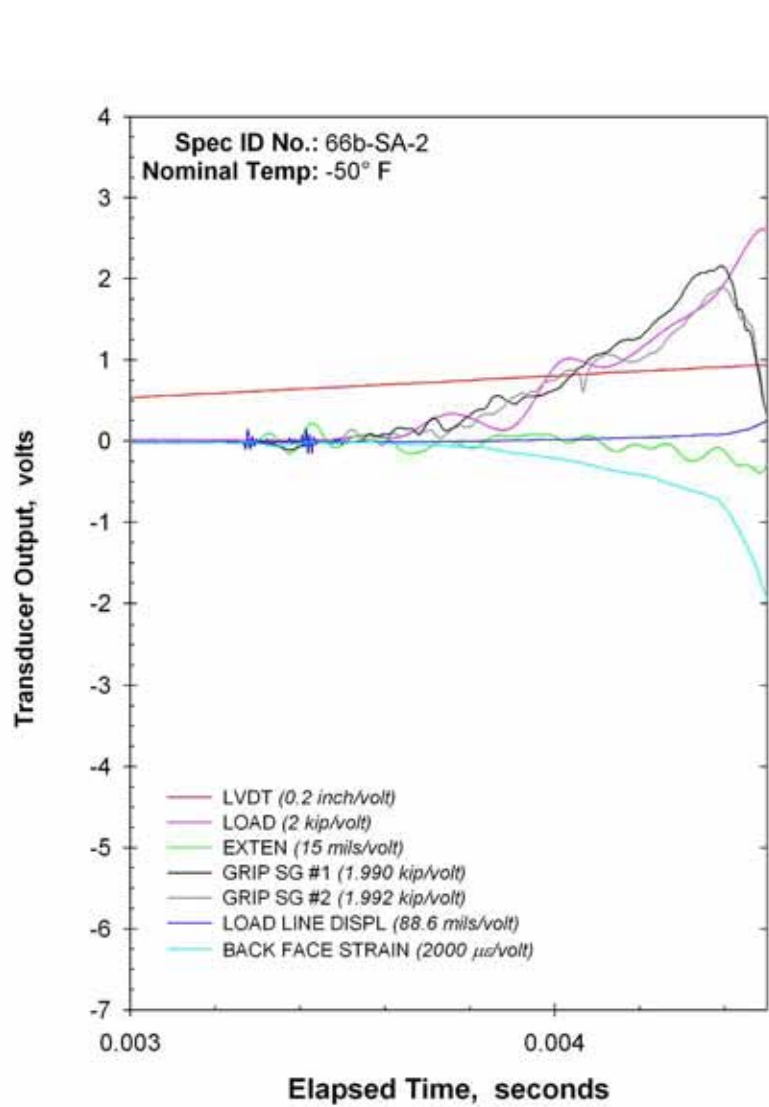


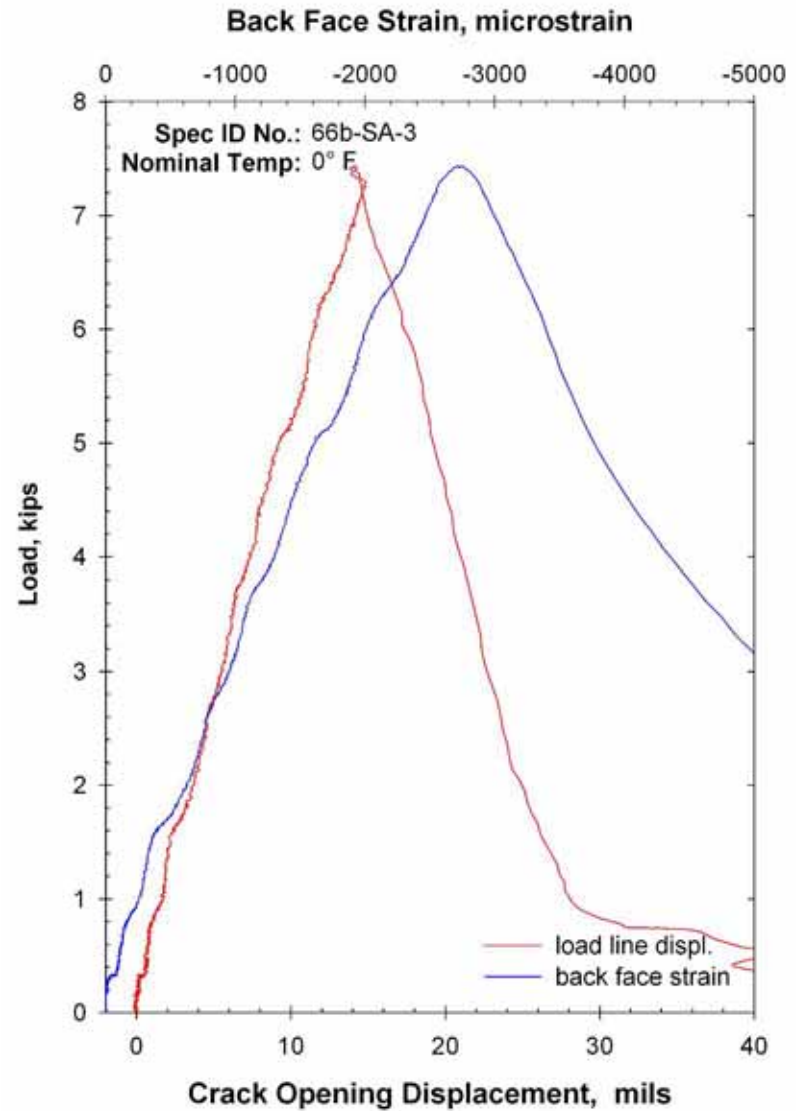
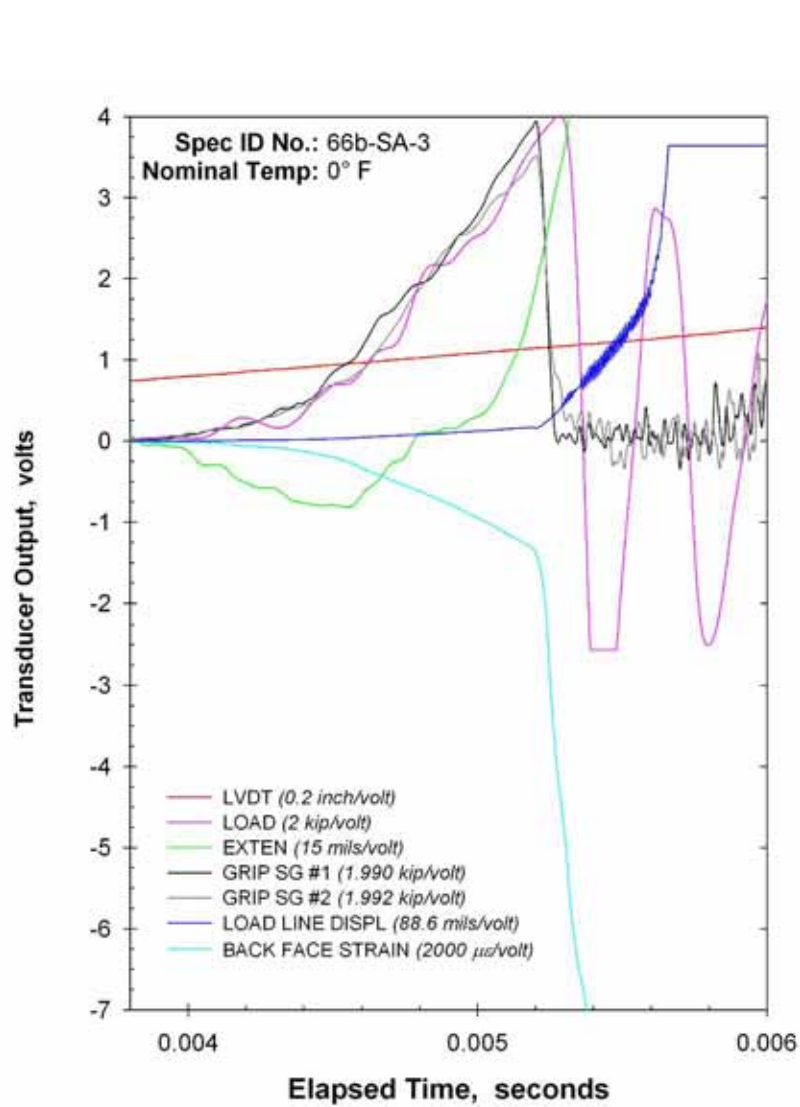


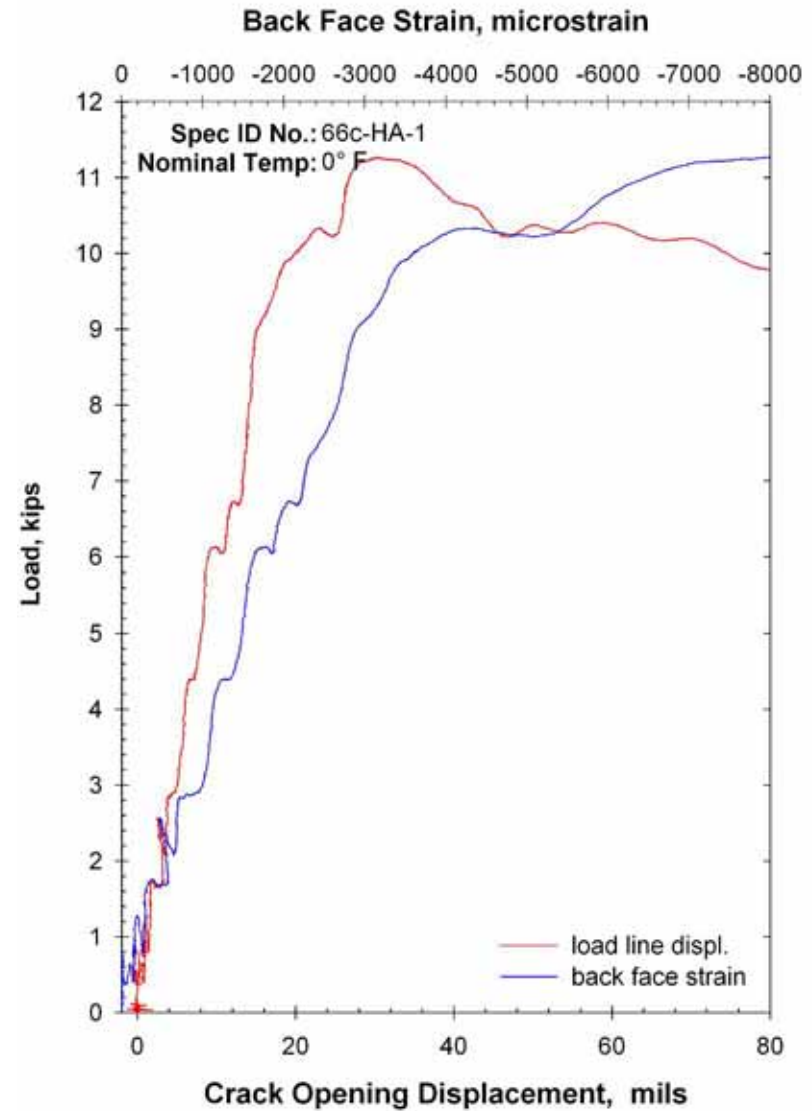
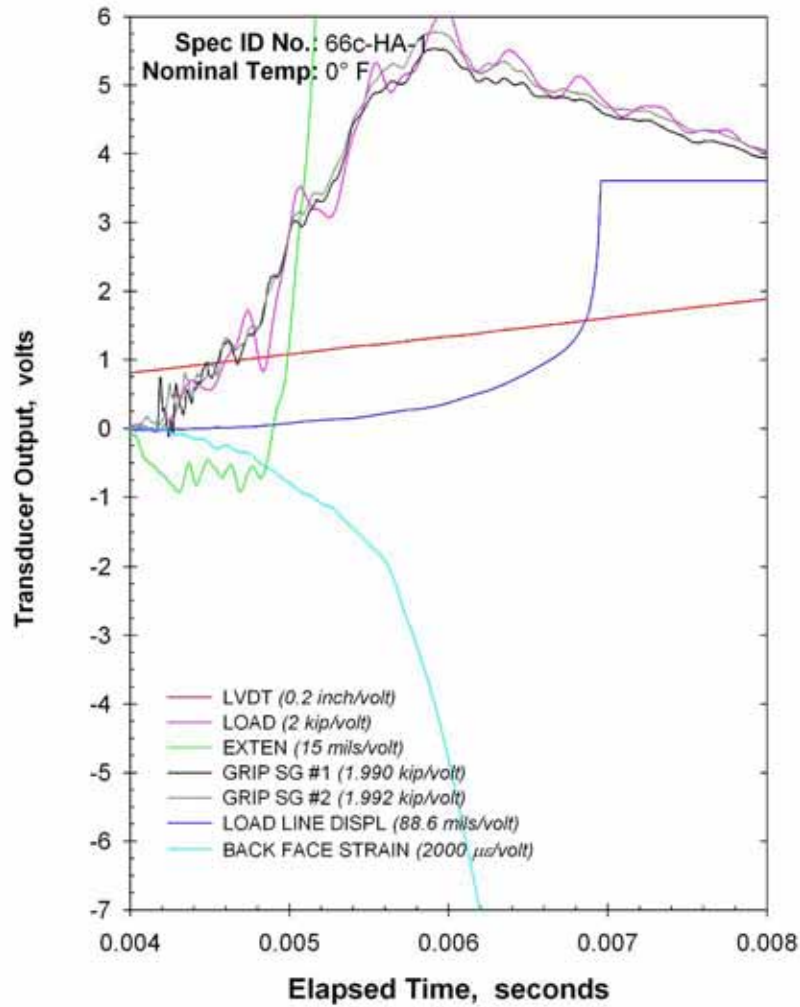


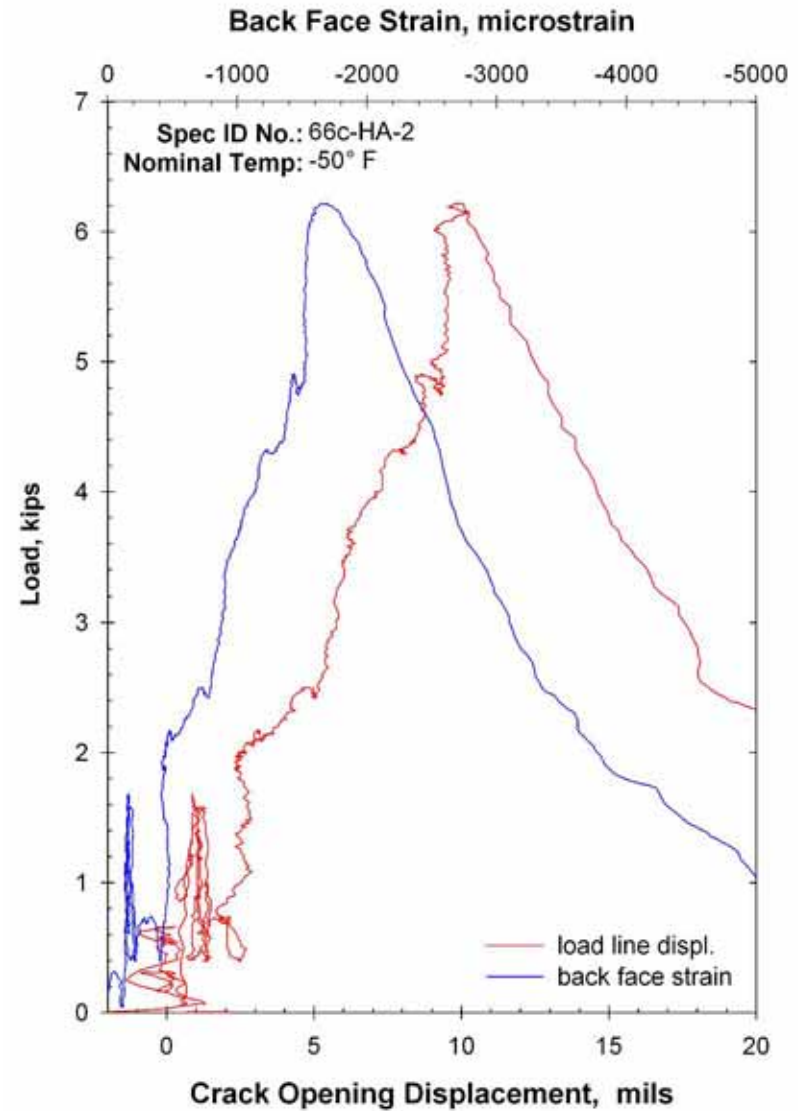
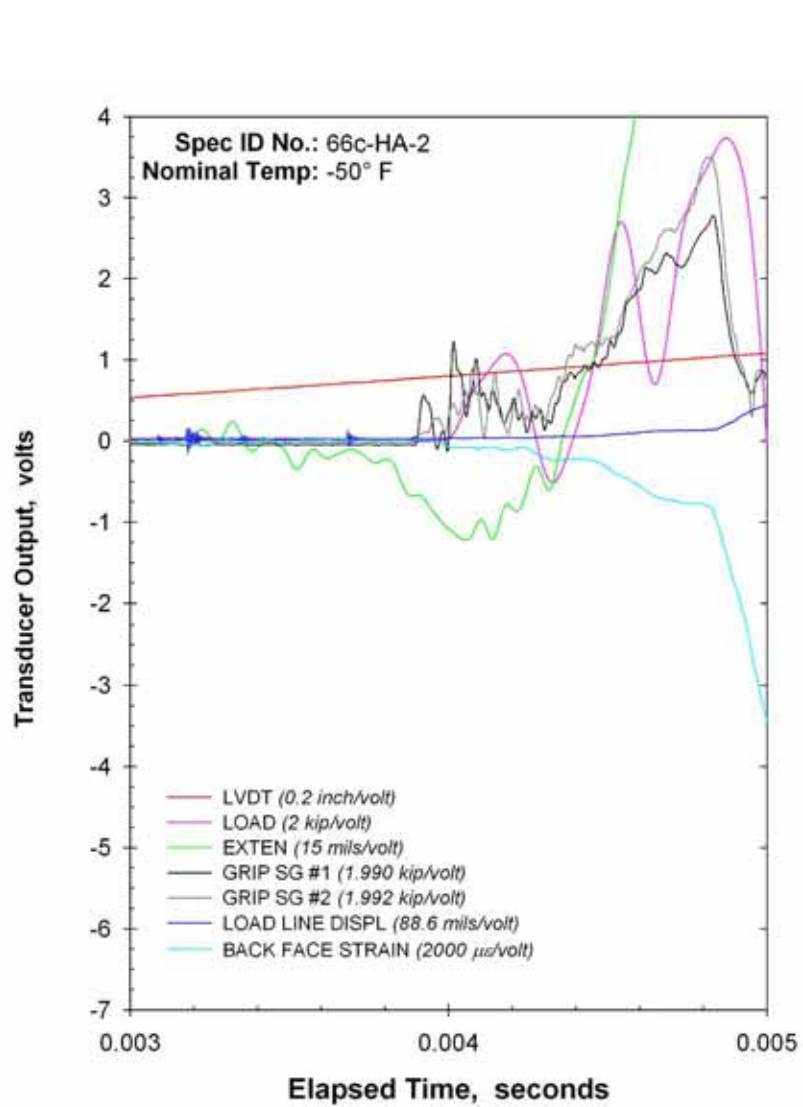


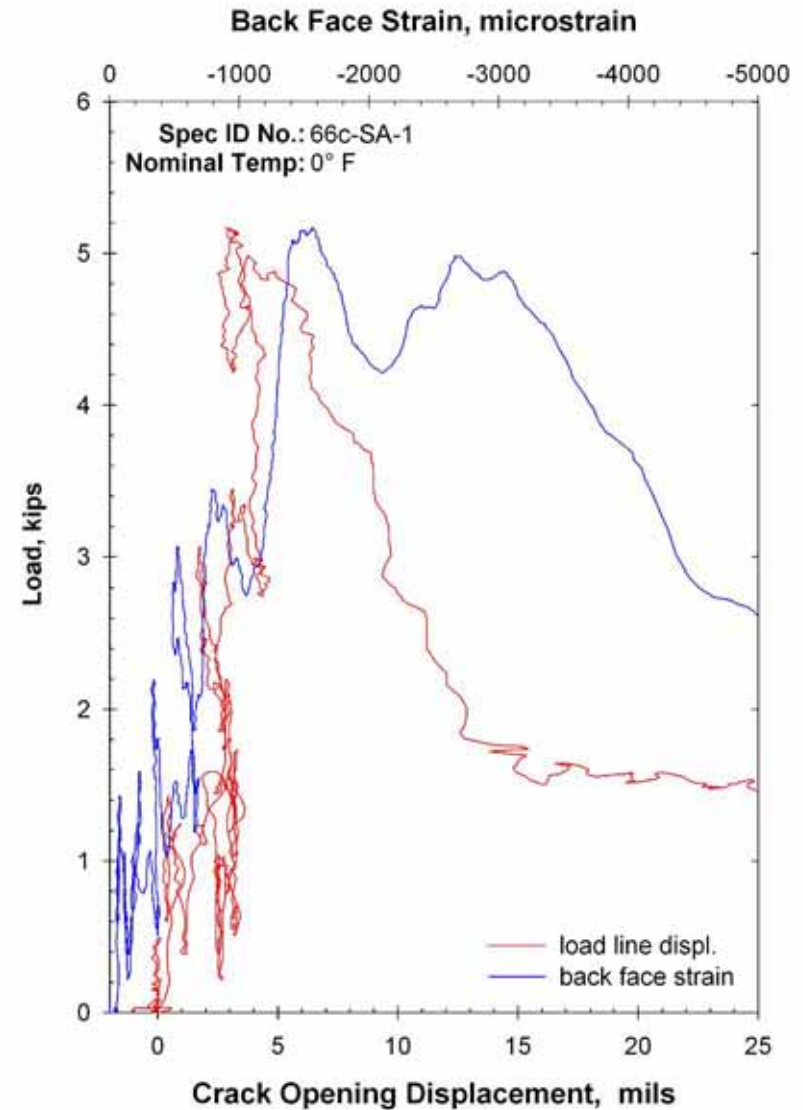
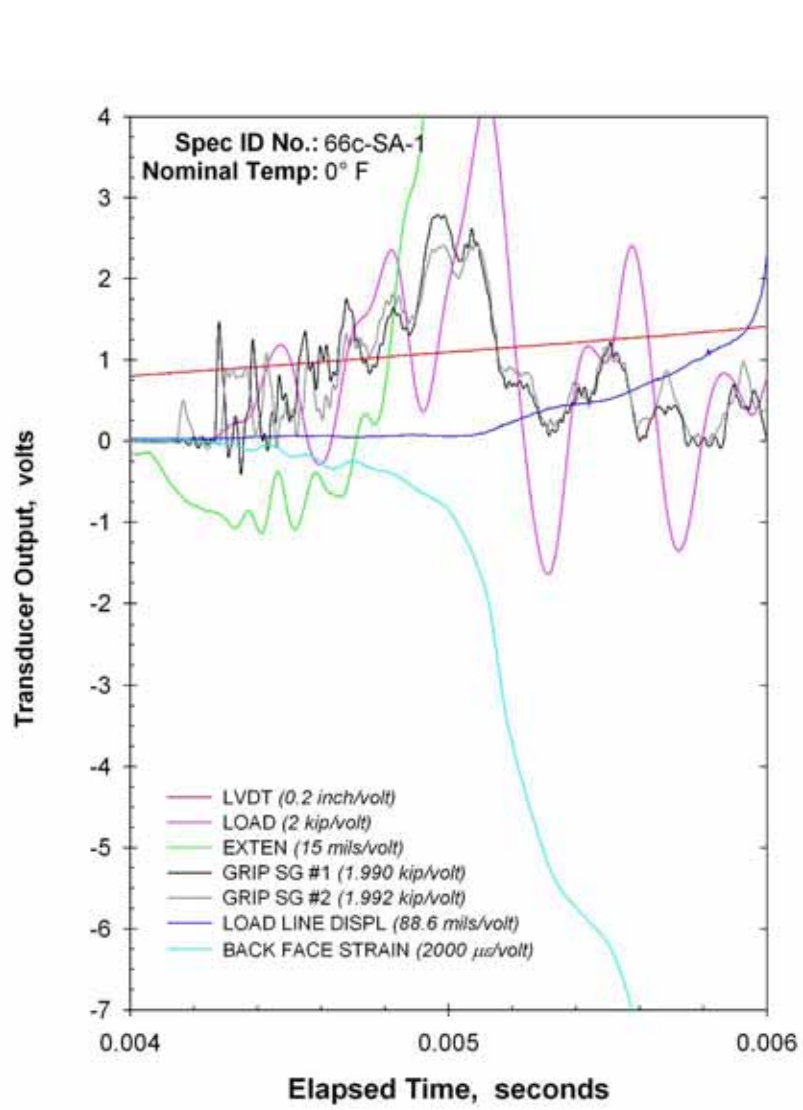


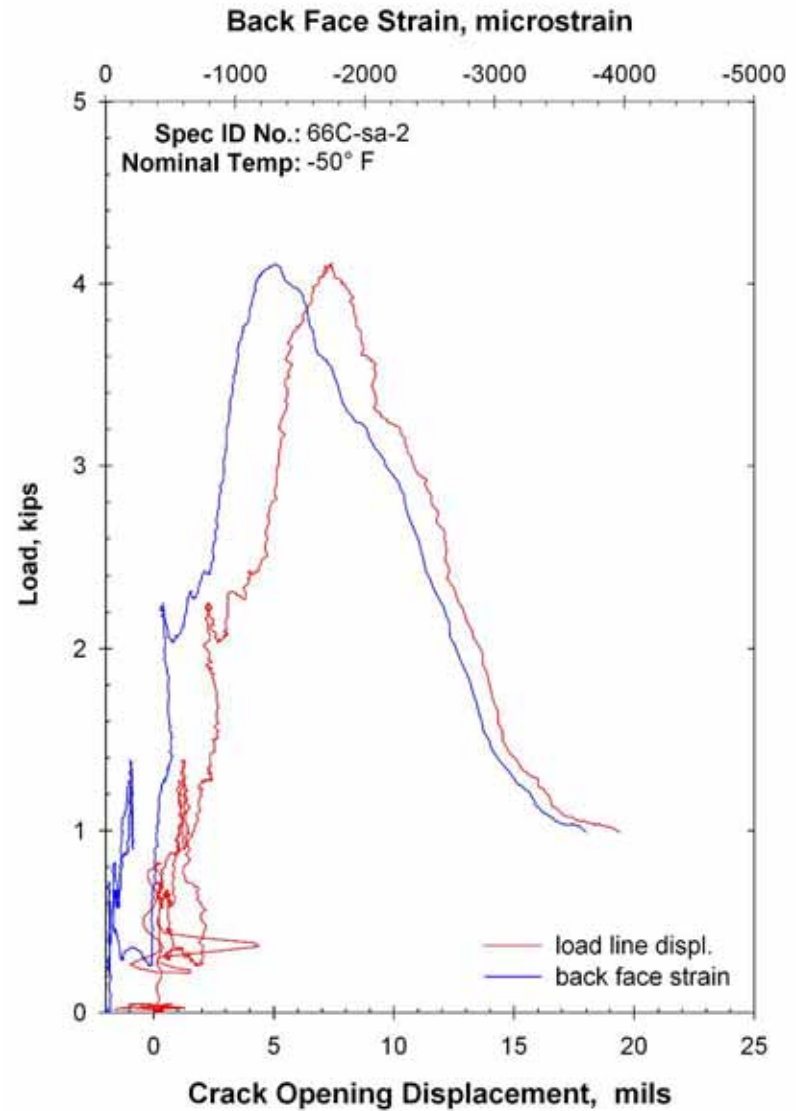
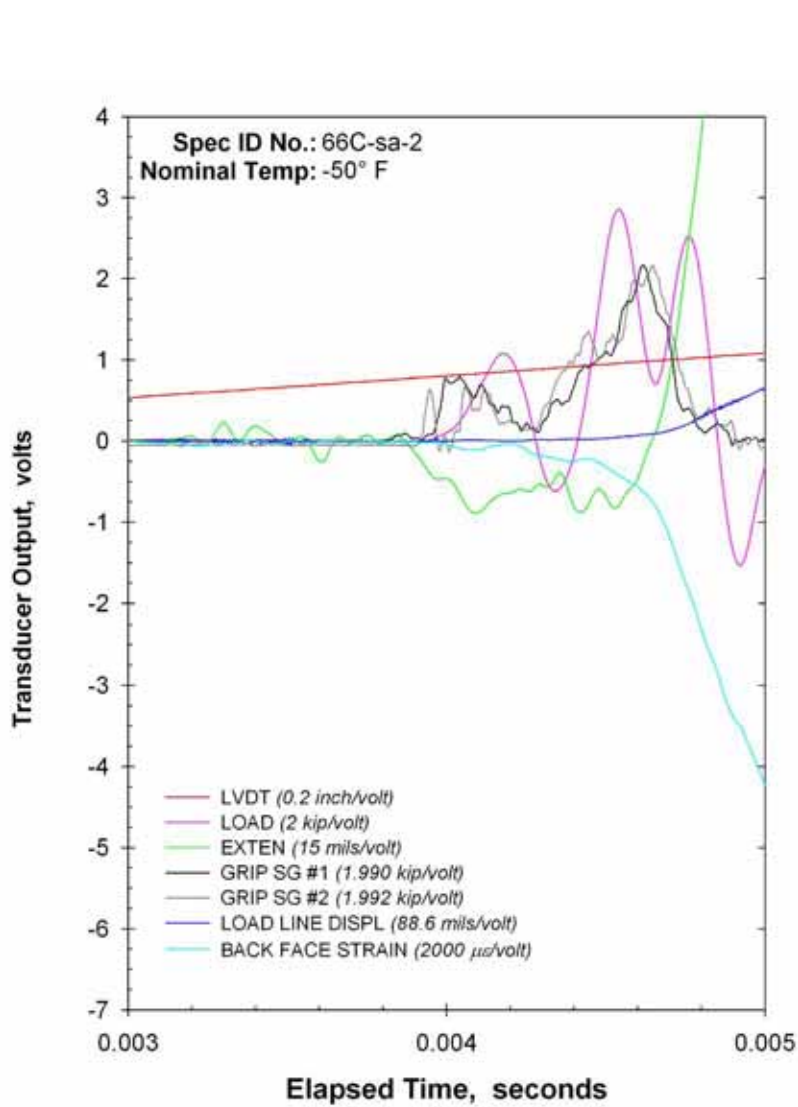


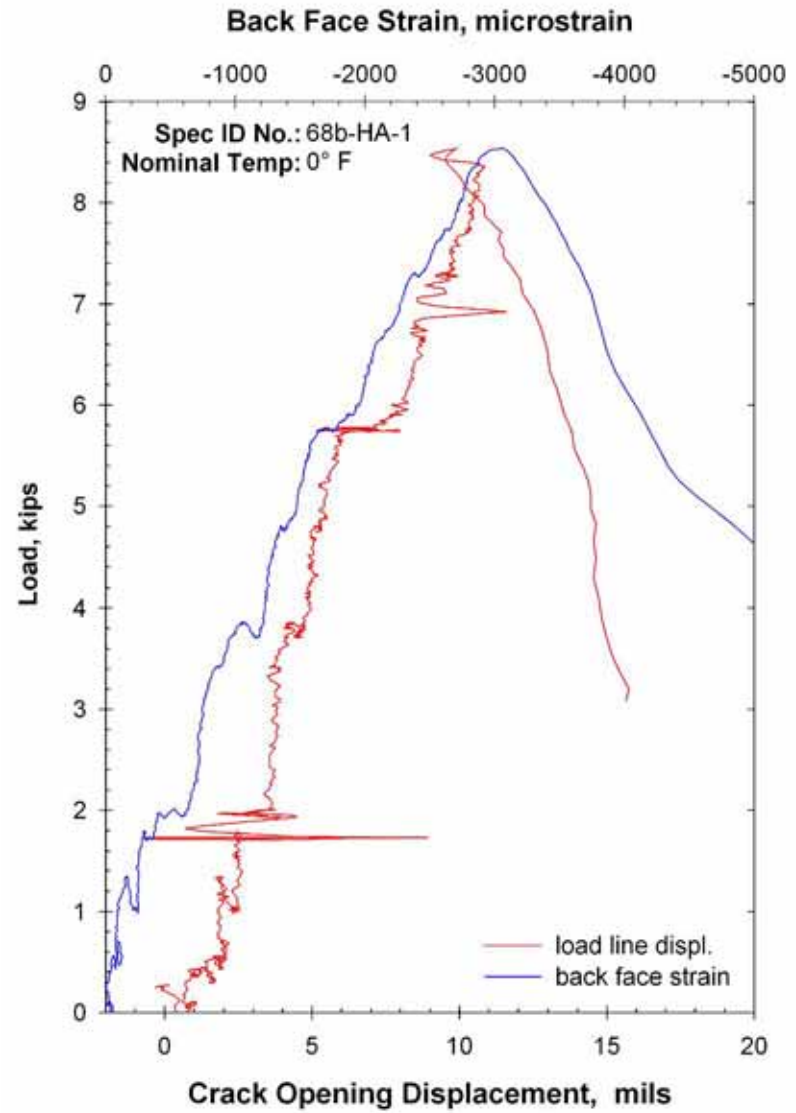
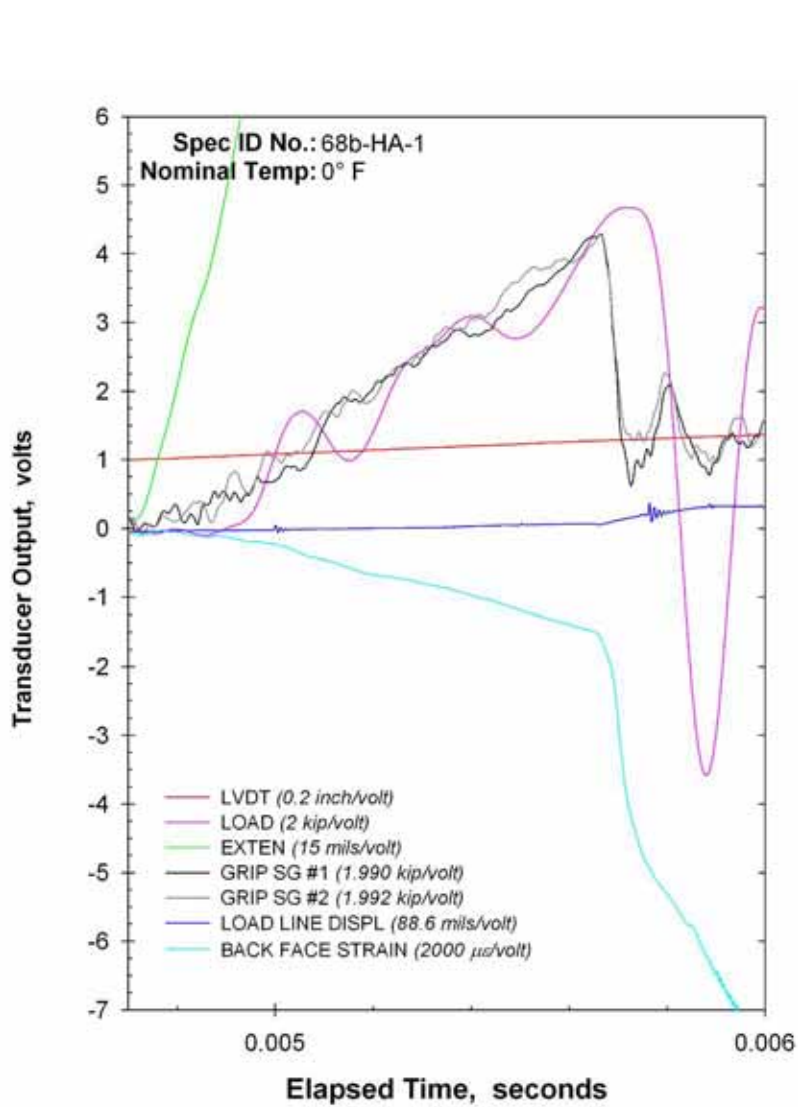


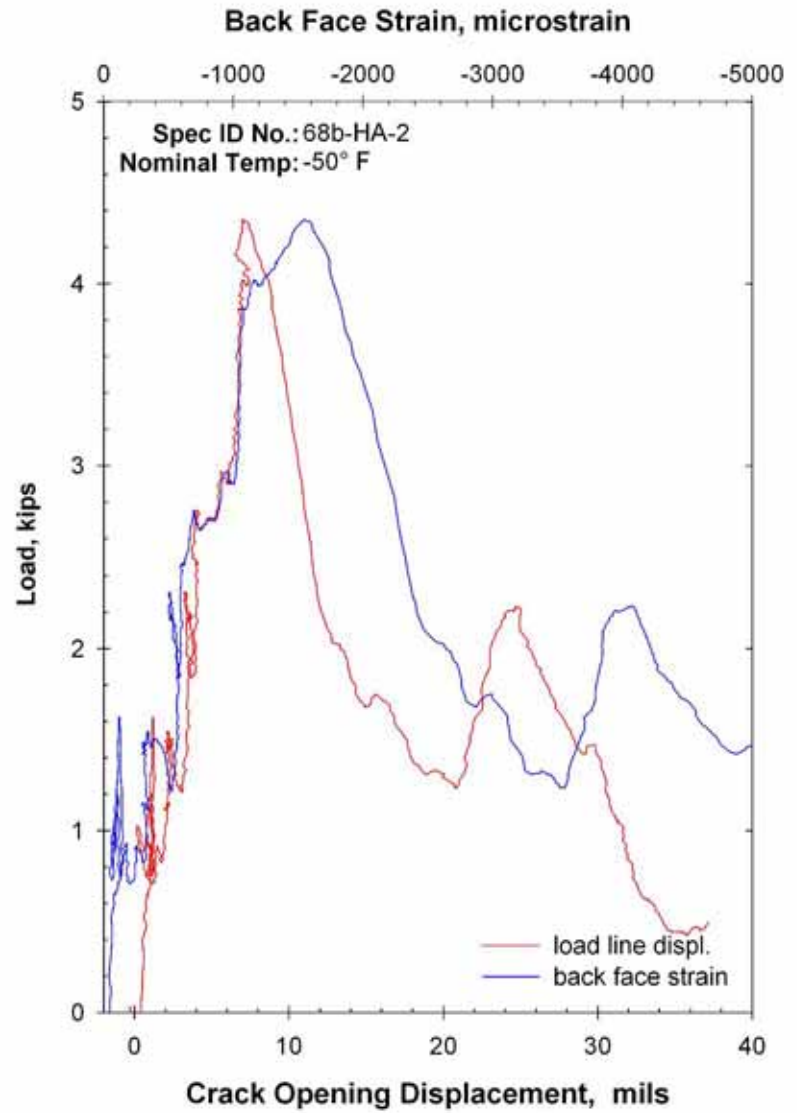
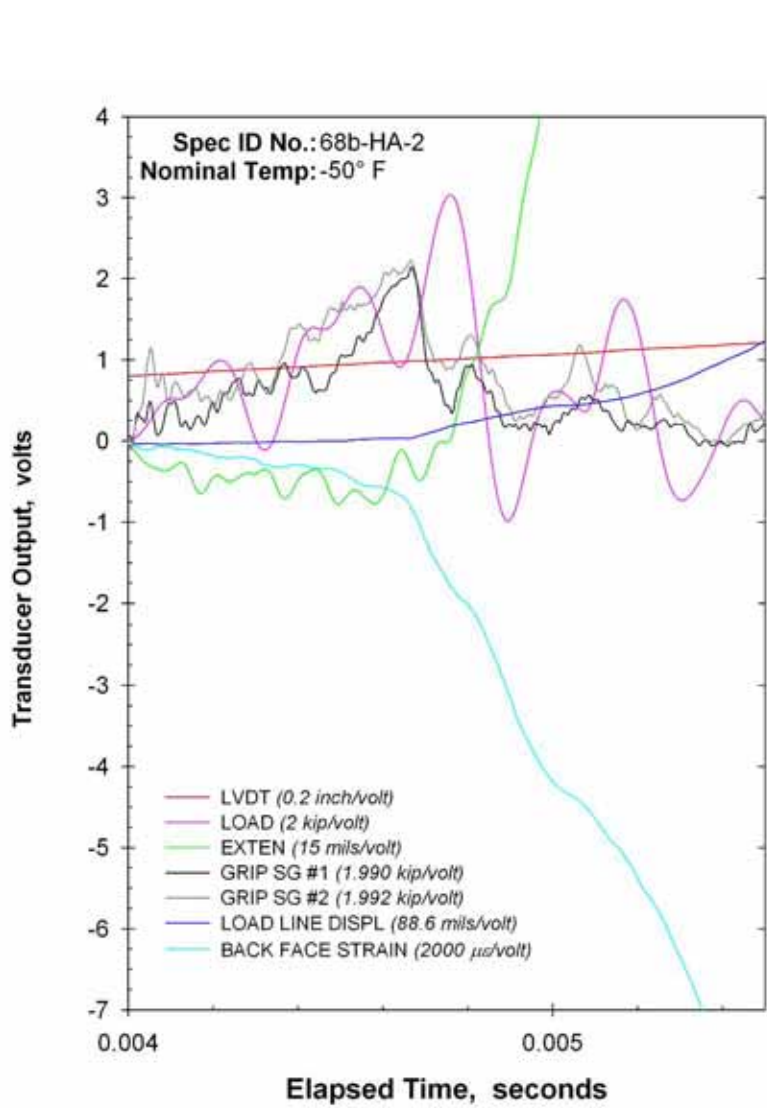


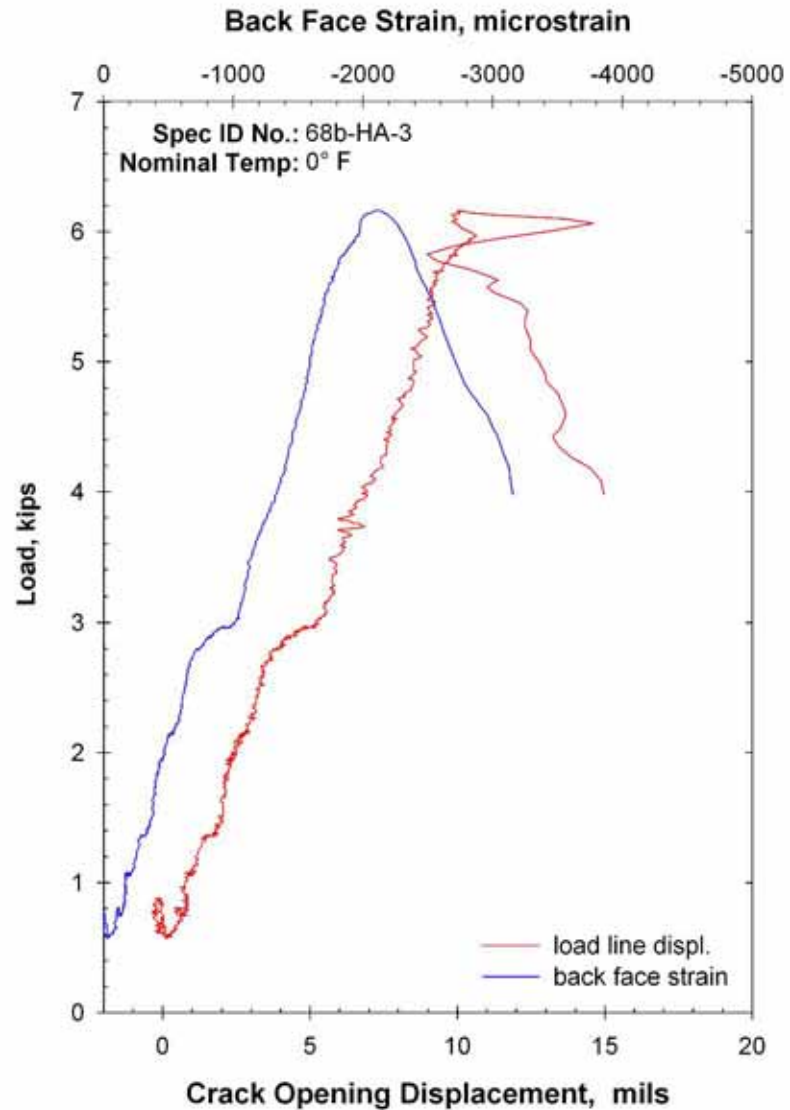
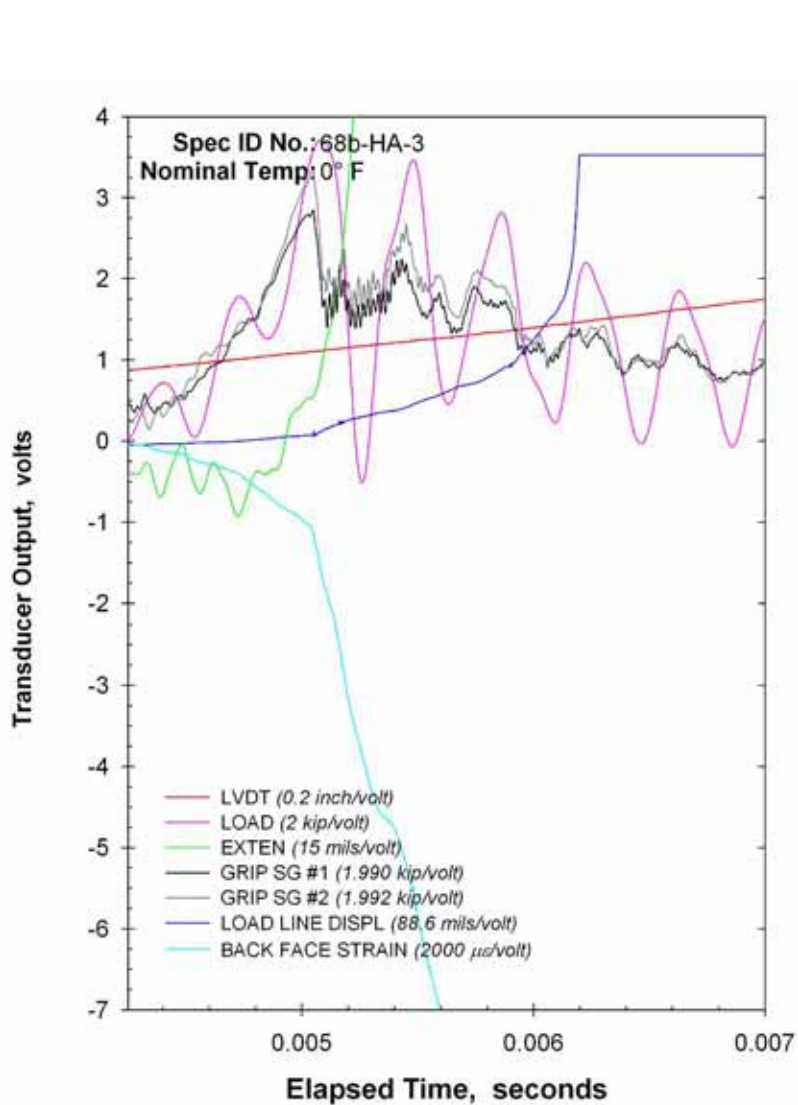


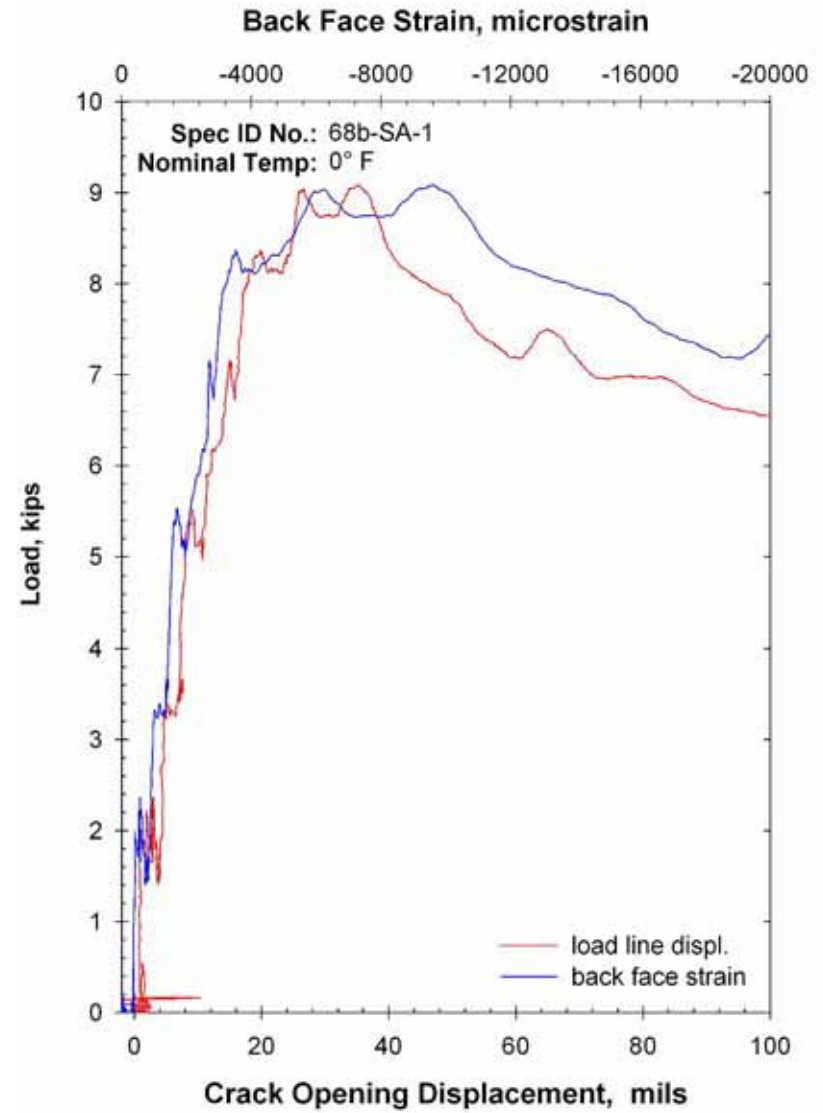
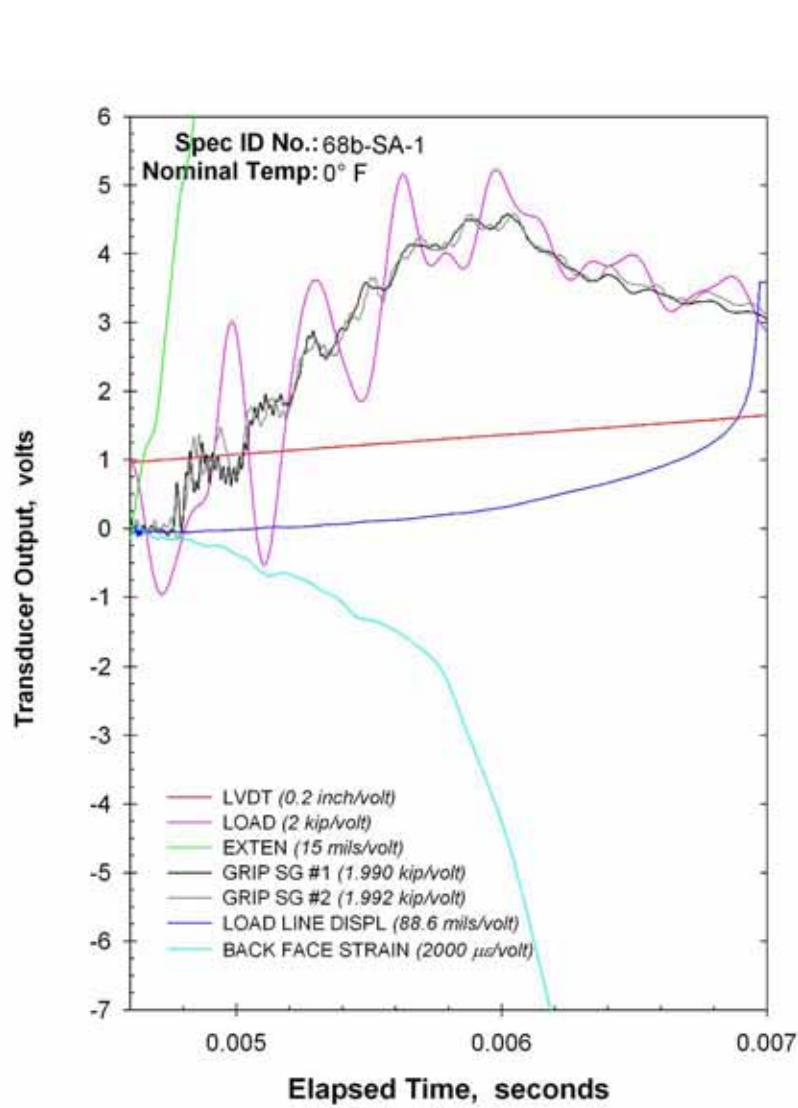


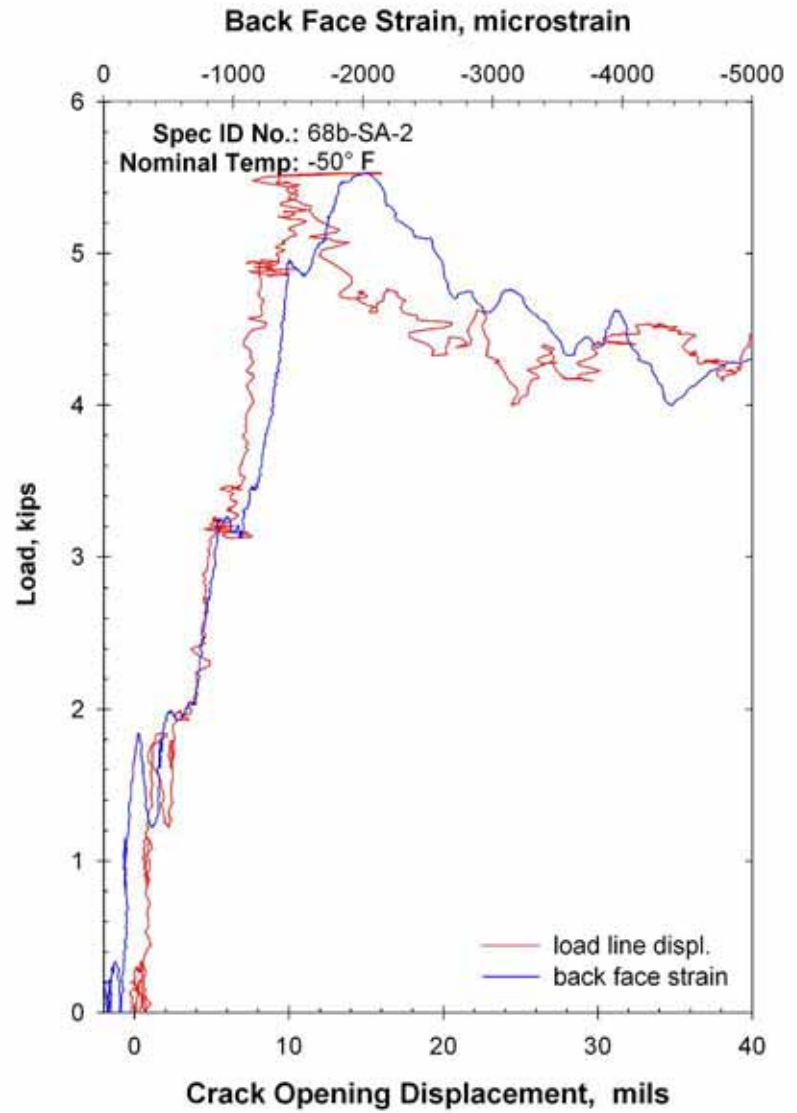
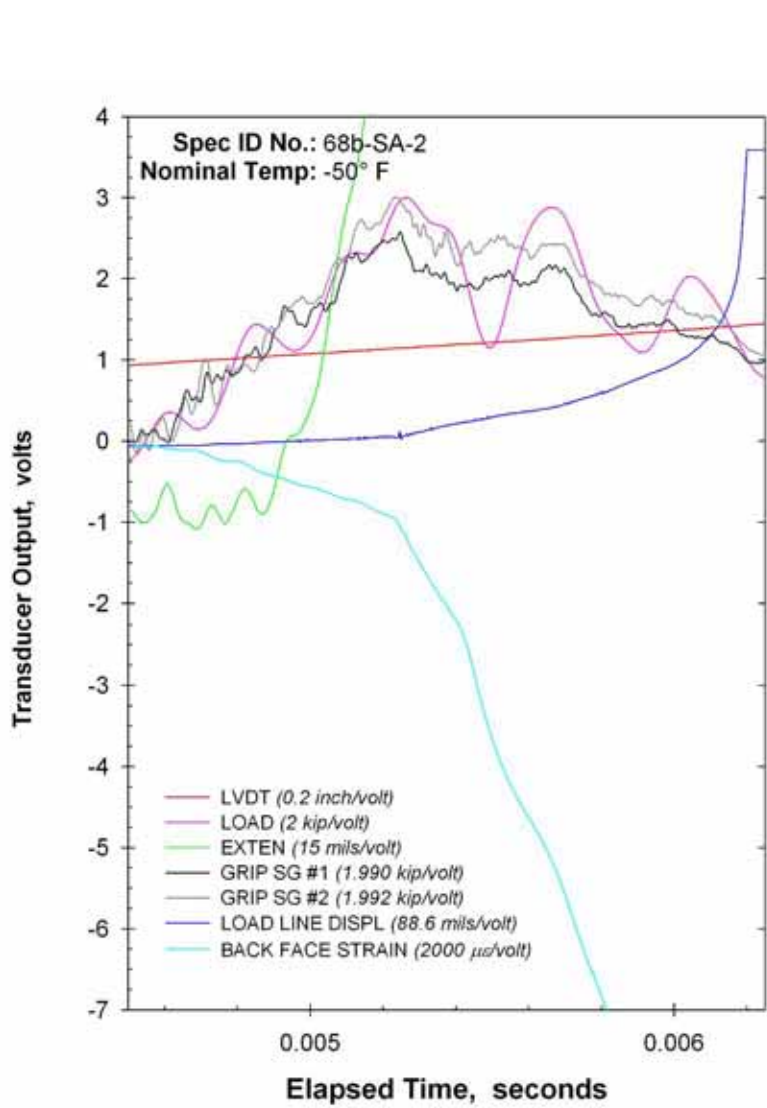


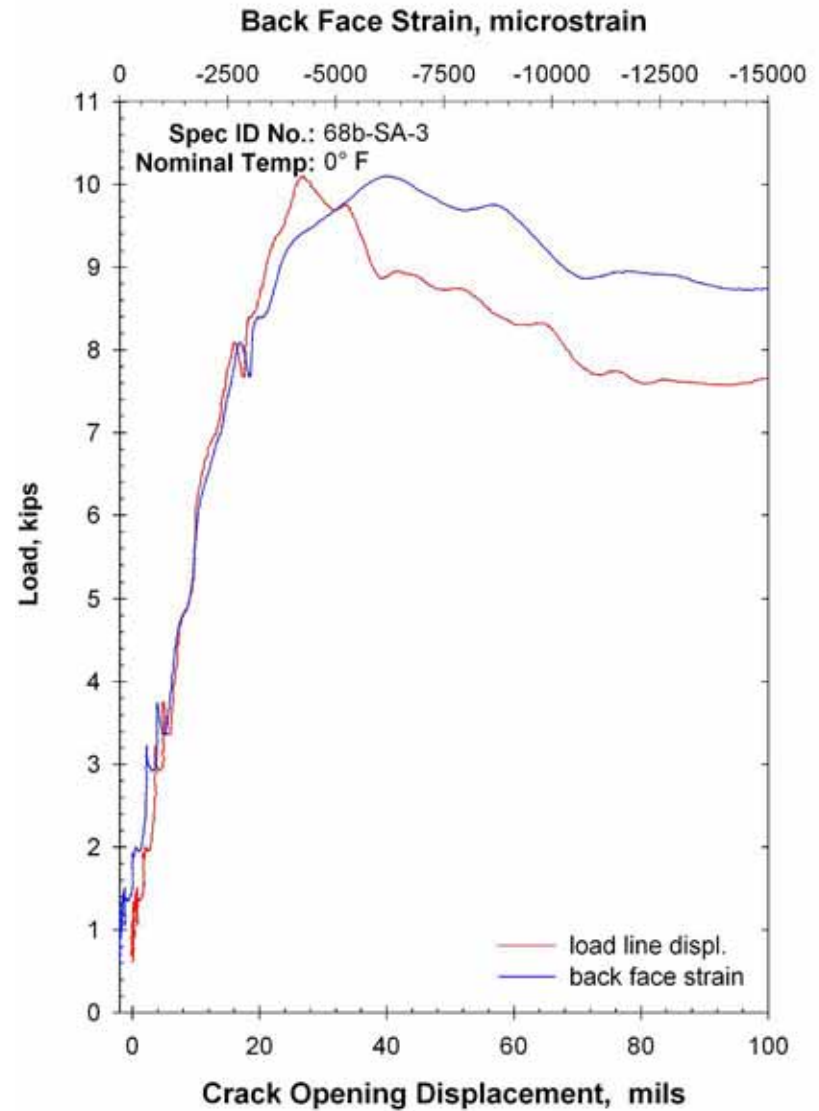
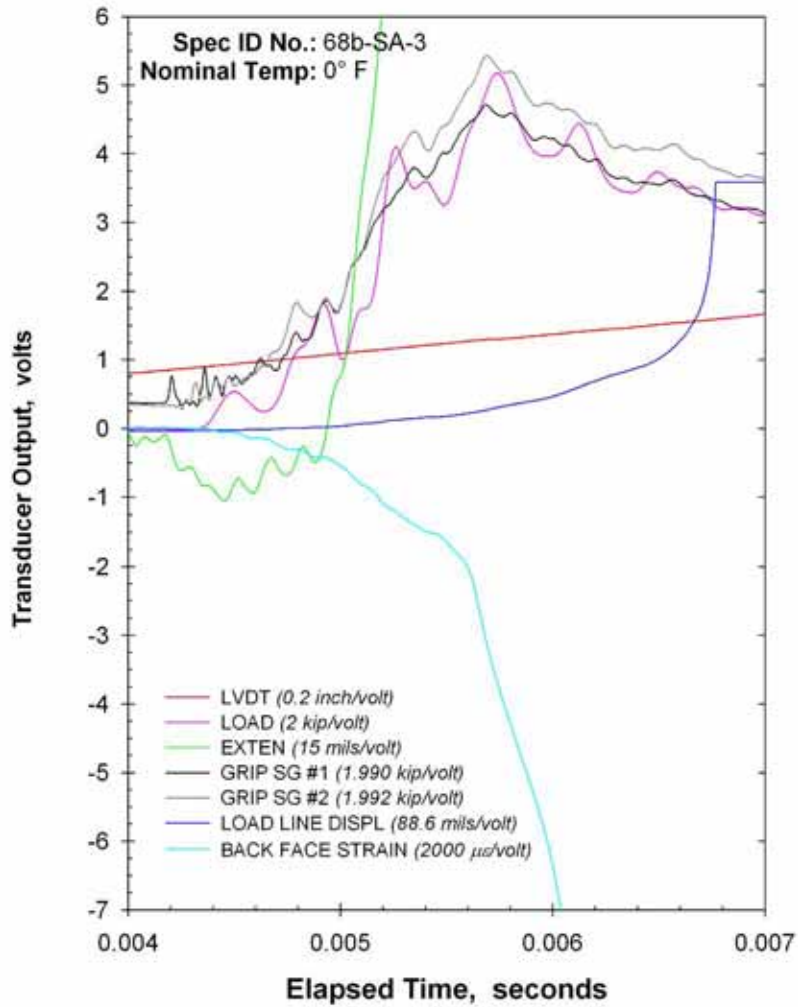


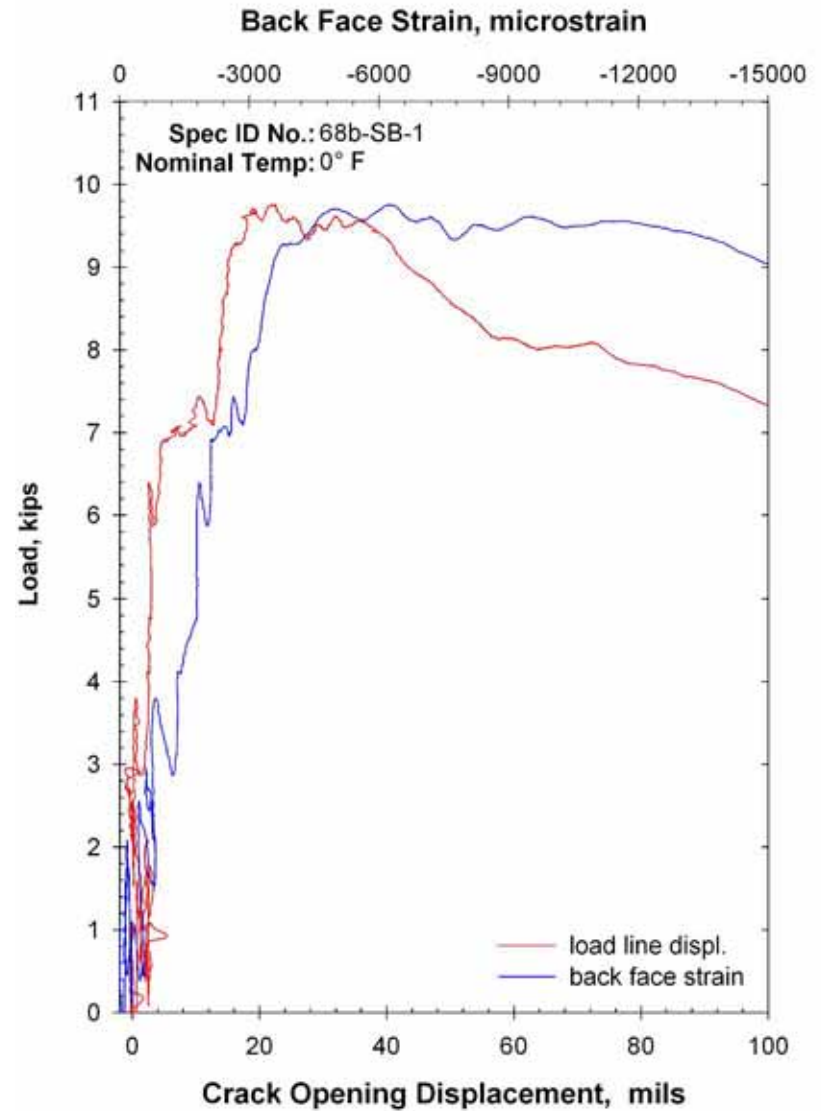
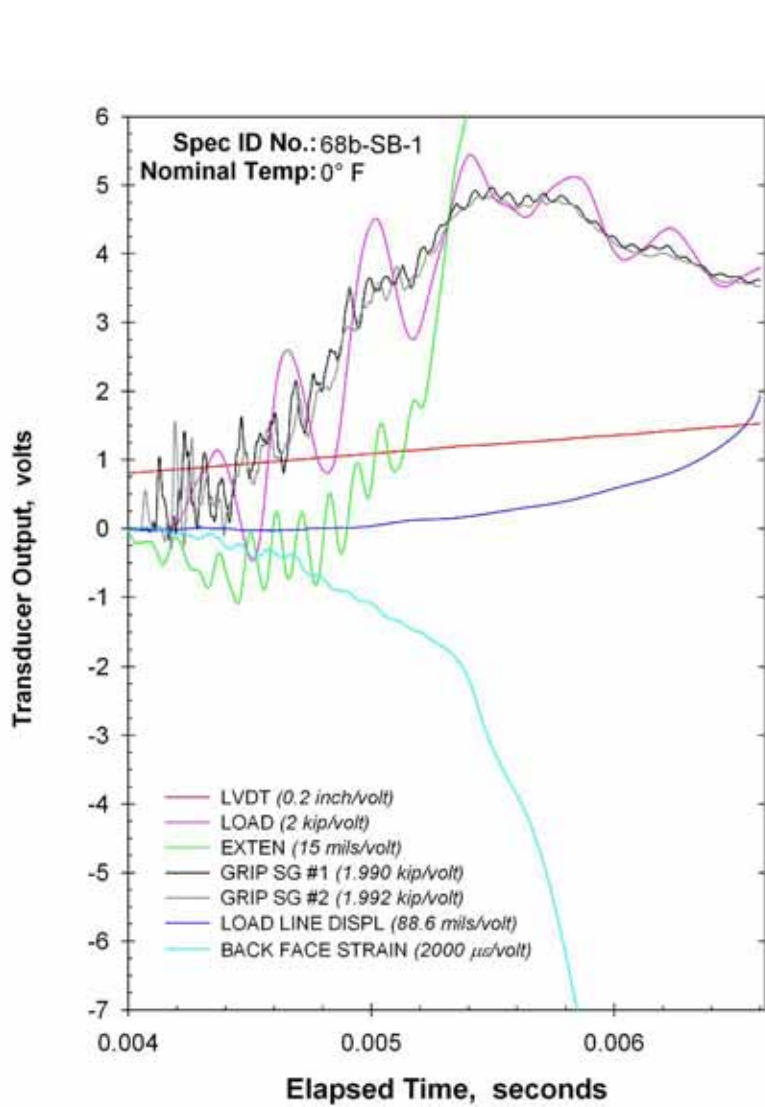


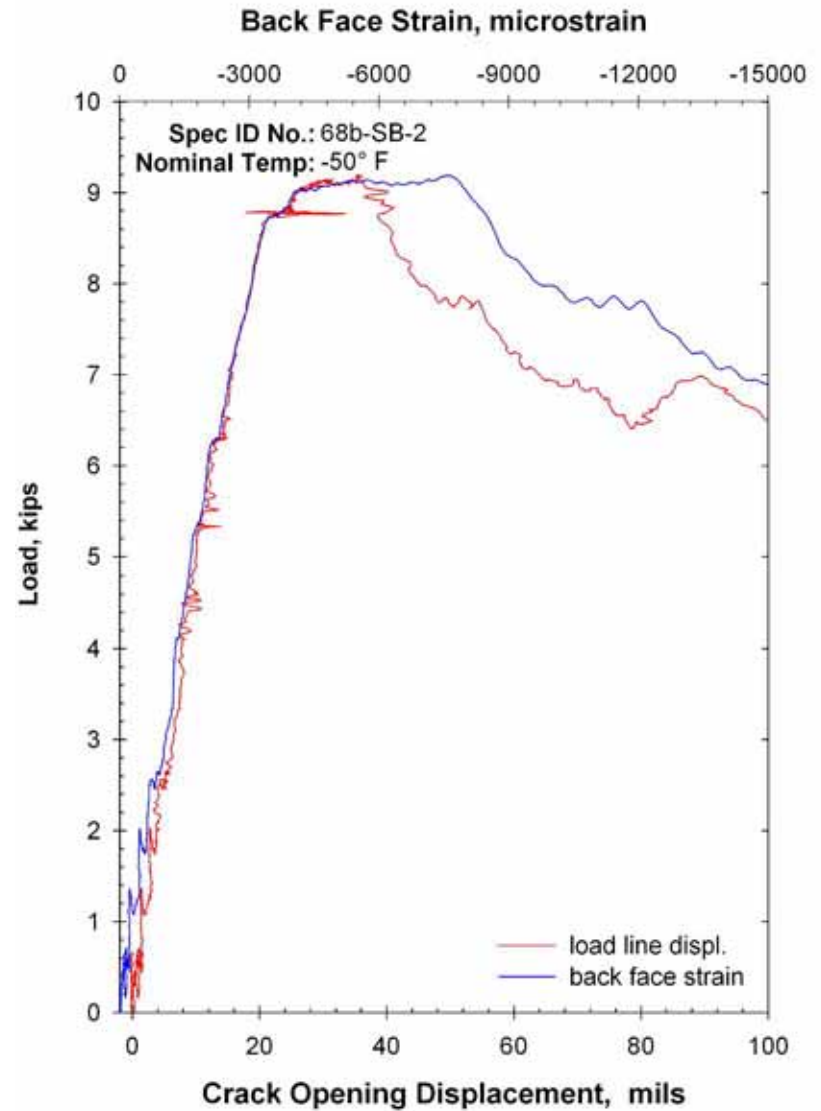
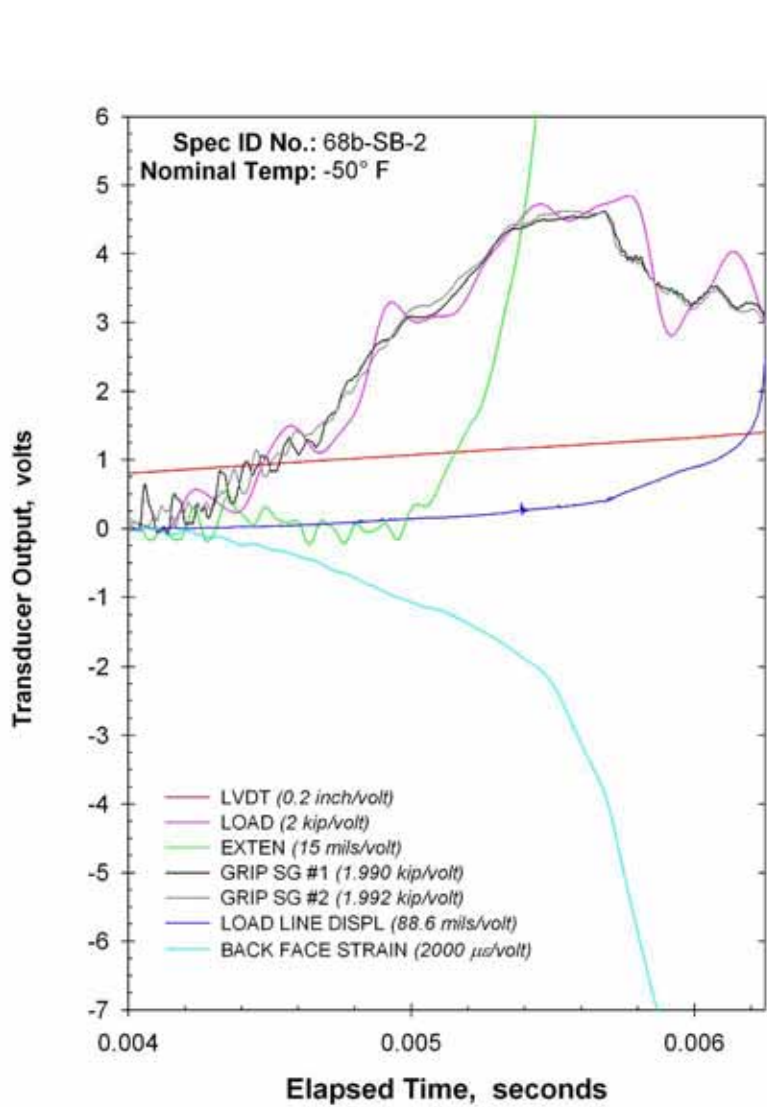


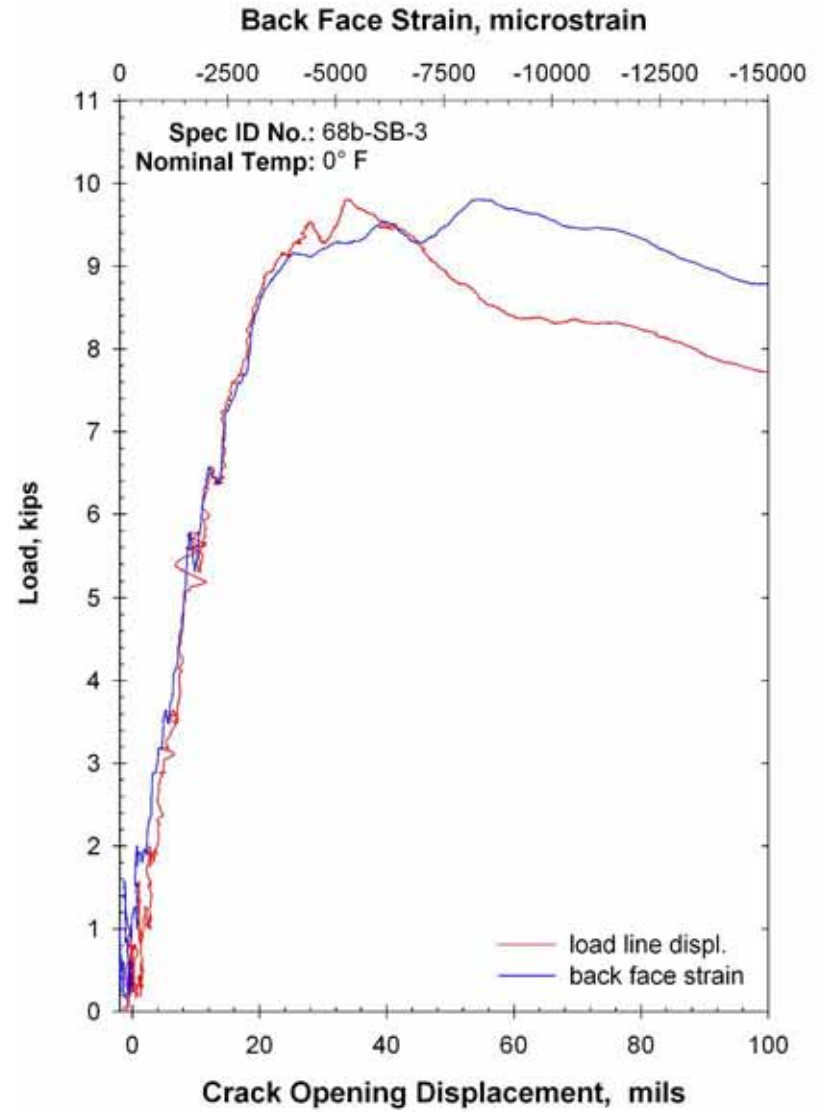
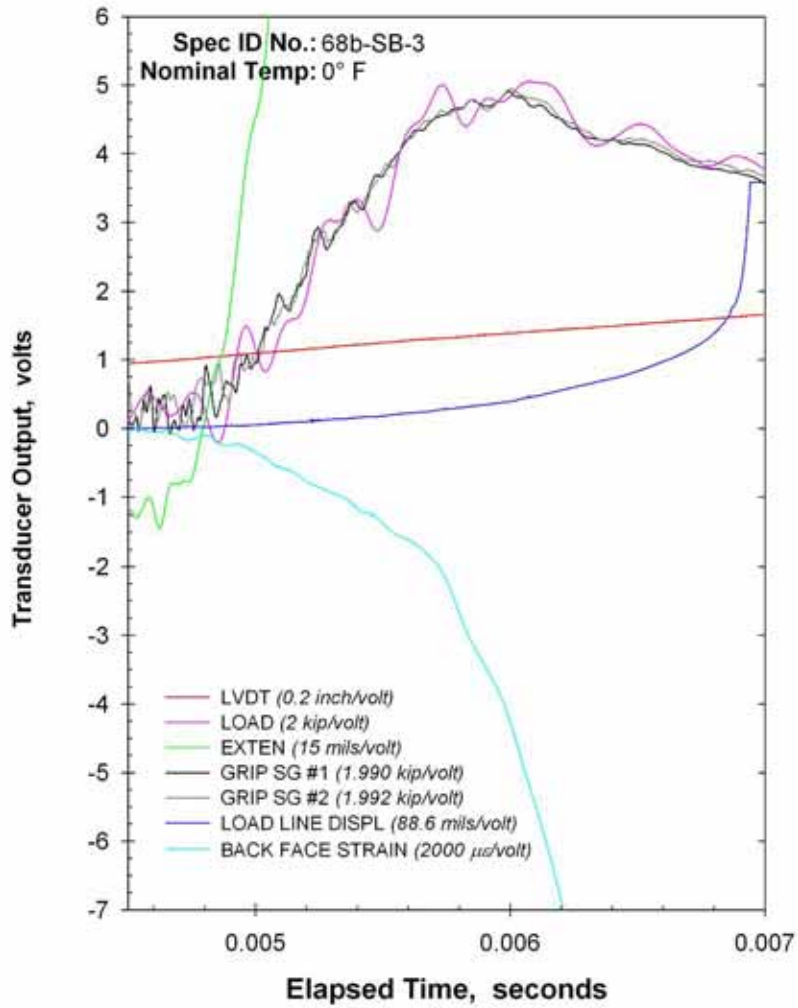


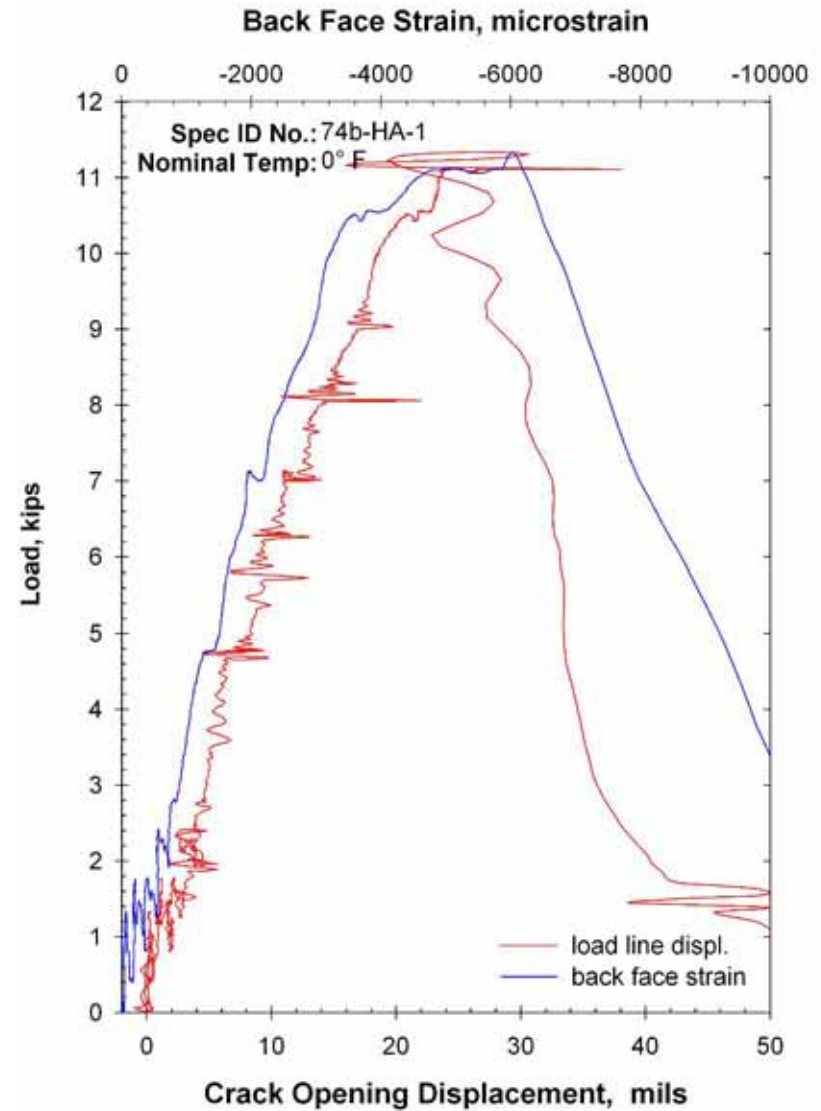
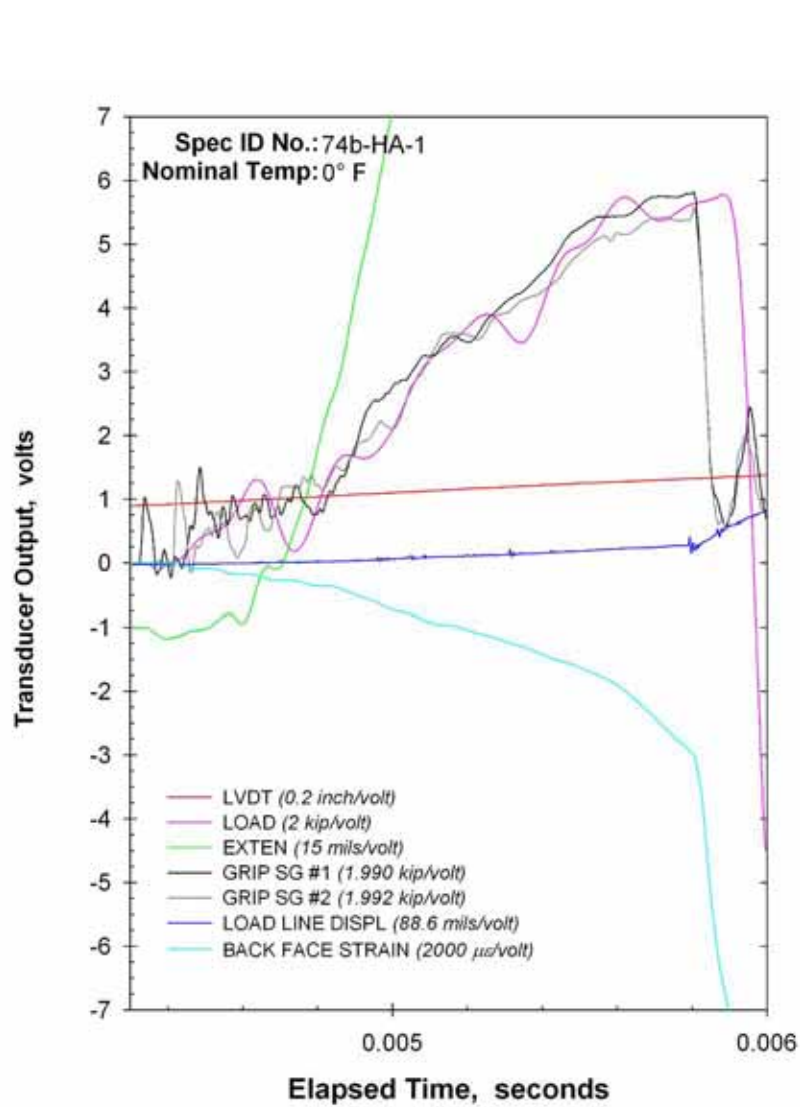


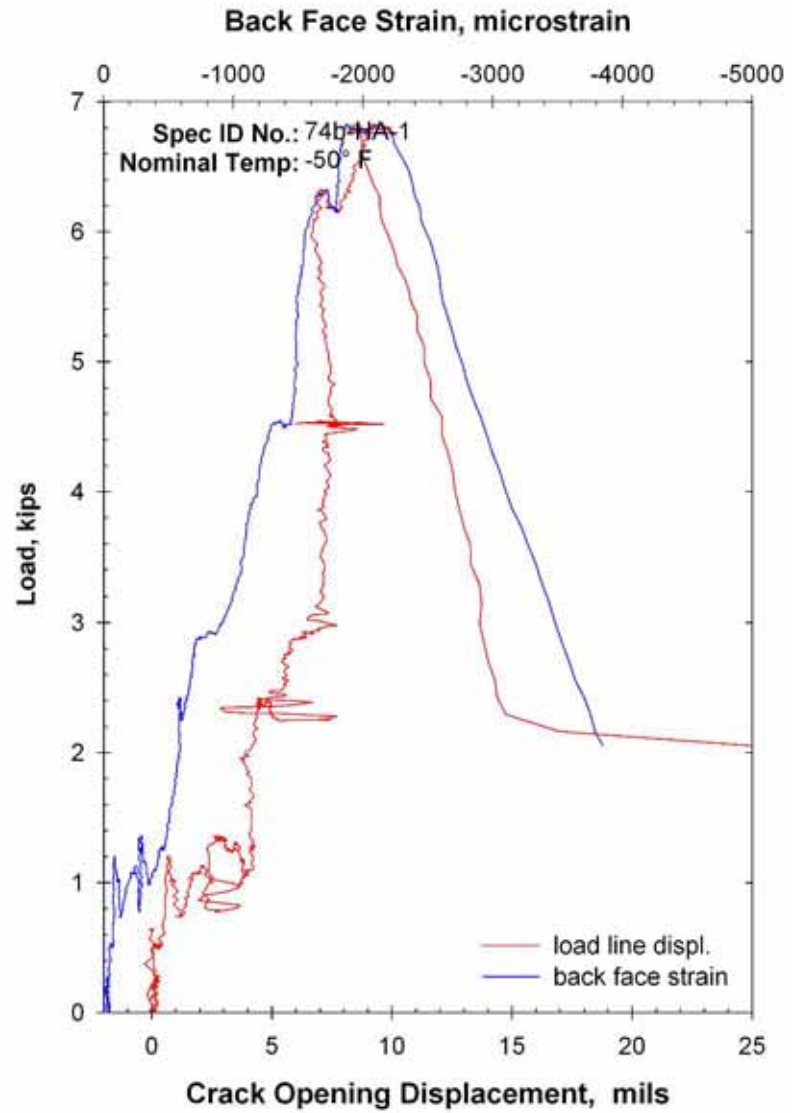
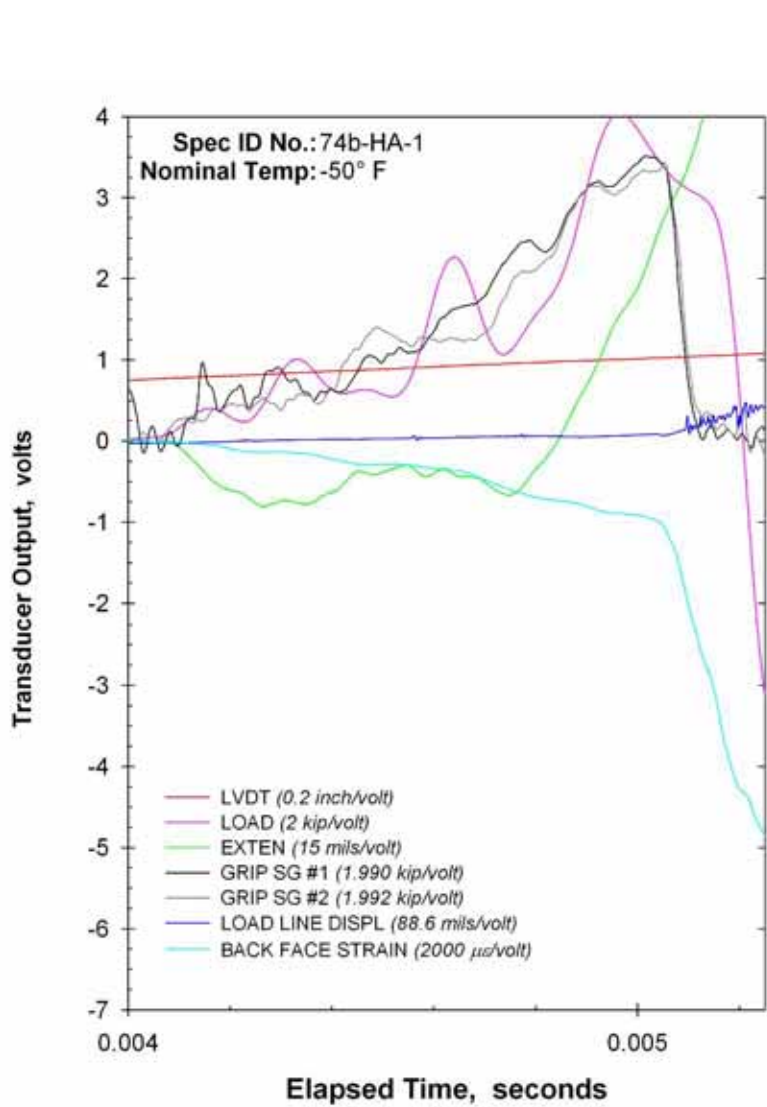


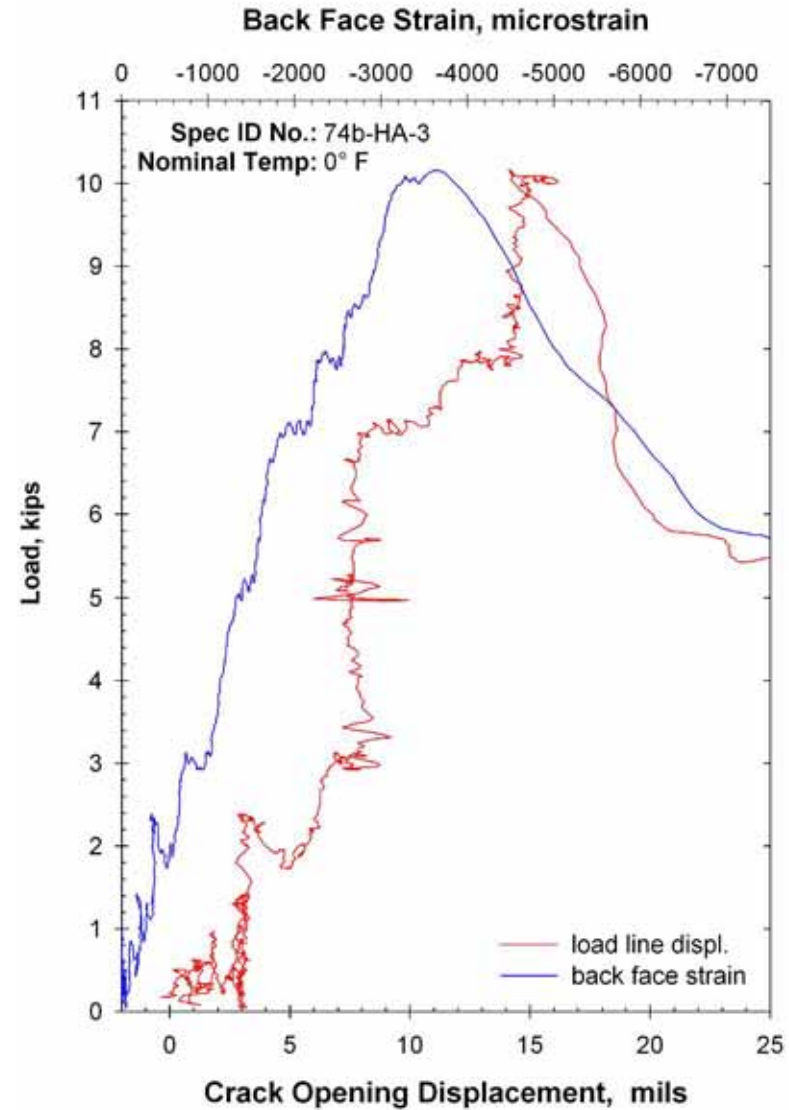
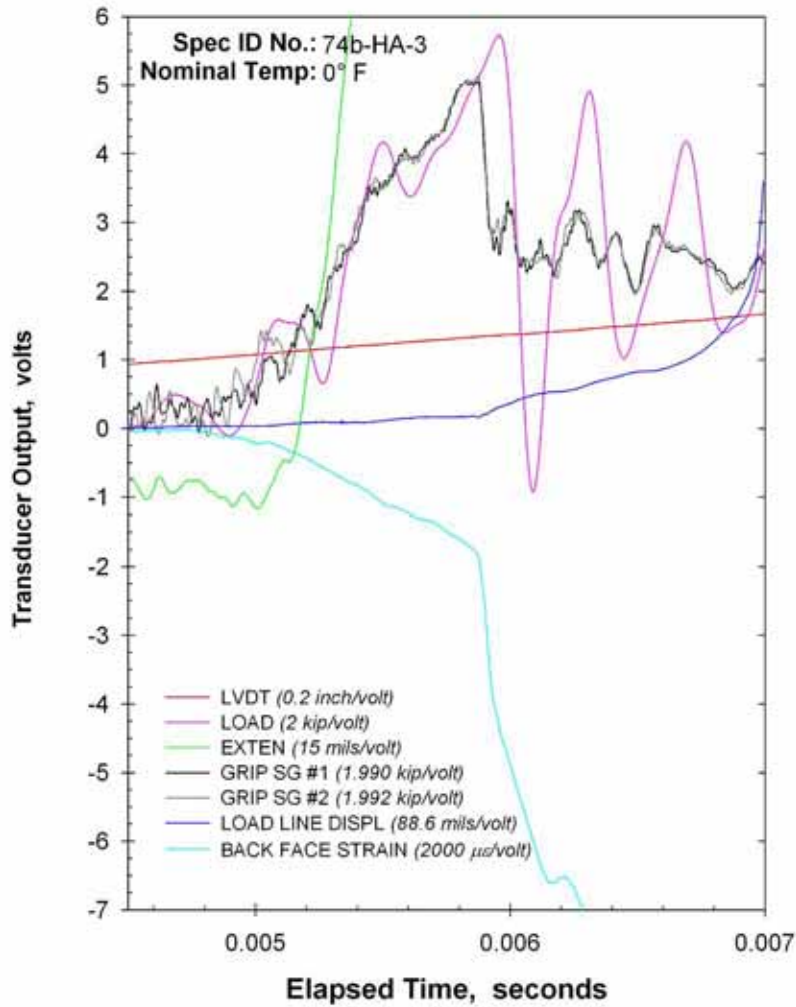


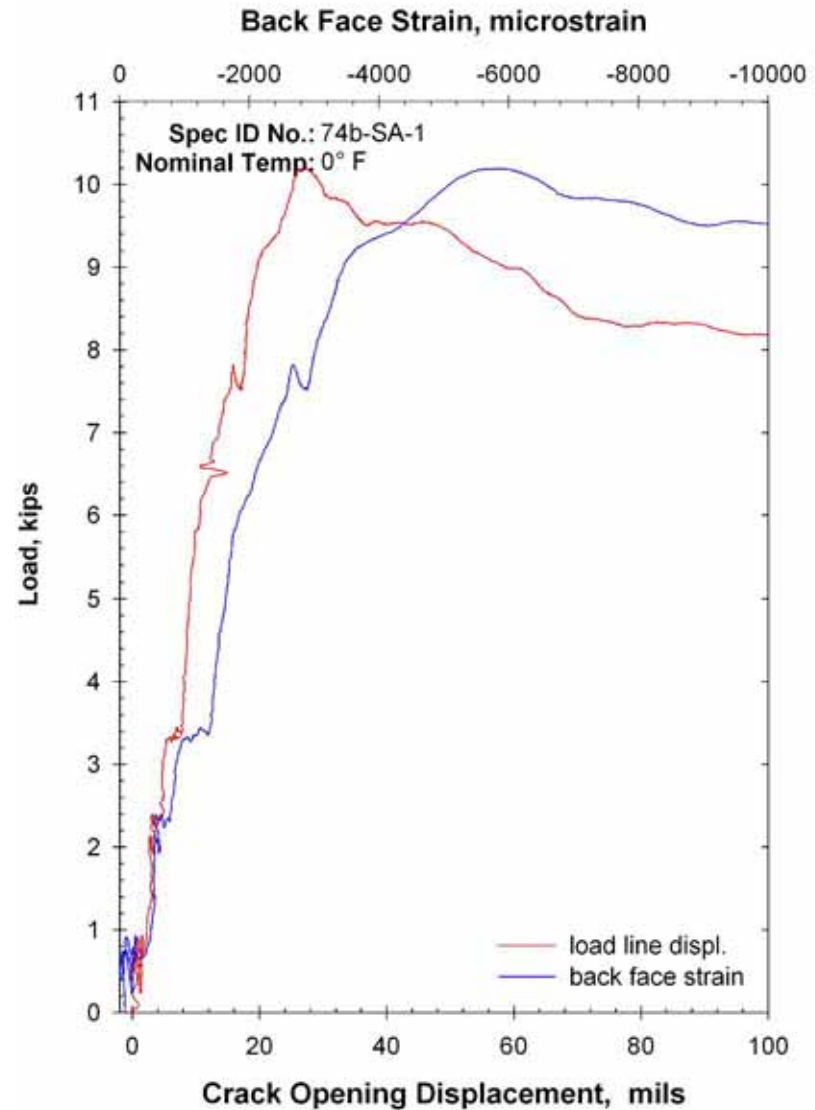
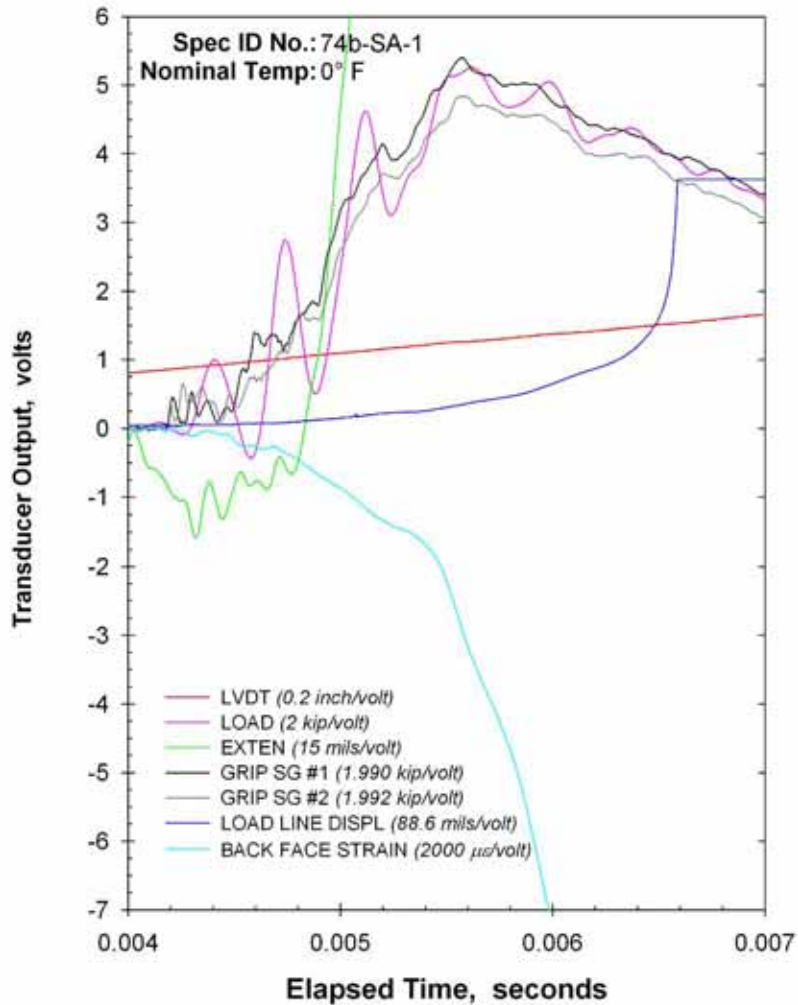


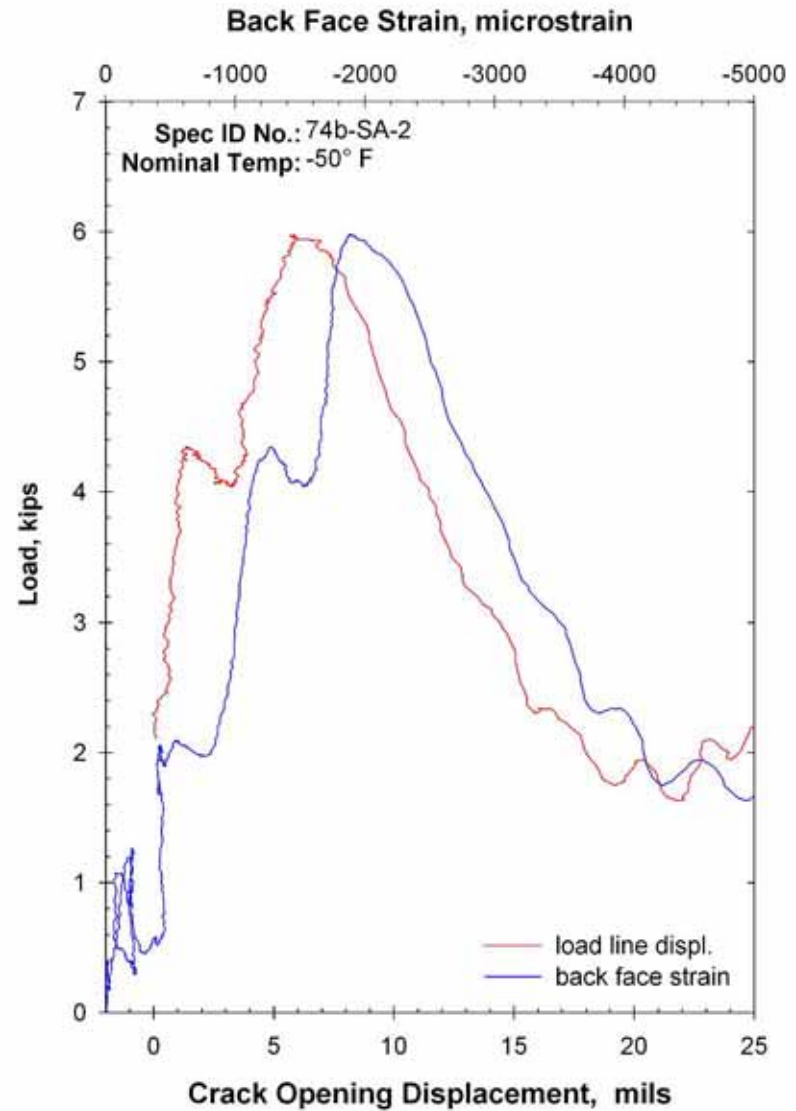
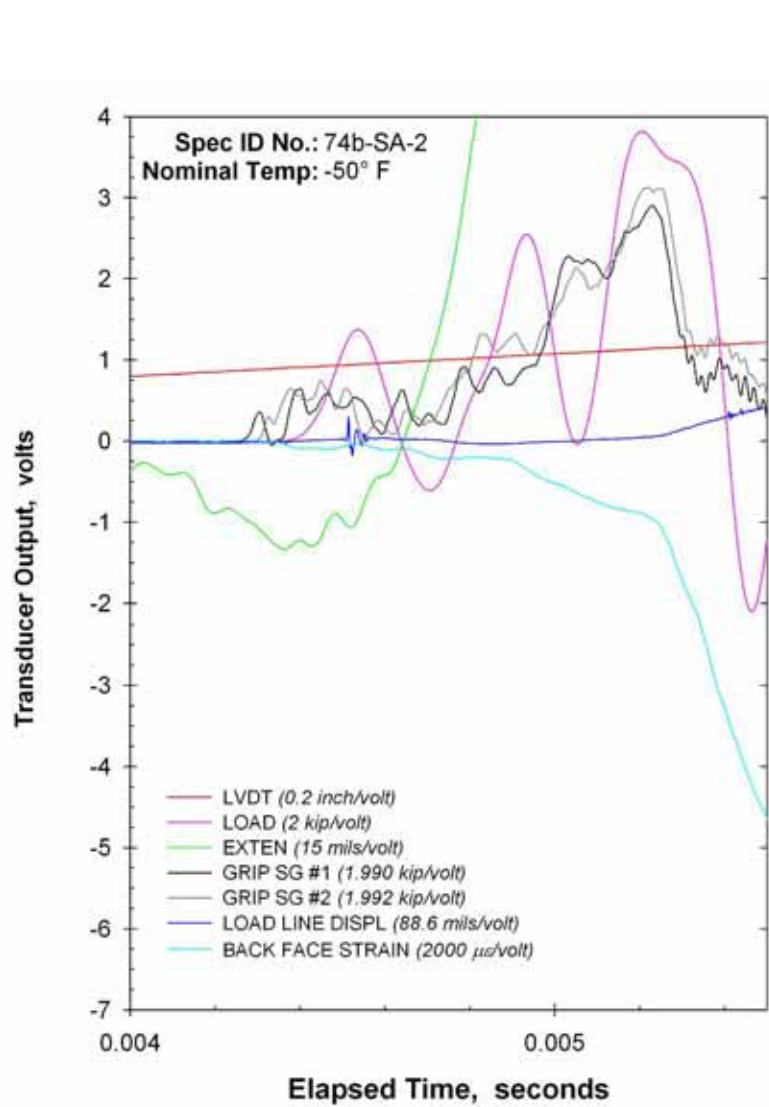


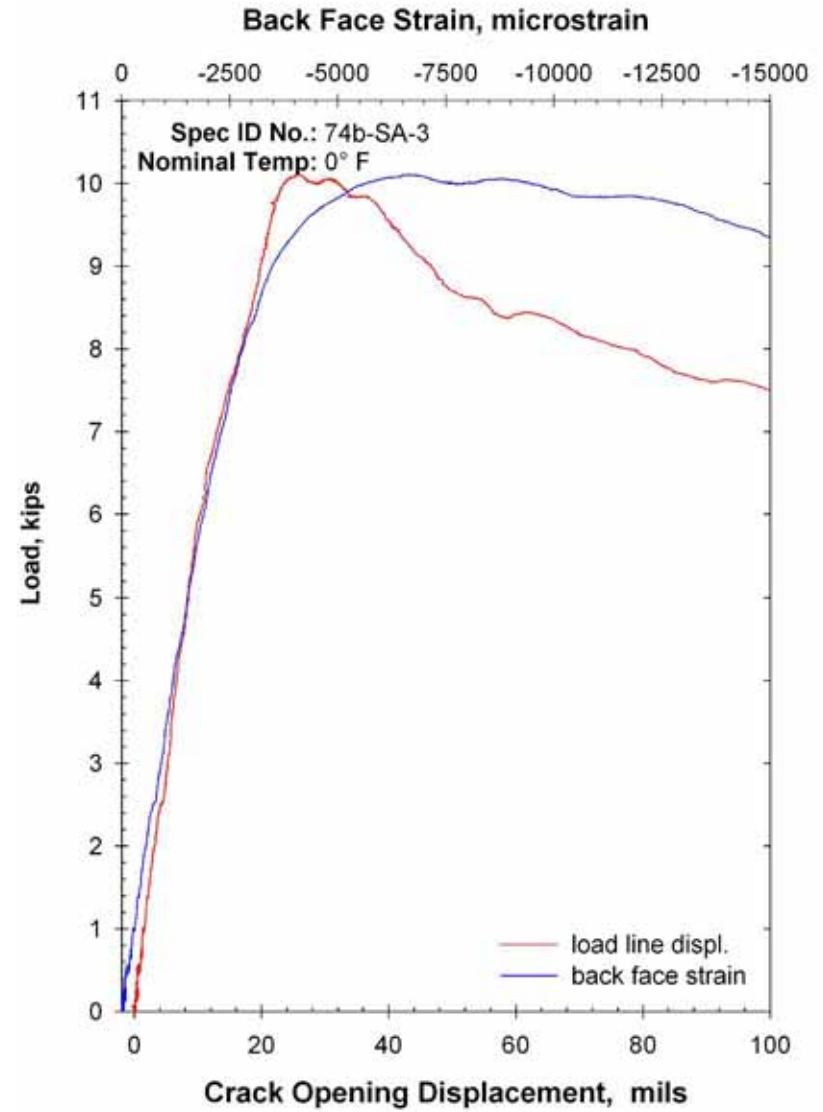
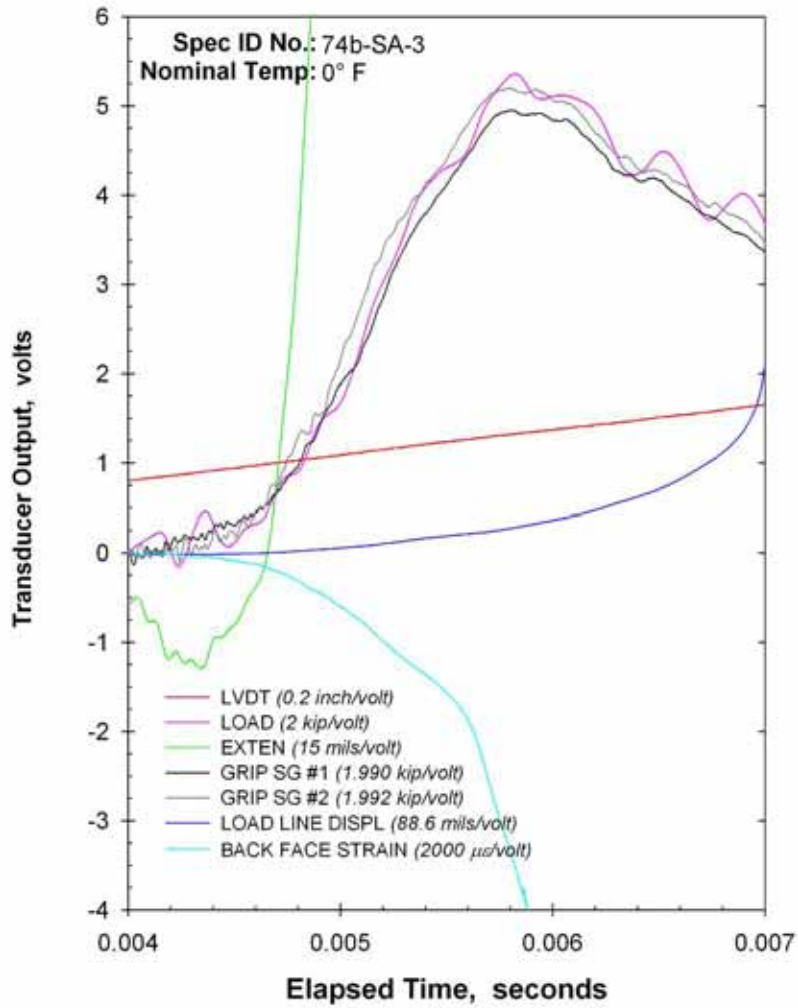


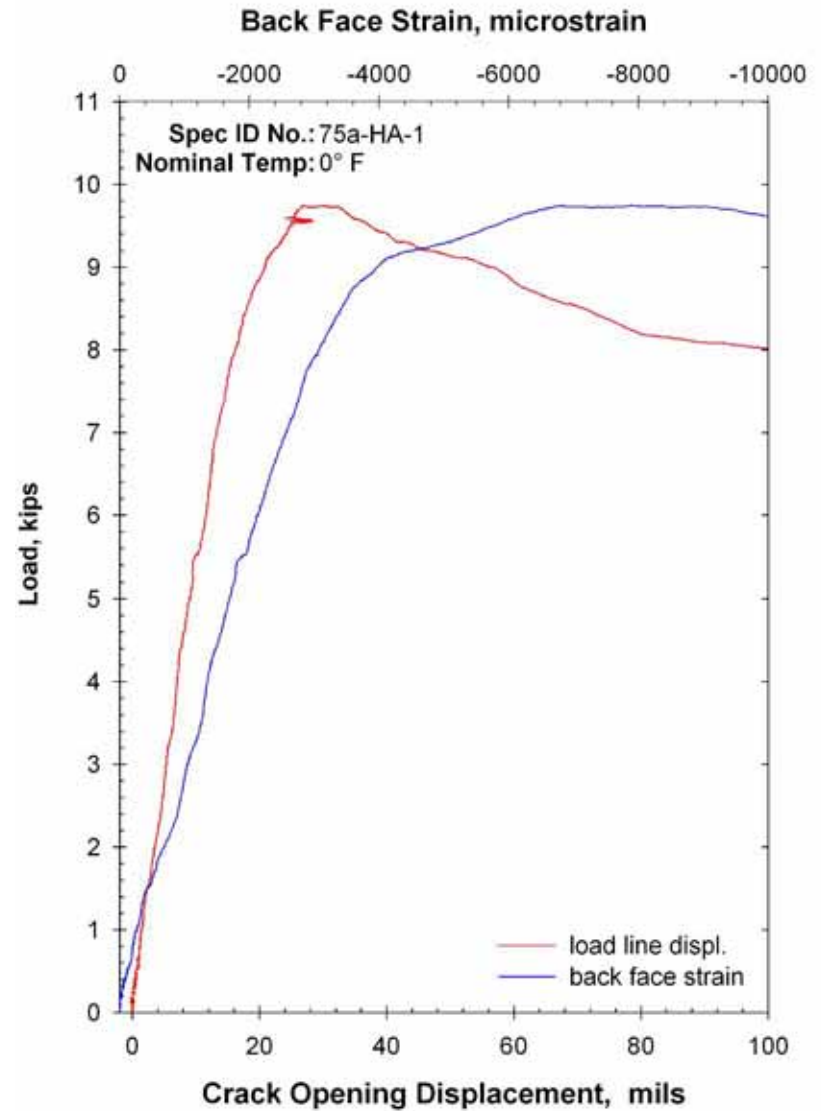
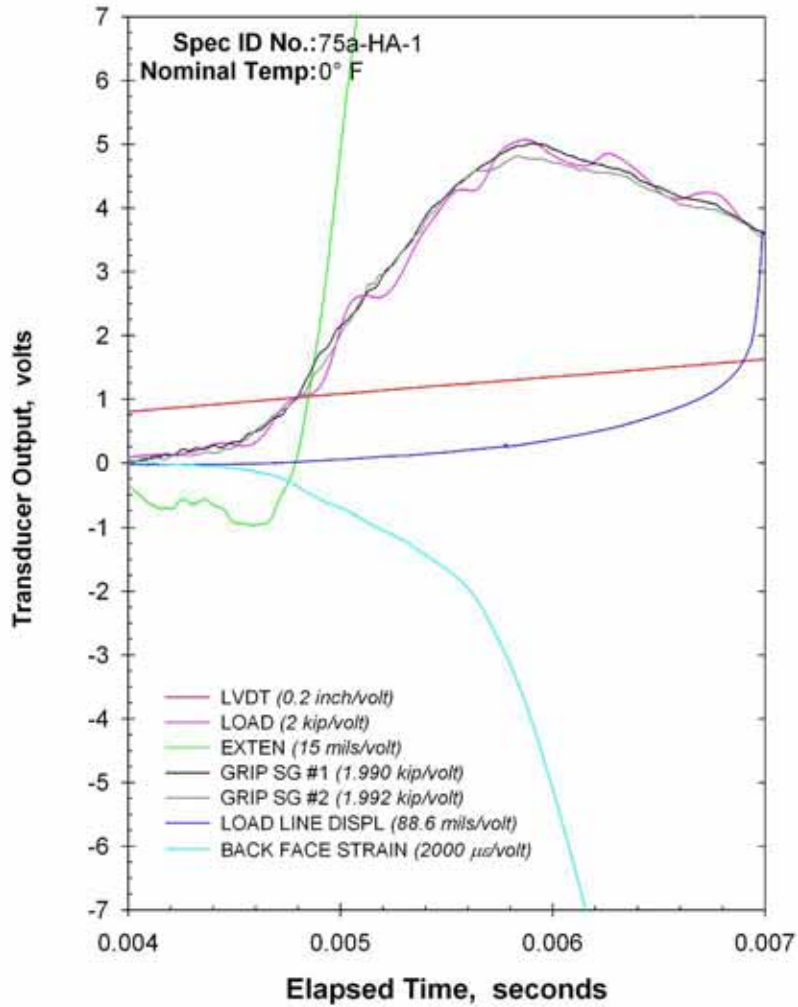


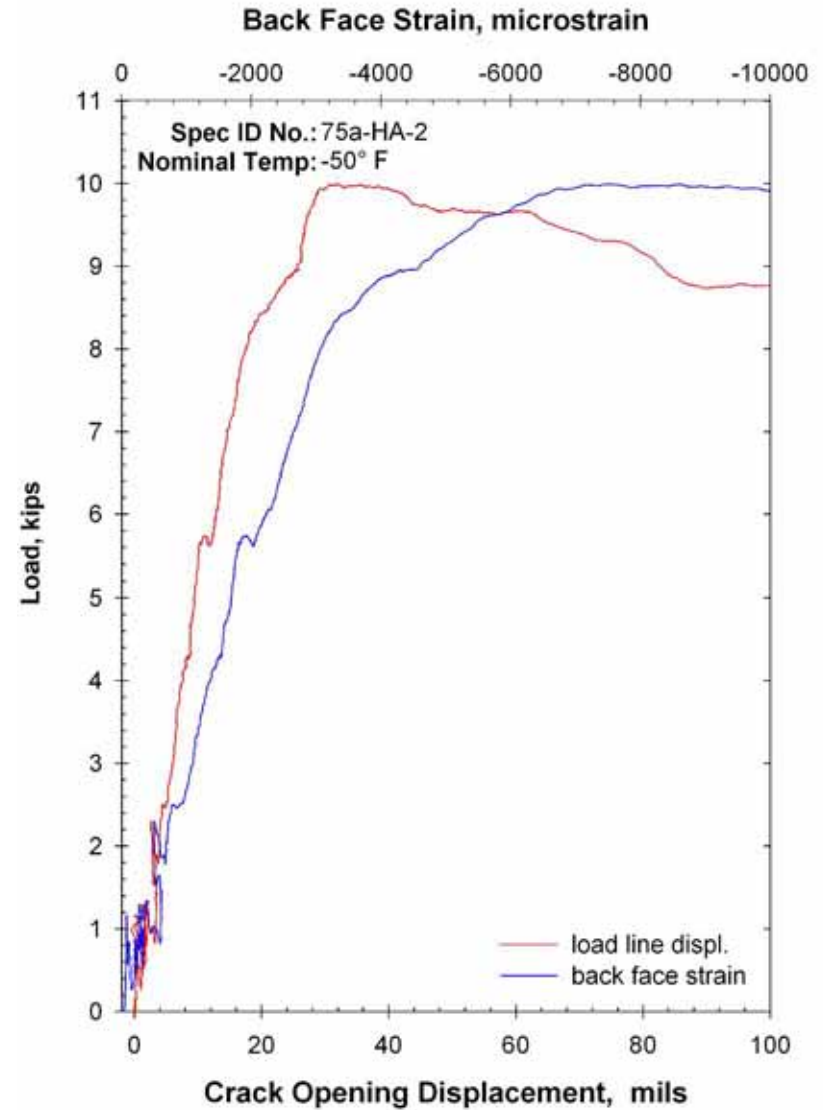
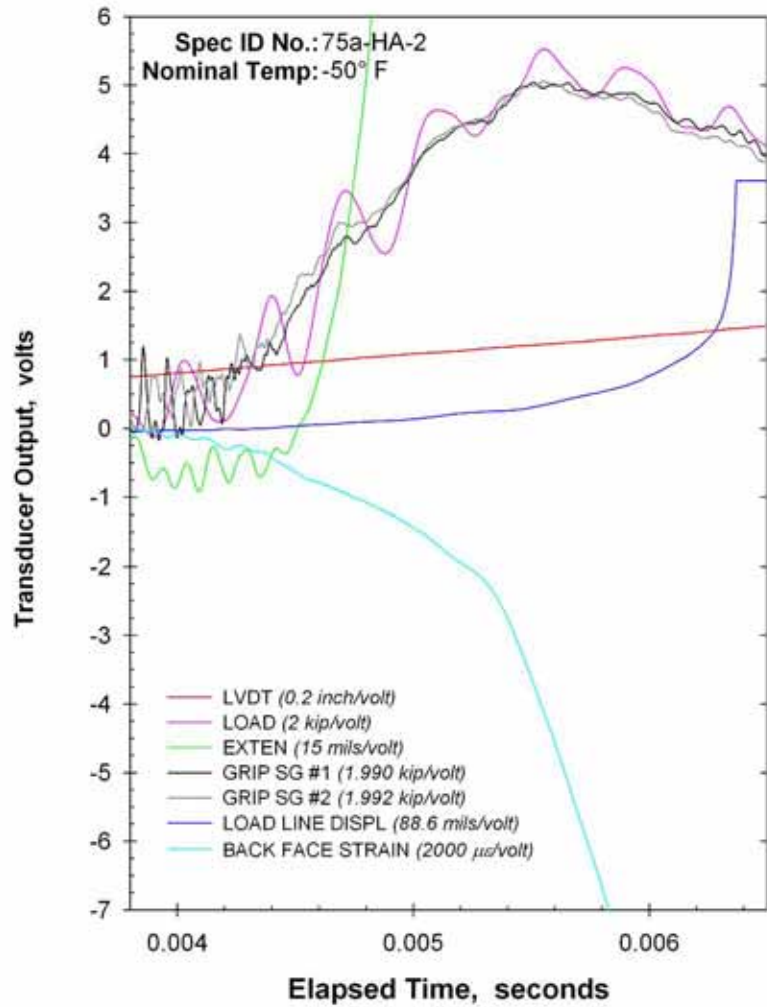


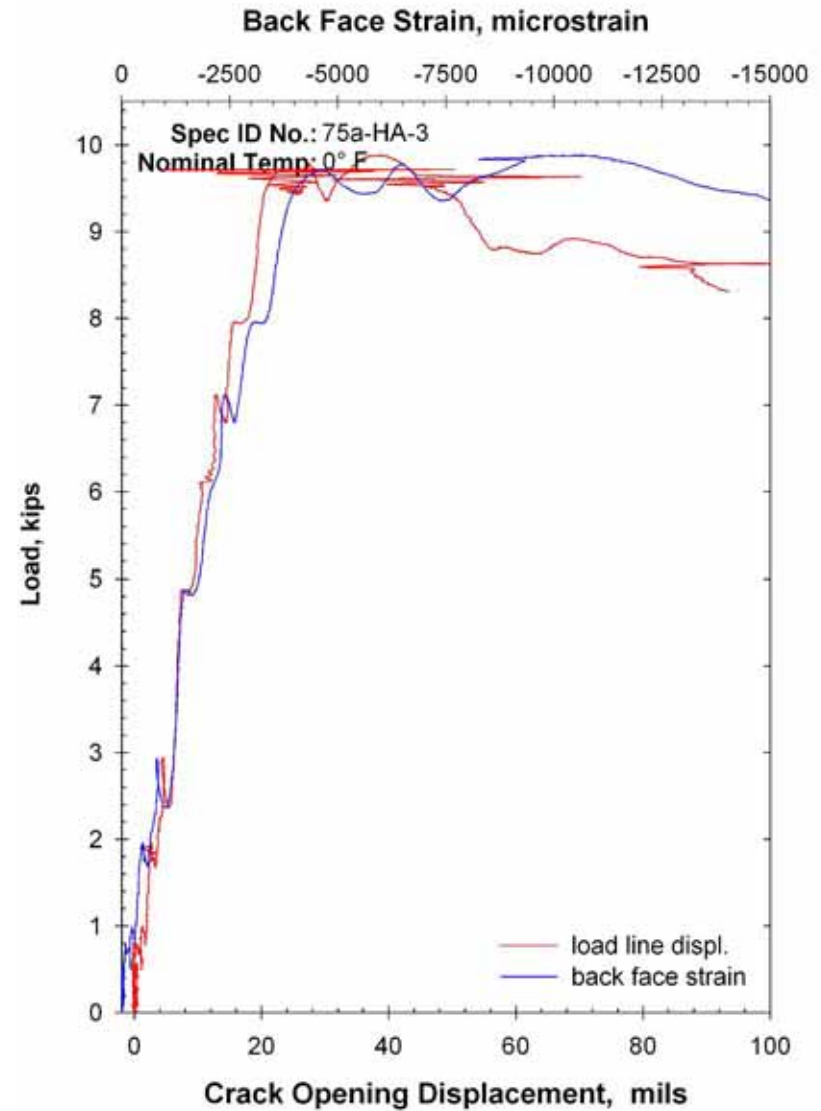
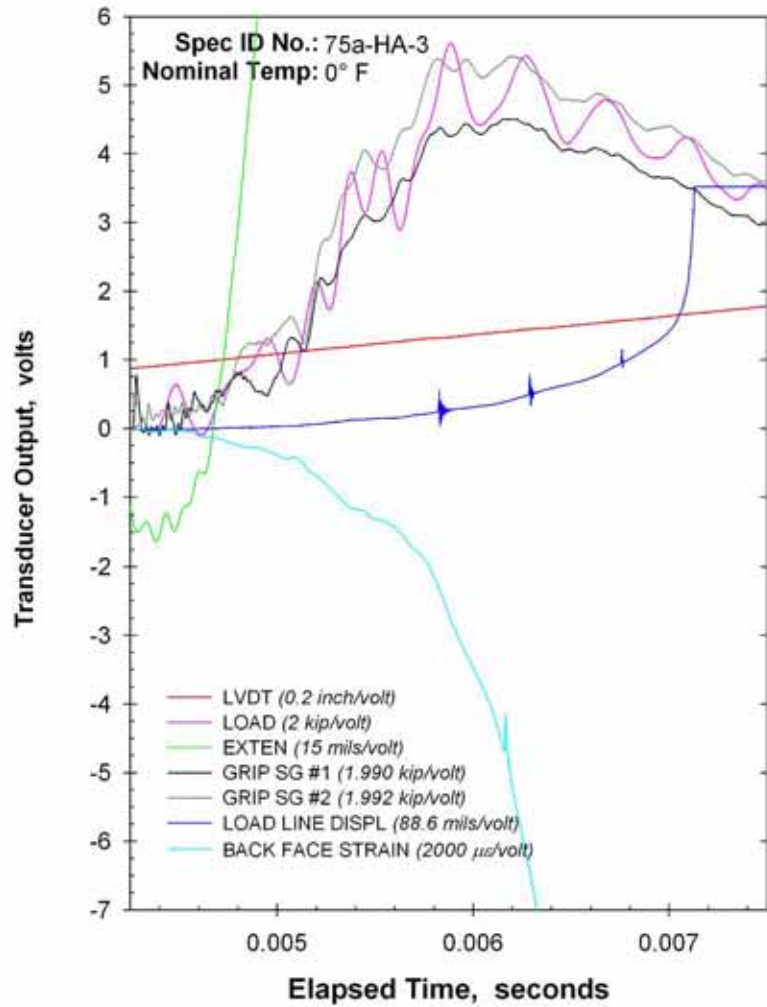


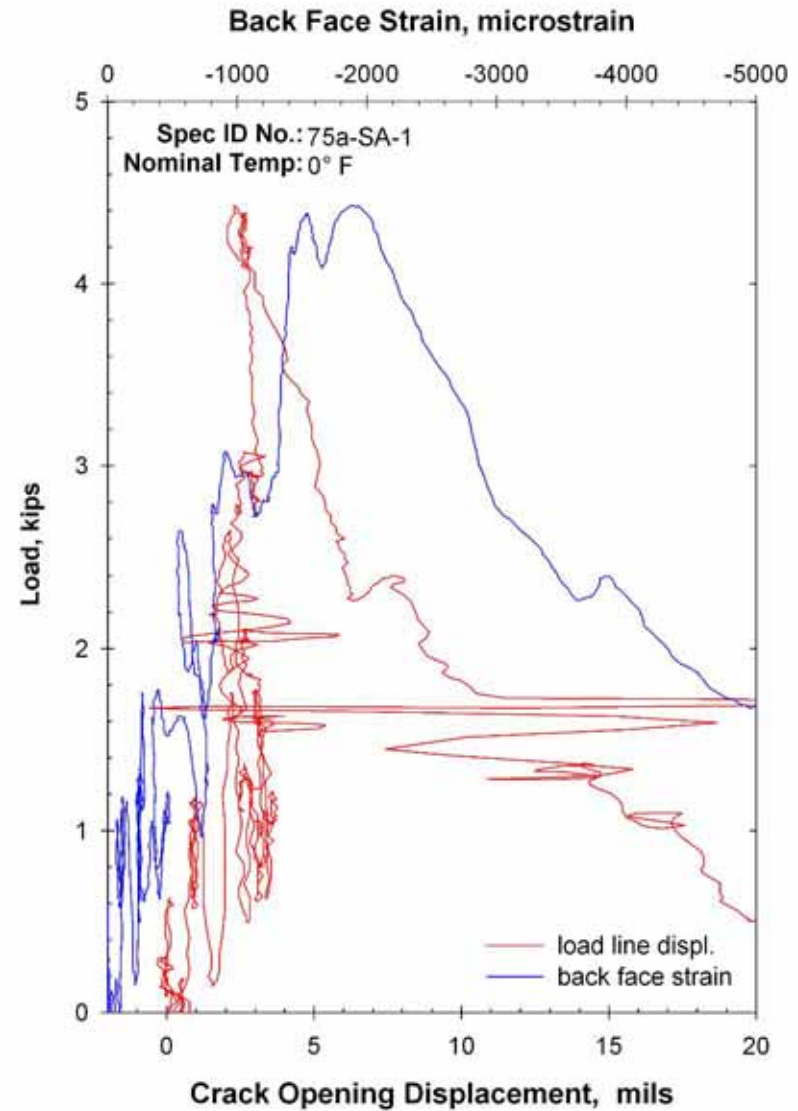
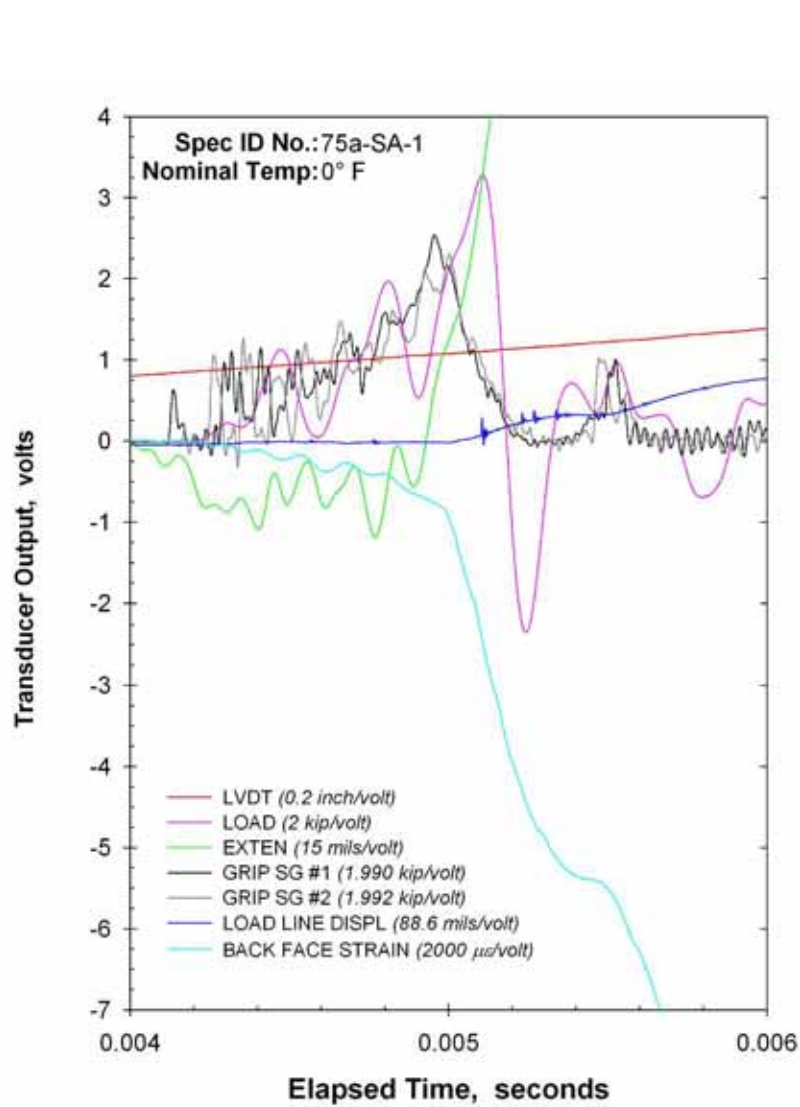


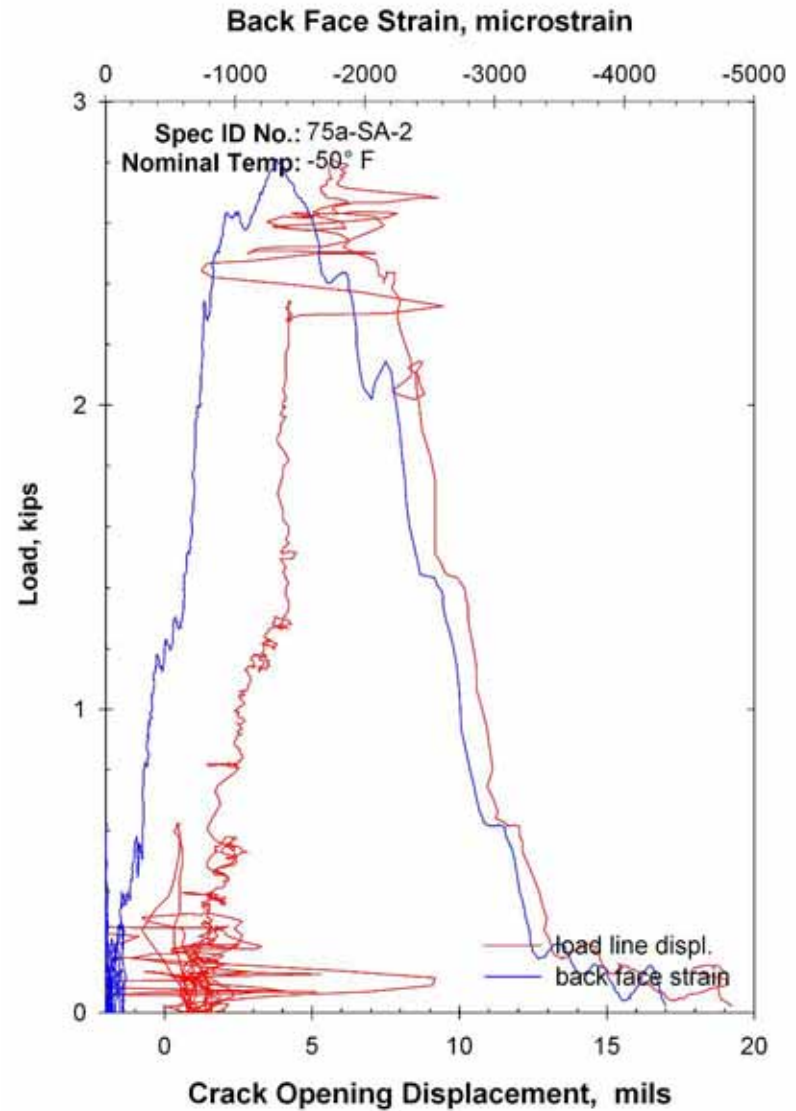
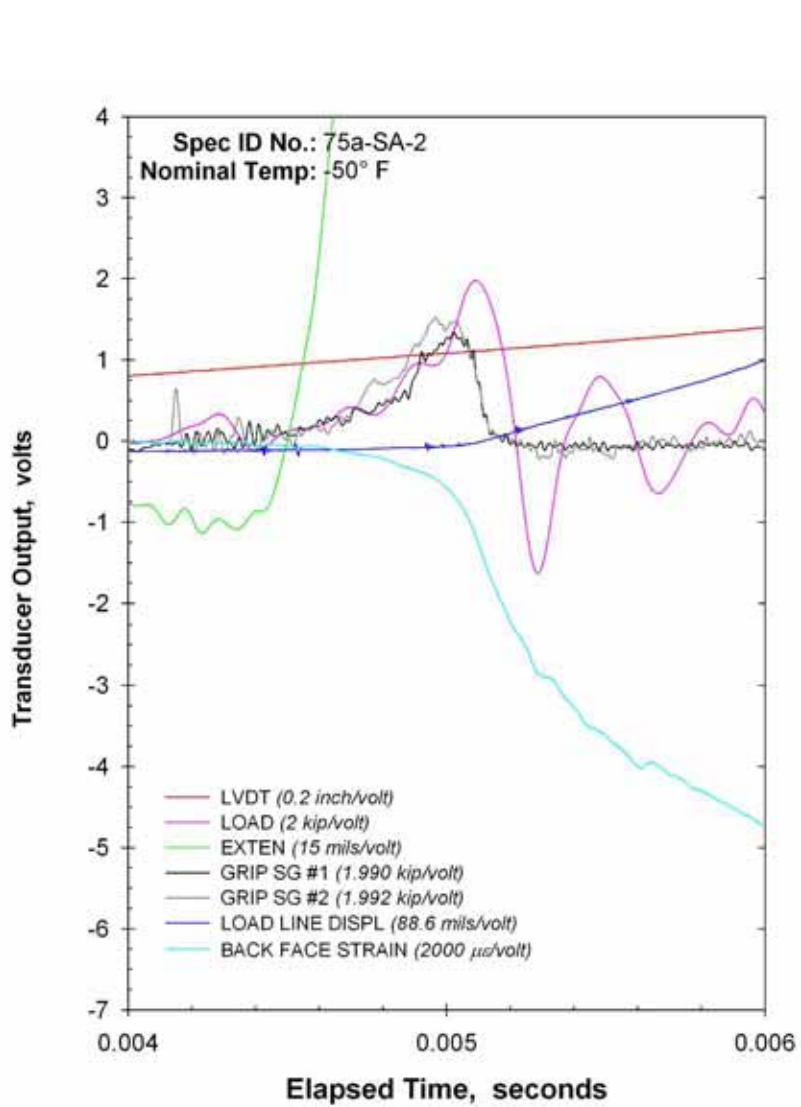


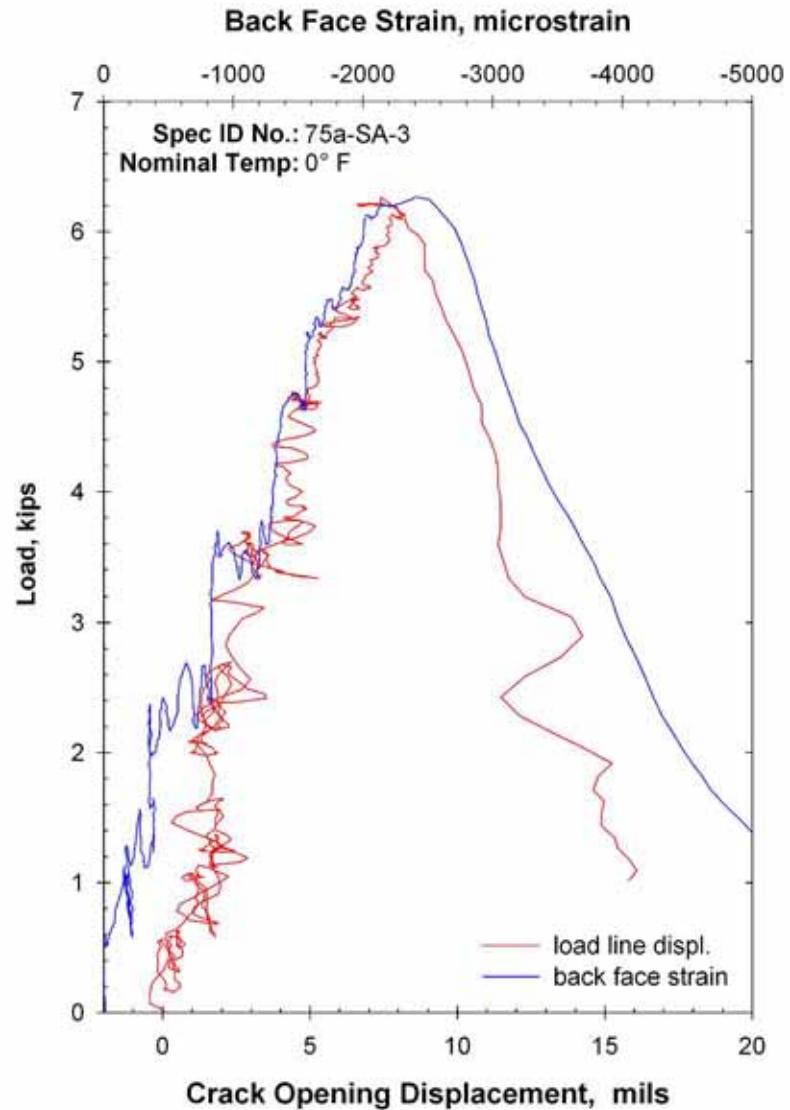
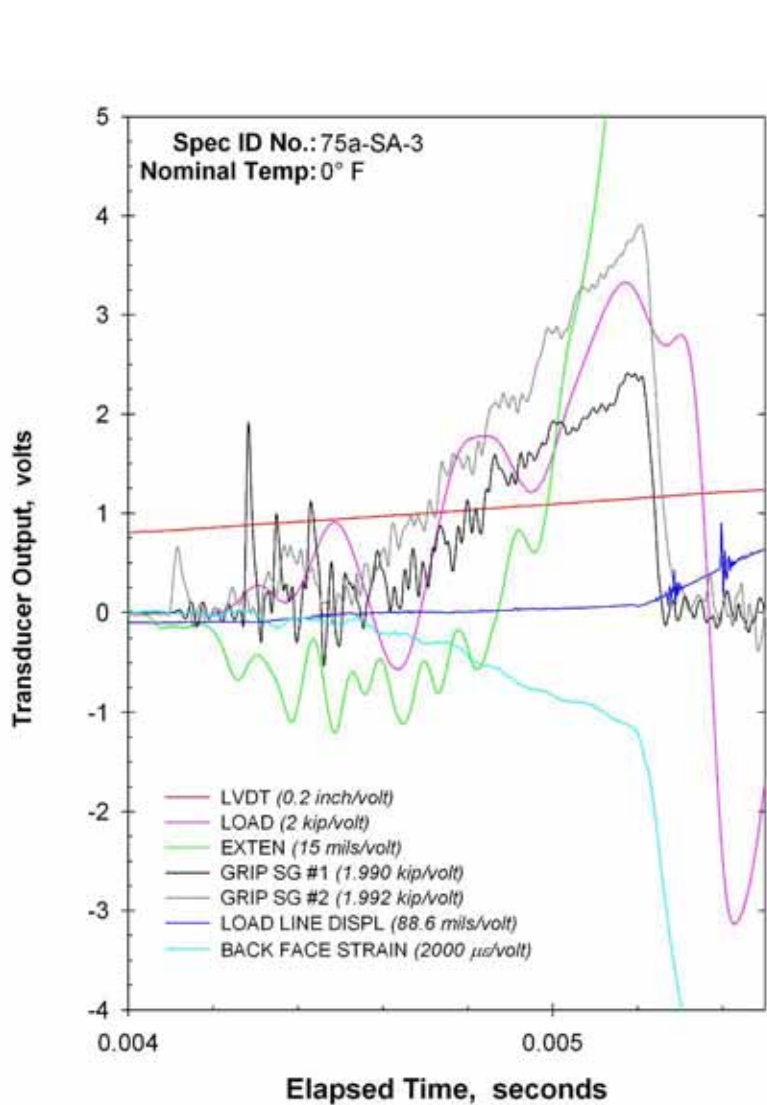


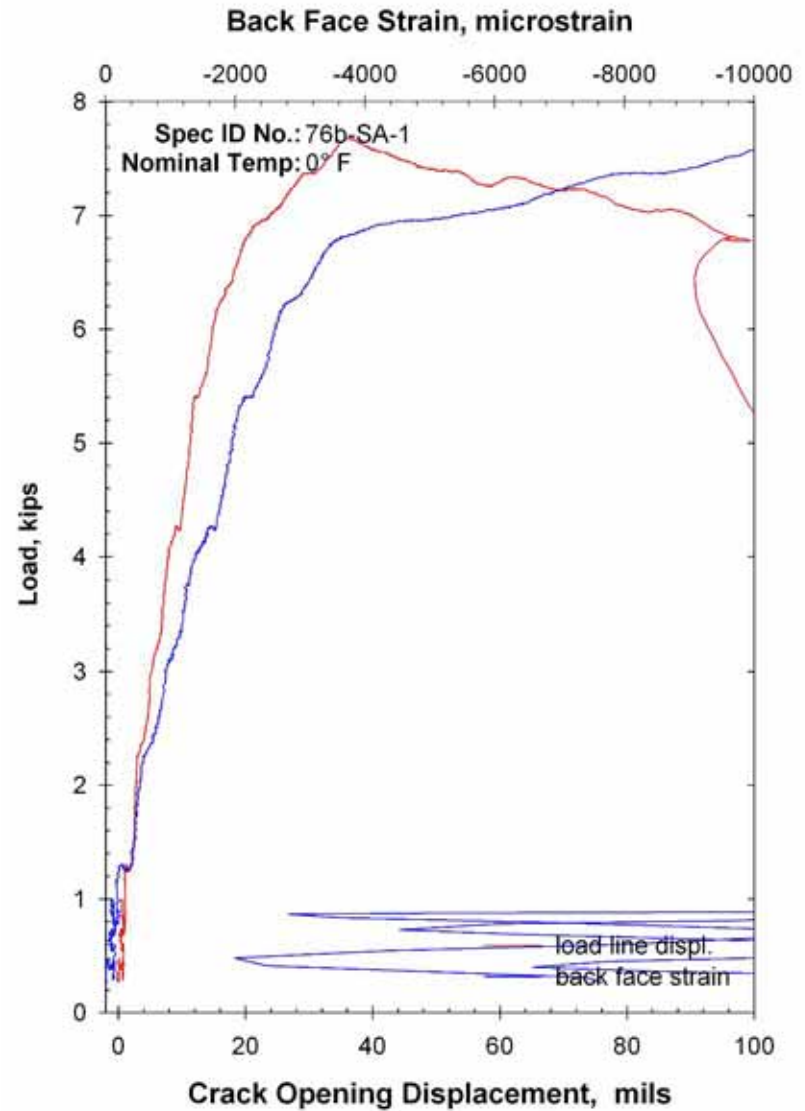
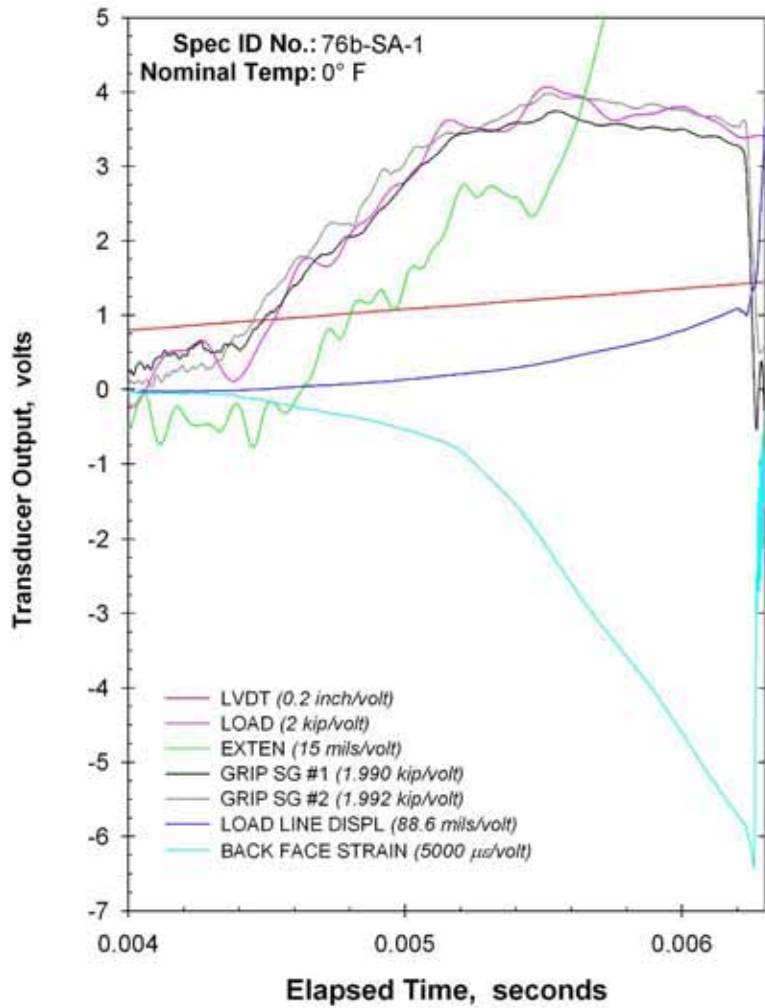


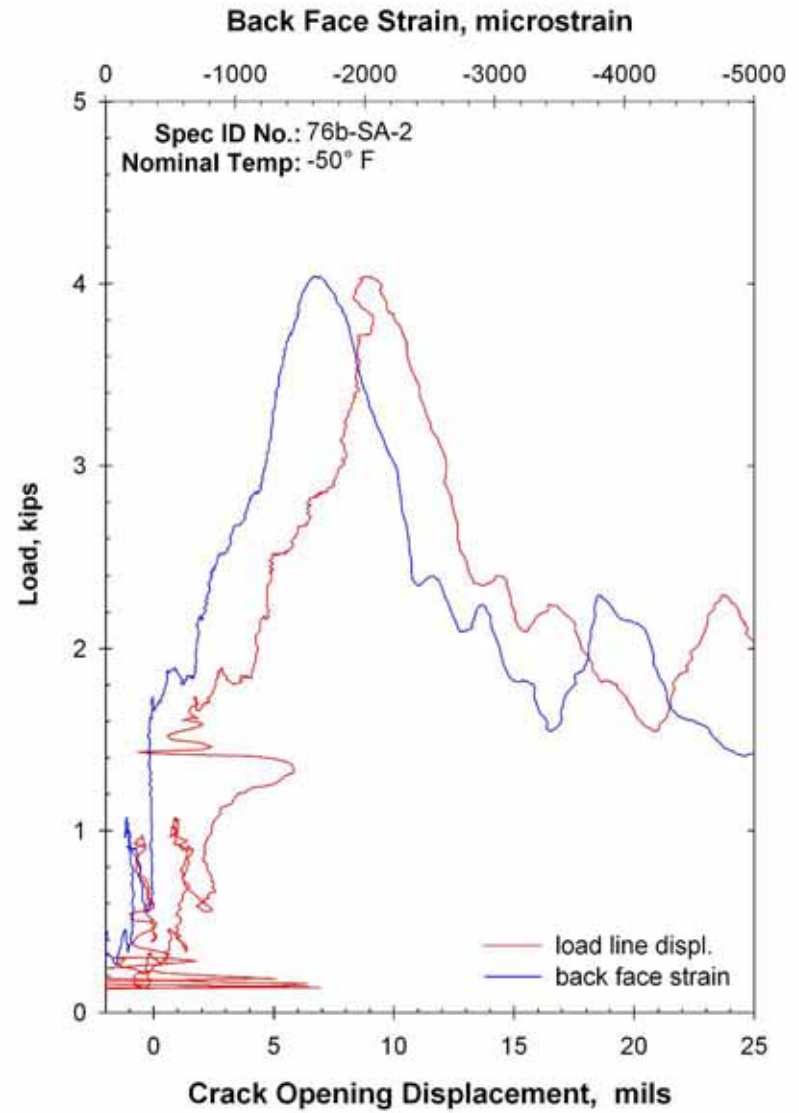
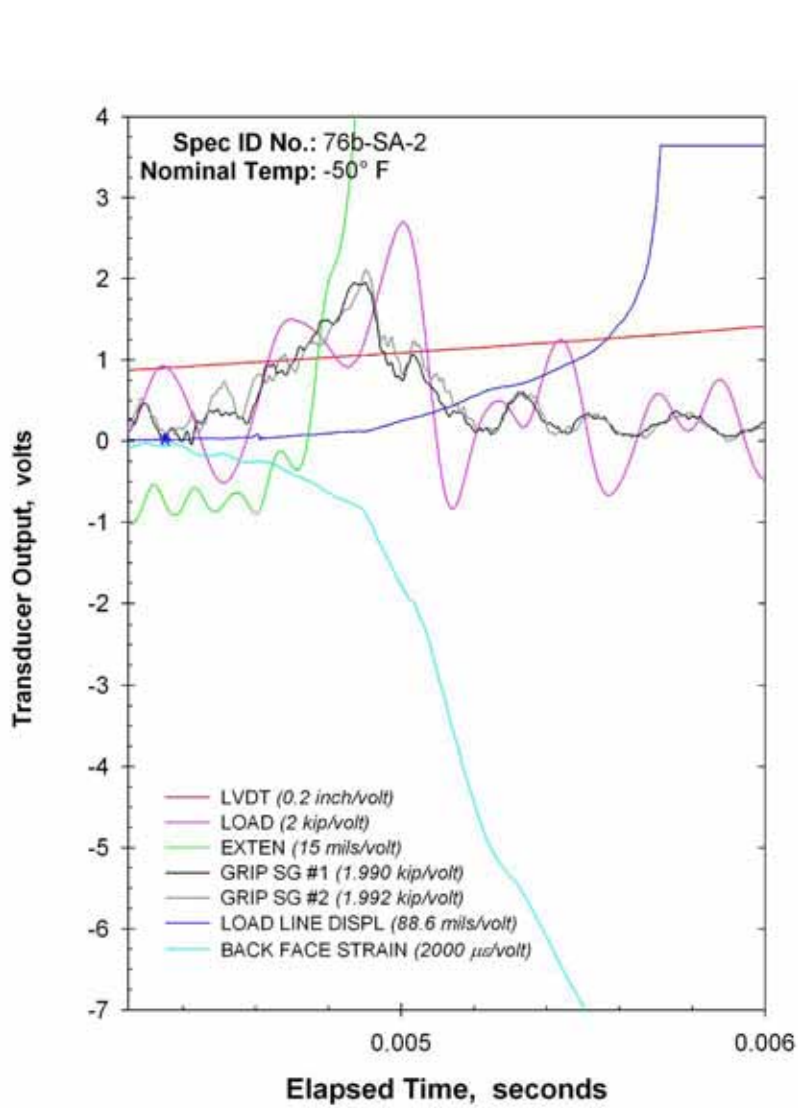


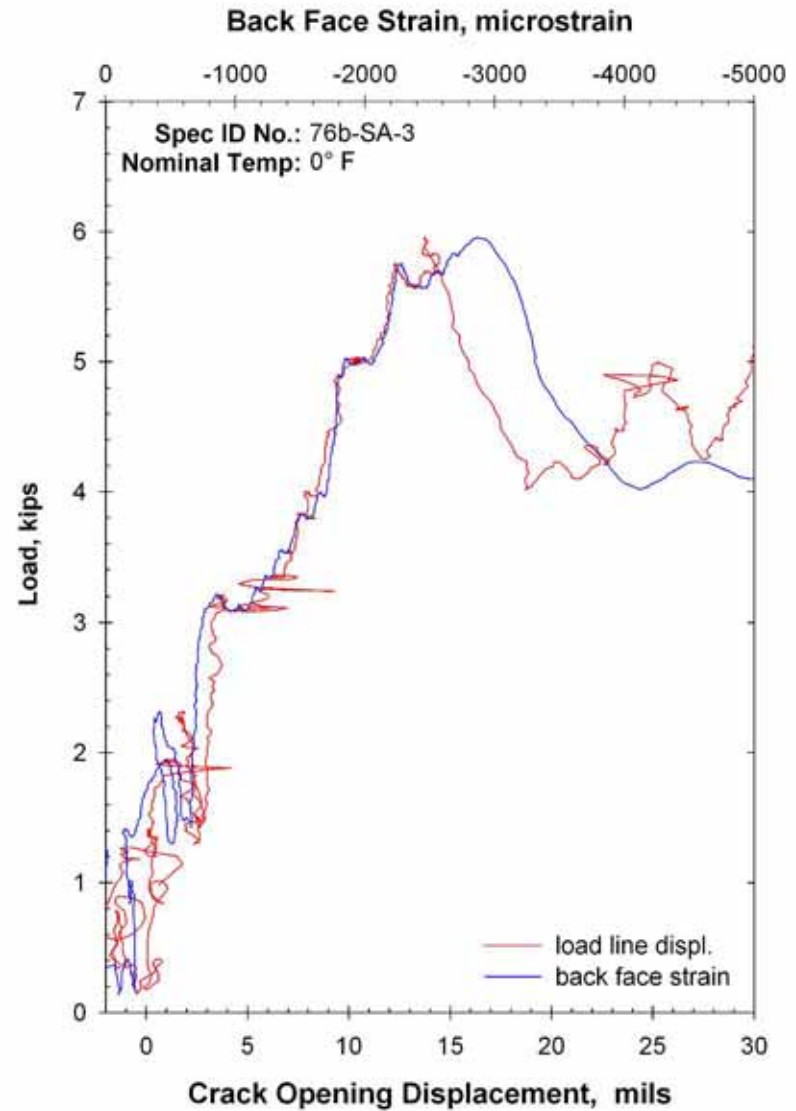
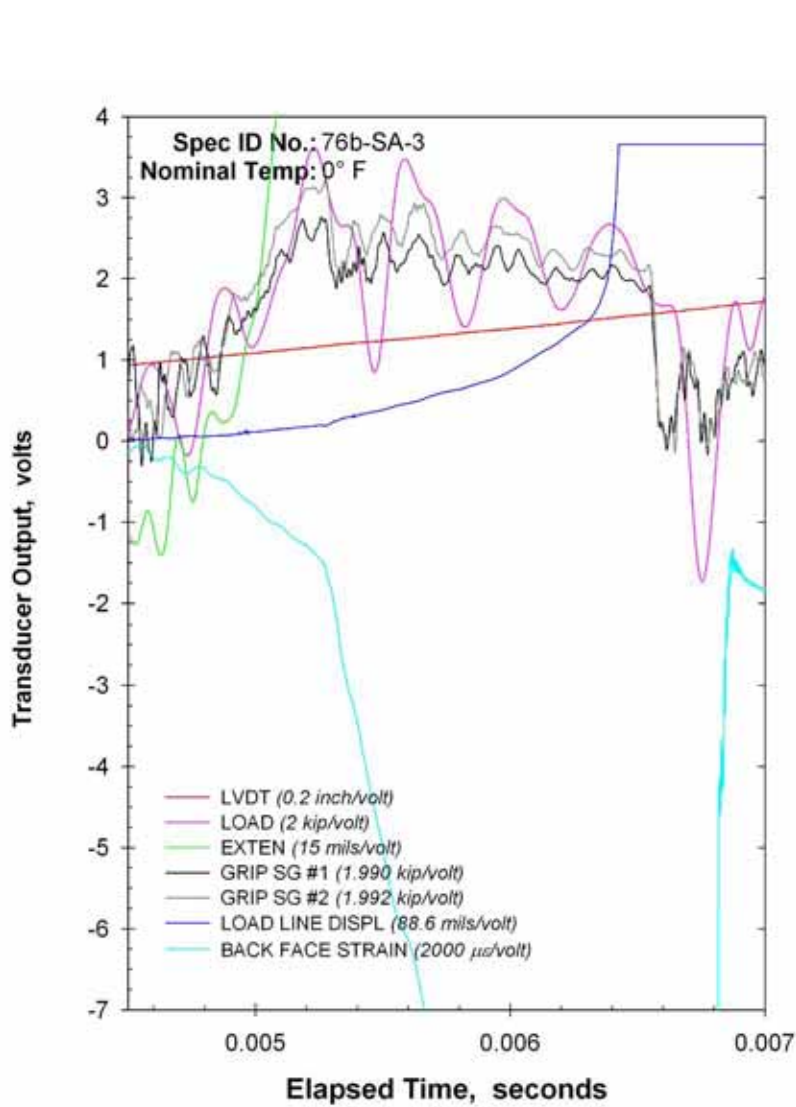


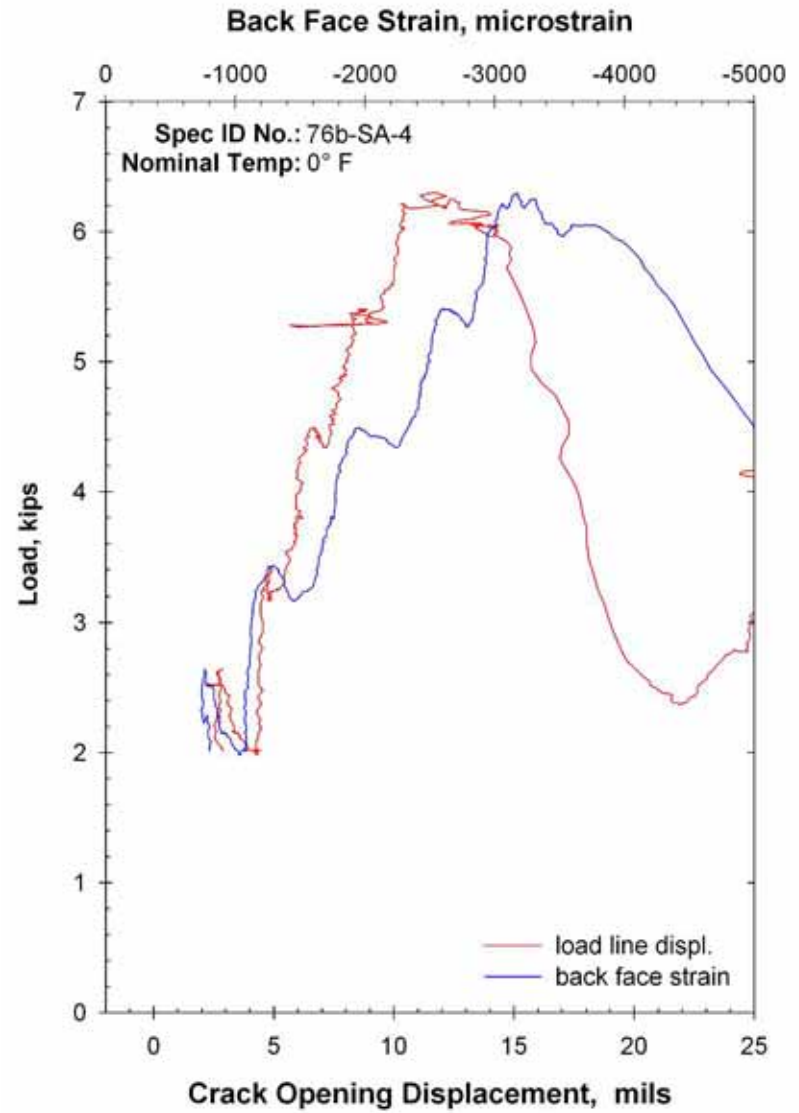
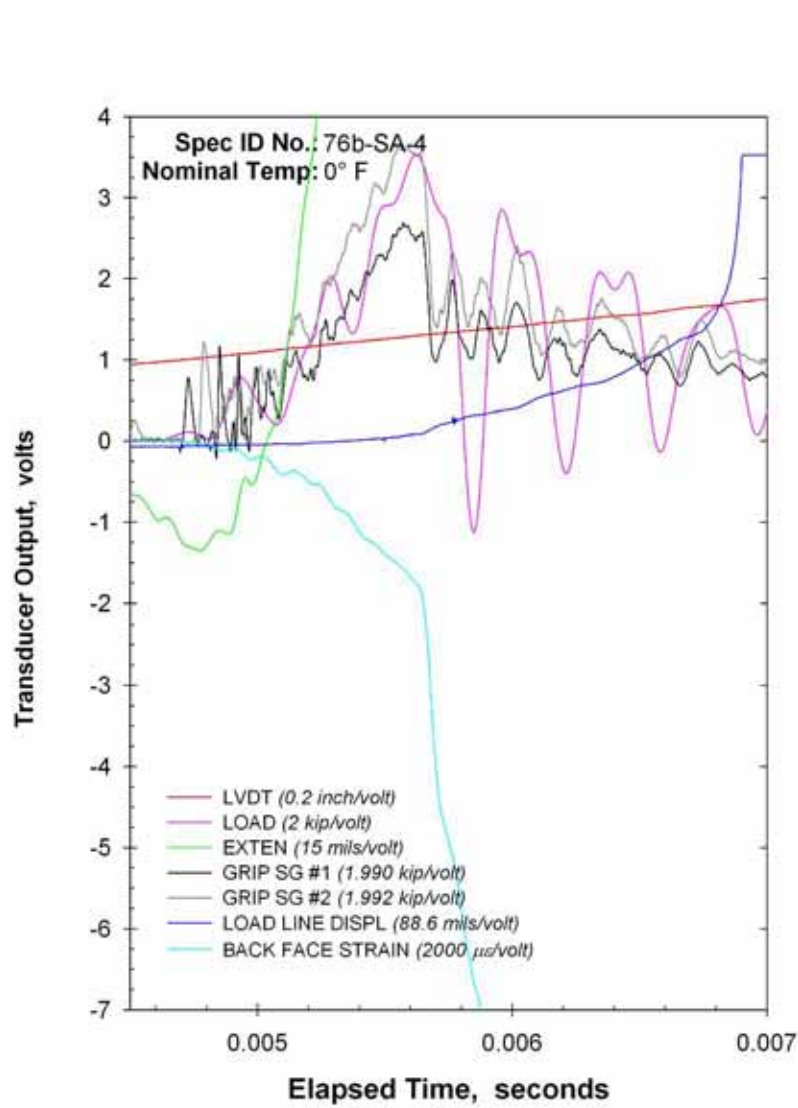


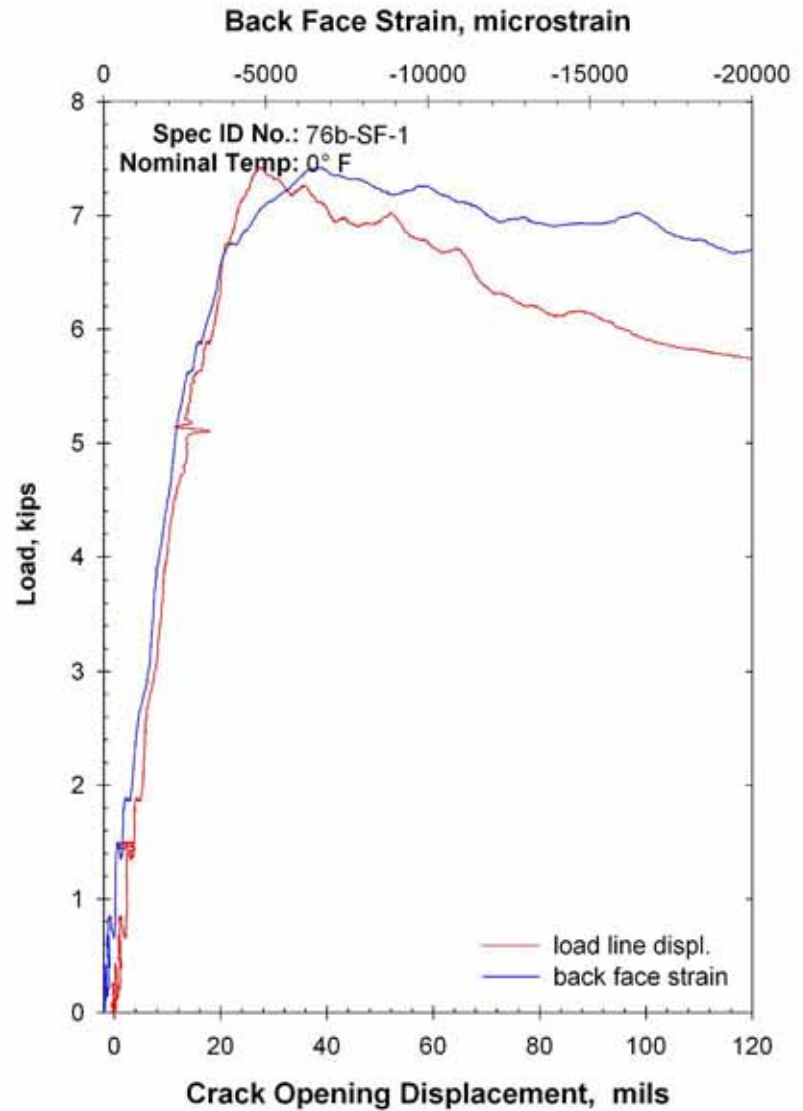
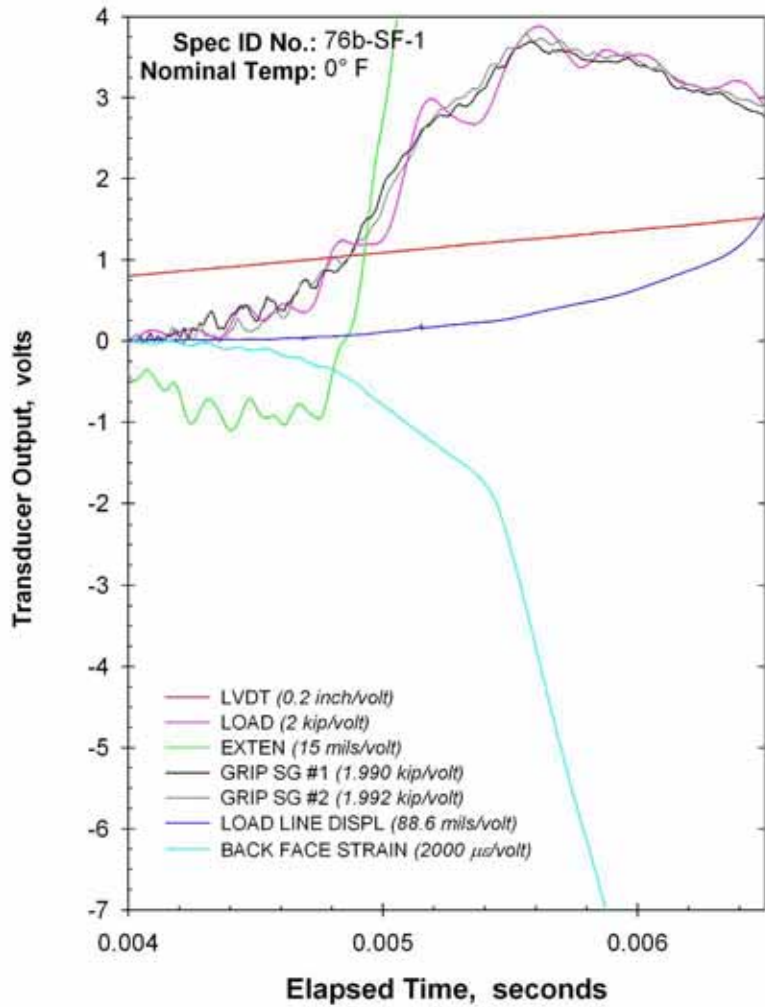


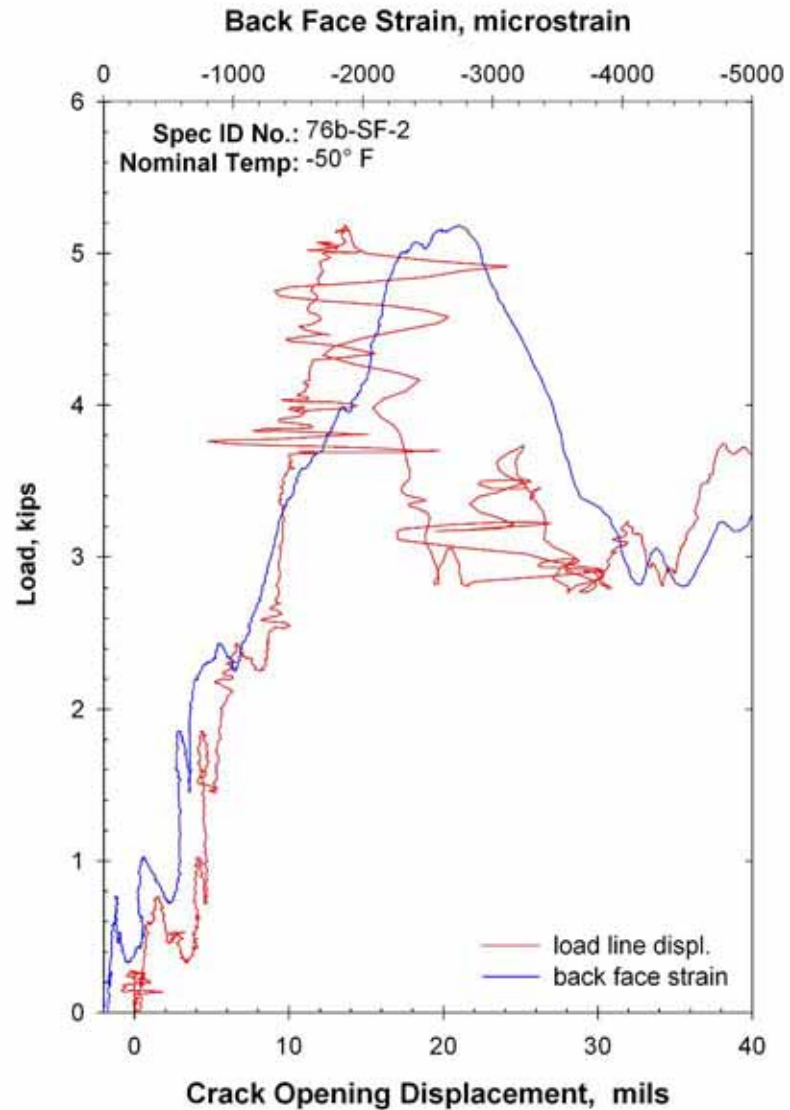
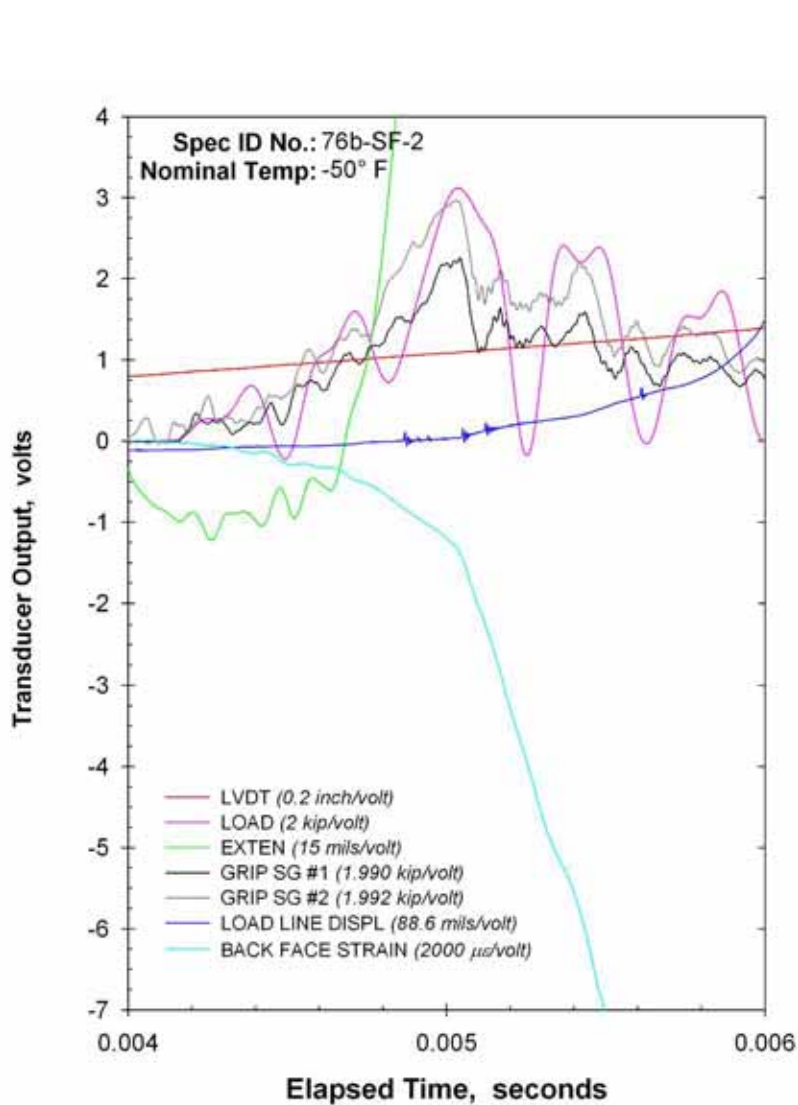


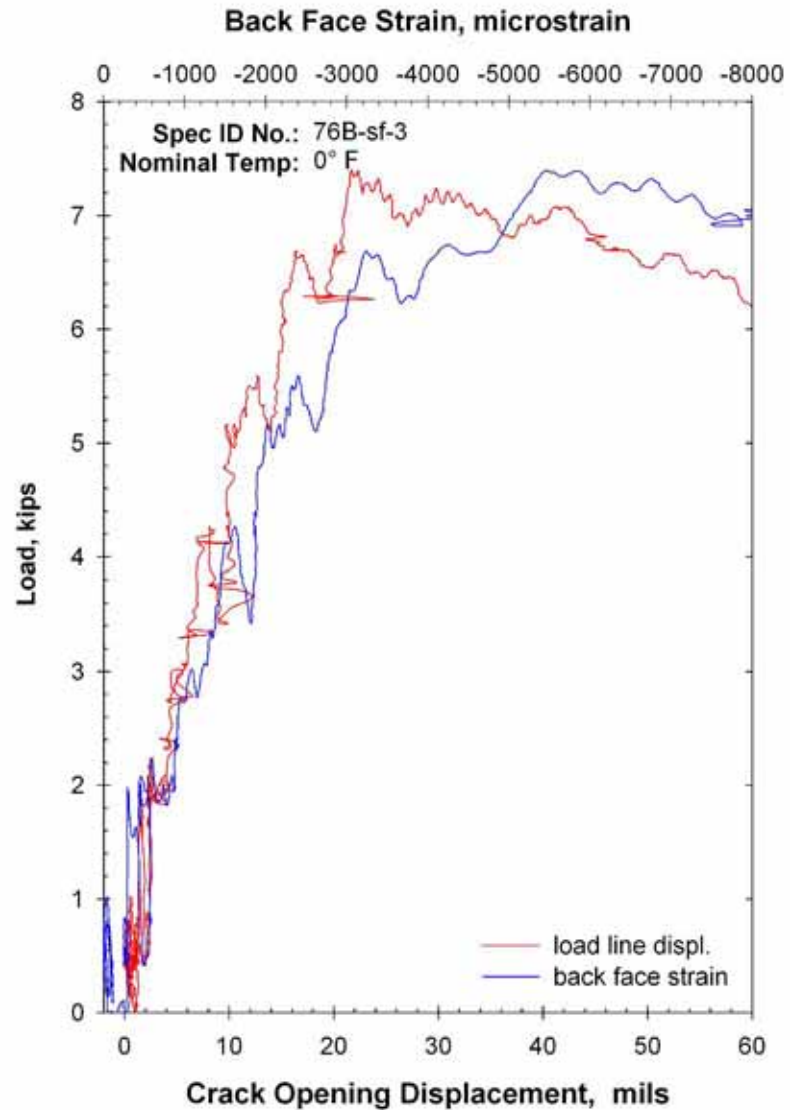
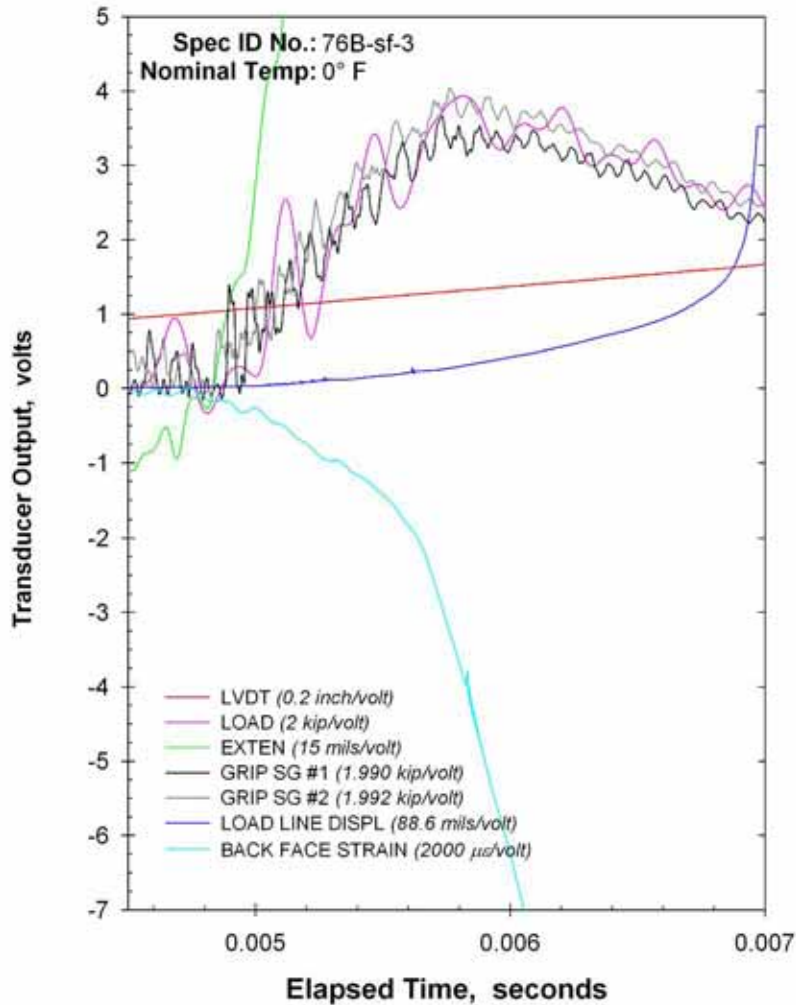


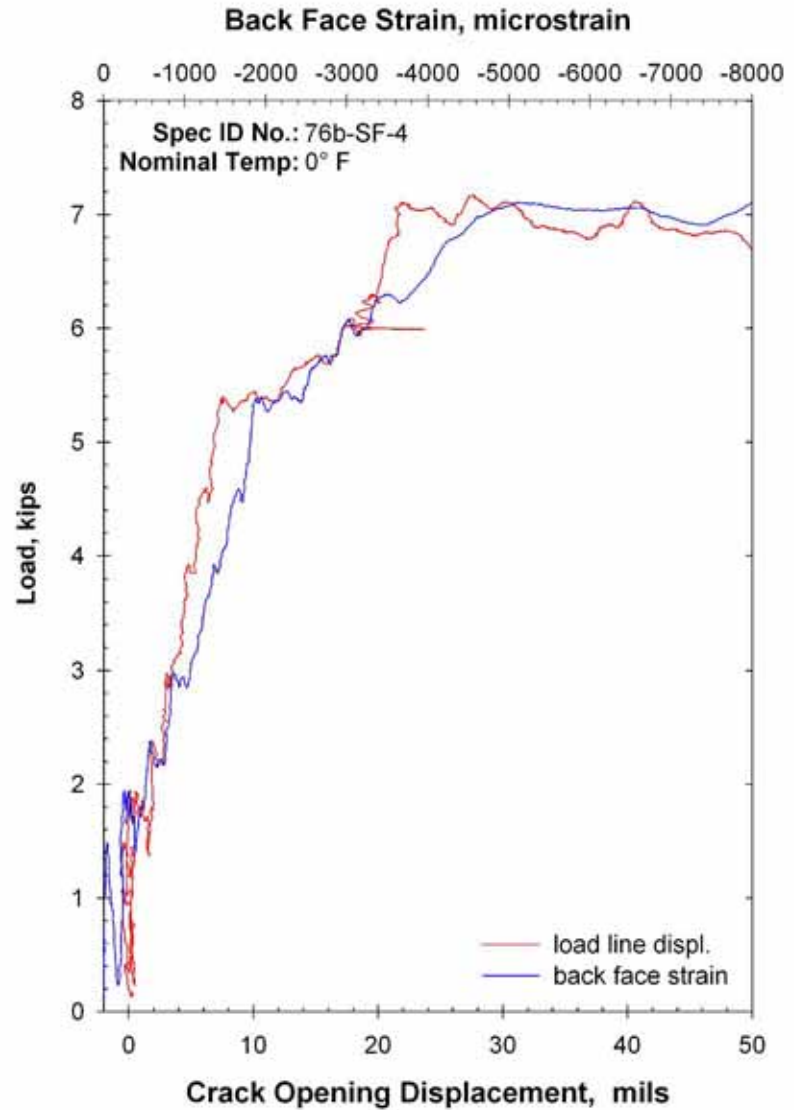
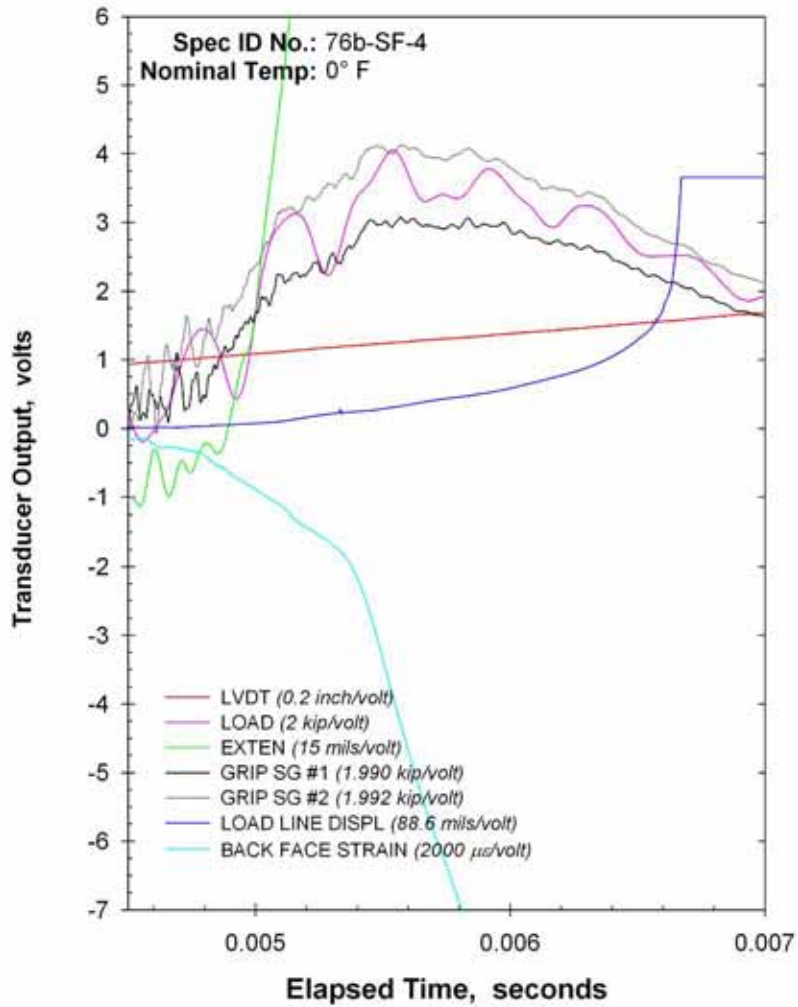


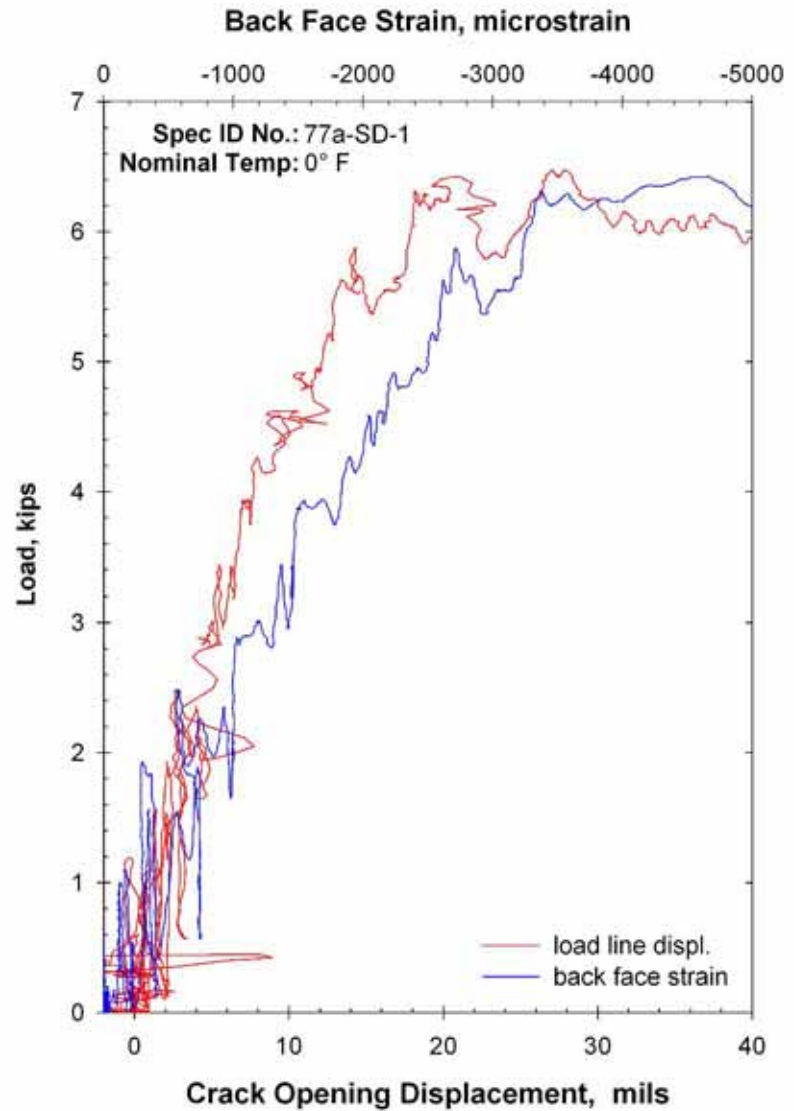
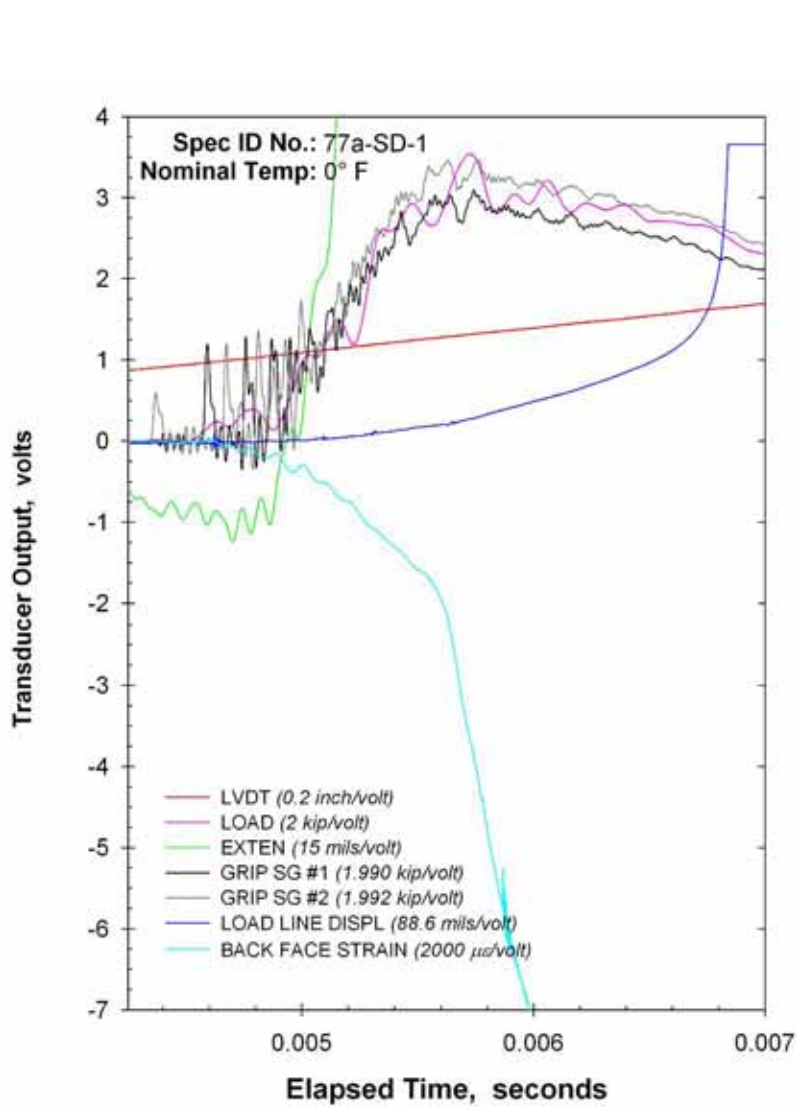


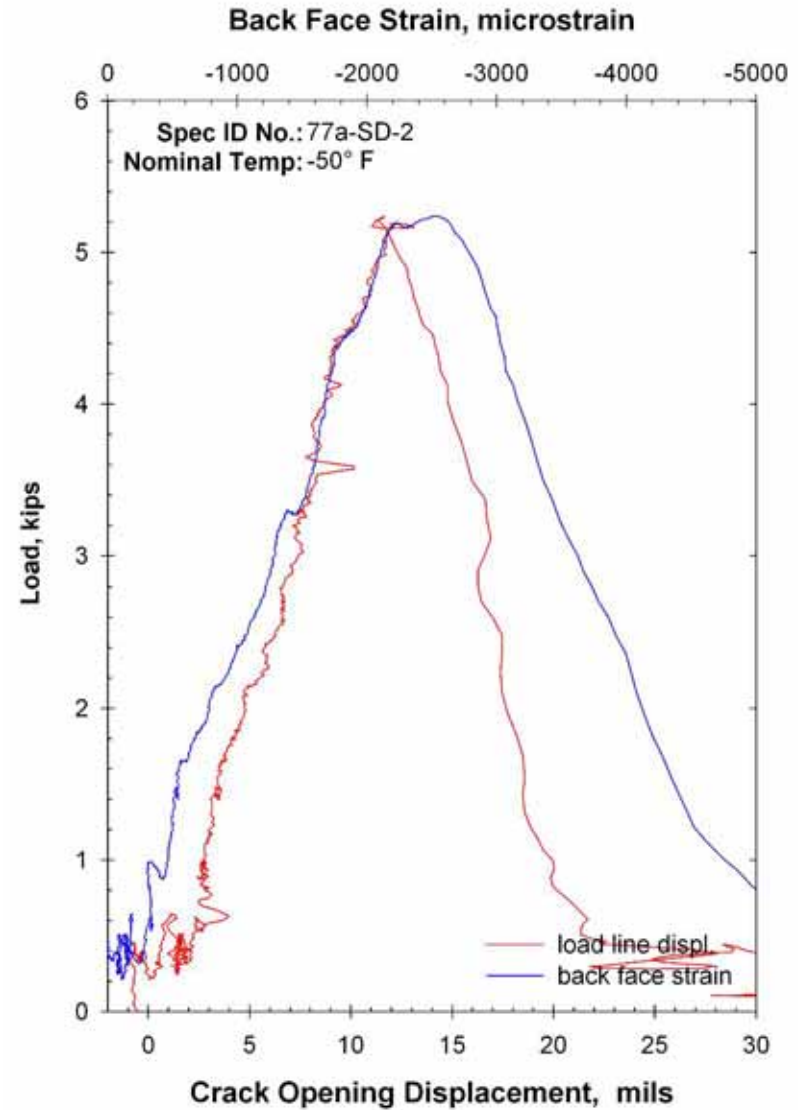
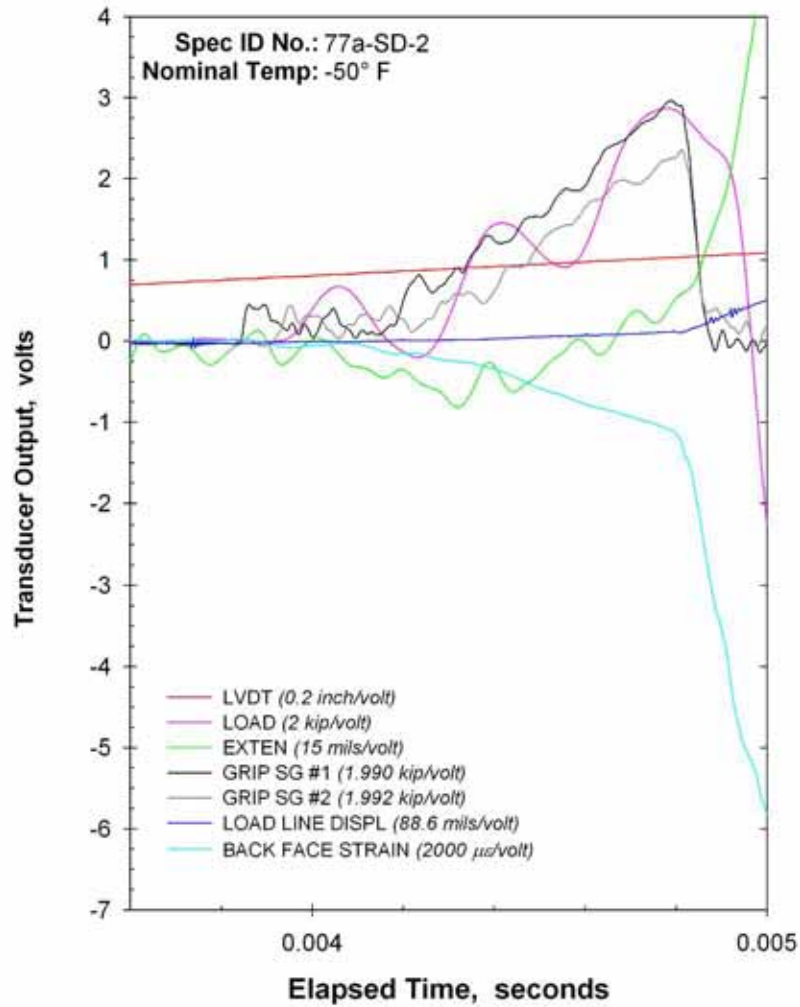


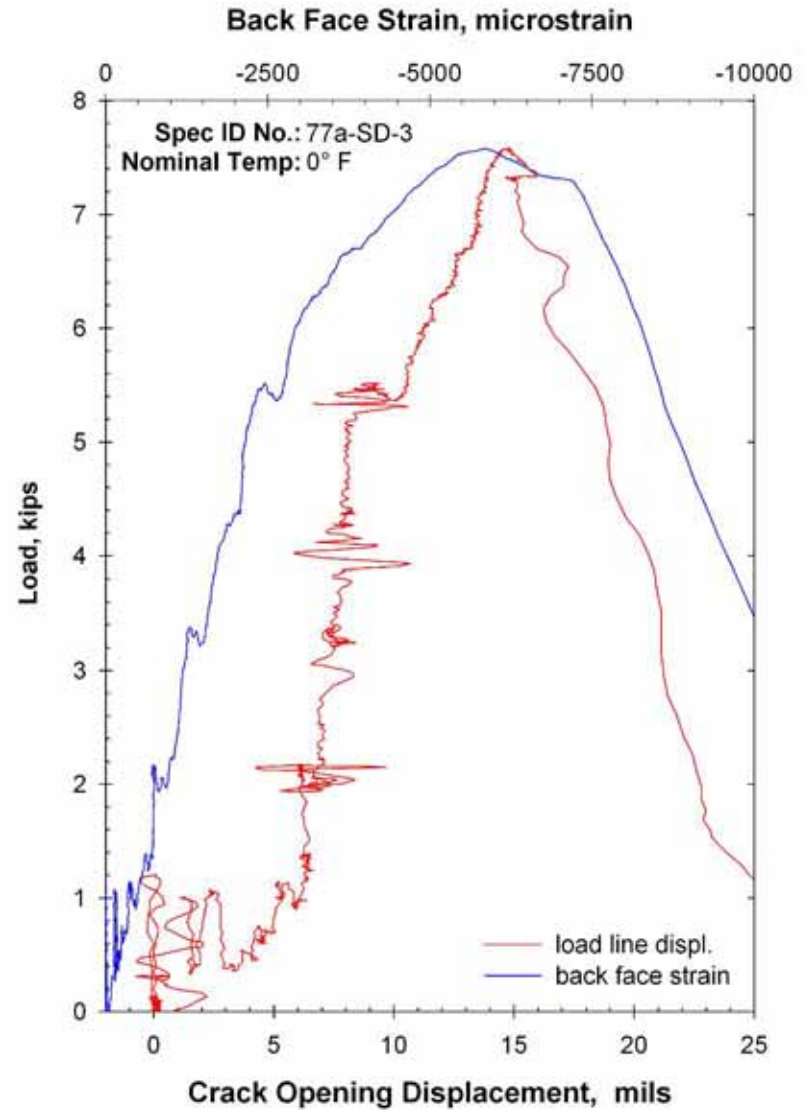
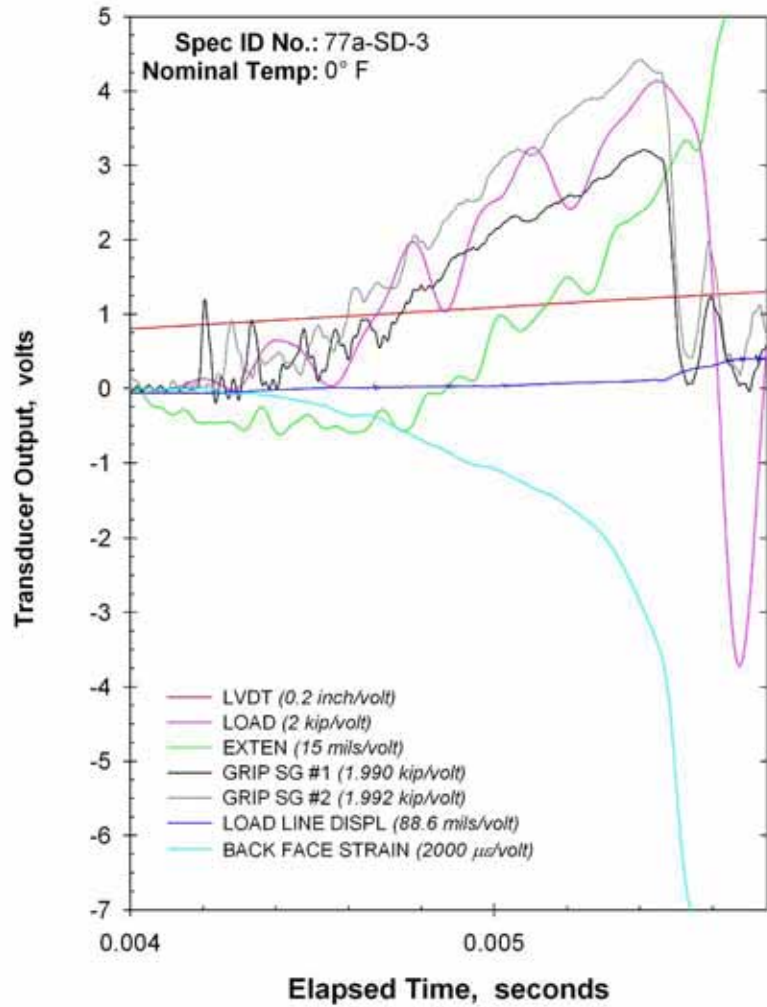


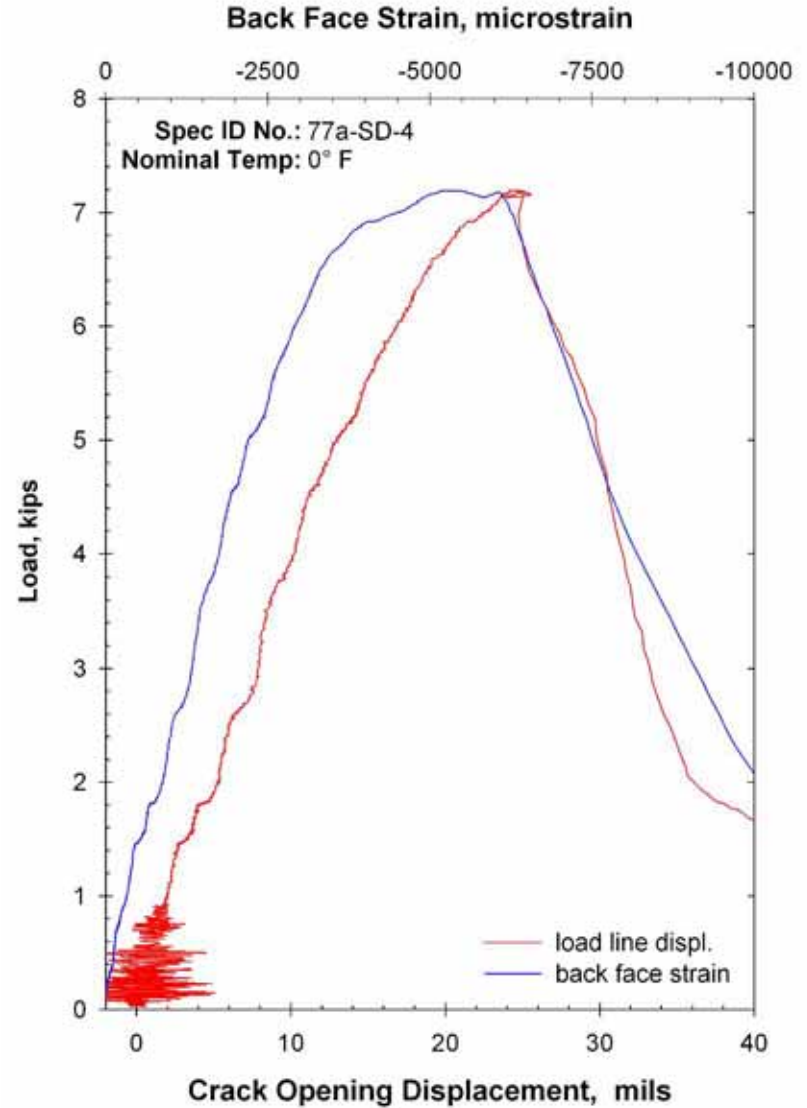
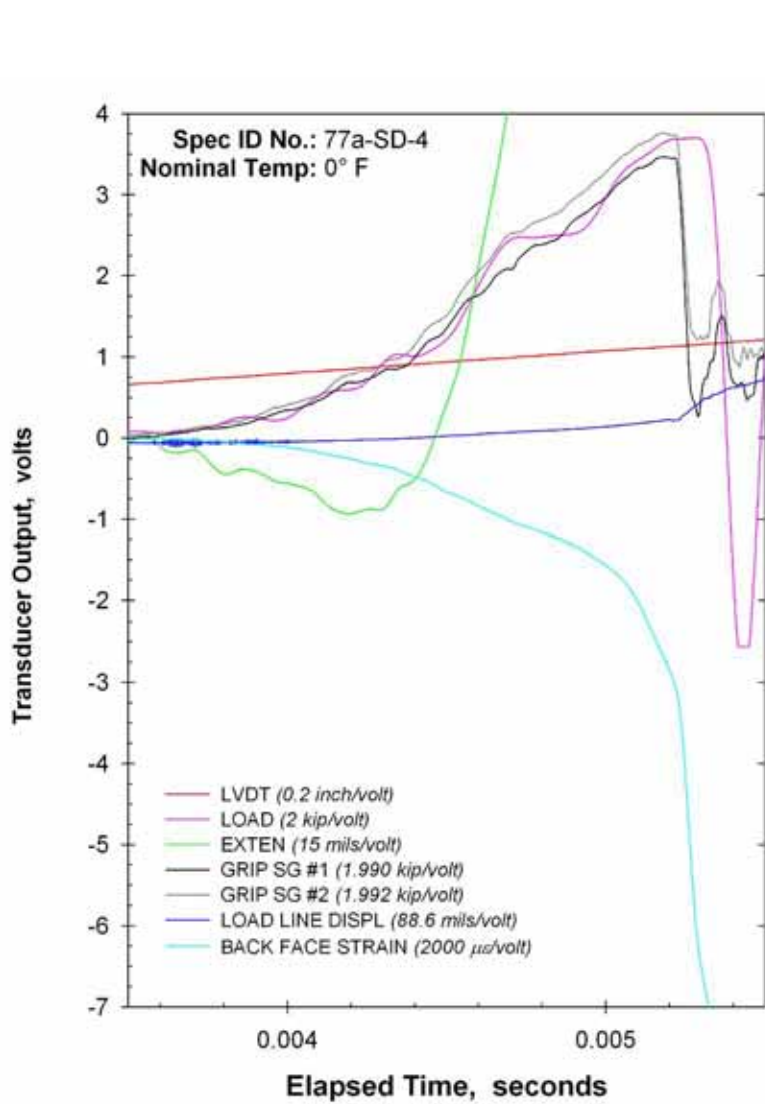


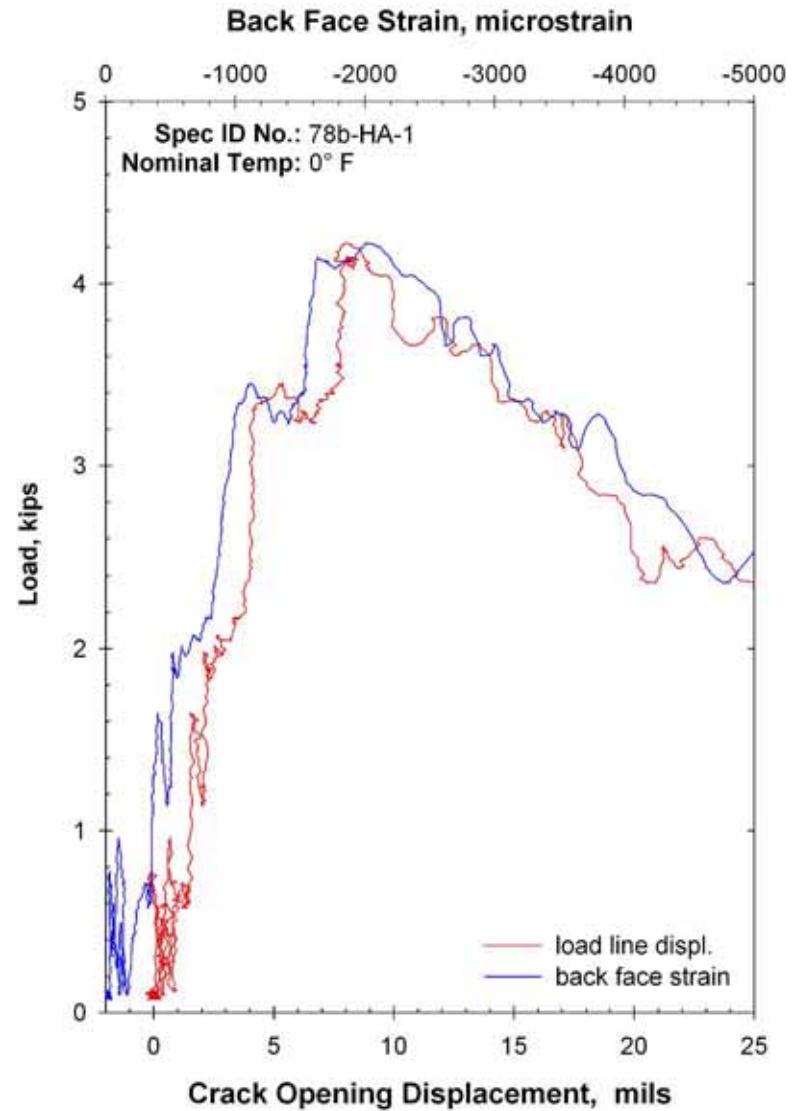
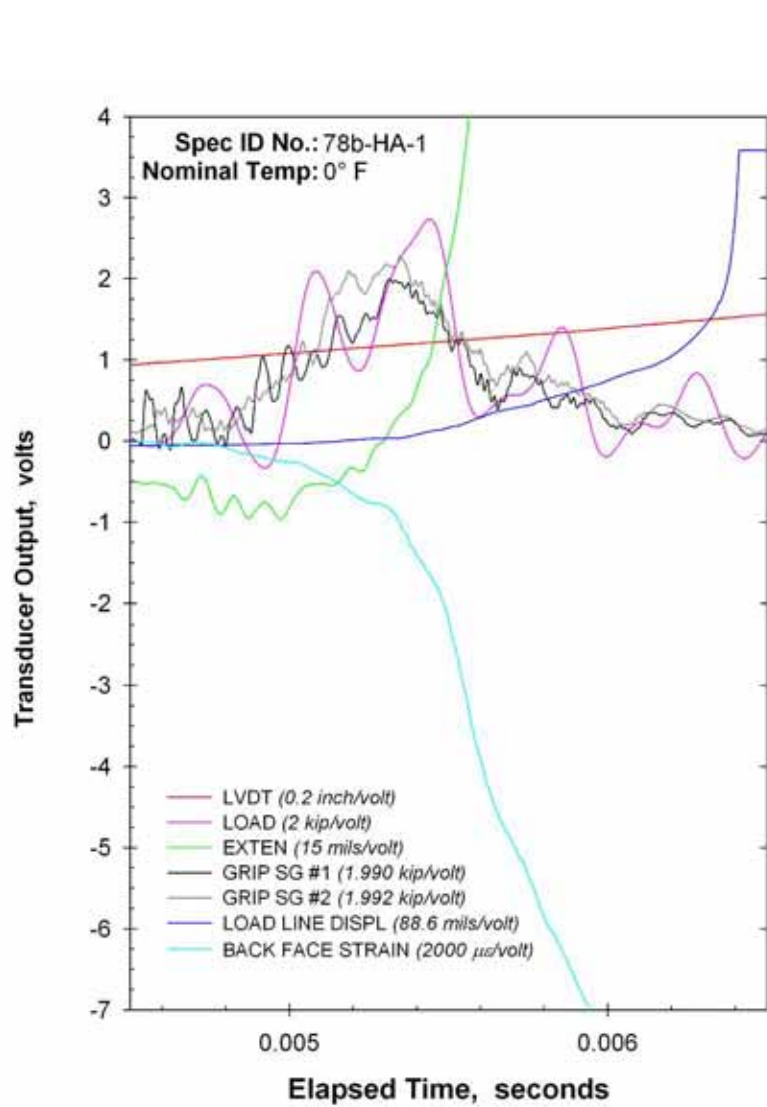


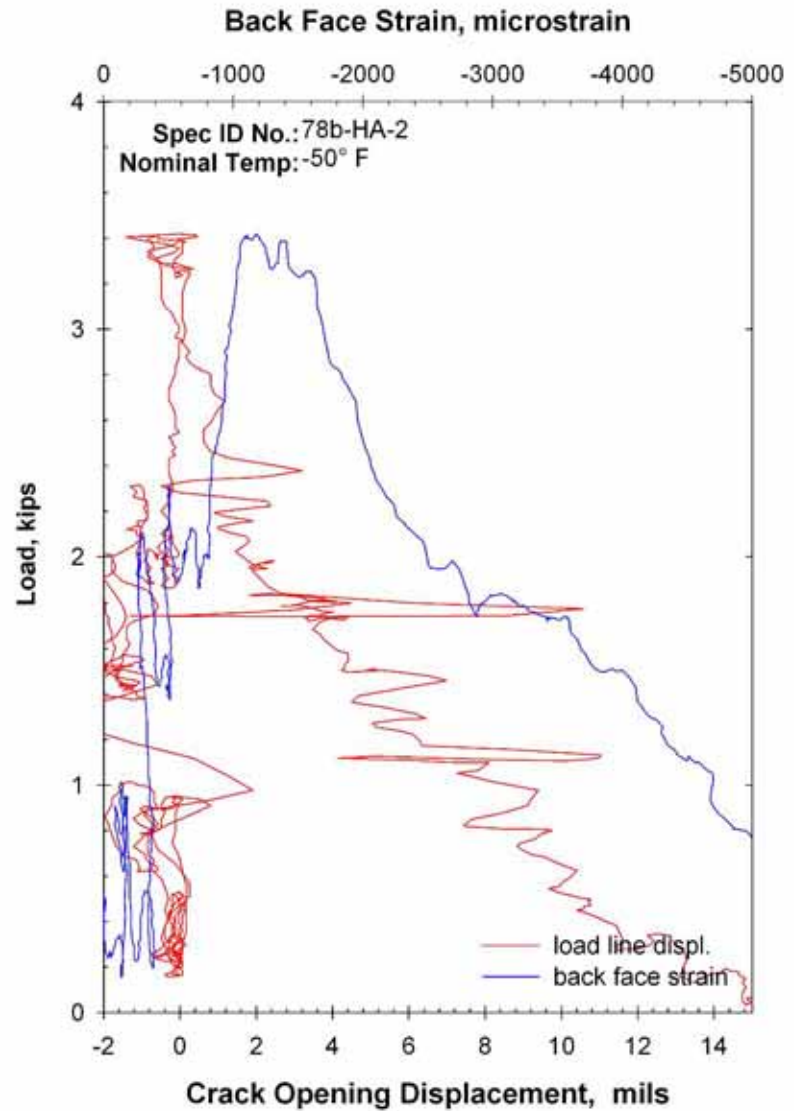
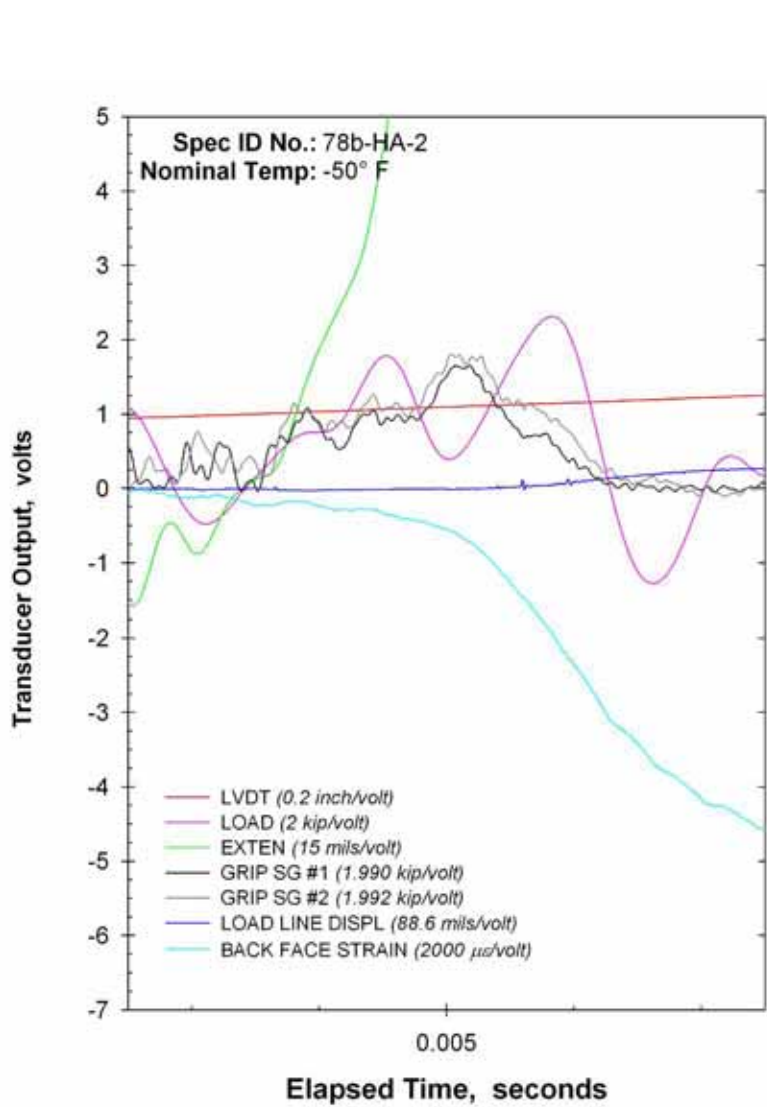


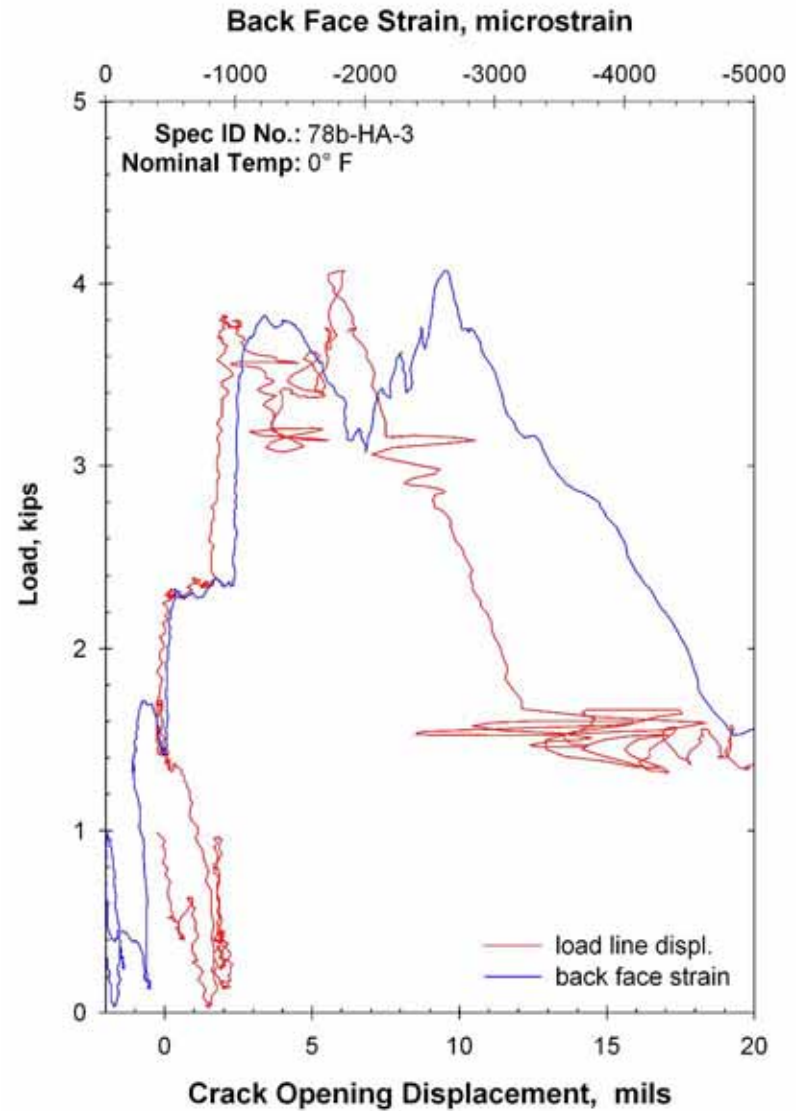
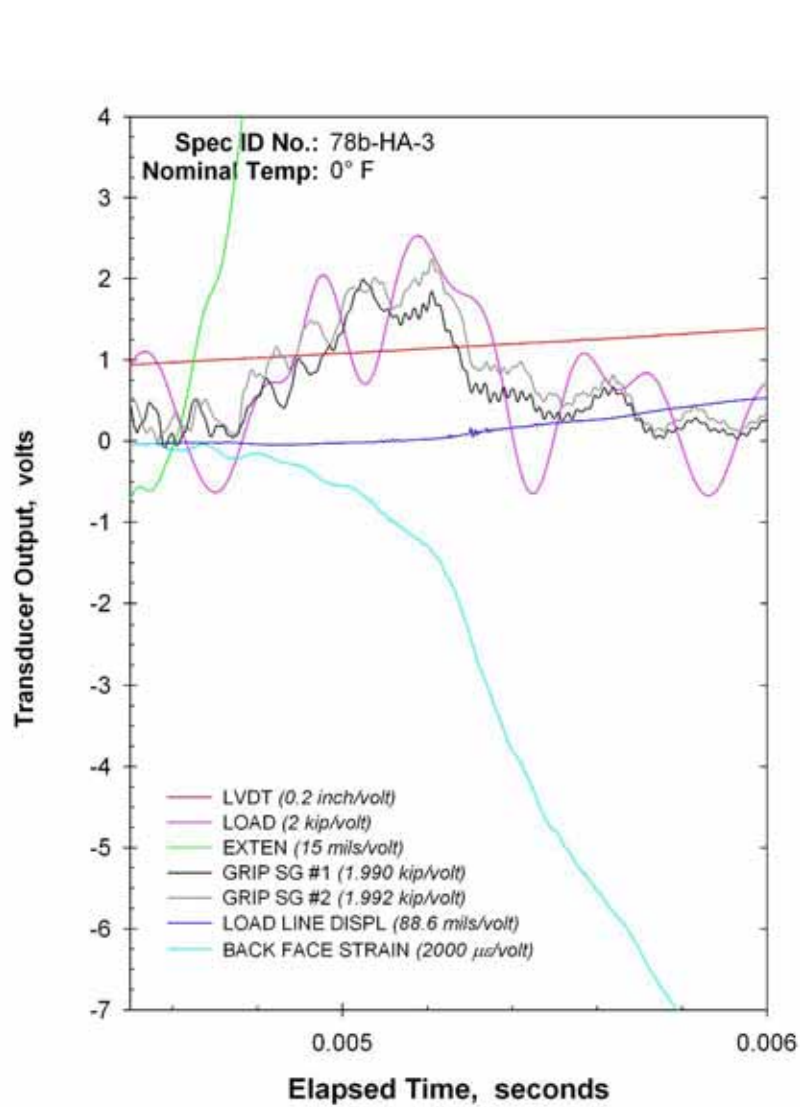


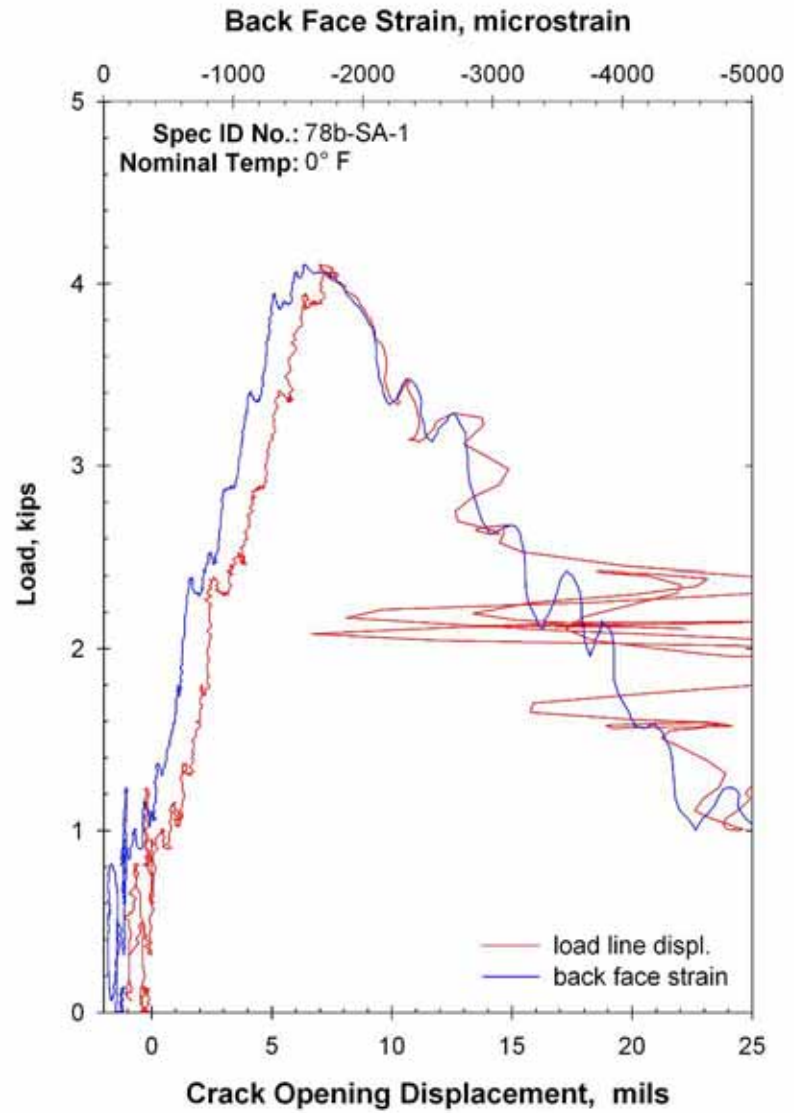
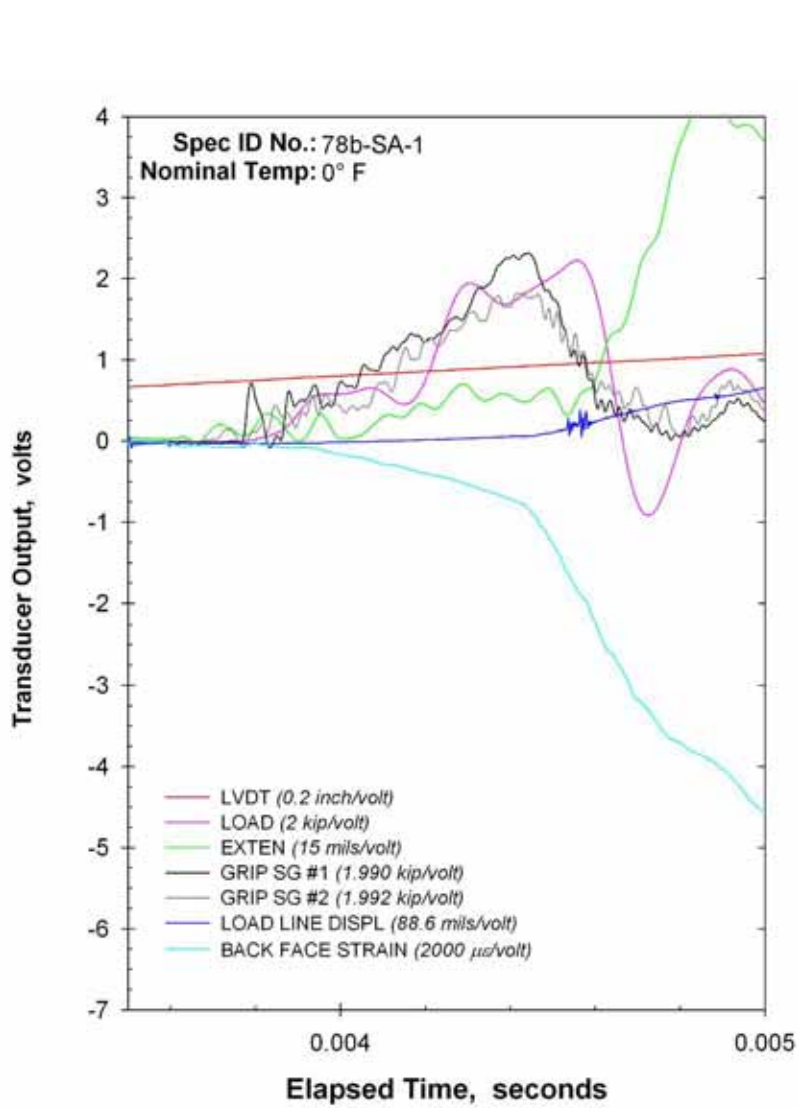


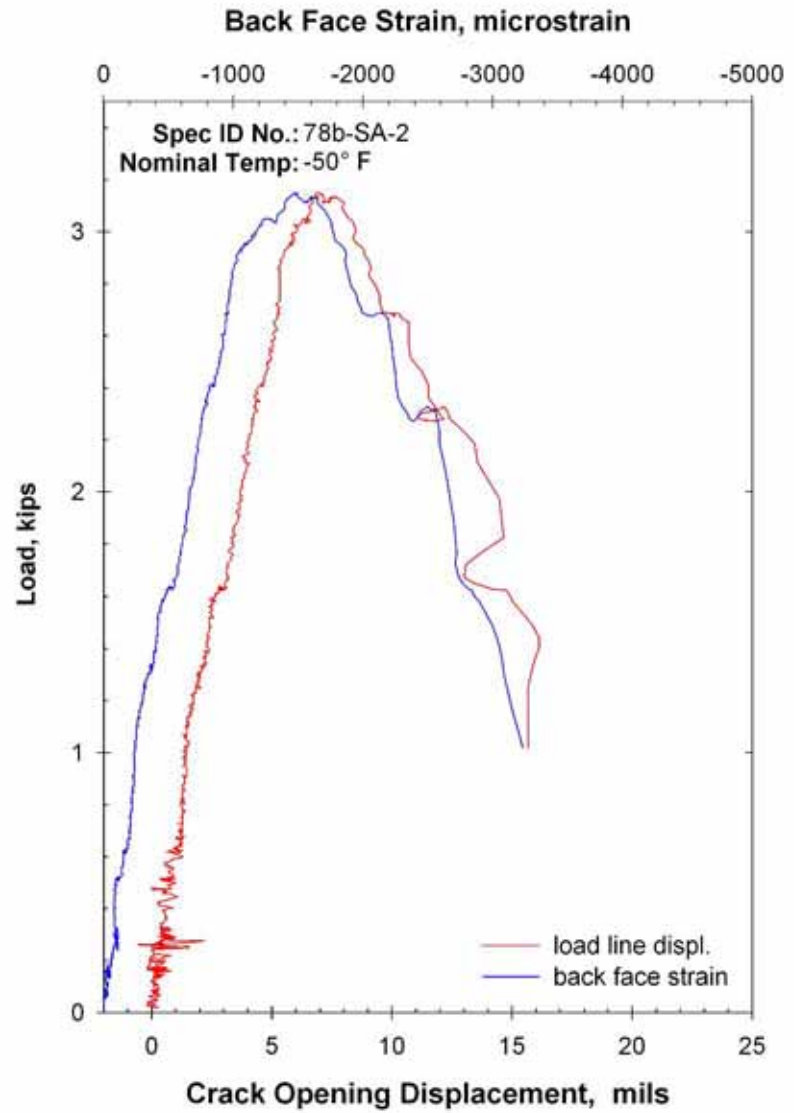
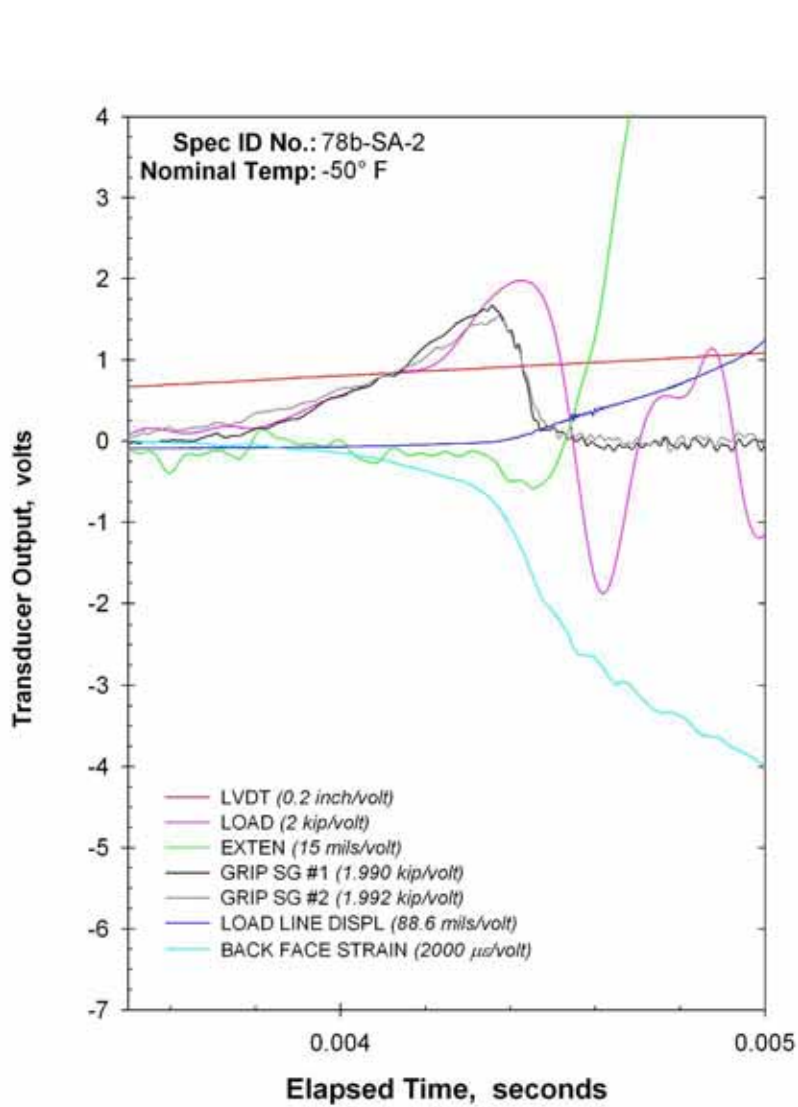


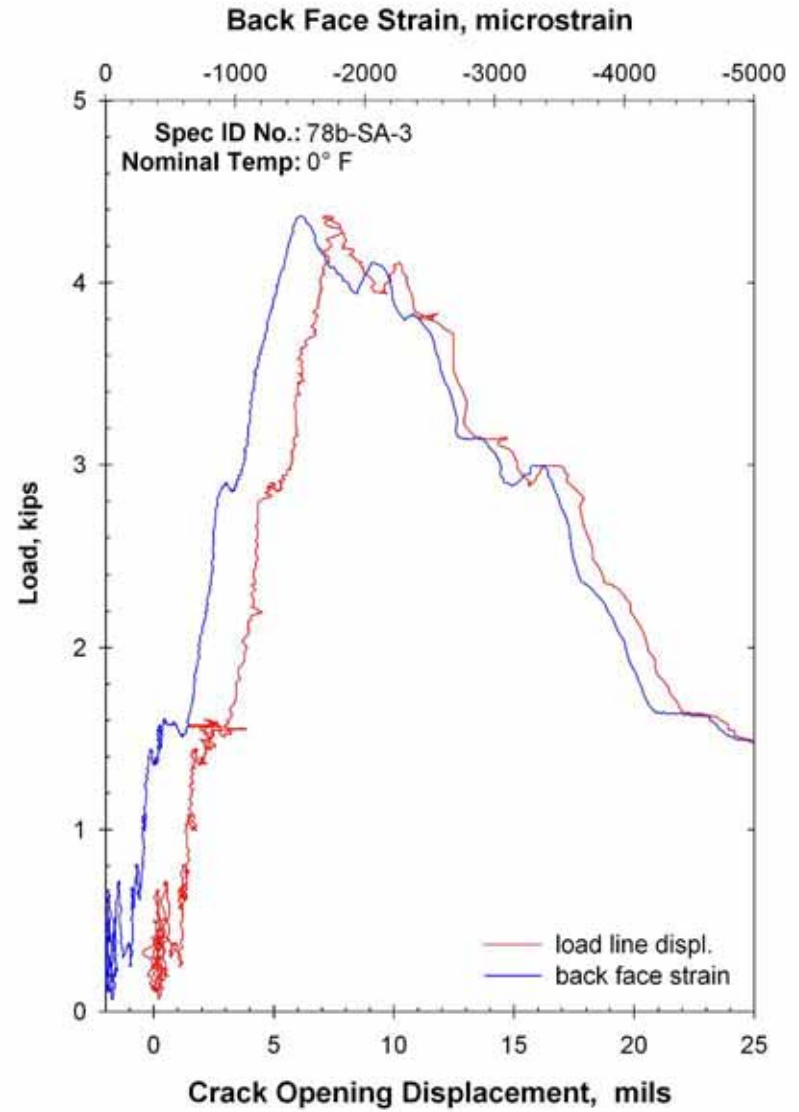
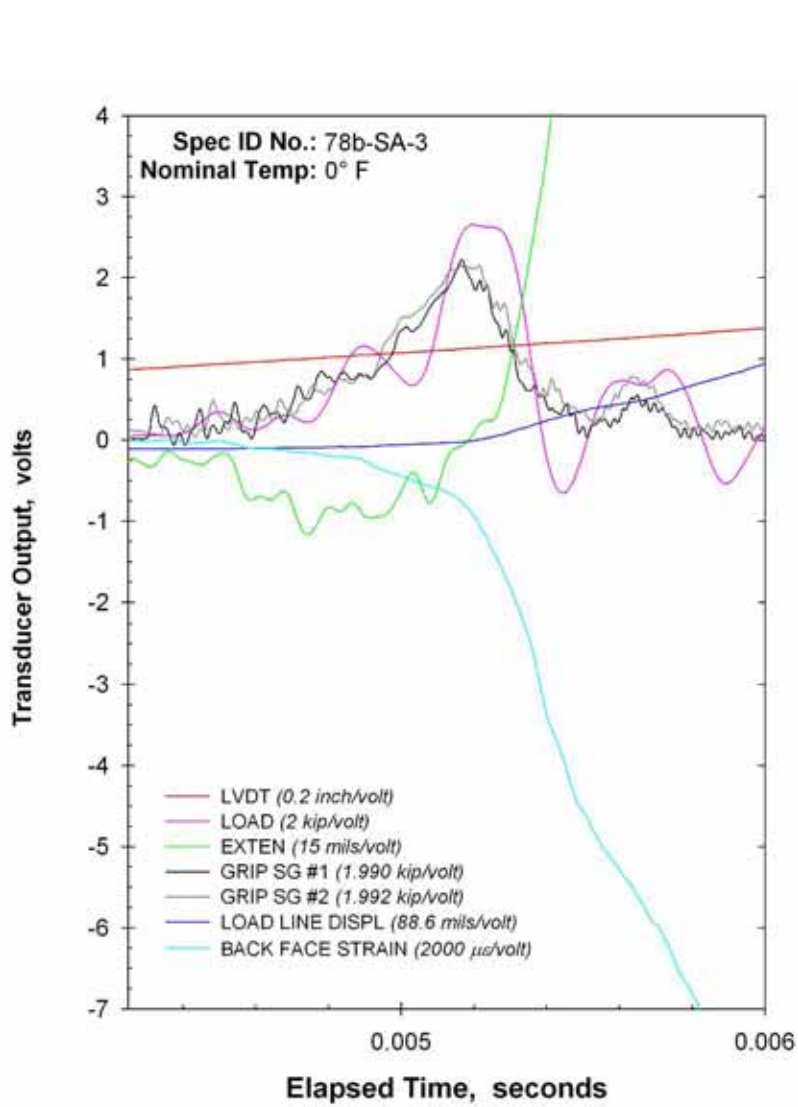


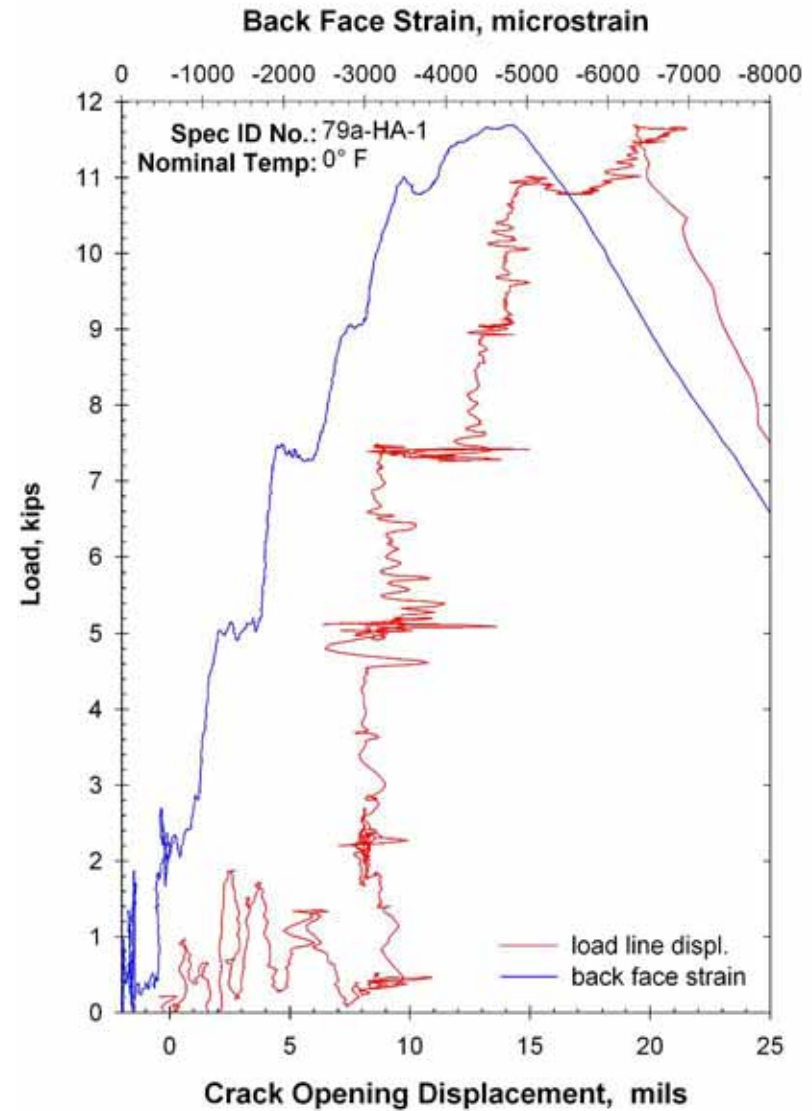
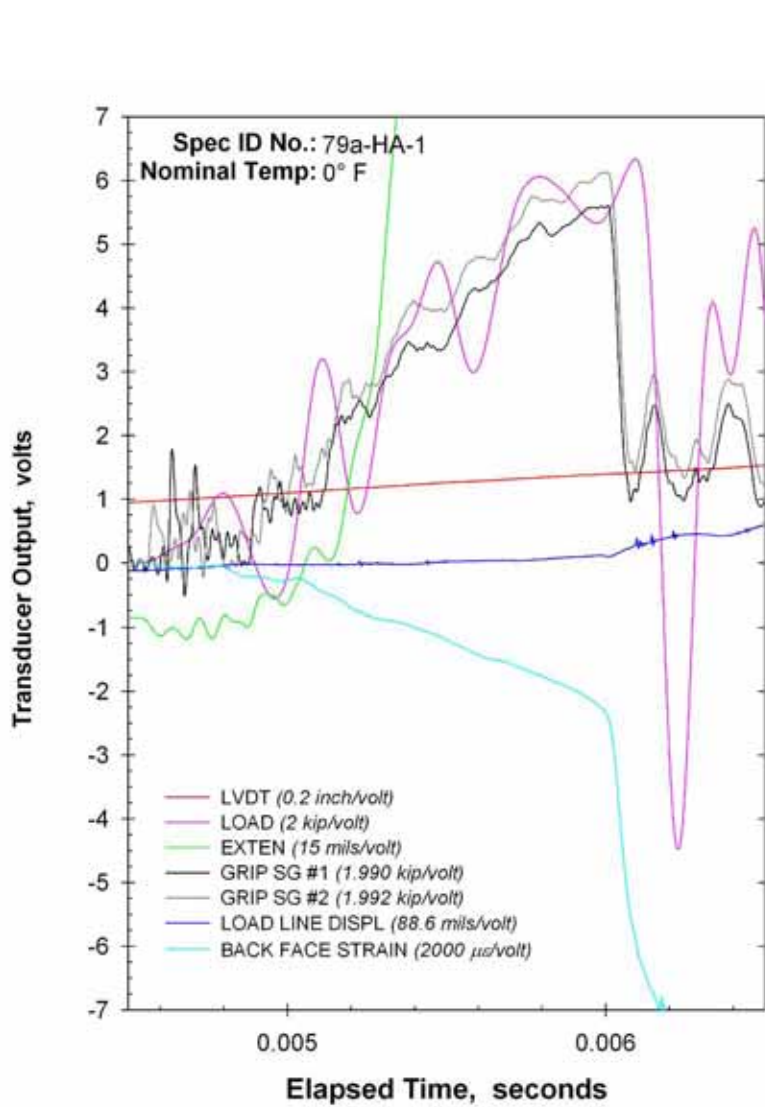


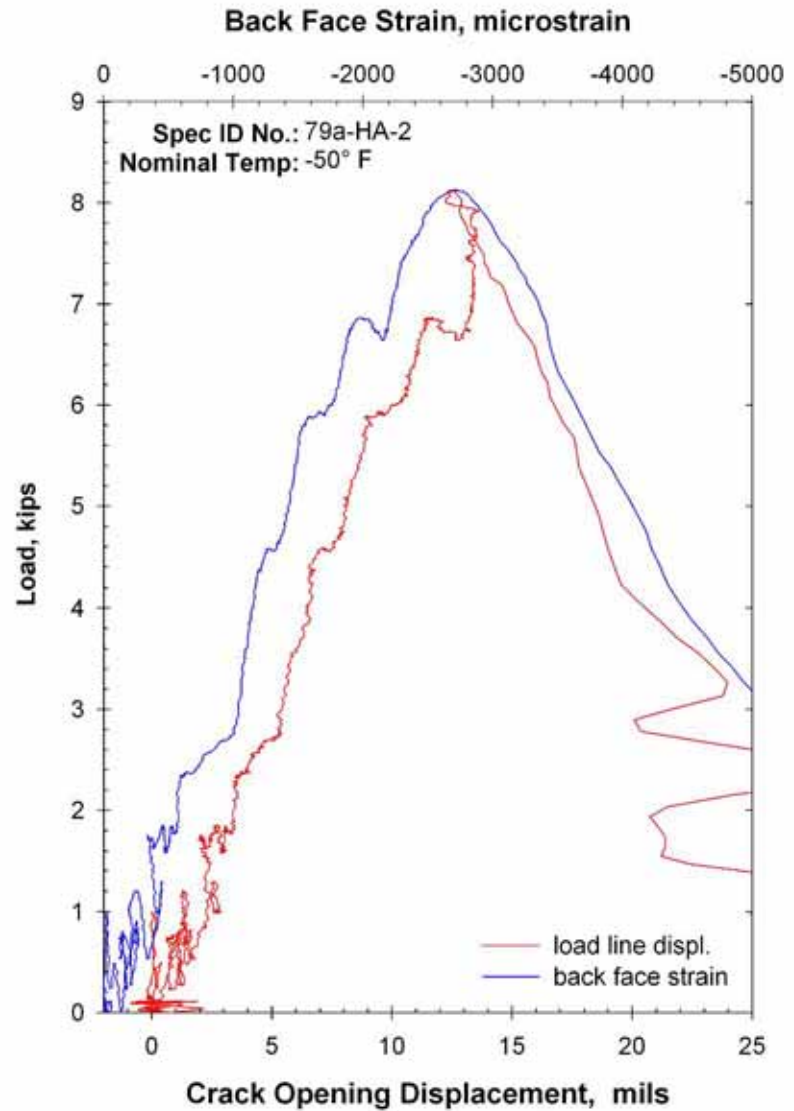
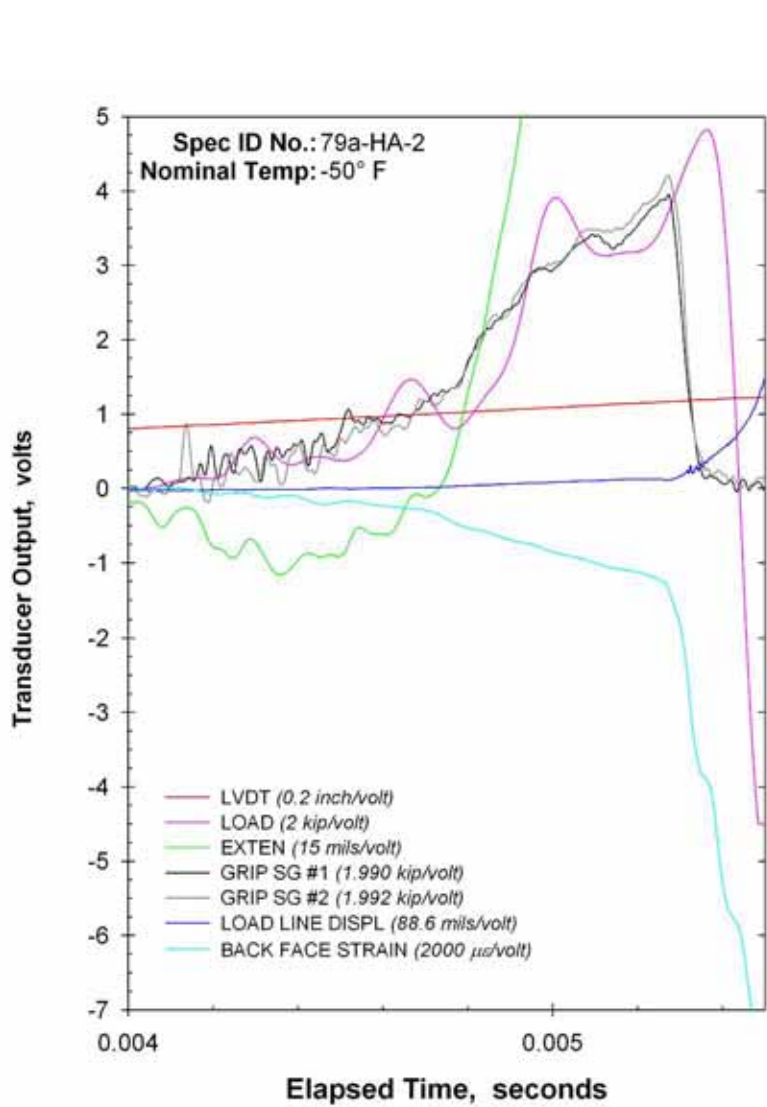


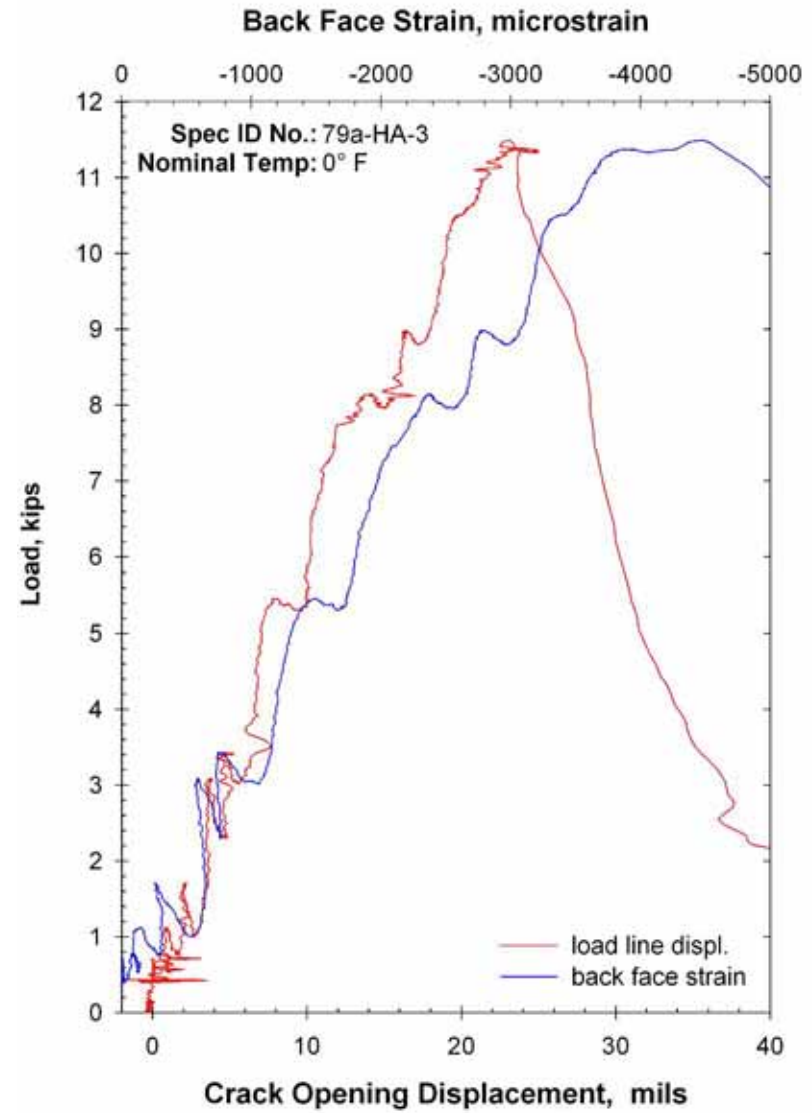
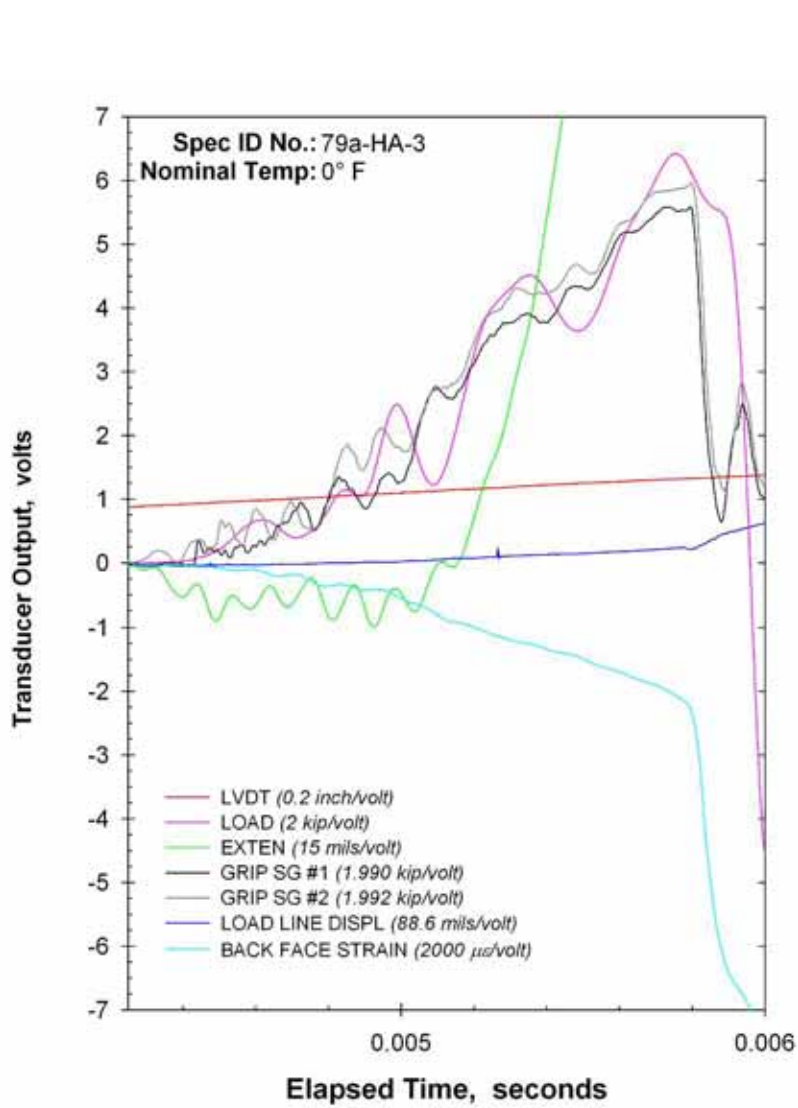


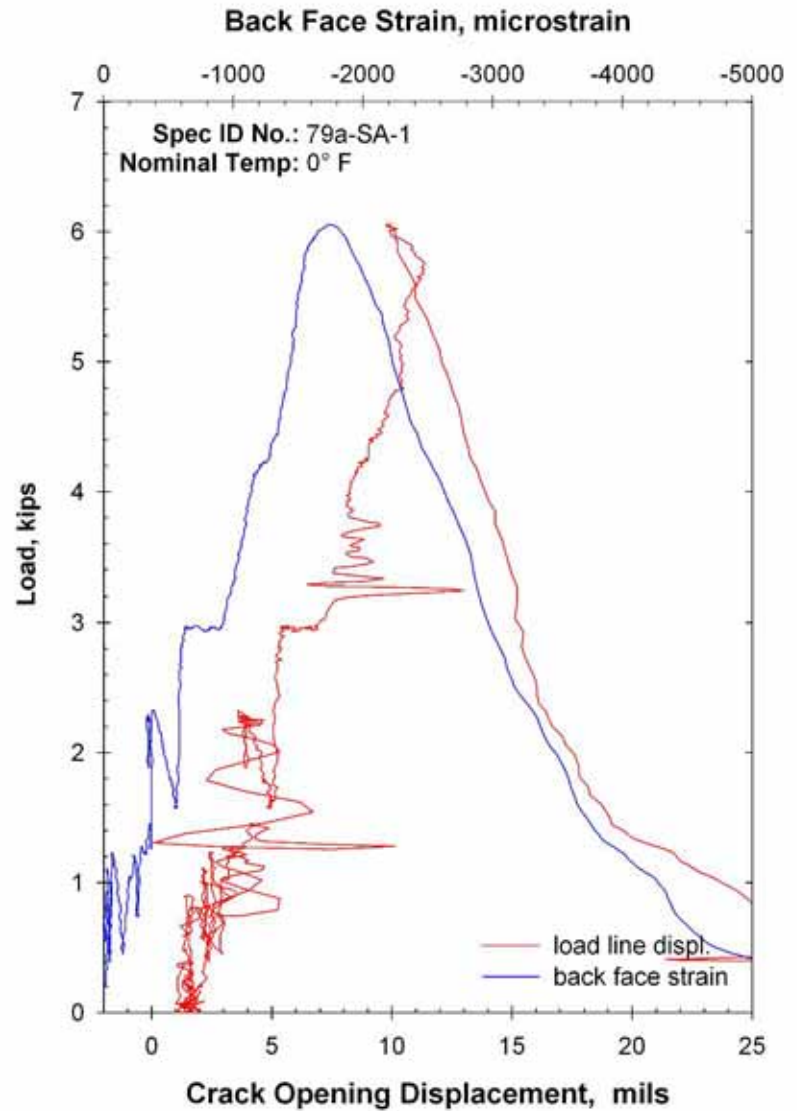
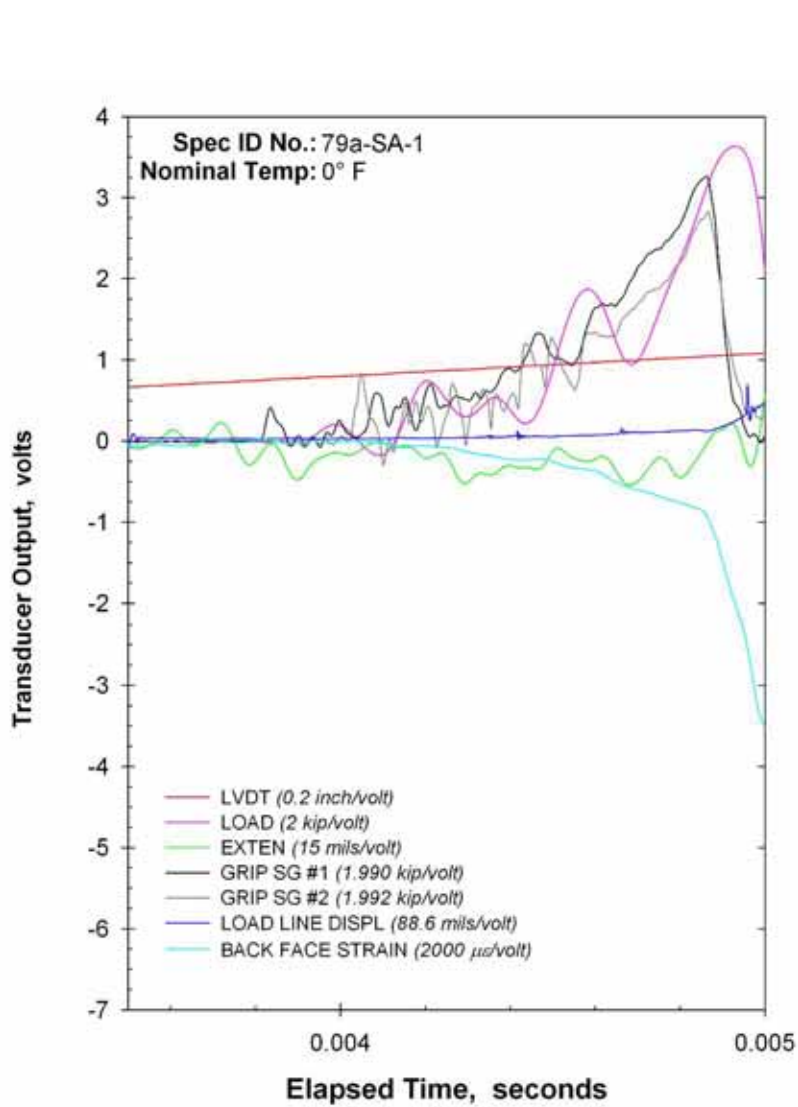


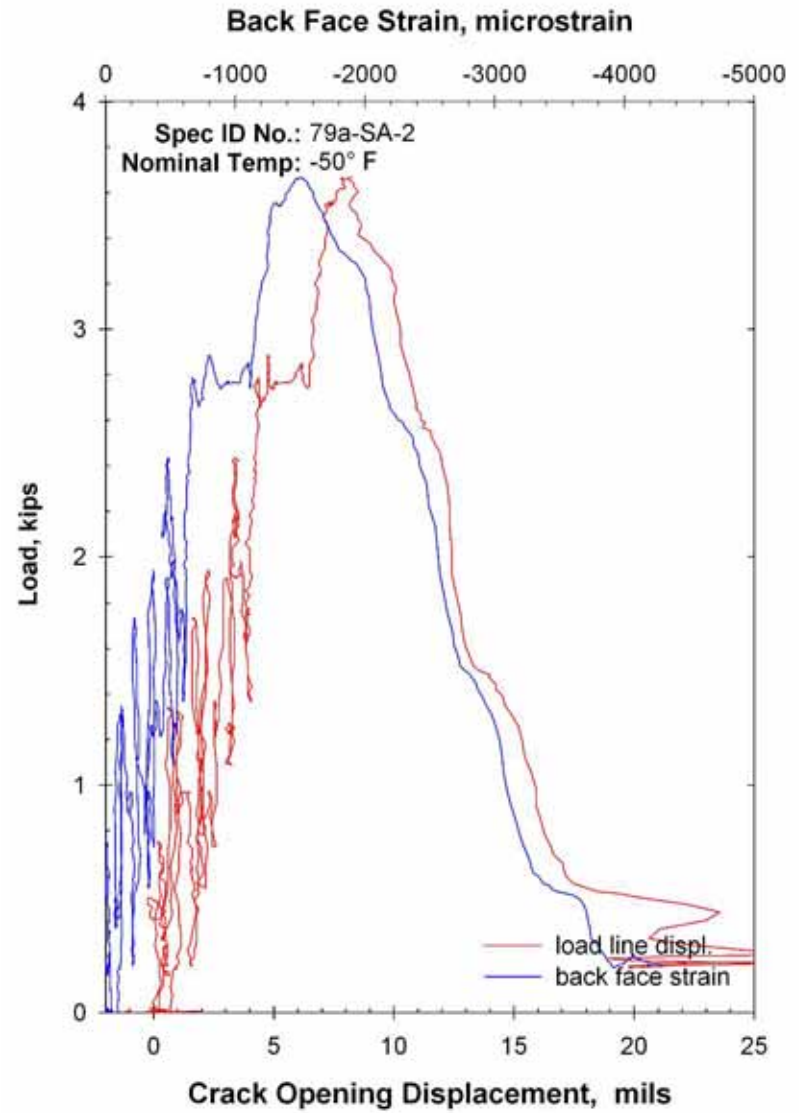
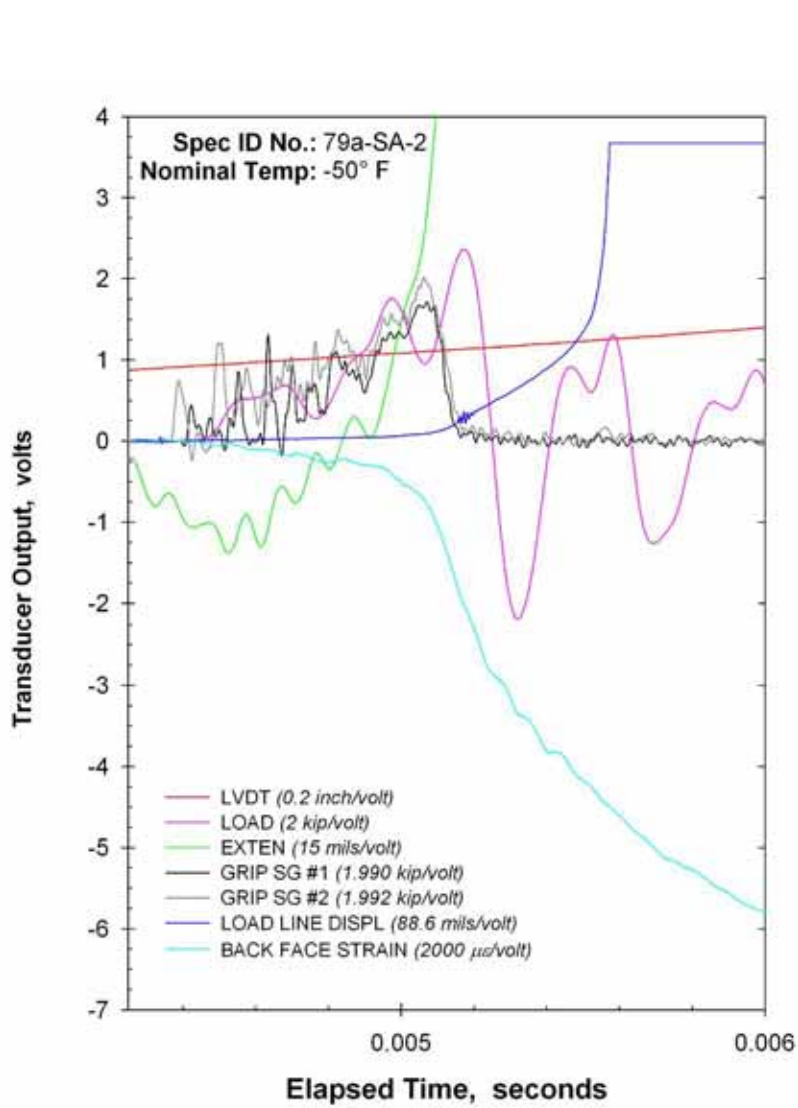


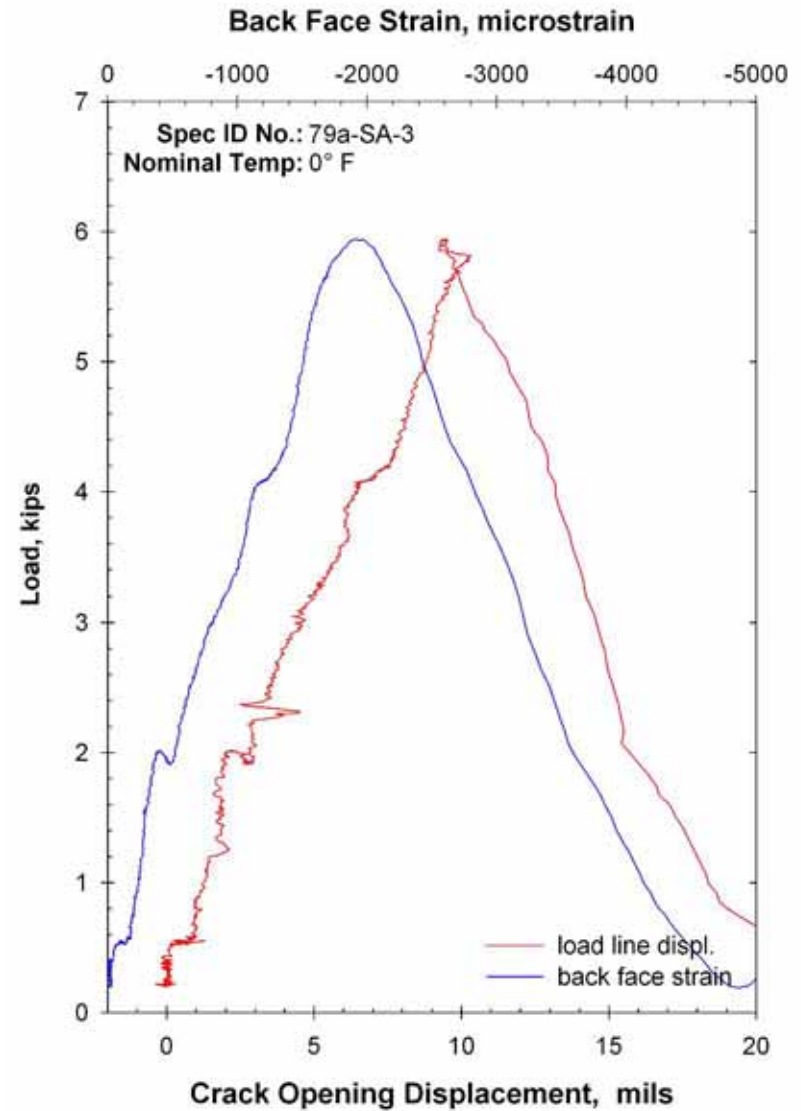
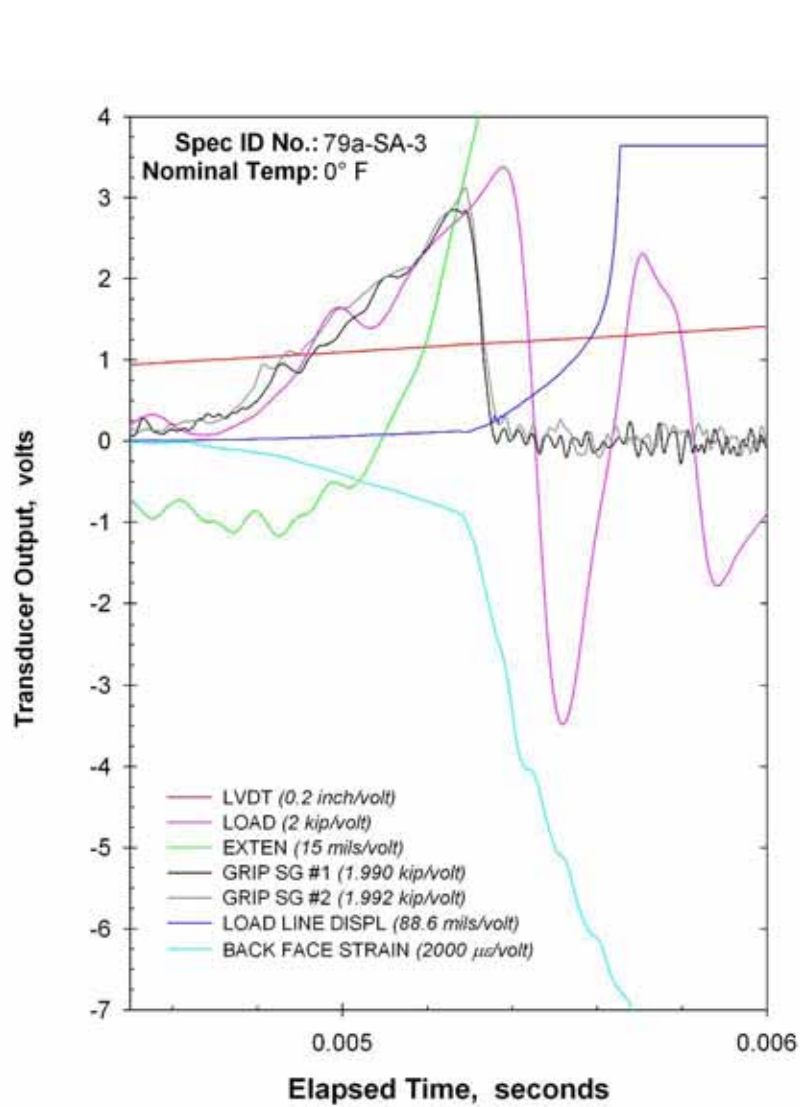


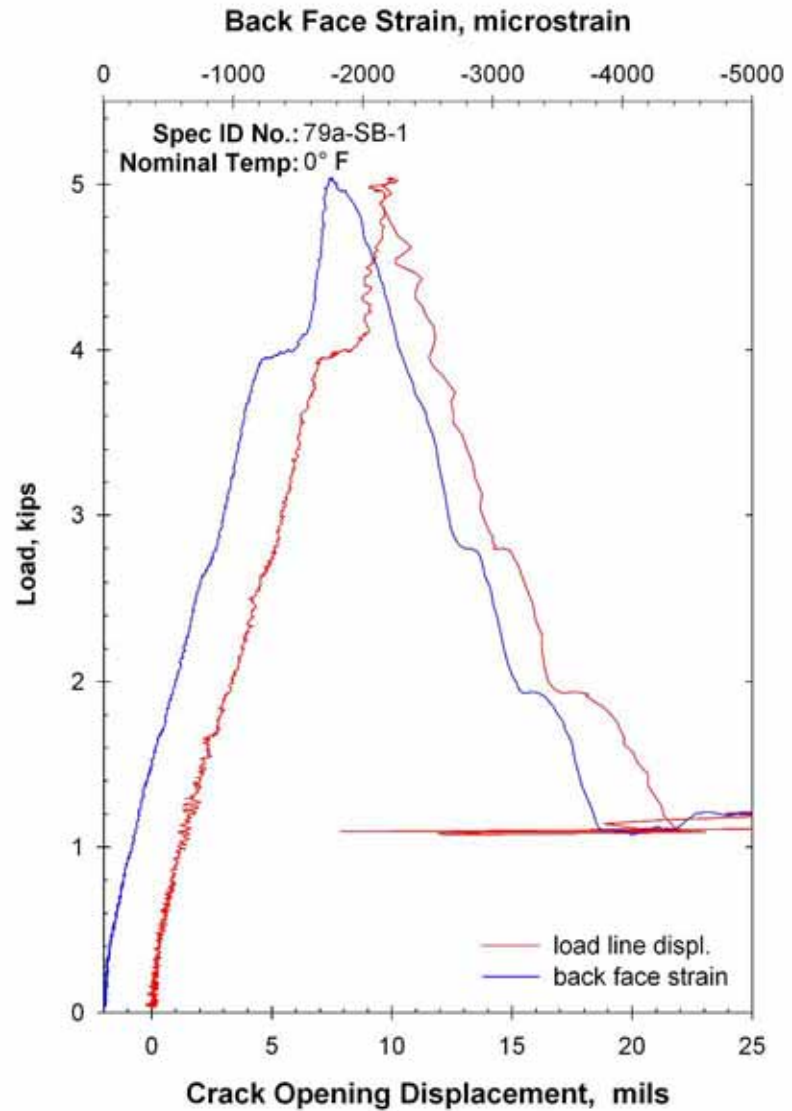
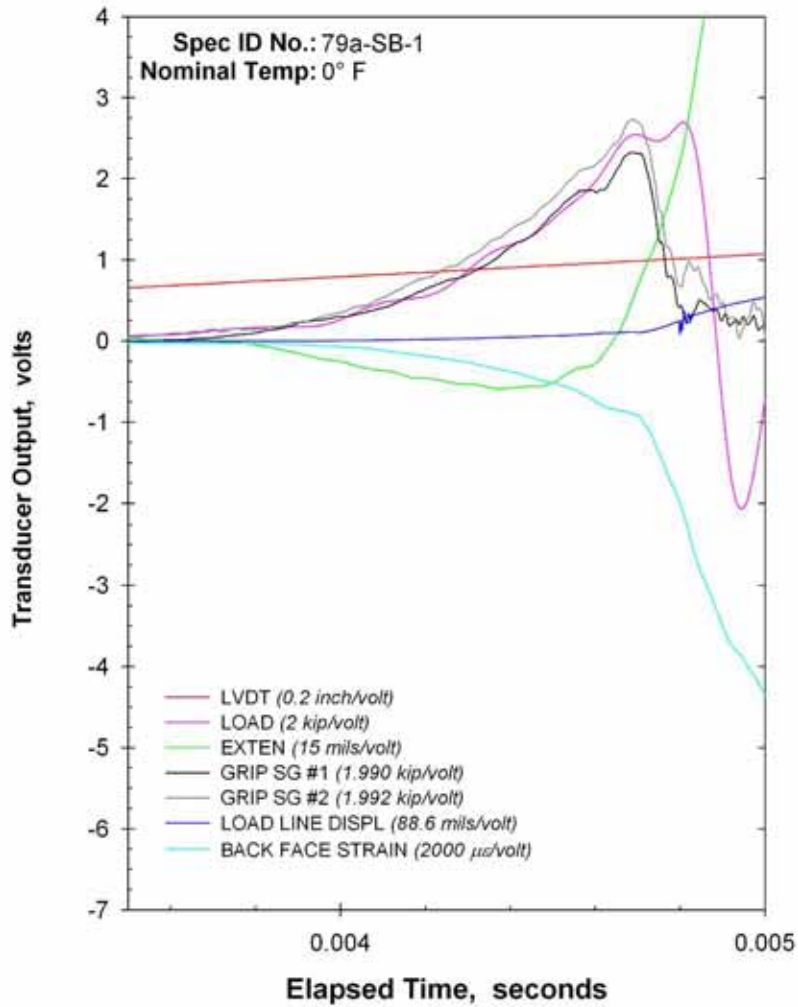


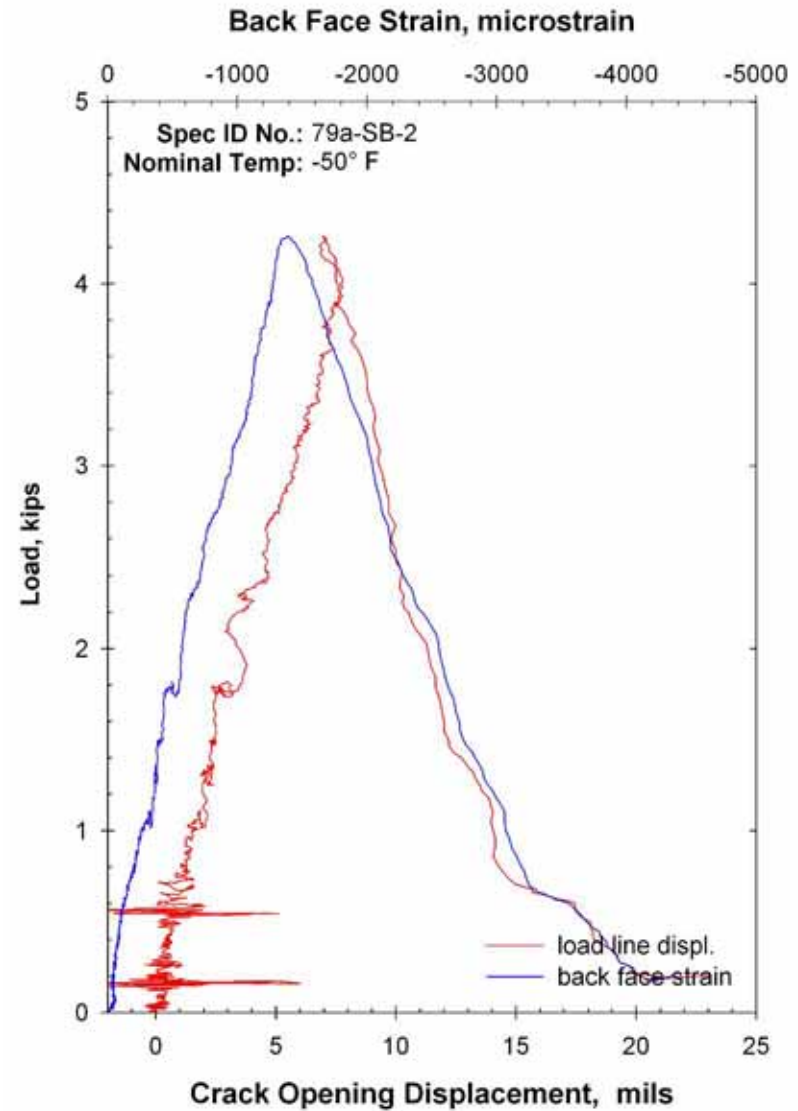
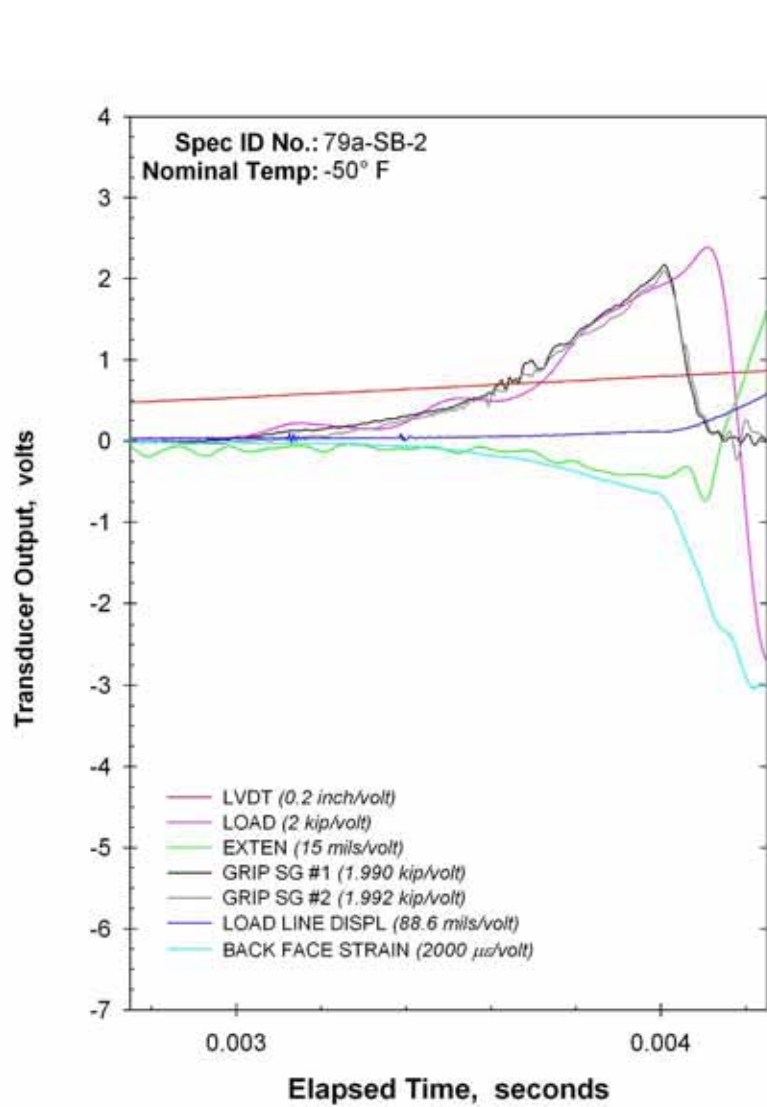


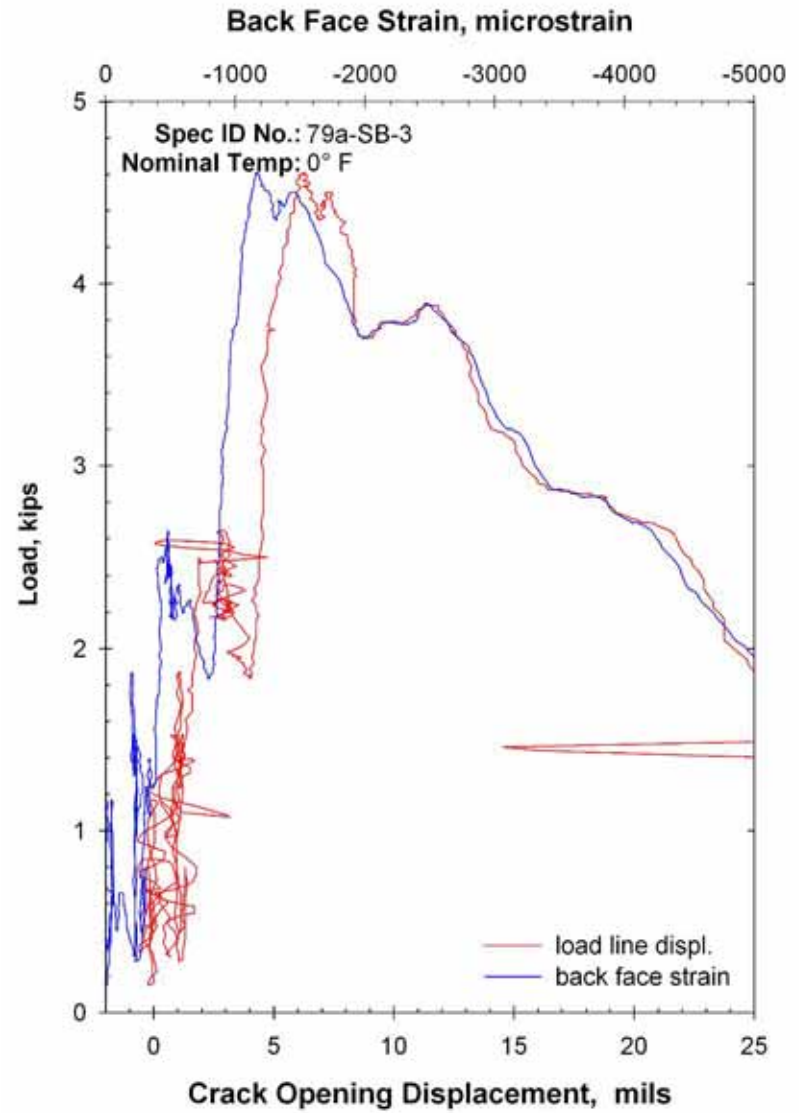
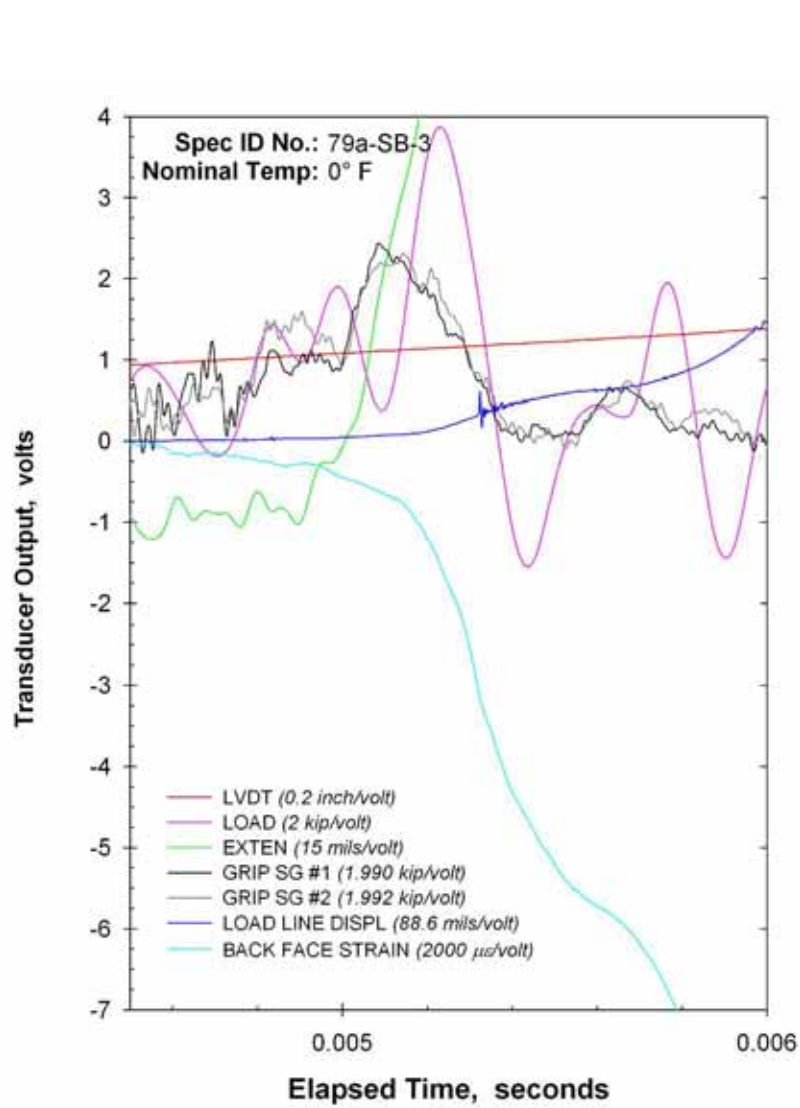


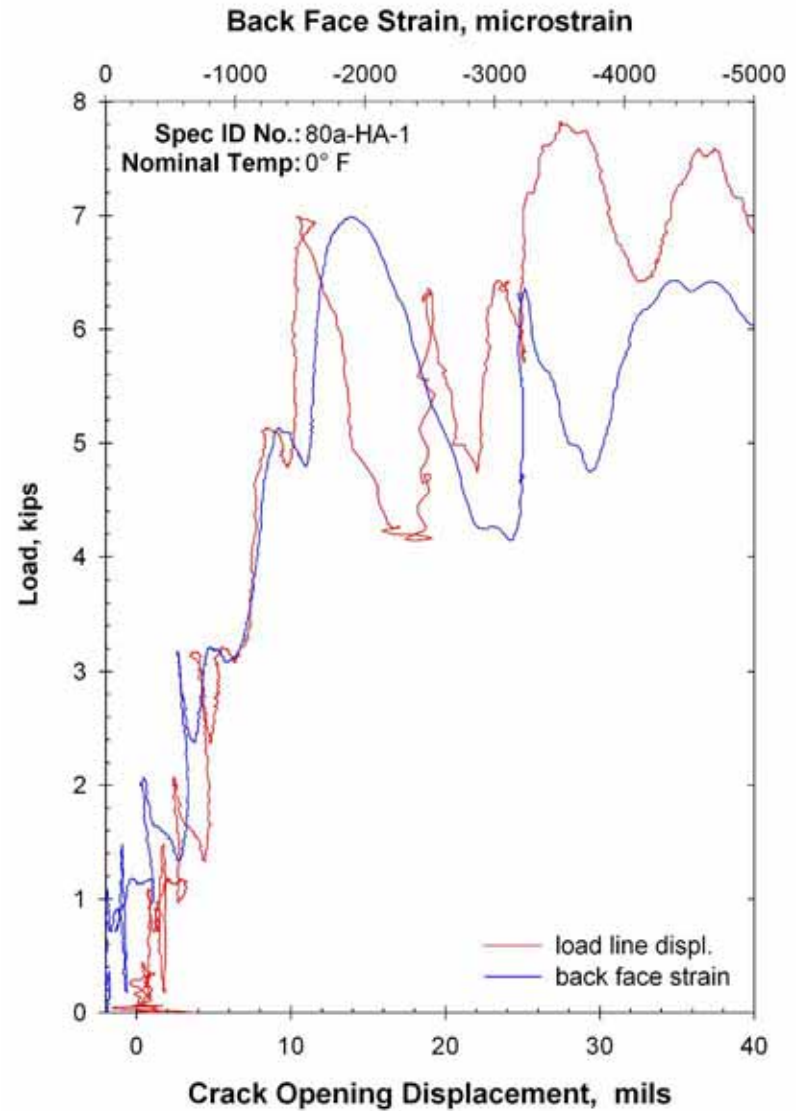
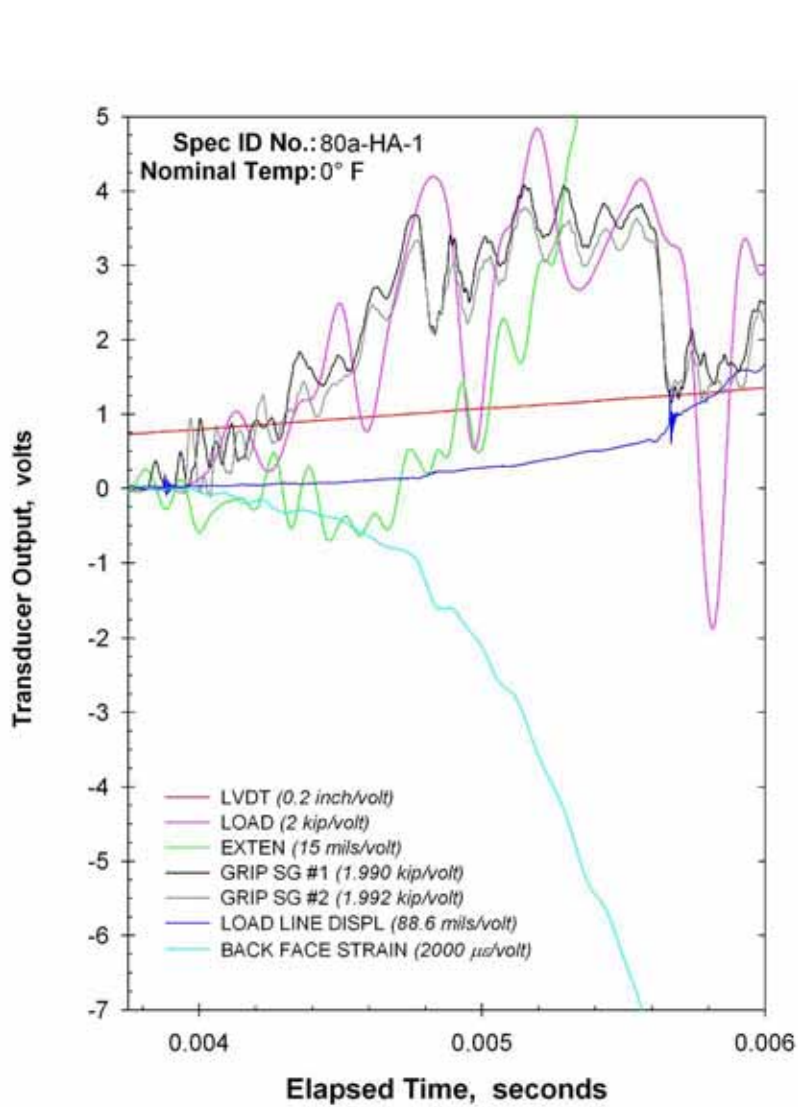


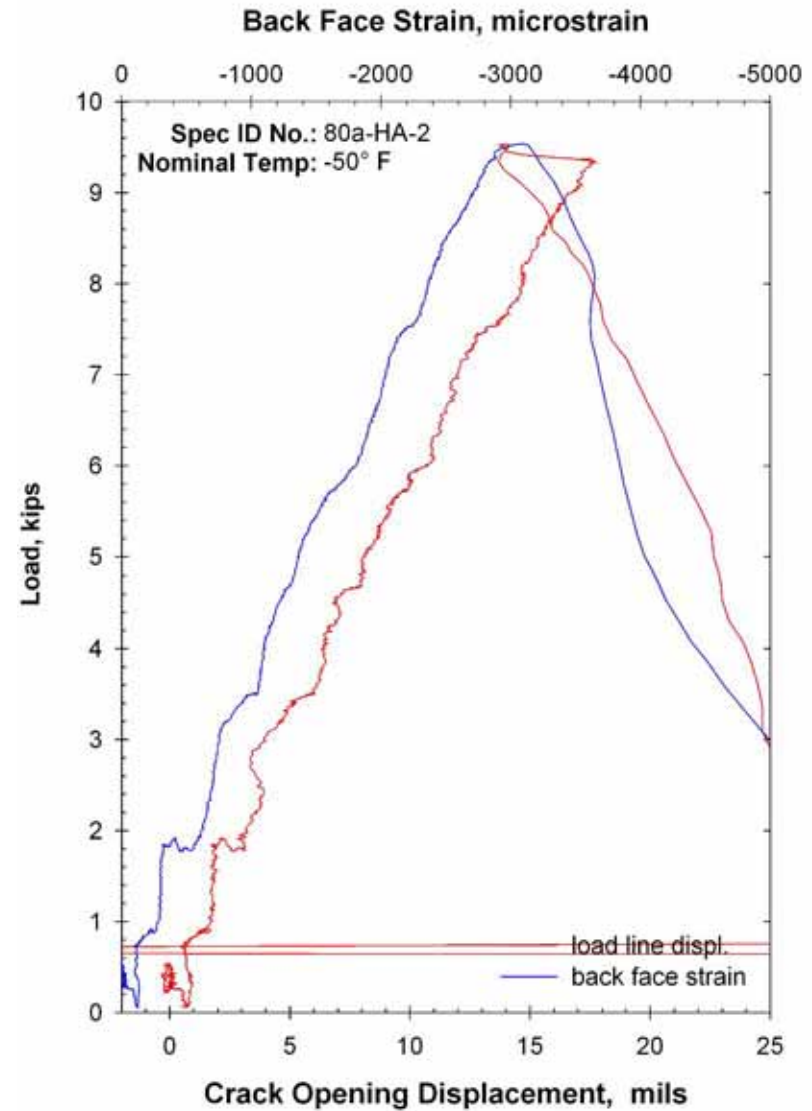
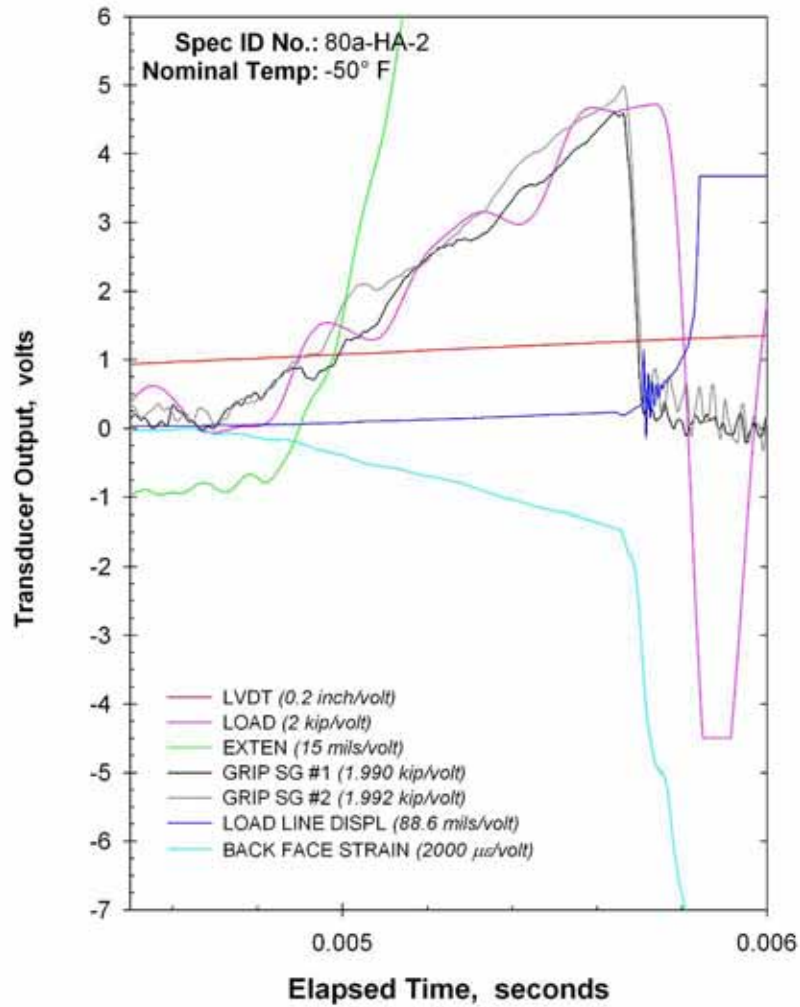


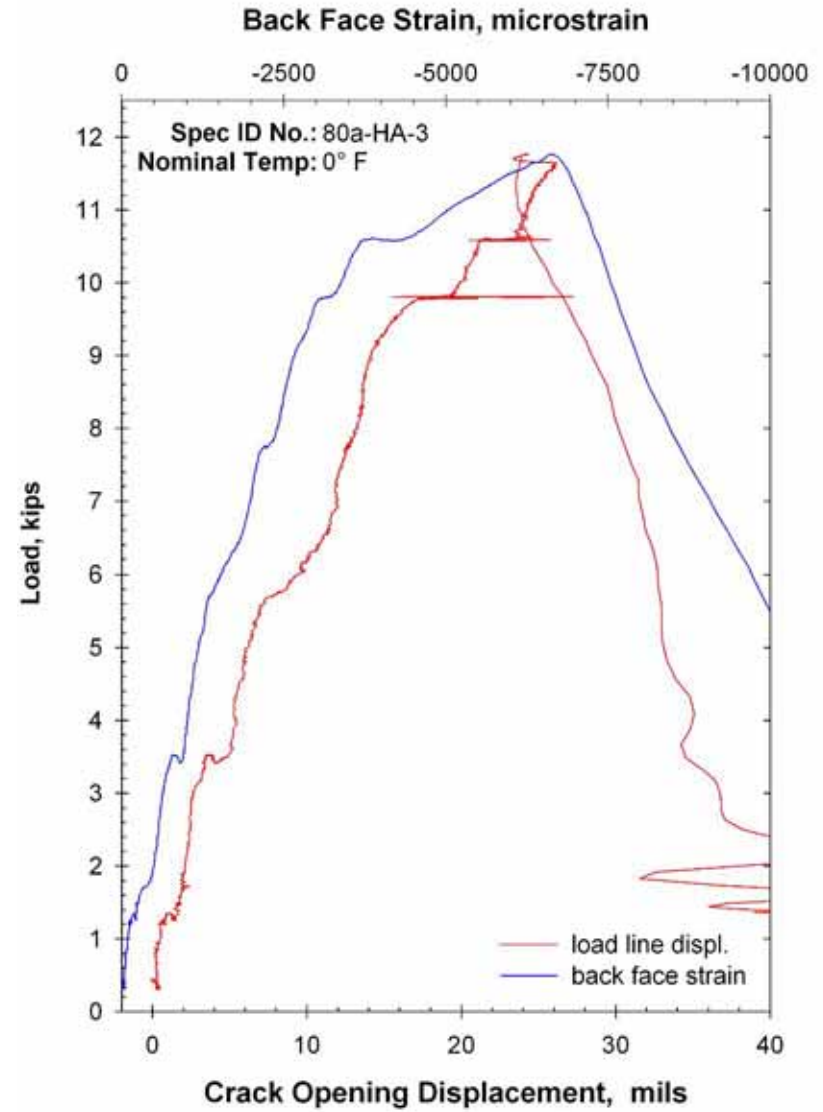
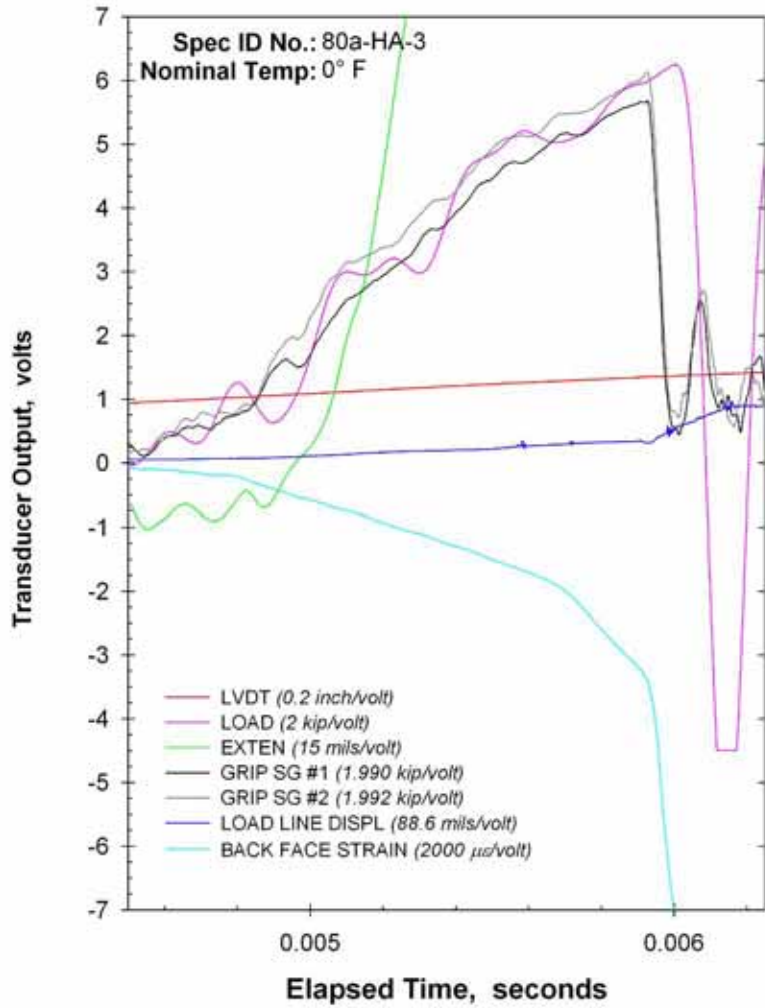


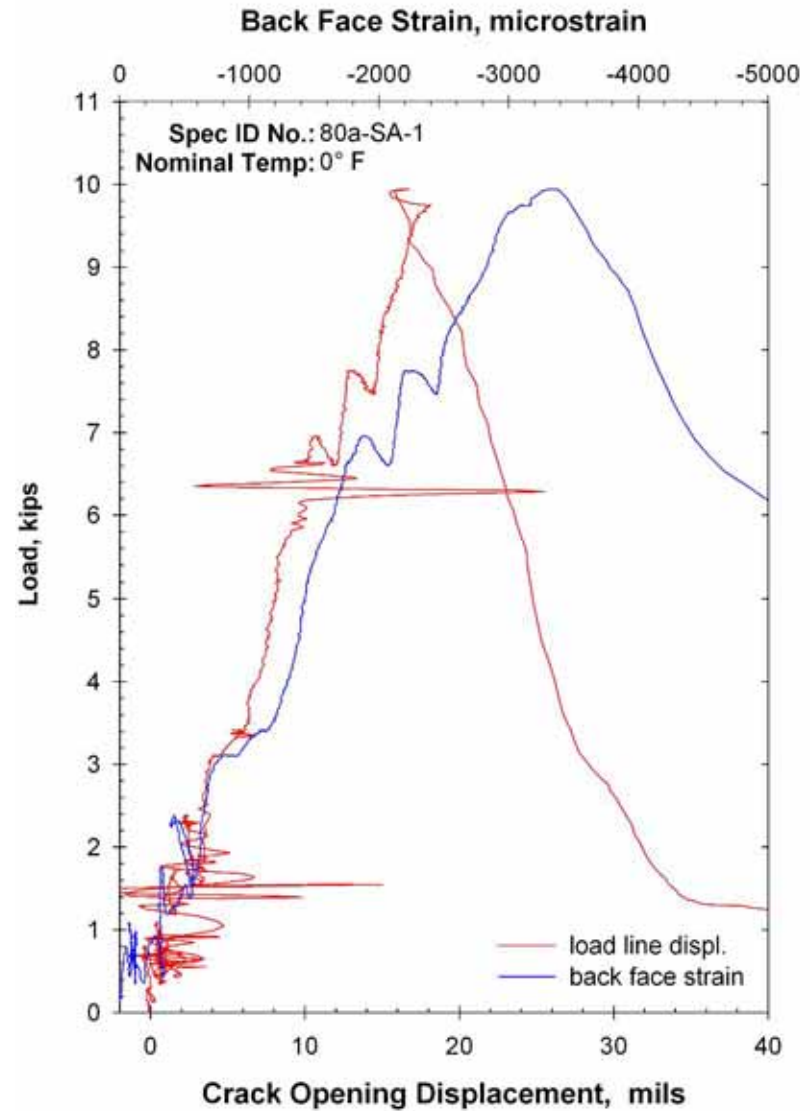
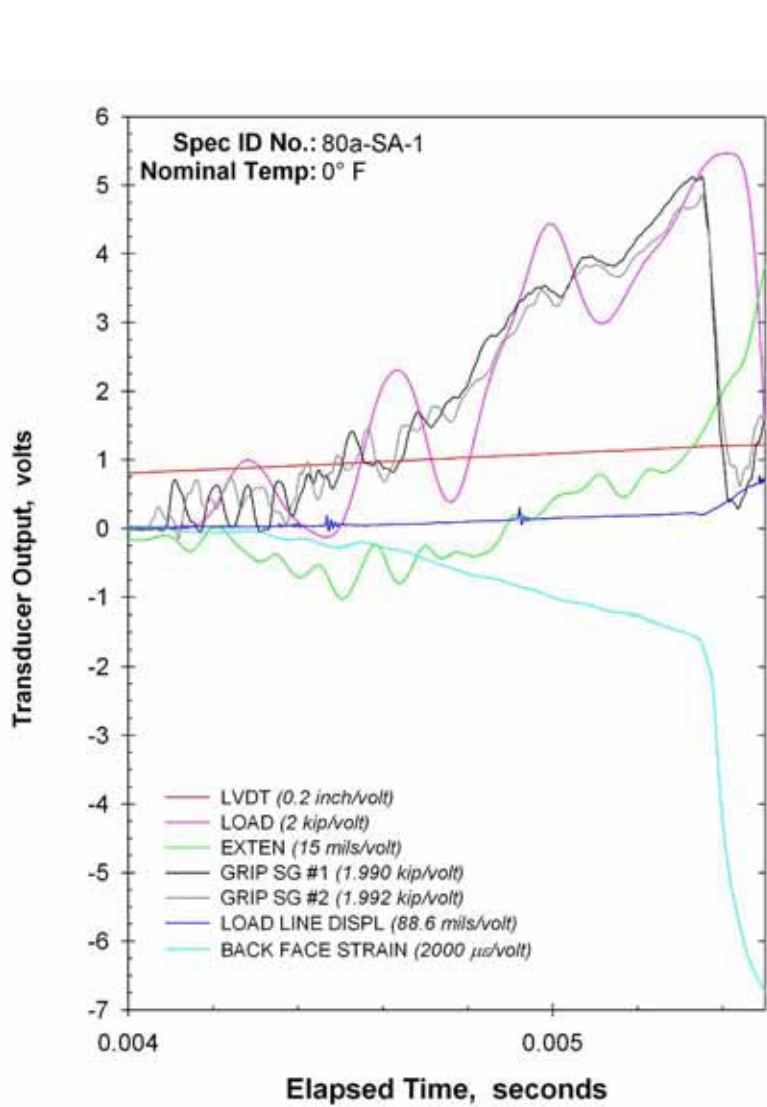


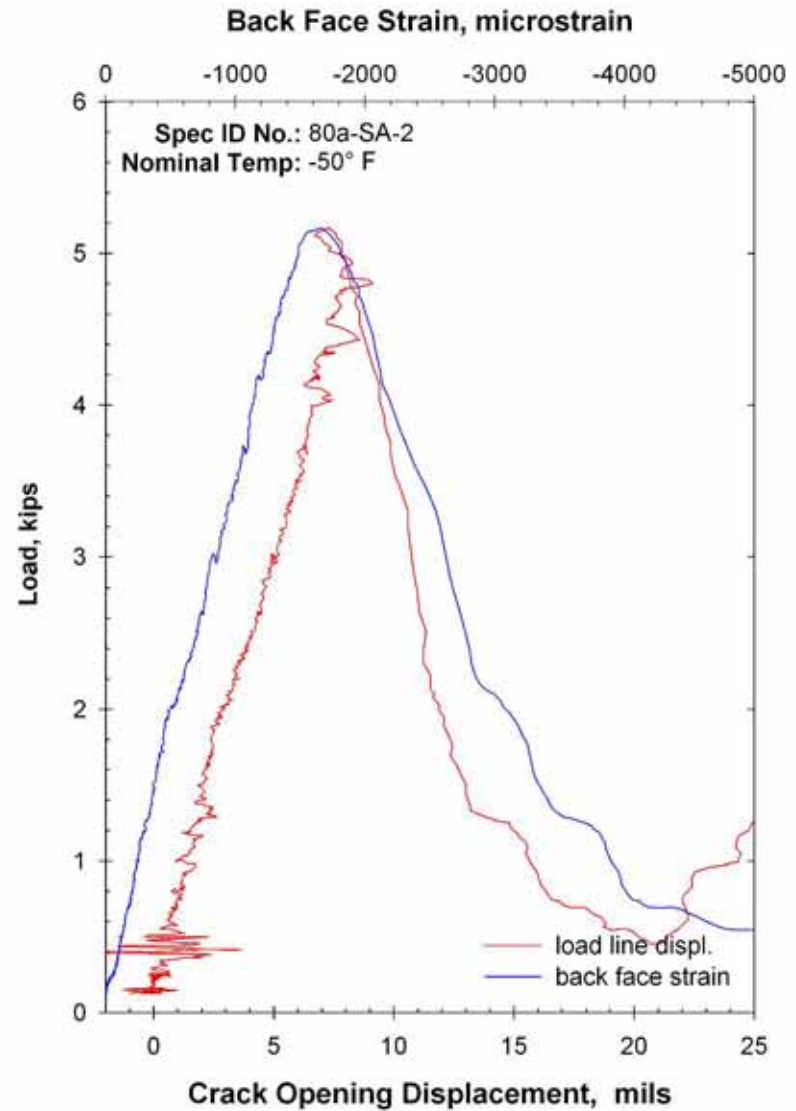
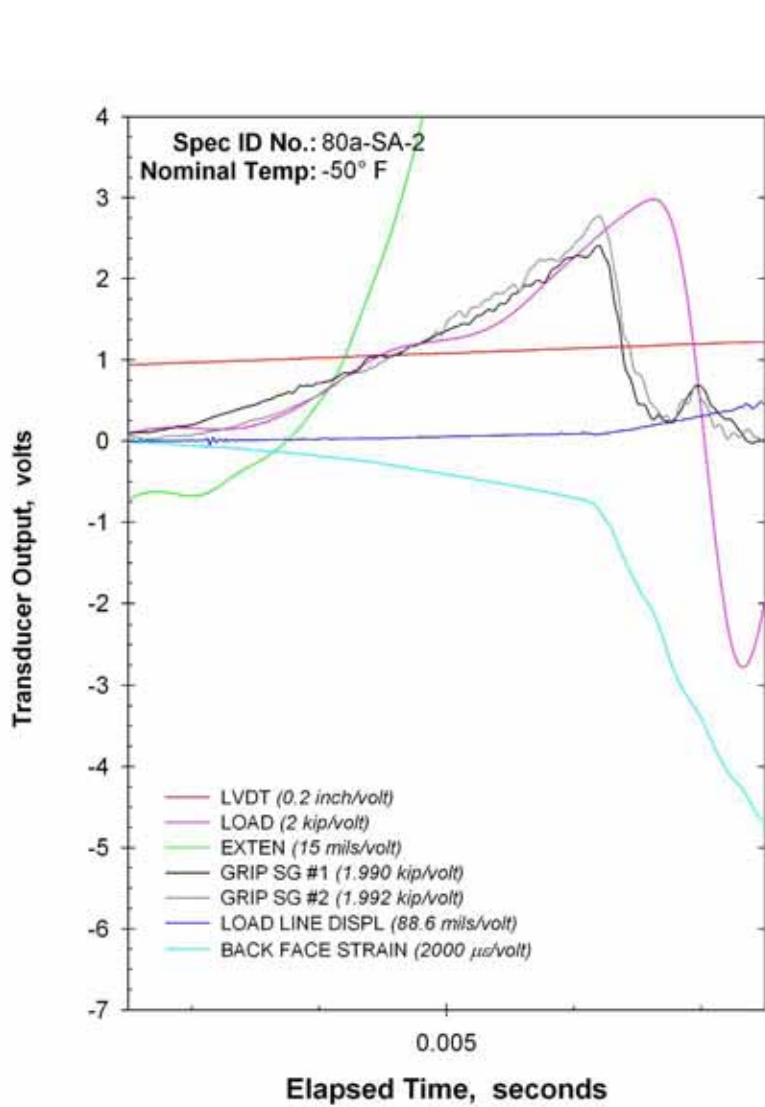


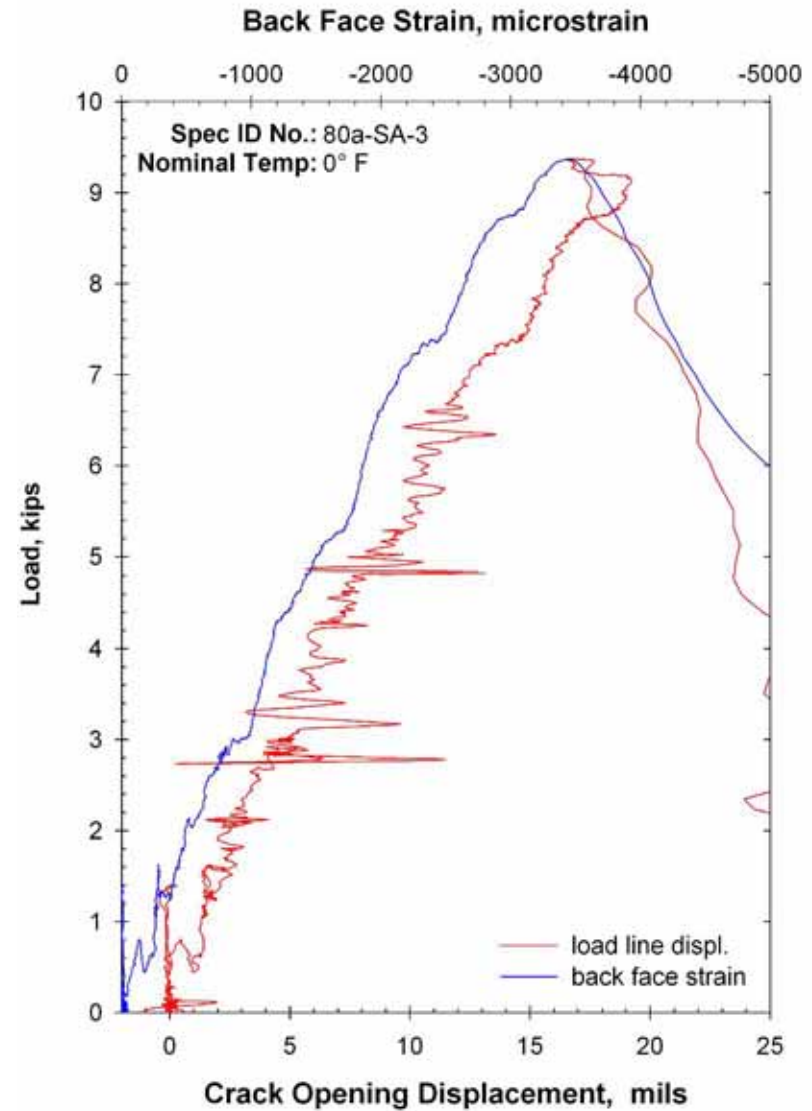
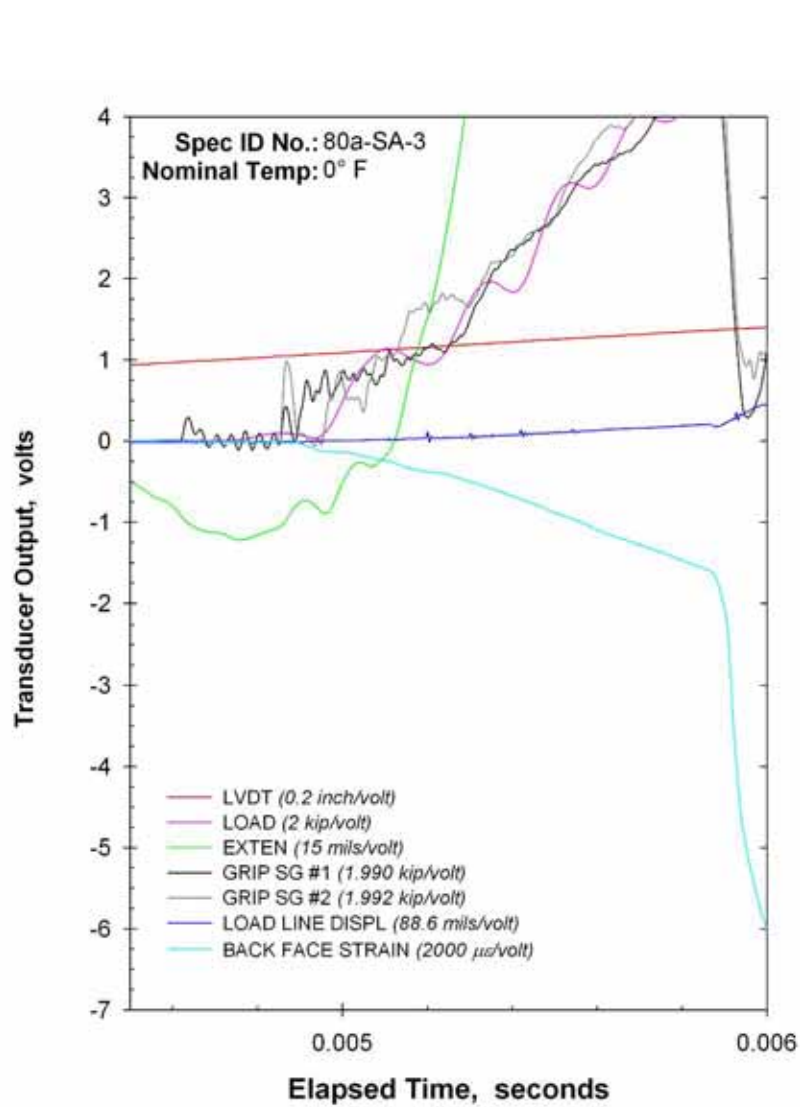


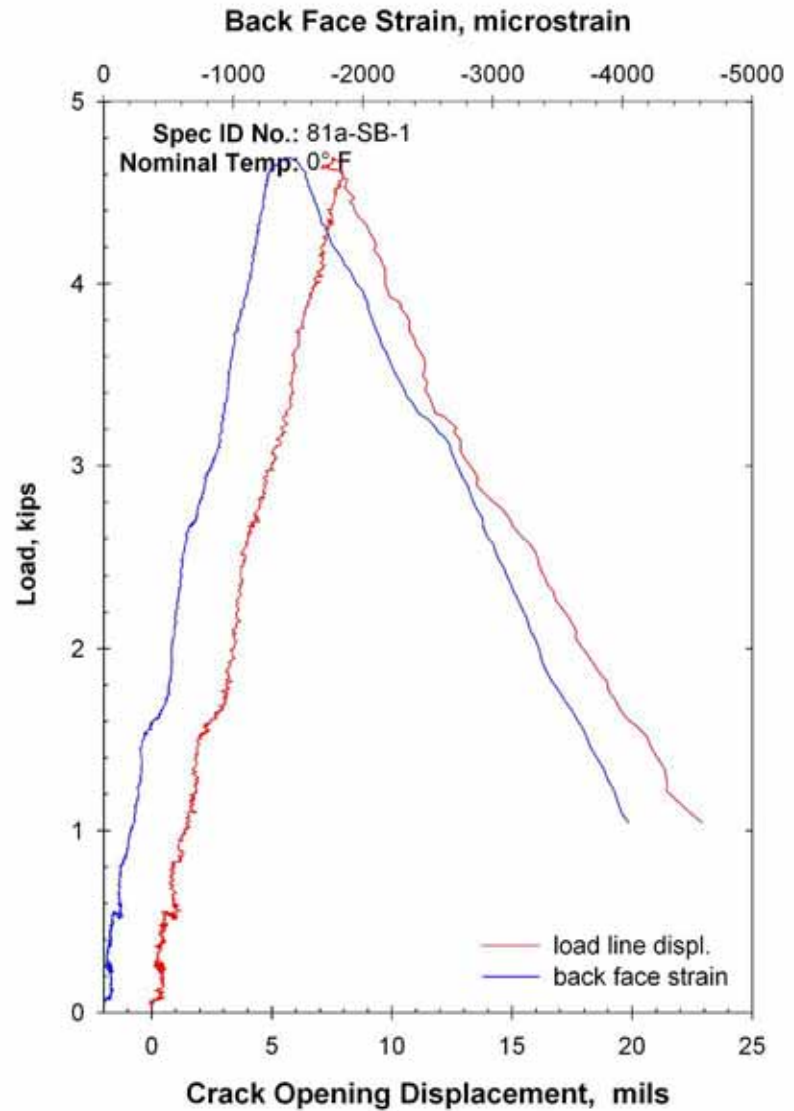
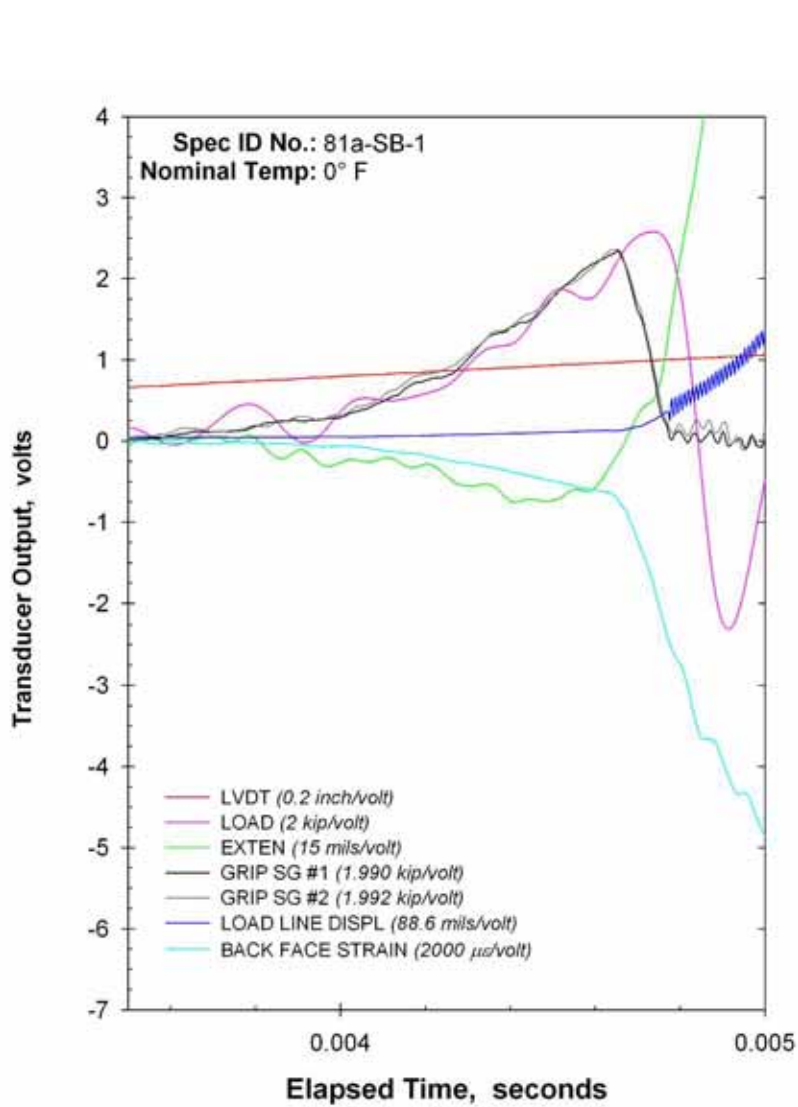


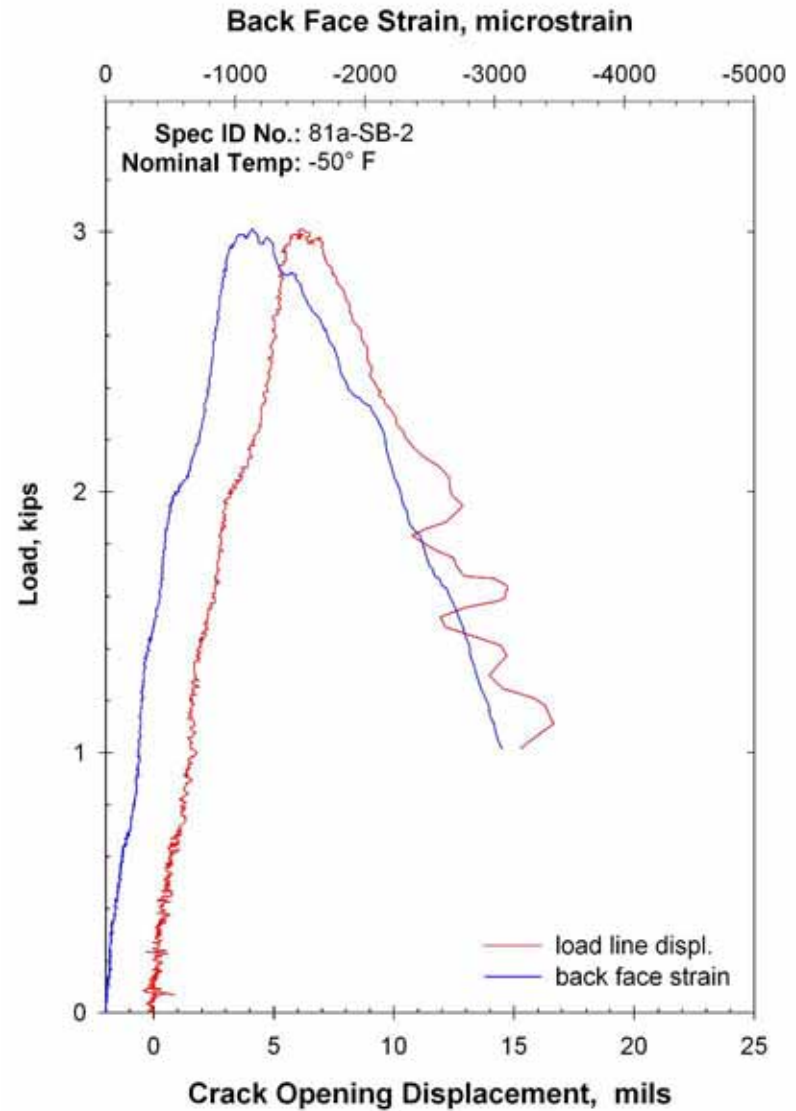
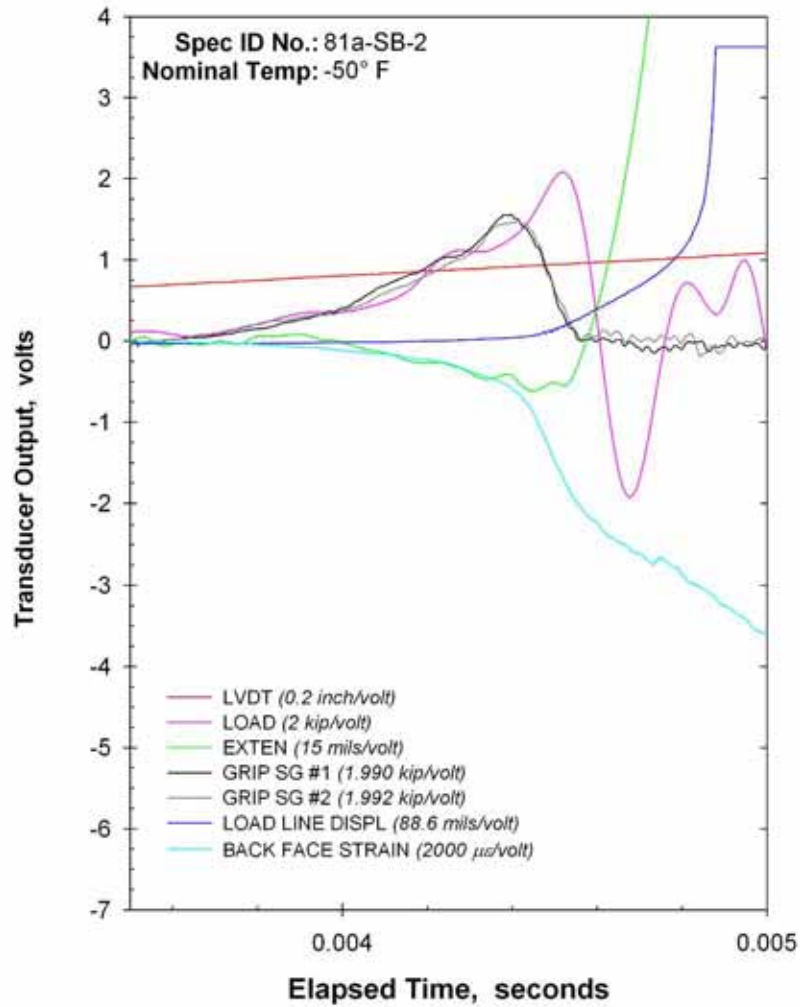


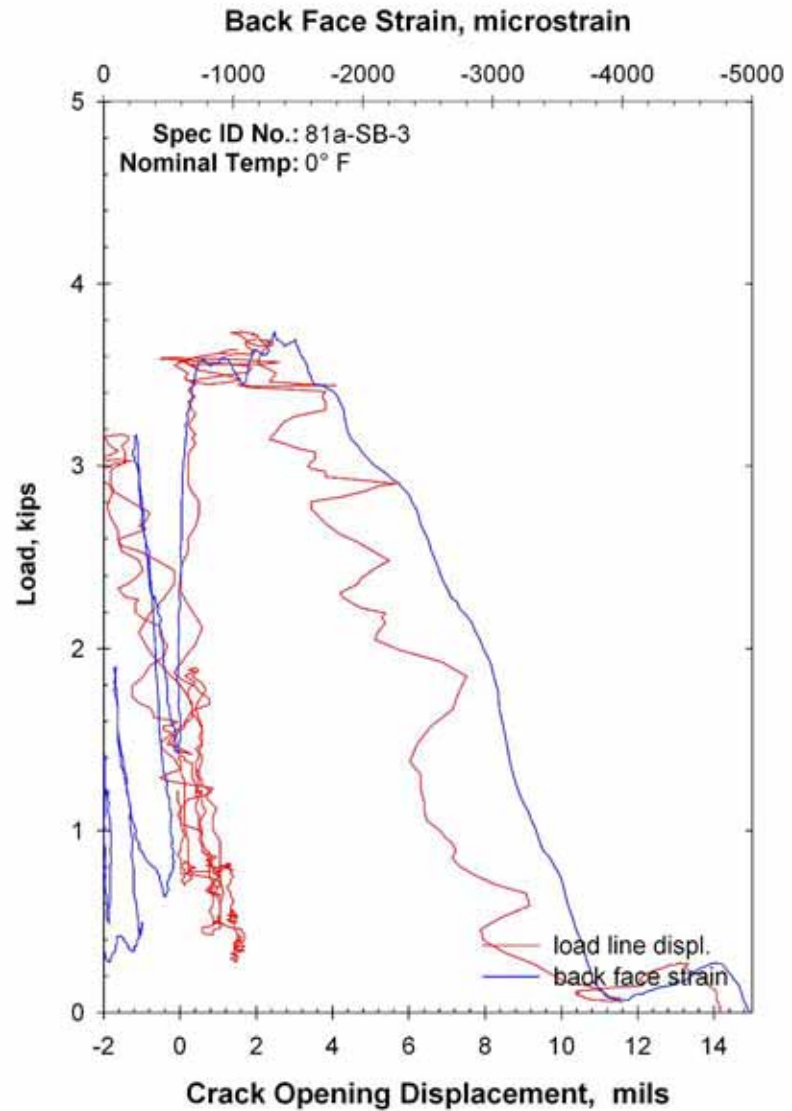
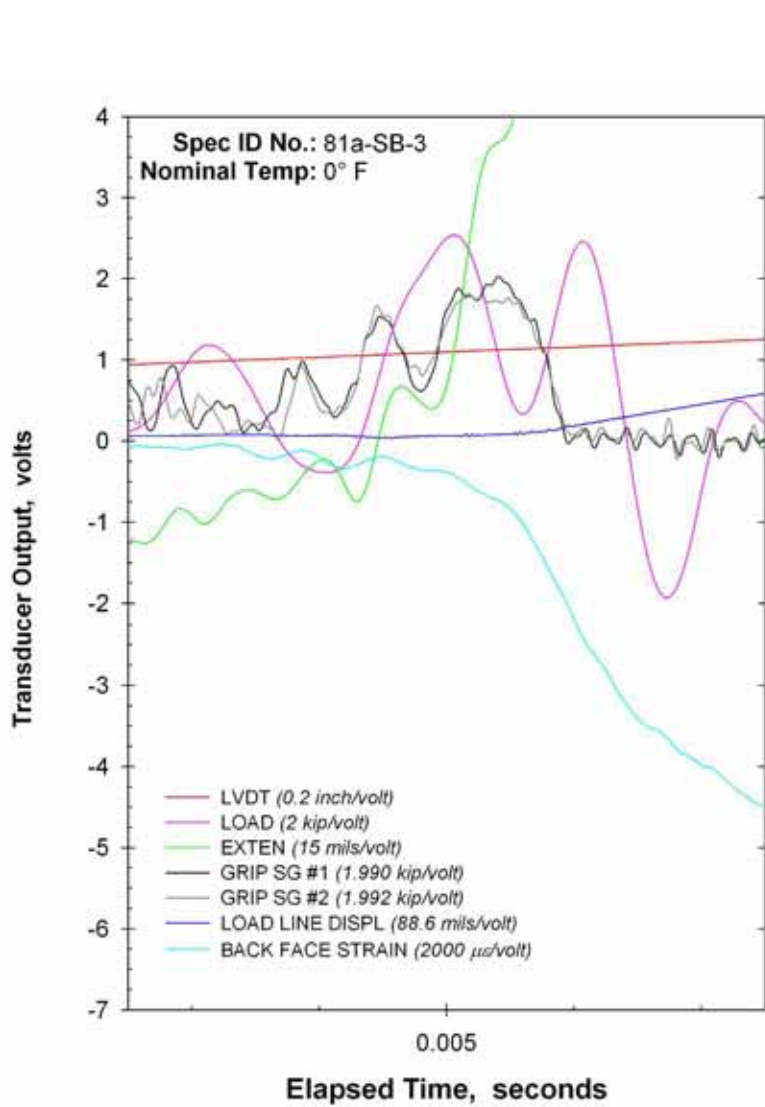


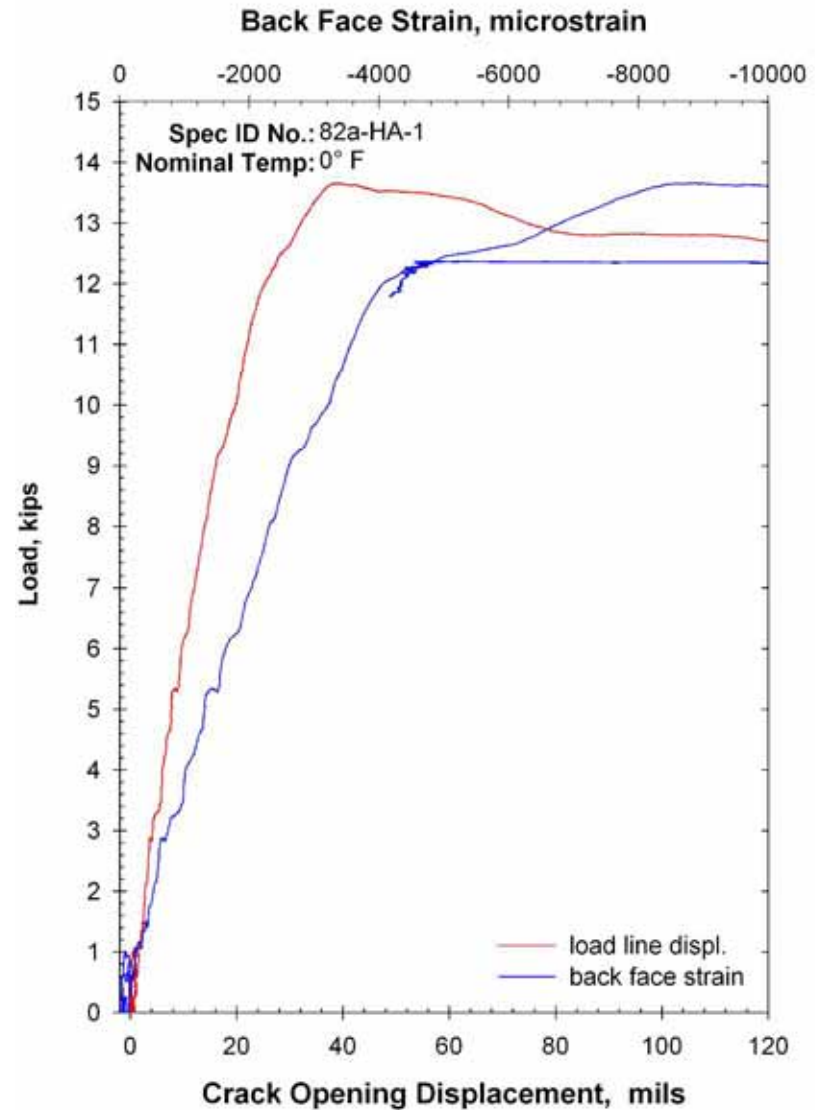
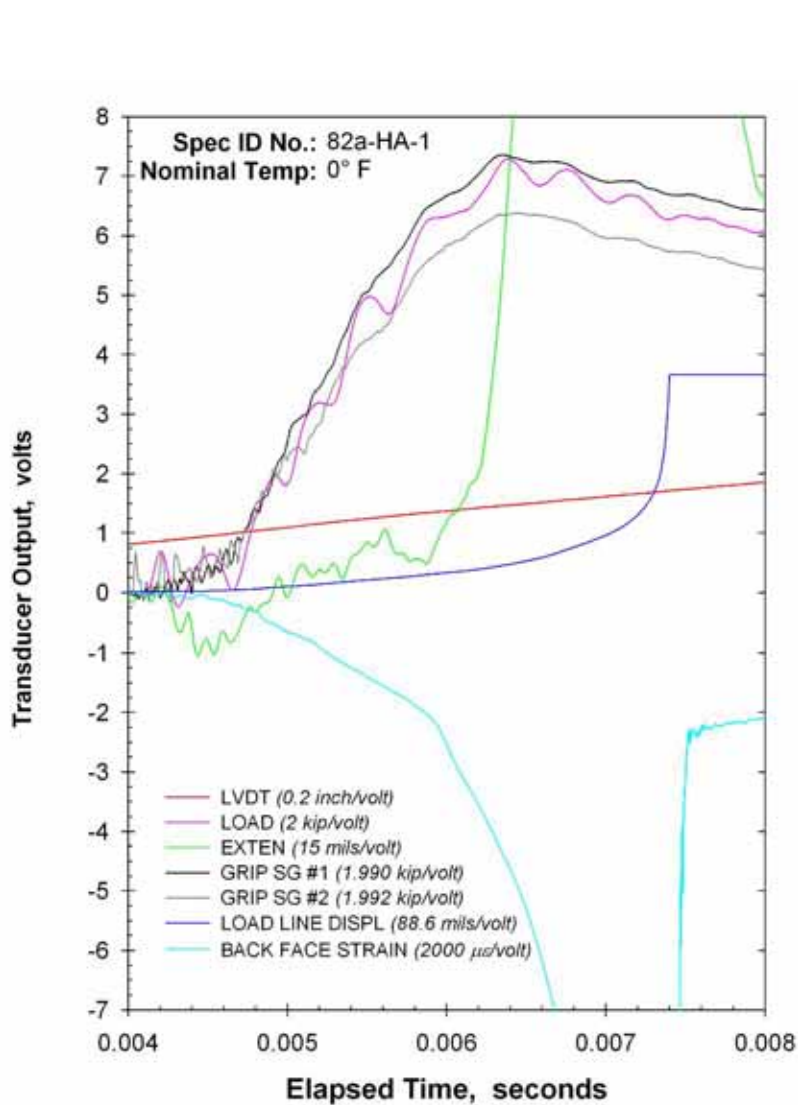


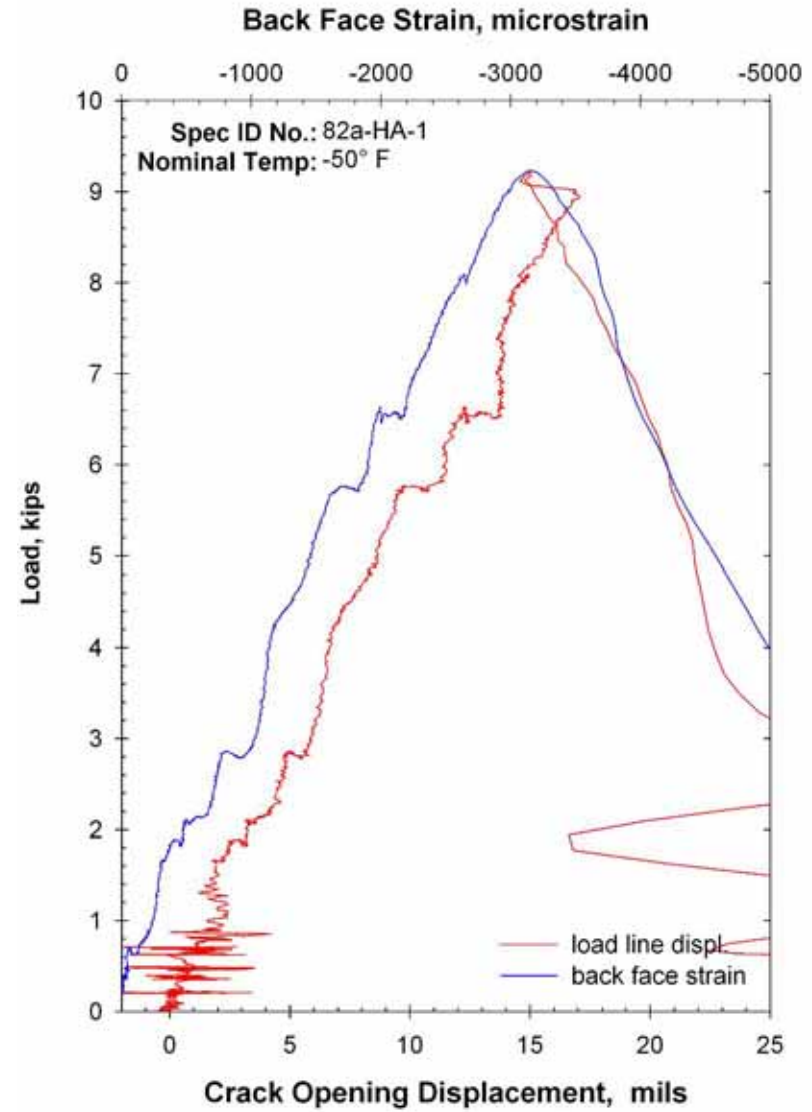
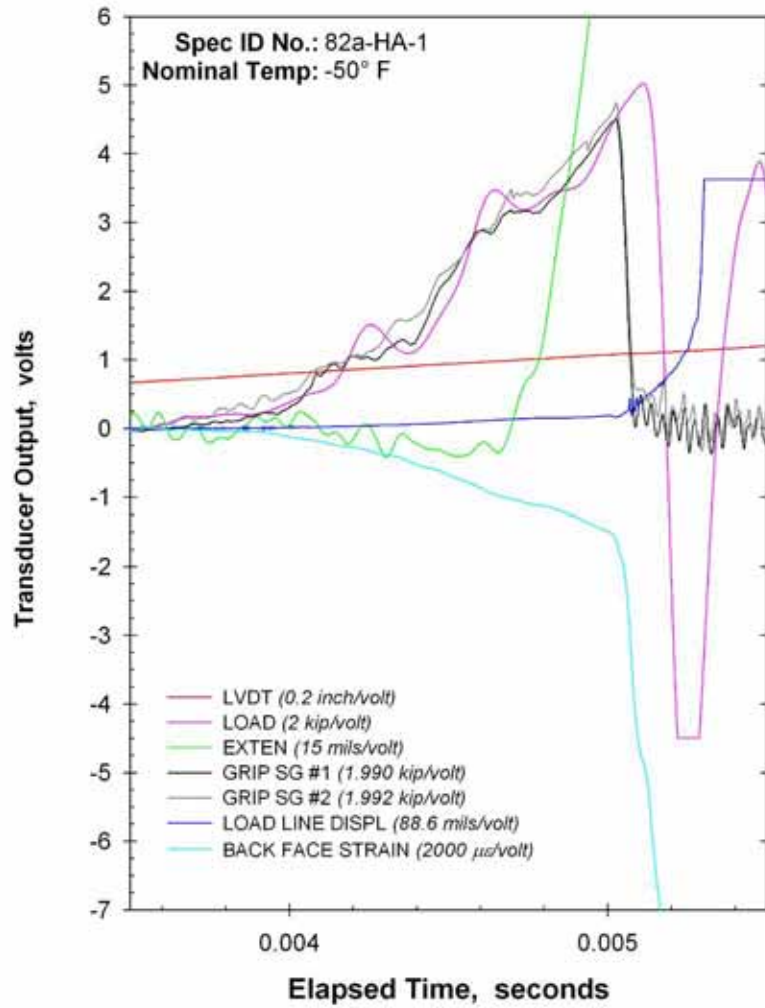


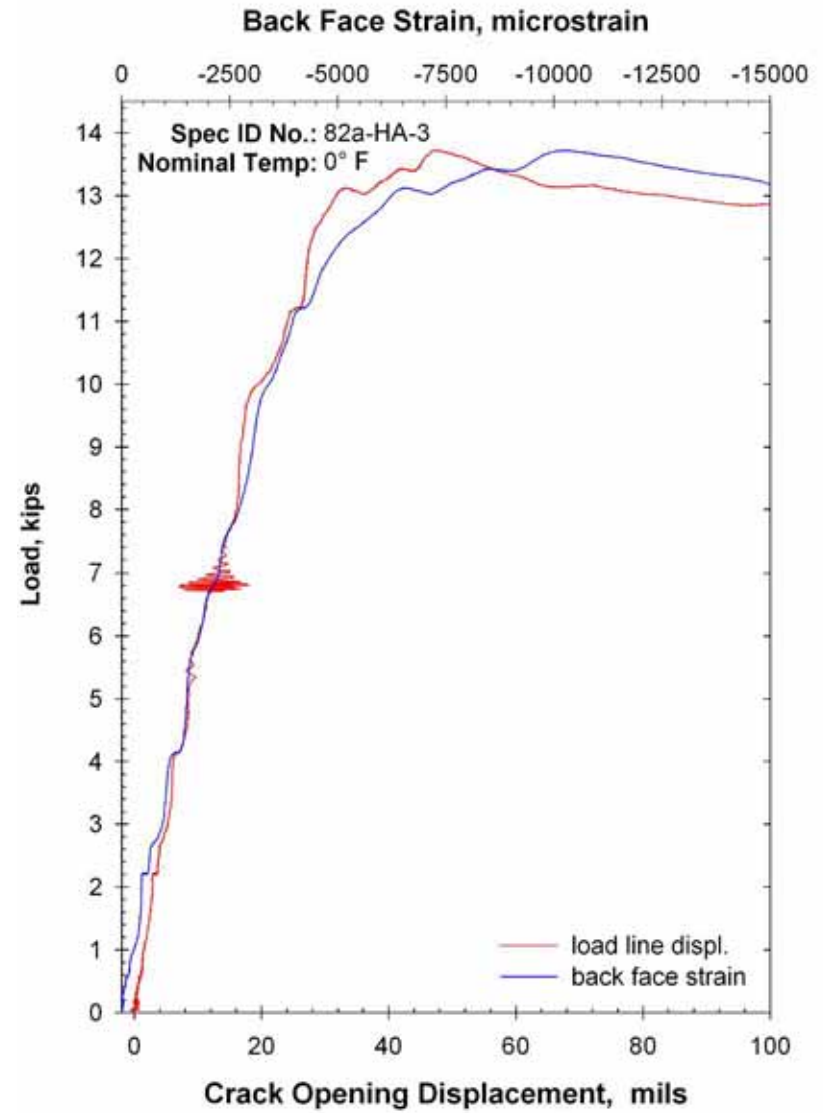
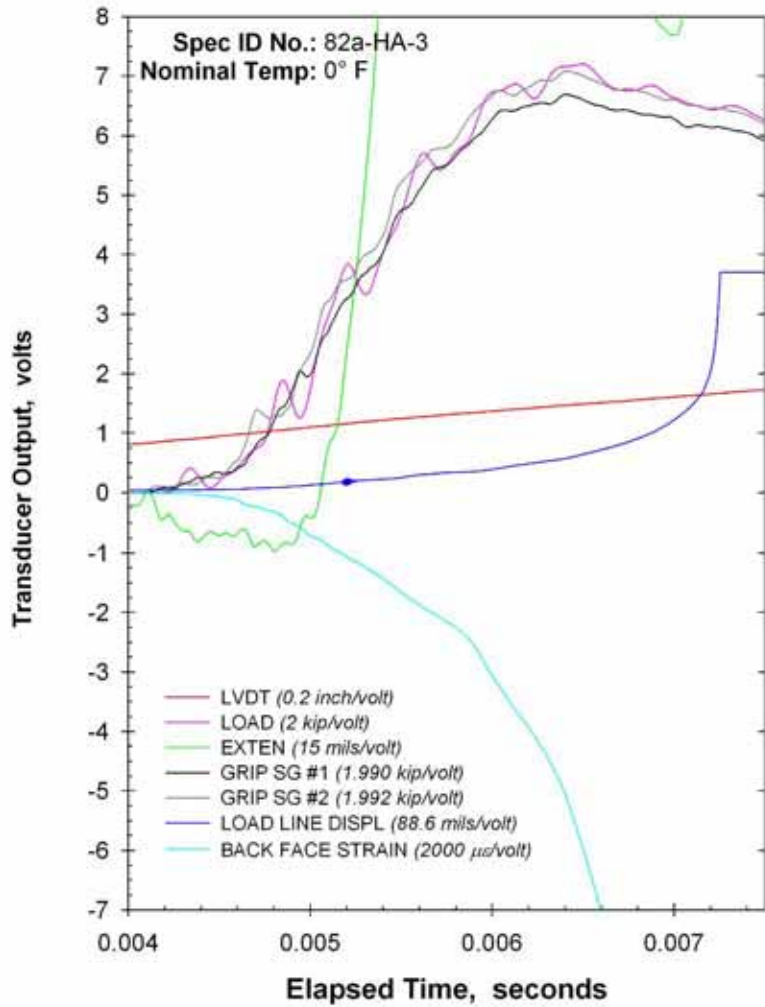


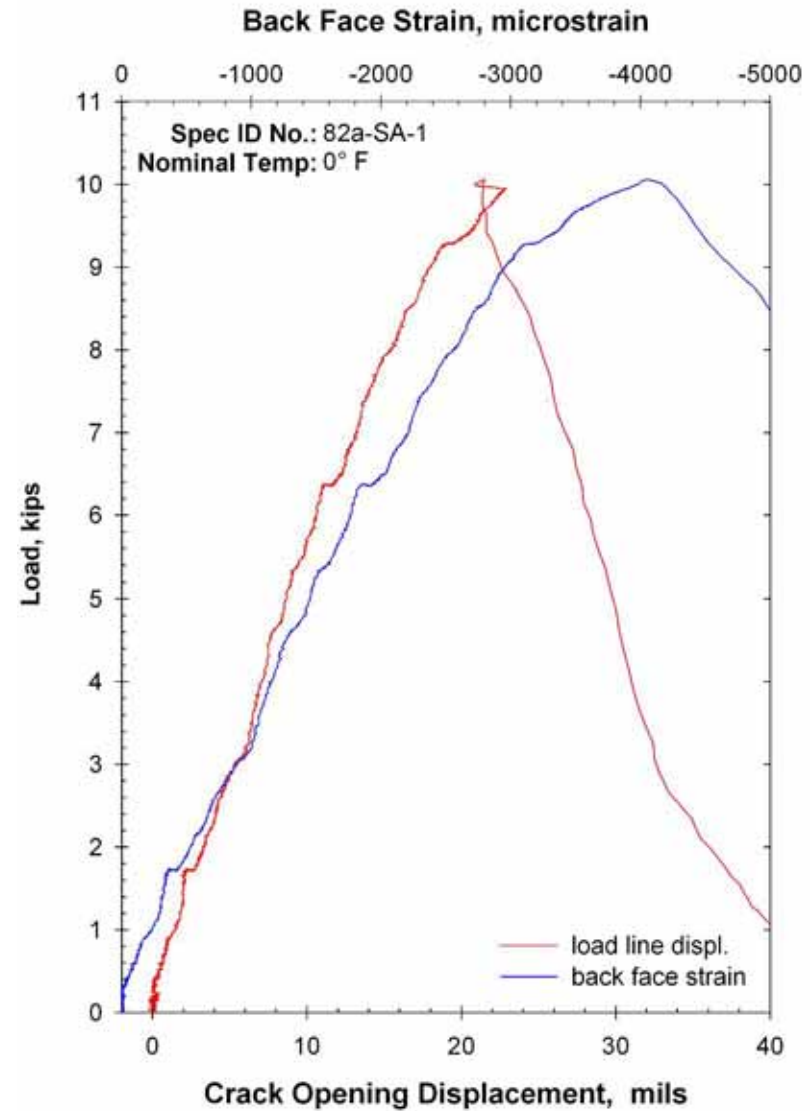
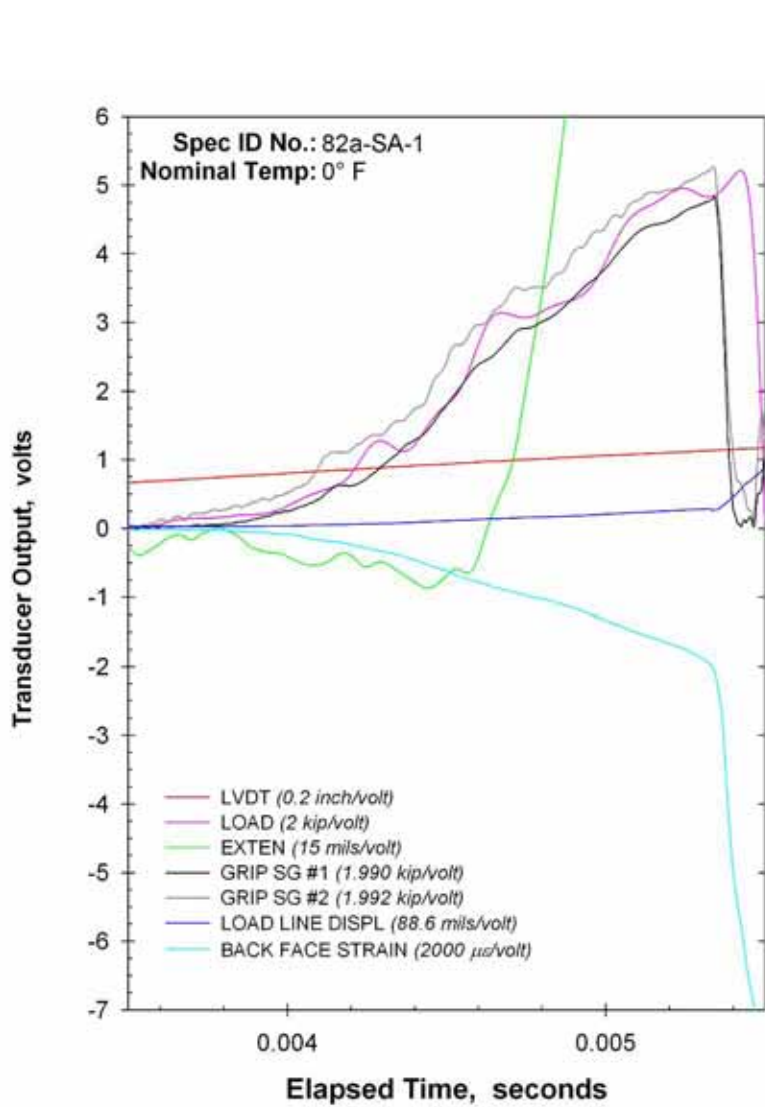


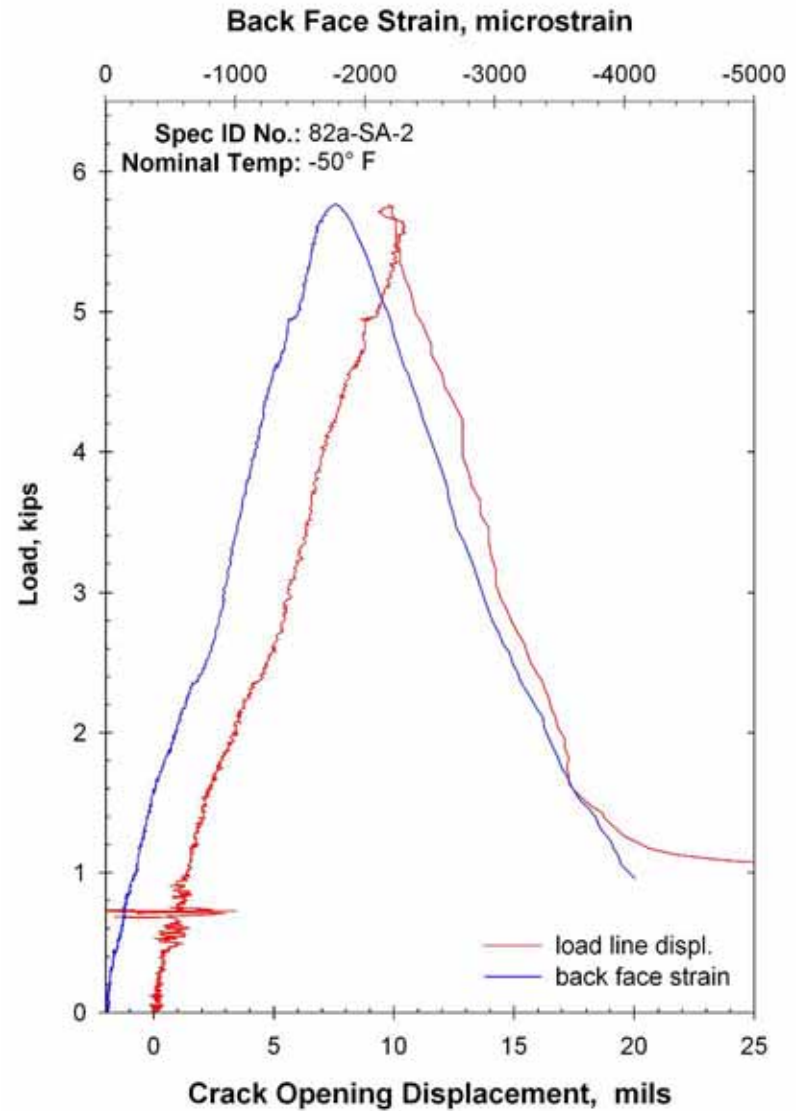
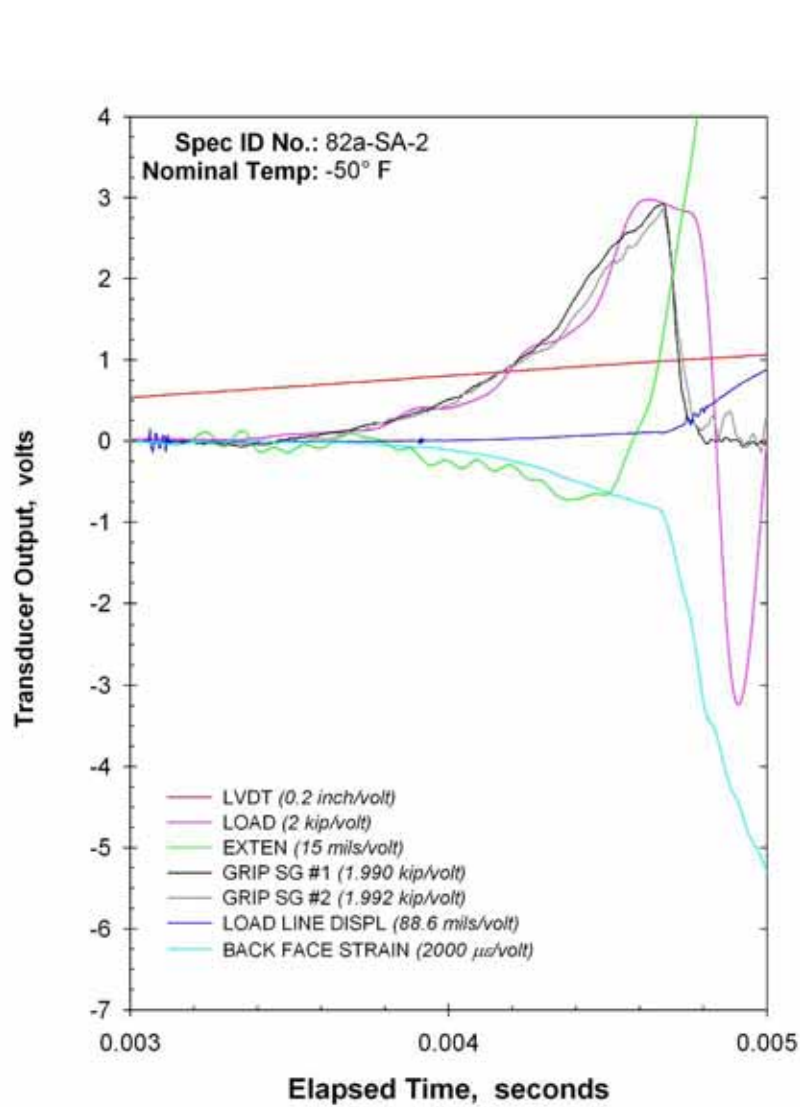


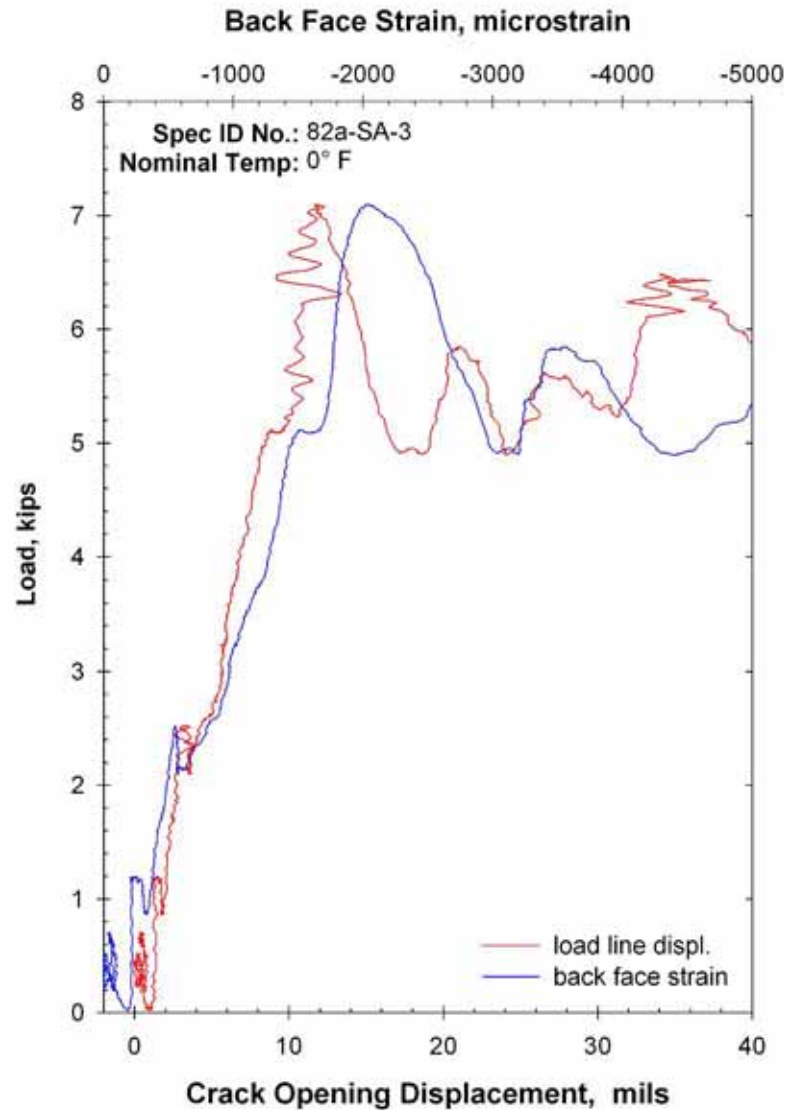
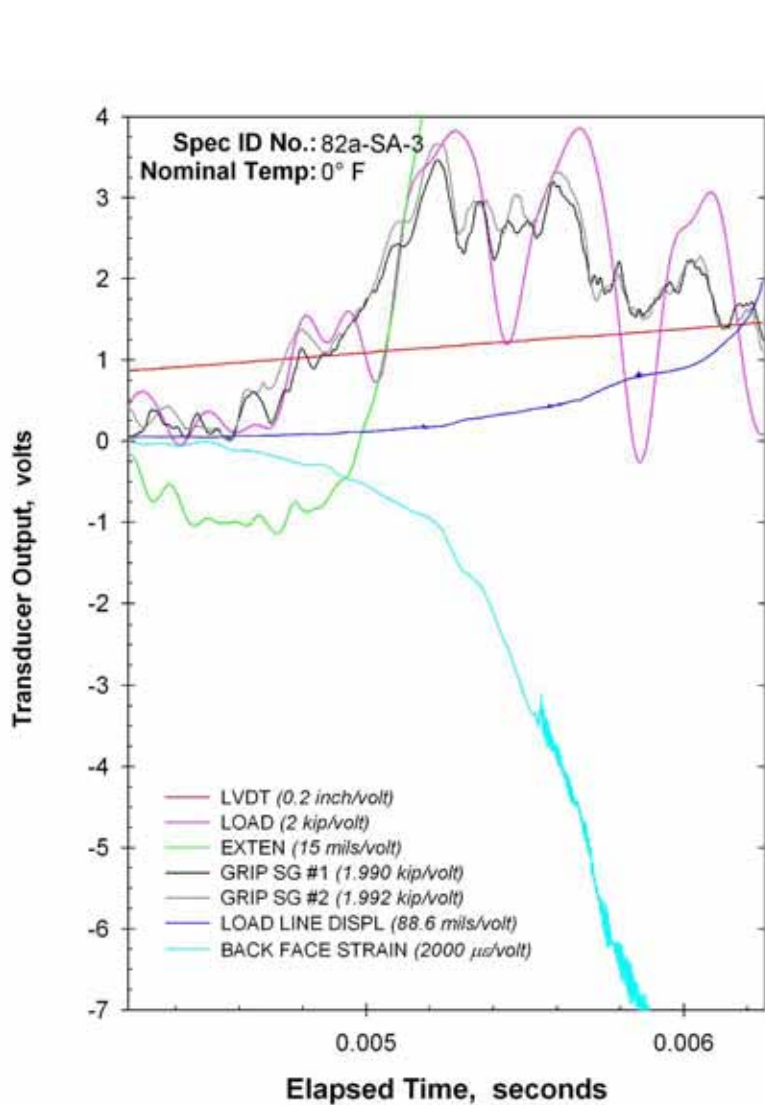


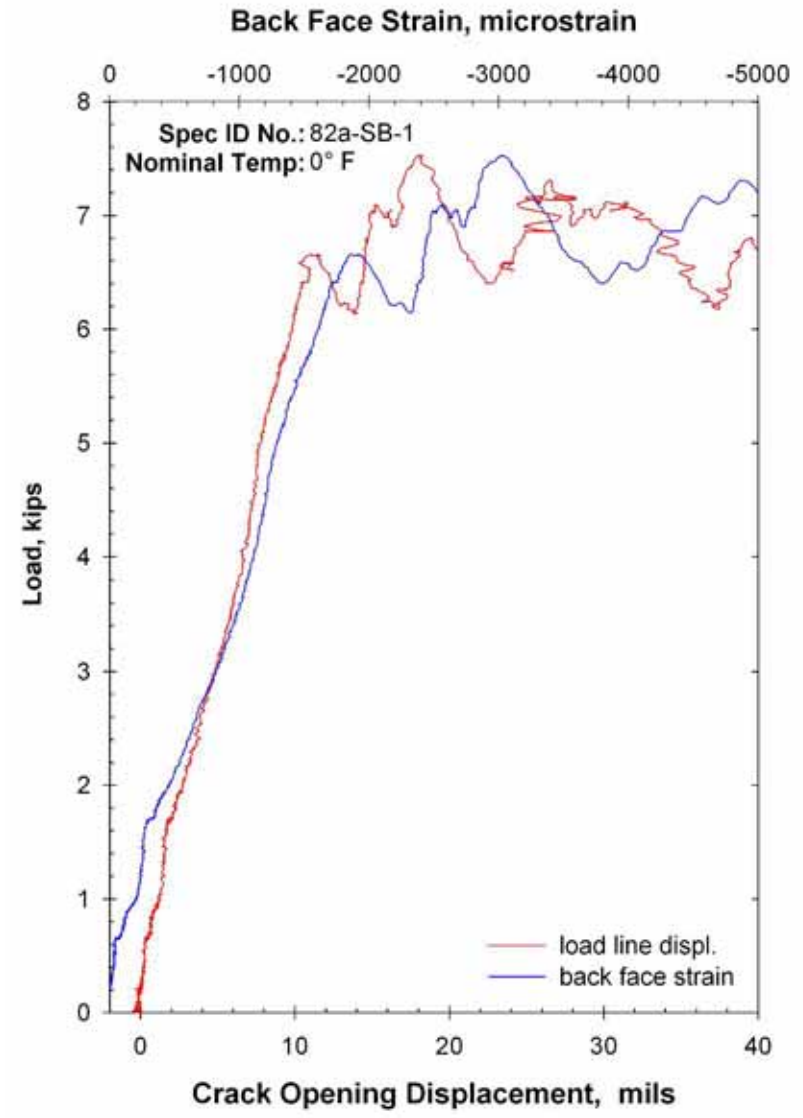
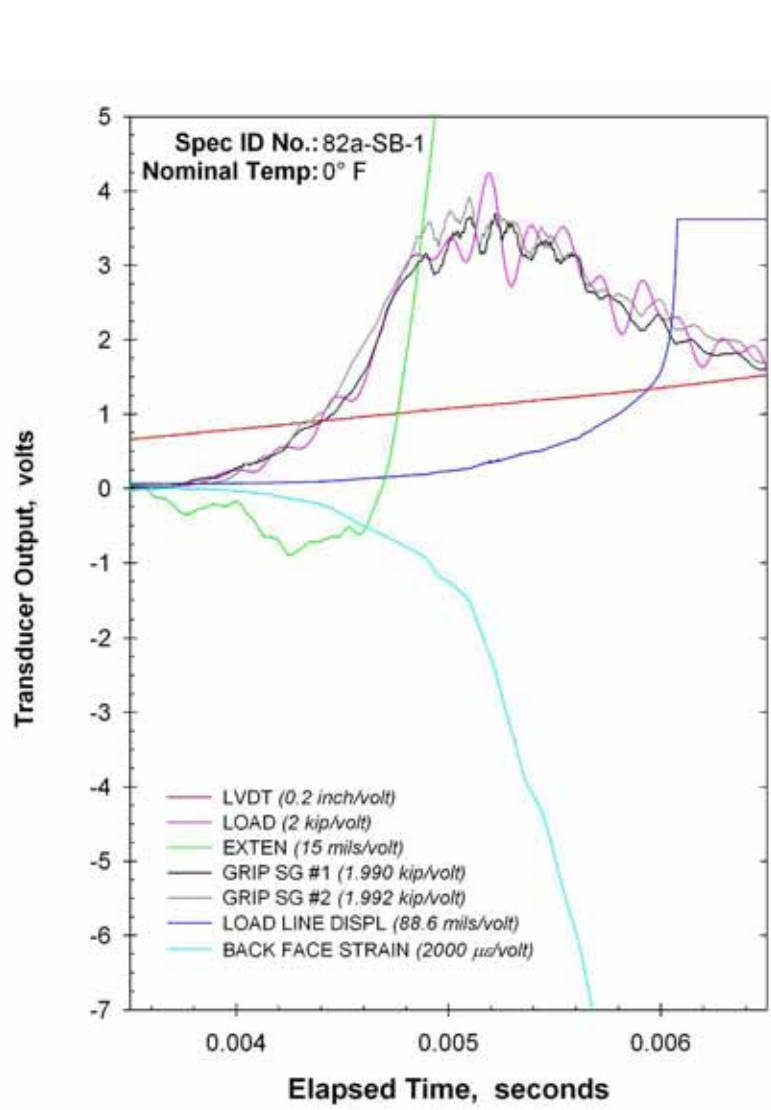


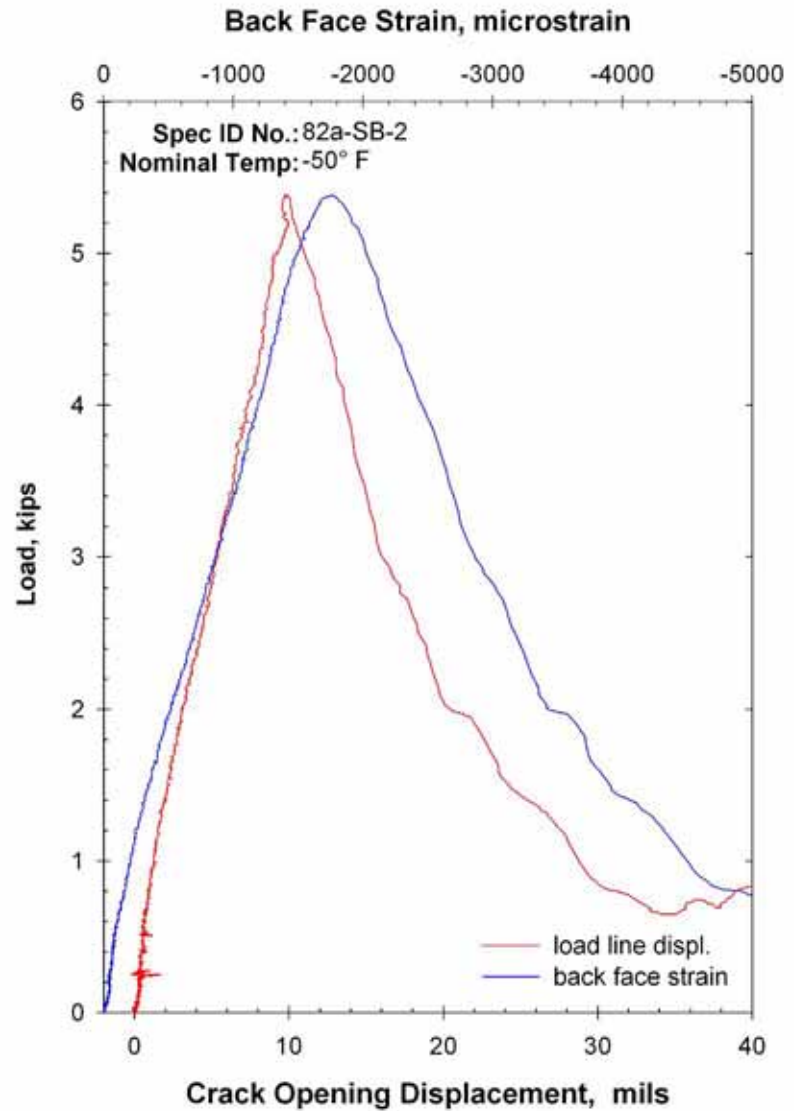
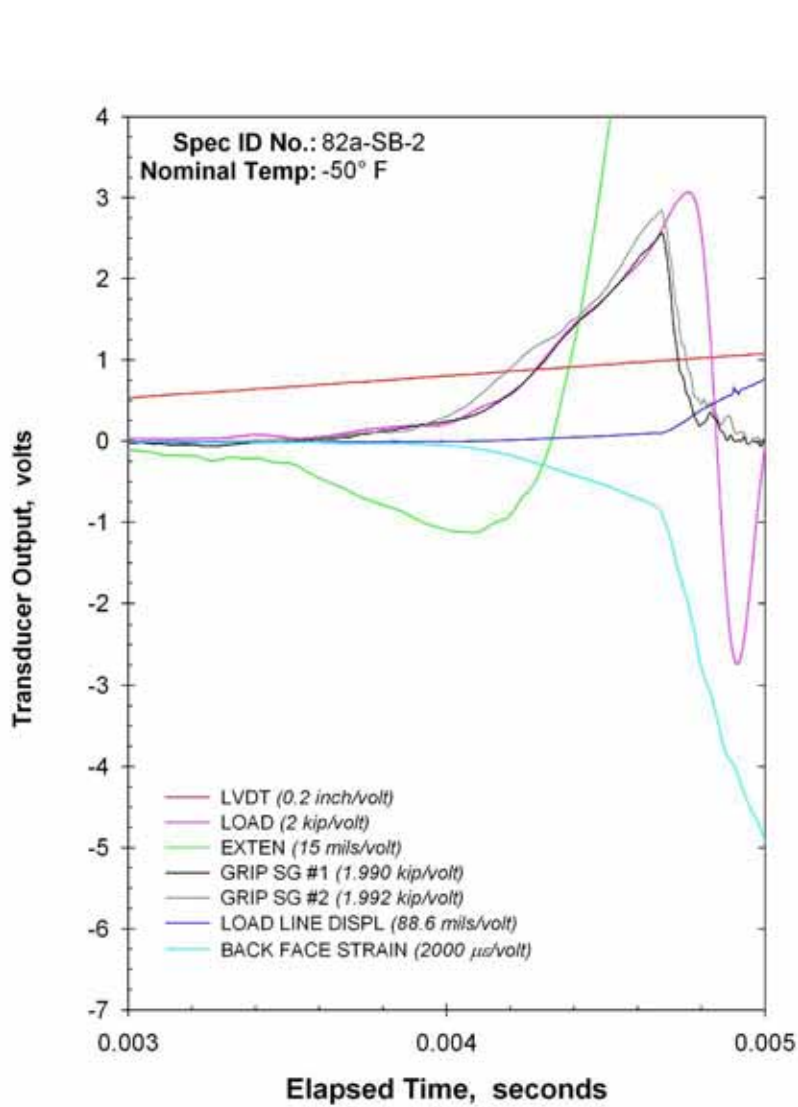


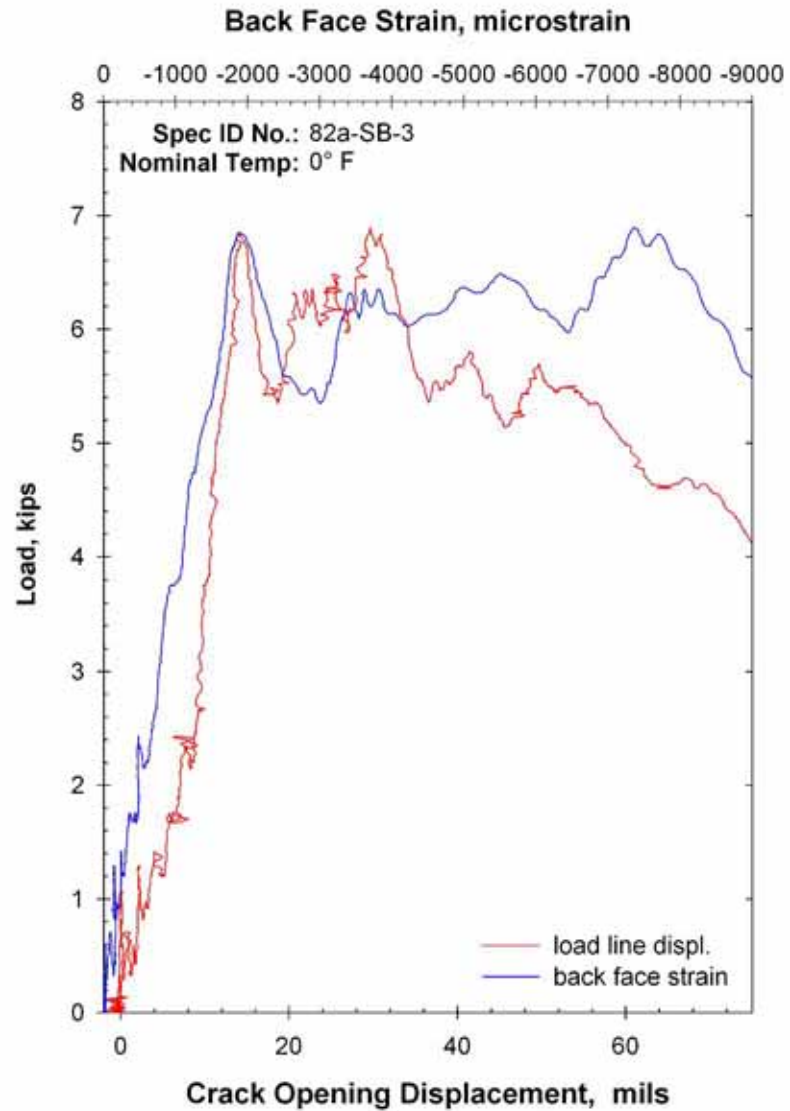
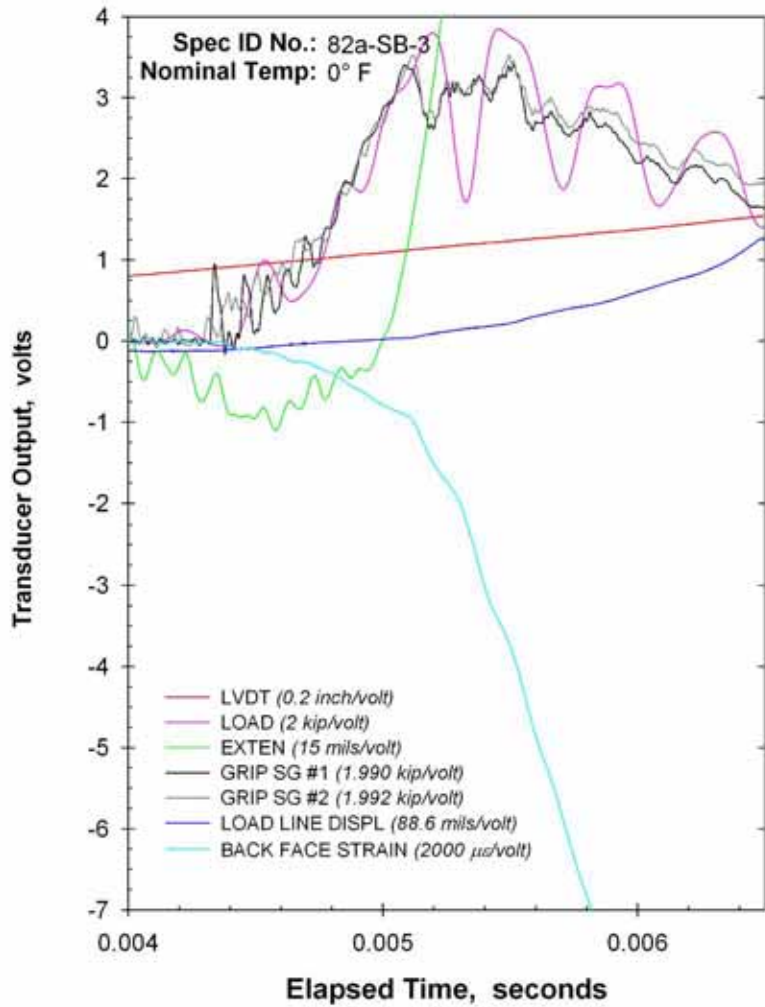


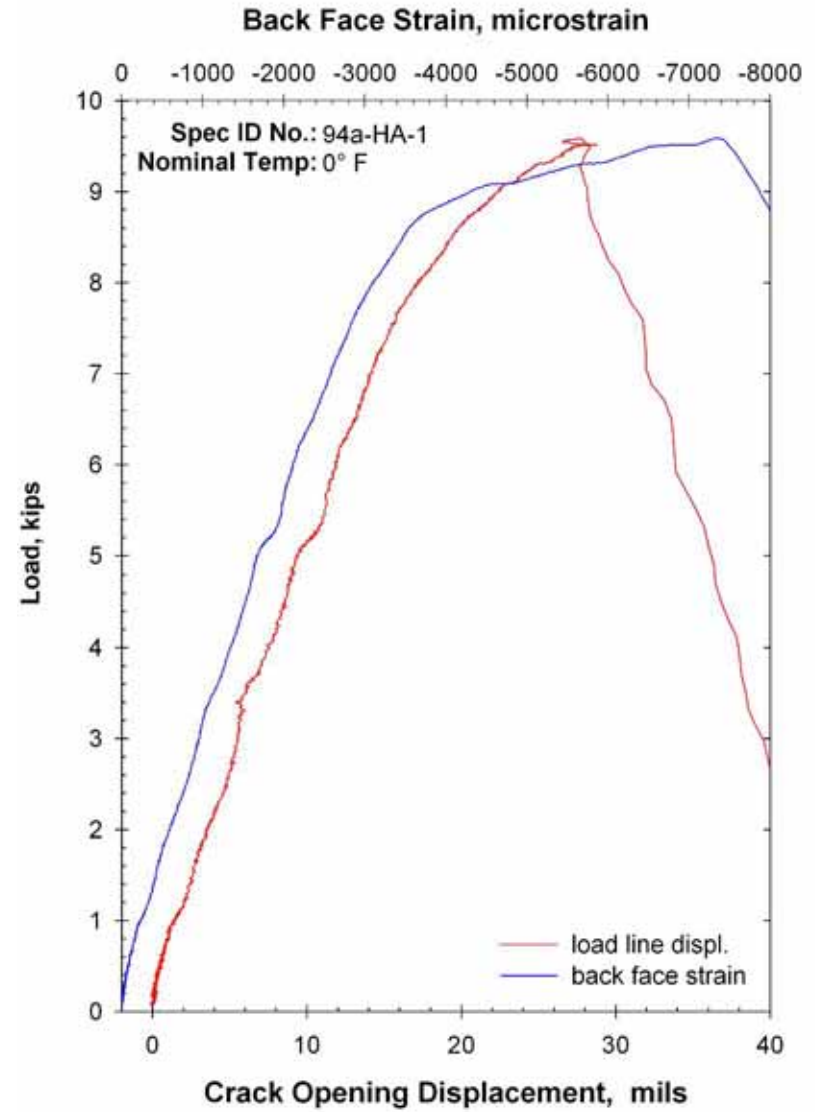
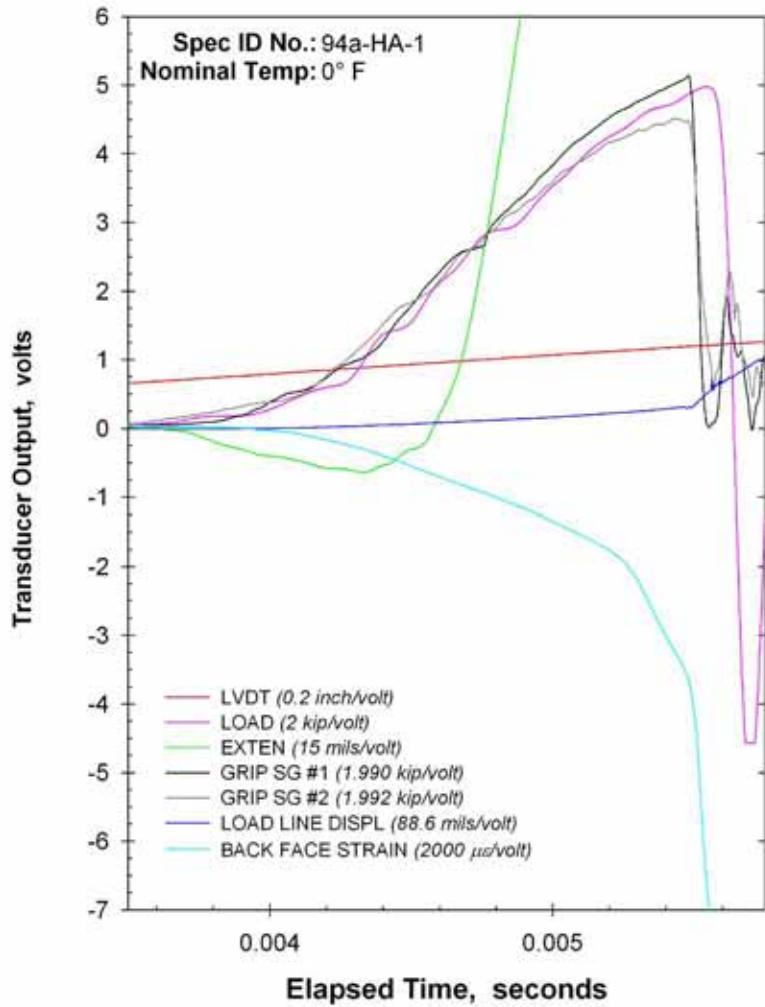


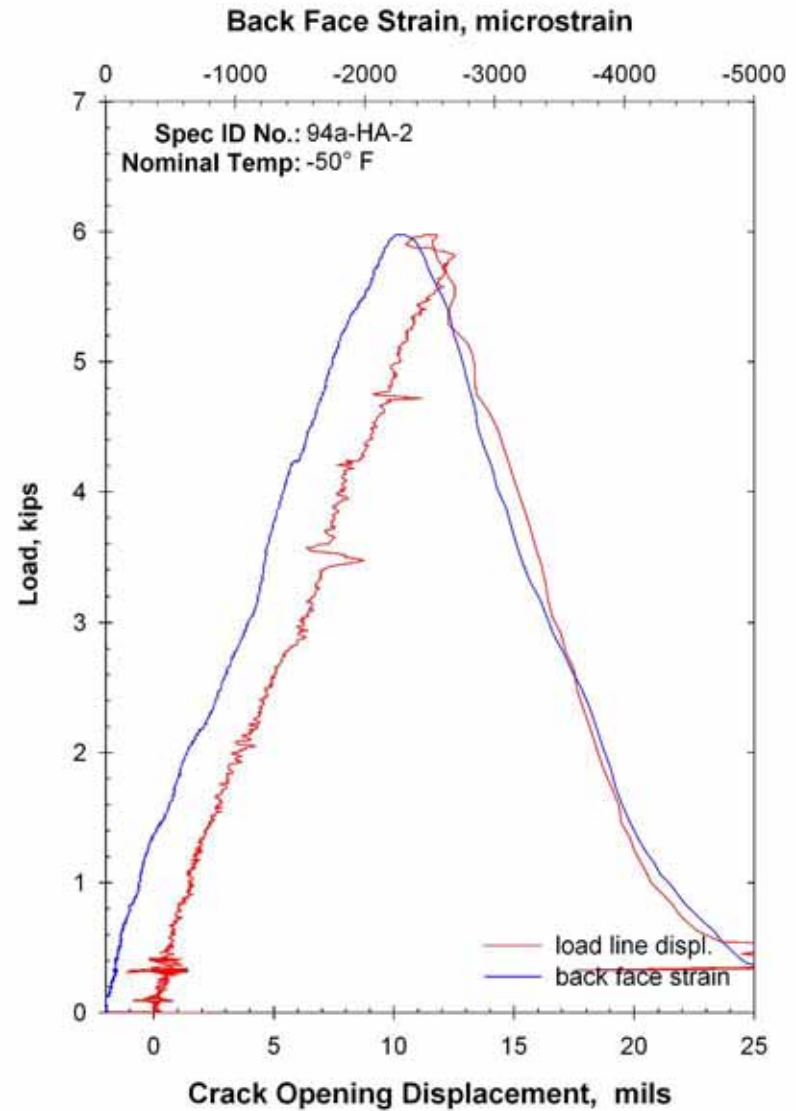
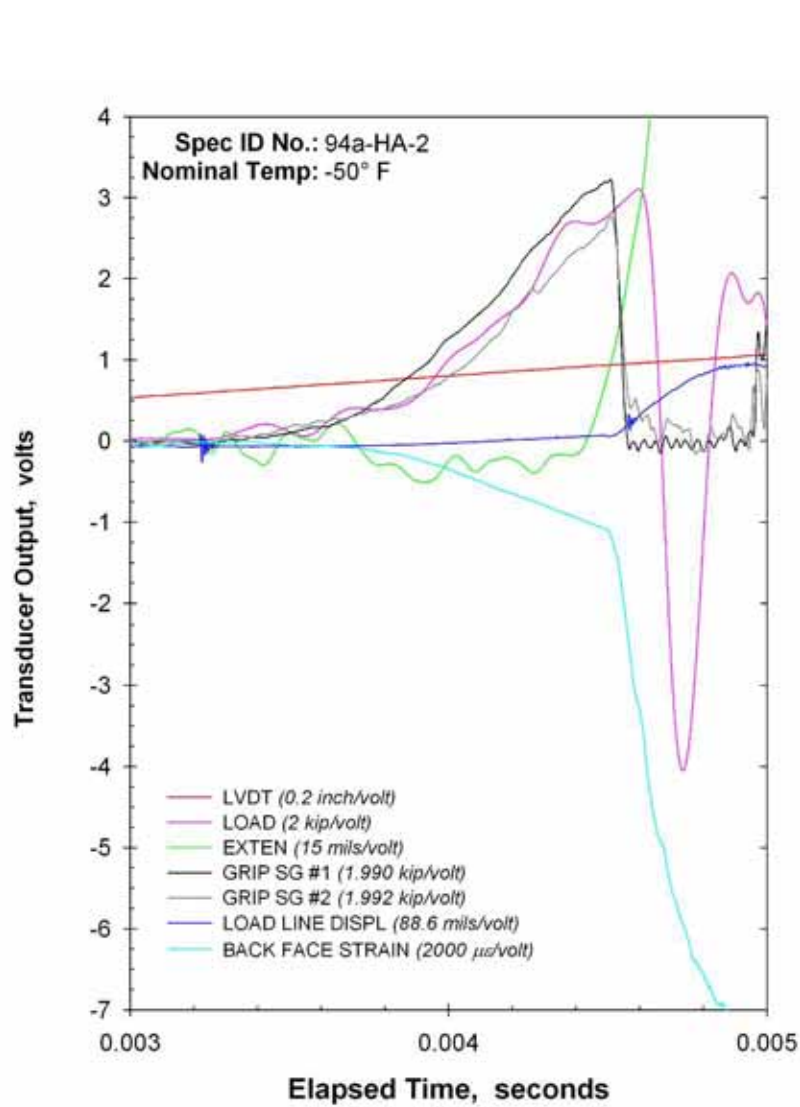


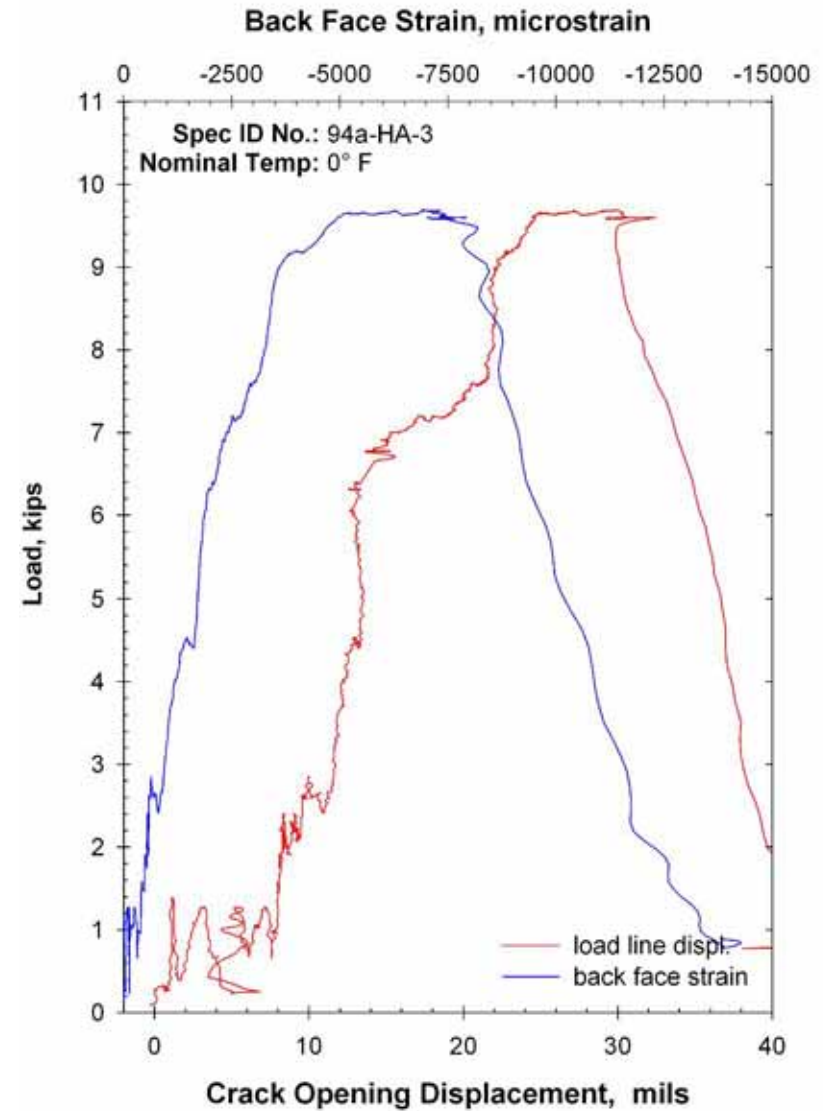
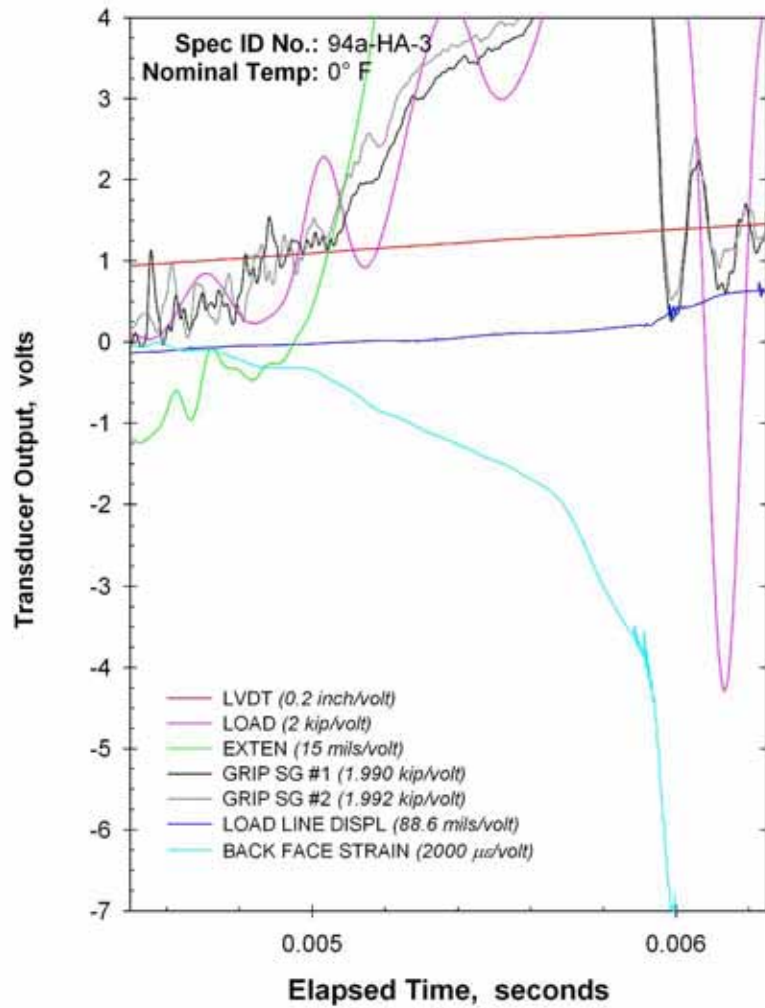


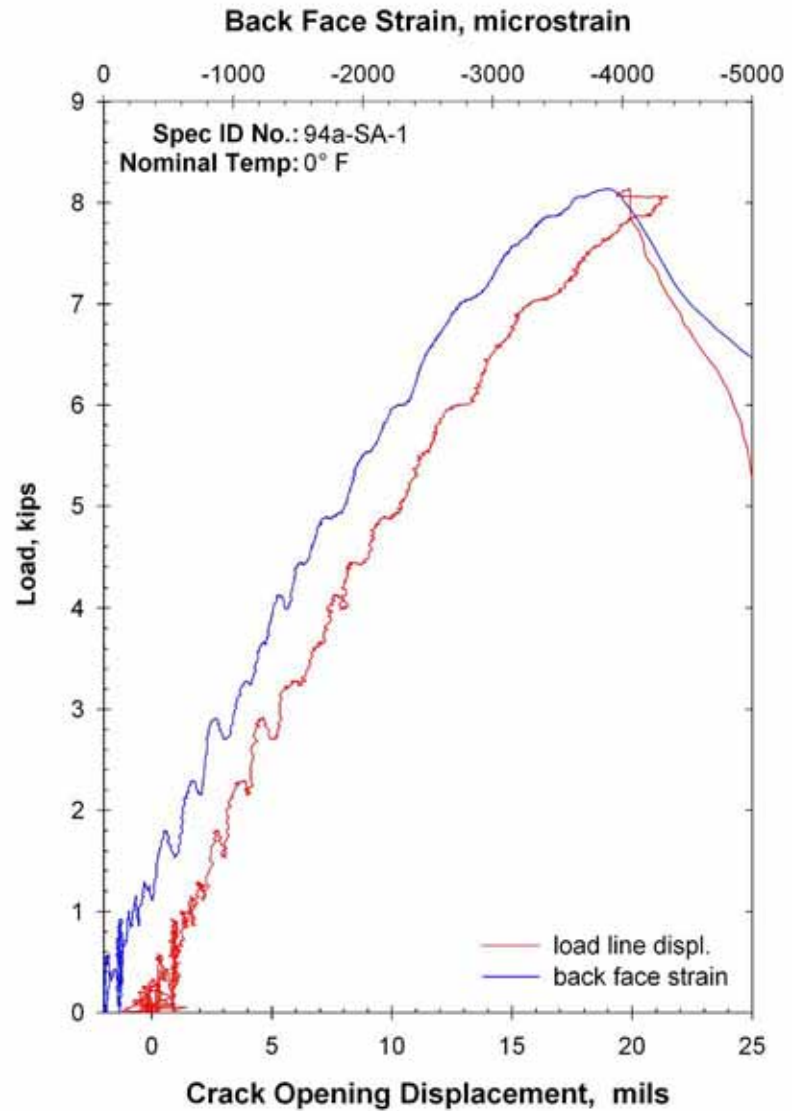
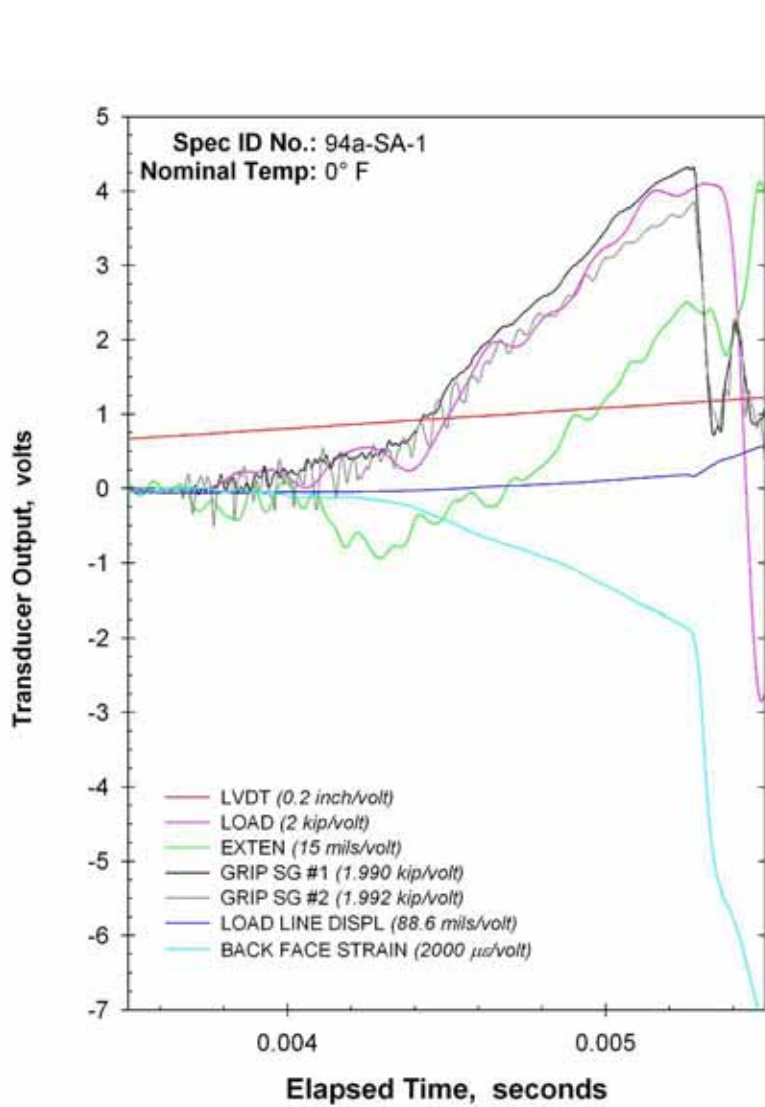


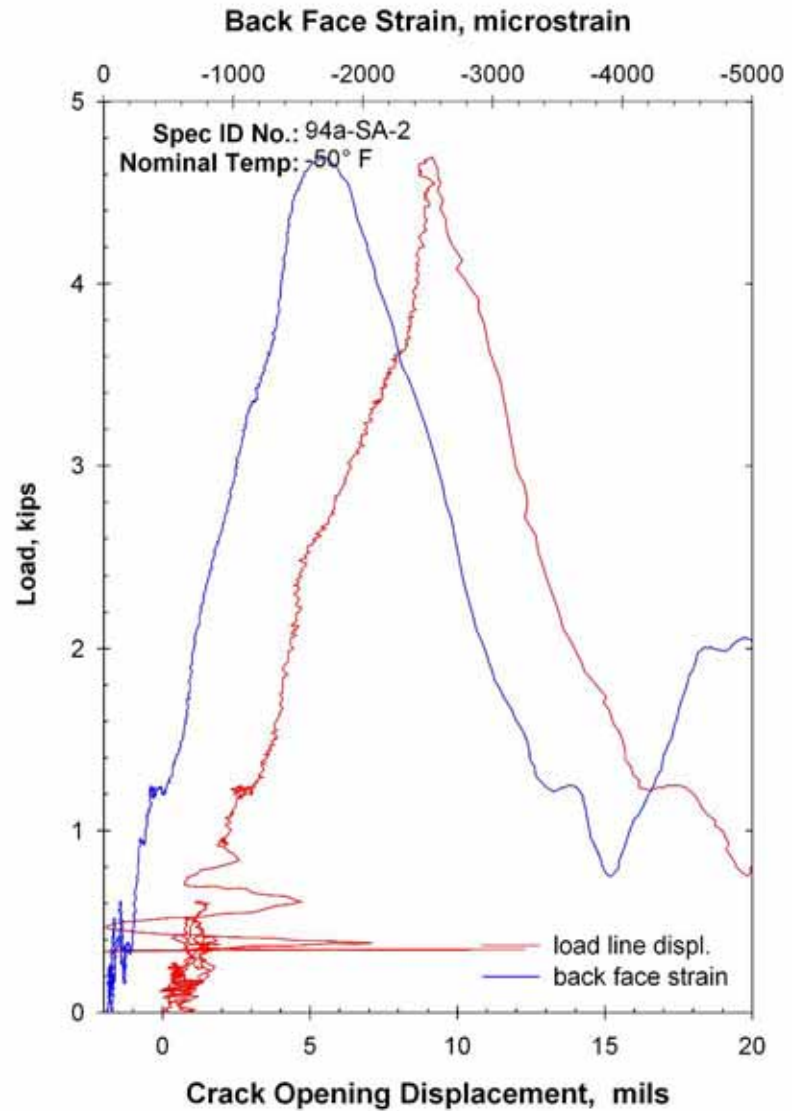
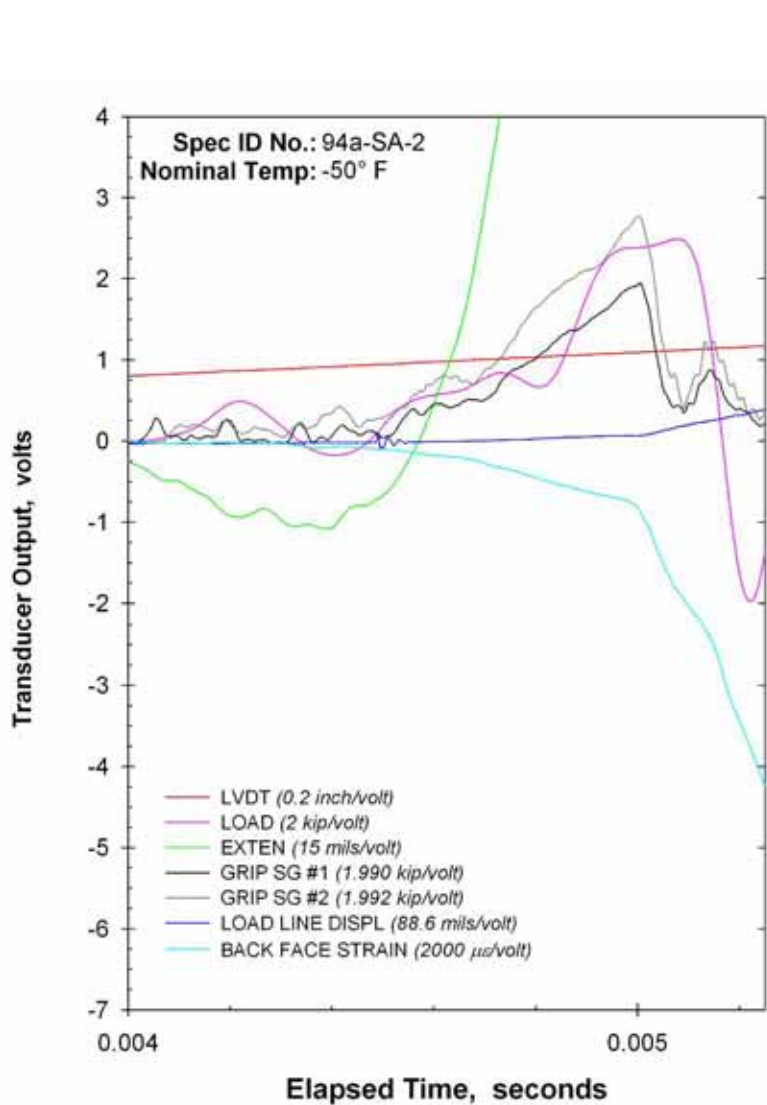


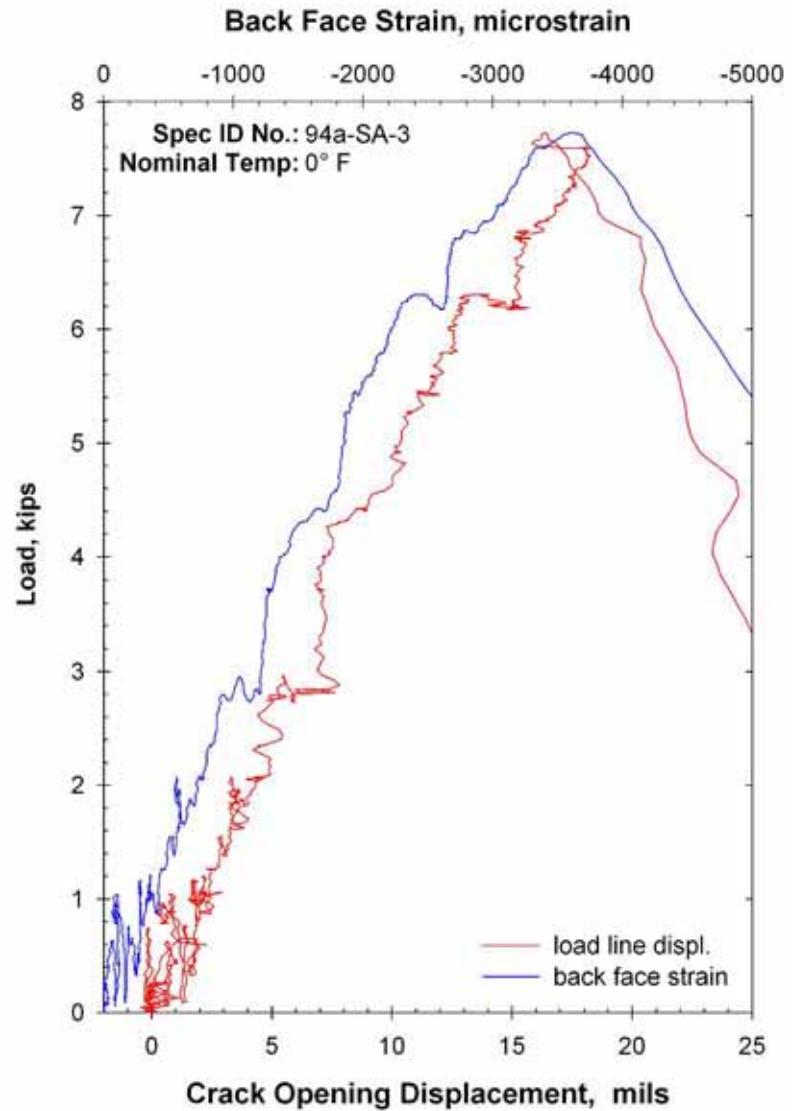
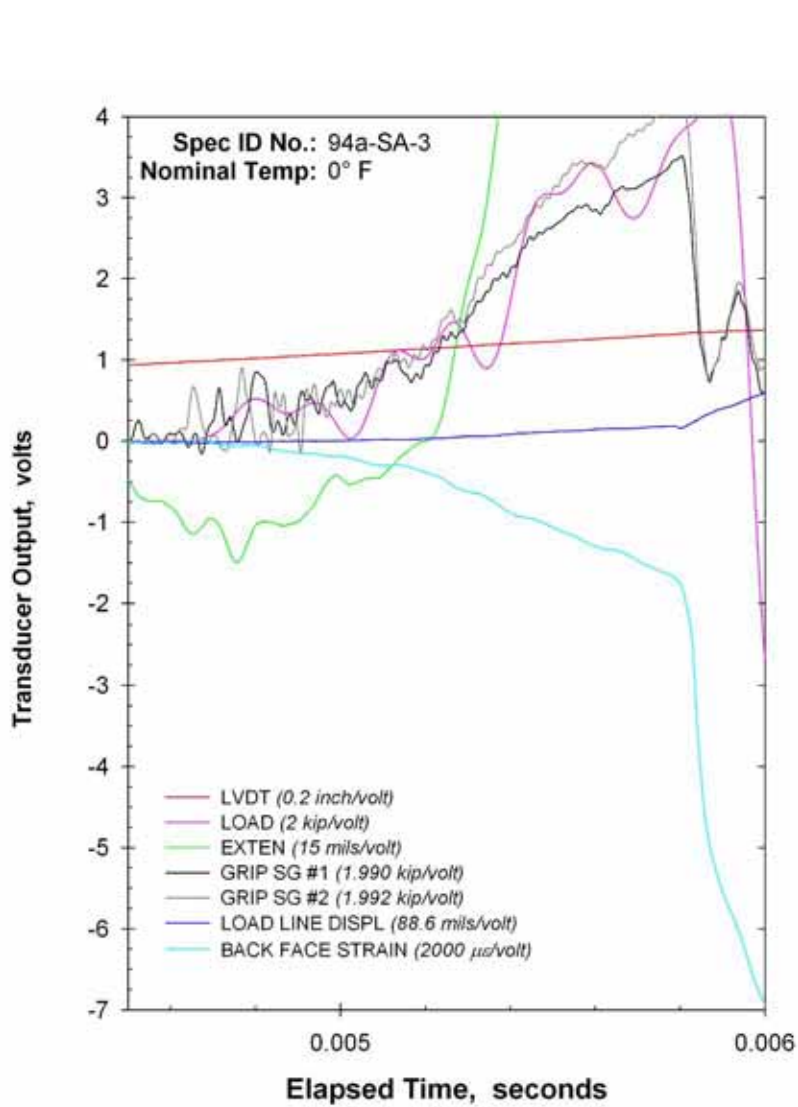


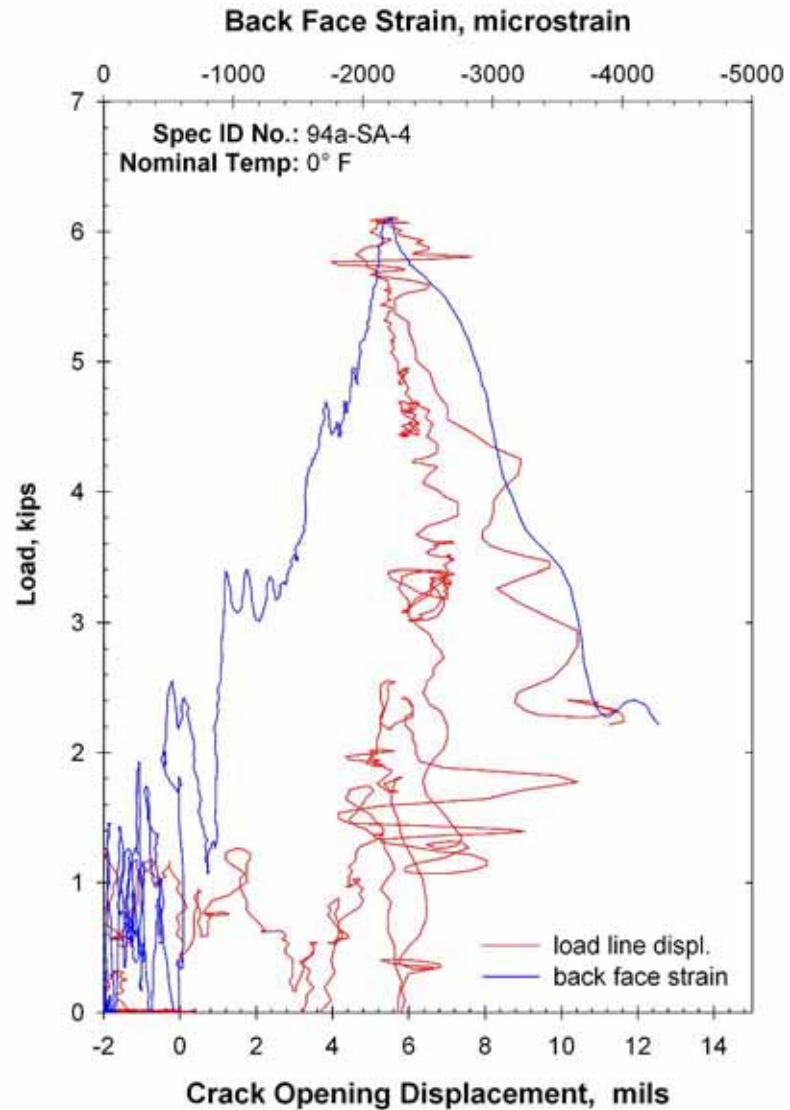
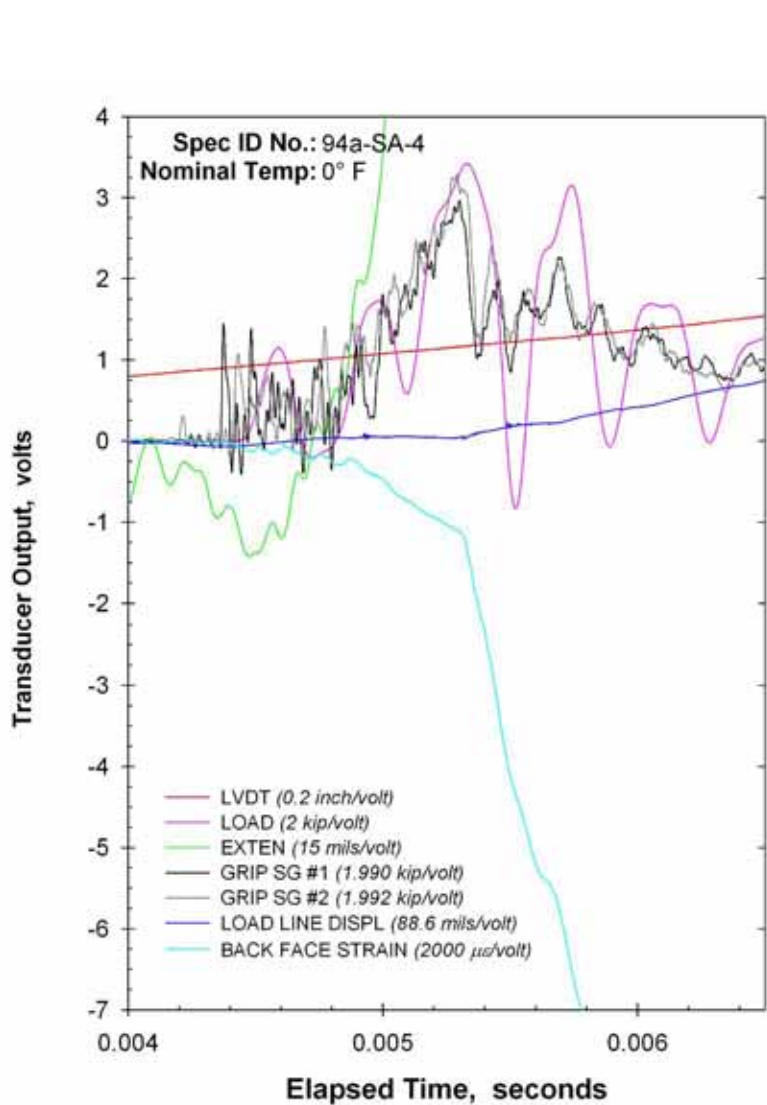


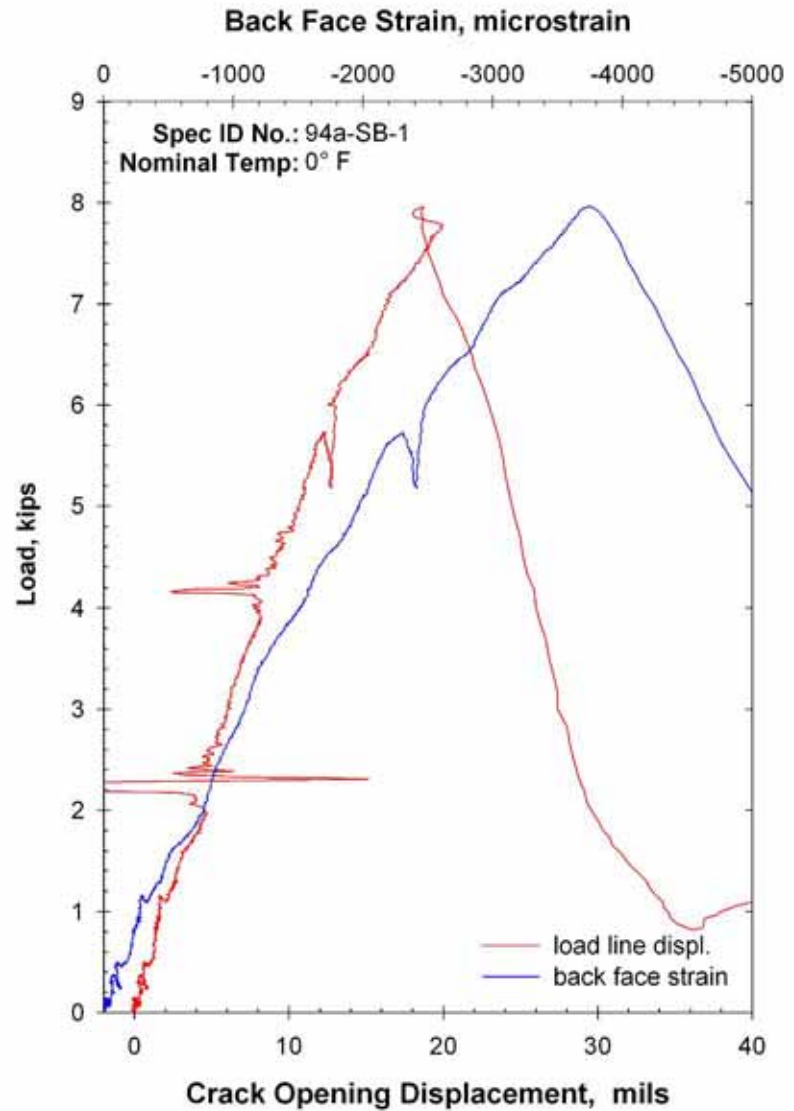
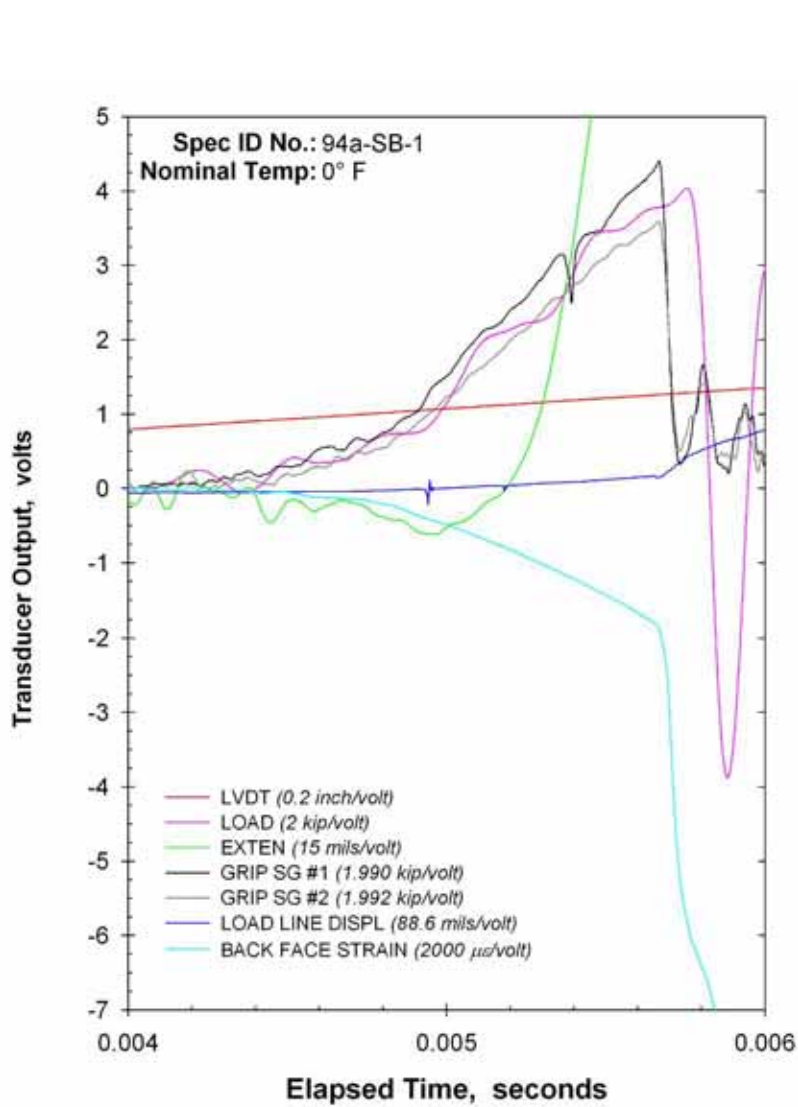


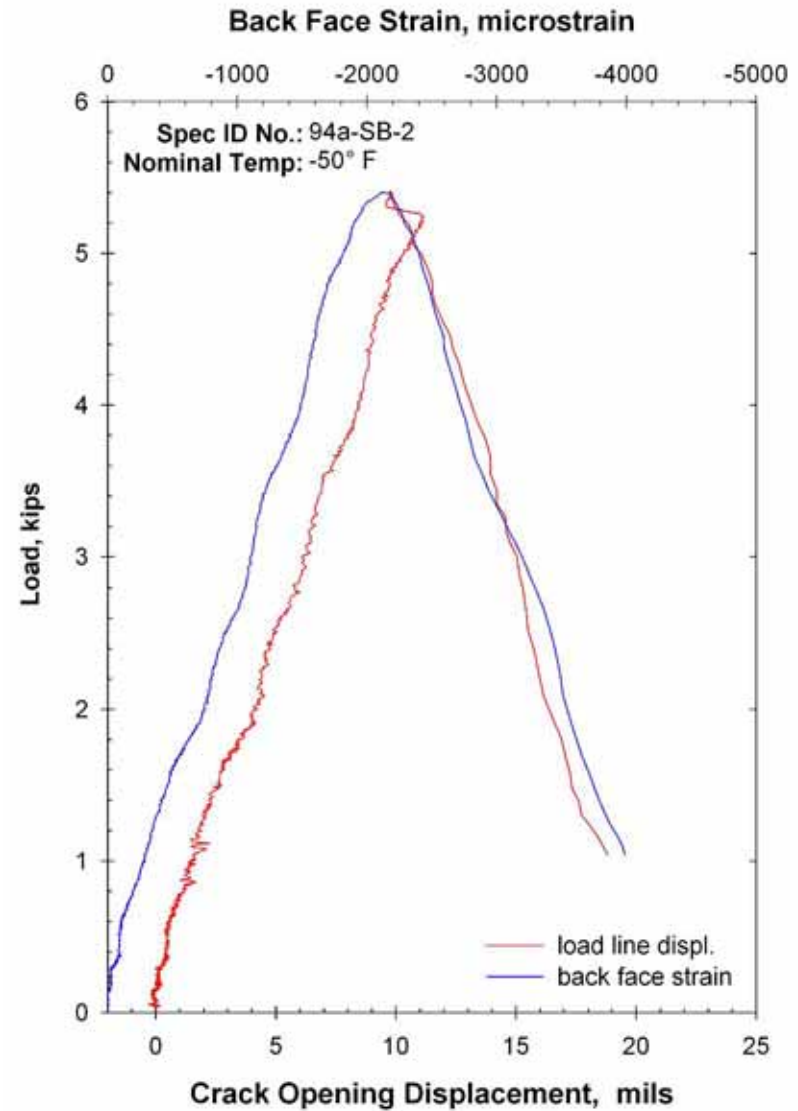
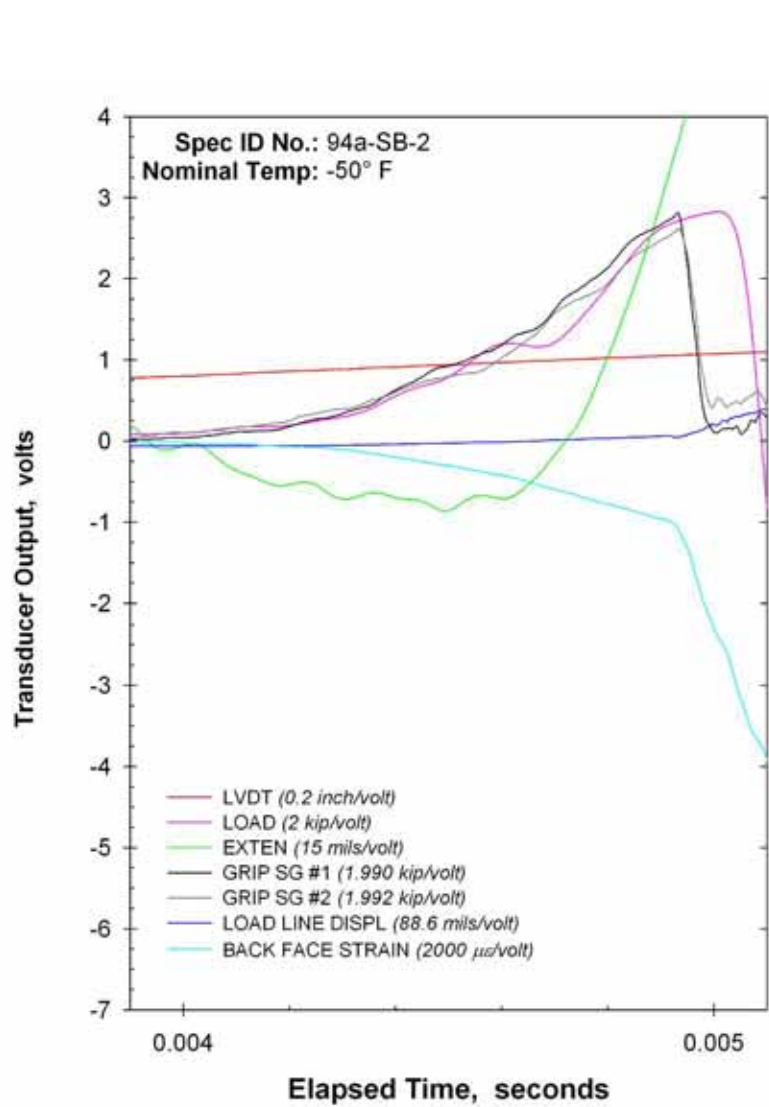


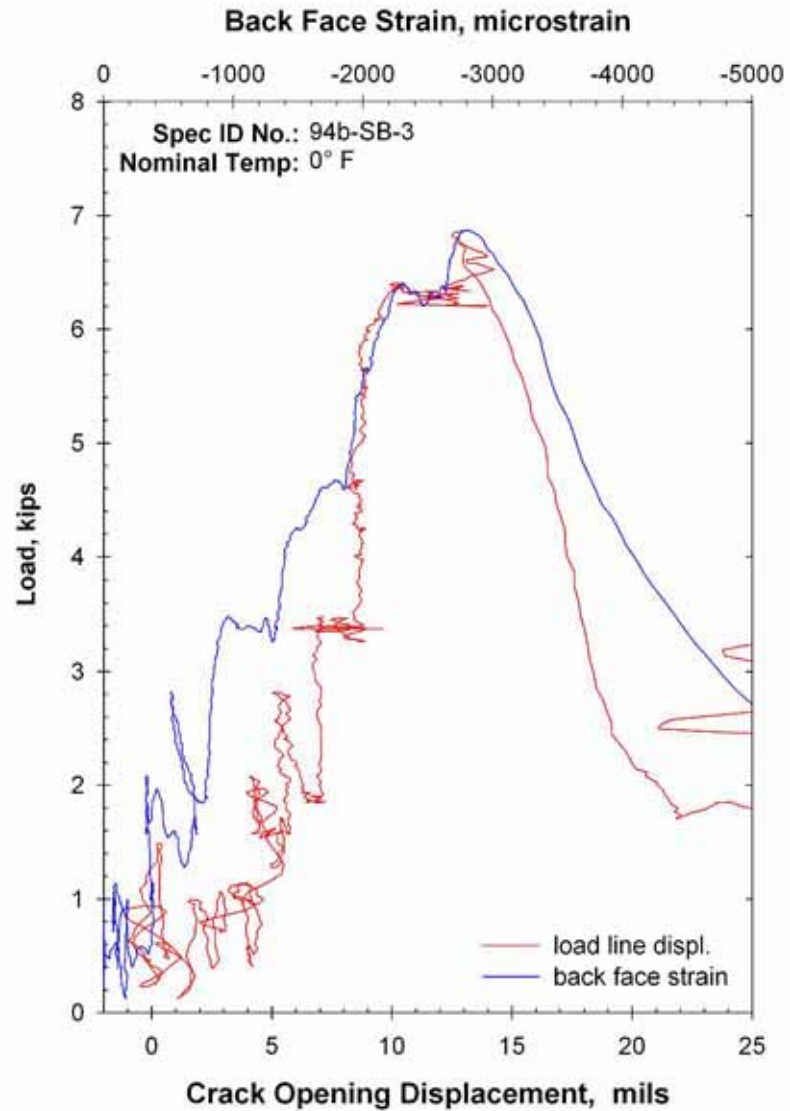
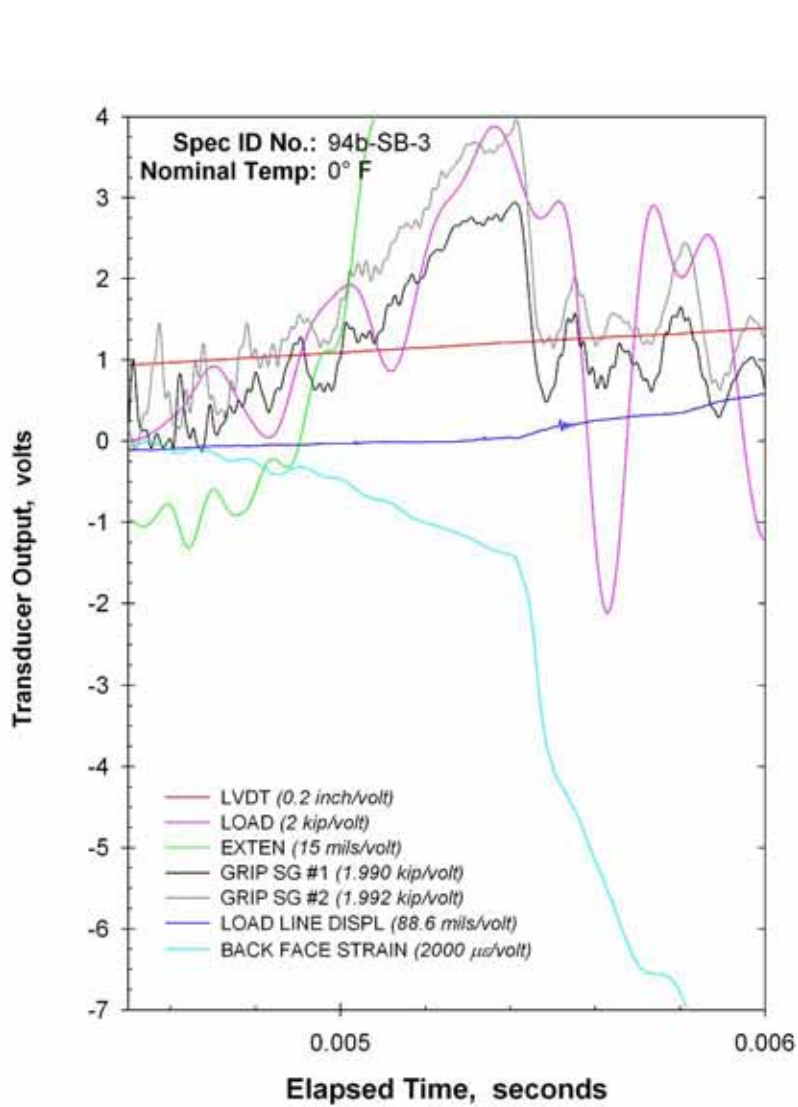


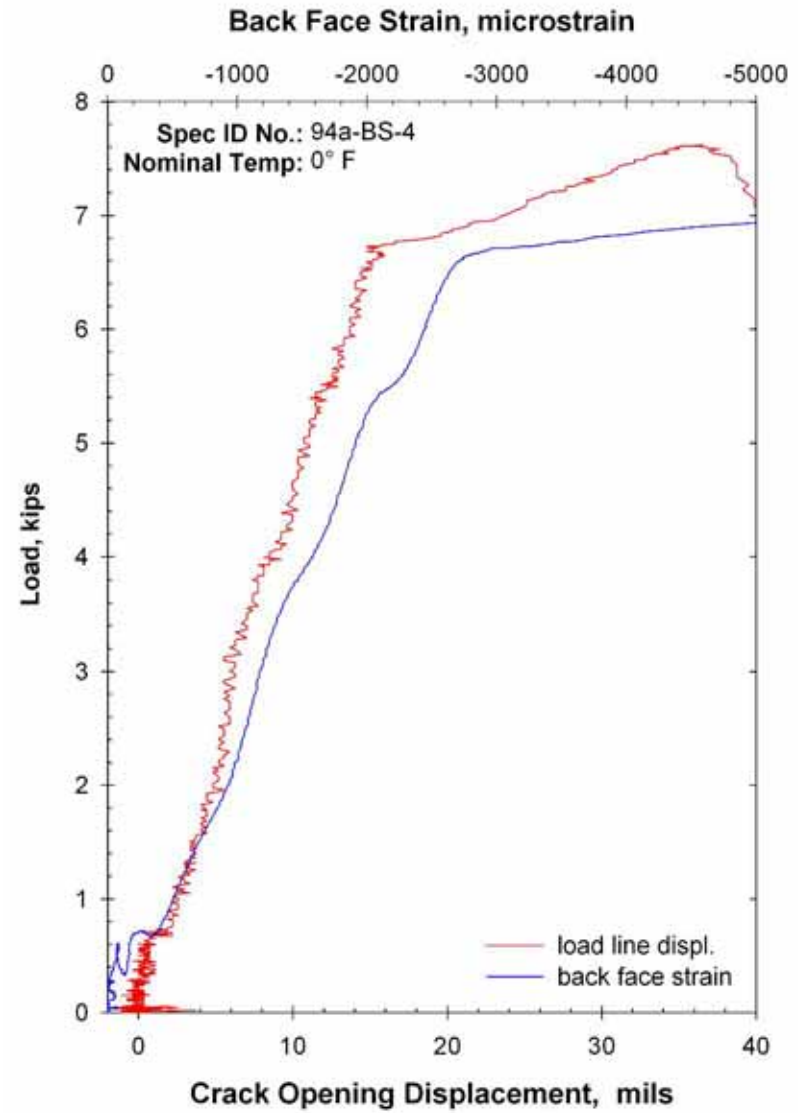
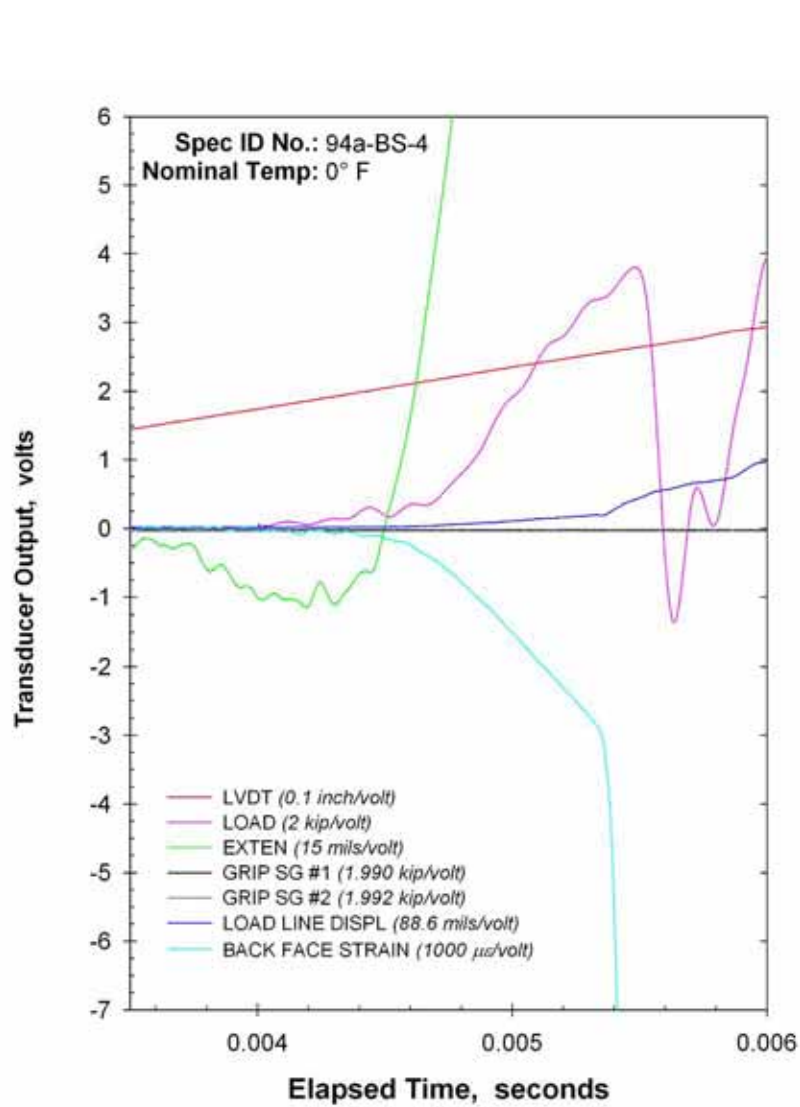


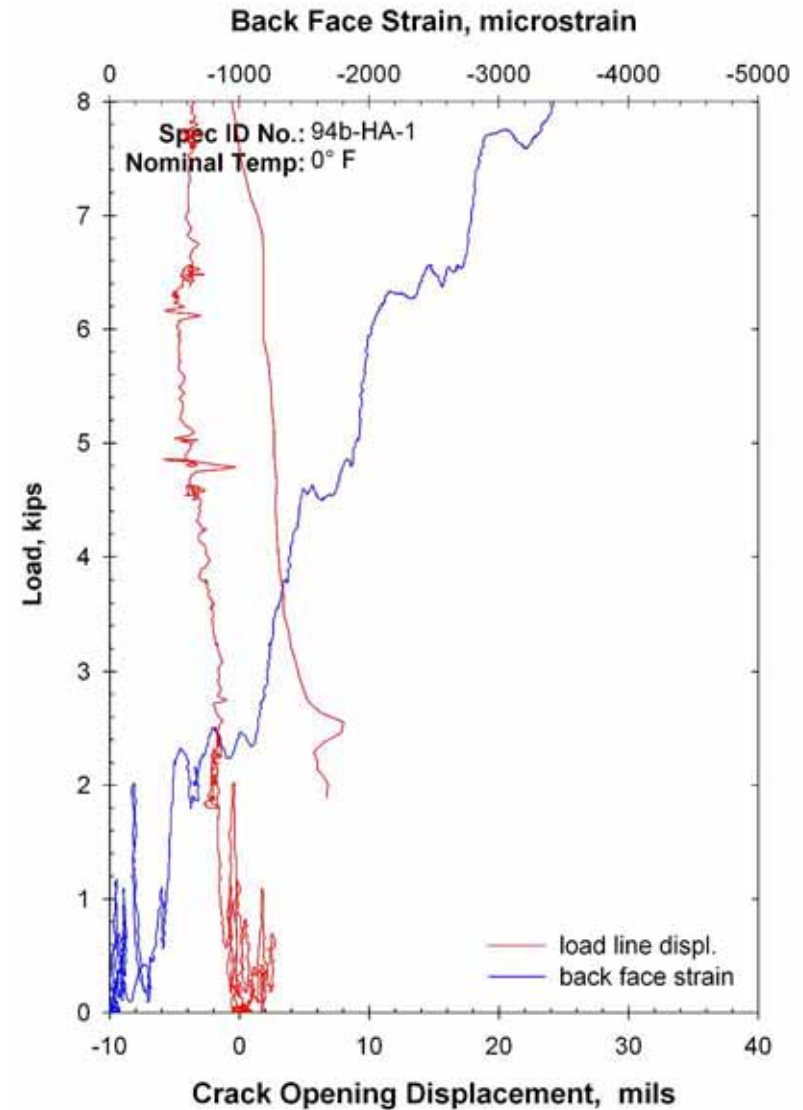
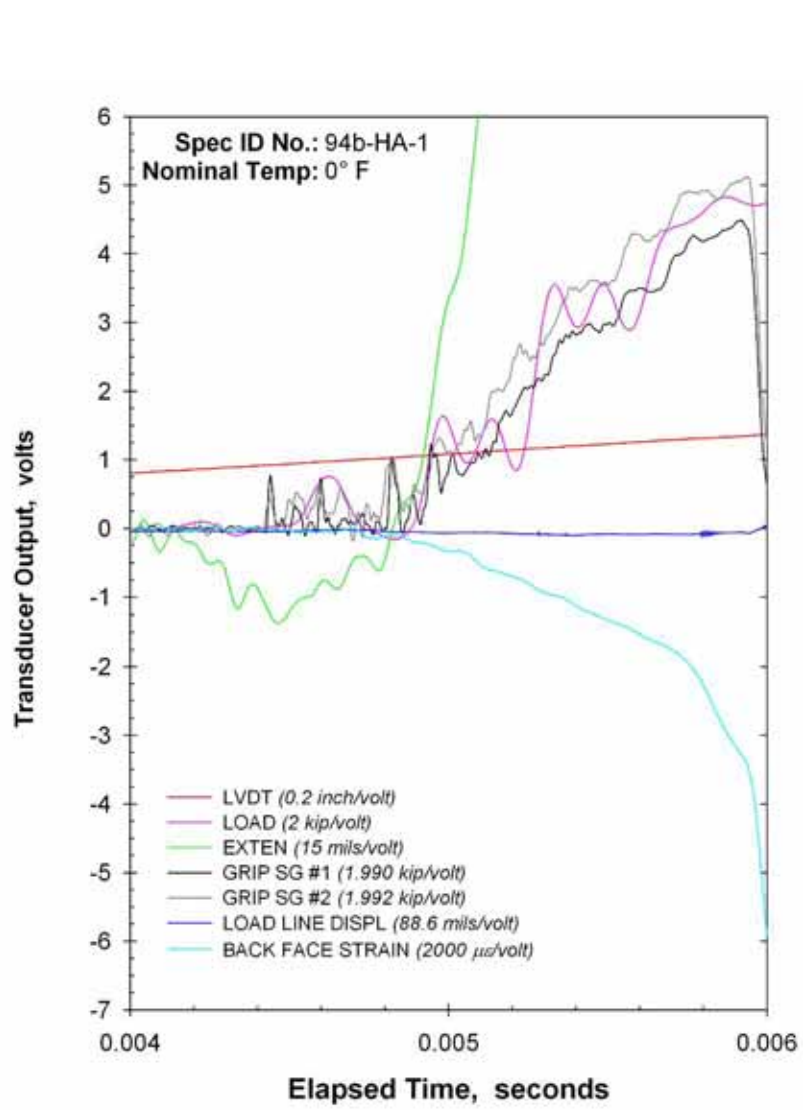


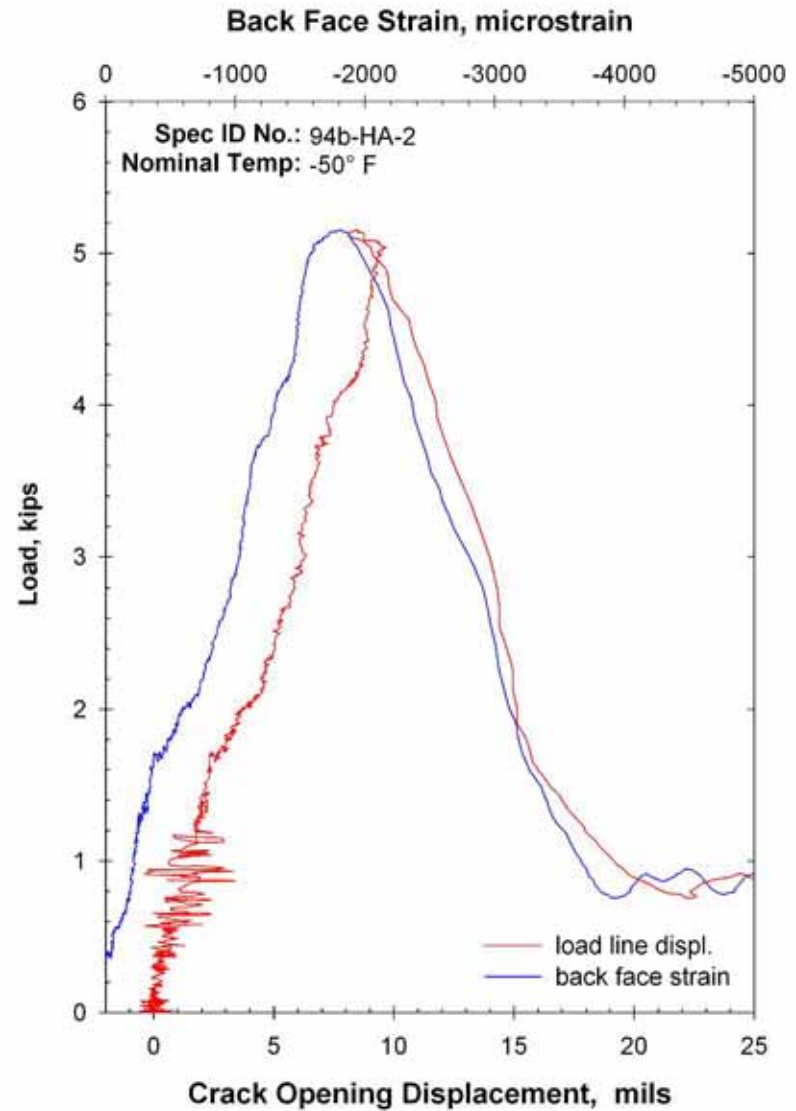
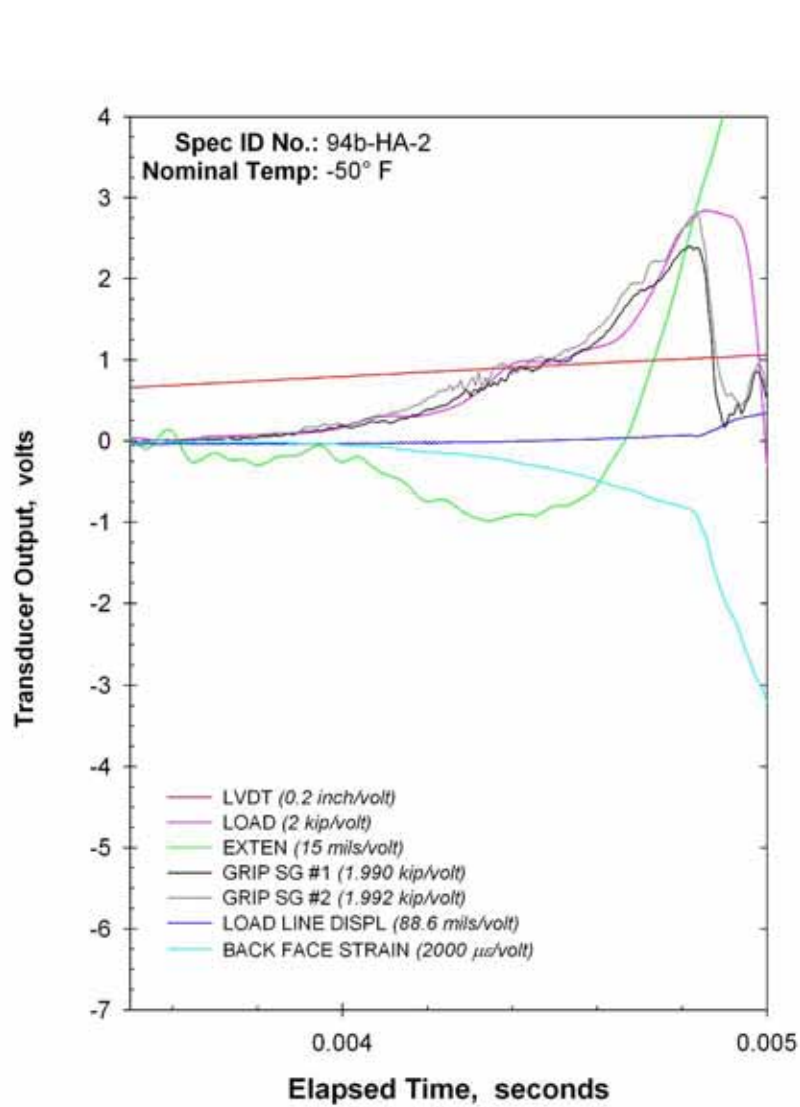


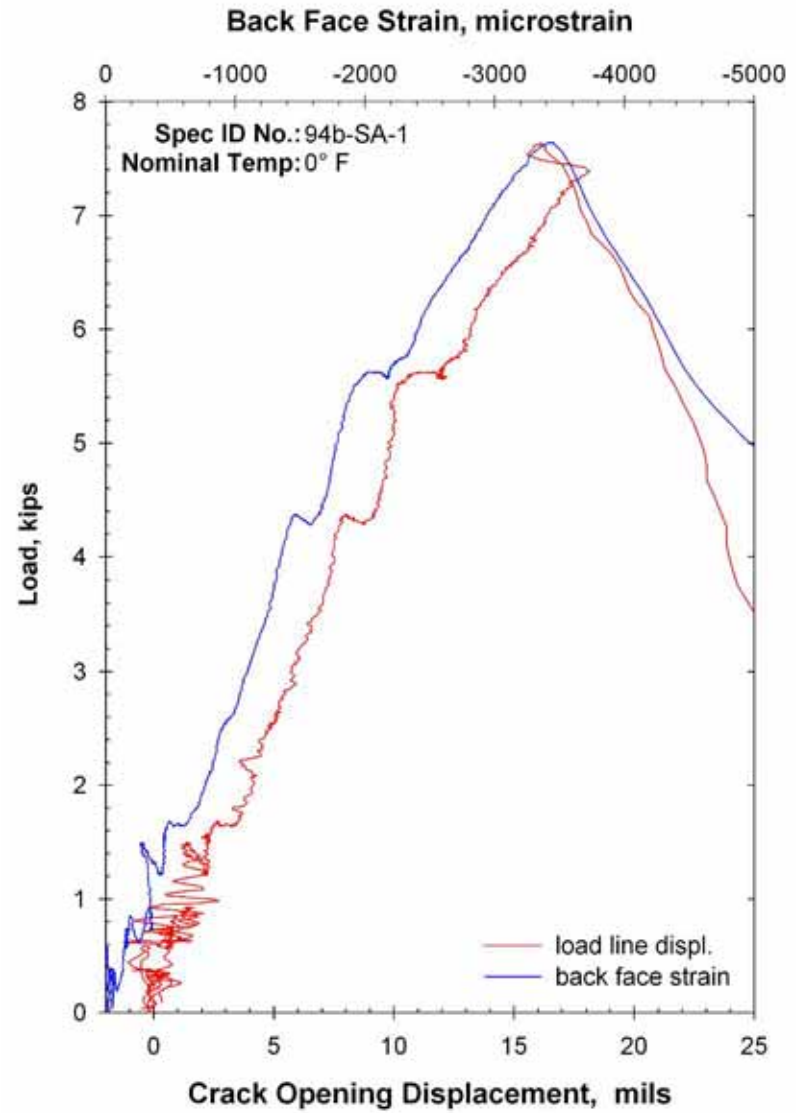
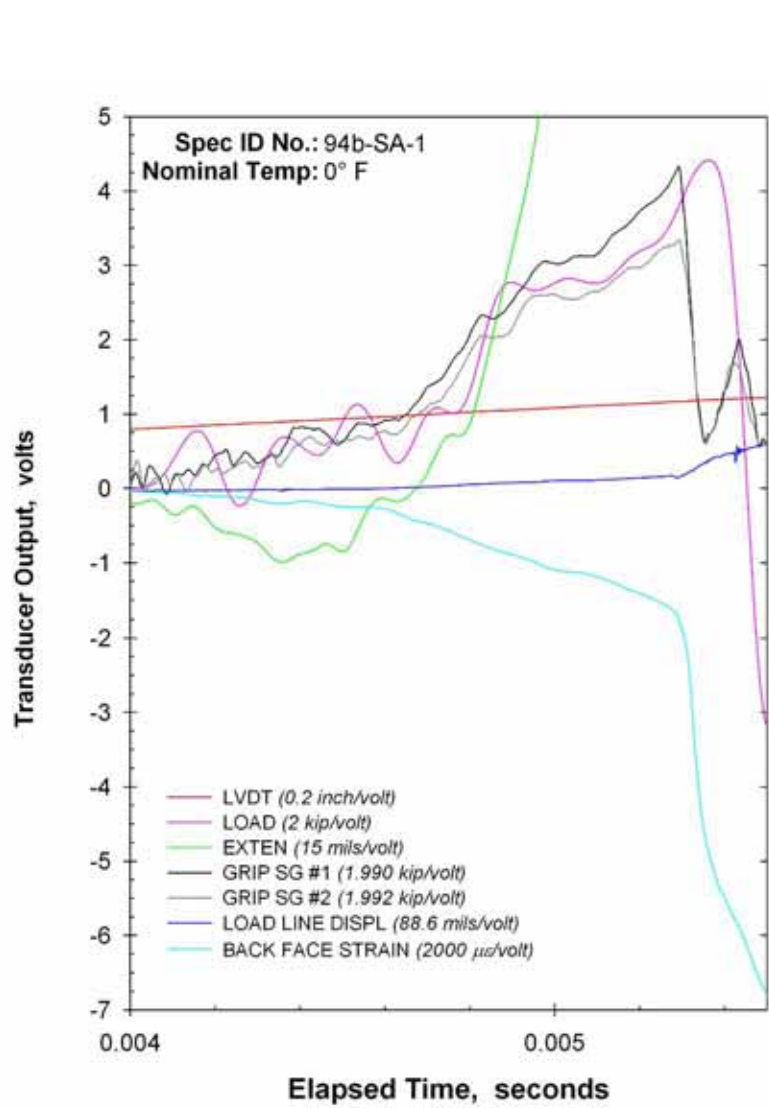


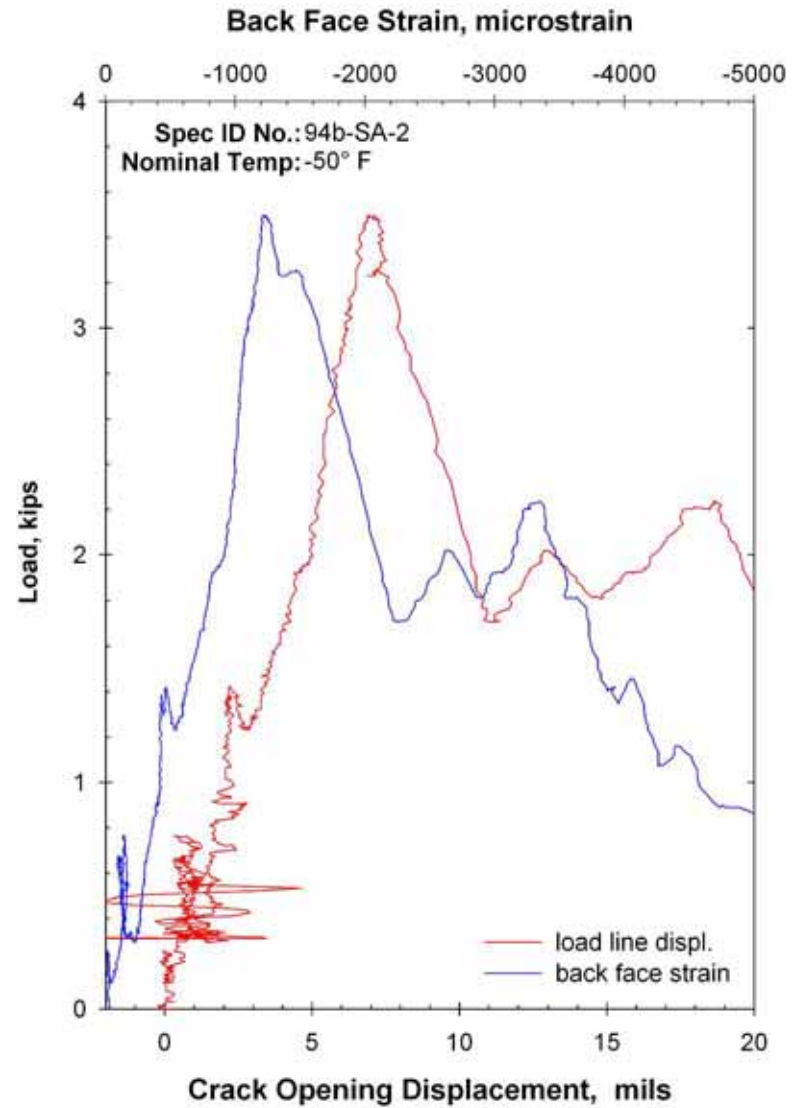
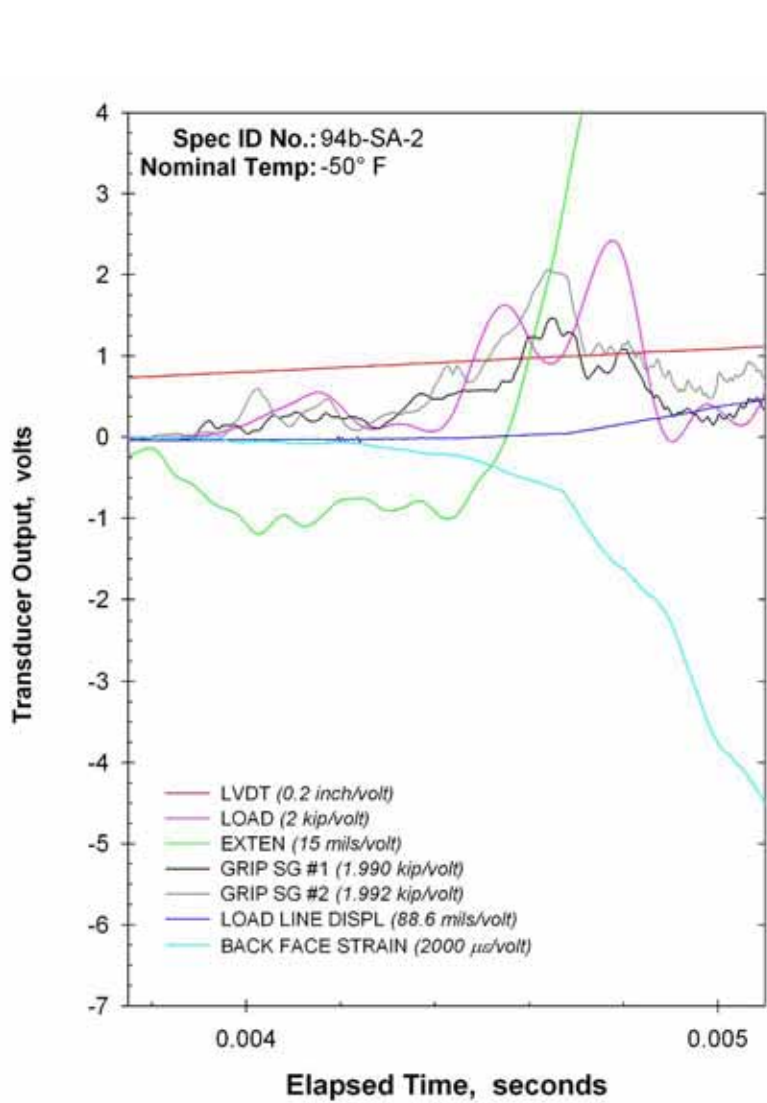












APPENDIX B

NTSB Assessment

This page intentionally left blank.

NTSB ASSESSMENT OF THE SIGNIFICANCE OF FRACTURE TOUGHNESS ON TANK CAR SAFETY IN RAILROAD ACCIDENTS

Alan S. Kushner
Chief Technical Advisor,
Research and Advanced Technology
February 23, 2007

EXECUTIVE SUMMARY:

Following the Safety Board's investigation of the release of anhydrous ammonia from derailed, ruptured tank cars during the derailment of a Canadian Pacific Railway train near Minot, North Dakota on January 18, 2002, recommendations were made to improve the impact and fracture resistance of tank cars carrying hazardous materials. These recommendations called for the characterization of the fracture behavior of tank car steels and the development of a predictive capability to define the dynamic loads on a railroad tank car under accident conditions. With this understanding, it was recommended that performance standards for tank cars be developed. The recommendations from the Minot, North Dakota accident were reiterated during the Board's investigations of the June 28, 2004, collision in Macdona, Texas and the January 6, 2005, in Graniteville, South Carolina. In both of these accidents, chlorine tank cars were breached, resulting in loss of life. The Federal Railroad Administration (FRA) has initiated several activities to address the Board's recommendations. This report addresses the FRA's efforts to characterize the fracture toughness of a specific tank car steel, non-normalized TC-128B. The information on the fracture toughness of non-normalized TC-128B steel called for in Minot recommendation R-04-4 has enabled a more complete assessment of the details needed to develop a valid predictive model for loads on tank cars during accidents called for in recommendation R-04-6. Specifically, a fully integrated approach, coupling the structural loads associated with derailment dynamics with the local loads caused by impacts is needed. Current and previous analyses have dealt only with the latter class of loads.

During the Minot investigation, the Board completed a comprehensive series of Charpy V-notch tests to characterize the impact fracture characteristics of steel from the ruptured tank cars. Such tests provide a relatively quick and simple procedure for characterizing the fracture mechanism of a material. The results of this testing confirmed that the tank car steels would have exhibited brittle, low energy, fracture behavior at the accident temperature. Because Charpy testing only provides a qualitative representation of the temperature dependence of dynamic fracture characteristics, no quantitative judgments of the conditions necessary to produce the ruptures in the Minot accident could be made during the investigation. In response to the Board's recommendation to characterize the fracture toughness of TC-128B steel, the FRA has contracted with Southwest Research

Institute (SwRI) to measure the fracture toughness of samples from tank cars involved in the Minot accident and from tank cars being retired from service.

An assessment of the initial results from the SwRI's testing program is included in this report. Questions are identified relative to the format in which SwRI computes their reported values of fracture toughness, however their data indicate that a safe, lower bound estimate of the 0° F fracture toughness of non-normalized TC-128B steel used in tank cars is 50 ksi-√in. Based on this result, an analysis is presented to identify the size of crack required for rupture of the tank cars under the operating conditions during the Minot accident. The analysis indicates very large cracks, several feet in length or more, would have been needed to initiate catastrophic failure. Because the field evidence from the investigation did not find any evidence of initiating cracks, the failure mechanism for the ruptured tank cars was assessed. It is shown that the most probable failure initiation mechanism is a structural failure under the stresses associated with large, geometrically non-uniform accelerations and impacts during the derailment. The low fracture toughness of the accident tank car steels facilitated the unstable growth of these failures resulting in the catastrophic ruptures. The FRA's future action on the Board's recommendations for characterizing dynamic loads on tank cars during accidents should enable judgments to be made on the adequacy of proposed designs for enhanced tank car safety.

I. BACKGROUND

In evaluating the ongoing programs on fracture toughness measurements for tank cars, it is essential to start from a perspective of how and when fracture toughness contributes to tank car safety. The critical fracture toughness, K_{Ic} , Anderson (1994), is a material property that relates the operating stress level to the crack size needed to have a crack begin to grow. To understand the significance of K_{Ic} one must first see the class of problems it relates to. In fracture mechanics, three modes of crack growth are defined, Figure 1.

- Mode I: Symmetric loading, opening mode (in-plane)
- Mode II: Antisymmetric loading, sliding mode (in-plane)
- Mode III: Antisymmetric loading, tearing mode (out-of-plane)

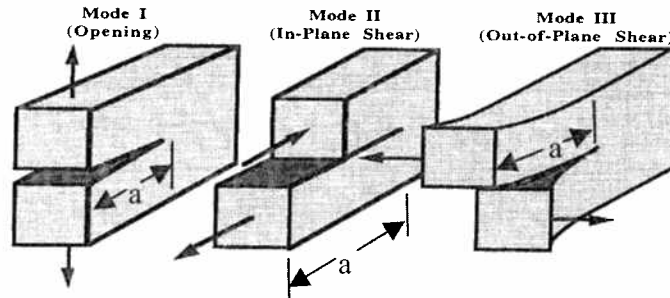


Figure 1. Deformation Mechanisms Associated with Three Fracture Modes

The most common mode is Mode I. If “a” denotes the crack length in the figures above, then a through crack in a tank car would have a total length of 2a. Mode III occurs for thin-walled structures such as tank car shells and heads after the crack has reached a critical length allowing the crack face surfaces to bulge out creating deformation induced stresses that lead to the tearing mode of crack propagation. This effect was studied extensively by the tank car community in the 70s and 80s and was shown to lead to the branching of axial cracks that causes circumferential separation of tank cars, Pellini (1983).

In the cylindrical portion of a tank car, without a crack present the circumferential stress is uniform and given by

$$\sigma_{\text{hoop}} = pr/t \quad (1)$$

where p is the internal pressure, r is the cylinder radius and t is the cylinder wall thickness. For fracture in a cylinder with an a crack of length 2a oriented in the axial direction, assuming the crack is small compared to the cylinder radius,

$$K_I = \sigma_{\text{hoop}} (\pi a)^{0.5} \quad (2)$$

A geometry factor could be included in (2), but for the current purposes this is not essential. A mode I crack grows when the combination of σ_{hoop} and crack half length, a , gives a value of K_I equal to K_{Ic} the value experimentally measured to initiate crack growth. For tank car safety, the role of K_{Ic} is to prevent the unconstrained growth of cracks initiated by impact denting and/or penetration before they reach a length sufficient to cause a transition to Mode III growth and tank car rupture, Pellini (1983). The critical toughness for mode III growth is, in general, much less than in mode I. It is important to recognize that K_{Ic} only relates to the growth of a crack, it in general cannot be used to define a tank car puncture or rupture resistance measure. Since leaks from punctures and/or subcritical cracks can potentially be just as severe from a safety perspective as complete rupture, considering fracture toughness by itself does not enable a complete assessment of tank car safety during accidents.

Most tank cars have internal diameters of 100 to 120 inches and wall thicknesses between 0.5 and 0.8 inches. For the chlorine tank car in the Macdona, Texas accident, NTSB (2006), r was approximately 50.0 inches and the nominal value of t was 0.775 inches. The chlorine had a pressure at filling of 37 psig, giving an operating value of σ_{hoop} equal to 2,400 psi. Figure 2 shows a plot of the critical crack size versus critical K_{Ic} based on the assumptions of equations 1 and 2, for this operating stress level. Measured values of K_{Ic} for TC128-B between approximately 50 and 200 $\text{ksi}\sqrt{\text{in}}$ have been reported in the literature. The plot covers this range even though the implied crack sizes are physically unrealistic and not consistent with the assumptions made about crack growth.

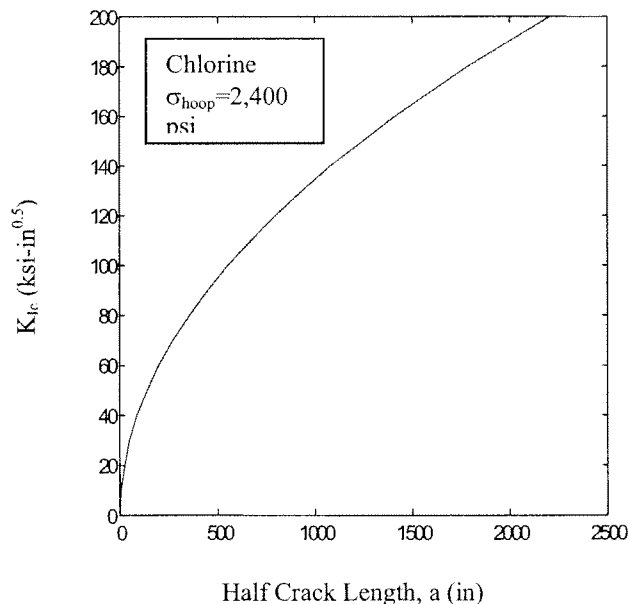


Figure 2. Relationship between Critical Fracture Toughness and Crack Size for Tank Car in Macdona, TX Accident

For a K_{Ic} of 20 $\text{ksi}\sqrt{\text{in}}$, a half crack length of 100 inches is required to initiate growth of a crack emanating from a puncture. Thus, the puncture and its associated tearing of

material would have to span 200 inches. A puncture of this size would allow for instantaneous release of product without any continued fracture. The Southwest Research Institute (SwRI) testing program, McKeighan (2005), has so far reported a minimum K_{Ic} at 0°F of 56 ksi- $\sqrt{\text{in}}$. To sustain crack growth in a chlorine tank car with this level of toughness would require a puncture and crack 400 inches long. This would appear to be consistent with the Macdona experience, where a crack driven by a head puncture moved through the normalized head material into the cylinder weld and about two inches into the non-normalized cylinder before arresting.

For a typical anhydrous ammonia tank car involved in the Minot, North Dakota accident, r was approximately 60.0 inches and the nominal value of t was 0.6 inches. The anhydrous ammonia had a pressure of approximately 55 psig, giving an operating value of $\sigma_{\text{hoop}}=5,800$ psi. Figure 3 shows the critical crack size versus critical K_{Ic} for this operating stress level. Because of the higher value of σ_{hoop} , the critical crack sizes are now seen to be almost an order of magnitude smaller than that found for the chlorine tank cars. For a material with K_{Ic} of 50 ksi- $\sqrt{\text{in}}$, a critical crack length would be approximately 40 inches. A crack of this length could be initiated by impacts during an accident. This analysis assumes that the impact deformation does not appreciably increase the local operating stresses at the crack above the nominal σ_{hoop} value. Work by Pellini (1983) found that for anhydrous ammonia cars, when cracks initiated by rail burn dents reached lengths of seven feet, the local stress state was elevated enough to cause crack growth and

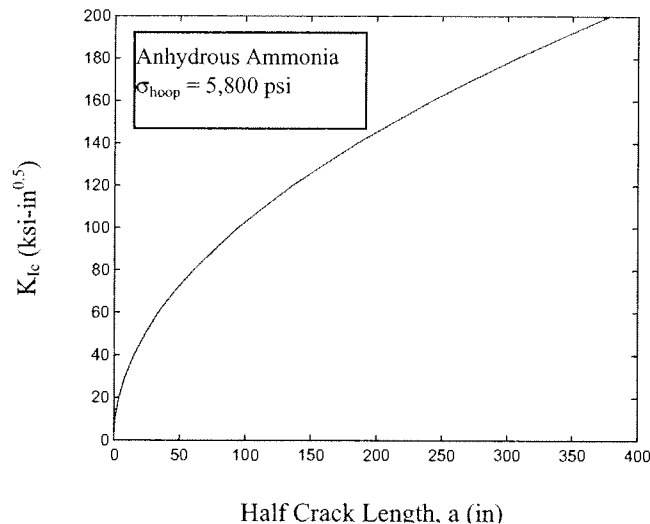


Figure 3. Relationship between Critical Fracture Toughness and Crack Size for Tank Car in Minot, ND Accident

branching into circumferential fracture. The testing being done by SwRI is reporting minimum K_{Ic} values for specimens from the Minot cars of about 70 ksi- $\sqrt{\text{in}}$ at 37° F. This would imply a critical crack size of approximately 90 inches, consistent with Pellini's results.

The preceding discussion looked at bounding behavior for cracks generated by an impact. It is possible that the combined loading from the impact process and the pressurization could lead to unstable crack growth. The puncture process is an extremely complex and non-unique structural/material process. It is highly dependent on impact speed, orientation, impactor characteristics and the operating environment of the tank car being impacted. Assuming the impact creates a crack, insight into the basic mechanics of crack growth during the penetration process can be obtained from the solution for a crack loaded by equal and opposite concentrated forces that pry the crack face open, as shown

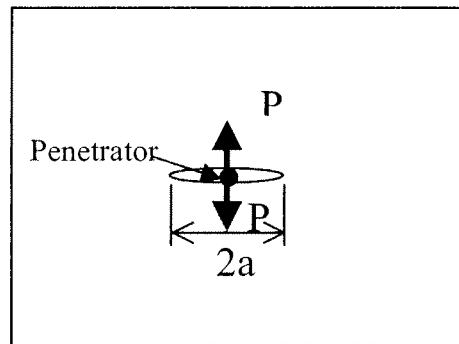


Figure 4. A Penetrator creates Opening forces on crack surfaces as it pushes open crack

in Figure 4. As the penetrating object moves through the puncture, it creates prying forces on the surface of the hole that try to push the surfaces apart (fracture) and bend the material inward (denting and tearing). Ignoring the denting and tearing, for the prying force P , modeling the puncture as a crack of length $2a$ gives a solution for the stress intensity factor,

$$K_I = \frac{P}{a} \sqrt{a} = \frac{P}{\sqrt{a}} \quad (3)$$

Thus, two competing factors are active for crack growth from punctures in a pressurized tank car. The tank stresses due to internal pressure create a crack tip stress state that causes increasing K_I as the crack grows as shown by equation 2, while for a constant penetrator force, equation 3 shows that the penetration process causes a stress state that leads to decreasing K_I as the crack grows.

It would appear that for chlorine tank cars the operating pressures are so low that catastrophic rupture cannot occur unless the impact and penetration process initiates it. An additional concern would be a fire that could raise the chlorine pressure. For anhydrous ammonia, very large impact generated cracks or severe deformation and moderate cracks are required for catastrophic rupture. The increased toughness from normalized steel does appear to play a role in this case, however it will be shown in later sections that it is probably secondary to that obtained by reducing the severity of the

impact caused deformation and penetration. For any tank car with multiple and/or severe denting, it is conceivable that the internal volume decrease caused by denting can equal or exceed the unfilled volume of the tank car. Under these conditions, further denting would cause large increases in the pressure of the liquid cargo. This could easily explain the rocketing of tank car sections seen in the Minot accident. For chlorine tank cars, a very large initial crack would be required for a catastrophic rupture. For example, if the internal pressure in a chlorine tank car increased by a factor of ten from 2,400 psi to 24,000 psi, for a K_{Ic} of 100 ksi- $\sqrt{\text{in}}$, the critical half-length would still be approximately 70 inches. An important question is, how safe would a fleet of cars with a K_{Ic} of 140 ksi- $\sqrt{\text{in}}$ be? This would require a puncture and crack approximately 350 inches in length. While this would appear to indicate a safe design, the real question that must be addressed is to quantify when the transition from simple mode I crack growth to the more complex structural deformation driven crack growth occurs. To answer this, the results of fracture toughness testing must be integrated into the structural analysis effort aimed at defining impact loads.

The SwRI sampling program has shown a large variation in toughness for non-normalized TC128-B from tank cars. It is doubtful that an expanded sampling program would drastically change the already large spread in measured K_{Ic} . In relating experiences from punctures and fractures during accidents, it is important to consider the failure process involved. The Macdona, TX accident is purely a leak caused by penetration, whereas the Minot, ND accident is an example of a catastrophic structural failure caused by impacts and derailment dynamics. No improvement in steel toughness alone would have prevented puncture in the Macdona accident, although the leaking may not have been as rapid. It is possible that the severity of the catastrophic ruptures seen in the Minot accident could have been reduced by tougher steels, however, not enough information is available to confidently make that conclusion.

II. EXPERIMENTAL MEASUREMENTS OF K_{Ic}

The SwRI program, McKeighan (2005), has provided measurements of mechanical characterization, strength, Charpy V-notch energies and fracture toughness of samples taken from rail tank cars involved in the Minot accident and other tank cars being retired from service. Two issues can be addressed based on the current data sets;

1. What does the data tell us about the expected variation in fracture toughness of the fleet of tank cars constructed of non-normalized TC128-B steel?
2. Can the fracture toughness data as presented by SwRI be used as the basis for establishing a standard for required toughness of tank car steels?

To address these points, one must first consider the experience from recent accidents and the basics of what can be expected in terms of operating conditions for tank cars carrying hazardous materials.

In the Minot accident, tank cars PLMX 4504, GATX 47814, and GATX 47982 all experienced catastrophic ruptures. Tank car PLMX 4644 experienced a puncture and tear and GATX 49248 experienced a puncture. Referring to Figure 5, it is observed that all of the cars that catastrophically ruptured had samples exhibiting a measured toughness below 90 ksi- $\sqrt{\text{in}}$. However, the large variation in the 0° F data from retired tank cars indicates that making car level judgments is not reliable. For tank car GATX 25008, a sample from the B-end shell showed a toughness of 56 ksi- $\sqrt{\text{in}}$ while samples from the A-end showed toughness values of 97.3 and 107.5 ksi- $\sqrt{\text{in}}$. Hence, it appears that the variation in toughness for samples taken from different sections of the same tank car is just as large as the variation in toughness found car-to-car. Therefore, it is probably not possible to define a tank car toughness value for tank cars made of non-normalized TC128-B steel. The statistical implications of this will be discussed later.

One aspect of the 0° F data that is troubling is the relationship between the static and dynamic toughness measurements. As previously noted, the data in Figure 5, shows the static toughness results for samples from retired tank cars to be on average lower than the dynamic results. In general, for the brittle, cleavage fracture regime, dynamic toughness is lower than the static toughness as is shown in Figure 6, Barsom (1975). The Charpy V-notch testing done on samples taken from the Minot accident cars showed the transition from lower to upper shelf to occur over the temperature range from 0° to 70°F. Charpy testing results reported by NTSB, Zakar (2003), for the Minot investigation are shown in Figure 7. At 0°F, non-normalized TC128-B should be brittle and normalized TC128-B should exhibit predominantly ductile fracture behavior. The data shows that normalized TC128-B plate should be above the mid-point in the transition curve from lower shelf, cleavage, to upper shelf, ductile fracture in the TL direction and fully in the ductile region in the LT direction at this temperature. Thus, at 0°F, brittle, cleavage, fracture behavior is expected for the non-normalized steels in the ruptured Minot and retired tank cars. As was pointed out, for cleavage, dynamic toughness is expected to be lower than static toughness. However, in terms of average values, an opposite trend in the data is seen. The average value of the static toughness for the normalized steel, 83.8 ksi- $\sqrt{\text{in}}$ is below the dynamic value, 85.5 ksi- $\sqrt{\text{in}}$ for samples from the same tank cars. Because of the very large spread in the dynamic data, standard deviation of 21.5 ksi- $\sqrt{\text{in}}$, as opposed to that for the static data, standard deviation of 2.9ksi- $\sqrt{\text{in}}$, one might assume this to be statistically insignificant. However, a closer inspection of the data shows that in all cases, samples taken from the same plate show lower static toughness values than dynamic toughness. The static toughness measurements are distributed in the mid 50% of the data of the corresponding dynamic data. The most striking characteristic of the 0°F data is the large spread in the data. The maximum toughness measured is 2.2 times the minimum and the standard deviation is approximately 20% of the mean. This large variability is consistent with what is typically found for materials that fail in a cleavage mode. Thus, it is quite doubtful that the characteristics of the data population will change as more retired tank cars constructed of non-normalized TC128-B steel are tested because the variability within a tank car is as large as the variability found between different cars. The implications of this will be discussed later when the manner SwRI uses to evaluate toughness is discussed.

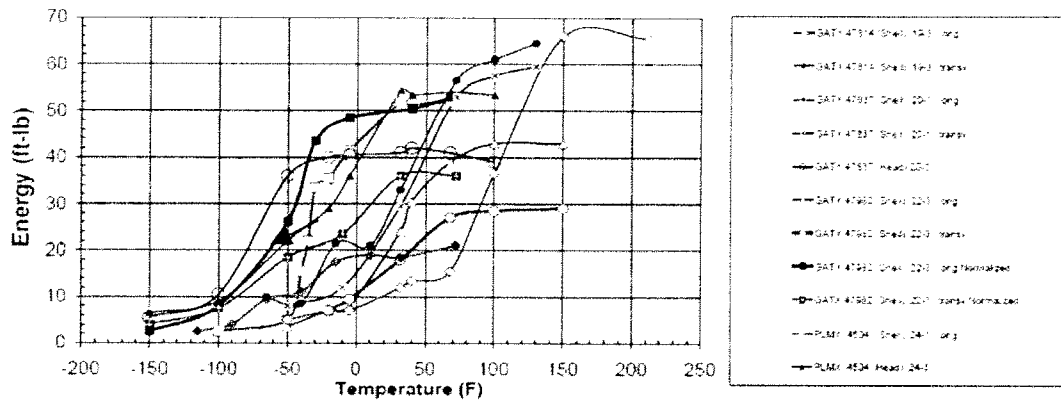


Figure 7. Ductile to Brittle Transition Temperature Curves Generated by Charpy V-notch Testing for Samples Taken from Tank Cars Involved in Minot Accident (Zakar, 2003)

Referring to the NTSB results shown in Figure 7, at 37°F, the specimens should exhibit a reasonable degree of ductility in their fracture behavior. The results in Figure 5, for samples from the Minot cars tested at 37°F, show an approximately 10% increase in average toughness when compared to the 0°F data. Additionally, the standard deviation of the 37°F data is approximately 40 to 50% lower than the 0°F data. The reduced spread of the measured toughness data is consistent with the expectation of some ductile fracture behavior at 37°F implied by the Charpy data. However, based on the large difference between lower and upper shelf Charpy energies, K_v , one would expect a larger increase in fracture toughness. K_v is not directly related to fracture toughness but has been shown to correlate well in many cases. For medium yield strength steels such as TC128-B, the Corten-Sailors empirical correlation has been found to be an accurate approximation:

$$K_{Id} = 15.87*(K_v)^{0.375} \tag{4}$$

where K_{Id} is the dynamic K_{Ic} . At 0°F, SwRI reports plate averaged K_v values between 7.7 and 27.3 ft.-lbs. These correspond to K_{Id} values of 34.2 and 54.85 ksi-√in respectively. What is most significant is that the SwRI Charpy V-notch energies correspond to K_{Id} values outside the range of measured K values (56 to 121 ksi-√in). This is consistent with the analysis of McKeighan, (2005), where the data is compared to the prediction of the Roberts-Newton empirical correlation. Thus, the toughness values reported by SwRI are not consistent with the measured K_v values. The K_v values reported by SwRI are consistent with the results reported by NTSB and others. Between 1975 and 1995, the National Institute of Standards and Technology (NIST) conducted a comprehensive evaluation of the mechanical and fracture toughness behavior of tank car steels. Their results are summarized in the report, *Materials and Fracture Mechanics Assessments of Railroad Tank Cars*, NISTIR 6266, NIST (1998). Some of the data from this report is shown in Figure 8. The minimum, TL direction, average toughness for normalized TC128-B at 0° F shown in Figure 8. is approximately 40% higher than the results reported by SwRI. Thus, while the high-rate toughness results for non-normalized TC128-B reported by SwRI appear high when correlated to Charpy data, the toughness

values for normalized TC128-B reported by SwRI is low when compared to that reported by NIST. It must be noted that the toughness values reported by SwRI are referred to as K_{max} values whereas the NIST values are ASTM standard K_{Ic} values. As will be discussed in the next section, the K_{max} values are always equal to or higher than K_{Ic} values.

Material Condition	Direction	Temperature °F	K_{Ic} ksi- $\sqrt{\text{in}}$
Normalized	TL	0	140
Normalized	LT	0	210
Normalized	TL	-40	85
Normalized	LT	-40	115
Normalized and Stress Relieved	TL	-40	155
Normalized and Stress Relieved	LT	-40	310
Normalized and Inclusion Shape Controlled	TL	-40	258
Normalized and Inclusion Shape Controlled	LT	-40	241

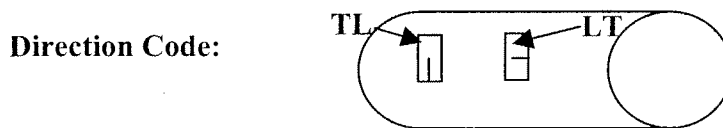


Figure 8. Fracture Toughness Values for TC128-B Measured by NIST

Interpretation of SwRI Data

Two issues that must be addressed before the measured toughness data can be used in any design/safety assessment application are how to handle the spread in the data and the correlation and processing of the measurement data into a useful format. Addressing the first of these requires setting a quantitative technical standard for what value of fracture toughness represents the data in a “safe” manner. In statistically based design standards one typically uses a reliability or confidence measure. A common approach is to use the B-basis, ASTM (2002), value for evaluating the data. A B-basis is defined as a number for which one has 95% confidence that only 10% of the specimens in the total (mostly unsampled) population will lie below. The actual computation of the B-basis is dependent on the assumed statistical variation and the size of the sample population. For small sample sizes the sensitivity to the assumed distribution function decreases and the variability of the data dominates. For sample sizes less than 29, the Hanson-Koopmans (1964) method has been found to be accurate for all of the distribution functions used for material strength and toughness data. Using this approach, the B-basis value for the SwRI 0°F toughness data is found to be ~56 ksi- $\sqrt{\text{in}}$, and for the 37°F data it is ~65 ksi- $\sqrt{\text{in}}$. In each case one observes that the B values for toughness are lower than the lowest measured data point. A simple explanation of this is that because of the small sample size and very large spread in the data, one cannot have confidence that they have found

the lower portion of the population. The total sample size for the 0° data is 28, and 21 samples were tested at 37°. If one assumes seven additional samples at 37° all with values equal to the mean, the equivalent sample size B value for 37° is 71 ksi-√in. Thus at both temperatures the test data indicates a 95% confidence that the lowest 10% of the population has not been found.

The second issue that must be addressed before using the SwRI data is the manner in

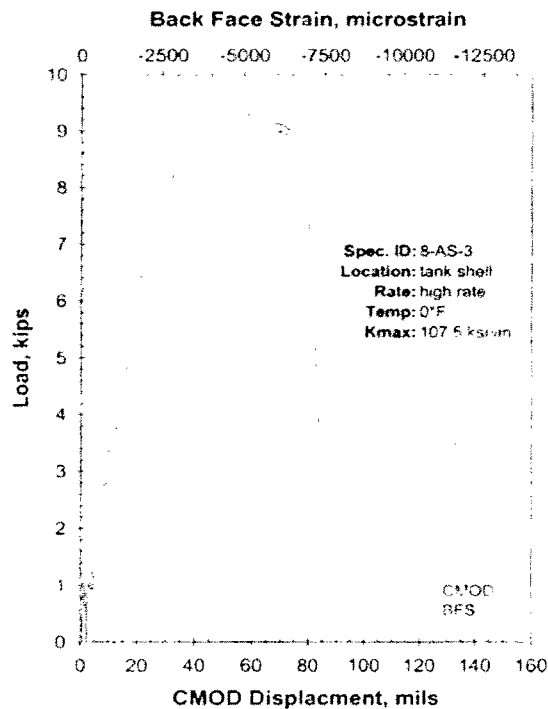


Figure 9. Resolved CMOD and BFS versus Load for Specimen from Retired Tank Car GATX 25008

which it is interpreted. The experimental procedure involves taking time history data of the applied load and certain displacement and strain measures. To calculate a fracture toughness value, the data must be combined to give a crack opening displacement versus load curve. ASTM standard E399-83, ASTM (1983), gives a rigorous definition of how the resulting data is to be evaluated for calculating a value of K_{Ic} , defined as the stress intensity factor at which crack growth initiates. Rather than following the ASTM procedure, SwRI has chosen to use the maximum value of load recorded during a test to compute a toughness they refer to as K_{max} . The following compares the values of load used for a K_{Ic} calculation to that used in a K_{max} calculation for two of the tests performed by SwRI.

Figure 9 shows the measured load versus crack mouth opening displacement (CMOD) and back face strain (BFS) for a sample taken from retired tank car GATX 25008. The response is seen to be reasonably linear until about 70% of the maximum load. The equation for computing K_{Ic} involves multiplying a load P_Q by a factor that involves only

specimen geometry and crack size. The procedure for identifying P_Q is standardized to

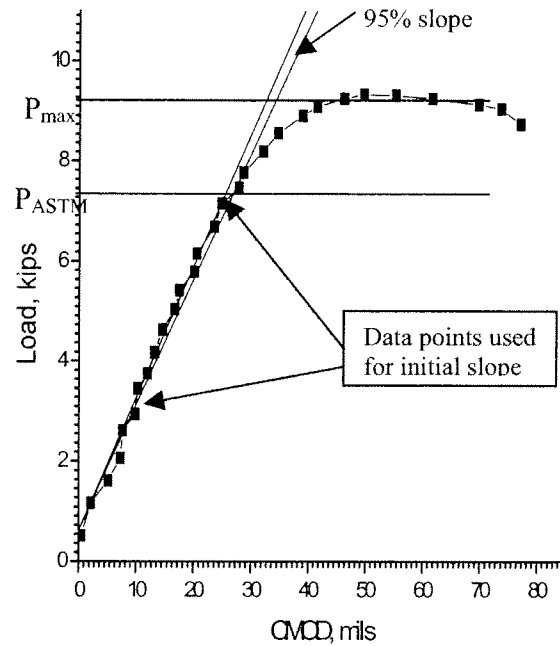


Figure 10. Computation of Load for Defining K_{Ic} from Data in Figure 9 According to ASTM Procedure

allow for crack blunting and some stable crack growth to occur. The K_{max} values reported by SwRI use the maximum value of load obtained during a test to compute a toughness referred to as K_{max} rather than computing P_Q and using it to compute K_{Ic} . In Figure 10, the initial portion of the load displacement curve has been reproduced and the ASTM procedure for computing the load for K_{Ic} has been followed. The K_{Ic} calculation uses the load labeled P_{ASTM} while the K_{max} calculation uses the P_{max} load level. In this case, the use of the ASTM procedure would lead to a 20% drop in the K value computed from $107.5 \text{ ksi}\sqrt{\text{in}}$ to $85 \text{ ksi}\sqrt{\text{in}}$. For comparison, Figures 11 and 12 show the corresponding data from a test that has a much more nonlinear load-displacement curve. For this case, the ratio of P_{ASTM} / P_{max} is 0.53. Thus, in this case the calculated value of K would drop from $103.2 \text{ ksi}\sqrt{\text{in}}$ to $55 \text{ ksi}\sqrt{\text{in}}$.

Inspection of the plots for all of the data presented in the SwRI reports indicates that the scaling from K_{max} to K_{Ic} would in general fall in the 0.5 to 0.9 range. According to McKeighan, the use of K_{max} is justified because

The K_{Ic} fracture test (ASTM E399) is best suited for brittle, linear-elastic behavior where at maximum load the crack reaches instability and instantaneously tears through the remaining specimen ligament..... However, under high rate loading

conditions the integrity of the load displacement behavior is often less than optimum (due primarily to dynamic effects from the displacement measurement transducer) hence making this approach somewhat ineffective. Therefore, during this testing the toughness that is reported is the K_{max} toughness.....

The explanation above is not completely consistent with the theory behind the ASTM procedure. The ASTM procedure for computing P_Q (referred to as P_{ASTM} in figures 10 and 12) recognizes that load will often continue to increase after crack growth is initiated. The conditions for having a valid test require that P_{MAX}/P_Q must be less than 1.1. The two examples just evaluated both fail this validity check. An additional validity check required by ASTM is that $2.5(K_Q/\sigma_{ys})^2$ be less than the specimen thickness, where σ_{ys} is the 0.2% offset yield stress. According to ASTM, when either of the constraints is not satisfied, the test results may be specimen size dependent and hence not representative of a material property. At 0°F, the measured yield stress is approximately 70 ksi. For a 0.7 inch thick specimen, this would limit the maximum acceptable values of K calculated to be 37 ksi-√in. For the Minot cars, this toughness would correspond to a two foot crack length. For the chlorine tank cars in the Graniteville accident, a twelve foot critical crack size is implied. Although the measured toughness values are not size independent, they are full thickness. Hence, they should be reasonable estimates of the apparent toughness exhibited in tank cars.

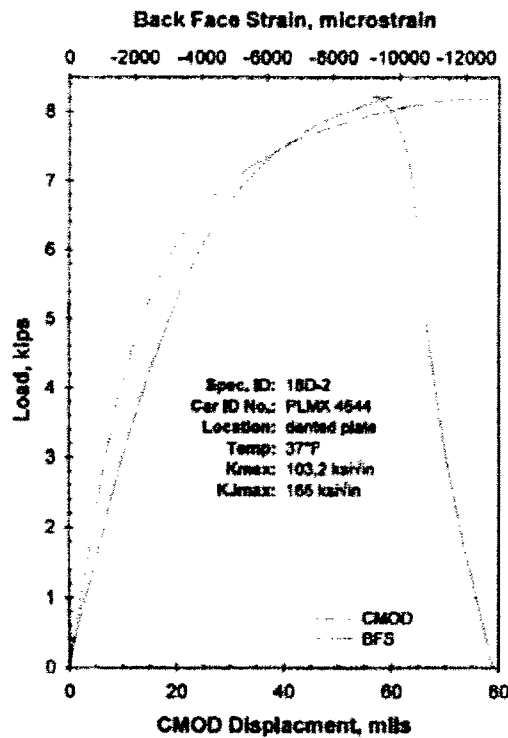


Figure 11. Resolved CMOD and BFS versus Load for Specimen from Tank Car PLMX 4644 Involved in Minot Accident

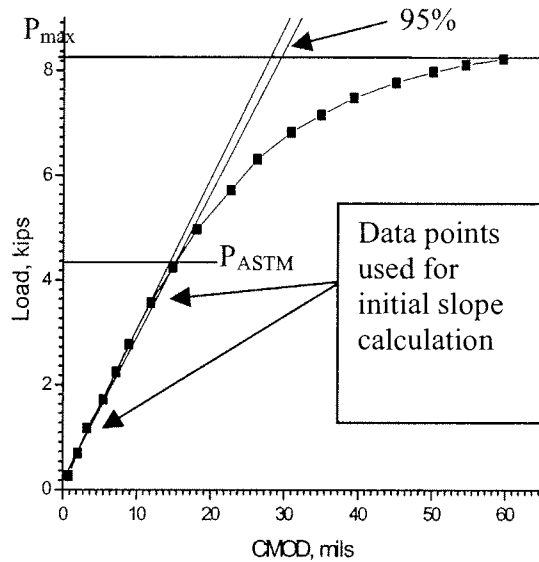


Figure 12. Computation of Load for Defining K_{Ic} from Data in Figure 11 According to ASTM Procedure

As shown, the scaling from K_{max} to K_{Ic} is not uniform. It is highly dependent on the shape of the load-displacement curve. In addition, by using the maximum load, one cannot rely on the ASTM consistency checks to guarantee a material rather than specimen property is reported. In assessing the utility of K_{max} , one must consider the possible reasons for load to continue to increase after crack growth initiates. For ductile fracture, crack tip blunting and inelastic deformation ahead of the crack tip can serve to reduce the effective stress intensity factor driving crack growth, allowing for stable crack growth under increasing load. For these cases, the J integral, Anderson (1994), is typically used to characterize the material toughness. The K_{Jmax} defined by McKeighan is not an established fracture parameter and is not consistently defined relative to K_{max} . The response time of the load adjustment is a strong function of the load cell sensitivity, load train inertia and the stiffness of the specimen. All of these effects influence the relationship between the maximum load recorded in a test, the K_{max} load, and the load corresponding to unstable crack growth, the K_{Ic} load. Most significantly, because K_{max} is not a standardized material characterization quantity, there is no established basis to compare the results to. In an informal August 2005 report to the Federal Railroad Administration (FRA) by Anderson and McKeighan, a framework for interpreting K-based fracture toughness results was proposed. They defined the following groupings and provided references to accepted industry design standards from ASME and API as justification;

- 25 – 50 ksi√in: Poor toughness
- 50 – 100 ksi√in: Adequate toughness
- 100 – 200 ksi√in: Good toughness
- >200 ksi√in: Excellent toughness.

It is important to note that the ASME and API standards are based on K_{Ic} . One can see that for the second example considered above, converting from a P_{max} to a P_{ASTM} based calculation moves the resulting K value from a K_{max} at the lower end of the good toughness region to a K_{Ic} value at the bottom of the adequate toughness region. The usefulness of the K_{max} data reported by SwRI must be assessed in terms of the manner in which the data is to be used. Traditional applications of fracture mechanics assume that cracks will develop and grow during the service life of the structure. Based on the operating stresses in the structure and the toughness of the construction material, one can then define a minimum crack size that must be reliably detected during routine inspections to guarantee continued safe operation. For tank cars carrying hazardous materials, no cracks can be tolerated in operation. As was shown in the Background section, even for a tank car constructed of steel with a K_{Ic} of 40 ksi√in, a crack of several feet in length would be needed before unstable crack growth initiated. Inspection of the load versus displacement curves for the Minot specimens tested at 0°F that have K_{max} values less than 70 ksi√in shows relatively linear behavior up to maximum load so that the reduction from K_{max} to K_{Ic} would be in the 10% range. These specimens would also satisfy the ASTM validity checks. Thus, one can confidently conclude that the 0° F toughness, K_{Ic} , for non-normalized TC128-B in railroad tank cars is above 50 ksi√in, ignoring the size dependency issues. This would place the material at the low end of the adequate toughness region defined by Anderson and McKeighan. However, because the normal operating stresses in railroad tank cars is so low, large cracks are necessary to induce unstable crack growth. Given the catastrophic failures of integrity that have occurred in the recent accidents at Minot, ND, Graniteville, SC and Macdona, TX, it is critical that the mechanisms leading to crack formation and structural failure be understood.

III. OBSERVATIONS OF TANK CAR STRUCTURAL FAILURES

Of the three accidents cited above, the tank car failures in the Minot, ND derailment accident are the most severe. This accident involved a derailment of a train traveling at 41 mph. Five derailed anhydrous ammonia tank cars sustained catastrophic structural failures. Figure 13 shows a photograph taken at the accident site of tank car PLMX 4504. This is one of the cars that rolled on its side after derailling and fractured into two sections. The inspection of this and the other fractured tank cars identified significant structural deformation and denting but did not identify any puncture or localized impact damage that could have served to initiate the cracking and splitting. In general, the fracture surfaces were identified as brittle. As is clearly shown in Figure 13, the tank car shell experienced significant ductile, inelastic deformation in the region where the catastrophic rupture occurred. Possible sources of this damage are impact with other tank cars or the ground, forces acting on the tank car couplers and wheel sets during the



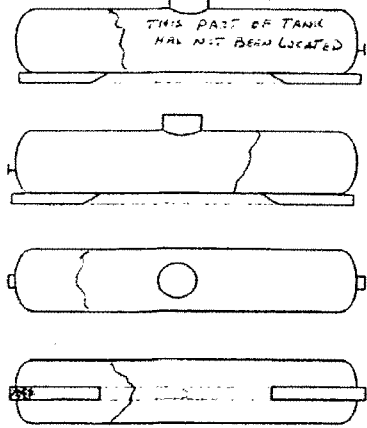
Figure 13. Photograph of B-end View of Tank Car PLMX 4504 at Minot Accident Site

derailment process and the inertia of the tank car components at the time of impact with the ground or other tank cars. The large-scale structural damage shown in Figure 13 is typical of what was observed in all of the tank cars that catastrophically ruptured during the Minot accident. In addition, investigators did not find any impact or penetration fracture initiation sites for any of these tank cars. Figure 14 shows excerpts from the *Tank Car Damage Assessment Worksheets*, Lasseigne, (2002), prepared at the Minot, ND accident site for four of the tanks cars that catastrophically ruptured. All four of these tank cars split in two along a failure surface that was primarily circumferential and projected vertically onto the stub sill area of the tank car. The combination of no identifiable damage initiation site and no signs of localized impacts implies that the fracture is the result of a structural deformation that loaded the tank car shell to failure. The common location of the failures would imply that the local stiffness and mass discontinuities where the stub sill attaches to the shell and/or the inertia of the wheel set and stub sill caused a bending of the tank cylindrical section that caused failure. The petaling at the failure plane observed in Figure 13 and similar photos from the other tank cars is characteristic of a tearing failure initiated by local hard points on a structure. All four of the tank cars exhibited measured K_{max} values below the mean at both 0° F and 37° F and hence it is feasible that while the rupture initiated as a local structural failure, it propagated as an unstable brittle fracture. Alternatively, the kinetic energy available from the derailment could create inertia loads sufficient to cause a stress driven failure of the entire cross section. The severe cross-sectional distortion illustrated in Figure 13 is also consistent with a decrease in tank volume that would lead to an increase in internal pressure. The internal pressure increase would contribute to the stresses driving fracture propagation and are the primary source of energy for projecting the tank car segments over large distances. Existing information does not allow for any conclusion as to the

actual failure initiation mechanism. A fully three dimensional finite element simulation of a tank car during derailment and non-normal impact with the ground and/or other tank cars is needed to define the magnitude and nature of the load state feasible during such a derailment. With this as initial conditions, a detailed finite element analysis could determine whether the failure is fully structural or a combination of structural and crack growth. Large scale simulations such as this are now routine in other crash analysis areas, but have not yet been applied for the rail tank car application. A critical output of the finite element analyses would be a clearer understanding of the denting processes responsible for the structural damage observed in tank cars that have been in accidents. Past work on denting was motivated by the need to understand the critical velocity for puncture when a coupler impacted a tank car. Thus, testing was performed with a fixed impactor causing the dent and over a limited range of impact velocities. Under these conditions, dent depth should correlate with penetration, Jeong (2001). Experience from accidents indicates extensive denting in tank cars, much of it appearing to not be caused by impacts. The most logical cause of this denting is local structural buckling caused by the accident loads.

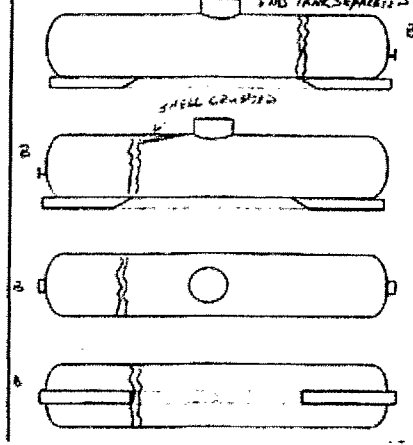
Figure 15 shows photographs of the puncture region for the tank car that was punctured and leaked chlorine gas in the Graniteville, SC accident. Typically, dents caused by localized impacts are somewhat symmetric about the impact region, with the point of maximum dent depth occurring under the impact region. As can be seen from the figure, the impression marks left by the coupler assembly are on an “upslope” region of the dent. The relatively mild surface damage at the impression marks indicates that the impacting surface did not itself puncture the tank. It is most likely that the denting and material failure that occurred in this tank car was caused by a combination of impact stresses and structural loads associated with the derailment dynamics. It is conceivable that the tearing failure initiated from impact in a highly stressed region caused by localized structural buckling or that the impact created a dent that acted as an imperfection and initiated the local buckling. The actual mechanism that initiated the fracture cannot be identified from the existing information. However, it can be concluded that the material failure process was initiated by a combination of stresses due to structural deformation from the derailment dynamics and local stresses associated with the impact.

APX 2 1/2 RINGS OF TANK PROPEL APX 1000 FT

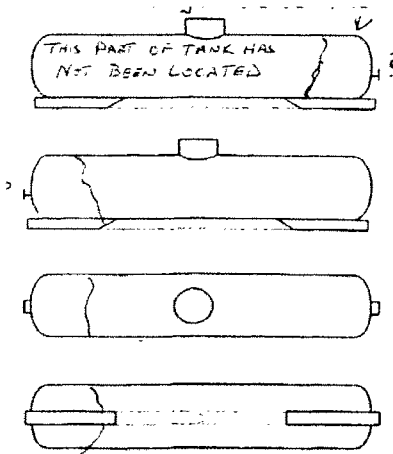


(a)

TANK IN 2 PIECES - 1 1/4 RINGS OF B' END TANK SEPARATED

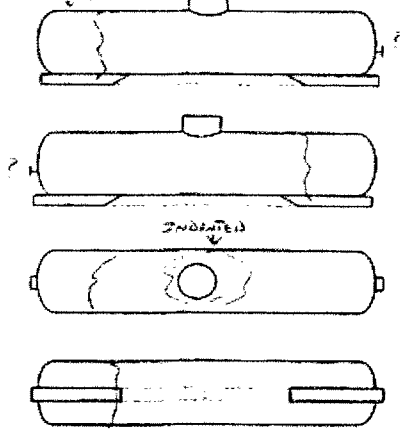


(b)



(c)

SECTION OF TANK MISSING

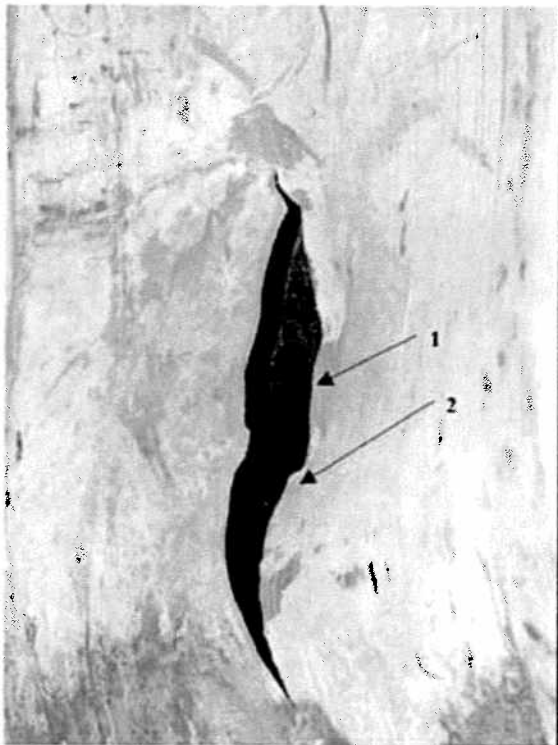


(d)

Figure 14. Results from Tank Car Damage Assessment Worksheets Prepared at Minot, ND Accident Site
 (a) GATX 47814; (b) GATX 47982; (c) GATX 48081; (d) PLMX 4504



View of the right side of the tank car after the patch was disassembled.



Close-up photograph of the fracture. Arrows "1" and "2" indicate the location of the two impression marks.

Figure 15. Photographs of Puncture Region in Tank Car UTLX900270 from the Graniteville, SC Accident, Zakar (2005)

IV. SUMMARY

In response to recommendations made by NTSB in the Minot, ND accident, the FRA is funding an extensive testing program at SwRI to characterize the mechanical and fracture properties of TC128-B steel found in railroad tank cars currently in service. Recent accidents in Graniteville, SC and Macdona, TX have demonstrated that punctures in hazmat tank cars are potentially just as dangerous to the public as catastrophic ruptures. Ideally, the fracture testing program would be based on a series of detailed tests and simulations to define the regime of impact velocities, structural loading and deformation rates and operating stress levels expected during accidents. Lacking this information, the fracture testing program undertaken at SwRI, under contract with the GATX Corporation and the Volpe Center, initiated a dynamic fracture toughness testing protocol where testing is done at the highest rate achievable in their servo-hydraulic machine. Although standard ASTM compact tension specimens are used, the results are presented in terms of K_{max} rather than either K_{Ic} or K_{Id} . Despite the concerns about the validity of this interpretation, it appears safe to conclude that a reliable estimate of the lower bound for the critical fracture toughness, K_{Ic} , of non-normalized TC128-B steel in tank cars is 50 ksi- $\sqrt{\text{in}}$ at 0° F and 70 ksi- $\sqrt{\text{in}}$ at 37° F, the approximate temperature of the anhydrous ammonia in the Minot tank cars that catastrophically ruptured. This would imply a critical crack length of approximately 80.0 inches for the tank cars that catastrophically ruptured in the Minot accident. Damage of this size scale should have been obvious during the post accident inspection of the tank cars. Post accident examination of the Minot tank cars did not show any indication of punctures or pre-existing cracks. Based on the physical evidence, it appears most likely that two factors contributed to the rupture of the tank car. The first is an increase in internal pressure for the anhydrous ammonia caused by cross section deformation of the tank car cylindrical section, resulting in a loss of internal volume. The vapor region of the tank cars occupied 2% of the volume. Hence, very little deformation is required to allow the liquid to fully occupy the internal volume of the tank car. At this point, further crushing would cause the internal pressure to increase rapidly. If the internal pressure in one of the Minot cars increased from 55 psig to 150 psig, the critical crack size for a toughness of 70 ksi- $\sqrt{\text{in}}$ would drop from approximately 80 inches to approximately 12 inches. While a significant drop, an impact puncture 12 inches long would have left a visible signature on the tank car fragments. Most probable is that the dynamics of the tank car during the derailment and impacts placed severe structural loads on the tank cars. These loads caused large stresses around the stiffness discontinuity associated the stub sill and wheel assemblies, initiating failure in the tank car material. Because of the relatively low toughness of the material, the fractures were driven dynamically up to separation.

The design of tank cars to withstand puncture and structural failure under conditions such as the Minot accident requires a fully integrated approach coupling structural response, material failure and fracture. Previous activities aimed at improving the puncture resistance of tank cars were oriented towards the problem of low speed impact with couplers. The information gathered from these activities is of little relevance to the problem encompassing the dynamics of tank cars during higher speed derailments. As a simple example of the importance of looking at the coupled structural/material problem,

one can consider the influence of the tank car jacket. It is recognized that the additional steel of the tank car jacket enhances the puncture resistance of the tank car, Jeong (2001). However, current designs have the insulation and steel jacket unbonded from the tank and each other. Structurally, they act independently. If they were bonded and the insulating material was capable of acting as a shear coupler between the inner tank and outer jacket, the local flexural stiffness of the “composite or sandwich” shell would easily be an order of magnitude higher than that of the current uncoupled designs. This increased stiffness would greatly reduce the local stress concentrations caused by the stub sill to tank attachment and would distribute the inertia loads from the wheel sets in a smoother manner, thereby reducing the probability of structurally initiated fractures.

REFERENCES

ASTM International, *Standard Test Method for Plane-Strain Fracture Toughness of Metallic Materials, Designation E399-3*, West Conshocken, PA, 2002

T.L. Anderson, *Fracture Mechanics: Fundamentals and Applications*, 2nd edition, CRC Press, 1994.

J.M. Barsom, *Effect of Loading Rate on the Cleavage Fracture Toughness of a Structural Steel, Engineering Fracture Mechanics*, Vol. 7, pp.605-618, 1975.

D.L. Hanson and L.H. Koopman, *Tolerance Limits for the Class of Distributions with Increasing Hazard Rates, Annals of Mathematical Statistics*, vol. 35, pp 1561-1570, 1964.

D.Y. Jeong, Y.H. tang, and A.B. Perlman, *Evaluation of Semi-Empirical Analyses for Railroad Tank Car Puncture Velocity, Part I: Correlations with Empirical Data, DOT/FRA/ORD-01/2.1*, Volpe National Transportation Systems Center, November 2001.

T. Lasseigne, *Hazardous Materials Factual Report, Appendix F.*, NTSB Accident ID No DCA 02 MR 002, National Transportation Safety Board, June, 2002.

NTSB, *Collision of Union Pacific Railroad Train MHOTU-23 with BNSF Railway Company Train MEAP-TUL-126-D with Subsequent Derailment and Hazardous Materials Release, Macdona, Texas, June 28, 2004, NTSB,RAR-06/03*, National Transportation Safety Board, July 6, 2006.

NTSB, *Derailment of Canadian Pacific Railway Freight Train 292-16 and Subsequent Release of Anhydrous Ammonia Near Minot, North Dakota, January 18, 2002*, Railroad accident Report, NTSB/RAR-04/01, March 9, 2004.

P.M. McKeighan, *High Rate Fracture Toughness, Tensile Properties, CVN and Composition of Various TC-128BS Steels; Phase A: Pre-1989 GATX Tank Cars and Modern Vintage Plate, Phase B: Tank Cars Involved in the Minot, SD Accident*, June, 2005.

W.S. Pellini, *Analysis of Tank Car Failures Related to Rail Burn Dents*, AAR R-551, Association of American Railroads, June, 1983.

F. Zakar, *Materials Laboratory Factual Report No. 05-071*, National Transportation Safety Board, September 8, 2005.

F. Zakar, *Materials Laboratory Factual Report No. 03-042*, National Transportation Safety Board, April 24, 2003.